Glykogen Synthase Kinase-3-Inhibitoren: Design, Synthese und Optimierung sowie die Evaluation in Modellen der Alzheimer-Krankheit

TECHNISCHE UNIVERSITÄT DARMSTADT

Vom Fachbereich Chemie
der Technischen Universität Darmstadt

zur Erlangung des akademischen Grades eines
Doctor rerum naturalium (Dr. rer. nat.)

genehmigte
kumulative Dissertation

vorgelegt von
Dipl.-Chemiker Thomas Kramer
aus Ochtrup

Referent: Prof. Dr. Boris Schmidt
Korreferentin: Prof. Dr. Katja Schmitz
Tag der Einreichung: 29. Oktober 2012
Tag der mündlichen Prüfung: 10. Dezember 2012

Darmstadt 2013
D17

Meiner Familie, besonders meiner Mutter

Die vorliegende Arbeit wurde unter der Leitung von Herrn Prof. Dr. Boris Schmidt am Clemens Schöpf-Institut für Organische Chemie und Biochemie der Technischen Universität Darmstadt von Oktober 2008 bis Dezember 2012 angefertigt.

Teile dieser Arbeit sind bereits veröffentlicht

1) **Thomas Kramer**, Boris Schmidt, und Fabio Lo Monte, „*Small-Molecule Inhibitors of GSK-3: Structural Insights and Their Application to Alzheimer's Disease Models*", International Journal of Alzheimer's Disease 2012, *2012*, 32 Seiten, doi:10.1155/2012/381029.

2) Fabio Lo Monte*, **Thomas Kramer***, Alexander Boländer, Batya Plotkin, Hagit Eldar-Finkelman, Ana Fuertes, Juan Dominguez, Boris Schmidt, „*Synthesis and biological evaluation of glycogen synthase Kinase-3 (GSK-3) inhibitors: An fast and atom efficient access to 1-aryl-3-benzylureas*", Bioorganic & Medicinal Chemistry Letters 2011, *21*, 5610-5615, http://dx.doi.org/10.1016/j.bmcl.2011.06.131.

3) Fabio Lo Monte, **Thomas Kramer**, Jiamin Gu, Upendra Rao Anumala, Luciana Marinelli, Valeria La Pietra, Ettore Novellino, Bénédicte Franco, David Demedts, Ana Fuertes, Juan Manuel Dominguez, Batya Plotkin, Hagit Eldar-Finkelman, Boris Schmidt, „*Identification of Glycogen Synthase Kinase-3 Inhibitors with a Selective Sting for Glykogen Synthase Kinase-3α*", Journal of Medicinal Chemistry 2012, *55*, 4407-4424, doi: 10.1021/jm300309a.

4) Fabio Lo Monte, **Thomas Kramer**, Jiamin Gu, Martin Brodrecht, Johannes Pilakowski, Ana Fuertes, Juan Manuel Dominguez, Batya Plotkin, Hagit Eldar-Finkelman, Boris Schmidt, „*Struture-based optimization of oxadiazole-based GSK-3 Inhibitors*", European Journal of Medicinal Chemistry 2012, im Druck, http://dx.doi.org/10.1016/j.ejmech.2012.06.006.

5) Boris Schmidt, Fabio Lo Monte, **Thomas Kramer**, Hagit Eldar-Finkelman, Fred Van Leuven, „*Verbindungen als Glykogen Synthase Kinase-3 (GSK-3) Inhibitoren für die Behandlung von GSK-3-vermittelten Erkrankungen*" Deutsche Patentanmeldung 2011, Nr.: DE 10 2011 106 990.2.

6) **Thomas Kramer***, Fabio Lo Monte*, Stefan Göring, Ghislaine Marlyse Okala Amombo, Boris Schmidt, „*Small Molecule Kinase Inhibitors for LRRK2 and Their Application to Parkinson´s Disease Models*", ACS Chemical Neuroscience 2012, *3*, 151-160, doi: 10.1021/cn200117j.

*Erstautor

7) Ghislaine Marlyse Okala Amombo*, **Thomas Kramer***, Fabio Lo Monte*, Stefan Göring, Matthias Fach, Steven Smith, Stephanie Kolb, Robert Schubenel, Karlheinz Baumann, Boris Schmidt, „*Modification of a promiscuous inhibitor shifts the inhibition from γ-secretase to FLT-3*", Bioorganic & Medicinal Chemistry Letters, angenommen im Oktober 2012, http://dx.doi.org/10.1016/j.bmcl.2012.10.016.

8) Jiamin Gu, Upendra Rao Anumala, Fabio Lo Monte, **Thomas Kramer**, Roland Heyny von Haußen, Jana Hölzer, Valérie Goetschy-Meyer, Gerhard Mall, Ingrid Hilger, Christian Czech, Boris Schmidt, „*2-Styrylindolium based fluorescent probes visualize neurofibrillary tangles in Alzheimer´s disease*", Bioorganic & Medicinal Chemistry Letters, angenommen im Oktober 2012, http://dx.doi.org/10.1016/j.bmcl.2012.09.109.

*Erstautor

Danksagung

Danken möchte ich…

… Prof. Dr. Boris Schmidt für die hervorragende fachliche Unterstützung während der Dissertation, die Förderung in Form von Fortbildungen und Tagungsreisen sowie die interessanten fachbezogenen und -fremden Gespräche.

… der EU und Noscira für die finanzielle Unterstützung im Rahmen des *European 7th Framework Programme*.

… Prof. Dr. Hagit Eldar-Finkelman, Dr. Juan Manuel Dominguez, Prof. Dr. Fred van Leuven, für die erfolgreiche Zusammenarbeit, Ratschläge und anregenden Diskussionen während des GSK-3-Projekts. Batya Plotkin, Ana Fuertes, Bénédicte Franco und David Demedts für die unermüdliche Aktivitätsmessung unserer Substanzen.

… Dr. Karlheinz Baumann und Robert Schübenel von der Firma Hoffmann-La Roche, Basel für die Beantwortung meiner Fragen und für die zahlreichen Tests unserer Verbindungen in Ihrem Sekretase-Assays.

… Prof. Dr. Luciana Marinelli und Valeria La Pietra für die GSK-3-Modellingstudien.

… Prof. Dr. Veerle Baekelandt und Dr. Jean-Marc Taymans für die hervorragende Zusammenarbeit und die Beantwortung meiner Fragen während des LRRK2-Projekts.

… Prof. Dr. Stefan Laufer für die sofortige Bereitschaft der Aktivitätsbestimmung unserer Verbindungen in seinem Kinase-Assay.

… meinen derzeitigen und ehemaligen Arbeitskollegen Fabio, Jiamin, Upendra, Stefan, Stephanie, Marlyse, Azadeh, Andrea, Binia, Eva, Daniel, Alexander, Nicole, Stefanie, Hannes und Estella für die schöne und abwechslungsreiche Zeit im Labor und Sozialraum sowie darüber hinaus.

… der Kickertruppe Fabio, Jiamin, Upendra und Stefan für die geniale Abwechslung nach dem Mittagessen.

… meinen Vertiefungs-, Bachelor-, Diplom- und Masterstudenten Stefan, Steven, Matthias, René, Johannes und Martin für Ihren Einsatz und die freundschaftliche Zusammenarbeit.

… der analytische Abteilung des Instituts für Organische Chemie für die Durchführung und die Hilfe bei der Interpretation von NMR- (Herr Dr. Meusinger, Frau Jung und Herr Runzheimer) und MS-Messungen (Frau Rudolph und Frau Sahinalp).

… Fabio, Stefan und Sina für das Korrekturlesen dieser Arbeit und die vielen Anregungen.

… Freunden von nah und fern für euer offenes Ohr und die abwechslungsreiche Zerstreuung neben dem Laboralltag. Insbesondere Jens, der selbst aus dem fernen Australien mir immer mit Rat und Tat zur Seite stand und den Ochtruper/Metelener Gentlemen für die geniale Zeit, die wir immer wieder mit einander verbringen.

… meiner Familie für den Rückhalt und Zusammenhalt in jeder Lebenslage.

… meiner Partnerin Sina für einfach alles!

Inhaltsverzeichnis

Abkürzungsverzeichnis

Abb.	Abbildung
AAV	Allgemeine Arbeitsvorschrift
Aβ	Amyloid β Peptid (der Länge zwischen 38-43 Aminosäuren)
$A\beta_{40}$	Amyloid β Peptid der Länge von 40 Aminosäuren
$A\beta_{42}$	Amyloid β Peptid der Länge von 42 Aminosäuren
AChEI	Acetylcholinesterase-Inhibitor (*Acetylcholinesterase-Inhibitor*)
AD	Alzheimer-Krankheit (*Alzheimer´s disease*)
ADI	*Alzheimer´s Disease International*
AICD	Intrazelluläre Domäne des APP
AKT	gleich Proteinkinase B (PKB)
APC	Adenomatös Polyposis Coli
APOE	Apolipoprotein E
APP	Amyloid Vorläufer Protein (*amyloid precursor protein*)
Arg	Arginin
Asp	Asparagin
ATP	Adenosintriphosphat
BBB	Blut-Hirnschranke (*blood-brain barrier*)
C85	83 Aminosäure langes, C-terminales Fragment des APP
C99	99 Aminosäure langes, C-terminales Fragment des APP
ca.	circa
CDK5	*Cyclin-dependent kinase 5*
CK1	Casein kinase 1
ClogP	kalkulierter Verteilungskoeffizient zwischen Oktanol und Wasser
CNS	Zentrales Nervensystem (*central nerve system*)
CNS-MPO	CNS-Multiparameteroptimierung (CNS-*Multiparameter Optimization)*
^{11}C-PIB	Pittsburgh compound B
CS_2	Kohlenstoffdisulfid
CSF	Zerebrospinalflüssigkeit (*cerebrospinal fluid*)
CT	Computertomographie
Cy	Cyclohexan
Cys	Cystein
DCM	Dichlormethan
dest.	destilliert
DIC	*N*,*N´*-Diisopropylcarbodiimid
DMAP	4-(Dimethylamino)-pyridin
DMF	*N*,*N*-Dimethylformamid
DMSO-d6	6-fach deuteriertes Dimethylsulfoxid
EE	Ethylacetat
EOAD	*Early-onset* AD
eq.	äquivalent

ERK2	*Extracellular signal-related kinase 2*
EtOH	Ethanol
FAD	Familiäre AD (*familial* AD)
FDA	Food and Drug Administration
^{18}F-FDG	2-[^{18}F]-Fluor-2-deoxy-D-glukose
fMRT	funktionelle MRT (*functional MRT*)
FRAT	humane Form des GBP (GBP = GSK-3 Bindungsprotein)
g	Gramm
Glu	Glutaminsäure
GS	Glykogen Synthase
GSK-3	Glykogen Synthase Kinase-3 (*glycogen synthase Kinase-3*)
h	Stunde
Het	Heterozyklus
HPLC	*high pressure liquid chromatography*
IDE	*Insulin degrading enzyme*
kDa	Kilodalton
konz.	konzentriert
LRP1	*low-density lipoprotein receptor related protein-1*
Leu	Leucin
LiCl	Lithiumchlorid
LOAD	*Late-onset* AD
Lys	Lysin
MCI	*Mild cognitive impairment*
MeOH	Methanol
mL	Milliliter
min.	Minute
Mio.	Millionen
MRT	Magnetresonanztomographie (*magnetic resonance imaging*)
N	Normal
NFT	Neurofibrillenbündel (*neurofibrillary tangles*)
NINCDS-ADRDA	National Institute of Neurological and Communicative Disorders and Stroke and Alzheimer´s Disease and Related Disorders Association
NMDA-Rezeptor	*N-Methyl-D-aspartat* Rezeptor
NMR	Kernspinresonanz (*nuclear magnetic resonance*)
PD	Parkinson Krankheit (Morbus Parkinson; *Parkinson´s disease*)
PDB	Proteindatenbank
PET	Positronen-Emissions-Tomographie (*positron emission tomography*)
ppm	*parts per million*
Pro	Prolin
PSEN1	Presenilin 1
PSEN2	Presenilin 2
pSer	phosphoryliertes Serin
pTau	phosphoryliertes Tau

pThr	phosphoryliertes Threonin
RAGEs	*Receptor for advanced glycation endproducts*
RT	Raumtemperatur
SAD	Sporadische AD (*sporadic* AD)
sAPPα	durch die α-Sekretase abgespaltene, N-terminale Ektodomäne des APPs
sAPPβ	durch die β-Sekretase abgespaltene, N-terminale Ektodomäne des APPs
Ser	Serin
SPECT	Einzelphotonen-Emissions-Computertomographie (*single-photon emission computed tomography*)
T2D	Typ 2 Diabetes
TEA	Triethylamin
THF	Tetrahydrofuran
Thr	Threonin
TPSA	*topological surface area*
t_R	Retentionszeit
tTau	*total tau*
Tyr	Tyrosin
Val	Valin
WHO	Weltgesundheitsorganisation (*World Health Organisation*)

1 Einleitung

1.1 Alzheimer-Krankheit

Anfang 2012 rückte der ehemalige Schalke 04 Manager Rudi Assauer mit seiner Autobiographie „Wie ausgewechselt: Verblassende Erinnerungen an mein Leben“ die Alzheimer-Krankheit (*Alzheimer´s disease*, AD) wieder in den öffentlichen Mittelpunkt.[1]

Die AD ist eine irreversible, neurodegenerative Erkrankung. Sie ist gekennzeichnet durch zwei pathologische Hauptmerkmale: die Bildung von amyloiden Plaques und Neurofibrillenbündeln (*neurofibrillary tangels*; NFTs), Abb. 1. Diese Veränderungen im Gehirn wurden im vorherigen Jahrhundert durch Alois Alzheimer entdeckt und spielen eine entscheidende Rolle in der AD-Diagnostik.[2-4] Bis heute kann eine definitive AD-Diagnose erst *post mortem* erfolgen.[5,6] Die Folgen der Alzheimer-Krankheit sind Gedächtnisverlust, Verlust der Sprachfähigkeit, Verwirrtheit und Desorientierung.[7,8] Aufgrund dieser Symptome benötigen AD-Patienten eine intensive und meist langjährige Betreuung, was die AD auch aus sozioökonomischer Sicht zur großen Herausforderung macht.[9]

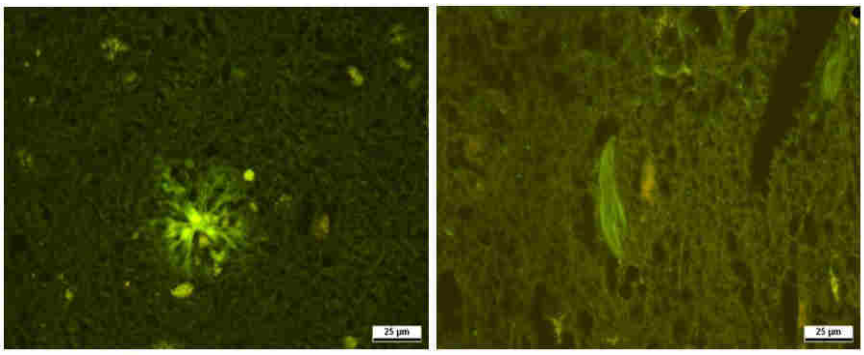

Abb. 1: Histopathologische Färbung von Gehirnschnitten, zur Verfügung gestellt von Dr. D. Kieser, in Zusammenarbeit mit dem Klinikum Darmstadt. Links: ein extrazelluläres amyloid Plaque; Rechts: ein intrazelluläres Neurofibrillenbündel (*neurofibrillary tangel*; NFT).

Neben der symptomatischen Behandlung der AD mit Acetylcholinesterase oder *N-Methyl-D*-aspartat Hemmern konnten verschieden Studien zeigen, dass auch eine Steigerung der kognitiven Belastung und der körperlichen Aktivität die Lebensqualität von AD-Patienten positiv beeinflusst.[10-12] Krankheitsbeeinflussende AD-Therapien

sind derzeit noch nicht bekannt, daher führt die Alzheimer-Krankheit unweigerlich zum Tod. Krankheitsbeeinflussende AD-Therapien sind jedoch Gegenstand intensiver Forschungsbemühungen. Dabei ist ein Schwerpunkt, die Entwicklung von Inhibitoren für die Glykogen Synthase Kinase-3 (GSK-3). Diese wird mit der Entwicklung beider pathologischer AD Merkmale in Verbindung gebracht.[13,14] Aktuell befinden sich potentielle Wirkstoffe unterschiedlicher Therapieansätze in der klinischen Entwicklung.[15]

1.1.1 Prävalenz und Inzidenz

Die bis dato unheilbare Alzheimer-Krankheit wird auch als „Krankheit des Alters“ bezeichnet, da sie verstärkt bei Menschen über 60 Jahren auftritt. Infolge des demographischen Wandels breitet sich die AD immer schneller und weiter aus.

Eine im Jahre 2005 veröffentlichte internationale Demenzstudie ergab, dass sich die für 2001 ermittelte Anzahl Demenzkranker (24,3 Mio.) alle 20 Jahre verdoppeln wird. Somit ist im Jahr 2040 von weltweit ca. 81,1 Mio. Menschen, die an einer Demenz erkrankt sind, auszugehen.[16] Bei ungefähr 70 % der Demenzpatienten wird die Erkrankung auf AD zurückgeführt.[17] Allein in Deutschland erkranken jedes Jahr schätzungsweise mehr als 290.000 Menschen im Alter von ≥ 65 Jahren an AD. Die geschätzte Gesamtanzahl deutscher AD-Patienten liegt bei knapp 1,2 Mio. Menschen. Bis zum Jahr 2030 wird mit einer Steigerung auf 2 Mio. Erkrankte gerechnet.[8,7] Eine von der Weltgesundheitsorganisation (*World Health Organisation*; WHO) veröffentlichte Studie über erwerbsunfähige Menschen ergab sogar, dass die Demenz mit 11,2 % bei Menschen älter als 60 Jahren die am häufigsten auftretende Krankheit darstellt, noch vor dem Schlaganfall, Herz-Kreislauf-Erkrankungen und Krebs.[18]

1.1.2 Pathologie

1.1.2.1 Amyloide Plaques und hyperphosphoryliertes Tau

Die Alzheimer-Krankheit zeichnet sich unter anderem durch eine erhöhte Immunantwort, Neuronendegeneration und Gehirnatrophie aus. Die Ursache dafür sind die pathologischen Hauptmerkmale amyloide Plaques und Neurofibrillenbündel.

Die extrazellulären amyloiden Plaques bestehen hauptsächlich aus Amyloid β (Aβ) Peptiden, die sich infolge des APP-Metabolismus (APP = Amyloid Vorläuferprotein; *amyloid precursor protein*) bilden.[19] Das APP ist ein Transmembranprotein, das mit der Bildung von Neuronen, deren Plastizität und dem Eisenexport in Verbindung steht.[20-22] Jedoch ist die genaue Funktion bis heute nicht geklärt. Das APP kann auf zwei Routen abgebaut werden, den nicht-amyloidogenen und amyloidogenen Weg, Abb. 2.[23]

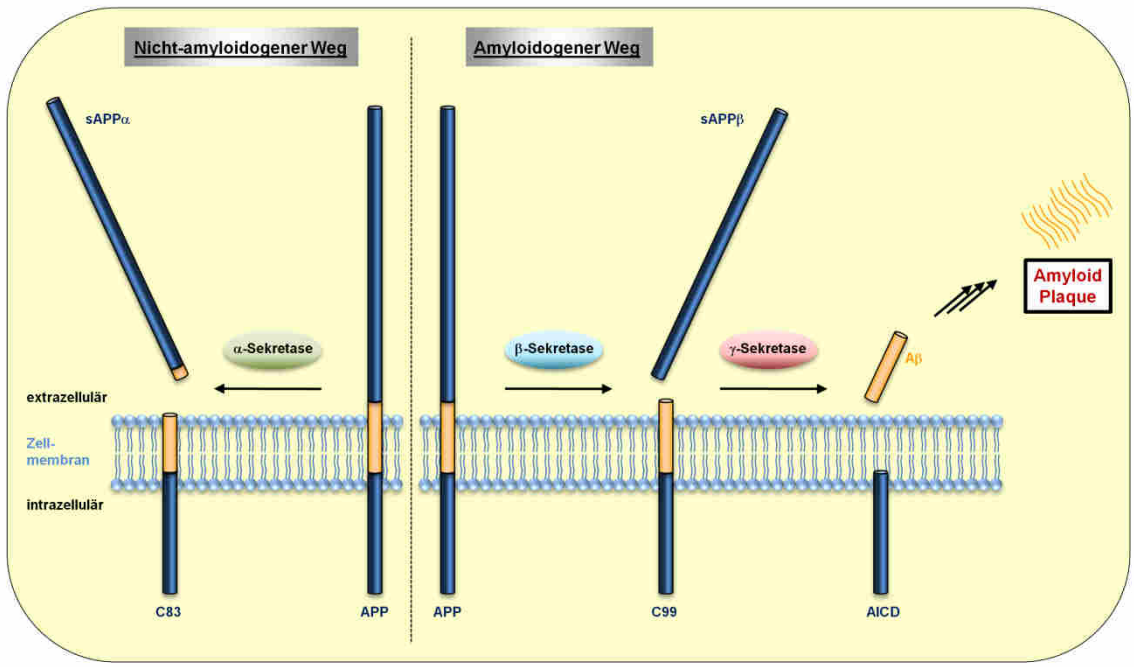

Abb. 2: Schematische Darstellung des nicht-amyloidogenen und amyloidogenen APP-Metabolismus; sAPPα = durch die α-Sekretase abgespaltene; N-terminale Ektodomäne des APPs; C83 = 83 Aminosäure langes, C-terminales Fragment; sAPPβ = durch die β-Sekretase abgespaltene, N-terminale Ektodomäne des APPs; C99 = 99 Aminosäure langes, C-terminales Fragment; AICD = intrazelluläre Domäne des APP; Aβ = amyloid β Peptide mit einer Aminosäureanzahl von 38-43.[23]

Bei gesunden Menschen dominiert der nicht-amyloidogene Weg. Dabei spaltet die α-Sekretase das APP und es werden nichttoxische Aβ-Peptide gebildet.[24,25] Treten

jedoch unter anderem Mutationen im APP auf, verschiebt sich der APP-Metabolismus in Richtung der amyloidogenen Route.[26] Hierbei wird das APP zunächst von der β-Sekretase gespalten. Anschließend spaltet die γ-Sekretase das transmembranständige C99 Peptid (99 Aminosäure langes, C-terminales Fragment). Dabei entstehen vor allem Peptide mit einer Länge von 40 Aminosäuren ($A\beta_{40}$), aber auch $A\beta_{42}$-Peptide. Insbesondere die $A\beta_{42}$-Peptide sind vergleichsweise hydrophob und weisen dadurch eine gesteigerte Tendenz zur Aggregation auf. Sie bilden letztlich die dominante Isoform der extrazellulären amyloiden Plaques.[27-31] Die Folgen der amyloiden Plaques sind oxydativer Stress, eine erhöhte Immunantwort und synaptische Fehlfunktionen. Diese werden neben den amyloiden Plaques mit der AD in Verbindung gebracht.[23]

Ein Vergleich von gesunden Menschen mit AD-Patienten ergab bei Letzteren eine achtmal höhere Konzentration des Proteins Tau im Gehirn.[32] Dieses Mikrotubuli-assoziierte Protein ist Hauptbestandteil der AD-assoziierten, intrazellulären Neurofibrillenbündel. Tau ist ein lösliches, weitgehend ungefaltetes Protein, welches sich infolge einer Hyperphosphorylierung zu den unlöslichen Aggregaten, NFTs, zusammenlagert, Abb. 3.[32-36] Für eine Vielzahl an AD-spezifischen Tau-Phosphorylierungsstellen konnten bereits die entsprechenden Kinasen wie *cyclin-dependent kinase 5* (CDK5), *extracellular signal-related kinase 2* (ERK2), Casein Kinase 1 (CK1) und Glykogen Synthase Kinase-3 (GSK-3) identifiziert werden.[37-39] Im Vergleich zu den anderen Kinasen phosphoryliert GSK-3 Tau an den meisten AD-spezifischen Phosphorylierungsstellen.[37] Laut der sogenannten Tau-Hypothese liegt im Fall der Alzheimer-Krankheit ein Ungleichgewicht zwischen der Kinase- und Phosphataseaktivität (Phosphatasen dephosphorylieren zuvor phosphorylierte Aminosäuren) in den Zellen des Gehirns vor.[38,39] Es folgt eine pathogene Hyperphosphorylierung von Tau, wodurch die Bindung an Mikrotubuli destabilisiert wird.[40,41] Die sich bildenden hyperphosphorylierten Tau-Monomere lagern sich zu Tau-Oligomeren zusammen. Diese formen paarig-helikale Filamente (PHFs), welche abschließend zu NFTs in Form von β-Faltblättern aggregieren. Die nun fehlende stabilisierende Wirkung des Tau-Proteins auf das Mikrotubuli führt letztlich zu dessen Depolymerisation. Dadurch wird der axonale Transport in den Neuronen und die Neurotransmission gestört.[34,36,40,41] Die Bildung von NFTs und die Störung des axonalen Transports hat die Degeneration der Neuronen und kognitive

Fehlfunktionen zur Folge. Beides wird mit der Alzheimer-Krankheit in Verbindung gebracht.

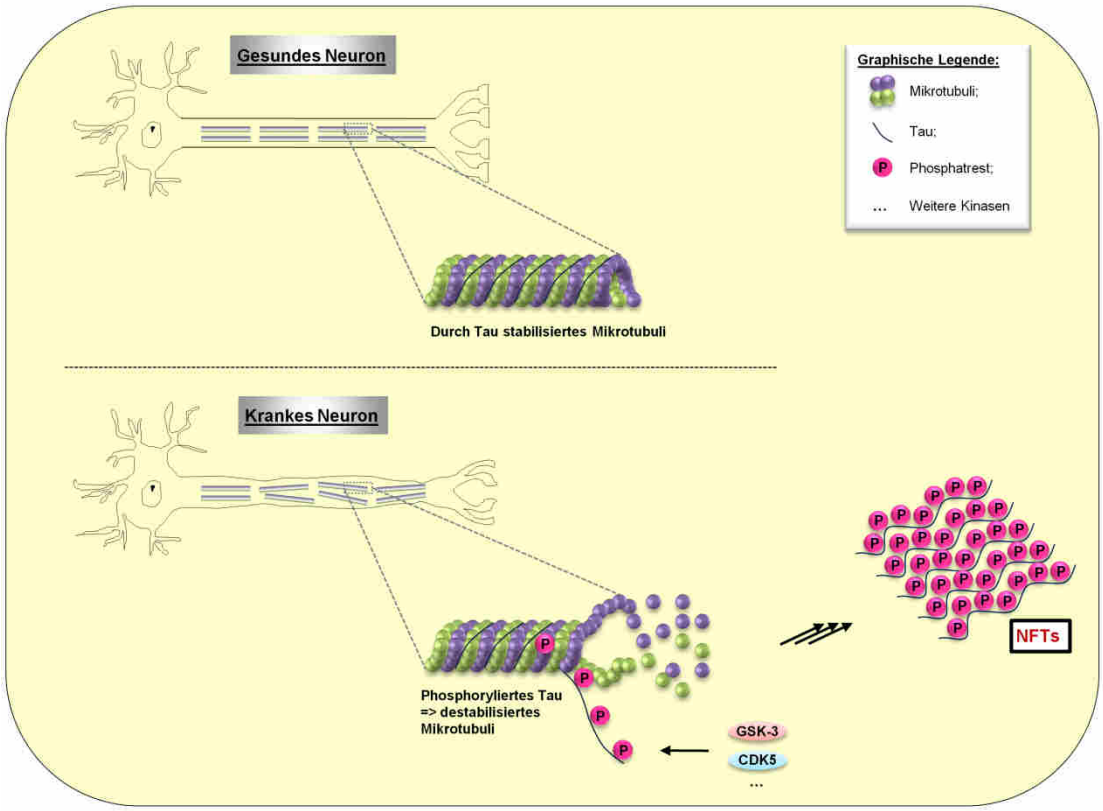

Abb. 3: Ein schematischer Vergleich eines gesunden und eines an einer Tauopathie wie beispielsweise die AD erkrankten Neurons sowie der Bildung von NFTs; CDK5 = *cyclin-dependent kinase 5*, GSK-3 = Glykogen Synthase Kinase-3.[42]

Der genaue Zusammenhang zwischen den amyloiden Plaques und NFTs ist bis heute nicht ganz verstanden. Ob die NFTs eine Folge der amyloiden Plaques sind oder umgekehrt ist Gegenstand aktueller Diskussionen.[43-47] Auf der einen Seite liegen wissenschaftliche Hinweise vor, dass eine toxische Konzentration an Aβ-Peptiden ausschlaggebend für die pathogene Veränderung von Tau (Bildung von NFTs) ist. Andererseits konnte nachgewiesen werden, dass eine erhöhte Tau-Expression die Bildung neurotoxischer, amyloider Peptide fördert.[37] Als verknüpfende Faktoren für die Entwicklung beider pathologischer Hauptmerkmale wurde die Kinase GSK-3 angeführt. GSK-3 wird nicht nur mit der Hyperphosphorylierung von Tau, sondern auch mit dem APP-Metabolismus in Verbindung gebracht.[36,48] Letzteres ist aktuell Gegenstand wissenschaftlicher Diskussionen.[45]

Derzeit werden jedoch nicht nur die amyloiden Plaques und NFTs als neurotoxisch betrachtet, vielmehr liegt der aktuelle wissenschaftliche Fokus auf deren löslichen

und neurotoxischen Vorläufern.[49-54] Neben den extrazellulären Aβ-Peptiden können auch Tau-Oligomere in unterschiedliche Gehirnregionen migrieren und dort ebenfalls neurotoxische Kaskaden auslösen.[55,56] Neben den angesprochenen Aβ- und Tau-Kaskaden gibt es eine Vielzahl epidemiologischer Faktoren, die die AD-Entwicklung fördern.[57]

1.1.2.2 Braak-Stadien

Die Verbreitung der NFTs im Gehirn lässt sich mit dem Schweregrad der AD eines Patienten korrelieren. Dies wird genutzt, um den Krankheitsfortschritt von AD-Patienten richtig einordnen zu können. Dabei werden die einzelnen Phasen der AD in sogenannte Braak-Stadien unterteilt, Abb. 4/Tabelle 1.[58,59]

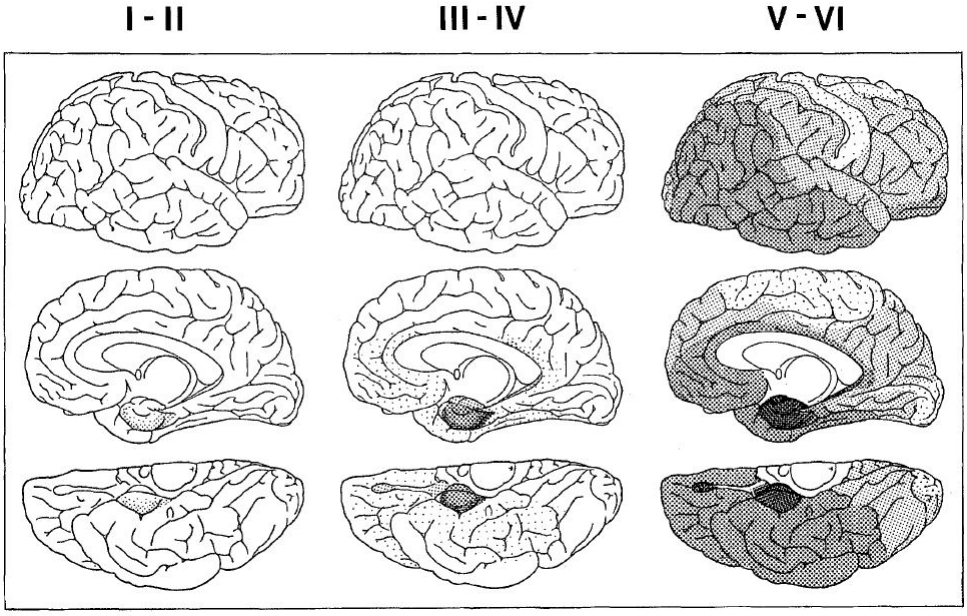

Abb. 4: Eine schematische Darstellung von NFT-Ablagerungen im Gehirn eingeteilt nach Braak-Stadien. – Mit freundlicher Genehmigung von *Springer*.[58]

Im ersten Braak-Stadium sind nur wenige NFTs in der transentorhinalen Gehirnregion detektierbar. Diese kommen im zweiten Braak-Stadium vermehrt vor und sind bereits teilweise auch im Hippocampus vorhanden. Weder im I. noch im II. Braak-Stadium sind klinische Symptome nachweisbar. Das ändert sich im dritten und vierten Braak-Stadium. Hier kommt es zu milden bis mäßigen kognitiven

Beeinträchtigungen und Persönlichkeitsveränderungen. Pathologisch breiten sich die Veränderungen bis zur äußeren entorhinalen Region und in die tiefere entorhinale Region (leitet Informationen zum Neocortex) aus. In den Braak-Stadien fünf und sechs können die NFTs im gesamten Hippocampus und in den angrenzenden Neocortex-Regionen nachgewiesen werden. Dies geht einher mit einer stark ausgeprägten Form der Demenz und motorischen Funktions- sowie Sprachstörungen.[58,59]

Auch die Entwicklung der Aβ-Ablagerungen wird in unterschiedliche Phasen eingeteilt.[60-64] Jedoch ist hierbei keine allgemeingültige Korrelation zwischen dem Ausmaß der Plaquebildung und der Schwere der AD zu erkennen.

Tabelle 1: Die Entwicklung der Alzheimer-Krankheit anhand der Tau-spezifischen Braak-Stadien.[58,59]

Braak-Stadium	Neuropathologie (Tau-spezifisch)	Klinische Pathologie (Verhaltensbeispiele)
1	wenige Neurofibrillenbündel in der transentorhinalen Gehirnregion	-
2	vermehrt Neurofibrillenbündel in der transentorhinalen Gehirnregion und teilweise auch im Hippocampus	-
3-4	Neurofibrillenbündel breiten sich bis zur äußeren entorhinalen Region und in die tiefere entorhinale Region aus	geringe kognitive Beeinträchtigungen und Persönlichkeitsveränderungen
5-6	Neurofibrillenbündel im gesamten Hippocampus und in den angrenzenden Neocortex-Regionen	stark ausgeprägte Form der Demenz und motorische Funktions- sowie Sprachstörungen

1.1.3 Genetik

Die Alzheimer-Krankheit wird in die zwei altersabhängigen Klassen *early-onset* AD (EOAD) und *late-onset* AD (LOAD) eingeteilt. AD-Patienten im Alter < 65 Jahren gehören zu EOAD und > 65 Jahren zu LOAD. Im Fall der EOAD wird in der Regel mit einem AD-Ausbruch in den späten 40igern bzw. frühen 50igern gerechnet. Ungefähr 1-5 % der AD-Patienten werden zur EOAD gezählt. Die Mehrheit (> 95 %) der AD-Patienten entwickelt die spätere LOAD. Klinisch sind EOAD und LOAD nicht zu unterscheiden.[17] Sie lassen sich jedoch anhand ihrer genetischen Ursachen differenzieren. Aufgrund der hohen Durchdringung mit genetischen Mutationen bei Patienten mit EOAD wird hier auch von einer familiären vererbbaren AD (*familial* AD, FAD) gesprochen. Die LOAD wird eher als sporadische AD (*sporadic* AD, SAD) angesehen, da sie neben den epigenetischen Faktoren auch von Umweltfaktoren beeinflusst und im geringeren Maße vererblich ist.[65]

APP (*Amyloid precursor protein*), *PSEN1* (Presenilin 1) und *PSEN2* (Presenilin 2) sind drei Gene, deren zumeist autosomal dominante Mutationen mit der EOAD in Verbindung gebracht werden, Tabelle 2.[66] Nach der Diagnose einer dieser Prädispositionen wird in > 85 % der Fälle im Laufe des Lebens AD festgestellt.[17] Aktuell sind 231 genetische Mutationen bekannt.[67] Genetische Mutationen von *APP*, *PSEN1* und *PSEN2* führen zu einem bevorzugten Abbau des Proteins APP durch den amyloidogenen Weg.[68,69]

Die einzige wissenschaftlich etablierte Prädisposition für LOAD ist der Polymorphismus des Gens Apolipoprotein E (APOE, Tabelle 2). Liegt ein APOE ε4 Allel vor, konnte ein 2- bis 3-fach erhöhtes AD Risiko festgestellt werden. Werden zwei APOE ε4 Allele bei einem Patienten bestimmt, besteht sogar ein mehr als 6-fach erhöhtes AD-Risiko. Mit jedem Allel beginnt die AD ca. sechs bis sieben Jahre eher.[70-72] Der mechanistische Zusammenhang zwischen APOE ε4 und AD konnte bisher nicht hinreichend aufgeklärt werden. Wissenschaftliche Untersuchungen weisen jedoch darauf hin, dass APOE ε4 das Ausschleusen von Aβ aus dem Gehirn vermindert und zudem die Aβ-Aggregation im Gehirn unterstützt.[73-76] Dennoch gibt es viele Menschen mit APOE Risikoallel, die demenzfrei älter als 90 Jahre werden. Dies lässt neben der genetischen Vorbelastung auf weitere genetische Einflüsse sowie Umweltfaktoren schließen, die letztlich in Kombination zu AD führen können.[66]

Tabelle 2: Prädispositionen der Alzheimer-Krankheit und deren Auswirkungen auf den β-amyloiden Phänotyp.

Gen Symbol	Gen Name	Chromosom	Erbgang	Phänotyp
APP	*Amyloid precursor protein*	21	Autosomal dominant	Steigert die Produktion von allen Aβ-Peptiden sowie im Speziellen die von $A\beta_{42}$
PSEN1	Presenilin 1	14	Autosomal dominant	Steigert die Produktion von $A\beta_{42}$
PSEN2	Presenilin 2	1	Autosomal dominant	Steigert die Produktion von $A\beta_{42}$
APOE	Apolipoprotein E	19	Sporadisch	Vermindert das Ausschleusen von Aβ aus dem Gehirn und unterstützt die Aβ-Aggregation

1.1.4 Diagnostik

Seit 1984 bilden die AD-Kriterien des *National Institute of Neurological and Communicative Disorders and Stroke and Alzheimer´s Disease and Related Disorders Association* (NINCDS-ADRDA) die Grundlage für die AD-Diagnostik.[6] Durch die fortwährende Einarbeitung neuer wissenschaftlicher Erkenntnisse im Bereich der prodromalen AD erfolgte eine stetige Weiterentwicklung. 2007 wurde durch die *International Working Group for New Research Criteria for the Diagnosis of AD* unter anderem festgelegt, dass sowohl die klinischen als auch pathologischen Merkmale vorliegen müssen, bevor eine definitive AD-Diagnose gestellt werden darf.[5] Klinische Merkmale umfassen beispielsweise die Verminderung des episodischen Gedächtnisses, aber auch Verhaltensauffälligkeiten wie Sprachstörungen und Verwirrtheit. Deren Charakterisierung und Klassifizierung erfolgt durch spezifische klinische Testverfahren, wie *Alzheimer´s Disease Assessment Scale-Cognitive Subset* (ADAS-Cog) oder *Mini-Mental State Examination* (MMSE).[11,12] Da bis heute die definitive Bestimmung der neuropathologischen AD-Merkmale der amyloiden Plaques und der NFTs nur *post mortem* möglich ist, gibt es derzeit intensive Forschungsbemühungen, spezifische Verfahren sowie Biomarker für die Diagnose zu Lebzeiten zu evaluieren.

1.1.4.1 Morphologische und funktionelle Diagnostik

Die bildgebenden Verfahren, die im Zuge der AD-Diagnostik zum Einsatz kommen, können grob in morphologische und funktionelle Methoden unterteilt werden. Die Magnetresonanztomographie (MRT) ist ein strukturell bildgebendes Verfahren basierend auf dem Prinzip der Kernspinresonanz (*nuclear magnetic resonance*, NMR).[77,78] Es ermöglicht den Abgleich zu unterschiedlichen Zeitpunkten aufgenommener Gehirnvolumina.[79-84] Die dabei ermittelten Gehirnatrophien konnten bereits mit Gedächtnisstörungen und einem erhöhten AD-Risiko in Verbindung gebracht werden.[85,86] Zudem konnte mit Hilfe der MRT die Unterscheidung zwischen

dem *mild cognitive impairment* (MCI), der Frontotemporalen Demenz und der AD verbessert werden.[87-90,17]

Durch die funktionell bildgebenden Verfahren, wie der funktionelle MRT (fMRT) und der Positronen-Emissions-Tomographie (PET), können neuronale Aktivitäten sichtbar gemacht werden.[91, 92,93] Dabei ermöglicht z. B. die Applikation einer PET-Sonde wie 2-[^{18}F]-Fluor-2-deoxy-D-glukose (**^{18}F-FDG**) die Messung des zerebralen Glukosemetabolismus, Abb. 5.[94,17] Dies ermöglicht auf indirektem Wege die Bestimmung der synaptischen Aktivität und somit die Wahrscheinlichkeit einer Demenzerkrankung.[95,96]

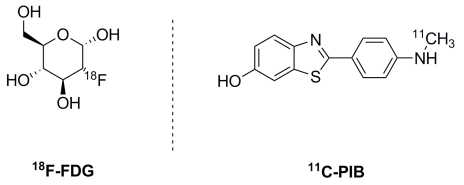

^{18}F-FDG **^{11}C-PIB**

Abb. 5: Links: Die zur Detektion des zerebralen Glukosemetabolismus verwendete PET-Sonde 2-[^{18}F]-Fluor-2-deoxy-D-glukose (**^{18}F-FDG**); Rechts: Die am häufigsten angewendete Aβ-Plaque spezifische PET-Probe im Bereich der AD **^{11}C-PIB** (PIB = Pittsburgh compound B).[97,94,17,98]

Um den direkten Einsatz funktionell bildgebender Verfahren in der AD-Diagnostik zu erhöhen, wurden eine Vielzahl an Aβ-Ablagerungen bindende, niedermolekulare Substanzen untersucht. Die am häufigsten verwendete und an Aβ-Ablagerungen bindende PET-Sonde ist Pittsburgh compound B (**^{11}C-PIB**, Abb. 5).[97,98] Durch **^{11}C-PIB**-PET-Messungen konnte das gesteigerte Vorkommen an Aβ-Ablagerungen bei AD-Patienten nachgewiesen werden, Abb. 6.[99] Es wird bei präklinischen Studien zur Unterscheidung von gesunden Menschen und zum Ausschluss von AD eingesetzt.[100] Avid Radiopharmaceuticals, ein Tochterunternehmen von Eli Lilly, entwickelte mit **Amyvid** (Florbetapir, 18F-AV-45) die erste an Aβ-bindende und von der *Food and Drug Administration* (FDA) zugelassene PET-Sonde, Tabelle 3.[101,102] Die im April 2012 zugelassene und seit Juni 2012 kommerziell erhältliche PET-Probe soll bei einem AD-Verdacht unterstützend zum Einsatz kommen. Unterstützend deshalb, da positive **Amyvid**-PET-Aufnahmen kein eindeutiger Hinweis auf AD sind. Der Grund liegt darin, dass Aβ-Ablagerungen auch bei älteren, gesunden Menschen vorkommen.[103] Dennoch lässt sich mit negativen **Amyvid**-PET-Aufnahmen die Alzheimer-Krankheit ausschließen. Dies liefert bei Patienten mit kognitiven

Schwächen und ohne Aβ-Ablagerungen einen Hinweis auf eine andere kognitive Erkrankung.[102,104]

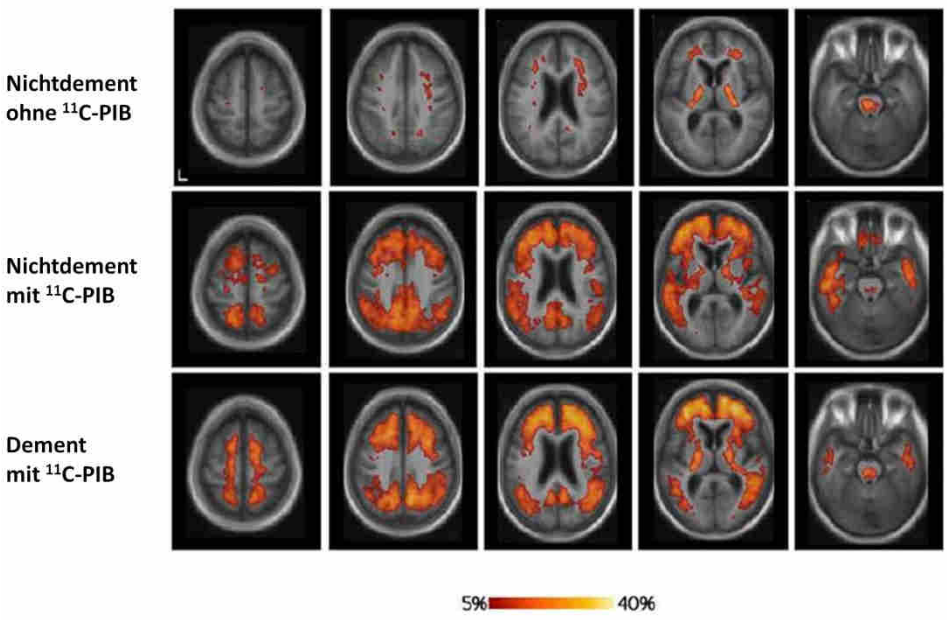

Abb. 6: ^{11}C-PIB-PET-Messungen zur Detektion von Aβ-Ablagerungen im Gehirn von nichtdementen Menschen und an Alzheimer erkrankten Menschen. Die Intensität der Aβ-Ablagerungen ist in einem prozentualen Bereich von 5-40 % farblich dargestellt. – Mit freundlicher Genehmigung der *Society for Neuroscience*.[105]

Tabelle 3: Amyvid, die erste an Aβ-bindende und von der FDA zugelasse PET-Sonde.[106,101,104,102,107-109]

Amyvid		
Firma:	Avid Radiopharmaceuticals (Eli Lilly)	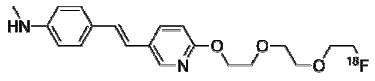
Bindungsmuster:	amyloide Plaques	
FDA Zulassung	April 2012	

Auf dem Gebiet der NFT-spezifischen Sonden gibt es noch keine von der FDA zugelassene PET-Probe. Jedoch wurde vor Kurzem mit **^{18}F-T808** der erste PET-Ligand publiziert, der 27-fach spezifischer an NFTs als Aβ-Plaques bindet, Abb. 7.[110,111] Erste präklinische Studien verliefen so positiv, dass laut der Autoren eine zukünftige klinische Prüfung geplant ist. Der Nutzen einer an NFTs bindenden Sonde besteht in der Möglichkeit, die gewonnenen PET-Aufnahmen mit den Braak-

Stadien vergleichen zu können. Das würde die Klassifizierung der AD eines Patienten und somit eine zielgerichtete Therapie ermöglichen.[112-114]

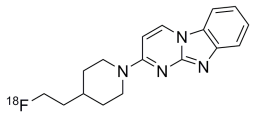

^{18}F-T808

Abb. 7: ^{18}F-T808, die erste NFT-spezifische PET-Sonde.[115,116,110,111]

1.1.4.2 Biomarker

$A\beta_{40}$, $A\beta_{42}$, pTau (phosphoryliertes Tau) und tTau (*total tau*) sind aktuell die gebräuchlichsten, löslichen Biomarker für die AD-Diagnostik. Sie kommen unter anderem im Plasma und der Zerebrospinalflüssigkeit (*cerebrospinal fluid*, CSF) vor. Im Vergleich zu gesunden Menschen lässt sich im CSF bei AD-Patienten eine erniedrigte $A\beta_{42}$-Konzentration feststellen.[117,118] Ein möglicher Grund könnten die Aβ-Ablagerungen und die damit verbundene Verringerung der löslichen Aβ-Konzentration sein. Entsprechende **^{11}C-PIB**-PET-Untersuchungen unterstützen diese Vermutung.[119] Dadurch könnten CSF-$A\beta_{42}$-Untersuchungen nicht nur als diagnostischer Biomarker für AD, sondern auch als Ersatzbiomarker für Aβ-Plaques verwendet werden.[4]

Die Konzentration an pTau und tTau im CSF ist bei AD-Patienten höher als bei gesunden Menschen.[120,121] Eine Kombination von CSF-$A\beta_{42}$-, pTau- und tTau-Untersuchungen könnte somit einen Weg darstellen, Prognosen über den kognitiven Verlauf vom normalen kognitiven Zustand bis hin zur AD zu ermöglichen.[122,117,123-125]

Die Detektion von $A\beta_{40}$, $A\beta_{42}$, pTau und tTau in Plasmaproben hängt entscheidend von der Blut-Hirnschranke (*blood-brain barrier*, BBB) ab. Im Fall der Plasmabiomarker $A\beta_{40}$ und $A\beta_{42}$ ist der genaue Mechanismus, der zum Gleichgewichtszustand zwischen dem Plasma- und Gehirn-$A\beta_{40}$- bzw. $A\beta_{42}$-Level führt, noch ungeklärt. Jedoch konnten mit den *receptor for advanced glycation endproducts* (RAGEs) und dem *low-density lipoprotein receptor related protein-1*

(LRP1) zwei unterschiedliche Arten von Aβ-Transporterproteinen bestimmt werden.[17] Dabei transportieren RAGEs Aβ-Peptide vom Plasma durch die BBB ins Gehirn und der LRP1 diese vom Gehirn zurück ins Plasma.[126-129] In einer Studie mit 1125 Probanden konnte ein Zusammenhang zwischen dem Plasma $A\beta_{40}/A\beta_{42}$-Verhältnis und einem Ausbruch der AD sowie einem fortgeschrittenen AD-Stadium bestimmt werden.[130] Obwohl dadurch das $A\beta_{40}/A\beta_{42}$-Verhältnis von Plasmaproben eine Aussage über die Entwicklung vom kognitiven Normalzustand bis hin zur AD zulässt, ergab sich bisher keine Korrelation mit den beim CSF erhaltenen Ergebnissen.[131-134]

1.1.5 Potentielle Risikofaktoren

Um mögliche Risikofaktoren für langwierige Demenzerkrankungen, wie z. B. die Alzheimer-Krankheit, vorbeugend begegnen zu können, wurden unterschiedliche klinische Studien und Beobachtungsstudien durchgeführt.[135] Dabei kam es bei Studien ähnlicher Rahmenbedingungen und Patientenkohorten oft zu widersprüchlichen Ergebnissen.[17] Deshalb wird im Folgenden nur eine Auswahl an Risikofaktoren, die einen belastbaren Zusammenhang zur Demenz bzw. AD aufweisen, aufgeführt: Tabelle 4.[10]

Tabelle 4: Eine Auswahl vorbeugender und risikobehafteter Faktoren der Alzheimer-Krankheit bzw. Demenz.

Risikofaktor	Folgen einer Steigerung	
	Verringert das AD/Demenz Risiko	Erhöht das AD/Demenz Risiko
Erhöhte kognitive Belastung	x	
Gesteigerte körperliche Aktivität	x	
Adipositas des mittleren Alters		x
Erhöhter Alkoholkonsum		x
Rauchen		x
Diabetes		x
Hirnschlag		x
Arterielle Hypertonie		x
Hypercholesterinämie		x

Die kognitive Belastung beinhaltet die Aspekte der Bildung, Erwerbstätigkeit und mentalen Aktivität.[136] Prospektive Studien hatten zum Ergebnis, dass kognitiv stimulierende Aktivitäten wie Lesen und Spiele spielen bei Menschen unterschiedlichen Alters eine geringere AD-Erwartung hervorrufen als bei Menschen, die diesen Aktivitäten nicht nachgehen.[137,138] Es werden jedoch nicht alle Gehirnregionen erreicht, wodurch beispielsweise alltägliche Gewohnheiten nicht beeinflusst werden.[139]

Körperliche Aktivitäten wie Aerobic haben einen positiven Einfluss auf die kognitiven Leistungen. Studien belegen, dass Bewegung eine gesteigerte Gehirnfunktion bei

Menschen im Alter > 55 Jahren zur Folge hatte. Sie wiesen eine erhöhte kognitive Auffassungsgabe, visuelle Aufmerksamkeit und ein besseres Hörvermögen auf.[140] Weitere Studien ergaben eine verbesserte Sauerstoffaufnahme, Glucoseverwertung und einen erhöhten zerebralen Blutfluss.[141]

Bei der Betrachtung des menschlichen Über- und Untergewichts wurde festgestellt, dass beides zu einem erhöhten Alzheimer-Krankheitsrisiko führt.[142-144] Dabei spielt jedoch der Zeitpunkt der Gewichtsmessung eine wichtige Rolle. Da Patienten im prodromalen Stadium der Demenz beispielsweise die Einnahme von Mahlzeiten vergessen, führt dies im Krankheitsverlauf zum Gewichtsverlust.[145] Bei starkem Übergewicht wird von einem bis zu 59 % erhöhten AD-Risiko ausgegangen.[146]

Ein dosisabhängiges Resultat ergaben 15 prospektive Studien, die den Alkoholkonsum als möglichen AD-Risikofaktor betrachtet haben.[147] Wird der Alkohol in geringem bis moderatem Maße konsumiert, wirkt er eventuell AD vermindernd. Steigert sich indes der Alkoholkonsum, erhöht sich das AD-Risiko.

Im Fall des Rauchens weisen acht empirische Studien auf einen protektiven Einfluss hin. Jedoch zeigen 14 Kohortenstudien auf, dass durch das Rauchen ein gesteigertes AD-Risiko besteht.[148,17] Rauchen kann durch verschiedene Mechanismen wie der Begünstigung des oxidativen Stresses der Beeinflussung des Immunsystems und der Förderung von zerebrovaskulären Krankheiten zu AD führen.[149]

Eine Vielzahl medikamentös behandelbarer Erkrankungen des mittleren Alters (zw. 31-50 Jahren) wurde mit einem erhöhten AD-Risiko in Verbindung gebracht. Dazu gehören beispielsweise der Diabetes Typ II (*type 2 diabetes*, T2D) und der Hirnschlag, sowie die arterielle Hypertonie und die Hypercholesterinämie, Tabelle 4. Einen direkten Zusammenhang zur AD gibt es jedoch nur im Fall des Diabetes.[10] Als Grund für die Verknüpfung des T2D und AD wurden verschiedene Mechanismen vorgeschlagen. Bei einer Hyperinsulinämie kommt es zu einer erhöhten Insulinausschüttung, das mit den Aβ-Peptiden um die Bindung an das *insulin degrading enzyme* (IDE) konkurriert. Dadurch wird das Ausschleusen des Aβ-Peptids aus dem Gehirn behindert und eine Akkumulation sowie die Bildung von AD unterstützt.[150] Liegt jedoch eine Insulinresistenz vor, kommt es zu einer reduzierten Aktivierung des Insulin-/AKT-Signalwegs. Eine Folge ist, dass GSK-3 nicht mehr

deaktiviert wird.[151] Aktives GSK-3 wird mit einer Hyperphosphorylierung von Tau und somit mit der Entstehung von NFTs und AD in Verbindung gebracht.[37] Die prospektiven Kohortenstudien zum Diabetes Typ II ergaben ein nahezu verdoppeltes AD-Risiko von T2D-Patienten.[152-154]

Ein Hirnschlag kann zerebrovaskuläre Veränderungen im Gehirn hervorrufen. Die Folge kann ein Gedächtnisverlust sein, der sich direkt zu einer Demenz ausweitet.[17] Eine weitere Konsequenz kann eine Hypoperfusion sein, welche eine Überexpression der CDK5 hervorruft. CDK5 wird neben GSK-3 mit einer anomalen Phosphorylierung von Tau und somit mit der Ausbildung von AD in Verbindung gebracht.[155] Darüber hinaus kann überexprimiertes CDK5 zu einer tödlichen, neuronalen Apoptose führen.[156]

Im mittleren Alter könnte die arterielle Hypertonie eine verminderte vaskuläre Integrität der BBB hervorrufen. Der dadurch entstehende Proteinfluss ins Gehirngewebe verursacht Zellschädigungen, Apoptose, Reduktion neuronaler oder synaptischer Funktionen und eine gesteigerte Aβ-Akkumulation führen.[157,158] Die Folge kann die Alzheimer-Krankheit sein. Durchgeführte Studien mit Blutdrucksenkern und deren Einfluss auf die Entwicklung von AD waren nicht eindeutig. Es müssen weitere Studien abgewartet werden, um eine genauere Aussage treffen zu können.[159]

Um den Zusammenhang zwischen Demenzerkrankungen und Hypercholesterinämie im mittleren Alter zu untersuchen, wurden klinische 18 Studien durchgeführt. Bei vier Studien konnte ein Zusammenhang zum gesteigerten Auftreten von Demenzerkrankungen bestimmt werden.[160,161] In Folgestudien mit Statinen (Cholesterinsenkern) zeigten sich jedoch keine positiven Effekte auf die Entwicklung der Alzheimer-Krankheit.[162]

Es bleibt festzuhalten, dass die wichtigsten selbst beeinflussbaren Faktoren die kognitive Belastbarkeit, körperliche Aktivität und die Adipositas des mittleren Alters sind.

1.2 Therapie und Therapieansätze

1.2.1 Aktuelle medikamentöse Therapien

Seit Mitte der 90iger Jahre ist die Behandlung der AD-Symptome möglich. Zu den Therapeutika gehören Acetylcholinesterase-Inhibitoren (AChEIs) und ein *N-Methyl-D*-aspartat (NMDA)-Rezeptor-Antagonist.

Neben den Aβ-Plaques und NFTs sind die Beschädigung und das Sterben von Neuronen Folgen der Alzheimer-Krankheit. Infolgedessen wird weniger des Neurotransmitters Acetylcholin produziert. Dies kann durch die Applikation von Acetylcholinesterase-Inhibitoren ausgeglichen werden. AChEIs hemmen den Abbau von Acetylcholin. Im Anfangsstadium einer AD kann dies die ungenügende Produktion von Acetylcholin kompensieren.[163,164] Der erste von der FDA zugelassene AChEI war das **Tacrin Hydrochlorid** (Cognex®), Tabelle 5.[165]

Tabelle 5: Von der FDA zugelassene Medikamente für die Therapie der Alzheimer-Krankheit.

Unternehmen	Wirkstoff/ Markenname	Struktur	Klassifikation
Shionogi Inc.	Tacrin Hydrochlorid/ Cognex®	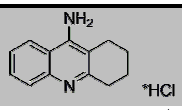	AChEI[a]
Eisai Inc.	Donepezil Hydrochlorid/ Aricept®	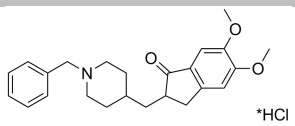	AChEI[a]
Novartis Pharmaceuticals Corp.	Rivastigmin Tartrat/ Exelon®	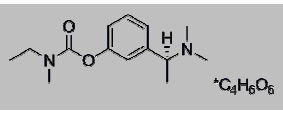	AChEI[a]
Janssen Pharmaceuticals NV	Galantamin Hydrobromid/ Razadyne®	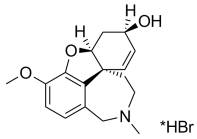	AChEI[a]
Forest Pharmaceuticals Inc.	Memantin Hydrochlorid/ Namenda®	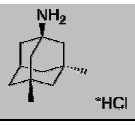	NMDA[b]-Rezeptor-Antagonist

[a] AChEI = Acetylcholinesterase-Inhibitor; [b] NMDA = *N-Methyl-D*-aspartat.

Der Wirkstoff besitzt eine relativ schwierige Applikationsroutine und weist zudem erhebliche Nebenwirkungen bis hin zur Hepatotoxizität auf. Heutzutage wird das **Tacrin** nicht mehr im signifikanten Maße angewendet. Darauffolgend wurden leichter

dosierbare und verträglichere AChEIs **Donepezil Hydrochlorid** (Aricept®; wird als Racemat verabreicht), **Rivastigmin Tartrat** (Exelon®) und **Galantamin Hydrobromid** (Razadyne®) entwickelt, Tabelle 5. Alle drei AChEIs sind am effektivsten, wenn sie bereits im Anfangsstadium der AD eingenommen werden und erzielen beim Patienten annähernd die gleichen kognitiven Effekt.[166-168] Sie verlangsamen den kognitiven Abbau und somit auch indirekt die Gemütsverfassung sowie die soziale Interaktion von AD-Patienten.[169-172] Neue Untersuchungsmethoden, wie das *Goal Attainment Scaling*, helfen zudem bei der individuellen Behandlung mit AChEIs und verbessern deren Wirkpotential.[173,174]

Das von der FDA zuletzt zugelassene Arzneimittel zur Behandlung von Alzheimer ist das **Memantin Hydrochlorid** (Namenda®), Tabelle 5.[175,168] Es ist ein nicht kompetitiver NMDA-Rezeptor Antagonist. **Memantin** blockiert die Bindung des erregenden Neurotransmitters Glutamat an NMDA-Rezeptoren. Lädierte bzw. sterbende Neuronen lassen sehr viel Glutamat in den synaptischen Spalt frei. Dies hat eine Überstimulation und Beschädigung der nachgeschalteten Neuronen sowie eine gesteigerte Aktivität der NMDA-Rezeptoren zur Folge. Letzteres führt zu einer übersteigerten Kalziumfreisetzung und schließlich zur Zellschädigung bzw. zum Zelltod.[176,177] Die Applikation von **Memantin** ermöglicht eine zeitlich begrenzte Unterdrückung dieser Exzitotoxizität, steigert die kognitive Leistung und wird zur Prävention bzw. Behandlung von Ruhelosigkeit und Aggressionen eingesetzt.[178,179] Es wird als Einzel- oder Kombinationstherapie zusammen mit AChEIs im mittleren bis fortgeschrittenen AD-Stadium eingesetzt.[180,175] Obwohl die angesprochenen Wirkstoffe eine Verlangsamung des kognitiven Abbaus hervorrufen, verringert sich jedoch ihre Effektivität im Verlauf der AD.[181] Der Grund liegt in dem nicht mehr kompensierbaren Neuronensterben.

Es gibt noch weitere Wirkstoffe, die in der AD-Therapie eingesetzt werden. Jedoch dienen diese der Behandlung potentieller AD-Begleiterscheinungen wie Depressionen oder Psychosen und sind nicht direkt für die AD-Therapie zugelassen. Sie kommen im Zuge einer zulassungsüberschreitenden Anwendung (*off-label use*) zum Einsatz.[12] Dabei muss immer das Verhältnis der geringen Behandlungserfolge gegenüber den eventuell auftretenden, starken Nebenwirkungen, wie einem Hirnschlag oder einer Erkrankung an Parkinson (Morbus Parkinson = *Parkinson´s disease* = PD), beachtet werden.[182,183]

Abschließend bleibt festzuhalten, dass obwohl eine Behandlung der AD Symptome in Grenzen möglich ist, eine krankheitsbeeinflussende Therapie Ziel der derzeitigen und zukünftigen Forschungsbemühungen sein muss.

1.2.2 Krankheitsbeeinflussende Therapieansätze

Es gibt eine Vielzahl an Hypothesen zur krankheitsbeeinflussenden Behandlung von AD, Tabelle 6.[184] Die entscheidenden, welche direkt mit den pathologischen Ursachen der AD in Verbindung stehen, sind die Aβ- und Tau-Hypothese.

Tabelle 6: Eine Auswahl an Hypothesen, die die Ursachen der Alzheimer-Krankheit beschreiben sollen.[184]

AD begründende Hypothese	Zugrundeliegender Effekt
Aβ	Aβ-Akkumulation
Cell cycle	Nicht normale Aktivität und Wiedereintritt neuronaler Zellen in den Zellzyklus
Entzündung	Nachhaltige Immunantwort unter Einbeziehung von Mikrogliazellen und Astrozyten
Oxidativer Stress	Überproduktion freier Radikale
Vaskuläre	Zerebrale Hypoperfusion und Auftreten vaskulärer Risikofaktoren
Tau	Hyperphosphoryliertes Tau und dessen Akkumulation

Die Aβ-Hypothese ist die bis dato am intensivsten untersuchte. Sie begründet die Entwicklung von AD mit der exzessiven Bildung von Aβ und dessen Akkumulation zu den extrazellulären Aβ-Plaques.[185] Im letzten Jahrzehnt wurden neuere Erkenntnisse über die neurotoxischen Eigenschaften löslicher Aβ-Oligomere und Protofibrillen mit der AD in Verbindung gebracht.[52] Infolge der Aβ-Hypothese ergaben sich diverse therapeutische Ansätze. Zu nennen wären die Modulation der Aβ-Produktion, die Unterdrückung der Aβ-Aggregation, die Förderung des Aβ-Abbaus und die Aβ-Immuntherapie, Abb. 8.[186] Die Immuntherapie kann in zwei Bereiche eingeteilt werden, in die aktive und passive Impfung. Bei der Aktiven handelt es sich um eine Impfung mit humanen fibrilliären $A\beta_{42}$-Peptiden. Deren subkutane Injektion über einen gewissen Zeitraum soll eine Immunantwort in Form von anti-Aβ-Antikörpern hervorrufen.[187,188] Jedoch konnten die positiven Ergebnisse der Tierversuche nicht in klinischen Tests bestätigt werden.[189,190] Ähnlich wie bei der aktiven Impfung erzielte

die passive Impfung mit monoklonalen Aβ-Antikörpern in Tiermodellen gute Ergebnisse, die jedoch nicht in klinischen Studien bestätigt werden konnten.[191,192] Die Förderung des Aβ-Abbaus kann ebenfalls in zwei Teilbereiche eingeteilt werden. Zum einen kann der direkte Abbau unterdrückt, zum anderen können Transporterproteine der BBB aktiviert oder deaktiviert werden. Die Aktivierung der Aβ-Degradationsenzyme Neprilysin, insulinabbauende Enzyme oder Plasmin gestaltet sich aus medizinalchemischer Sicht eher kompliziert.

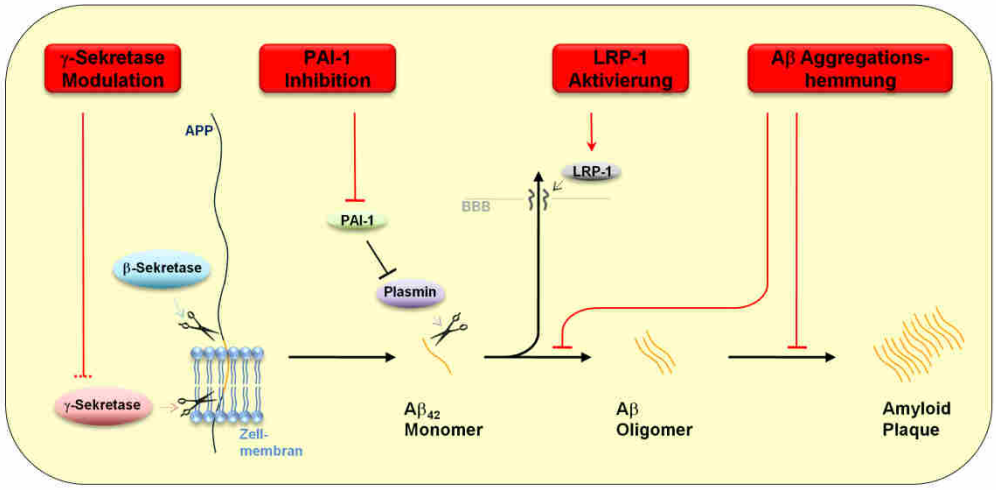

Abb. 8: Ein Auszug möglicher Aβ Therapien zur Behandlung von AD (Alzheimer-Krankheit); APP = Amyloid Vorläufer Protein (*amyloid precursor protein*), PAI-1 = *plasminogen activator inhibitor 1*, LRP1 = *low-density lipoprotein receptor-related protein 1*, BBB = Blut-Hirnschranke (*blood-brain barrier*).[186]

Ein Zugang ist die Inhibition der Enzyme, die die Aβ-Degradationsenyzme hemmen.[193] Dies wurde bereits in Form eines PAI-1-Inhibitors (PAI-1 = *plasminogen activator inhibitor 1*) erfolgreich umgesetzt.[194] Mit RAGE sowie LRP1 konnten zwei entscheidende Aβ-Transporterproteine benannt werden. Hierbei ist RAGE für den Aβ-Zustrom ins Gehirn und LRP1 für dessen Ausschleusen verantwortlich.[157] Jedoch gab es bisher keine positiven klinischen Ergebnisse für Aktivatoren/Inhibitoren auf den Gebieten der Aβ-Transporter und Aβ-Degradationsenzyme.

Aβ-Aggregationshemmer sind niedermolekulare Substanzen, die an Aβ-Aggregate binden und deren Aneinanderlagern verhindern sollen. Allerdings ergaben auch hierbei klinische Studien bisher kein positives Resultat.[195]

Die Modulation der Aβ-Produktion geht einher mit der Beeinflussung der Sekretaseaktivität. Sie bildet den Schwerpunkt aktueller Sekretaseforschung und es wurden bereits eine Vielzahl an γ-Sekretasemodulatoren publiziert, Abb. 9.[196-199]

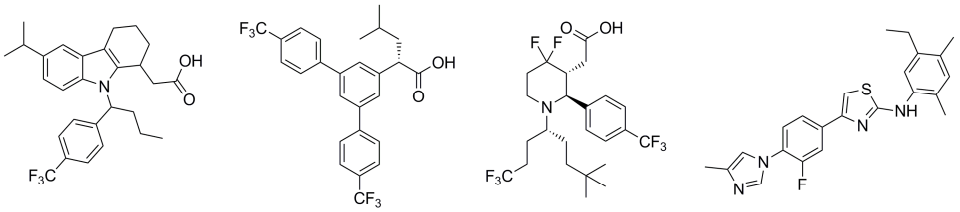

Carbazolderivat **JNJ-40418677** **Piperidinderivat** **2-Aminothiazolderivat**

Abb. 9: Eine Auswahl an γ-Sekretasemodulatoren, die die Aβ-Sekretion vom pathologischen $Aβ_{42}$ Zugunsten des unbedenklichen $Aβ_{38}$ reduziert.[196-199]

Die γ-Sekretase wird moduliert (d.h. die Bildung von $Aβ_{42}$ unterdrückt und die Bildung vom unbedenklichen $Aβ_{38}$ unterstützt) und nicht inhibiert, da sie ansonsten auch den Notch-Signalweg beeinflussen würde. Ist letzteres der Fall, können unerwünschte Nebenwirkungen, in Form von Metaplasie intestinaler Becherzellen, Alterung der Milz B-Zellen und Hemmung der Thymozytendifferenzierung auftreten.[200,201] Bis heute konnten sich weder γ-Sekretasemodulatoren noch γ-Sekretaseinhibitoren in den klinischen Phasen durchsetzen.[181]

Mit der Tau-Hypothese wird das zweite pathologische Merkmal der AD betrachtet, die intrazellulären NFTs.[32,202] Sie treten auch im Rahmen sogenannter Tauopathien wie der Pick-Krankheit (*Pick´s Disease* oder auch bekannt unter der Frontotemporalen-Demenz) oder der progressiven supranukleären Blickparese auf. Dennoch besteht eine enge Korrelation zwischen der Alzheimer-Krankheit und den Tau-Ablagerungen.[203-205] Wie bei der Entstehung der Aβ-Plaques gibt es auch bei der Bildung der NFTs mehrere therapeutische Ansätze, Abb. 10. Einer davon ist die Unterdrückung der Tau-Aggregation. Ein zweiter ist die Hemmung der Tau-Hyperphosphorylierung.[206,207] Auf dem Gebiet der Tau-Aggregationshemmer wurde bereits eine Vielzahl potentieller Leitstrukturen veröffentlicht.[42,208] Jedoch konnten die positiven Resultate aus den vorangegangenen *in vivo* Tests in den klinischen Studien nicht bestätigt werden.

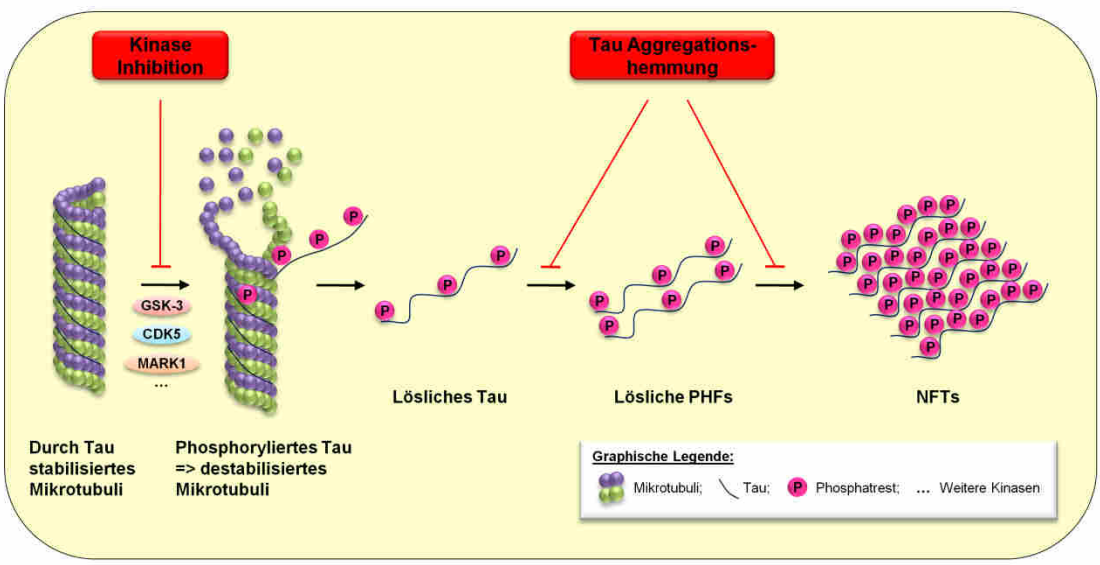

Abb. 10: Ein Auszug möglicher Tau-Therapien zur Behandlung von AD (Alzheimer-Krankheit); GSK-3 = Glykogen Synthase Kinase-3, CDK5 = *cyclin-dependent kinase 5*, MARK1 = MAP/*microtubule affinity-regulating kinase 1*.[186,38]

Für die Hyperphosphorylierung von Tau sind Kinasen wie GSK-3, CDK5 und die MAP/*microtubule affinity-regulating kinase 1* (MARK1) verantwortlich.[209,37,38] Deren Inhibition ist ein weiterer therapeutischer Ansatz, um die Bildung von NFTs zu verhindern. Im Fall von GSK-3 gibt es eine Fülle von Inhibitorleitstrukturen, Abb. 11, deren einzelne Vertreter bereits in AD-spezifischen *in vivo* Modellen getestet wurden.[210] Aktuell befindet sich ein Inhibitor der TDZD-Klasse (TDZD = Thiadiazolindion), **Tideglusib**, in der klinischen Phase IIb.[211]

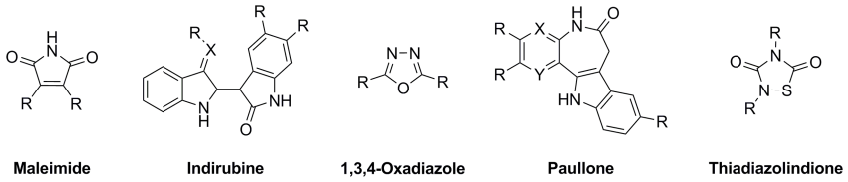

Abb. 11: Eine Auswahl an Inhibitorleitstrukturen für die Glykogen Synthase Kinase-3.[212,210,213]

Derzeit sind unterschiedlichste klinische Studien potentieller Arzneimittel mit dem Indikationsgebiet AD aktiv. Sei es auf dem Gebiet der Aβ-Impfstoffe (z. B. Novartis mit **CAD-106**, Elan Pharmaceuticals mit **ACC-001**), wie eben erwähnt auf dem Gebiet der GSK-3 Inhibitoren (Noscira mit **Tideglusib**) oder der Anwendung „alter“, bereits von der FDA zugelassener Arzneistoffe mit AD als neuem Indikationsgebiet (Amgen Inc. mit **Etanercept** – TNF-α Inhibitor).[15,211,214-218] Da bisher alle klinischen Studien negativ verliefen, wird derzeit über eine Modifikation der klinischen AD-

Studien nachgedacht. Dadurch soll eine verbesserte Erprobung potentieller AD-Wirkstoffe ermöglicht werden.[186,219]

Abschließend sei noch zu erwähnen, dass es auch nichtmedikamentöse Behandlungsansätze, wie beispielsweise kognitive Trainingseinheiten, für AD-Patienten gibt.[220] Spezifische Übungen sind online frei zugänglich.[221]

1.3 Die Glykogen Synthase Kinase-3 als therapeutisches Zielenzym zur Behandlung der Alzheimer-Krankheit

1.3.1 Glykogen Synthase Kinase-3

Die Glykogen Synthase Kinase-3 (GSK-3) ist eine prolingerichtete (P+1) Serin/Threonin Kinase. Sie zählt zur CMCG Kinasefamilie. Dazu gehören neben GSK-3 auch die MAP-Kinasen und CDKs.[222-225] 1980 wurde die Glykogen Synthase Kinase-3 im Zusammenhang mit der Phosphorylierung der Glykogen Synthase (GS) identifiziert.[226] Sie katalysiert die Übertragung des γ-Phosphatrests vom Adenosintriphosphat (ATP) auf das jeweilige Substrat, Abb. 12.

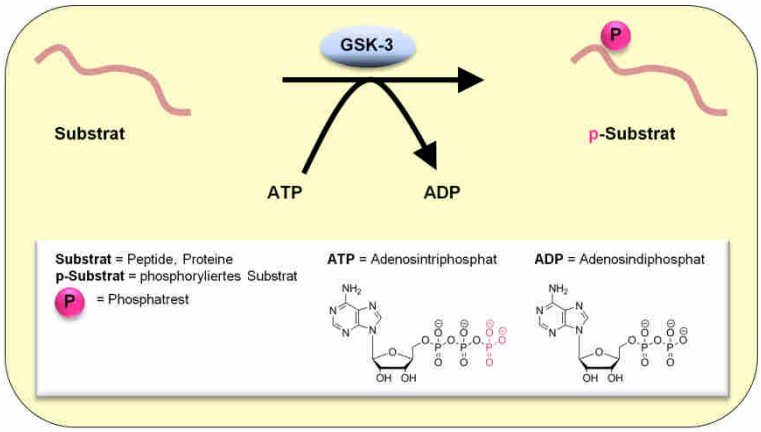

Abb. 12: Allgemeine Darstellung der Übertragung von einem γ-Phosphatrest eines Adenosintriphosphats auf ein Substrat, z. B. GS.

GSK-3 phosphoryliert eine Vielzahl von Substraten. Dazu gehören Transkriptionsfaktoren wie β-Catenin, Strukturproteine wie Tau und metabolische Enzyme wie APP, PSEN1 oder GS.[224] Ein Großteil der Substrate liegt geprimt (= vorphosphoryliert, *primed*) vor und weist eine P+4 Erkennungssequenz, Ser/Thr-XXX-pSer/pThr (X = beliebige Aminosäure, pSer/pThr = phosphoryliertes Serin bzw. Threonin), auf.[232, 235] GSK-3 konnte mit mehreren Signalwegen wie dem WNT-Signalweg und dem Insulin/AKT Signalweg in Verbindung gebracht werden.[227] Eine anomal gesteigerte Aktivität bzw. Überexpression von GSK-3 wird mit Krankheiten wie T2D, Krebs, Bipolarer Störung und AD in Beziehung gesetzt.[228-230] GSK-3 ist stark konserviert.[231] Ihre Orthologen wurden in diversen Organismen wie Pilzen, Würmern, Fliegen und Menschen identifiziert.[229, 230] Die konstitutiv aktive Kinase wird ubiquitär exprimiert.

Beim Menschen wird GSK-3 am stärksten im Gehirn, in Neuronen sowie Gliazellen, exprimiert.[232,233,231,234] Es gibt zwei humane GSK-3 Isoformen, GSK-3α und GSK-3β. GSK-3α ist durch seine erweiterte, glycinreiche N-terminale Domäne mit 51 kDa (483 Aminosäuren) größer als GSK-3β mit 47 kDa (433 Aminosäuren).[235,231] Beide besitzen eine hohe Sequenzhomologie von 85 %. In der ATP-Bindungstasche liegt sogar eine Übereinstimmung von 98 % vor.[231] Neben GSK-3α und GSK-3β wurde mit GSK-3β2 eine humane Splicevariante von GSK-3β entdeckt. Diese zeichnet sich durch eine 13 Aminosäure umfassende Insertion zwischen den GSK-3β Aminosäuren 303 und 304 aus. Sie wird hauptsächlich in neuronalem Gewebe exprimiert.[233, 234]

Die genauen Funktionen der GSK-3 Isoformen sind bis heute nicht geklärt. Einen Hinweis auf deren metabolische Zusammenhänge könnte beispielsweise eine detaillierte Untersuchung von Vögeln als natürlichem GSK-3α *knockout* Model liefern.[236]

1.3.2 Struktur

Die röntgenkristallographisch gelöste Struktur von GSK-3β ermöglicht einen Blick auf deren dreidimensionalen Aufbau, Abb. 13 (links).[235,237]

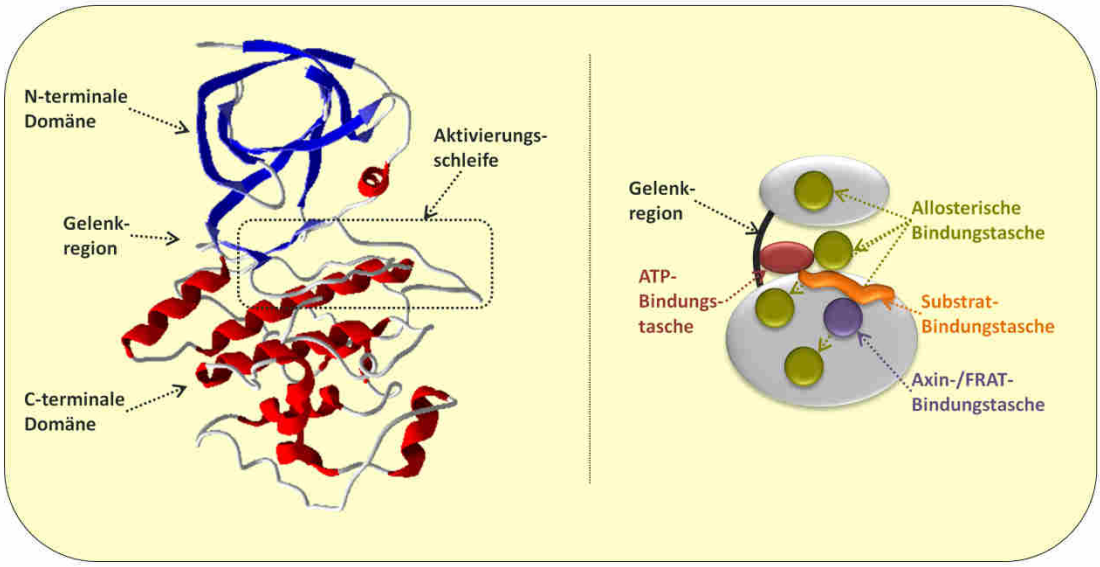

Abb. 13: Die Tertiärstruktur der Glykogen Synthase Kinase-3 (GSK-3) (links; PDB: 3F88; verwendete Software: Molegro Virtual Docker 5) und eine schematische Darstellung von GSK-3 inklusive potentieller Bindungstaschen (rechts).[238,239,237]

Die Proteinstruktur von GSK-3β entspricht einer allgemeinen zwei Domänen-Konformation. Sie besteht aus einer kleineren, N-terminalen β-Strang-Domäne und einer größeren, C-terminalen, α-helikalen Domäne.[240,241] Zwischen den beiden Domänen im Bereich der Gelenkregion befindet sich die ATP-Bindungstasche.[237] Direkt neben der ATP-Bindungstasche ist die Substratbindetasche, welche von einer Aktivierungsschleife umrahmt wird, lokalisiert. Die Aktivierungsschleife liegt dabei in einer aktiven Konformation vor, was der Grund dafür ist, warum GSK-3 als konstitutiv aktiv gilt. Diese Konformation ermöglicht den Zugang von Substraten zur Substratbindetasche und zu einer kleinen, benachbarten Phosphatbindetasche (bestehend aus Arg96, Arg180 und Lys205). Letztere bindet den Phosphatrest eines geprimten Substrats und erleichtert so dessen Interaktion mit der Substrat-bindetasche von GSK-3β.[232, 235] Die Axin-/FRAT-Bindetasche ermöglicht die Bindung von Axin bzw. FRAT (FRAT = humane Form des GBP, GSK-3 Bindungsprotein) und somit zur Bildung von Proteinkomplexen. Durch Dockingstudien konnten vier weitere allosterische Bindungstaschen bestimmt werden.[238]

Alle GSK-3-Bindungstaschen sind potentielle Ziele für GSK-3-Inhibitoren. Jedoch sollte im Fall von allosterischen Inhibitoren darauf geachtet werden, dass potentielle Interaktionen mit Bindungstaschen im N-terminalen Bereich weniger konformationsändernd und somit aktivitätsbeeinflussend wirken als solche im C-terminalen Bereich.[242]

1.3.3 Regulation

Es gibt mehrere Mechanismen zur Regulation der Aktivität von GSK-3. Sie kann durch Phosphorylierung, Proteinkomplexbildung, subzelluläre Lokalisation und *„primed“* Substrate erfolgen.[224,243]

Wird GSK-3 phosphoryliert, kann dies sowohl inhibierend als auch aktivierend wirken. Im Fall des Ser21 bei GSK-3α bzw. Ser9 bei GSK-3β wird die Kinaseaktivität inhibiert.[244-246] Dies erfolgt über einen Autoinhibitionsmechanismus. Zunächst werden die am N-Terminus lokalisierten Serine 21 bzw. 9 von einer anderen Kinase wie AKT (AKT = PKB, Proteinkinase B) phosphoryliert. Anschließend dient diese N-terminale Aminosäuresequenz als Pseudosubstrat und faltet sich so zurück, dass sie ihre eigene Substratbindetasche blockiert, Abb. 14.[232, 235]

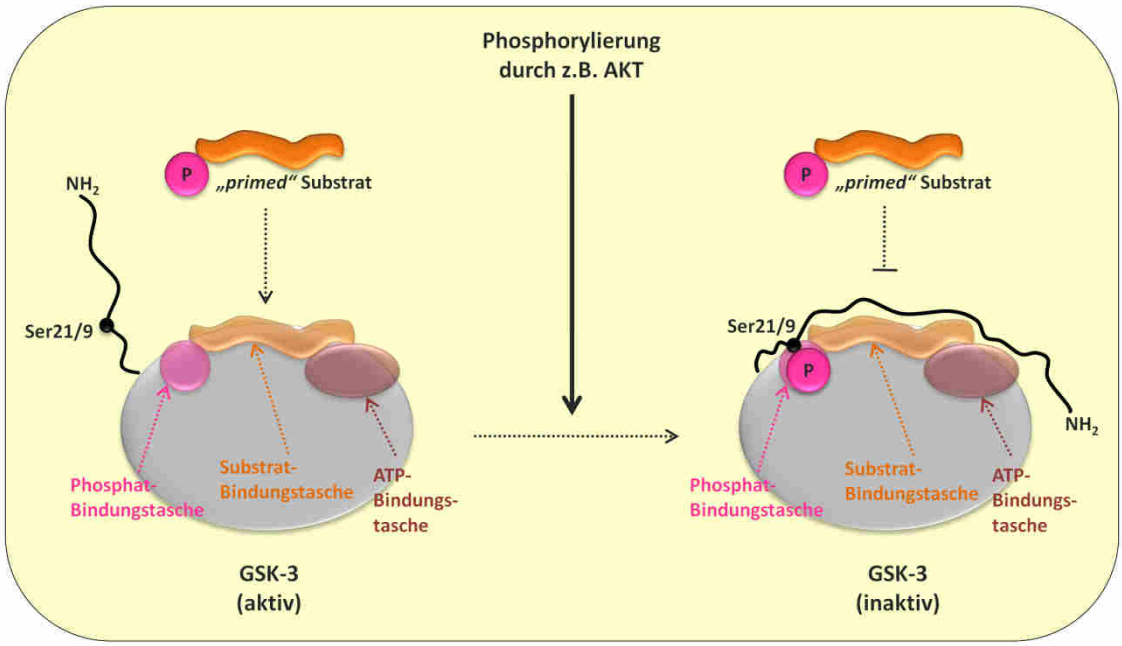

Abb. 14: Schematische Darstellung der Konformationsänderung von GSK-3 hervorgerufen durch die Phosphorylierung von Ser21 (GSK-3α) bzw. Ser9 (GSK-3β).[232, 235]

Für GSK-3β konnten mit Thr43, Ser389 und Thr390 drei weitere inhibierend wirkende Phosphorylierungsstellen bestimmt werden.[247,248] Erfolgt dahingegen die Phosphorylierung am Tyr279 bei GSK-3α bzw. Tyr216 bei GSK-3β kommt es zu einer Aktivitätssteigerung. Der zugrunde liegende Mechanismus ist noch nicht geklärt. Eine aktivierende Phosphorylierung von GSK-3β durch humane Kinasen konnte bisher nicht nachgewiesen werden.[235,249,250,243] Allerdings wurde vor Kurzem

eine Autophosphorylierung von humanem Tyr216 vorgeschlagen. Diese hat zur Folge, dass sich das auf der Aktivierungsschleife lokalisierte Tyr216 nach der Phosphorylierung so anordnet, dass Substrate von GSK-3β uneingeschränkten Zugang zur Substratbindetasche erhalten.[251-253]

Im WNT-Signalweg kann GSK-3 erst dann das Substrat β-Catenin phosphorylieren, wenn es mit Axin, Adenomatös Polyposis Coli (APC) und β-Catenin einen Proteinkomplex bildet. Kommt es zur Proteinkomplexbildung mit FRAT, kann dies entweder aktivierend oder inhibierend auf GSK-3 wirken.[254-256]

Neben der Proteinkomplexbildung spielt auch die subzelluläre Lokalisation von GSK-3 eine Rolle bei Aktivitätsregulierung. GSK-3 kommt nicht nur im Zytoplasma, sondern auch im Nukleus sowie in den Mitochondrien vor.[257-259] Dabei ist der intrazelluläre Transport von GSK-3α und GSK-3β unter anderem von der posttranslationalen Modifikation der N-terminalen Reste abhängig. Somit kann es zu isoenzymspezifischen Transporten oder Anhäufungen kommen.[260,261] Hierdurch kann eine isoenzymspezifische Phosphorylierung von Substraten erfolgen.

Die GSK-3 Substrate selbst tragen auch zur Phosphorylierungsaktivität durch GSK-3 bei. Viele der GSK-3 Substrate liegen als *„primed“* Substrate vor. Auf Grund dieser Vorphosphorylierung kann das *„primed“* Substrat effektiver an GSK-3 binden und wird dadurch ca. 100- bis 1000-mal schneller durch GSK-3 phosphoryliert.[262]

Es kann festgehalten werden, dass obwohl es sich bei GSK-3 um eine konstitutiv aktive Kinase handelt, dessen Aktivität dennoch durch diverse Mechanismen reguliert wird.

1.3.4 Verbindung zur Alzheimer-Krankheit

GSK-3 phosphoryliert nicht nur eine Vielzahl an unterschiedlichen Substraten aus dem Bereich der metabolischen Enzyme, Transkriptionsfaktoren oder Strukturproteine, sondern konnte mit diversen Erkrankungen in Verbindung gebracht werden.[263-269,224,270,271] Seit Ende des letzten Jahrhunderts richtete sich der Forschungsschwerpunkt der pharmazeutischen Industrie und der akademischen Forschungsgruppen auf die Entwicklung von GSK-3 Inhibitoren als Therapeutikum für die Alzheimer-Krankheit.[227] Dafür gibt es zwei entscheidende Gründe. Zum einen wird GSK-3 im Gehirn höher exprimiert als im restlichen Körper.[232,233,231,234] Zum anderen steht GSK-3 durch die Phosphorylierung von APP, Presenilin 1 und Tau im Zusammenhang mit den pathologischen Merkmalen von AD.[272,232,37,273-275] Die Inhibition von GSK-3 erzielte in *in vitro* und *in vivo* Modellen positive Resultate bzgl. der AD-spezifischen Ablagerungen und Verhaltensmustern.[224] Ein GSK-3-spezifisches Therapeutikum stellt somit eine vielversprechende Möglichkeit zur Behandlung der Alzheimer-Krankheit dar. Bis heute wurde eine Vielzahl an potenten GSK-3-Inhibitoren synthetisiert.[212,210,213] Jedoch hat es bisher kein Wirkstoff zur Marktreife geschafft. Gründe dafür waren unter anderem eine zu geringe Hirngängigkeit, metabolische Instabilität und unerwünschte Nebenwirkungen.[276]

1.3.5 Inhibition

1.3.5.1 Small molecules als potentielle Inhibitoren/Wirkstoffe

Ein Großteil der zugelassenen Arzneimittel sind *small molecules* (niedermolekulare Moleküle). Mit der Lipinski „*rule of five*“ kann deren potentielle Löslichkeit, Membrandurchdringung und somit Bioverfügbarkeit abgeschätzt werden.[277] Die Lipinski „*rule of five*“ besteht aus folgenden Vorgaben: 1. weniger als fünf Wasserstoffdonatoren (*hydrogen bond donators*, HBD), 2. weniger als zehn Wasserstoffakzeptoren, 3. eine molekulare Masse (MW) geringer als 500 g/mol und 4. einen ClogP (ClogP = kalkulierter Verteilungskoeffizient zwischen Oktanol und Wasser) kleiner als 5. Im Zuge der Wirkstoffentwicklung für die Alzheimer-Krankheit müssen jedoch noch weitere Faktoren betrachtet werden. Unter anderem die Durchdringung der BBB. Um diese vor der eigentlichen Synthese potentieller Inhibitoren abschätzen zu können, haben vor kurzem Forscher eine Multiparameter Optimierung für das zentrale Nervensystem durchgeführt (CNS-*Multiparameter Optimization*, CNS-MPO).[278]

Tabelle 7: Die CNS-MPO-Parameter und deren bevorzugte und weniger bevorzugte Bereiche für die potentielle Hirngängigkeit von *small molecules*.[278]

Parameter	Bevorzugter Bereich	Weniger bevorzugter Bereich
ClogP	≤ 3	> 5
ClogD	≤ 2	> 4
MW	≤ 360	> 500
TPSA	40 < TPSA ≤ 90	20 ≤ TPSA > 120
HBD	≤ 0.5	> 3.5
pK_a	≤ 8	> 10

ClogP = kalkulierter Verteilungskoeffizient zwischen Oktanol und Wasser; ClogD = Verteilungskoeffizient bei einem pH-Wert von 7,4; MW = molekulare Masse; TPSA = *topological polar surface area*; HBD = Wasserstoffdonatoren (*hydrogen bond donators*); pK_a = basischstes Zentrum.

Dabei wurden 119 zugelassene CNS-Wirkstoffe untersucht. Es resultierte eine Zusammenstellung folgender Parameter: ClogP, ClogD (Verteilungskoeffizient bei einem pH-Wert von 7.4), MW, *topological polar surface area* (TPSA), Anzahl der

HBD und das basischste Zentrum (pK_a), Tabelle 7. Diese ermöglichen eine Abschätzung der Hirngängigkeit zukünftiger *small molecules* als potentielle CNS-Wirkstoffe.

1.3.5.2 Therapeutisches Fenster

Lithium in Form von **LiCl** ist der am häufigsten in *in vivo* Tests verwendete GSK-3-Inhibitor. Es inhibiert GSK-3 im millimolaren Bereich und ist ein zugelassenes Therapeutikum zur Behandlung von bipolaren Störungen.[279,212,280,281] Bei einer therapeutischen Lithiumdosis im niedrigen millimolaren Bereich wird mit einer GSK-3-Inhibition von ca. 25 % gerechnet. Die mit einer GSK-3-Inhibition in Verbindung gebrachten Erkrankungen der Hyperglykämie bis hin zur Tumorgenese konnten dabei nicht beobachtet werden. Dadurch wurde gefolgert, dass eine moderate GSK-3-Inhibition im Menschen denkbar und relativ sicher zu sein scheint.[14]

1.3.5.3 GSK-3-Inhibition – Schwerpunktlegung: ATP-kompetitive Inhibition

Es gibt mehrere publizierte Wege GSK-3 erfolgreich zu inhibieren, Abb. 15. Diese lassen sich in die irreversible und reversible Inhibition unterteilen. GSK-3 irreversibel inhibierende Substanzen sind beispielsweise die Halomethylketone, Abb. 16.[282-284] Sie inhibieren GSK-3 mit einem IC_{50} von bis zu 0,5 µM und binden irreversibel an das Cys199. Das Cys199 ist Teil der aktiven ATP-Bindungstasche von GSK-3. Ein weiteres Beispiel sind die Thiadiazolinone (TDZDs; IC_{50} von bis zu 105 nM). Die TDZDs galten zunächst als allosterische Inhibitoren. Jedoch lieferte eine vor kurzem veröffentlichte Publikation Belege für eine irreversible Bindung an das Cys199.[211]

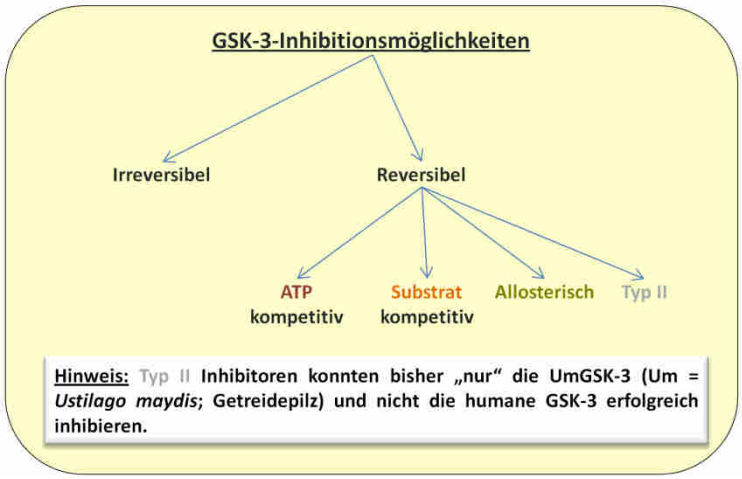

Abb. 15: Schematische Darstellung der Möglichkeiten GSK-3 zu inhibieren.

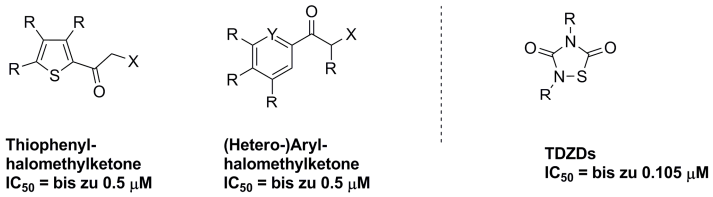

Abb. 16: Allgemeine Darstellung von Halomethylketonleitstrukturen und Thiadiazolinone (TDZDs) für die irreversible GSK-3-Inhibition; R = Alkyl, Halogenid, usw.; X = Br, Cl; Y = CH, N.[282,211,283,284]

Bei der reversiblen Inhibition von GSK-3 muss weiter differenziert werden, Abb. 17. So wurden bereits ATP-kompetitive, substratkompetitive, allosterische und sogenannte Typ-II-Inhibitoren veröffentlicht, Abb. 18. Letztere binden nicht nur an Aminosäuren der ATP-Bindungstasche, sondern auch an Aminosäuren einer benachbarten allosterischen Tasche. Sie stellen eine strukturelle Verknüpfung von ATP-kompetitiven und allosterischen Inhibitoren dar. Typ-II-Inhibitoren konnten bisher „nur“ die UmGSK-3 aus *Ustilago maydis* mit einem IC_{50} von bis zu 57 nM inhibieren, Abb. 18. Humane GSK-3 konnte indes durch Typ-II-Inhibitoren noch nicht gehemmt werden. Der Grund liegt voraussichtlich in der höheren Flexibilität der UmGSK-3-Struktur verglichen mit der Humanen. Dadurch kann die UmGSK-3 im Gegensatz zur humanen GSK-3 in eine inaktive Konformation überführt werden.[285]

Abb. 17: Schematische Darstellung erfolgreicher, reversibler Inhibitionsansätze GSK-3.

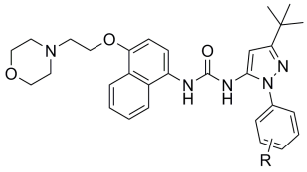

Leitstruktur basierend
auf dem bekannten
Typ II Inhibitor
BIRB-796
IC_{50} = bis zu 1.06 μM

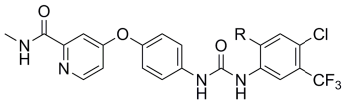

Leitstruktur basierend
auf dem bekannten
Typ II Inhibitor
Sorafenib
IC_{50} = bis zu 0.057 μM

Abb. 18: Allgemeine Darstellung unterschiedlicher Leitstrukturen für die Typ-II-Inhibition von GSK-3; R = Alkyl, Amin, usw.[285]

Kinetische Studien belegen eine allosterische Inhibition von GSK-3 mit dem Inhibitor **VP0.7**, Abb. 19. **VP0.7** inhibiert GSK-3 mit einem IC_{50} von ca. 3 µM. Bindungsstudien lassen auf eine Koordination von **VP0.7** an eine der C-terminalen, allosterischen Bindungstaschen schließen.[238]

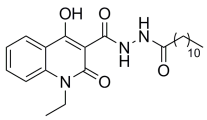

VP0.7
IC_{50} = 3.01 μM

Abb. 19: Strukturformel des allosterischen GSK-3-Inihibitors **VP0.7**.[238]

Neben dem Naturstoff **Manzamine A** wirkt auch das Peptid **L803-mts** substratkompetitiv, Abb. 20.[238,286-288] **Manzamine A** inhibiert GSK-3β mit einem IC_{50} von 10 μM.[289] Dabei ist zu beachten, dass es mit einem IC_{50} von 1.5 μM ein noch besserer Inhibitor für CDK5 ist. Das Peptid **L803-mts** inhibiert GSK-3β mit einem IC_{50} von 40 μM.[290] Obwohl es substratkompetitiv wirkt, haben Bindungsstudien ergeben, dass **L803-mts** nur einen Teil der Substratbindungstasche von GSK-3 besetzt. Hauptsächlich interagiert es mit einer benachbarten, hydrophoben Tasche.[286-288] Kürzlich wurden weitere **L803-mts** Analoga veröffentlicht. Sie sind bis zu 10-fach aktiver als **L803-mts**.[288]

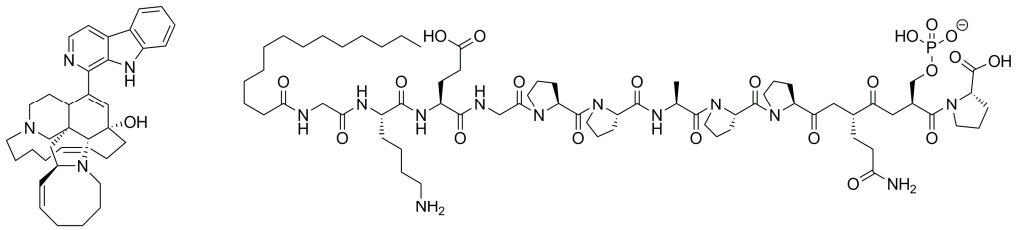

Manzamine A
IC_{50} = 10 μM

L803-mts
IC_{50} = 40 μM

Abb. 20: Strukturformeln der substratkompetitiven GSK-3-Inihibitoren **Manzamine A** und **L803-mts**.[289,290]

Ein Großteil der Forschungsbemühungen der pharmazeutischen Industrie und akademischer Arbeitsgruppen gilt der ATP-kompetitiven Inhibition von GSK-3.[210] Ein Grund dafür ist beispielsweise die schnelle und kostengünstige Synthese von *small molecules* als potentielle GSK-3-Inhibitoren. Darüber hinaus ist die Applikation und Darreichungsform von *small molecules* als Wirkstoff zahlreich erprobt und etabliert. Dennoch ist zu beachten, dass ATP-kompetitive Inhibitoren mit der hohen zellulären ATP-Konzentration (millimolarer Bereich) konkurrieren. Somit müssen sie um ein vielfaches inhibierender wirken als beispielsweise substratkompetitive Inhibitoren. Die Aktivität potentieller ATP-kompetitiver Inhibitoren sollte im niedrigen nanomolaren Bereich liegen, was eine hohe Bindungsaffinität voraussetzt. Daneben spielt die Selektivität von ATP-kompetitiven GSK-3-Inhibitoren eine entscheidende

Rolle. Der Grund liegt in der evolutionär stark konservierten ATP-Bindungstasche aller Kinasen.[291-293] Somit muss ein potentieller ATP-kompetitiver GSK-3-Inhibitor so passgenau designt werden, dass selbst engste Kinaseverwandte von GSK-3, wie z. B. die CDKs, nicht inhibiert werden. Es wurde bereits eine Vielzahl selektiver und hoch potenter ATP-kompetitiver Kinaseinhibitoren unterschiedlichster Leitstrukturen synthetisiert, Abb. 21.[212,210,213]

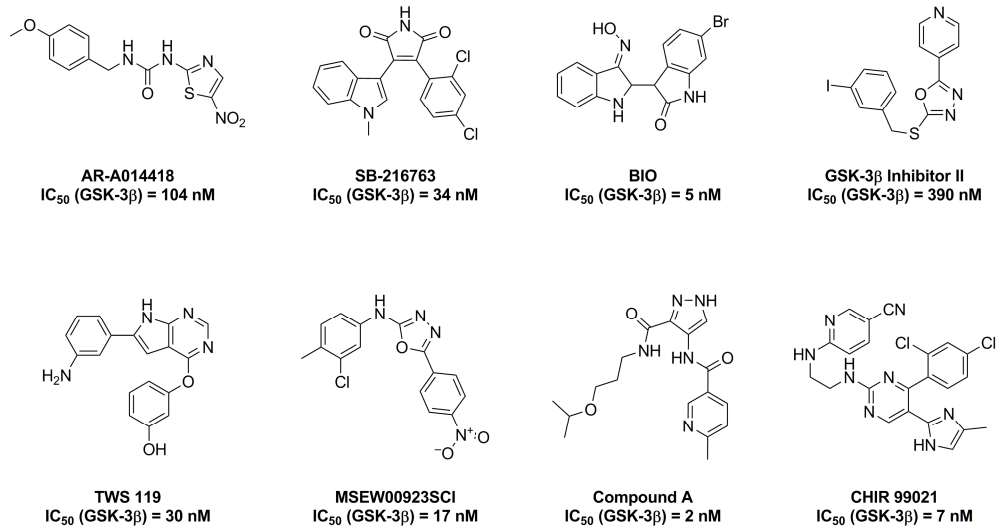

Abb. 21: Eine Auswahl von kommerziell erhältlichen, ATP-kompetitiven GSK-3-Inhibitoren unterschiedlichster Leitstrukturen.[294,210]

Interessant ist, dass es eine Fülle von selektiven GSK-3-Inhibitoren gibt, diese jedoch nicht entscheidend zwischen GSK-3α und GSK-3β differenzieren. Dabei konnte bereits gezeigt werden, dass die einzelnen Isoenzyme verschiedene Krankheitsbilder unterschiedlich stark beeinflussen. Beispielsweise spielt in der akuten myeloischen Leukämie GSK-3α eine entscheidendere Rolle als GSK-3β.[295] Im Fall der Alzheimer-Krankheit wird der Einfluss der unterschiedlichen Isoenzyme von GSK-3 derzeit diskutiert.[296,45,48] Isoenzymspezifische GSK-3-Inhibitoren könnten eventuell dabei helfen, einen detaillierteren Einblick in die metabolischen und krankheitsspezifischen Zusammenhänge der einzelnen GSK-3-Isoenzyme zu bekommen. Aktuell gibt es mit **Λ-OS1** nur einen moderat isoenzymspezifischen GSK-3-Inhibitor, Abb. 22.[297] **Λ-OS1** inhibiert GSK-3α mit einem IC_{50} von 0.9 nM und GSK-3β mit einem IC_{50} von 6 nM. Somit hemmt es GSK-3α ca. 7-fach spezifischer als GSK-3β. Zwar ergab eine Co-Kristallisation mit GSK-3β beispielsweise mögliche Interaktionen mit der Gelenkregion und der glycinreichen Schleife von GSK-3β, jedoch konnte diese keinen Aufschluss über die Selektivität erbringen. Da die ATP-

Bindungstaschen von GSK-3α und GSK-3β zu 98 % identisch ist, wurde als möglicher Grund eine potentielle Konformationsänderung in dem erweiterten Bereich der ATP-Bindungstasche angeführt.[231, 297]

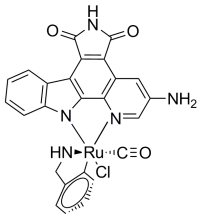

Λ-OS1
IC_{50} (GSK-3α) = 0.9 nM
IC_{50} (GSK-3β) = 6.0 nM

Abb. 22: Strukturformel von **Λ-OS1** (ca. 7-fach selektiver für GSK-3α).[297]

Somit wäre die Entwicklung neuer isoenzymspezifischer GSK-3-Inhibitoren nicht nur für die Aufklärung der isoenzymspezifischen Bindungsmuster hilfreich, sondern auch für weitere Einblicke in die mit GSK-3 in Verbindung stehenden Krankheiten.

Auch wenn keine isoenzymspezifische Inhibition von GSK-3 vorliegt, wurden dennoch viele der potenten, GSK-3α/β selektiven und ATP-kompetitiven Inhibitoren in AD-spezifischen *in vivo* Studien getestet.[212,224,210] **AR-A014418** (AstraZeneca) ist ein Beispiel eines in unterschiedlichen Studien getesteten, ATP-kompetitiven GSK-3-Inhibitors, Abb. 22/23.[298-300] Es inhibiert GSK-3β mit einem IC_{50} von 104 nM und zeigte gegenüber 26 weiteren Kinasen keine inhibierende Wirkung. **AR-A014418** ist einer der ersten ATP-kompetitiven Inhibitoren, die mit GSK-3β kristallisiert werden konnten (PDB Code = 1Q5K). Dies ermöglichte einen Einblick in wichtige Interaktionen zwischen **AR-A014418** und der ATP-Bindungstasche von GSK-3β. Für dessen Aktivität und Selektivität wichtige direkte Interaktionen erfolgten mit den Aminosäuren Val135, Pro136 und Arg141. Darüber hinaus wurden indirekte Interaktionen über mehrere Wassermoleküle mit den Aminosäuren Lys85, Glu97 und Arg200 beschrieben, Abb. 23. Diese Interaktionen konnten auch in fast allen darauffolgenden Co-Kristallisationen von Inhibitoren mit GSK-3β detektiert werden.[298] In stabil transfizierten und Tau-exprimierenden 3F3-Fibroblasten reduzierte **AR-A014418** via GSK-3β-Inhibition die Tau-Phosphorylierung. **AR-A014418** verringerte in Zellkulturversuchen das Sterben von Neuroblastomzellen (N2A) sowie die Aβ-induzierte Neurodegeneration und verursachte selbst keine neurotoxischen Effekte.[298] Durch die intraperitoneale Applikation von **AR-A014418** in humanes Tau überexprimierenden JNPL3-Mäusen konnte ein signifikanter Rückgang der

unlöslichen Tau-Ablagerungen im Hirnstamm der Mäuse beobachtet werden.[299] Jedoch konnten diese Effekte nicht in neuronenähnlichen Zellen, LUHMES, sowie in weiblichen Wistar-Raten beobachtet werden. Eine vorgeschlagene Begründung ist, dass die Inhibitoren für eine potentielle Wirkung im Gehirn 7-mal stärker inhibierend wirken müssen als in rekombinanten und zellbasierten Assays.[300] Somit müsste ein potentieller Inhibitor GSK-3 im niedrigen nanomaloren Bereich inhibieren, um im Gehirn wirksam zu sein.

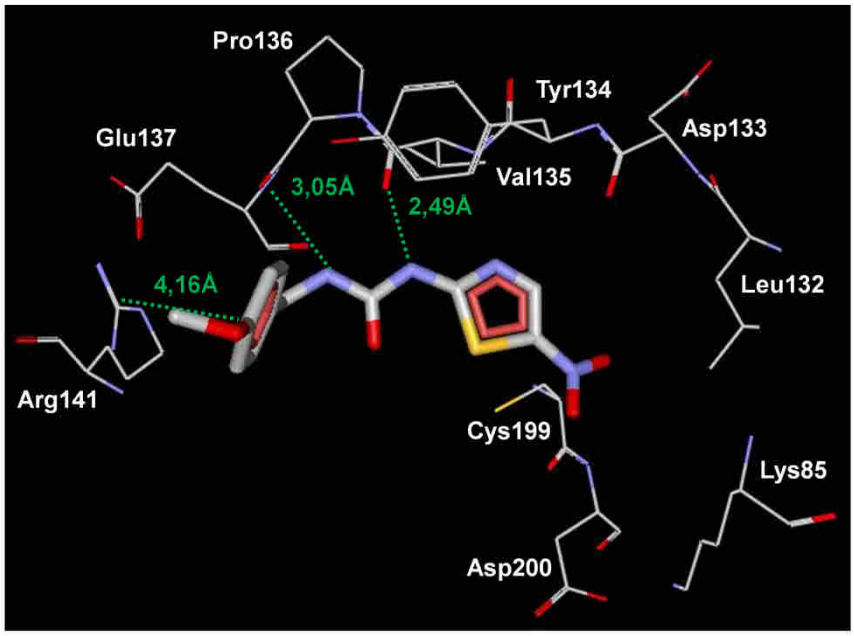

Abb. 23: Schematische Darstellung der Interaktionen der ATP-Bindungstasche von GSK-3β mit dem Harnstoff **AR-A014418** (AstraZeneca); hervorgehoben sind die direkten Interaktionen mit den Aminosäuren Val135, Pro136 und Arg141; verwendete Software: Molegro Virtual Docker 5; PDB Code = 1Q5K.[298]

Obwohl eine Vielzahl potenter ATP-kompetitiver Inhibitoren in unterschiedlichsten zellbasierten und *in vivo* Studien untersucht wurden, erreichten seit 2006 nur zwei von ihnen (Indikationsgebiet AD) die klinischen Phasen. **AZD-1080** (AstraZeneca) wurde bereits in der klinischen Phase I gestoppt. Der Grund dafür war eine beobachtete Nephrotoxizität.[212] Der zweite ist **Tideglusib** (NP-12; Noscira), Tabelle 7. **Tideglusib** ist ein irreversibel an GSK-3 bindender Inhibitor, der Ende Oktober 2012 die klinische Phase II absolvieren wird. Er soll nicht nur zur Behandlung von AD, sondern auch zur Behandlung der progressiven supranukleären Blickparese zugelassen werden. In den bisherigen Studien konnten keine entscheidenden Nebenwirkungen am Menschen festgestellt werden. Darüber hinaus

ergab die Applikation von **Tideglusib** einen Rückgang der Gehirnatrophie als Folge der Demenzerkrankung.[15,301,302,211,303-305]

Tabelle 7: Tideglusib der Firma Noscira, S.A.[15,301,302,211,303-305]

Tideglusib		
Firma:	Noscira, S.A. (Spain)	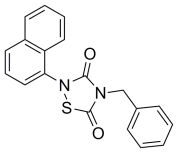
Inhibitionsmuster:	Irreversibel	
IC_{50} (ohne Vorinkubationszeit):	105 nm	
Klinische Phase:	II (Ende: Okt. 2012)	

Zusammenfassend bleibt festzuhalten, dass, obwohl eine komplexe metabolische Verknüpfung von GSK-3 vorliegt, moderat wirkende, selektive, hirngängige und eine gute Pharmakokinetik aufweisende GSK-3-Inhibitoren eine probate Möglichkeit zur Behandlung der Alzheimer-Krankheit darstellen.

2 Zielsetzung

Ein aktueller Bericht der Weltgesundheitsorganisation (WHO) in Zusammenarbeit mit *Alzheimer´s Disease International* (ADI) geht davon aus, dass im Jahr 2010 weltweit ca. 35,6 Mio. Menschen eine Demenzerkrankung aufwiesen. Mit 60-70 % wird die Mehrheit von ihnen mit der Alzheimer-Krankheit in Verbindung gebracht.[9] Derzeit gibt es für die AD noch keine krankheitsbeeinflussenden Medikamente, so dass sie unweigerlich zum Tode führt. Die medizinische Chemie setzt an diesem Punkt an und versucht Wirkstoffe für die AD-Therapie zu entwickeln. Dabei gibt es unterschiedlichste Ansätze.

Mit der Glykogen Synthase Kinase-3 wurde ein Enzym evaluiert, welches mit beiden pathologischen Merkmalen der AD, den Aβ-Plaques und Neurofibrillenbündel, zusammenhängt.[13,224] Eine Inhibition der konstitutiv aktiven GSK-3 konnte bereits in *in vitro* und *in vivo* Studien die Unterdrückung der AD belegen.[224] Dennoch ist bis heute kein GSK-3-spezifischer Inhibitor mit AD als Indikationsgebiet auf dem Markt.

GSK-3 mittels potentiell ATP-kompetitiver Inhibitoren zu inhibieren, die Bindungsinteraktionen der potentiellen Inhibitoren mit GSK-3 *in silico* Modellen zu untersuchen und die Inhibitoren in *in vivo* Studien zu testen, sind Schwerpunkte der Dissertation. Dabei sollen zunächst die Daten der zurückliegenden, 30-jährigen Forschung an ATP-kompetitiven GSK-3-Inhibitoren aufbereitet werden. Um die theoretischen Datensätze experimentell zu verifizieren, soll im Anschluss eine kostenbewusste und schnell zugängliche Substanzbibliothek erstellt werden. Die resultierenden Ergebnisse zur Strukturaktivitätsbeziehung zwischen den Inhibitoren und der ATP-Bindungstasche von GSK-3 sollen anschließend dazu genutzt werden, eine neue, patentierbare Leitstruktur zu generieren.

Ein detailliertes Ziel dieser Dissertation ist die organische Synthese und biochemische Evaluation von Imidazo[4,5-*b*]pyridin-2-aminderivaten als potentiellen ATP-kompetitiven Inhibitoren von GSK-3, Abb. 24.

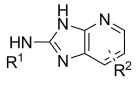

Abb. 24: Allgemeine Strukturformel von Imidazo[4,5-*b*]pyridin-2-aminderivaten.

3 Kumulativer und allgemeiner Teil

3.1 *Small molecule* GSK-3-Inhibitoren: Strukturelle Einblicke und ihre Applikation in Modellen der Alzheimer-Krankheit

Der Inhalt dieses Kapitels wurde bereits veröffentlicht: Thomas Kramer, Boris Schmidt, und Fabio Lo Monte, „*Small-Molecule Inhibitors of GSK-3: Structural Insights and Their Application to Alzheimer's Disease Models*", International Journal of Alzheimer's Disease **2012**, *2012*, 32 Seiten, doi:10.1155/2012/381029.

Die Weltgesundheitsorganisation (WHO) hat in Zusammenarbeit mit der *Alzheimer´s Disease International* (ADI) einen Bericht zur aktuellen Lage der Demenzerkrankungen herausgebracht.[9] Aus diesem geht hervor, dass im Jahr 2010 voraussichtlich gut 35 Mio. Menschen weltweit mit einer Demenzerkrankung in Zusammenhang gebracht werden konnten. Zudem wird davon ausgegangen, dass es sich bei ca. zweidrittel aller Erkrankten um Alzheimer Patienten handelt. Ein bereits 1980 identifiziertes Enzym namens Glykogen Synthase Kinase-3 konnte Ende des 20igsten Jahrhunderts mit beiden pathologischen Merkmalen, den Aβ-Plaques und Neurofibrillenbündel, der Alzheimer-Krankheit in Verbindung gebracht werden.[227,13] Seitdem wurde eine Vielzahl an Inhibitoren für die konstitutiv aktive GSK-3 entwickelt. Die angefügte Publikation gibt einen strukturellen Überblick der ATP-kompetitiven GSK-3-Inhibitoren, ergänzt durch deren *in vitro* und *in vivo* Ergebnisse, sowie einer Zusammenfassung aktueller vorklinischer und klinischer Studien. Die Auswertung der publizierten und hier zusammengetragenen Co-Kristallisationen von diversen Inhibitoren mit GSK-3β wurde in einem allgemeinen Aktivitäts- und Selektivitätsschema für zukünftige Inhibitorsynthesen zusammengefasst, Abb. 25. In diesem sind wichtige Aminosäuren als potentielle Interaktionspartner für ATP-kompetitive GSK-3-Inhibitoren hervorgehoben. Derzeit gibt es zwar eine Fülle an GSK-3-spezifischen Inhibitoren, es gibt jedoch nur einen Inhibitor (**Λ-OS1**), der eine die GSK-3-Isoenzyme, GSK-3α und GSK-3β, unterschiedlich stark inhibiert (7-fach spezifischer für GSK-3α). Wobei davon auszugehen ist, dass eine isoenzymspezifische Inhibition von GSK-3, weitere

Erkenntnisse in ihrem metabolischen Zusammenwirken mit anderen Proteinen und somit auch in diversen Erkrankungen ergeben würde.

Abschließend ist festzuhalten, dass es sich bei der AD um eine derzeit nur symptomatisch behandelbare Krankheit handelt, und dass krankheitsbeeinflussende Wirkstoffe, wie beispielsweise GSK-3-Inhibitoren, dringend benötigt werden.

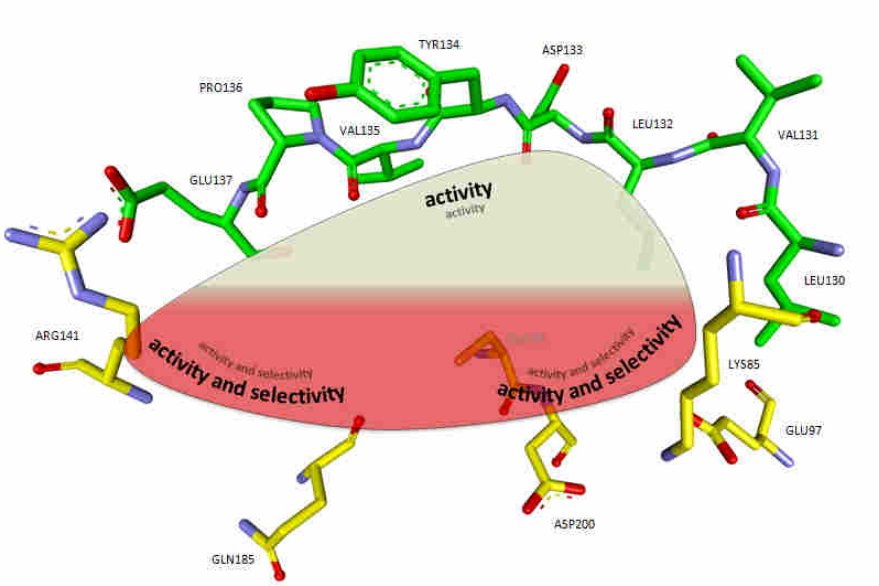

Abb. 25: Schematische Darstellung der ATP-Bindungstasche von GSK-3β; wichtige Aminosäuren und Bereiche für die Aktivität und Selektivität sind vermerkt (Hinweis: Originalschema aus der Publikation).

Hindawi Publishing Corporation
International Journal of Alzheimer's Disease
Volume 2012, Article ID 381029, 32 pages
doi:10.1155/2012/381029

Review Article

Small-Molecule Inhibitors of GSK-3: Structural Insights and Their Application to Alzheimer's Disease Models

Thomas Kramer, Boris Schmidt, and Fabio Lo Monte

Clemens Schöpf-Institute of Organic Chemistry and Biochemistry, Technische Universität Darmstadt, 64287 Darmstadt, Germany

Correspondence should be addressed to Boris Schmidt, schmidt_boris@t-online.de and Fabio Lo Monte, fabio.lo-monte@gmx.de

Received 8 December 2011; Accepted 31 January 2012

Academic Editor: Kurt A. Jellinger

The world health organization (WHO) estimated that 18 million people are struck by Alzheimer's disease (AD). The USA, France, Germany, and other countries launched major programmes targeting the identification of risk factors, the improvement of caretaking, and fundamental research aiming to postpone the onset of AD. The glycogen synthase kinase 3 (GSK-3) is implicated in multiple cellular processes and has been linked to the pathogenesis of several diseases including diabetes mellitus, cancer, and AD. Inhibition of GSK-3 leads to neuroprotective effects, decreased β-amyloid production, and a reduction in tau hyperphosphorylation, which are all associated with AD. Various classes of small molecule GSK-3 inhibitors have been published in patents and original publications. Herein, we present a comprehensive summary of small molecules reported to interact with GSK-3. We illustrate the interactions of the inhibitors with the active site. Furthermore, we refer to the biological characterisation in terms of activity and selectivity for GSK-3, elucidate *in vivo* studies and pre-/clinical trials.

1. Introduction

Protein kinases regulate diverse cellular functions and thus are frequently exploited in drug discovery programmes [1]. They regulate signal transduction processes by phosphorylating serine, threonine and tyrosine residues in key proteins. The signalling pathways involved contribute to the pathology in many diseases [2, 3]. Glycogen synthase kinase 3 (GSK-3) was identified in the late 1970s and is a constitutively active, ubiquitous expressed serine/threonine kinase, which participates in a number of physiological processes ranging from glycogen metabolism to gene transcription [4]. Initially, the focus of pharmaceutical companies concerning GSK-3 was on diabetes mellitus, but since GSK-3 was linked to Alzheimer's disease (AD), the focus has moved from diabetes to AD. GSK-3 has been linked to all primary abnormalities associated with AD. GSK-3 interacts with different components of the plaque producing amyloid system, participates in phosphorylating the microtubule binding protein tau that contributes to the formation of neurofibrillary tangles, and has an influence on presenilin and other AD-associated proteins [4–8]. Two related isoforms of GSK-3 are present in mammalians, GSK-3α and β, which share 98% homology in their catalytic domains and have similar biochemical properties [9]. The isoforms are similar in their catalytic domains, yet differ significantly in their N-terminal regions [10]. Alois Alzheimer's first report of the neuropathological hallmarks of AD dates back to 1907 [11, 12]. The histopathology of the AD brain is characterized by the presence of abnormal filamentous tau-protein inclusions in nerve cells and extracellular amyloid deposits [13, 14]. Partially phosphorylated tau contains sequence motifs that support association with tubulin, which entails the stabilization of microtubules in AD-uneffected cells. The pathological hyperphosphorylation of these motifs destabilizes microtubules and consequently interferes with tubulin binding. The misfolding of hyperphosphorylated tau involves the E/Z-isomerisation of a phosphorylated Ser-Pro motive, which leads to the formation of insoluble neurofibrillary tangles (NFTs) and intraneuronal aggregates of paired helical filaments (PHFs) [9, 15]. GSK-3 phosphorylates multiple sites on tau both *in vitro* and *in vivo* [9]. It exerts a central and crucial role in the pathogenesis of both familial and sporadic forms of AD. Early-onset forms of familial Alzheimer's disease (FAD) have been linked to

mutations in amyloid precursor protein (APP), presenilin-1 (PS-1), and presenilin-2 (PS-2). These mutations adversely affect APP processing and result in the increased production of the 40–42 amino acid long β-Amyloid (Aβ) peptides, which are the major component of amyloid deposits. Several risk factors have been associated with sporadic Alzheimer's disease (SAD). The most prevalent factors are aging and the presence of specific ApoE isoforms, which have been implicated in Aβ clearance. Sporadic Alzheimer's disease can be caused by the activation of β-secretase, which results in enhanced formation of Aβ. Enhanced Aβ production or deficiency in Aβ clearance will result in the deposition of Aβ aggregates [4, 16]. Recent work suggests that enhanced GSK-3 activity increases Aβ production [17]. Several studies support that GSK-3 inhibition leads to decreased Aβ production and a reduction in tau hyperphosphorylation [1].

A plethora of GSK-3 inhibitors has been described, and most of the biological effects were reported for *in vitro* and cellular studies [17]. These studies, the number of patent applications, and a successful phase II trial indicate that GSK-3 is a promising drug target for AD therapy, but the ultimate proof of concept has not been presented yet. GSK-3 is highly enriched in the brain, and several publications indicate that the GSK-3β isoform is a key kinase required for abnormal hyperphosphorylation of tau [18, 19]. Spittaels et al. generated a double-transgenic mouse overexpressing human protein tau and constitutively active human GSK-3β and ascertained that this kinase is implicated in aberrant tau phosphorylation and in addition reduced tau binding capacity to microtubules [15, 20]. The homology of the ATP-binding pocket in GSK-3α and GSK-3β presents an obstacle for the development of isoform selective inhibitors. All GSK-3 inhibitors developed until now are able to inhibit the two isoforms with similar potency, except Λ–**OS1** (**36**), which showed a selectivity (up to 7 fold) for GSK-3α [8, 21, 22].

The structures of GSK-3β cocrystallized with several inhibitors have been solved by X-ray crystallography recently. These structures provide a remarkable possibility to design both novel and selective GSK-3 inhibitors. There are two fundamental options to inhibit GSK-3: non-ATP competitive inhibition and ATP competitive inhibition.

The non-ATP competitive inhibitors, for example, substrate competitive inhibitors, usually engage in a weak-binding interaction with the enzyme [23]. Non-ATP competitive inhibitors do not compete with the high intracellular ATP-concentration and thus offer a distinct pharmacological advantage. Moreover, the involvement of GSK-3 in several essential signalling pathways imposes a limit on the GSK-3 inhibition, complete inhibition will result in adverse events.

Thus GSK-3 inhibitors suitable for AD therapy have to strike a balance between the different pathways. This delicate balance may be achieved by moderate inhibition in combination with excellent pharmacokinetics. Thiadiazolindiones (TDZDs) are non-ATP competitive GSK-3 inhibitors, which delivered a candidate for phase IIb trials recently [24]. The extended phase II trial (60-day treatment) did not reveal adverse effects [25]. However, the majority of the known GSK-3 inhibitors are ATP competitive and target the ATP binding pocket of GSK-3. Several small-molecule inhibitor/GSK-3 complexes can be extracted from the Protein Data Bank (PDB) (PDB codes: 3PUP (15), 1Q4L (25), 1Q3D (25), 1Q41 (25), 1Q3W (25), 1R0E (34), 2OW3 (40), 2JLD (55), 3M1S (56), 1UV5 (65), 3I4B (113), 3F7Z (119), 3F88 (119), 3GB2 (120), 1Q5K (124), 2O5K (127), 3L1S (130), 3Q3B (136), 1I09 (138)). A closer view at the interactions of these inhibitors with GSK-3 will be provided in the following sections.

2. Small-Molecule Inhibitors of Glycogen Synthase Kinase 3

Several ATP competitive GSK-3 inhibitors from different structural classes are highlighted in this paper. The *in vitro* and *in vivo* data are summarized if available. It should be noted that the IC_{50} values strongly depend on assay conditions and thus may vary 100 fold depending on ATP and enzyme concentration as well as incubation time. The interactions between the inhibitors and the ATP binding pocket are depicted.

2.1. Lithium Chloride. **Lithium chloride** (**LiCl**) was the first GSK-3 inhibitor to be discovered. However, there are several other biological targets for lithium resulting in adverse events and a rather small therapeutic window. This effectively rules out the use of **LiCl** in the therapy of AD. The mechanism by which **lithium** inhibits GSK-3 is unknown, but two hypotheses were proposed: (a) **lithium** (Li^+) is a competitive inhibitor of GSK-3 with respect to **magnesium** (Mg^{2+}), but neither competitive to substrate nor to ATP (b) **lithium** inhibits **potassium** deprivation [25–27]. This paper focuses on small organic molecules that target specifically GSK-3, thus the activity of lithium salts will not be reviewed. Also covalent or irreversible inhibitors, like the TDZD **NP-12**, will be noted, but not further discussed as well as the **FRATtide**, a peptide derived from FRAT1, which binds to GSK-3 and blocks GSK-3 from interacting with axin [28, 29].

2.2. Maleimide Derivatives. Maleimide derivatives have been reported as scaffolds for ATP competitive GSK-3 inhibitors. Researchers at SmithKline Beecham Pharmaceuticals reported that 3-anilino-4-arylmaleimides **1–3** (Table 1) are potent and selective inhibitors of GSK-3 [30]. The compounds displayed GSK-3 inhibition (IC_{50}) at low nanomolar concentrations. The selectivity of compound **2** was evaluated using a panel of 25 kinases. The majority of the kinases showed less than 30% inhibition at an inhibitor concentration of 10 μM. The complex of **3** (named **I-5**) with GSK-3β (Figure 1) elucidated the binding mode to the ATP pocket [31]. Herein, the maleimide nitrogen interacts with the carbonyl oxygen of Asp133 and the oxygen of compound **3** with the backbone nitrogen of Val135. Two additional interactions are observed between a carboxylate oxygen and Arg141 and with Gln185. Compound **4** (**SB-216763**) inhibited GSK-3α with an IC_{50} of 34 nM (Table 2). Derivative **4** exhibited little or no inhibition of the 24 kinases tested in the panel [32]. Incubation of cerebellar granule neurones with this compound reduced the death rate in a concentration-dependent manner in response to

Table 1: Examples of maleimide inhibitors with biological activity against GSK-3, selectivity, X-ray and reference.

No.	R^1	R^2	IC_{50} (nM)	Kinase panel	*In vivo*	X-ray	Year/lit.
1		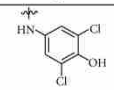	*α*: 20	—	—	—	2001 [30]
2		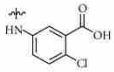	*α*: 26	*β* + 24	—	—	2001 [30]
3		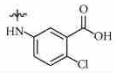	*α*: 76	—	—	1Q4L	2001, 2003 [30, 31]

α: GSK-3*α*; *β*: GSK-3*β*.

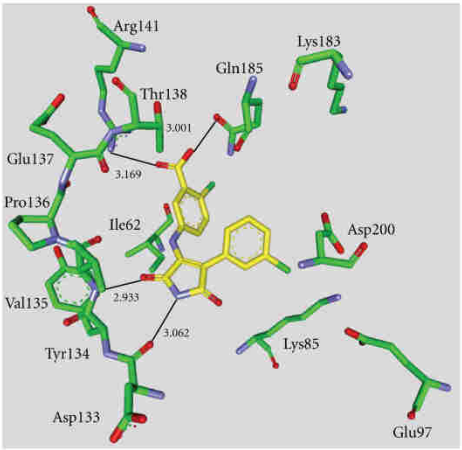

Figure 1: Compound **3** (**I-5**) in the ATP binding pocket of GSK-3*β*; important protein-inhibitor interactions are shown. The distance is denoted by Å. PDB code 1Q4L [31].

either stimulus. The maximal neuroprotection was observed with 3 μM of **SB-216763** [33]. A 60% reduction in GSK-3*β* activity levels was observed in the hippocampus, but not in the cortex of **SB-216763** treated animals versus vehicle-treated rats [34]. The compounds **5–11** revealed good potencies against GSK-3. Concerning compounds **7** and **9–11**, much higher potencies (IC_{50} < 4 nM) were ascertained in comparison to compound **1** (Table 2) [36–38]. The compounds **10** and **11** demonstrated very good GSK-3 inhibition and improved selectivity against PKC*β*II, CDK2, and CDK4 and inhibit tau phosphorylation in a neuronal cell line [38]. Whereas compound **12** was analyzed by *in silico* docking, the binding mode of **13** (IC_{50} = 0.6 nM) was determined by X-ray crystallographic analysis (Figure 2) [40]. Similar to compound **3**, the maleimide nitrogen of **13** interacts with the carbonyl oxygen of Asp133 and its oxygen with the backbone nitrogen of Val135. Furthermore, compound **13** forms a crucial hydrogen bond to Gln185. Maleimide **13** was screened against 317 kinases to provide data on kinase selectivity in order to predict potential safety issues. It was found that compound **13** inhibits only 36 kinases with >90% inhibition at 10 μM [40]. Compounds **14** and **15** are reversible GSK-3 inhibitors in the low micromolar or high nanomolar range and can be used as chemical precursors for the corresponding halomethylketones (HMKs). These HMKs are irreversible inhibitors, they alkylate Cys199, which is located in the ATP binding site of GSK-3 [41]. Further maleimide derivatives are listed in Table 3. All of them, compounds **16–27** showed IC_{50}/K_i values in the low nanomolar range [42–48]. The majority of these structures was synthesized by Johnson & Johnson Pharmaceutical R & D. The compounds **17** and **18** were evaluated against a broad panel of 55 protein kinases. 10 μM of derivative **17** or **18** inhibited GSK-3*β* kinase activity by 100% in the presence of 10 μM ATP. Compound **18** exhibited excellent selectivity for GSK-3*β* except for the moderate selectivity against PKC*β*II. Meanwhile, the bis-7-azaindolylmaleimide **17** exhibited high selectivity at GSK-3*β* against all kinases tested [43]. The activity of compound **23** was tested in a kinase panel containing 100 diverse protein kinases. An IC_{50} of 3 nM and a 460 fold selectivity for GSK-3*β* over PKC*β*II was reported [46]. The X-ray structure analysis of cocrystallized compound **23** and GSK-3*β* is illustrated in Figure 3.

The maleimide establishes key hydrogen bond contacts with the residues Asp133 and Val135. The compounds **25** and **26** were docked into the ATP binding site of GSK-3*β* (PDB code 1R0E). Similar to other maleimide derivatives, the maleimide nitrogen interacts with the carbonyl oxygen of Asp133 and the oxygen with the backbone NH of Val135. In addition to these main interactions, the hydroxymethyl group of compound **26** interacts with the side chain of Arg141 [48].

Table 2: Examples of indolyl-maleimide inhibitors with biological activity against GSK-3, selectivity, X-ray, and reference.

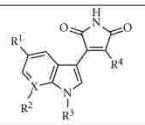

No.	R^1	X	R^2	R^3	R^4	IC_{50}/K_i (nM)	Kinase panel	*In vivo*	X-ray	Year/lit.
4	H	C	H	Me		α: 34[a]	β + 24	Yes	—	2000, 2001, 2007 [32–34]
5	H	N	—			β: 25[b]	β + 79	Yes	—	2004 [35]
6	H	N	—			β: 6[b]	β + 79	Yes	—	2004 [35]
7	H	N	—			β: 4[a]	—	—	—	2004 [36]
8	H	N	—			β: 26[a]	β + 69	Yes	1Q3D[c]	2004 [36]
9	H	C		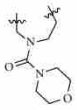		β: 1.3[a]	β + 36	Yes	—	2004 [37]
10	H	C		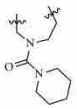		GSK-3: 2.0[a]	GSK-3 + 3	Yes	—	2005 [38]
11	H	C		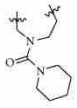		GSK-3: 0.7[a]	GSK-3 + 3	Yes	—	2005 [38]
12	Br	C	H	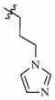		β: 140[a]	β + 5	Yes	1Q3D[c]	2009 [39]
13	F	C	H	Me	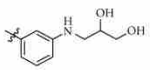	β: 0.6[a]	α & β + 315	Yes	1R0E	2010 [40]
14	H	C	H	H		β: 4470[a]	—	—	—	2011 [41]
15	H	C	H	Me		β: 890[a]	—	—	—	2011 [41]

[a] IC_{50} value; [b] K_i value; [c] docking studies, PDB code; α: GSK-3α; β: GSK-3β.

Table 3: Examples of bisindolyl maleimide and benzofuranyl-indolyl maleimide inhibitors with biological activity against GSK-3, selectivity, X-ray and reference.

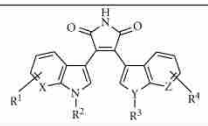

No.	R^1	X	R^2	R^3	Y	Z	R^4	IC_{50}/K_i (nM)	Kinase panel	*In vivo*	X-ray	Year/lit.
16	H	CH	Me	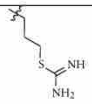	N	CH	H	β: 2.8[a]	—	Yes	—	1999 [42]
17	H	N			N	N	H	β: 48[a]	$\beta + 54$	Yes	—	2003 [43]
18	H	N			N	N	H	β: 34[a]	$\beta + 54$	Yes	1H8F[c]	2003 [43]
19	H	CH			N	CH	H	β: 25[a]	$\beta + 18$	Yes	—	2003 [44]
20	H	CH			N	CH	H	β: 4[a]	—	Yes	—	2003 [44]
21	H	N			N	N	H	β: 11[b]	$\beta + 65$	Yes	—	2004 [45]
22	H	N			N	N	H	β: 36[b]	$\beta + 65$	Yes	1H8F[c] + 1AQ1[c]	2004 [45]
23	H	CH		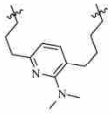	N	CH	H	β: 3[a]	α & $\beta + 98$	—	2OW3	2007 [46]
24	5-Br	CH	Me	—	O	CH	H	β: 7.0[a] (4.6[b])	$\beta + 22$	Yes	1Q3D[c]	2007 [47]
25	5-F	CH	Me	—	O	CH	6-CH_2OH	β: 0.35[a]	$\beta + 1$	—	1R0E[c]	2009 [48]
26	7-CH_2OH	CH	Me	—	O	CH	H	β: 5.4[a]	$\beta + 1$	—	1R0E[c]	2009 [48]
27	7-CH_2OMe	CH	Me	—	O	CH	H	β: 0.23[a]	$\beta + 1$	Yes	—	2009 [48]

[a]IC_{50} value; [b]K_i value; [c]Docking studies, PDB code; α: GSK-3α; β: GSK-3β.

The benzo[e]isoindole-1,3-dione **28** (Table 4) displays an IC_{50} of 304 nM in the presence of 100 μM ATP. It was evaluated in a panel of 22 representative kinases. 5 μM of compound **28** inhibited 91% of GSK-3β activity as well as 71% of CDK2/cyclin A and 53% of KDR (VEGFR2) [49]. The inhibition of GSK-3 leads to ectopic activation of the Wnt pathway during zebrafish development, resulting in a headless embryo. Thus, zebrafish embryos, which were treated with compound **28**, had highly restricted brain defects that ranged from smaller eyes and forebrain to a complete loss of these structures [49]. Compound **29** displayed a lower IC_{50} *in vitro* than **30**, whereas compound **30** displayed better *in vivo* efficacy. 25 μM of derivative **30** resulted in the eyeless phenotype of zebrafish embryos after

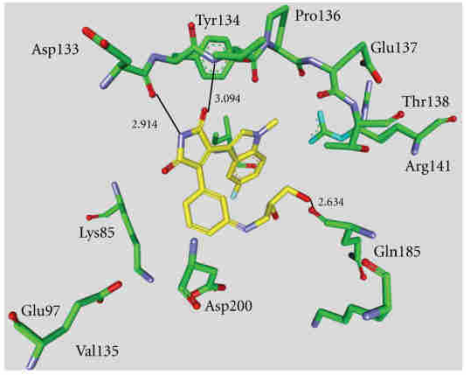

FIGURE 2: Compound **13** in the ATP binding pocket of GSK-3β; important protein-inhibitor interactions are shown. The distance is denoted by Å. PDB code 1R0E [40].

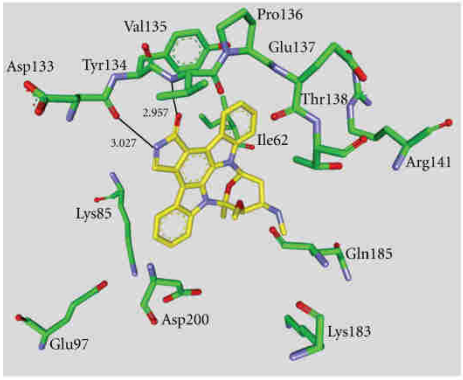

FIGURE 4: Compound **31** in the ATP binding pocket of GSK-3β; important protein-inhibitor interactions are shown. The distance is denoted by Å. PDB code 1Q3D [31].

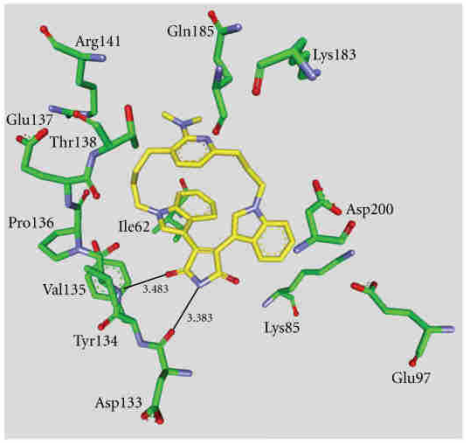

FIGURE 3: Compound **23** in the ATP binding pocket of GSK-3β; important protein-inhibitor interactions are shown. The distance is denoted by Å. PDB code 2OW3 [46].

3 days of incubation [50]. The synthetic activity dedicated to this structural class has been strong and is ongoing [51–55].

2.3. Staurosporine and Organometallic Inhibitors. **Staurosporine** (**31**) is a natural product from the bacterium *Streptomyces staurosporeus* [56]. It exerts antimicrobial, hypotensive, and cytotoxic activity [57]. **Staurosporine** (**31**) is also a potent GSK-3β inhibitor with a reported IC_{50} value of 15 nM (Table 5) [58]. The cocrystal structure of **Staurosporine** (**31**) with GSK-3β is elucidated in Figure 4. Again, the maleimide **31** interacts with the Asp133 carbonyl oxygen and the backbone nitrogen of Val135. These are the only direct hydrogen bonds observed between GSK-3β and this inhibitor [31]. The other polar interactions, for example, water-mediated interactions are not denoted. The organometallic ruthenium complex **32** is a remarkably potent inhibitor of GSK-3 (Table 5). The IC_{50} for GSK-3α is 3 nM and 10 nM for GSK-3β. The compound was evaluated against 10 kinases and displayed activity against GSK-3 and RSK1 (IC_{50} = 100 nM) only. The authors observed a water-mediated contact between the carbonyl ligand and the carbamide of Gln185 and assumed that this contributes to the specificity of GSK-3 [59]. Compound **33** showed improved selectivity. A test panel of more than 50 kinases was not significantly inhibited at 100 nM. Compound **33** was reported to activate the Wnt signaling pathway in cell culture experiments at nanomolar concentrations. The treatment of zebrafish embryos in early development by compound **33** caused malformations, for example, a head structure lacking the eyes and a stunted tail [60]. The S-diastereomer of compound **34** is a weaker GSK-3β inhibitor than the R-diastereomer: IC_{50} of 0.22 nM at 100 μM. Compound **34** (R-diastereomer, Table 5) exerts the highest reported potency against GSK-3β with an IC_{50} of 40 pM. Unfortunately, the evaluation in a kinase panel was not reported yet [61]. The complex of derivative **34** with GSK-3β (Figure 5) provided insight into the binding mode in the ATP pocket of GSK-3β. The interactions between the imide NH and the carbonyl oxygen of Asp133 and between the imide carbonyl and the NH of Val135 are typical. Another interaction is marked between the carbonyl oxygen of Val135 and the indolyl OH. The compound **34**, and the analogues **35** (**(*R*)-DW 12**) and **36** (**Λ-OS1**) contain a carbonyl, which interacts with the flexible glycine-rich loop of GSK-3β (Figures 6 and 7). Thereby Ile62, Gly63, Phe67 and Val70 form a small hydrophobic pocket (Figure 6(b), compound **35**). The structure activity analysis of ruthenium-based GSK-3 inhibitors

Table 4: Examples of maleimide inhibitors with biological activity against GSK-3, selectivity, X-ray and reference.

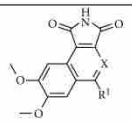

No.	X	R^1	IC_{50} (nM)	Kinase panel	*In vivo*	X-ray	Year/lit.
28	N	Et	β: 304	β + 21	Yes	1UV5[a]	2009 [49]
29	CH	Et	β: 92	β + 2	Yes	1UV5[a]	2010 [50]
30	CH	Me	β: 270	β + 2	Yes	1UV5[a]	2010 [50]

[a]Docking studies, PDB code; β: GSK-3β.

Table 5: Staurosporine and organometallic inhibitors with biological activity against GSK-3, selectivity, X-ray and reference.

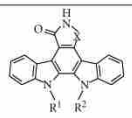

No.	X	R^1	R^2	IC_{50} (nM)	Kinase panel	*In vivo*	X-ray	Year/lit.
31	CH_2			β: 15	β + 2	—	1Q3D	1977, 1994, 2001, and 2003 [31, 56–58]

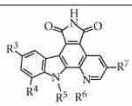

No.	R^3	R^4	R^5	R^6	R^7	IC_{50}/K_i (nM)	Kinase Panel	*In vivo*	X-ray	Year/lit.
32	H	H			H	α: 3 β: 10	α & β + 8	Yes	—	2004 [59]
33	OH	Br	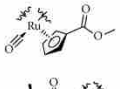		H	α: 0.35[a] β: 0.55[a]	α & β + 55	Yes	—	2006 [60]
34	OH	H	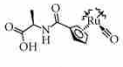		F	β: 0.04[a] (0.005[b])	—	—	2JLD	2008 [61]
35	OH	H			H	α: 0.5[a] β: 1.00[a]	—	—	3M1S	2011 [62]
36	H	H			NH_2	α: 0.9[a] β: 6[a]	α & β + 100	—	3PUP	2011 [22]

[a]IC_{50} value; [b]K_i value; α: GSK-3α; β: GSK-3β.

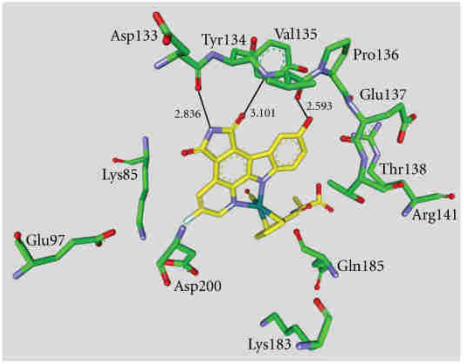

FIGURE 5: Compound **34** in the ATP binding pocket of GSK-3β; important protein-inhibitor interactions are shown. The distance is denoted by Å. PDB code 2JLD [61].

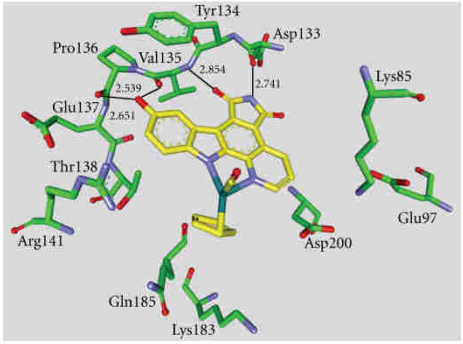

(a) Compound **35** in the ATP binding pocket of GSK-3β

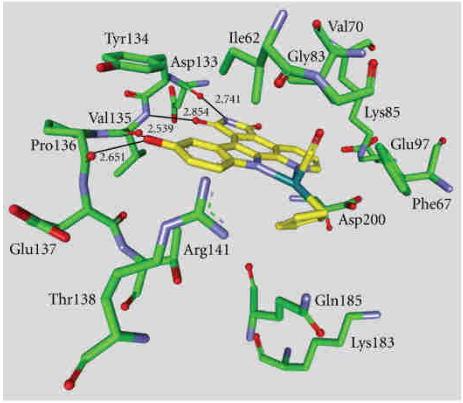

(b) Rotated (a) to reveal the hydrophobic pocket containing Ile62, Phe67, Gly83, Val70, Lys85, and Glu97

FIGURE 6: Compound **35** in the ATP binding pocket of GSK-3β; important protein-inhibitor interactions are shown. The distance is denoted by Å. PDB code 3M1S [62].

lacking the carbonyl revealed the contribution of this carbonyl to potency and selectivity [22, 61, 62].

2.4. Indole Derivatives. Several pharmaceutical companies have reported and patented indole derivatives as GSK-3 inhibitors [67–74]. Indirubins are likewise indole derivatives. They are related to the naturally occurring indigo dyes, and their pharmacological properties have long been known in traditional Chinese medicine, for example, in the treatment of leukemias [15]. Except for the dye indirubin **38**, all other noted indole derivatives (**37**, **39–50**) revealed an IC_{50} below 100 nM. Compound **37**, the **indirubin-3′-monoxime**, was reported to display an IC_{50} of 22 nM on GSK-3 inhibition (Table 6). This unselective compound is a strong inhibitor of the closely related kinases CDK1 and CDK5 [58]. Compound **37** did not affect p-tau levels in neither cortex nor hippocampus of P12 rats despite the high concentration of the compound in the brain (13 μM) [34]. Three important interactions of compound **37** and GSK-3β are displayed in the X-ray in Figure 8 [31]. Maternal Wnt activityz is necessary for dorsal axis formation in *Xenopus laevis* embryos, whereas head formation requires the inhibition of zygotic Wnt activity. The *Xenopus laevis* embryos were treated with compound **39** (**BIO**) or **LiCl**, respectively; in order to challenge these two GSK-3 regulated events *in vivo*. **LiCl** treatment leads to a hyper dorsoanteriorization at the expense of trunk and tail when applied during early cleavage stage. **39** exerted the same effect on the embryos. Compound **39** inhibited GSK-3 with an IC_{50} of 5 nM, but also CDK1, CDK2, and CDK5 in a nanomolar range [63, 64]. The binding mode of **39** in the ATP pocket of GSK-3β has been determined by X-ray crystallographic analysis. The four major interactions between the inhibitor and GSK-3β are shown in Figure 9. The nitrogen interacts with the carbonyl oxygen of Asp133 and the oxygen with the backbone nitrogen of Val135. Moreover, interactions with the oxygens of Val135 and Pro136 as well as the van der Waals contact between the bromine and Leu132 were observed. Compounds **41** and **43** are potent GSK-3 inhibitors and very selective against CDK1/cyclin B and CDK5/p25 [64]. In 2007, this class of indirubine derivatives was patented by Meijer et al. [75]. This patent lists *in vivo* activity for several compounds. The derivatives **44–46** feature an extended amino side chain at position R^1. They were prepared to enhance selectivity and water solubility versus compound **39**. These compounds were reported to inhibit β-catenin Ser33/37/Thr41 phosphorylation by GSK-3. Compounds **44–46** were also less cytotoxic than compound **39** in the MTS reduction assay of SH-SY5Y neuroblastoma cells [65]. The compounds **47–50** are potent, yet unselective GSK-3 inhibitors [66].

Table 6: Examples of indirubine inhibitors with biological activity against GSK-3, selectivity, X-ray, and reference.

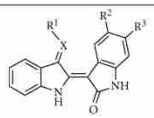

No.	X	R^1	R^2	R^3	IC_{50} (nM)	Kinase panel	*In vivo*	X-ray	Year/lit.
37	N	OH	H	H	β: 22	$\beta + 2$	Yes	1Q41	2001, 2003, 2007 [31, 34, 58]
38	O	—	H	H	β: 600	$\beta + 2$	—	—	2001 [58]
39	N	OH	H	Br	α/β: 5	$\alpha/\beta + 19$	Yes	1UV5 + 1Q41[a]	2003, 2004 [63, 64]
40	N	OAc	H	Br	α/β: 10	$\alpha/\beta + 19$	—	—	2003 [63]
41	O	—	H	Br	β: 45	$\beta + 2$	—	—	2004 [64]
42	N	OAc	Cl	Cl	β: 4	$\beta + 2$	—	—	2004 [64]
43	N	OAc	CH_3	Br	β: 7	$\beta + 2$	—	—	2004 [64]
44	N	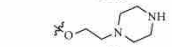	H	Br	α/β: 3.3	$\alpha/\beta + 2$	Yes	1UV5[a]	2008 [65]
45	N	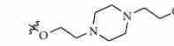	H	Br	α/β: 5.0	$\alpha/\beta + 2$	Yes	1UV5[a]	2008 [65]
46	N	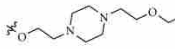	H	Br	α/β: 14	$\alpha/\beta + 2$	Yes	—	2008 [65]
47	O	—	NH_2	H	α/β: 80	$\alpha/\beta + 4$	Yes	—	2009 [66]
48	O	—	NHAc	H	α/β: 7.5	$\alpha/\beta + 4$	Yes	—	2009 [66]
49	N	OH	H	NO_2	α/β: 40	$\alpha/\beta + 4$	—	—	2009 [66]
50	N	OH	NO_2	H	α/β: 2.1	$\alpha/\beta + 4$	—	—	2009 [66]

[a] Docking studies; PDB code; β: GSK-3β; α/β: GSK-3α/β.

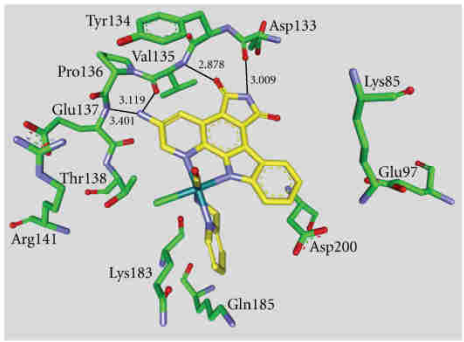

Figure 7: Compound **36** in the ATP binding pocket of GSK-3β; important protein-inhibitor interactions are shown. The distance is denoted by Å. PDB code 3PUP [22].

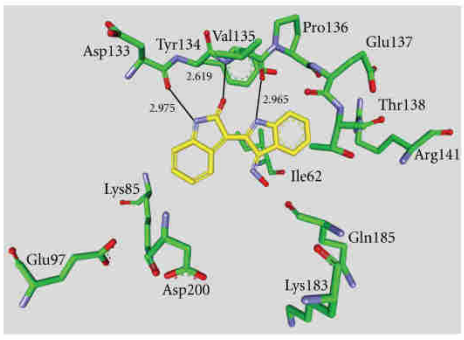

Figure 8: Compound **37** in the ATP binding pocket of GSK-3β; important protein-inhibitor interactions are shown. The distance is denoted by Å. PDB code 1Q41 [31].

2.5. Paullone Derivatives. Paullones have been reported as potent ATP competitive inhibitors of CDKs and GSK-3β [76, 77]. Compounds **51–55** revealed that a defined derivatisation of one substituent only can increase the GSK-3β inhibition up to 155 fold. Alsterpaullone **55** (**9-nitro-paullone**) is one of the most potent GSK-3β inhibitors and competes with ATP for binding to GSK-3β (Table 7).

Compound **55** was evaluated in a kinase panel with 25 kinases and exhibited high selectivity for GSK-3α/β, CDK1/cyclin B, CDK2/cyclin A, CDK2/cyclin E, and CDK5/p35.

Table 7: Examples of paullone inhibitors with biological activity against GSK-3, selectivity, X-ray, and reference.

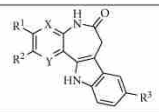

No.	X	Y	R^1	R^2	R^3	IC_{50} (nM)	Kinase panel	*In vivo*	X-ray	Year/lit.
51	CH	CH	H	H	H	β: 620	α/β + 2	—	—	1999, 2000 [76, 77]
52	CH	CH	H	H	Cl	β: 24	α/β + 2	—	—	1999, 2000 [76, 77]
53	CH	CH	H	H	Br	β: 23	α/β + 2	—	—	1999, 2000 [76, 77]
54	CH	CH	H	H	CN	β: 10	α/β + 2	—	—	1999, 2000 [76, 77]
55	CH	CH	H	H	NO_2	α: 4 β: 4	α & β + 23	Yes	1Q3W	1999, 2000, 2003, 2007 [31, 34, 76, 77]
56	CH	CH		H	Br	β: 30	β + 2	—	—	2002 [78]
57	CH	CH	H		Br	β: 40	β + 2	—	—	2002 [78]
58	CH	N	H	H	Br	β: 18	β + 2	—	—	2004 [79]
59	N	CH	H	H	Br	β: 6000	β + 2	—	—	2004 [79]
60	CH	CH	H		NO_2	β: 6	β + 2	—	—	2005 [80]
61	CH	CH	H		NO_2	β: 2.5	β + 2	—	—	2005 [80]
62	CH	CH	H		NO_2	β: 6.5	β + 2	—	—	2005 [80]
63	CH	CH	H		NO_2	β: 34	β + 2	—	—	2005 [80]
64	CH	CH	H		NO_2	β: 0.8	β + 21	—	—	2005 [80]

α: GSK-3α; β: GSK-3β.

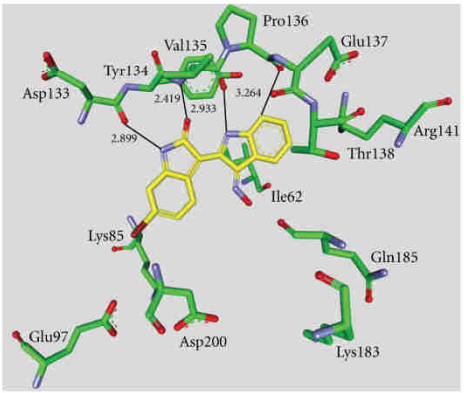

Figure 9: Compound **39** in the ATP binding pocket of GSK-3β; important protein-inhibitor interactions are shown. The distance is denoted by Å. PDB code 1UV5 [63].

All measured IC_{50} values were in the nanomolar range. Alsterpaullone **55** was reported to inhibit the *in vivo* phosphorylation of tau at AD-specific sites by GSK-3β [76]. Paullone **55** formulated in 20% DMSO/25% Tween-80 and injected *s.c.* led to a reduction in 43 kDa tau phosphorylation in cortex after 2 h, though not in the 49 kDa isoform. Furthermore, the phosphorylation levels of the 43 kDa and 49 kDa isoforms in the hippocampus were significantly decreased [34]. Most of the paullone derivatives were patented by Meijer and Kunick in 2001 [81]. The binding mode of **55** has been determined by X-ray crystallographic analysis (Figure 10) [31]. The interactions of alsterpaullone and GSK-3β include two hydrogen bonds with Val135 and one interaction between the nitro group and the side chain amino group of Lys85. The compounds **56** and **57** inhibited GSK-3 as well as CDK1/cyclin B and CDK5/p25 in the nanomolar range [78]. The exchange of nitrogen and carbon in compound **58** and **59** decreased the inhibitory activity, but provided selectivity to **58,** which is void of CDK-inhibitory effects [79]. However, compound **58** was tested against three kinases (GSK-3β, CDK1/cyclin

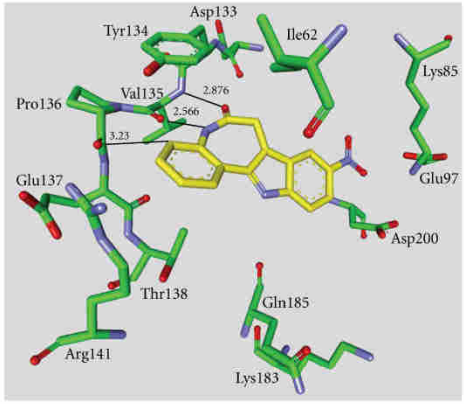

FIGURE 10: Compound **55** in the ATP binding pocket of GSK-3β; important protein-inhibitor interactions are shown. The distance is denoted by Å. PDB code 1Q3W [31].

B, and CDK5/p2) only. The derviatisation of the R^2 motif, see compounds **57** and **60–64** in Table 7, leads to the most potent inhibitor **64**. Compound **64**, with an IC_{50} of 0.8 nM is likewise nonselective for GSK-3. It preferentially inhibited the CDK/GSK-3 family in the nanomolar range and VEGFR-2, VEGFR-3, and Src in the submicromolar range [80].

2.6. Pyrazolamide Derivatives. GlaxoSmithKline identified another class of GSK-3 inhibitors in 2003 (Table 8). The precursor was identified by a pharmacophore search of the in house database. The compounds **65–67** were profiled against a panel of 25 kinases including GSK-3β. An excellent selectivity was obtained against the majority of the kinases. However, a significant inhibition of CDK2/cyclin A was reported [82]. Compounds **68** and **69** displayed improved potency, but nevertheless inhibited CDK2/cyclin A. Only compound **70** showed an excellent GSK-3 potency and improved CDK-2/cyclin A selectivity [83]. The IC_{50} comparison of compounds **71–73** revealed that the Ph-4-OH motif is the best. The most potent inhibitor **74** (IC_{50} = 0.8 nM) was tested against a panel of kinases and showed a reduction in the overall selectivity profile [84, 85]. Compounds **75–77** showed an excellent selectivity against CDK-2/cyclin A. In addition, compound **77** demonstrated an excellent overall selectivity profile against all kinases of the panel [85]. Unfortunately, no further studies were published concerning this series.

Takeda Pharmaceutical disclosed compound **78** in 2009. It is a very potent inhibitor of GSK-3 with an IC_{50} of 2.3 nM for GSK-3α and 2.0 nM for GSK-3β. It had no inhibitory effect on 23 kinases, and only a weak inhibition was detected for CDK1/cyclin B, CDK2/cyclin A, CDK5, and JNK1. The cold-water stress model (CWS) with male C57BL/6Njcl mice was used to evaluate the *in vivo* efficacy of compound **78**. CWS transiently induces *in vivo* tau hyperphosphorylation as reported in previous studies. The compound displayed highly potent inhibition of *in vivo* phosphorylation in CWS mice and reduced sarkosyl insoluble tau in old homozygous JNPL3 mice. Furthermore, compound **78** inhibited tau phosphorylation at GSK-3-directed sites in rat primary neuronal cells and mouse brain tissue [86]. Several structures containing a pyrazole core have shown promising results in animal models of diabetes, for structural information see denoted references.

The pyrazolamides developed by Wyeth-Ayerst Research, now Pfizer, showed significant plasma glucose-lowering activity (16–42% reduction) in genetically obese, diabetic db/db mice [87, 88]. Novartis published a series of compounds with ED_{50} values for glucose reduction in ob/ob mice of 3.0 mg/kg/day [89]. In 2011, the Merck Research Laboratories disclosed a potent human glucagon receptor antagonist with good pharmacokinetic profiles in four preclinical species. One of these compounds showed excellent oral pharmacodynamic efficacy in rhesus monkeys and transgenic mice by blocking glucagon-induced hyperglycemia [90].

2.7. Pyrimidine and Furopyrimidine Derivatives. GSK-3 inhib-itors bearing the pyrimidine moiety are listed in Tables 9 and 10. This series is characterized by a high number of patent applications, particularly by Vertex Pharmaceuticals [97–122]. Compounds **79** and **81** inhibited GSK-3β in the nanomolar range. The *in silico* docking of compound **80** into the ATP binding pocket of GSK-3β suggested that **80** makes two hydrogen bonds with the hinge region and one interaction with the positively charged Arg141 [28, 91]. Unfortunately, the activity of these compounds in a kinase panel was not disclosed. The compounds **82–90** are weak inhibitors of GSK-3, and there are no public data for *in vivo* activity nor selectivity. Docking of **90** into the PDB structure 1Q5K of GSK-3β suggested that one nitrogen and the secondary amine form hydrogen bonds to the hinge region at the Val135 NH and carbonyl, respectively. The following compounds **91–93** showed IC_{50} values below 100 nM, but **91** and **92** inhibit Aurora A in the nanomolar range. Derivative **93** (GSK-3α IC_{50} = 61 nM, GSK-3β IC_{50} = 41 nM) inhibited Aurora A at micromolar concentration only. *In vivo* studies of this compound in rats showed 34% oral bioavailability and good exposure [92]. Compound **94**, a lead compound for ERK2 inhibition, is a nonselective GSK-3 inhibitor and inhibited all 5 kinases in the panel, which included GSK-3 [93]. The complex of compound **94** with GSK-3β (Figure 11) provided the binding mode in the ATP pocket of GSK-3. The secondary amine interacts with the carbonyl oxygen of Val135 and the nitrogen of compound **94** with the backbone NH of Val135. Two additional interactions are present between OH and Asp200 and between the carbonyl and the primary amine of Lys85. The arylimidazoles **95** (**CHIR 99021**) and **96** (**CHIR 98014**) are very effective ATP competitive inhibitors of murine and rat GSK-3 ($IC_{50} \leq 10$ nM). Both compounds exhibited 500 to 10000 fold selectivity for GSK-3 versus 20 other kinases tested. These GSK-3 inhibitors rapidly lower blood glucose levels in diabetic rodent models and enhance glucose transport as well as GS activation in insulin-resistant oxidative skeletal muscle from

Table 8: Examples of pyrazolamide inhibitors with biological activity against GSK-3, selectivity, X-ray, and reference.

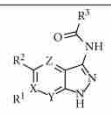

No.	X	Y	Z	R^1	R^2	R^3	IC_{50} (nM)	Kinase panel	*In vivo*	X-ray	Year/lit.
65	C	N	CH	H	Ph	Propyl	α: 56	β + 24	—	—	2003 [82]
66	C	N	CH	H	2-F-Ph	Propyl	α: 18	β + 24	—	—	2003 [82]
67	C	N	CH	H	3-Pyridyl	Propyl	α: 11	β + 24	—	—	2003 [82]
68	N	N	CH	—	Ph	Propyl	α: 4	β + 24	—	PDB n.p.[a]	2003 [83]
69	N	CH	CH	—	Ph	Propyl	α: 7	—	—	—	2003 [83]
70	N	N	CH	—	Ph		α: 22	β + 24	—	PDB n.p.[a]	2003 [83]
71	C	N	CH	Ph	H		α: 425	—	—	—	2003 [84]
72	C	N	CH	Ph-4-OMe	H		α: >5000	—	—	—	2003 [84]
73	C	N	CH	Ph-4-OH	H		α: 8	α + 23	—	PDB n.p.[a]	2003 [84, 85]
74	C	N	CH	Ph-4-OH	Br		α: 0.8	α + 23	—	PDB n.p.[a]	2003 [84, 85]
75	C	N	CH	Ph	Br		α: 75	α + 23	—	—	2003 [85]
76	C	CH	CH	5-Indolyl	H		α: 42	α + 1	—	—	2003 [85]
77	C	N	CH	2-Furyl	Br		α: 7	β + 23	—	—	2003 [85]

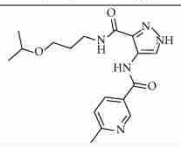

No.	IC_{50}/K_i (nM)	Kinase panel	*In vivo*	X-ray	Year/lit.
78	α: 2.3 β: 2.0	α & β + 27	Yes	—	2009 [86]

[a] Not published as PDB; α: GSK-3α; β: GSK-3β.

type 2 diabetic rats [94]. The nitropyridine **96** exerts a very potent reduction of Ser396 tau phosphorylation in a human neuronal cell line. P12 rats were injected *i.v.* with 30 mg/kg of **CHIR 98014** (**96**, dissolved in DMSO) to test the efficacy on tau phosphorylation *in vivo*, resulting in a maximal brain concentration of 7 μM. Tissue analysis by Western blotting using a p-tau Ser396 antibody showed approximately 40% reduction in the phosphorylation of 43 kDa and 49 kDa tau in the cortex and a significant 3 fold reduction of the 43 kDa isoform in the hippocampus. Moreover, a 50% reduction of GSK-3β activity was observed in compound **96** treated animals versus vehicle [34].

The denoted furopyrimidines **97–102** inhibited GSK-3β with an IC_{50} below 40 nM (Table 10). Compound **100** (GSK-3β IC_{50} = 5 nM) displayed excellent selectivity against 25 kinases, including CDK2/cyclin A, which was inhibited with an IC_{50} of 0.46 μM. Compound **100** was examined in a glycogen accumulation assay in L6 cells and exhibited excellent induction of glycogen accumulation

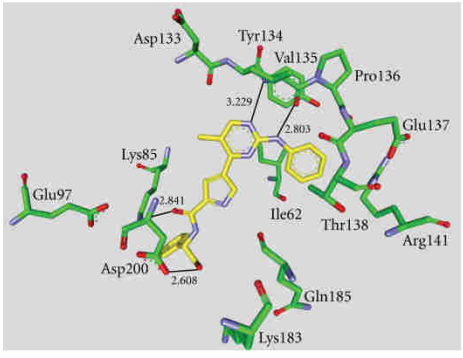

Figure 11: Compound **94** in the ATP binding pocket of GSK-3β; important protein-inhibitor interactions are shown. The distance is denoted by Å. PDB code 3I4B [93].

Table 9: Examples of pyrimidine inhibitors with biological activity against GSK-3, selectivity, X-ray, and reference.

No.	R^1	R^2	R^3	R^4	IC_{50}/K_i (nM)	Kinase panel	*In vivo*	X-ray	Year/lit.
79		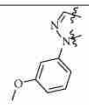	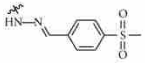	H	β: 2.5[a]	—	Yes	—	2004 [91]
80			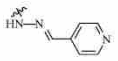	H	β: 100[a]	—	Yes	1GNG[c]	2001; and 2004 [28, 91]
81			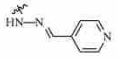	H	β: 4.0[a]	—	Yes	1GNG[c]	2001; and 2004 [28, 91]
82		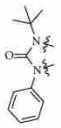	H		β: 2400[a]	—	—	—	2008 [92]
83		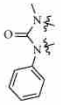	H		β: 1700[a]	—	—	—	2008 [92]
84		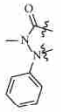	H	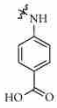	α: 1020[a] β: 960[a]	—	—	—	2008 [92]
85			H	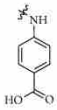	α: 1900[a] β: 760[a]	—	—	—	2008 [92]
86		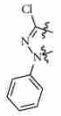	H	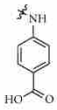	α: 350[a] β: 180[a]	—	—	—	2008 [92]

Table 9: Continued.

									
87	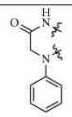		H	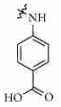	α: 6700[a] β: 3500[a]	—	—	—	2008 [92]
88		NO_2	H	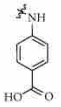	α: 270[a] β: 150[a]	—	—	—	2008 [92]
89		CF_3	H	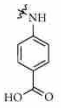	α: 750[a] β: 490[a]	—	—	—	2008 [92]
90			H		α: 330[a] β: 628[a]	α and β + 1	—	1Q5K[c]	2008 [92]
91		NO_2	H	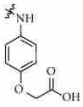	α: 74[a] β: 92[a]	α and β + 1	—	—	2008 [92]
92			H	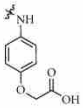	α: 9[a] β: 13[a]	α and β + 1	—	—	2008 [92]
93		CF_3	H		α: 61[a] β: 41[a]	α and β + 1	Yes	—	2008 [92]
94	H	Me	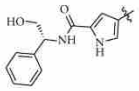		GSK-3: 7[b]	GSK-3 + 4	—	3I4B	2009 [93]
95			H	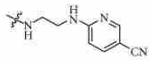	α: 10 β: 6.7[a] (9.8[b])	α and β + 20	Yes	—	2003, and 2007 [34, 94]
96			H	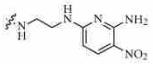	α: 0.65 β: 0.58[a] (0.87[b])	α and β + 20	Yes	—	2003, and 2007 [34, 94]

[a]IC_{50} value; [b]K_i value; [c]docking studies, PDB code (n.d.: not denoted); α: GSK-3α; β: GSK-3β.

(EC_{50} = 0.39 μM) [95]. Compound **101** was also profiled by cross-screening against a variety of kinases and showed an excellent overall selectivity against all kinases tested including CDK2. The docking of **101** into the ATP binding site of GSK-3β provided a likely interaction. One nitrogen and NH_2 of aminopyrimidine are anchored to the carbonyl moiety and NH of Val135 via hydrogen bond interactions. The 3-pyridine moiety is located close to Lys85 of the conserved salt

Table 10: Examples of furopyrimidine inhibitors with biological activity against GSK-3, selectivity, X-ray, and reference.

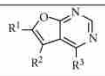

No.	R^1	R^2	R^3	IC_{50} (nM)	Kinase panel	*In vivo*	X-ray	Year/lit.
97		H		β: 5	β + 2	Yes	—	2004 [95]
98		H		β: 32	β + 2	—	—	2004 [95]
99		H		β: 23	β + 2	Yes	—	2004 [95]
100		H		β: 5	β + 24	Yes	PDB n.d.[a]	2004 [95]
101		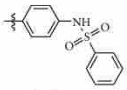	NH_2	β: 30	β + 9	Yes	PDB n.d.[a]	2008 [96]
102		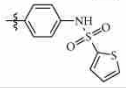	NH_2	β: 23	—	—	—	2008 [96]

[a] Docking studies, PDB code (n.d.: not denoted); β: GSK-3β.

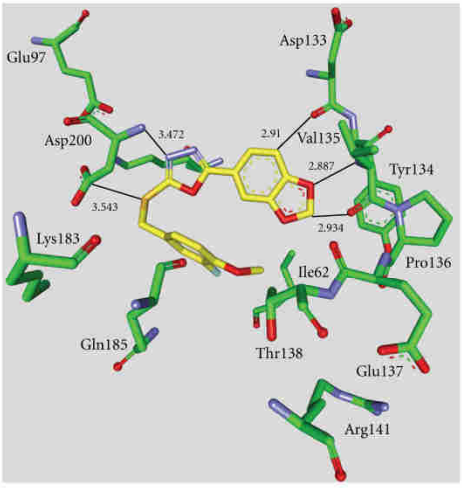

Figure 12: Compound **110** in the ATP binding pocket of GSK-3β; important protein-inhibitor interactions are shown. The distance is denoted by Å. PDB code 3F7Z [125].

bridge (Lys85/Glu97). The EC_{50} value of compound **101** in the glycogen accumulation assay in L6 cells was 3.2 μM and thus 9 fold higher than for compound **100** [96].

2.8. Oxadiazole Derivatives. Tables 11–13 list GSK-3 inhibitors featuring the oxadiazole moiety. The depicted 1,2,5-oxadiazoles, **103–109**, revealed IC_{50} values from 0.1 μM to more than 1.1 μM. Compounds **104–106** were screened for inhibitory activity against a panel of 32 kinases at 100 μM ATP concentration. All compounds gave at least 100 fold selectivity for GSK-3 compared to CDK2. However, 10 μM of compound **104** inhibited other kinases like MSK1 and DYRK1A, the latter activity is of interest for neurodegenerative diseases. The above mentioned compounds **104–106** displayed both sufficient cell penetration and suitable water solubility [123]. The dioxolane **110** was identified as GSK-3β inhibitor (IC_{50} = 65 nM; Table 12) by high throughput screening. The X-ray analysis of the GSK-3β cocrystallized compound confirmed the interaction with the ATP binding site (Figure 12). One oxygen and a neighbouring hydrogen atom of the benzodioxole establish hydrogen bonds with the amide NH hydrogen and carbonyl oxygen of Val135 in the hinge region. The nitrogen atoms of the oxadiazole engage in an unique hydrogen bond relay network between Lys85-Glu97-Asp200 via two water molecules (interactions not shown). Further interactions are denoted in Figure 12. After an extensive derivatisation, for example, **111–114**, compound **114** (Figure 13) exerts a 28 fold increased activity (GSK-3β IC_{50} = 2.3 nM) compared to its homologue **110** (Table 12). The selectivity of **114** was evaluated in a panel of more than 20 kinases to reveal more than 1000 fold selectivity against CDK1, CDK2, and CDK5. In addition, rat cassette dosing experiments of compound **114** were performed, which revealed low oral bioavailability. The cocrystal

Table 11: Examples of 1,2,5-oxadiazole inhibitors with biological activity against GSK-3, selectivity, X-ray, and reference.

No.	R^1	R^2	IC_{50} (nM)	Kinase panel	*In vivo*	X-ray	Year/lit.
103	NH_2	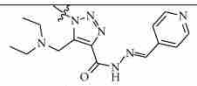	β: 410	—	—	—	2003 [123]
104	NH_2	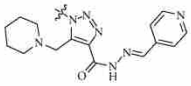	β: 100	β + 31	Yes	—	2003 [123]
105	NH_2	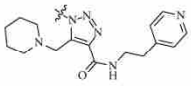	β: 1160	β + 31	Yes	—	2003 [123]
106	NH_2	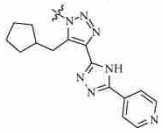	β: 280	β + 31	Yes	—	2003 [123]
107	NH_2	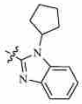	β: 210	β + 3	—	—	2009 [124]
108	NH_2	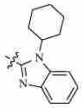	β: 240	β + 3	—	—	2009 [124]
109	NH_2		β: 290	β + 3	—	—	2009 [124]

β: GSK-3β.

structure of **114** bound to GSK-3β was not fully characterized due to the cleavage of the S–C bond in the X-ray beam (Figure 13) [125]. The cocrystal structure indicated that the nitrogen of the benzimidazole forms a hydrogen bond with the backbone NH of the hinge region at Val135, and one nitrogen of the oxadiazole ring makes a hydrogen bond with the NH of Asp200. The hydrogen atom on the carbon of the benzimidazole made an additional hydrogen bond with the carbonyl oxygen of Val135 [125]. The compounds **115** and **116** are enantiomers just as compounds **117** and **118**. The S-isomers **116** and **118** were found to be eutomers. It was reported that the S-isomers possessed good oral absorption in nonfasted Crl: CD(SD)IGS rats with a bioavailability of 72.8% for derivative **116** and 65.5% for derivative **118**. Furthermore, the compounds exhibited favourable blood-brain barrier (BBB) permeability. Compounds **116** and **118** were tested for inhibitory activity against more than 20 kinases and displayed no significant activity. This indicates that these compounds are highly selective GSK-3 inhibitors. The binding mode of **116** in the ATP pocket of GSK-3β has been determined by X-ray crystallographic analysis (Figure 14) [126]. One of the nitrogen atoms of the oxadiazole was revealed to interact via a hydrogen bond with the side chain of Lys85 and the other with Asp200. The oxygen atom and one carbon hydrogen of the benzofuran ring interact with the main chain of Val135. Another interaction was observed between one carbon hydrogen and the carbonyl of Asp133. Derivatives **116** and **118** were tested *in vivo* using the CWS model in mice. Here, tau phosphorylation was induced at several GSK-3β-directed sites such as Ser199, Thr205, Thr231, and Ser396 in mice. As reported, tau phosphorylation was significantly reduced by 35% for compound **116** and 38% for compound **118** [126]. Compound **116** was further investigated and revealed significantly decreased hippocampal tau phosphorylation as well as suppression of tau pathology without affecting amyloid β pathology [127].

A multistage virtual screening of 289903 molecules resulted in 59 hits of potential GSK-3β inhibitors, for example,

Table 12: Examples of 1,3,4-oxadiazole inhibitors with biological activity against GSK-3, selectivity, X-ray, and reference.

No.	R^1	R^2	IC_{50} (nM)	Kinase panel	*In vivo*	X-ray	Year/lit.
110	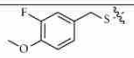		β: 65	—	—	3F7Z	2009 [125]
111	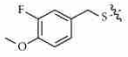		β: 44	—	—	—	2009 [125]
112	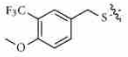		β: 3.1	—	—	—	2009 [125]
113	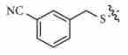	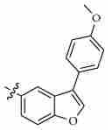	β: 3.5	—	—	—	2009 [125]
114	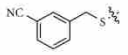	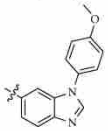	β: 2.3	β + 23	Yes	3F88	2009 [125]
115	Me	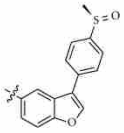	β: 140	—	—	—	2009 [126]
116	Me	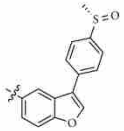	α: 37; β: 34 (53)[a]	β + 22	Yes	3GB2	2009, 2011 [126, 127]
117	Me	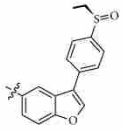	β: 190	—	—	—	2009 [126]
118	Me	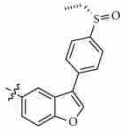	β: 20	β + 22	Yes	—	2009 [126]
119			β: 17	β + 1	Yes	1UV5[b]	2010 [128]
120	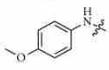		β: 53	—	—	—	2010 [128]

Table 12: Continued.

							
121	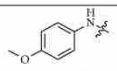		β: 18	—	—	—	2010 [128]
122	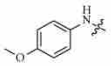		β: 7	—	—	1UV5[b]	2010 [128]

[a]Results of different publications; [b]docking studies, PDB code (n.d.: not denoted); β: GSK-3β.

Table 13: Examples of 1,2,4-oxadiazole inhibitors with biological activity against GSK-3, selectivity, X-ray, and reference.

							
No.	R^1	R^2	IC_{50} (nM)	Kinase panel	*In vivo*	X-ray	Year/lit.
123	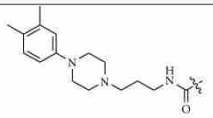		β: 350	β + 8	Yes	—	2008 [129]
124	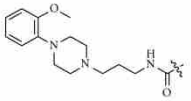		β: 410	β + 8	Yes	—	2008 [129]
125	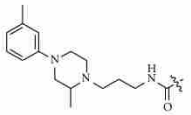		β: 690	β + 8	Yes	—	2008 [129]
126	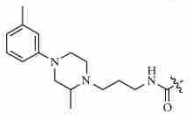		β: 710	—	Yes	—	2008 [129]
127	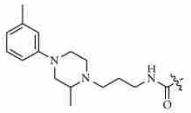		β: 1130	—	Yes	—	2008 [129]

β: GSK-3β.

compound **119**. Biological tests confirmed the IC_{50} of 17 nM and good selectivity versus CDK2. It crosses the BBB and has a good hepatic glycogen effect in mice. The derivatisation, for example, **120–122**, of compound **119** lead to compound **122** with an IC_{50} of 7 nM. Surprisingly, docking experiments of compound **122** revealed a different binding mode in comparison to the cocrystallized oxadiazoles **110**, **114** and **116**. The *in silico* docked oxadiazole motif coordinates to the GSK-3β hinge region, Val135, Tyr134, and Asp133, instead of binding to the polar region, Lys85, Cys199, and Asp200 [128].

The last denoted oxadiazoles are the 1,2,4-oxadiazoles **123–127**, which exert moderate inhibition of GSK-3β only (Table 13). A subset of these oxadiazoles (**123–125**) exhibited weak inhibition of Pim-1 and no detectable inhibition towards seven other kinases tested at 10 μM concentration [129].

2.9. Thiazole Derivatives. The benzothiazoles **128** and **129** (Table 14) are nonselective GSK-3 inhibitors and showed moderate activity against CDKs [130]. This stands in contrast to the thiazolylurea **130** (**AR-A014418**), which strongly inhibited GSK-3 (IC_{50} = 104 nM) but not any other kinase in the panel. **AR-A014418** inhibited tau phosphorylation in transfected 3T3-fibroblasts in a dose-dependent fashion exhibiting an IC_{50} of 2.7 μM. The neuronal loss was reduced

Table 14: Examples of thiazole inhibitors with biological activity against GSK-3, selectivity, X-ray, and reference.

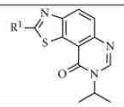

No.	R^1	IC_{50} (nM)	Kinase panel	*In vivo*	X-ray	Year/lit.
128	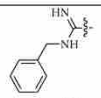	α/β: 130	α/β + 2	—	1J1B[b]	2008 [130]
129	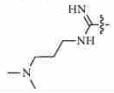	α/β: 560	α/β + 2	—	—	2008 [130]

No.	R^2	R^3	IC_{50}/K_i (nM)	Kinase Panel	*In Vivo*	X-ray	Year/Lit.
130	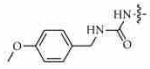	NO_2	β: 104[b] (38[c])	β + 26	Yes	1Q5K	2003, 2005, 2007 [34, 131, 132]

[a]Docking studies, PDB code; [b]IC_{50} value; [c]K_i value; α/β: GSK-3α/β; β: GSK-3β.

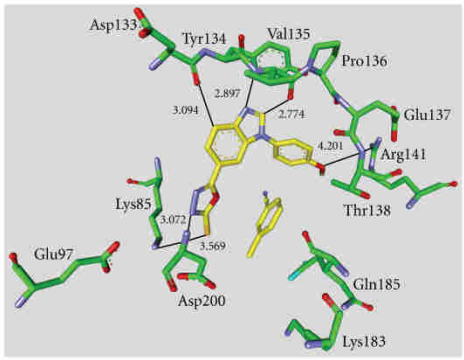

Figure 13: Compound **114** in the ATP binding pocket of GSK-3β; important protein-inhibitor interactions are shown. The distance is denoted by Å. PDB code 3F88 [125].

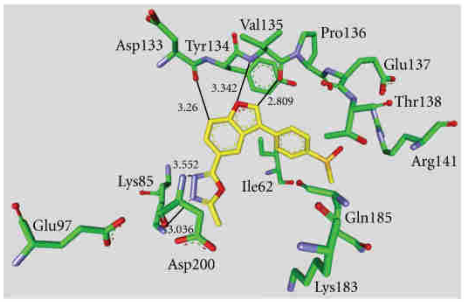

Figure 14: Compound **116** in the ATP binding pocket of GSK-3β; important protein-inhibitor interactions are shown. The distance is denoted by Å. PDB code 3GB2 [126].

in the organotypic culture (N2A cells) and compound **130** by itself did not affect neuronal viability. The cocrystal structure analysis of **AR-A014418** and GSK-3β revealed that this compound binds to the hinge region via three hydrogen bond interactions (Figure 15) [131]. Furthermore, compound **130** significantly reduced insoluble tau levels in the brainstem of JNPL3 mice when compared with vehicle treated animals [132]. Surprisingly, another research group reported that **AR-A014418** showed no effect on the phosphorylation levels of neither 43 kDa nor 49 kDa tau in the cortex or hippocampus of postnatal model rats [34]. Novel compounds based on the scaffold of **AR-A014418** were synthesized recently. They showed improved *in vitro* activity and reduced toxicity in the wildtype zebrafish embryo assay [133].

2.10. Miscellaneous Heterocyclic Derivatives with GSK-3 Activity. Table 15 lists GSK-3 inhibitors featuring a benzimidazole core. There are neither *in vivo* assays nor selectivity data published for these potential metal chelators **131–134**

Table 15: Examples of miscellaneous heterocyclic inhibitors with biological activity against GSK-3, selectivity, X-ray and reference.

(a)

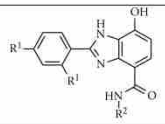

No.	R^1	R^2	IC_{50} (nM)	Kinase panel	*In vivo*	X-ray	Year/lit.
131	H		—	—	—	1I09[a]	2007 [134]
132	H		β: 580	—	—	—	2007 [134]
133	H	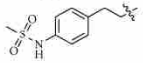	β: 25	—	—	—	2007 [134]
134	Cl	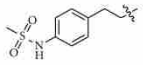	β: 15	—	—	2O5K	2007 [134]

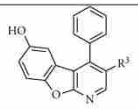

No.	R^3	K_i (nM)	Kinase panel	*In vivo*	X-ray	Year/lit.
135	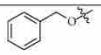	β: 5800	β + 4	—	PDB n.d.[a]	2008 [135]
136		β: 4100	β + 4	—	PDB n.d.[a]	2008 [135]
137		β: 1500	β + 4	—	PDB n.d.[a]	2008 [135]

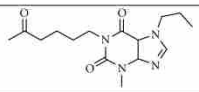

No.	IC_{50} (nM)	Kinase panel	*In vivo*	X-ray	Year/lit.
138	—	—	Yes	—	2005 [136]

[a] Docking studies, PDB code (n.d.: not denoted); β: GSK-3β.

(b)

No.	R^1	R^2	K_i (nM)	Kinase panel	*In vivo*	X-ray	Year/lit.
139	H		β: 1490	—	—	1Q3D[b]	2010 [137]
140			β: 0.8	β + 13	—	—	2010 [137]
141			β: 2	β + 13	—	—	2010 [137]
142			β: <2	—	—	3L1S	2010 [137]

(b) Continued.

143	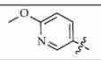		β: 4.5	β + 13	—	—	2010 [137]

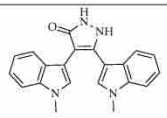

No.	IC_{50} (nM)	Kinase panel	*In vivo*	X-ray	Year/lit.
144	α: 34	β + 39	Yes	1Q3D[b]	2011 [138]

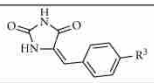

No.	R^3	IC_{50} (nM)	Kinase panel	*In vivo*	X-ray	Year/lit.
145		β: 4200	—	Yes	1Q4l[b]	2009 [139]
146		β: 6400	—	—	—	2009 [139]
147	SCH_2CH_3	β: 7800	—	—	—	2009 [139]

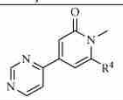

No.	R^4	IC_{50} (nM)	Kinase panel	*In vivo*	X-ray	Year/lit.
148	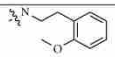	β: 17.4	β + 2[a]	Yes	—	2011 [140]
149		β: 8.5	β + 2[a]	Yes	—	2011 [140]
150	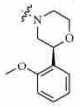	β: 16.1	β + 2[a]	Yes	—	2011 [140]

[a] Further, it was noted that the compound was screened against a broad panel of kinases; [b] docking studies, PDB code; β: GSK-3β.

(c)

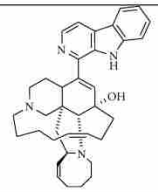

No.	Name	IC_{50} (nM)	Kinase panel	*In vivo*	X-ray	Year/lit.
151	Manzamine A	β: 10200	α and β + 4	Yes	—	2007 [141]

(c) Continued.

No.	Name	IC_{50} (nM)	Kinase panel	*In vivo*	X-ray	Year/lit.
152	Meridianin D	β: 2500	β + 5	Yes	—	2004 [142]

No.	Name	IC_{50} (nM)	Kinase panel	*In vivo*	X-ray	Year/lit.
153	Hymenialdisine	β: 10	β + 31	Yes	—	2000 [143]

No.	Name	IC_{50} (nM)	Kinase panel	*In vivo*	X-ray	Year/lit.
154	Dibromocantharelline	β: 3000	β + 3	—	1H8F[a]	2010, 2011 [143, 144]

[a] Docking studies, PDB code; β: GSK-3β.

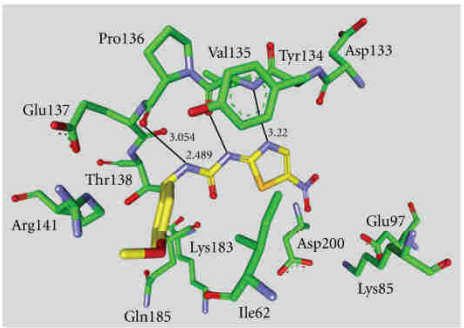

FIGURE 15: Compound **130** in the ATP binding pocket of GSK-3β; important protein-inhibitor interactions are shown. The distance is denoted in Å. PDB code 1Q5K [131].

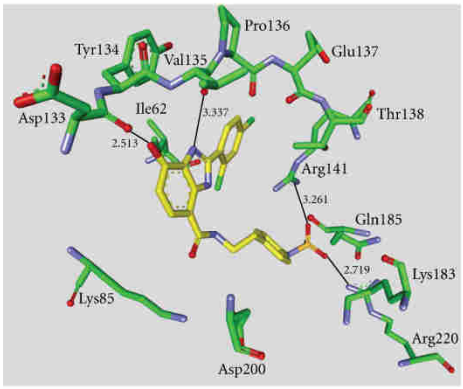

FIGURE 16: Compound **134** in the ATP binding pocket of GSK-3β; important protein-inhibitor interactions are shown. The distance is denoted in Å. PDB code 2O5K [134].

(Table 15(a)). However, compound **134** (GSK-3β IC_{50} = 15 nM) was cocrystallized with GSK-3β (Figure 16) [134].

Herein, the secondary amine interacts with the carbonyl oxygen of Val135 and the phenolic OH of **134** with the carbonyl of Asp133. Two more interactions are established between the SO_2 of compound **134** and the arginines Arg141 and Arg220. The 1-aza-9-oxafluorenes **135–137** are moderately active GSK-3β inhibitors, but showed activity for CDKs (Table 15(a)) [135].

There is no report for an *in vitro* IC_{50} of the synthetic xanthine **propentofylline** (PPF, compound **138**, Table 15(a)), but studies in the Tg mouse model of AD indicated that

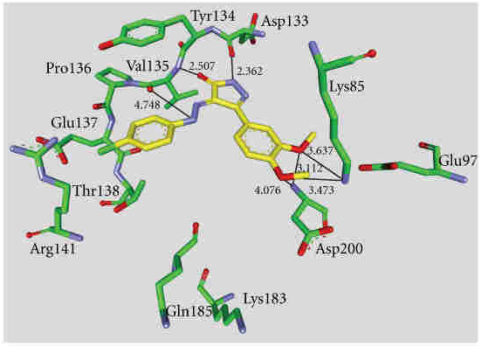

FIGURE 17: Compound **142** in the ATP binding pocket of GSK-3β; important protein-inhibitor interactions are shown. The distance is denoted in Å. PDB code 3L1S [137].

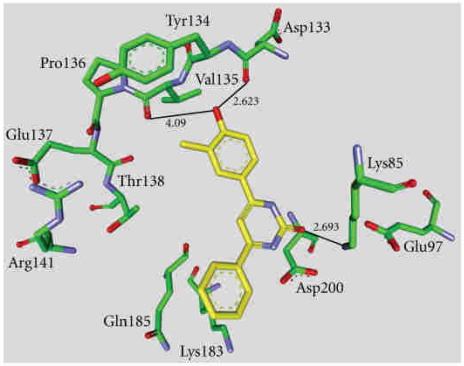

FIGURE 18: The HTS hit named **Compound 1** in the ATP binding pocket of GSK-3β; important protein-inhibitor interactions are shown. The distance is denoted in Å. PDB code 3Q3B [140].

PPF exerts a dual effect: reduction of both pathological amyloidogenesis and tau phosphorylation while reducing the ratio of activated versus inactivated GSK-3β [136].

The pyrazolone **139** was identified as potential scaffold in a compound screen for novel GSK-3 inhibitors. Derivatisation has increased the potency of the derivatives (K_i from 1.49 mM to 0.8 nM (Table 15(b)). The compounds **140**, **141**, and **143** showed selectivity in a kinase panel of 14 kinases. A cocrystallization was realized with compound **142** (Figure 17) and provided the interactions of the pyrazole moiety with the GSK-3 backbone aminoacids Asp133 and Val135. In addition, the methoxy substituents make hydrogen-bonding contacts with both Asp200 and Lys85. These interactions and the hydrophobic contacts of the phenyl rings are thought to be responsible for the potency and selectivity [137]. A recent docking study of the pyrazolone **144** confirmed the interactions of compound **142** with GSK-3β. It is an active (IC_{50} of 34 nM) and selective (kinase panel of 40 kinases) structural analogue to the previously described maleimides **9–27** (Tables 2 and 3). Furthermore, compound **144** was evaluated in a model of oxidative stress induced by homocysteic acid and displayed full neuroprotective activity at 1 μM. Additionally, it was able to reduce locomotor activity in the chlordiazepoxide/amphetamine-induced hyperactivity model *in vivo* [138]. The compounds **145–147** are moderate GSK-3 inhibitors and were not tested against other kinases to evaluate their selectivity (Table 15(b)). Compound **145** increased the glycogen content in the liver of Sprague-Dawley rats in a dose-dependent manner [139].

Compound 1 is a HTS hit, which was cocrystallized with GSK-3β and solved by X-ray crystallography (Figure 18). The overlap of the inhibitor **Compound 1** with a pyridone derivative revealed interactions with the catalytic triad, especially Lys85, and the protein backbone aminoacid Val135 of GSK-3β [140]. This leads to the latest ATP competitive GSK-3 inhibitors, the pyridones **148–150** (Table 15(b)). Compound **150** revealed potent *in vitro* inhibition with an IC_{50} of 16.1 nM against GSK-3β. It was selective in a broad panel of kinases, including CK2 and CLK1. Compared to compound **148**, compound **150** exhibited an improved *in vitro* human liver microsome intrinsic clearance value of 16.3 mL/min/kg. The *in vivo* CNS penetration assay demonstrated a good free brain to free plasma ratio and the assessment of potential genetic toxicology hazards was negative for compound **150** [140]. Last but not least, there were several GSK-3 inhibitors isolated from marine organisms. These alkaloids have the potential to provide new scaffolds comparable to the established indirubines. Manzamines, meridianins, hymenialdisine and dibromocantharelline inhibit GSK-3β in the μM range and display promising selectivity and *in vivo* results (Table 15(c); compounds **151–154**) [141–144].

3. Activity and Selectivity Profiling

A plethora of GSK-3 inhibitors was discovered in recent years, and most of these displayed good-to-excellent inhibition of this kinase. However, selectivity and safety against other kinases remains to be a challenge. The structural analysis of the ATP competitive inhibitors may guide the development of more selective GSK-3 inhibitors. All ATP competitive inhibitors establish hydrogen bonds with the backbone atoms of Asp133 and Val135. Contact to these aminoacids is a key to enhance affinity to GSK-3, but it does not provide selectivity over other kinases. Moreover, Pro136 appears in several complexes to strengthen the interaction of the inhibitor with the backbone (Figure 19). One region of GSK-3 may offer privileged access to enhanced activity and selectivity: it is the region characterized by the aminoacids Lys85, Glu97, and Asp200. Lys85 was observed to form a salt-bridge with Glu97 and simultaneously with Asp200, which is expected to be less significant and potent as the one with Glu97 [145]. The interaction of an inhibitor with this region holds potential to increase activity and selectivity for GSK-3. This interaction can be mediated via water molecules, as

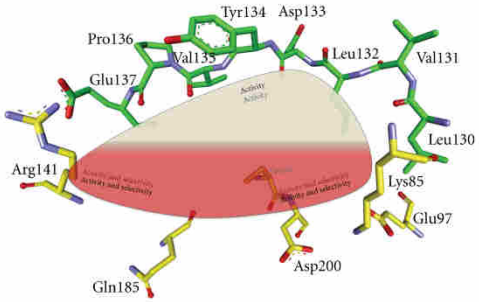

FIGURE 19: Schematic view in the ATP binding pocket of GSK-3β; important areas for activity and selectivity are denoted by PDB code 1I09 [146].

observed for **AR-A014418** (**130**), or be established by direct contact. We observed in our dataset that a direct interaction with this region may cause a loss of selectivity (data not shown). There is a salt-bridge formed by Glu137 and Arg141 in the entrance area of the ATP pocket of GSK-3β. This region seems to contribute to the activity and selectivity of several inhibitors.

Another important interaction between GSK-3 and an organometallic inhibitor was reported by Bregman et al. They observed a water-mediated contact between the carbonyl ligand of the inhibitor and the carboxylate of Gln185 [59]. This water molecule was also found in other GSK-3β inhibitor complexes and seems to be responsible for an increased activity and especially for an improved selectivity towards GSK-3.

Docking studies with our inhibitors confirmed this interaction and further explained the selectivity of these inhibitors (data not shown). Feng et al. observed that the ruthenium-coordinated CO ligand of their inhibitor interacts with the flexible glycine-rich loop formed by Ile62, Gly63, Phe67, and Val70. This pocket, which is not shown in Figure 18, seems to be crucial for potency and selectivity [22]. Figure 18 illustrates in a simple scheme how to enhance activity and selectivity of inhibitors. The interaction with at least two of the three areas deems necessary to provide active and selective inhibitors.

4. Examples of *In Vivo* Tests

Over the last decade, several animal models have been developed to study tauopathies and other neurodegenerative disorders *in vivo*. Despite some obvious advantages of the diverse AD invertebrate systems, the vertebrate animal models of AD are generally favoured (for detailed invertebrate reviews, see [147–149]). Vertebrate models are evolutionary and morphologically closer related to humans, which makes the direct translation of experimental results easier and more reliable. A conditionally GSK-3β overexpressing mouse was reported by Lucas et al. in 2001. They demonstrated that GSK-3β overexpressed *in vivo* results in neurodegeneration and proposed that these mice can be used to study some aspects of AD [150]. In 2005, Perez et al. and Ribe et al. developed and characterized a double-transgenic mouse line based on overexpression of human mutant APP and tau [151, 152]. They treated this transgenic mouse model with **NP12**, a non-ATP competitive GSK-3β inhibitor, and observed lower levels of tau phosphorylation, decreased amyloid deposition and prevention of memory deficits [18]. The APP-V7171 $\times$ Tau-P301L mice with combined amyloid and tau pathology and the GSK-3β $\times$ Tau-P301L mice with tauopathy only were reported by Terwel et al. in 2008. These models offer the possibility to explore molecular signals that act upstream and downstream of, or in parallel with GSK-3 isozymes [153]. Two transgenic mice models were developed to study the interaction between APP or Aβ and tau: the triple-transgenic model (3 $\times$ Tg-AD) harboring $PS1_{M146V}$, APP_{Swe} and tau_{P301L} transgenes and the TAPP mice [154, 155].

The transgenic mice have been the major species used for modelling AD and frontotemporal dementia (FTD). JNPL3 mice are well-characterized transgenic mice that express human 4R0N tau with a FTDP-17 (P301L) mutation [156]. In particular, the levels of sarkosyl insoluble tau in JNPL3 mice increase in an age-dependent manner and comigrate with insoluble tau from AD and FTDP-17 brains. Thus, treatment with GSK-3 inhibitors should result in a significant reduction of sarkosyl insoluble tau, see, for example, compound **78** [86, 132]. Besides JNPL3 mice, the transgenic zebrafish larvae have advanced as an AD model system. It combines many of the advantages of invertebrate and vertebrate models. The latest model is a Gal4/UAS-based vector system that efficiently generates transgenic zebrafish overexpressing high levels of human Tau-P301L or other disease-associated proteins. This tau-transgenic fish model could be an effective *in vivo* screening tool to identify quickly promising GSK-3 inhibitors and eliminate compounds without reasonable *in vivo* activity early in the screening process [157, 158].

GSK-3 inhibitors have also specific effects on early wild-type zebrafish development when treatment occurs between 4 and 24 hpf. Thus this animal model can be used to test the efficacy of GSK-3 inhibitors *in vivo* [133, 157]. Furthermore, there are two *in vivo* model systems with transiently induced tau hyperphosphorylation that were used to evaluate the activity of GSK-3 inhibitors. One of them is the cold-water stress (CWS) model, which causes a rapid and reversible enhancement of tau phosphorylation in the mouse brain at several GSK-3β directed sites such as pSer199, pThr205, pThr231, and pSer396 [125, 159]. The CWS-model proves the significant reduction of tau phosphorylation in **LiCl**- or compound **78**-treated mice [86, 160]. The *in vivo* activities of several other GSK-3 inhibitors (e.g., compound **55** and **96**) were demonstrated in the postnatal rat model [34]. This *in vivo* model takes advantage of the well-characterized GSK-3β expression level in the early and later life cycle of rats [161, 162].

5. Compounds in Preclinical and Clinical Trials

Currently, several GSK-3 inhibitors pass through preclinical or clinical trials. Subsequently GSK-3 inhibitors are listed with the therapeutic indication of AD. These examples are taken from the database of PharmaProjects by searching for the criteria GSK-3 and Alzheimer (March 2010), the MEDD report of GESENT (May 2009) and ClinicalTrials.gov (August 2011).

The Wayne State University is currently in phase IV with **lithium carbonate** against bipolar disorder whereas the University of Sao Paulo is in phase II with **lithium carbonate** against GSK-3 for AD and cognitive impairment. **Lithium** against AD was submitted by the National Institute of Neurological Disorder and Stroke and is in phase II, but there was no update since March 2008. Two compounds from Noscira, **NP-12** (TDZD) and **NP-103**, are in the pre-/clinical trials. **NP-12** (**NP031112**, **tideglusib**) is currently in a phase IIb clinical trial for AD. At the moment, **NP-103** and **CG-301338** from CrystalGenomics and an GSK-3β inhibitor from Takeda are in preclinical trials. The development status of **XD-4241** from Cambrex, **SB-415286** from GlaxoSmith-Kline, a GSK-3β inhibitor from Amphora, **SAR-502250** from Sanofi-Aventis, **CEP-16805** from Cephalon, and an GSK-3β inhibitor from Lundbeck are not reported. The failure or progress of these compounds into preclinical and clinical trials will stimulate or discourage further research.

6. Summary

The moderate inhibition of GSK-3 by selective inhibitors with excellent pharmacokinetic properties and excellent blood-brain barrier permeation holds high potential for the treatment of AD. The failure of the first potent GSK-3 inhibitor by Astra-Zeneca indicates the complexity of this target and the therapeutic window of GSK-3 inhibition in adult mammals. Information on the failure is rather limited, it may be due to potential toxicity of the chemical scaffold: P450-mediated metabolism of thiazoles has resulted in hepatotoxicity and thus failure of phase III candidates previously.

Biological characterization has advanced GSK-3 as a potential drug target, and the inhibition of this protein kinase by small molecules resulted in significant inhibition of tau phosphorylation. We have described a wide range of molecules that inhibit GSK-3 and discussed their properties. We focused on several inhibitors interacting with the ATP binding pocket of GSK-3β. The water molecule interactions are not incorporated in the figures; however, they may play a crucial role in the hydrogen bond network between the inhibitor and the aminoacids. The aminoacids, which are responsible for strong interaction with the enzyme, have been identified. Noteworthy are Asp133, Val135, Glu137, Arg141, Gln185, Asp200, and Arg220, which constitute important aminoacids for interactions with the binding pocket of GSK-3. The conserved salt bridge Lys85/Glu97 materializes as an interesting interaction partner. We summarized crucial biological findings and provided an overview on the *in vivo* effects of some inhibitors. Additional *in vivo* assays can be retrieved via the references denoted in the tables next to the structures. We summarized the GSK-3 inhibitors, which are in pre-/clinical trials with the therapeutic indication of AD. Yet, a review will be biased, and we request your pardon or input, if your favourite inhibitor or *in vivo* studies are not adequately referred to.

7. Outlook

GSK-3 is an intriguing enzyme, which plays important roles in the pathogenesis of several diseases, for example, diabetes, cancer, and AD. The literature is immense and quite often provides conflicting statements and observations for this kinase. For example, a few studies observed that Pin1 (peptidyl-prolyl cis-trans isomerase) knockout mice display tau hyperphosphorylation and that this enzyme might have an inhibitive role in phosphorylating tau and GSK-3β, thus protecting against AD [163]. Whereas another study ascertained that the GSK-3 inhibitor **BIO** (compound **39**) may be useful in regenerative medicine, by reversibly maintaining human embryonic stem cells in an undifferentiated state [164]. A plethora of GSK-3 inhibitors has been published since it has been linked to AD. Naturally, the vast majority thereof was reported by pharmaceutical companies. Many potent inhibitors with good selectivity have been disclosed so far. The challenge of medicinal chemists will be to develop inhibitors, which translate their potent enzymatic inhibition into cellular settings and finally humans, who will tolerate a moderate GSK-3 inhibition only. A mild GSK-3 inhibition (~35%) is needed because such an inhibition level provides sufficient insulin sensitization without elevation of β-catenin levels. Thus a moderate inhibition minimizes significant mechanism-based toxicities, ranging from hypoglycemia to tumorigenesis [165, 166]. A further indication of a moderate GSK-3 inhibition is the application of lithium for the treatment of bipolar disorder. The GSK-3 inhibitor lithium is estimated to inhibit approximately 25% of total GSK-3 activity. It was used for the treatment of bipolar disorder since the 1950s without association of hypoglycemia, increased levels of tumorigenesis, or deaths from cancer [167]. Nevertheless, the established *in vivo* studies have to be accompanied by the investigation of pleiotropic activity and the determination of a safe therapeutic window for chronic GSK-3 inhibition in humans. The X-ray analysis of cocrystallized structures revealed how the inhibitors interact with the ATP-binding pocket and provide information about essential interaction partners to improve potency and selectivity. The comparison of the IC_{50} values will be much easier, if only one stringent GSK-3 *in vitro* assay would be utilized, which employs a defined final ATP and inhibitor concentration as well as a standardized incubation time. Currently, Alon et al. determined that GSK-3β is responsible for the phosphorylation of the embryonic tau isoforms in birds, which harbors the GSK-3β gene only. In consideration of their and former studies, Alon et al. assume that GSK-3α and β have distinct roles in phosphorylating tau in adult and embryonic brain in nonvertebrates. Furthermore, they raise the hypothesis that specific inhibition of GSK-3α may be useful for therapeutic intervention in AD [168]. This supposition is enhanced by

former siRNA experiments [169]. But all GSK-3 inhibitors developed until now inhibit the two isoforms of GSK-3 equipotently, except Λ-**OS1** (**36**) (~7 fold more selective for GSK-3α). Still most of the GSK-3 inhibitors fail in model animals despite of their good inhibitory activity in cell free assays. This is frequently due to the lack of selectivity, insufficient cell permeation, and poor blood-brain barrier permeability. Appropriate animal models were developed in transparent zebrafish to study preclinical efficacy, metabolic stability and toxicity, but their potential is not fully exploited. These *in vivo* tests are fast (3 days), relatively inexpensive and suitable for larger screening efforts in 96-well format. Furthermore, it has been observed that resistance arises during the therapy. The problem is that most of the kinase inhibitors are ATP competitive type I inhibitors. A new generation of type II inhibitors, which binds to the ATP site and extends into an allosteric site, may provide a solution [15, 170, 171]. Such novel type II inhibitors must be active, selective and permeate the human blood-brain barrier, which bears further limitations for drug development. However, several pharmaceutical companies continue to develop ATP competitive GSK-3 inhibitors [172, 173]. Just a few pharmaceutical companies have started pre-/clinical trials addressing the druggability of GSK-3 inhibition. Noscira launched the phase IIb trial ARGO of **Tideglusib** (**NP-12**) to treat mild-to-moderate AD patients in April 2011. The trial period will be 65 weeks with 2 dosage regimes of **Tideglusib** (500 and 1000 mg/day oral suspension, ClinicalTrials.gov identifier: NCT01350362). The ongoing clinical trials may lead to a paradigm shift, if the GSK-3 inhibitors display efficacy and safety.

Abbreviations

Å: Angstrom
AD: Alzheimer's disease
ApoE: Apolipoprotein E
APP: Amyloid precursor protein
Arg: Arginine
Asp: Aspartic acid
ATP: Adenosine triphosphate
Aβ: β-Amyloid
BBB: Blood-brain barrier
CDK: Cyclin-dependent kinase
CK2: Casein kinase 2
CLK1: Dual specificity protein kinase 1
CWS: Cold-water stress
Cys: Cysteine
DMSO: Dimethyl sulfoxide
DYRK1A: Dual specificity tyrosine phosphorylation-regulated kinase 1A
EC50: Half maximal effective concentration
ERK: Extracellular signal-regulated kinase
FAD: Familial Alzheimer's disease
FTD: Frontotemporal dementia
GESENT: Gesellschaft für experimentelle und klinische Neurotherapeutika
Gln: Glutamine
Glu: Glutamic acid
Gly: Glycine
GS: Glycogen synthase
GSK-3: Glycogen synthase kinase 3
h: hour
HMK: Halomethylketone
i.v.: Intravenous
IC50: Half maximal inhibitory concentration
Ile: Isoleucine
JNK: c-Jun N-terminal kinase
kDa: kilodalton
KDR: Kinase insert domain receptor
kg: kilogram
K_i: Dissociation constant for the inhibitor
Leu: Leucine
LiCl: Lithium chloride
Lys: Lysine
MED-D: Medikamentenentwicklung für Demenzen in Deutschland
mg: milligram
MSK1: Mitogen- and stress-activated protein kinase
MTS: 3-(4,5-dimethylthiazol-2-yl)-5-(3-carboxy-methoxyphenyl)-2-(4-sulfophenyl)-2*H*-tetrazolium
μM: micromolar
NFTs: Neurofibrillary tangles
nM: nanomolar
PDB: Protein Data Bank
Phe: Phenylalanine
PHFs: Paired helical filaments
Pim-1: Proto-oncogene serine/threonine-Protein kinase
Pin1: Peptidyl-prolyl cis-trans isomerase
PKCβII: Protein kinase C βII
PPF: Propentofylline
Pro: Proline
PS-1/2: Presenilin-1/2
pSer: phosphorylated Serine
pThr: phosphorylated Threonine
RSK1: Ribosomal protein S6 kinase alpha-1, also known as RPS6KA1
s.c.: Subcutane
SAD: Sporadic Alzheimer's disease
Ser: Serine
Src: Proto-oncogene tyrosine-protein kinase
TDZD: Thiadiazolidine
Thr: Threonine
Tyr: Tyrosine
Val: Valine
VEGFR: Vascular endothelial growth factor receptor
WHO: World health organization
Wnt: Signaling pathway
X-ray: X-radiation.

References

[1] L. K. Chico, L. J. van Eldik, and D. M. Watterson, "Targeting protein kinases in central nervous system disorders," *Nature Reviews Drug Discovery*, vol. 8, no. 11, pp. 892–909, 2009.
[2] D. Bossemeyer, "Protein kinases—structure and function," *The FEBS Letters*, vol. 369, no. 1, pp. 57–61, 1995.

[3] C. Peifer and D. R. Alessi, "Small-molecule inhibitors of PDK1," *ChemMedChem*, vol. 3, no. 12, pp. 1810–1838, 2008.

[4] C. Hooper, R. Killick, and S. Lovestone, "The GSK3 hypothesis of Alzheimer's disease," *Journal of Neurochemistry*, vol. 104, no. 6, pp. 1433–1439, 2008.

[5] I. Ferrer, T. Gomez-Isla, B. Puig et al., "Current advances on different kinases involved in tau phosphorylation, and implications in Alzheimer's disease and tauopathies," *Current Alzheimer Research*, vol. 2, no. 1, pp. 3–18, 2005.

[6] F. Hernandez, E. Gomez de Barreda, A. Fuster-Matanzo, J. J. Lucas, and J. Avila, "GSK3: a possible link between beta amyloid peptide and tau protein," *Experimental Neurology*, vol. 223, no. 2, pp. 322–325, 2010.

[7] A. Leroy, I. Landrieu, I. Huvent et al., "Spectroscopic studies of GSKβ phosphorylation of the neuronal tau protein and its interaction with the N-terminal domain of apolipoprotein E," *The Journal of Biological Chemistry*, vol. 285, no. 43, pp. 33435–33444, 2010.

[8] A. Martinez, A. Castro, I. Dorronsoro, and M. Alonso, "Glycogen synthase kinase-3 (GSK-3) inhibitors as new promising drugs for diabetes, neurodegeneration, cancer, and inflammation," *Medicinal Research Reviews*, vol. 22, no. 4, pp. 373–384, 2002.

[9] H. Eldar-Finkelman, "Glycogen synthase kinase-3: an emerging therapeutic target," *Trends in Molecular Medicine*, vol. 8, no. 3, pp. 126–132, 2002.

[10] S. Frame and P. Cohen, "GSK3 takes centre stage more than 20 years after its discovery," *Biochemical Journal*, vol. 359, no. 1, pp. 1–16, 2001.

[11] A. Alzheimer, "Über eine eigenartige Erkrankung der Hirnrinde," *Allgemeine Zeitschrift für Psychiatrie und psychisch-gerichtiliche Medizin*, vol. 64, pp. 146–148, 1907.

[12] R. A. Stelzmann, H. N. Schnitzlein, and F. R. Murtagh, "An English translation of Alzheimer's 1907 paper, 'uber eine eigenartige erkankung der hirnrinde'," *Clinical Anatomy*, vol. 8, no. 6, pp. 429–431, 1995.

[13] D. Dickson, Weller R. O. et al., *Neurodegeneration: The Molecular Pathology of Dementia and Movement Disorders*, Wiley-Blackwell, 2nd edition, 2011.

[14] C. Duyckaerts, B. Delatour, and M. C. Potier, "Classification and basic pathology of Alzheimer disease," *Acta Neuropathologica*, vol. 118, no. 1, pp. 5–36, 2009.

[15] M. P. Mazanetz and P. M. Fischer, "Untangling tau hyperphosphorylation in drug design for neurodegenerative diseases," *Nature Reviews Drug Discovery*, vol. 6, no. 6, pp. 464–479, 2007.

[16] F. Hernández and J. Avila, "The role of glycogen synthase kinase-3 in the early stages of Alzheimers' disease," *The FEBS Letters*, vol. 582, no. 28, pp. 3848–3854, 2008.

[17] P. Cohen and M. Goedert, "GSK3 inhibitors: development and therapeutic potential," *Nature Reviews Drug Discovery*, vol. 3, no. 6, pp. 479–487, 2004.

[18] L. Sereno, M. Coma, M. Rodriguez et al., "A novel GSK-3β inhibitor reduces Alzheimer's pathology and rescues neuronal loss *in vivo*," *Neurobiology of Disease*, vol. 35, no. 3, pp. 359–367, 2009.

[19] A. Takashima, "Drug development targeting the glycogen synthase kinase-β(GSK- 3β)-mediated signal transduction pathway: role of GSK-β in adult brain," *Journal of Pharmacological Sciences*, vol. 109, no. 2, pp. 174–178, 2009.

[20] K. Spittaels, C. van den Haute, J. van Dorpe et al., "Glycogen synthase kinase-β phosphorylates protein tau and rescues the axonopathy in the central nervous system of human four-repeat tau transgenic mice," *The Journal of Biological Chemistry*, vol. 275, no. 52, pp. 41340–41349, 2000.

[21] R. V. Bhat, S. L. Budd Haeberlein, and J. Avila, "Glycogen synthase kinase-3: a drug target for CNS therapies," *Journal of Neurochemistry*, vol. 89, no. 6, pp. 1313–1317, 2004.

[22] L. Feng, Y. Geisselbrecht, S. Blanck et al., "Structurally sophisticated octahedral metal complexes as highly selective protein kinase inhibitors," *Journal of the American Chemical Society*, vol. 133, no. 15, pp. 5976–5986, 2011.

[23] H. Eldar-Finkelman, A. Licht-Murava, S. Pietrokovski, and M. Eisenstein, "Substrate competitive GSK-3 Inhibitors—strategy and Implications," *Biochimica et Biophysica Acta*, vol. 1804, no. 3, pp. 598–603, 2010.

[24] A. Martinez, M. Alonso, A. Castro, C. Perez, and F. J. Moreno, "First non-ATP competitive glycogen synthase kinase-3β (GSK-β) inhibitors: thiadiazolidinones (TDZD) as potential drugs for the treatment of Alzheimer's disease," *Journal of Medicinal Chemistry*, vol. 45, no. 6, pp. 1292–1299, 2002.

[25] A. Martinez, "Preclinical efficacy on GSK-3 inhibitors: towards a future generation of powerful drugs," *Medicinal Research Reviews*, vol. 28, no. 5, pp. 773–796, 2008.

[26] A. Mora, G. Sabio, R. A. Gonzalez-Polo et al., "Lithium inhibits caspase 3 activation and dephosphorylation of PKB and GSK3 induced by K^+ deprivation in cerebellar granule cells," *Journal of Neurochemistry*, vol. 78, no. 1, pp. 199–206, 2001.

[27] W. J. Ryves and A. J. Harwood, "Lithium inhibits glycogen synthase kinase-3 by competition for magnesium," *Biochemical and Biophysical Research Communications*, vol. 280, no. 3, pp. 720–725, 2001.

[28] B. Bax, P. S. Carter, C. Lewis et al., "The structure of phosphorylated GSK-β complexed with a peptide, FRATtide, that inhibits β-catenin phosphorylation," *Structure*, vol. 9, no. 12, pp. 1143–1152, 2001.

[29] J. M. Domínguez, A. Fuertes, L. Orozco, M. del Monte-Millán, E. Delgado, and M. Medina, "Evidence for the irreversible inhibition of glycogen synthase kinas-3β by tideglusib," *The Journal of Biological Chemistry*, vol. 287, pp. 893–904, 2012.

[30] D. G. Smith, M. Buffet, A. E. Fenwick et al., "3-Anilino-4-arylmaleimides: potent and selective inhibitors of glycogen synthase kinase-3 (GSK-3)," *Bioorganic and Medicinal Chemistry Letters*, vol. 11, no. 5, pp. 635–639, 2001.

[31] J. A. Bertrand, S. Thieffine, A. Vulpetti et al., "Structural characterization of the GSK-β active site using selective and non-selective ATP-mimetic inhibitors," *Journal of Molecular Biology*, vol. 333, no. 2, pp. 393–407, 2003.

[32] M. P. Coghlan, A. A. Culbert, D. A. E. Cross et al., "Selective small molecule inhibitors of glycogen synthase kinase-3 modulate glycogen metabolism and gene transcription," *Chemistry and Biology*, vol. 7, no. 10, pp. 793–803, 2000.

[33] D. A. E. Cross, A. A. Culbert, K. A. Chalmers, L. Facci, S. D. Skaper, and A. D. Reith, "Selective small-molecule inhibitors of glycogen synthase kinase-3 activity protect primary neurones from death," *Journal of Neurochemistry*, vol. 77, no. 1, pp. 94–102, 2001.

[34] M. L. Selenica, H. S. Jensen, A. K. Larsen et al., "Efficacy of small-molecule glycogen synthase kinase-3 inhibitors in the postnatal rat model of tau hyperphosphorylation," *British Journal of Pharmacology*, vol. 152, no. 6, pp. 959–979, 2007.

[35] D. J. O'Neill, L. Shen, C. Prouty et al., "Design, synthesis, and biological evaluation of novel 7-azaindolyl-heteroaryl-maleimides as potent and selective glycogen synthase kinase-β

(GSK-β) inhibitors," *Bioorganic and Medicinal Chemistry*, vol. 12, no. 12, pp. 3167–3185, 2004.

[36] H. C. Zhang, H. Ye, B. R. Conway et al., "3-(7-Azaindolyl)-4-arylmaleimides as potent, selective inhibitors of glycogen synthase kinase-3," *Bioorganic and Medicinal Chemistry Letters*, vol. 14, no. 12, pp. 3245–3250, 2004.

[37] T. A. Engler, J. R. Henry, S. Malhotra et al., "Substituted 3-imidazo[1,2-a]pyridin-3-yl-4-(1,2,3,4-tetrahydro-[1,4] diazepino-[6,7,1-hi]indol-7-yl)pyrrole-2,5-diones as highly selective and potent inhibitors of glycogen synthase kinase-3," *Journal of Medicinal Chemistry*, vol. 47, no. 16, pp. 3934–3937, 2004.

[38] T. A. Engler, S. Malhotra, T. P. Burkholder et al., "The development of potent and selective bisarylmaleimide GSK3 inhibitors," *Bioorganic and Medicinal Chemistry Letters*, vol. 15, no. 4, pp. 899–903, 2005.

[39] Q. Ye, G. Xu, D. Lv, Z. Cheng, J. Li, and Y. Hu, "Synthesis and biological evaluation of novel 4-azaindolyl-indolyl-maleimides as glycogen synthase kinase-β (GSK-β) inhibitors," *Bioorganic and Medicinal Chemistry*, vol. 17, no. 13, pp. 4302–4312, 2009.

[40] L. Gong, D. Hirschfeld, Y. C. Tan et al., "Discovery of potent and bioavailable GSK-β inhibitors," *Bioorganic and Medicinal Chemistry Letters*, vol. 20, no. 5, pp. 1693–1696, 2010.

[41] D. I. Perez, V. Palomo, C. Perez et al., "Switching reversibility to irreversibility in glycogen synthase kinase-3 inhibitors: clues for specific design of new compounds," *Journal of Medicinal Chemistry*, vol. 54, no. 12, pp. 4042–4056, 2011.

[42] I. Hers, J. M. Tavare, and R. M. Denton, "The protein kinase C inhibitors bisindolylmaleimide I (GF 109203x) and IX (Ro 31-8220) are potent inhibitors of glycogen synthase kinase-3 activity," *The FEBS Letters*, vol. 460, no. 3, pp. 433–436, 1999.

[43] G. H. Kuo, C. Prouty, A. de Angelis et al., "Synthesis and discovery of macrocyclic polyoxygenated bis-7-azaindolylmaleimides as a novel series of potent and highly selective glycogen synthase kinase-β inhibitors," *Journal of Medicinal Chemistry*, vol. 46, no. 19, pp. 4021–4031, 2003.

[44] H. C. Zhang, K. B. White, H. Ye et al., "Macrocyclic bisindolylmaleimides as inhibitors of protein kinase C and glycogen synthase kinase-3," *Bioorganic and Medicinal Chemistry Letters*, vol. 13, no. 18, pp. 3049–3053, 2003.

[45] L. Shen, C. Prouty, B. R. Conway et al., "Synthesis and biological evaluation of novel macrocyclic bis-7-azaindolylmaleimides as potent and highly selective glycogen synthase kinase-β (GSK-β) inhibitors," *Bioorganic and Medicinal Chemistry*, vol. 12, no. 5, pp. 1239–1255, 2004.

[46] H. C. Zhang, L. V. R. Bonaga, H. Ye, C. K. Derian, B. P. Damiano, and B. E. Maryanoff, "Novel bis(indolyl)maleimide pyridinophanes that are potent, selective inhibitors of glycogen synthase kinase-3," *Bioorganic and Medicinal Chemistry Letters*, vol. 17, no. 10, pp. 2863–2868, 2007.

[47] A. P. Kozikowski, I. N. Gaisina, H. Yuan et al., "Structure-based design leads to the identification of lithium mimetics that block mania-like effects in rodents. Possible new GSK-β therapies for bipolar disorders," *Journal of the American Chemical Society*, vol. 129, no. 26, pp. 8328–8332, 2007.

[48] I. N. Gaisina, F. Gallier, A. V. Ougolkov et al., "From a natural product lead to the identification of potent and selective benzofuran-3-yl-(indol-3-yl)maleimides as glycogen synthase kinase-β inhibitors that suppress proliferation and survival of pancreatic cancer cells," *Journal of Medicinal Chemistry*, vol. 52, no. 7, pp. 1853–1863, 2009.

[49] H. Zhong, H. Zou, M. V. Semenov et al., "Characterization and development of novel small-molecules inhibiting GSK3 and activating Wnt signaling," *Molecular Biosystems*, vol. 5, no. 11, pp. 1356–1360, 2009.

[50] H. Zou, L. Zhou, Y. Li et al., "Benzo[e]isoindole-1,3-diones as potential inhibitors of glycogen synthase kinase-3 (GSK-3). Synthesis, kinase inhibitory activity, zebrafish phenotype, and modeling of binding mode," *Journal of Medicinal Chemistry*, vol. 53, no. 3, pp. 994–1003, 2010.

[51] A. Kozikowski and I. Gaysina, "3-Benzofuranyl-4-indolyl maleimides as potent GSK3 inhibitors for neurogenerative disorders," WO 2008/077138 A1, 2008.

[52] A. Kozikowski and I. Gaysina, "Benzofuran-3-yl(indol-3-yl) maleimides as potent GSK3 inhibitors," US 2010/0004308 A1, 2010.

[53] P. von Matt and J. Wagner, "Indolylmaleimide derivatives," EP 2075249 A2, Novartis AG., 2009.

[54] H. Zhang, B. Maryanoff, and H. Ye, "Substituted indazoly(indoly)maleimide derivatives as kinase inhibitors," US 7439363 B2, Janssen Pharmaceutica N.V., 2008.

[55] H. Zhang, B. Maryanoff, and H. Ye, "Substituted indazolyl (indolyl) maleimide derivatives as kinase inhibitors," EP 1654255 B1, Janssen Pharmaceutica N.V., 2008.

[56] S. Omura, Y. Iwai, A. Hirano et al., "A new alkaloid AM 2282 of Streptomyces origin taxonomy, fermentation, isolation and preliminary characterization," *Journal of Antibiotics*, vol. 30, no. 4, pp. 275–282, 1977.

[57] N. Funato, H. Takayanagi, Y. Konda et al., "Absolute configuration of staurosporine by X-ray analysis," *Tetrahedron Letters*, vol. 35, no. 8, pp. 1251–1254, 1994.

[58] S. Leclerc, M. Garnier, R. Hoessel et al., "Indirubins inhibit glycogen synthase kinase-β and CDK5/P25, two protein kinases involved in abnormal tau phosphorylation in Alzheimer's disease. A property common to most cyclin-dependent kinase inhibitors?" *The Journal of Biological Chemistry*, vol. 276, no. 1, pp. 251–260, 2001.

[59] H. Bregman, D. S. Williams, G. E. Atilla, P. J. Carroll, and E. Meggers, "An organometallic inhibitor for glycogen synthase kinase-3," *Journal of the American Chemical Society*, vol. 126, no. 42, pp. 13594–13595, 2004.

[60] G. E. Atilla-Gokcumen, D. S. Williams, H. Bregman, N. Pagano, and E. Meggers, "Organometallic compounds with biological activity: a very selective and highly potent cellular inhibitor for glycogen synthase kinase-3," *ChemBioChem*, vol. 7, no. 9, pp. 1443–1450, 2006.

[61] G. E. Atilla-Gokcumen, N. Pagano, C. Streu et al., "Extremely tight binding of a ruthenium complex to glycogen synthase kinase-3," *ChemBioChem*, vol. 9, no. 18, pp. 2933–2936, 2008.

[62] G. E. Atilla-Gokcumen, L. di Costanzo, and E. Meggers, "Structure of anticancer ruthenium half-sandwich complex bound to glycogen synthase kinase-3β," *Journal of Biological Inorganic Chemistry*, vol. 16, no. 1, pp. 45–50, 2011.

[63] L. Meijer, A. L. Skaltsounis, P. Magiatis et al., "GSK-3-selective inhibitors derived from Tyrian purple indirubins," *Chemistry and Biology*, vol. 10, no. 12, pp. 1255–1266, 2003.

[64] P. Polychronopoulos, P. Magiatis, A. L. Skaltsounis et al., "Structural basis for the synthesis of indirubins as potent and selective inhibitors of glycogen synthase kinase-3 and cyclin-dependent kinases," *Journal of Medicinal Chemistry*, vol. 47, no. 4, pp. 935–946, 2004.

[65] K. Vougogiannopoulou, Y. Ferandin, K. Bettayeb et al., "Soluble 3′,6-substituted indirubins with enhanced selectivity toward glycogen synthase kinase-3 alter circadian period," *Journal of Medicinal Chemistry*, vol. 51, no. 20, pp. 6421–6431, 2008.

[66] A. Beauchard, H. Laborie, H. Rouillard et al., "Synthesis and kinase inhibitory activity of novel substituted indigoids," *Bioorganic and Medicinal Chemistry*, vol. 17, no. 17, pp. 6257–6263, 2009.

[67] D. Beher, M. Bettai, I. Churcher et al., "1-alkyl-3-thio-substituted indole-2-alkynoic acids useful for the treatment for Alzheimer's disease and related conditions," EP 1708997 B1, Merck and Company, Inc., 2009.

[68] S. Berg, S. Hellberg, M. Nylöf, and Y. Xue, "3-Heterocyclyl-indole inhibitors of glycogen synthase kinase-3," US 7399780 B2, Astra Zeneca AB., 2008.

[69] S. Berg, S. Hellberg, M. Nylöf, and Y. Xue, "2-hydroxy-3-heteroarylindole derivatives as GSK3 inhibitors," EP 1492785 B1, Astra Zeneca AB., 2008.

[70] J. Green, A. Miller, J. Jimenez et al., "Azaindoles useful as inhibitors of rock and other protein kinases," US 7514448 B2, Vertex Pharmaceuticals Inc., 2009.

[71] A. Heckel, G. Roth, J. Kley, S. Hoerer, and I. Uphues, "Novel alkyl-containing 5-acylindolinones, their preparation and their use as pharmaceutical products," WO 2005/087727 A1, Boehringer Ingelheim Pharma GmbH & Company KG., 2005.

[72] A. Heckel, G. Roth, J. Kley, S. Hoerer, and I. Uphues, "Cycloalkyl—containing 5-acylindolinones, the preparation thereof and their use as medicaments," WO 7262206 B2, Boehringer Ingelheim International GmbH., 2007.

[73] A. Heckel, G. Roth, J. Kley, S. Hoerer, and I. Uphues, "Aryl-containing 5-acylindolinones, the preparation thereof and their use as medicaments," US 7176231 B2, Boehringer Ingelheim International GmbH., 2007.

[74] A. Heckel, G. Roth, J. Kley, S. Hoerer, and I. Uphues, "Alkyl-containing 5-acylindolinones, the preparation thereof and their use as medicaments," US 7560480 B2, Boehringer Ingelheim Pharma GmbH & Company KG., 2009.

[75] L. Meijer, P. Greengard, M. Knockaert, and A. Skaltsounis, "Indirubin-type compounds, compositions, and methods for their use," US 2007/0276025 A1, 2007.

[76] M. Leost, C. Schultz, A. Link et al., "Paullones are potent inhibitors of glycogen synthase kinase-β and cyclin-dependent kinase 5/p25," *European Journal of Biochemistry*, vol. 267, no. 19, pp. 5983–5994, 2000.

[77] C. Schultz, A. Link, M. Leost et al., "Paullones, a series of cyclin-dependent kinase inhibitors: synthesis, evaluation of CDK1/cyclin B inhibition, and *in vitro* antitumor activity," *Journal of Medicinal Chemistry*, vol. 42, no. 15, pp. 2909–2919, 1999.

[78] M. Knockaert, K. Wieking, S. Schmitt et al., "Intracellular targets of paullones: identification following affinity purification on immobilized inhibitor," *The Journal of Biological Chemistry*, vol. 277, no. 28, pp. 25493–25501, 2002.

[79] C. Kunick, K. Lauenroth, M. Leost, L. Meijer, and T. Lemcke, "1-Azakenpaullone is a selective inhibitor of glycogen synthase kinase-β," *Bioorganic and Medicinal Chemistry Letters*, vol. 14, no. 2, pp. 413–416, 2004.

[80] C. Kunick, Z. Zeng, R. Gussio et al., "Structure-aided of optimization of kinase inhibitors derived from alsterpaullone," *ChemBioChem*, vol. 6, no. 3, pp. 541–549, 2005.

[81] L. Meijer and C. Kunick, "Use of paullone derivatives for making medicines," WO 2001/060374 A1, 2001.

[82] J. Witherington, V. Bordas, S. L. Garland et al., "5-Aryl-pyrazolo[3,4-b]pyridines: potent inhibitors of glycogen synthase kinase-3 (GSK-3)," *Bioorganic and Medicinal Chemistry Letters*, vol. 13, no. 9, pp. 1577–1580, 2003.

[83] J. Witherington, V. Bordas, D. Haigh et al., "5-Aryl-pyrazolo[3,4-b]pyridazines: potent inhibitors of glycogen synthase kinase-3 (GSK-3)," *Bioorganic and Medicinal Chemistry Letters*, vol. 13, no. 9, pp. 1581–1584, 2003.

[84] J. Witherington, V. Bordas, A. Gaiba et al., "6-Aryl-pyrazolo[3,4-b]pyridines: potent inhibitors of glycogen synthase kinase-3 (GSK-3)," *Bioorganic and Medicinal Chemistry Letters*, vol. 13, no. 18, pp. 3055–3057, 2003.

[85] J. Witherington, V. Bordas, A. Gaiba et al., "6-Heteroaryl-pyrazolo[3,4-b]pyridines: potent and selective inhibitors of glycogen synthase kinase-3 (GSK-3)," *Bioorganic and Medicinal Chemistry Letters*, vol. 13, no. 18, pp. 3059–3062, 2003.

[86] Y. Uno, H. Iwashita, T. Tsukamoto et al., "Efficacy of a novel, orally active GSK-3 inhibitor 6-Methyl-N-[3-[[3-(1-methylethoxy)propyl]carbamoyl]-1H-pyrazol-4-yl]pyridine-3-carboxamide in tau transgenic mice," *Brain Research*, vol. 1296, pp. 148–163, 2009.

[87] K. L. Kees, T. J. Caggiano, K. E. Steiner et al., "Studies on new acidic azoles as glucose-lowering agents in obese, diabetic db/db mice," *Journal of Medicinal Chemistry*, vol. 38, no. 4, pp. 617–628, 1995.

[88] K. L. Kees, J. J. Fitzgerald Jr., K. E. Steiner et al., "New potent antihyperglycemic agents in db/db mice: synthesis and structure-activity relationship studies of (4-substituted benzyl)(trifluoromethyl)pyrazoles and -pyrazolones," *Journal of Medicinal Chemistry*, vol. 39, no. 20, pp. 3920–3928, 1996.

[89] G. R. Bebernitz, G. Argentieri, B. Battle et al., "The effect of 1,3-diaryl-[1H]-pyrazole-4-acetamides on glucose utilization in ob/ob mice," *Journal of Medicinal Chemistry*, vol. 44, no. 16, pp. 2601–2611, 2001.

[90] D. M. Shen, E. J. Brady, M. R. Candelore et al., "Discovery of novel, potent, selective, and orally active human glucagon receptor antagonists containing a pyrazole core," *Bioorganic and Medicinal Chemistry Letters*, vol. 21, no. 1, pp. 76–81, 2011.

[91] A. J. Peat, D. Garrido, J. A. Boucheron et al., "Novel GSK-3 inhibitors with improved cellular activity," *Bioorganic and Medicinal Chemistry Letters*, vol. 14, no. 9, pp. 2127–2130, 2004.

[92] C. Lum, J. Kahl, L. Kessler et al., "2,5-Diaminopyrimidines and 3,5-disubstituted azapurines as inhibitors of glycogen synthase kinase-3 (GSK-3)," *Bioorganic and Medicinal Chemistry Letters*, vol. 18, no. 12, pp. 3578–3581, 2008.

[93] A. M. Aronov, T. Qing, G. Martinez-Botella et al., "Structure-guided design of potent and selective pyrimidylpyrrole inhibitors of extracellular signal-regulated kinase (ERK) using conformational control," *Journal of Medicinal Chemistry*, vol. 52, no. 20, pp. 6362–6368, 2009.

[94] D. B. Ring, K. W. Johnson, E. J. Henriksen et al., "Selective glycogen synthase kinase-3 inhibitors potentiate insulin activation of glucose transport and utilization *in vitro* and *in vivo*," *Diabetes*, vol. 52, no. 3, pp. 588–595, 2003.

[95] Y. Maeda, M. Nakano, H. Sato et al., "4-Acylamino-6-arylfuro[2,3-d]pyrimidines: potent and selective glycogen synthase kinase-3 inhibitors," *Bioorganic and Medicinal Chemistry Letters*, vol. 14, no. 15, pp. 3907–3911, 2004.

[96] Y. Miyazaki, Y. Maeda, H. Sato, M. Nakano, and G. W. Mellor, "Rational design of 4-amino-5,6-diaryl-furo[2,3-d]pyrimidines as potent glycogen synthase kinase-3 inhibitors," *Bioorganic and Medicinal Chemistry Letters*, vol. 18, no. 6, pp. 1967–1971, 2008.

[97] D. Bebbington, Binch H., R. Knegtel et al., "Pyrazole compounds useful as protein kinase inhibitors," US 6660731 B2, Vertex Pharmaceuticals Inc., 2003.

[98] D. Bebbington, H. Binch, R. Knegtel et al., "Fused pyrimidyl pyrazole compounds useful as protein kinase inhibitors," US 7008948 B2, Vertex Pharmaceuticals Inc., 2006.

[99] D. Bebbington and J. Charrier, "Pyrazole compounds useful as protein kinase inhibitors," US 6656939 B2, Vertex Pharmaceuticals Inc., 2003.

[100] D. Bebbington, J. Charrier, R. Davies et al., "Pyrazole compounds useful as protein kinase inhibitors," US 6989385 B2, Vertex Pharmaceuticals Inc., 2006.

[101] D. Bebbington, J. Charrier, R. Davies et al., "Pyrazole compounds useful as protein kinase inhibitors," WO 2002/059111 A2, Vertex Pharmaceuticals Inc., 2002.

[102] D. Bebbington, J. Charrier, R. Davies et al., "Pyrazole compounds useful as protein kinase inhibitors," US 6653301 B2, Vertex Pharmaceuticals Inc., 2003.

[103] D. Bebbington, J. Charrier, J. Golec, A. Miller, and R. Knegtel, "Pyrazole compounds useful as protein kinase inhibitors," WO 2002/057259 A2, Vertex Pharmaceuticals Inc., 2002.

[104] D. Bebbington, J. Charrier, J. Golec, A. Miller, and R. Knegtel, "Pyrazole compounds useful as protein kinase inhibitors," US 6664247 B2, Vertex Pharmaceuticals Inc., 2003.

[105] D. Bebbington, J. Charrier, J. Golec, and F. Pierard, "Pyrazole compounds useful as protein kinase inhibitors," US 6727251 B2, Vertex Pharmaceuticals Inc., 2004.

[106] D. Bebbington, J. Charrier, J. Golec, and F. Pierard, "Pyrazole compounds useful as protein kinase inhibitors," US 7427681 B2, Vertex Pharmaceuticals Inc., 2008.

[107] R. Davies, D. Bebbington, R. Knegtel et al., "Fusion joining device for plastic tubes," US 39081 B2, Vertex Pharmaceuticals Inc., 2008.

[108] R. Davies, P. Li, J. Golec, J. Charrier, R. Knegtel, and D. Bebbington, "Pyrazole compounds useful as protein kinase inhibitors," US 6610677 B2, Vertex Pharmaceuticals Inc., 2003.

[109] E. Freyne, C. Love, L. Cooymans et al., "Triazolopyrimidine derivatives as glycogen synthase kinase 3 inhibitors," US 7449465 B2, Janssen Pharmaceutica, 2008.

[110] E. Freyne, C. Love, L. Cooymans et al., "Triazolopyrimidine derivatives as glycogen synthase kinase-3 inhibitors," US 7560458 B2, Janssen Pharmaceutica, 2009.

[111] A. Garcia, T. Gallet, A. Taki Li et al., "2-pyridinyl-6,7,8,9-tetrahydropyrimido[1,2-a] pyrimidin-4-one and 7-pyridinyl-2,3-dihydroimidazo[1,2-a] pyrimidin-5(1H)one derivatives," US 7566720 B2, Sanofi-Aventis Mitsubishi Pharma Corporation, 2009.

[112] P. George, A. Lochead, M. Saady, F. Slowinski, and P. Yaiche, "Substituted 8′-pyridinyl-dihydrospiro-[cycloalkyl]-pyrimido[1,2-a] pyrimidin-6-one and 8′-pyrimidinyl-dihydrospiro-[cycloalkyl]-pyrimido[1,2-a] pyrimidin-6-one derivatives," US 7507743 B2, Sanofi-Aventis Mitsubishi Pharma Corporation, 2009.

[113] D. Goff, S. Harrison, J. Nuss, D. Ring, and X. Zhou, "Inhibitors of glycogen synthase kinase 3," US 6417185 B1, Chiron Corporation, 2002.

[114] K. Kataoka, T. Kosugi, T. Ishii et al., "Substituted pyrrolo[3,2-d]pyrimidines as glycogen synthase kinase (GSK) inhibitors," US 7528140 B2, Teijin Limited, 2009.

[115] K. Kataoka, T. Kosugi, T. Ishii et al., "Pyrrolopyrimidine derivative," EP 1477490 A1, Teijin Limited, 2004.

[116] R. Knegtel, D. Bebbington, H. Binch et al., "Pyrazole compounds useful as protein kinase inhibitors," US 6613776 B2, Vertex Pharmaceuticals Inc., 2003.

[117] A. Lochead, S. Marguerie, M. Saady, and P. Yaiche, "1-[alkyl], 1-[(heteroaryl)alkyl] and 1-[(aryl)alkyl]-7-pyridinyl-imidazo[1,2-a]pyrimidin-5(1h)-one derivatives," US 7608624 B2, Sanofi-Aventis Mitsubishi Pharma Corporation, 2009.

[118] M. Nakano and Y. Maeda, "Novel chemical compounds," WO 2005/061516 A1, Smithkline Beecham Corporation, 2005.

[119] J. Nuss, S. Harrison, D. Ring et al., "Inhibitors of glycogen synthase kinase-3," US 6489344 B1, Chiron Corporation, 2002.

[120] J. Nuss, S. Harrison, D. Ring et al., "Inhibitors of glycogen synthase kinase-3," US 7037918 B2, Chiron Corporation, 2006.

[121] J. Nuss, S. Harrison, D. Ring et al., "Inhibitors of glycogen synthase kinase-3," US 7045519 B2, Chiron Corporation, 2006.

[122] T. Tsutsumi, S. Sugiura, M. Koga et al., "Substituted pyrrolo[3,2-d]pyrimidine derivatives," US 7557113 B2, Teijin Pharma Limited, 2009.

[123] P. H. Olesen, A. R. Sorensen, B. Urso et al., "Synthesis and *in vitro* characterization of 1-(4-aminofurazan-3-yl)-5-dialkylaminomethyl-1H-[1,2,3]triazole-4-carboxylic acid derivatives. A new class of selective GSK-3 inhibitors," *Journal of Medicinal Chemistry*, vol. 46, no. 15, pp. 3333–3341, 2003.

[124] U. Bandarage, B. Hare, J. Parsons et al., "4-(Benzimidazol-2-yl)-1,2,5-oxadiazol-3-ylamine derivatives: potent and selective p70S6 kinase inhibitors," *Bioorganic and Medicinal Chemistry Letters*, vol. 19, no. 17, pp. 5191–5194, 2009.

[125] M. Saitoh, J. Kunitomo, E. Kimura et al., "Design, synthesis and structure-activity relationships of 1,3,4-oxadiazole derivatives as novel inhibitors of glycogen synthase kinase-β," *Bioorganic and Medicinal Chemistry*, vol. 17, no. 5, pp. 2017–2029, 2009.

[126] M. Saitoh, J. Kunitomo, E. Kimura et al., "2-{3-[4-(Alkylsulfinyl)phenyl]-1-benzofuran-5-yl}-5-methyl-1,3,4-oxadiazole derivatives as novel inhibitors of glycogen synthase kinase-β with good brain permeability," *Journal of Medicinal Chemistry*, vol. 52, no. 20, pp. 6270–6286, 2009.

[127] T. Onishi, H. Iwashita, Y. Uno et al., "A novel glycogen synthase kinase-3 inhibitor 2-methyl-5-(3-{4-[(S)-methylsulfinyl]phenyl}-1-benzofuran-5-yl)-1,3,4-oxadiazole decreases tau phosphorylation and ameliorates cognitive deficits in a transgenic model of Alzheimer's disease," *Journal of Neurochemistry*, vol. 119, no. 6, pp. 1330–1340, 2011.

[128] M. A. Khanfar, R. A. Hill, A. Kaddoumi, and K. A. El Sayed, "Discovery of novel GSK-β inhibitors with potent *in vitro* and *in vivo* activities and excellent brain permeability using combined ligand- and structure-based virtual screening," *Journal of Medicinal Chemistry*, vol. 53, no. 24, pp. 8534–8545, 2010.

[129] A. G. Koryakova, Y. A. Ivanenkov, E. A. Ryzhova et al., "Novel aryl and heteroaryl substituted N-[3-(4-phenylpiperazin-1-yl)propyl]-1,2,4-oxadiazole-5-carboxamides as selective GSK-3 inhibitors," *Bioorganic and Medicinal Chemistry Letters*, vol. 18, no. 12, pp. 3661–3666, 2008.

[130] C. Loge, A. Testard, V. Thiery et al., "Novel 9-oxothiazolo[5,4-f]quinazoline-2-carbonitrile derivatives as dual cyclin-dependent kinase 1 (CDK1)/glycogen synthase kinase-3 (GSK-3) inhibitors: synthesis, biological evaluation and molecular modeling studies," *European Journal of Medicinal Chemistry*, vol. 43, no. 7, pp. 1469–1477, 2008.

[131] R. Bhat, Y. Xue, S. Berg et al., "tructural insights and biological effects of glycogen synthase kinase-3-specific inhibitor AR-A014418," *The Journal of Biological Chemistry*, vol. 278, no. 46, pp. 45937–45945, 2003.

[132] W. Noble, E. Planel, C. Zehr et al., "Inhibition of glycogen synthase kinase-3 by lithium correlates with reduced tauopathy and degeneration *in vivo*," *Proceedings of the National Academy of Sciences of the United States of America*, vol. 102, no. 19, pp. 6990–6995, 2005.

[133] F. Lo Monte, T. Kramer, A. Bolander et al., "Synthesis and biological evaluation of glycogen synthase kinase-3 (GSK-3) inhibitors: an fast and atom efficient access to 1-aryl-3-benzylureas," *Bioorganic and Medicinal Chemistry Letters*, vol. 21, no. 18, pp. 5610–5615, 2011.

[134] D. Shin, S. C. Lee, Y. S. Heo et al., "Design and synthesis of 7-hydroxy-1H-benzoimidazole derivatives as novel inhibitors of glycogen synthase kinase-β," *Bioorganic and Medicinal Chemistry Letters*, vol. 17, no. 20, pp. 5686–5689, 2007.

[135] B. Voigt, M. Krug, C. Schachtele, F. Totzke, and A. Hilgeroth, "Probing novel 1-aza-9-oxafluorenes as selective GSK-β inhibitors," *ChemMedChem*, vol. 3, no. 1, pp. 120–126, 2008.

[136] N. B. Chauhan, G. J. Siegel, and D. L. Feinstein, "Propentofylline attenuates tau hyperphosphorylation in Alzheimer's Swedish mutant model Tg2576," *Neuropharmacology*, vol. 48, no. 1, pp. 93–104, 2005.

[137] M. Arnost, A. Pierce, E. ter Haar et al., "3-Aryl-4-(arylhydrazono)-1H-pyrazol-5-ones: highly ligand efficient and potent inhibitors of GSKβ," *Bioorganic and Medicinal Chemistry Letters*, vol. 20, no. 5, pp. 1661–1664, 2010.

[138] W. Chen, I. N. Gaisina, H. Gunosewoyo et al., "Structure-guided design of a highly selective glycogen synthase kinase-3β inhibitor: a superior neuroprotective pyrazolone showing antimania effects," *ChemMedChem*, vol. 6, pp. 1587–1592, 2011.

[139] M. A. Khanfar, B. A. Asal, M. Mudit, A. Kaddoumi, and K. A. El Sayed, "The marine natural-derived inhibitors of glycogen synthase kinase-β phenylmethylene hydantoins: *in vitro* and *in vivo* activities and pharmacophore modeling," *Bioorganic and Medicinal Chemistry*, vol. 17, no. 16, pp. 6032–6039, 2009.

[140] K. Coffman, M. Brodney, J. Cook et al., "6-amino-4-(pyrimidin-4-yl)pyridones: novel glycogen synthase kinase-3β inhibitors," *Bioorganic and Medicinal Chemistry Letters*, vol. 21, pp. 1429–1433, 2011.

[141] M. Hamann, D. Alonso, E. Martin-Aparicio et al., "Glycogen synthase kinase-3 (GSK-3) inhibitory activity and structure-activity relationship (SAR) studies of the manzamine alkaloids. Potential for Alzheimer's disease," *Journal of Natural Products*, vol. 70, no. 9, pp. 1397–1405, 2007.

[142] M. Gompel, M. Leost, E. B. de Kier Joffe et al., "Meridianins, a new family of protein kinase inhibitors isolated from the ascidian Aplidium meridianum," *Bioorganic and Medicinal Chemistry Letters*, vol. 14, no. 7, pp. 1703–1707, 2004.

[143] L. Meijer, A. M. W. H. Thunnissen, A. W. White et al., "Inhibition of cyclin-dependent kinases, GSK-β and CK1 by hymenialdisine, a marine sponge constituent," *Chemistry and Biology*, vol. 7, no. 1, pp. 51–63, 2000.

[144] N. Zhang, R. Zhong, H. Yan, and Y. Jiang, "Structural features underlying selective inhibition of GSK3β by dibromocantharelline: implications for rational drug design," *Chemical Biology and Drug Design*, vol. 77, no. 3, pp. 199–205, 2011.

[145] V. Pande and M. J. Ramos, "Structural basis for the GSK-β binding affinity and selectivity against CDK-2 of 1-(4-aminofurazan-3yl)-5-dialkylaminomethyl-1H-[1,2,3] triazole-4-carboxylic acid derivatives," *Bioorganic and Medicinal Chemistry Letters*, vol. 15, no. 23, pp. 5129–5135, 2005.

[146] E. ter Haar, J. T. Coll, D. A. Austen, H. M. Hsiao, L. Swenson, and J. Jain, "Structure of GSKβ reveals a primed phosphorylation mechanism," *Nature Structural Biology*, vol. 8, no. 7, pp. 593–596, 2001.

[147] J. Gotz and L. M. Ittner, "Animal models of Alzheimer's disease and frontotemporal dementia," *Nature Reviews Neuroscience*, vol. 9, no. 7, pp. 532–544, 2008.

[148] K. Iijima-Ando and K. Iijima, "Transgenic drosophila models of Alzheimer's disease and tauopathies," *Brain Structure and Function*, vol. 214, no. 2-3, pp. 245–262, 2010.

[149] J. Wentzell and D. Kretzschmar, "Alzheimer's disease and tauopathy studies in flies and worms," *Neurobiology of Disease*, vol. 40, no. 1, pp. 21–28, 2010.

[150] J. J. Lucas, F. Hernandez, P. Gomez-Ramos, M. A. Moran, R. Hen, and J. Avila, "Decreased nuclear β-catenin, tau hyperphosphorylation and neurodegeneration in GSK-3β conditional transgenic mice," *The EMBO Journal*, vol. 20, no. 1-2, pp. 27–39, 2001.

[151] M. Perez, E. Ribe, A. Rubio et al., "Characterization of a double (amyloid precursor protein-tau) transgenic: tau phosphorylation and aggregation," *Neuroscience*, vol. 130, no. 2, pp. 339–347, 2005.

[152] E. M. Ribe, M. Perez, B. Puig et al., "Accelerated amyloid deposition, neurofibrillary degeneration and neuronal loss in double mutant APP/tau transgenic mice," *Neurobiology of Disease*, vol. 20, no. 3, pp. 814–822, 2005.

[153] D. Terwel, D. Muyllaert, I. Dewachter et al., "Amyloid activates GSK-β to aggravate neuronal tauopathy in bigenic mice," *American Journal of Pathology*, vol. 172, no. 3, pp. 786–798, 2008.

[154] J. Lewis, D. W. Dickson, W. L. Lin et al., "Enhanced neurofibrillary degeneration in transgenic mice expressing mutant tau and APP," *Science*, vol. 293, no. 5534, pp. 1487–1491, 2001.

[155] S. Oddo, A. Caccamo, J. D. Shepherd et al., "Triple-transgenic model of Alzheimer's disease with plaques and tangles: intracellular Aβ and synaptic dysfunction," *Neuron*, vol. 39, no. 3, pp. 409–421, 2003.

[156] J. Lewis, E. McGowan, J. Rockwood et al., "Neurofibrillary tangles, amyotrophy and progressive motor disturbance in mice expressing mutant (P301L)tau protein," *Nature Genetics*, vol. 25, no. 4, pp. 402–405, 2000.

[157] D. Paquet, R. Bhat, A. Sydow et al., "A zebrafish model of tauopathy allows *in vivo* imaging of neuronal cell death and drug evaluation," *Journal of Clinical Investigation*, vol. 119, no. 5, pp. 1382–1395, 2009.

[158] D. Paquet, B. Schmid, and C. Haass, "Transgenic zebrafish as a novel animal model to study tauopathies and other neurodegenerative disorders *in vivo*," *Neurodegenerative Diseases*, vol. 7, no. 1–3, pp. 99–102, 2010.

[159] Y. Okawa, K. Ishiguro, and S. C. Fujita, "Stress-induced hyperphosphorylation of tau in the mouse brain," *The FEBS Letters*, vol. 535, no. 1–3, pp. 183–189, 2003.

[160] S. Yoshida, M. Maeda, S. Kaku, H. Ikeya, K. Yamada, and S. Nakaike, "Lithium inhibits stress-induced changes in tau phosphorylation in the mouse hippocampus," *Journal of Neural Transmission*, vol. 113, no. 11, pp. 1803–1814, 2006.

[161] K. Leroy and J. P. Brion, "Developmental expression and localization of glycogen synthase kinase-β in rat brain," *Journal of Chemical Neuroanatomy*, vol. 16, no. 4, pp. 279–293, 1999.

[162] M. Takahashi, K. Tomizawa, and K. Ishiguro, "Distribution of tau protein kinase I/glycogen synthase kinase-β, phosphatases 2A and 2B, and phosphorylated tau in the developing rat brain," *Brain Research*, vol. 857, no. 1-2, pp. 193–206, 2000.

[163] S. H. Min, J. S. Cho, J. H. Oh et al., "Tau and GSKβ dephosphorylations are required for regulating Pin1 phosphorylation," *Neurochemical Research*, vol. 30, no. 8, pp. 955–961, 2005.

[164] N. Sato, L. Meijer, L. Skaltsounis, P. Greengard, and A. H. Brivanlou, "Maintenance of pluripotency in human and mouse embryonic stem cells through activation of Wnt signaling by a pharmacological GSK-3-specific inhibitor," *Nature Medicine*, vol. 10, no. 1, pp. 55–63, 2004.

[165] T. D. Gould, N. A. Gray, and H. K. Manji, "Effects of a glycogen synthase kinase-3 inhibitor, lithium, in adenomatous polyposis coli mutant mice," *Pharmacological Research*, vol. 48, no. 1, pp. 49–53, 2003.

[166] A. Martinez, A. Castro, and M. Medina, *Glycogen Synthase Kinase-3 (GSK-3) and Its Inhibitors*, John Wiley & Sons, Hoboken, NJ, USA, 2006.

[167] A. Martinez, C. Gil, and D. I. Perez, "Glycogen synthase kinase-3 inhibitors in the next horizon for Alzheimer's disease treatment," *International Journal of Alzheimer's Disease*, vol. 2011, Article ID 280502, 7 pages, 2011.

[168] L. T. Alon, S. Pietrokovski, S. Barkan et al., "Selective loss of glycogen synthase kinase-3α in birds reveals distinct roles for GSK-3 isozymes in tau phosphorylation," *The FEBS Letters*, vol. 585, no. 8, pp. 1158–1162, 2011.

[169] C. J. Phiel, C. A. Wilson, V. M. Y. Lee, and P. S. Klein, "GSK-3α regulates production of Alzheimer's disease amyloid-β peptides," *Nature*, vol. 423, no. 6938, pp. 435–439, 2003.

[170] M. I. Davis, J. P. Hunt, S. Herrgard et al., "Comprehensive analysis of kinase inhibitor selectivity," *Nature Biotechnology*, vol. 29, no. 11, pp. 1046–1051, 2011.

[171] D. Rauh, "Inaktive Kinasekonformationen stabilisieren," *Nachrichten aus der Chemie*, vol. 58, no. 2, pp. 118–121, 2010.

[172] K. Okada, T. Sato, Y. Kohno, and M. Nomura, "7-Cycloalkylaminoquinolones as GSK-3 inhibitors," WO 2010/104205 A1, Kyorin Pharmaceutical Company Limited, 2010.

[173] S. C. Turner, M. H. M. Bakker, W. Hornberger, and F. E. Wolter, "Heterocyclic compounds and their use as glycogen synthase kinase-3 inhibitors," WO 2010/109005 A1, Abbott GmbH & Co. KG., 2010.

3.2 Synthese und biologische Evaluation von Glykogen Synthase Kinase-3 (GSK-3) Inhibitoren: Ein schneller und atomeffizienter Zugang zu 1-Aryl-3-benzylharnstoffen

Der Inhalt dieses Kapitels wurde bereits veröffentlicht: Fabio Lo Monte*, Thomas Kramer*, Alexander Boländer, Batya Plotkin, Hagit Eldar-Finkelman, Ana Fuertes, Juan Dominguez, Boris Schmidt, „*Synthesis and biological evaluation of glycogen synthase Kinase-3 (GSK-3) inhibitors: An fast and atom efficient access to 1-aryl-3-benzylureas*“, Bioorg. Med. Chem. Lett. **2011**, *21*, 5610-5615, http://dx.doi.org/10.1016/j.bmcl.2011.06.131.

Mit freundlicher Genehmigung von *Elsevier*.

Seitdem die Glykogen Synthase Kinase-3 mit diversen zellulären Prozessen, insbesondere der pathologischen Merkmale der Alzheimer-Krankheit, in Verbindung gebracht werden konnte, ist es ein therapeutisches Zielenzym der akademischen und industriellen Forschung. Um die in Kapitel 5.1 beschriebenen Daten experimentell zu stützen, wurde ein kostengünstiges und schnell zu synthetisierendes Strukturmotiv gesucht. Die Entscheidung fiel auf die 1-Aryl-3-benzylharnstoffe als Basisstrukturmotiv. Der Grund liegt in den Vorarbeiten unseres Arbeitskreises und der Kenntnis des bereits intensiv erforschten GSK-3-Inhibitor **AR-A014418** (AstraZeneca).[306,298,307] Durch die gezielte Verwendung unterschiedlicher *building blocks* und die Etablierung einer chromatographiefreien Aufarbeitung wurden innerhalb kürzester Zeit diverse Harnstoffe synthetisiert. Im Anschluss wurden einige dieser Produkte durch Suzukireaktionen und Mikrowellen-unterstützte Reaktionsführung weiter umgesetzt. Der systematische Aufbau der Produktbibliothek ergab einen empirischen Einblick in die Strukturaktivitätsbeziehung zwischen den Harnstoffen und GSK-3. Darüber hinaus konnte beispielsweise mit dem Benzothiazolylharnstoff **66** eine gesteigerte Aktivität und geringere Toxizität (in einem *zebrafish embryo phenotype assay*) im Vergleich zur Referenz **AR-A014418** erzielt werden, Abb. 26.

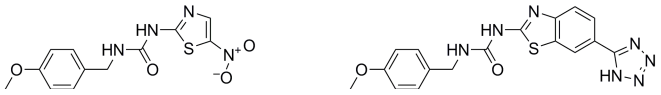

AR-A014418
IC_{50} = 330 nM

66
IC_{50} = 140 nM

Abb. 26: Graphische Darstellung der Referenz **AR-A014418** (links) und des Benzothiazolylharnstoffs **66** (rechts). Hinweis: Um die Aktivitäten der synthetisierten Harnstoffe mit **AR-A014418** vergleichen zu können, wurde letzterer im gleichen Assay vermessen.

Die im Rahmen dieser Arbeit synthetisierten Verbindungen sind: **1 (BSc4158), 3 (BSc4189), 5 (BSc4109), 8 (BSc4169), 9 (BSc4243), 11 (BSc4162), 12 (BSc4160), 14 (BSc4191), 16 (BSc4193), 17 (BSc4167), 20 (BSc4171), 22 (BSc4146), 26 (BSc4152), 31 (BSc4150), 33 (BSc4195), 35 (BSc4197), 37 (BSc4199), 40-43 (BSc4103, BSc4110, BSc4107), 46 (BSc4105), 47 (BSc4112), 54 (BSc4114), 57 (BSc4201), 59 (BSc4203), 61 (BSc4241), 62 (BSc4420), 64 (BSc4156), 65 (BSc4164).**

Bioorganic & Medicinal Chemistry Letters 21 (2011) 5610–5615

Contents lists available at ScienceDirect

Bioorganic & Medicinal Chemistry Letters

journal homepage: www.elsevier.com/locate/bmcl

Synthesis and biological evaluation of glycogen synthase kinase 3 (GSK-3) inhibitors: An fast and atom efficient access to 1-aryl-3-benzylureas

Fabio Lo Monte [a,†], Thomas Kramer [a,†], Alexander Boländer [a], Batya Plotkin [b], Hagit Eldar-Finkelman [b], Ana Fuertes [c], Juan Dominguez [c], Boris Schmidt [a,*]

[a] Clemens Schöpf—Institute of Organic Chemistry and Biochemistry, Technische Universität Darmstadt, 64287 Darmstadt, Germany
[b] Department of Human Molecular Genetics and Biochemistry, Sackler School of Medicine, Tel Aviv University, Tel Aviv 69978, Israel
[c] Noscira, Tres Cantos, 28760 Madrid, Spain

ARTICLE INFO

Article history:
Received 15 April 2011
Revised 11 June 2011
Accepted 13 June 2011
Available online 18 July 2011

Keywords:
Glycogen synthase kinase 3 (GSK-3)
Alzheimer disease
Structure–activity relationship (SAR)
Suzuki coupling
Microwave irradiation

ABSTRACT

The glycogen synthase kinase 3 (GSK-3) is implicated in multiple cellular processes and has been linked to the pathogenesis of Alzheimer's disease (AD). In the course of our research topic we synthesized a library of potent GSK-3 inhibitors. We utilized the urea scaffold present in the potent and highly selective GSK-3 inhibitor AR-A014418 (AstraZeneca). This moiety suits both (a) a convergent approach utilizing readily accessible building blocks and (b) a divergent approach based on a microwave heating assisted Suzuki coupling. We established a chromatography-free purification method to generate products with sufficient purity for the biological assays. The structure–activity relationship of the library provided the rationale for the synthesis of the benzothiazolylurea **66** (IC_{50} = 140 nM) and the pyridylurea **62** (IC_{50} = 98 nM), which displayed two to threefold enhanced activity versus the reference compound **18** (AR-A014418: IC_{50} = 330 nM) in our assays.

Alzheimer's disease (AD) is a neurodegenerative disorder defined by progressive memory loss and cognitive impairment.[1] The definite diagnosis of AD is possible postmortem only. It is based on the presence of extracellular plaques of β-amyloid (Aβ), and intracellular neurofibrillary tangles (NFTs) consisting of hyperphosphorylated tau protein.[2] Glycogen synthase kinase 3 (GSK-3) interacts with several neuronal proteins that are directly linked to AD.[3] There are two GSK-3 genes, GSK-3α and GSK-3β. Both are ubiquitously expressed and constitutively active proline-directed serine/threonine kinases.[1] Several GSK-3 inhibitors have been studied in kinase assays and cellular test panels. Among these inhibitors are paullones, indirubin, aminomaleimides and other small molecules. The potent and specific GSK-3 inhibitor AR-A014418 (**18**) was reported by AstraZeneca and its interactions with the essential amino acids of GSK-3β are denoted in Figure 1.[4]

AR-A014418 (**18**) is selective against Cdk2, Cdk5 and 26 other kinases tested. It inhibits GSK-3 activity with a strongly assay dependent IC_{50}, the highest activity was reported as IC_{50} = 104 nM.[4] AR-A014418 constitutes a lead compound in our kinase inhibitor programe targeting neurodegenerative diseases.[5]

There is a need of a robust and inexpensive approach to AR-A014418 (**18**), suitable for combinatorial chemistry, which provides straightforward access to related ureas displaying enhanced GSK-3 inhibition. The generation of chemical diversity and the limitation by commercial building blocks stimulated a search for mild reaction conditions, rapid purification strategy and access to the reactive intermediate isocyanates without destillation.[6] The two step protocol utilized the in situ generation of

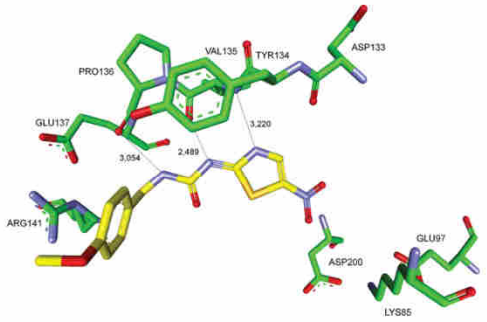

Figure 1. Potent and highly selective GSK-3 inhibitor AR-A014418 (AstraZeneca) in the ATP binding pocket of GSK-3β; important protein–inhibitor interactions are shown. The distance is denoted in Å. PDB code 1Q5K (Accelrys Discovery Studio Visualizer 2.5).

* Corresponding author. Tel.: +49 6151 164531; fax: +49 6151 163278.
E-mail address: schmidt_boris@t-online.de (B. Schmidt).
† These authors contributed equally to this work.

0960-894X/$ - see front matter © 2011 Published by Elsevier Ltd.
doi:10.1016/j.bmcl.2011.06.131

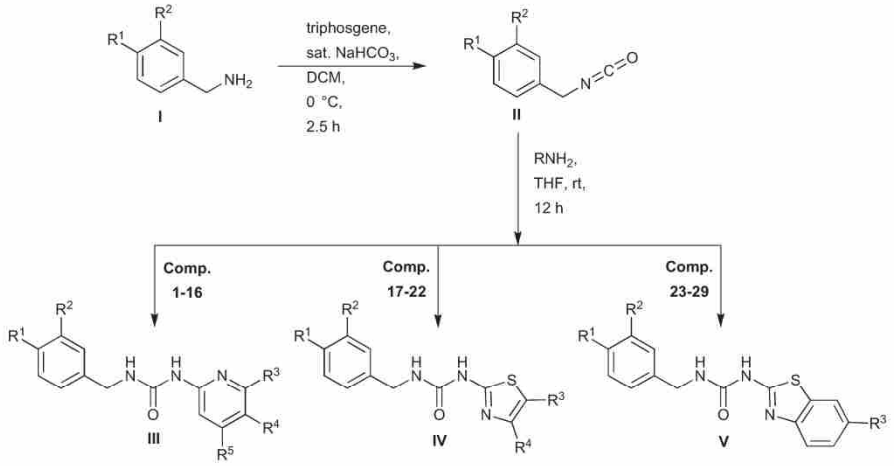

Scheme 1. Mild synthesis and rapidly purified ureas.

Table 1
Mild synthesis provides crystalline ureas free of chromatography

Compd	R^1	R^2	R^3	R^4	R^5	Yield[a] (%)	*c* Log *P*[c]
1	F	H	H	I	H	11	3.74
2	F	H	Br	H	H	52	3.48
3	MeO	H	Br	H	H	41	3.25
4	F	H	H	Br	H	54	3.48
5	MeO	H	H	Br	H	48	3.25
6	MeO	H	H	H	Br	75	3.25
7	F	H	H	H	Cl	31	3.33
8	MeO	H	H	H	Cl	34	3.10
9	MeO	H	H	H	CN	63[b]	2.00
10	F	H	H	NO_2	H	21[b]	2.51
11	MeO	H	H	NO_2	H	13[b]	2.28
12	F	H	H	CN	H	63[b]	2.22
13	MeO	H	H	CN	H	58[b]	2.00
14	Br	H	H	CN	H	34[b]	2.94
15	OCF_3	H	H	CN	H	13[b]	3.10
16	$-OCH_2O-$	H	CN	H		19[b]	2.04
17	F	H	NO_2	H	—	21[b]	2.34
18	MeO	H	NO_2	H	—	26[b]	2.11
19	F	H	COOEt	Me	—	35[b]	3.02
20	MeO	H	COOEt	Me	—	24[b]	2.80
21	F	H	H	4-Me-Ph	—	29[b]	5.00
22	MeO	H	H	4-Me-Ph	—	46[b]	4.77
23	F	H	Br	—	—	24[b]	4.87
24	MeO	H	F	—	—	52[b]	3.92
25	F	H	CF_3	—	—	31[b]	4.96
26	MeO	H	CF_3	—	—	50[b]	4.74
27	MeO	H	NO_2	—	—	26[b]	3.64
28	F	F	NO_2	—	—	36[b]	3.93
29	MeO	H	CN	—	—	70[b]	3.34

[a] Yields of analytically pure products; products recrystallized from methanol or ethanol.
[b] Amines preactivated with *n*-BuLi.
[c] Determined by CS ChemOffice 2008.

isocyanates from benzylamine and triphosgene. These crude intermediates were dissolved in dry *N*,*N*-dimethylformamide or dry tetrahydrofurane and reacted with nonactivated or *n*-buthyllithium (*n*-BuLi) activated amines (Scheme 1 and Table 1).

Initially, the reaction of aminopyridines was dominated by the dimerization of benzylamines. This resulted in the isolation of known benzylamine adducts **30** and **31** (Scheme 2 and Table 2).[7,8]

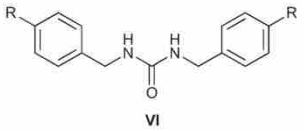

Scheme 2. Commonly observed dimerization product.

Table 2
Dimerization derived products

Compd	R	Yield[a] (%)	*c* Log *P*[b]
30[6,7]	4-F	37	3.17
31[6]	4-MeO	43	2.72

[a] Yields of analytically pure products; products recrystallized from methanol.
[b] Determined by CS ChemOffice 2008.

Using *n*-BuLi for the deprotonation of the heterocyclic amines solved this problem. Furthermore, high-pressure liquid chromatography (HPLC) controls showed that the *n*-BuLi preactivated amines reacted with the isocyanates immediately, but nevertheless the reactions were stirred 12 h at room temperature. Afterward the reaction solution was suspended in vigorously stirred water and precipitation occured promptly. The purification of the crude urea was achieved by filtration and recrystallization. These reaction and purification conditions were standardized for a variety of amines, including benzylamines, aminopyridines and aminothiazoles.

AR-A014418 (**18**) was synthesized without heating and chromatographic purification, which were employed by AstraZeneca 2003.[4] The initial yields of the standard methodology were moderate at best, but they did not require chromatography and the yield of compound **6** obtained by the standard protocol was optimized in scaled up experiments to 75%. Thus the atom efficiency of the total process, which includes the purification, is actually sufficiently high as it produces very little waste material.

The required diversity was introduced by the Suzuki-coupling of arylbromides and boronic acids (Scheme 3 and Table 3).

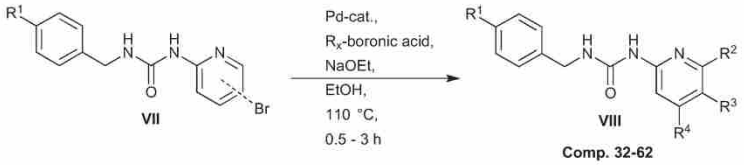

Scheme 3. Suzuki reactions.

Table 3
Urea enlargement supported by Suzuki reaction

Compd	R^1	R^2	R^3	R^4	Yield[a] (%)	*c* Log *P*[d]
32	F	Ph	H	H	40[b]	4.58
33	MeO	Ph	H	H	71[b]	4.36
34	F	3-F-Ph	H	H	29[b]	4.75
35	F	3-MeO-Ph	H	H	31[b]	6.37
36	MeO	3-MeO-Ph	H	H	34[b]	6.13
37	F	3-BnO-Ph	H	H	51[b]	6.37
38	F	4-Py	H	H	67[b]	3.26
39	MeO	4-Py	H	H	50[b]	3.04
40	F	H	Ph	H	70[c]	4.37
41	MeO	H	Ph	H	47[c]	4.15
42	F	H	4-Me-Ph	H	34[c]	4.87
43	MeO	H	4-Me-Ph	H	32[c]	4.65
43	MeO	H	4-Me-Ph	H	32[c]	4.65
44	F	H	3-F-Ph	H	68[c]	4.54
45	MeO	H	3-F-Ph	H	33[c]	4.32
46	F	H	3-MeO-Ph	H	37[c]	4.39
47	MeO	H	3-MeO-Ph	H	34[c]	4.17
48	F	H	3-Isopro-poxy-Ph	H	43[c]	5.23
49	MeO	H	3-Isopro-poxy-Ph	H	61[c]	5.01
50	F	H	3-BnO-Ph	H	26[c]	6.16
51	MeO	H	3-BnO-Ph	H	19[c]	5.94
52	MeO	H	3-CF_3-Ph	H	27[c]	5.07
53	F	H	2,3-di-F-Ph	H	83[c]	4.62
54	MeO	H	2,3-di-F-Ph	H	26[c]	4.40
55	F	H	4-Vinyl-Ph	H	85[c]	5.09
56	MeO	H	4-Vinyl-Ph	H	87[c]	4.87
57	MeO	H	H	Ph	77[b]	4.15
58	MeO	H	H	3-F-Ph	57[b]	4.32
59	MeO	H	H	3-MeO-Ph	62[b]	4.17
60	MeO	H	H	2-MeO-Ph	47[c]	3.61
61	MeO	H	H	2-Thio-phen	33[c]	4.06
62	MeO	H	H	2-F-Py	67	3.03

[a] Yields of analytically pure products; products were recrystallized from methanol.
[b] $Pd(OAc)_2$.
[c] $Pd(PPh_3)_4$.
[d] Determined by CS ChemOffice 2008.

The Suzuki coupling of phenylboronic acids and brominated arylureas was catalyzed by $Pd(OAc)_2$ under standard conditions or subtle modifications thereof.[9,10] Some reactions required catalyst exchange to $Pd(PPh_3)_4$. The boronic acids were activated by sodium ethanolate. The starting materials were suspended in dry ethanol and the reactions were carried out in a sealed, argon flushed vessel. Again, the crude products of the Suzuki reaction were purified by atom efficient recrystallization.

Finally, we obtained four tetrazole derivatives (**63–66**) using microwave radiation in a Biotage Initiator 300. These products were purified by recrystallization and isolated in very good yields requiring no further optimization at this stage (Scheme 4 and Table 4), although the reaction conditions can be improved by using ionic liquids.[11] Be careful while working with azides, they can be explosive and should be handled with great care. During our study we encountered no adverse events.[12]

The arylureas were evaluated for their inhibition of GSK-3 activity. Several compounds were identified to reduce in vitro GSK-3β activity beneath 50% at a concentration of 10 μM (Table 5).[13]

Two derivatives (**66** and **62**) are more potent than our reference compound AR-A014418 (**18**). Five derivatives (**29**, **63**, **11**, **60, and 13**) display comparable inhibitory activity and four of them are not associated with toxicity alerts (Fig. 2). It should be noted that the tetrazoles, for example, compound **63** with a topological polar surface area of 111.83 Å (ChemOffice2008) may not permeate the blood brain barrier.

A docking study of compound **66** and PDB structure 1Q5K of GSK-3β suggested a binding mode along the hinge region of the ATP-binding pocket approximately like AR-A014418 (**18**) (Fig. 3).[4,14] There are two hydrogen bond interactions between **66** and the amino acid Glu137. Furthermore we assume two other interactions, one between the Asp133 carbonyl and a hydrogen of the phenyl group and the other between the tetrazol moiety and the polar pocket consisting of Lys85, Glu97 and Asp200. We hypothesize that the latter interaction is the reason for the enhanced potency of derivative (**66**).

Via the expeditious structure–activity relationship (SAR) we ascertained that the aminothiazole, used by AstraZeneca, can be

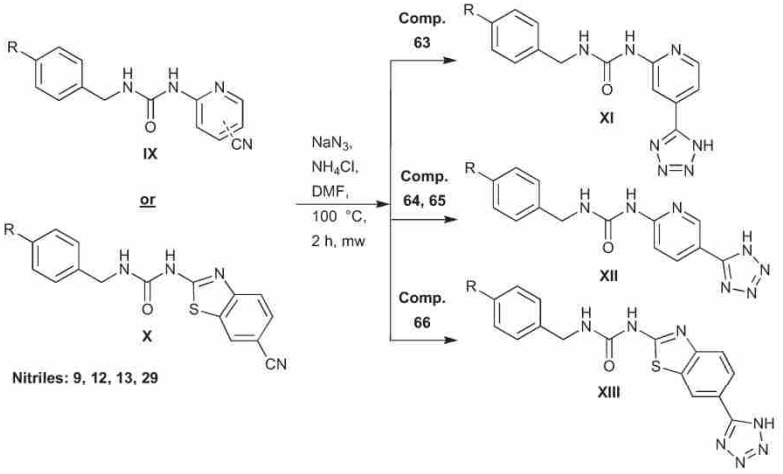

Scheme 4. Microwave reactions.

Table 4
Urea aryl tetrazole formation by microwave reaction

Compd	R	Yield[a] (%)	*c* Log *P*[b]
63	MeO	87	1.75
64	F	81	1.98
65	MeO	88	1.75
66	MeO	91	3.26

[a] Yields of analytically pure products; products recrystallized from methanol.
[b] Determined by CS ChemOffice 2008.

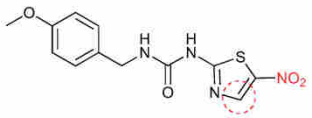

Figure 2. Potential toxic alerts: 1. Nitro group; 2. P450 associated-hepatotoxicity alert.

replaced by aminopyridines and aminobenzothiazoles. We found that an elongation in position R^3 and R^4 of structure **III** entailed reduced activity. However, an acceptor like NO_2 or CN is needed in position R^4 of structure **III** as long as no acceptor is allocated in position R^5. Our future research is focused on structure **V** and position R^5 of structure **III** from which we expect to obtain improved activity.

Table 5
GSK-3β inhibitory activity of selected compounds

Compd	Structure	GSK-3β activity in[a] (%)	
		1 μM of compd	10 μM of compd
62	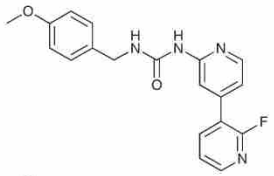	–	12
66	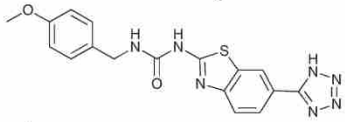	69	18
18	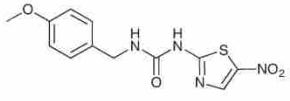	55	20

(*continued on next page*)

Table 5 (*continued*)

Compd	Structure	GSK-3β activity in[a] (%)	
		1 μM of compd	10 μM of compd
29	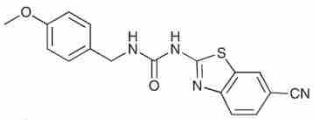	57	24
63	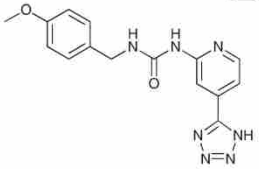	82	24
11	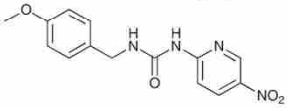	75	31
60	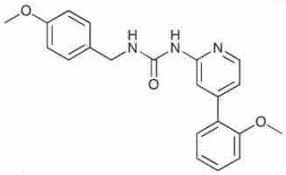	91	32
13	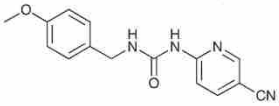	79	40
9	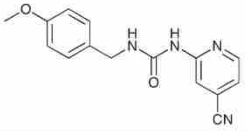	101	42

[a] Conditions for GSK-3β in vitro assay see Supplementary data.[10]

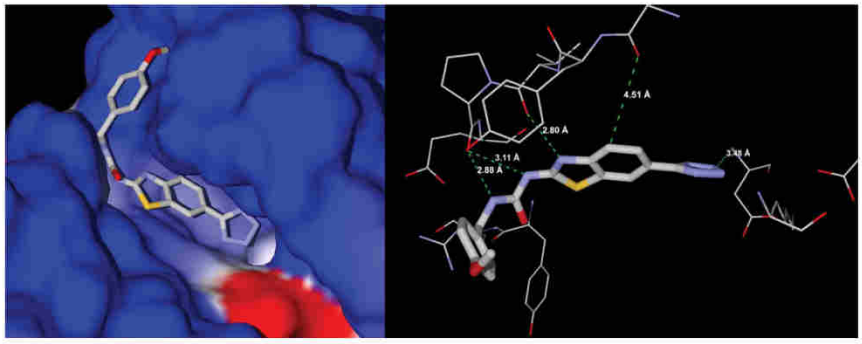

Figure 3. Docking of compound **66** into PDB structure 1Q5K of GSK-3β; Surface illustration of the ATP-binding pocket with **66** (left); Hydrogen bond interactions of **66** with the amino acids of the ATP-binding pocket (right).[4,14]

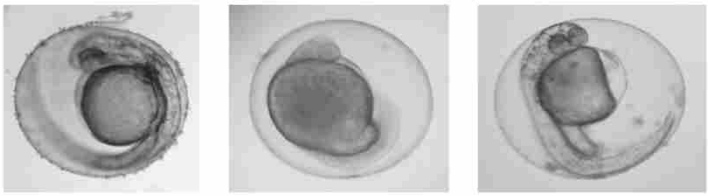

Figure 4. Exposure of zebrafish embryos to 1% DMSO (left), 100 mM **18** (AR-A14418, middle), and 100 mM **66** (right). The embryos were collected and maintained in E2 medium at 30 °C, compounds were added at 8–15 somites, and the phenotypes were compared after 25 h.

Table 6
GSK3 selectivity panel

Compound	IC_{50} values (mM)					
	GSK-3β	GSK-3α	Cdk5/p35	CKIε	AurKA	PKCα
18 (AR-A014418)	0.33	0.07	>100	>100	>100	>100
9	1.43	1.12	>100	>100	>100	>100
27	3.64	0.22	>100	>100	>100	>100
63	0.51	0.37	>100	>100	>100	>100
66	0.14	0.13	26.4	15.3	4.8	24.2

To evaluate the specificity of the family against GSK-3β, four of the synthesized compounds (**9**, **27**, **63** and **66**) were selected and tested against five human protein kinases (GSK-3α, PKCα, AurKA, Cdk5/p35 and CKIε) (Table 6).

Compound **66** with an IC_{50} of 140 nM for GSK3β was the only one able to inhibit all of the kinases tested (PKCα, AurKA, Cdk5/p35 and CKIε) but the IC_{50} values were one or two orders of magnitude above those found for the GSK-3 isoforms, indicating a fair degree of selectivity for this compound towards these latter enzymes. Such selectivity is even larger for the other three compounds tested, which were inactive (or poorly active) against the former kinases when tested up to 100 μM.

In order to demonstrate the utility and nontoxicity of the pyridine and benzothiazole moiety in whole organisms, we performed a zebrafish embryo phenotype assay.[15,16] We exposed the zebrafish embryos to the compounds **66**, **18** (AR-A014418) and **63** at early stages of development (8 till 15 somites, Fig. 4).

Controls after 18 h and 25 h showed that **18** (AR-A014418) is indeed toxic. This toxicity could be diminished by replacement of the thiazole with a benzothiazole (**66**) or pyridine (**63**) moiety (CHIR98014 is not toxic and compound **19** precipitates—data not shown). We observed some deformation in the fishtail at 100 μM (**66**, **63** and at 25 μM of CHIR98014—data not shown) and after eclosion we observed these fishes were swimming in circles only. This correlates with the observation that Wnt signaling, and thus GSK-3β, plays a crucial role in the development of metazoan and that known GSK-3 inhibitors like LiCl and the ruthenium complex (**R**)-**7** perturbe the zebrafish development.[15]

We have established a fast and atom efficient approach to generate kinase targeting urea derivatives. Hereby, it is feasible to diversify the scaffold in a time efficient manner. Thereby we expect to identify novel GSK-3 inhibitors displaying enhanced activity and selectivity. A preview of the biological activity and selectivity of the synthesized compounds is depicted in Tables 5 and 6. They are of comparable potency and selectivity to the reference compound **18** (AR-A014418). The aminothiazole used by AstraZeneca was replaced by other heterocycles. We have also shown that a selection of our compounds compared to **18** (AR-A014418) were less toxic in a zebrafish embryo phenotype assay, albeit some of these are not expected to be brain penetrant. This is subject of ongoing and future research in animal models of Alzheimer's disease.

Acknowledgment

This work was supported by a collaborative project financed by the 7th Framework Program of the European Union.

Supplementary data

Supplementary data associated with this article can be found, in the online version, at doi:10.1016/j.bmcl.2011.06.131.

References and notes

1. Hooper, C.; Killick, R.; Lovestone, S. *J. Neurochem.* **2008**, *104*, 1433.
2. Bhat, R. V.; Haeberlein, S. L. B.; Avila, J. *J. Neurochem.* **2004**, *89*, 1313.
3. Eldar-Finkelman, H. *Trends in Mol. Med.* **2002**, *8*, 126.
4. Bhat, R.; Xue, Y.; Berg, S.; Hellberg, S.; Ormö, M.; Nilsson, Y.; Radesäter, A.; Jerning, E.; Markgren, P.; Borgegard, T.; Nylöf, M.; Giménez-Cassina, A.; Hernández, F.; Lucas, J.; Díaz-Nido, J.; Avila, J. *J. Biol. Chem.* **2003**, *278*, 45937.
5. Hoettecke, N.; Liebeck, M.; Baumann, K.; Schubenel, R.; Winkler, E.; Steiner, H.; Schmidt, B. *Bioorg. Med. Chem. Lett.* **2010**, *20*, 2958.
6. Tsai, J. H.; Takaoka, L. R.; Powell, N. A.; Nowick, J. S. *Org. Synth.* **2002**, *78*, 220.
7. Wiley, R.; Beasley, P.; Knabeschuh, L. *J. Am. Chem. Soc.* **1954**, *76*, 311.
8. Shelton, P.; Zhang, Y.; Nguyen, T.; McElwee-White, L. *Chem. Commun.* **2009**, 947.
9. Miyauro, N.; Suzuki, A. *Chem. Rev.* **1995**, *95*, 2457.
10. Kotha, S.; Lahiri, K.; Kashinath, D. *Tetrahedron* **2002**, *48*, 9633.
11. Schmidt, B.; Meid, D.; Kieser, D. *Tetrahedron* **2007**, *63*, 492.
12. (a) Prudent Practice for Handling Hazardous Chemicals in Laboratories, National Academic: Washington, DC, 1983, 87.; (b) Bräse, S.; Gil, C.; Knepper, K.; Zimmermann, V. *Angew. Chem.* **2005**, *117*, 5320.
13. Liberman, Z.; Eldar-Finkelman, H. *J. Biol.Chem.* **2005**, *280*, 4422.
14. Molegro Virtual Docker, Version 4.2.0 (October 4th, 2010).
15. Atilla-Gokcumen, G. E.; Williams, D. S.; Bregman, H.; Pagano, N.; Meggers, E. *ChemBioChem* **2006**, *7*, 1443.
16. Paquet, D.; Bath, R.; Sydow, A.; Mandelkow, E.; Berg, S.; Hellberg, S.; Fälting, J.; Distel, M.; Köster, R.; Schmid, B.; Haass, C. *J. Clin. Invest.* **2009**, *119*, 1382.

3.2.1 Variation/Austausch des Harnstoffstrukturmotivs als Erweiterung der empirischen Strukturaktivitätsbeziehungsstudie

Neben der in der Publikation „*Synthesis and biological evaluation of glycogen synthase Kinase-3 (GSK-3) inhibitors: An fast and atom efficient access to 1-aryl-3-benzylureas*“ bereits angesprochenen Variation der benzylischen und heterozyklischen Strukturmotive wurde weitere Modifikationen des Harnstoffstrukturmotivs vorgenommen, Abb. 27 (Synthese siehe Kapitel: Experimenteller Teil – Ein Auszug).

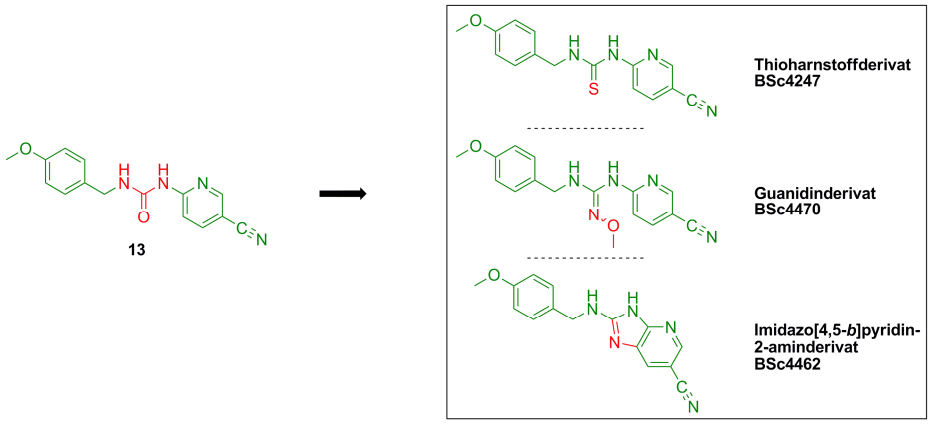

Abb. 27: Schematische Darstellung der Derivatisierung des Harnstoffstrukturmotivs am Beispiel vom Harnstoff **13**.

Der Austausch des Harnstoffstrukturmotivs durch ein Thioharnstoff-, Guanidin- oder gar durch ein Imidazo[4,5-*b*]pyridin-2-aminstrukturmotiv erzielte keine nennenswerte Hemmung von GSK-3 bei einer Probenkonzentration von 10 µM. Dies lässt darauf schließen, dass der Verlust möglicher Interaktionen des Carbonylsauerstoffs mit dem in der ATP-Bindungstasche vorliegendem Wassernetzwerk zu hoch ist und nicht durch andere Interaktionen kompensiert werden kann. Ferner ergab auch die Abkehr vom Harnstoffleitmotiv mit gleichbleibendem Heterozyklus hin zu Amid- bzw. Sulfonamidderivaten keine nennenswerte Inhibition von GSK-3 bei einer Probenkonzentration von 10 µM, Abb. 28 (Synthese siehe Kapitel: Experimenteller Teil – Ein Auszug). Dies belegt die Wichtigkeit der Interaktionen des Harnstoffstrukturmotivs und des 4-Methoxybenzylrests (siehe z. B. bei **13** oder **AR-A014418**) mit den Aminosäuren Val135, Pro136 und Arg141 der ATP-Bindungstasche von GSK-3, Abb. 23.[298]

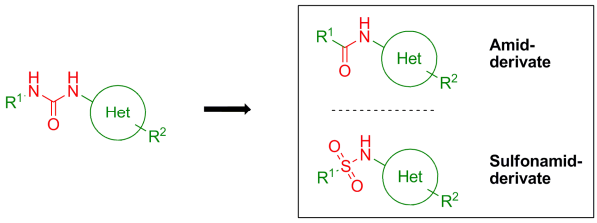

Abb. 28: Schematischer Strukturvergleich vom Harnstoff- über das Amid- bis hin zum Sulfonamidstrukturmotiv; Het = Thiazole/Benzothiazole, R^1 = Aryle/Benzyle, R^2 = NO_2/CN/OMe/H.

Die im Rahmen dieser Arbeit synthetisierten Verbindungen sind: **BSc4247, BSc4457, BSc4458, BSc4459, BSc4460, BSc4461, BSc4462, BSc4463, BSc4464, BSc4465, BSc4466, BSc4467, BSc4468, BSc4469, BSc4470, BSc4471, BSc4472, BSc4473, BSc4474, BSc4475.**

3.3 Identifikation von Glykogen Synthase Kinase-3-Inhibitoren mit einem selektiven Stachel für die Glykogen Synthase Kinase-3α

Der Inhalt dieses Kapitels wurde bereits veröffentlicht: Fabio Lo Monte, Thomas Kramer, Jiamin Gu, Upendra Rao Anumala, Luciana Marinelli, Valeria La Pietra, Ettore Novellino, Bénédicte Franco, David Demedts, Ana Fuertes, Juan Manuel Dominguez, Batya Plotkin, Hagit Eldar-Finkelman, Boris Schmidt, „*Identification of Glycogen Synthase Kinase-3 Inhibitors with a Selective Sting for Glykogen Synthase Kinase-3α*", J. Med. Chem. **2012**, *55*, 4407-4424, doi: 10.1021/jm300309a.

Mit freundlicher Genehmigung der *American Chemical Society (ACS)*.

Die humane Glykogen Synthase Kinase-3 liegt hauptsächlich in zwei Isoenzymen, GSK-3α und GSK-3β, vor. Sie werden mit einer Vielzahl an Krankheiten in Verbindung gebracht.[228-230] GSK-3β spielt beispielsweise eine Rolle bei der Diabetes, dem Down Syndrom, der Bipolaren Störung, dem Darmkrebs und der Alzheimer-Krankheit. GSK-3α beeinflusst nicht nur den β-adrenergen Signalweg (Verbindung zu Herzrhythmusstörungen), sondern auch die Alzheimer-Krankheit und die akute myeloische Leukämie.[295,308] Die spezifische Rolle beider Isoenzyme insbesondere in den Bereichen der AD und der Krebsforschung sind Schwerpunkt aktueller Diskussionen.[296,45,48] Die Entwicklung und Anwendung isoenzymspezifischer Inhibitoren könnte einen detaillierteren Einblick in die metabolischen Zusammenhänge von GSK-3 ermöglichen.

Obwohl bereits eine Fülle von GSK-3-Inhibitoren synthetisiert wurde, gibt es bisher mit **ΛOS-1** nur einen moderaten, GSK-3α spezifischen Inhibitor (7-fach aktiver im Bezug auf GSK-3α).[297] Die Gründe liegen in der hohen Sequenzhomologie beider GSK-3 Isoenzyme von 85 % und der mit 98 % fast identischen ATP-Bindungstasche.[231]

Eine detaillierte Analyse veröffentlichter Co-Kristallisationen von GSK-3β mit diversen Inhibitoren und die darauf aufbauende Synthese von Oxadiazolderivaten resultierte in einer Reihe GSK-3α spezifischer Inhibitoren. Die selektivsten Inhibitoren sind **14d** und **15b**, Abb. 29. **14d** inhibiert GSK-3α im einstelligen nanomolaren Bereich und zudem ca. 52-fach stärker als GSK-3β (IC_{50} = 6 nM für GSK-3α und 316 nM für

GSK-3β). Der isoenzymspezifischste GSK-3-Inhibitor ist **15b**. Dieser inhibiert GSK-3α 92-fach intensiver als GSK-3β (IC_{50} = 2 nM für GSK-3α und 185 nM für GSK-3β). Trotz intensiver Dockingversuche können keine genauen Gründe für diese Selektivität angeführt werden. Jedoch gibt es Hinweise, die auf eine Konformationsänderung in der C-terminalen Schleife hindeuten, hervorgerufen durch Interaktionen von **14d** und **15b** mit den Aminosäuren der ATP-Bindungstasche. Die weiterführende Selektivität von **14d** wurde in einem Kinase-Panel bestehend aus 50 humanen Kinasen getestet. Dabei wiesen 48 Kinasen eine Restaktivität von über 80 % auf. Neben GSK-3α wurde nur GSK-3β signifikant inhibiert (Restaktivität von 27 %).

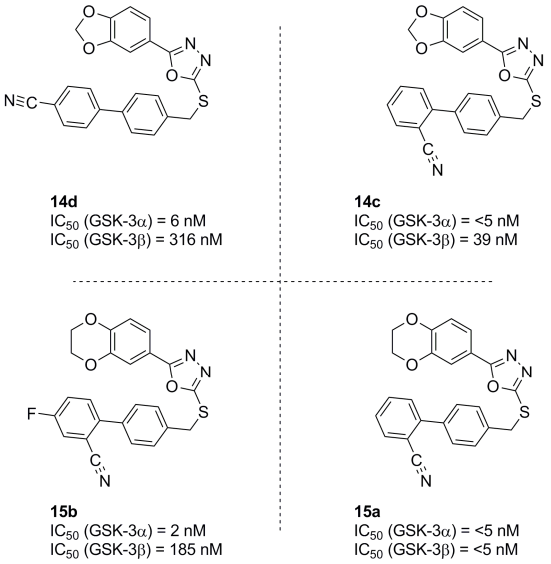

Abb. 29: Strukturformeln der Glykogen Synthase Kinase-3α Inhibitoren **14d** und **15b** sowie der weniger isoenzymspezifischen GSK-3-Inhibitoren **14c** und **15a**.

Im Anschluss wurden die GSK-3α-selektiven Inhibitoren **14d** und **15b** als auch die weniger GSK-3α selektiven Inhibitoren **14c** und **15a** auf ihre *in vivo* Aktivität in einem *zebrafish embryo phenotype assay* untersucht. Infolge der Applikation der Inhibitoren **14c** und **15a** ergaben sich phänotypische Veränderungen wie fehlende Augenpigmentierung und ein verkürztes bzw. gekrümmtes Rückgrat der Zebrafischembryos. Diese Beobachtungen gehen mit dem Einfluss von GSK-3β auf den WNT-Signalweg von Metazoan und den zuvor veröffentlichten Resultaten eines *zebrafish embryo phenotype assay* mit bekannten GSK-3-Inhibitoren wie **LiCl** und dem Rutheniumkomplex **(R)-7** einher.[309,310] Zudem belegt dies die Aufnahme und Zellpenetration von Biphenylderivaten. Die Ergebnisse des *zebrafish embryo phenotype assay* konnten mit den GSK-3α-spezifischen Inhibitoren **14d** und **15b**

nicht erzielt werden. Dies spricht entweder für eine verringerte Rolle von GSK-3α im WNT-Signalweg des Zebrafisches oder für eine verminderte Zellpenetration. Letzteres wird auch von einem von Cerep durchgeführten Bioverfügbarkeitsprofil von **14d** unterstützt. Wie auch immer, die letztgenannte These wiederspricht den Beobachtungen mit den strukturähnlichen und vergleichbar löslichen Inhibitoren **14c** und **15a**. Eine weitergehende Untersuchung der GSK-3α-spezifischen Inhibitoren **14d** und **15b** bezogen auf deren möglichen Einfluss auf den β-adrenergen Signalweg und somit auf den Herzrhythmus der Zebrafische ergab keinen Effekt. Dahingegen konnte durch die Applikation der GSK-3 Inhibitoren **14c** und **15a** auf stabil mit Tau.P301L transfizierten SH-SY5L-Neuroblastomzellen eine verringerte Phosphorylierung GSK-3-spezifischer Phosphorylierungsstellen am Tau-Protein festgestellt werden.

Es bleibt festzuhalten, dass mit den Oxadiazolbiphenylderivaten eine Substanzklasse synthetisiert werden konnte, die nicht nur *in vitro* und *in vivo* aktiv ist, sondern auch eine erstmalige Differenzierung der Isoenzyme GSK-3α und GSK-3β ermöglicht.

Journal of Medicinal Chemistry

Article

pubs.acs.org/jmc

Identification of Glycogen Synthase Kinase-3 Inhibitors with a Selective Sting for Glycogen Synthase Kinase-3α

Fabio Lo Monte,*[,†] Thomas Kramer,[†] Jiamin Gu,[†] Upendra Rao Anumala,[†] Luciana Marinelli,[‡] Valeria La Pietra,[‡] Ettore Novellino,[‡] Bénédicte Franco,[§] David Demedts,[§] Fred Van Leuven,[§] Ana Fuertes,[∥] Juan Manuel Dominguez,[∥] Batya Plotkin,[⊥] Hagit Eldar-Finkelman,[⊥] and Boris Schmidt*[,†]

[†]Clemens Schöpf—Institute of Organic Chemistry and Biochemistry, Technische Universität Darmstadt, 64287 Darmstadt, Germany

[‡]Dipartimento di Chimica Farmaceutica e Tossicologica, Università di Napoli "Federico II", 80131 Napoli, Italy

[§]Experimental Genetics Group, Department of Human Genetics, Katholieke Universiteit Leuven, 3000 Leuven, Belgium

[∥]Noscira SA, Drug Discovery, Tres Cantos 28760-Madrid, Spain

[⊥]Department of Human Molecular Genetics and Biochemistry, Sackler School of Medicine, Tel Aviv University, 69978 Tel Aviv, Israel

Supporting Information

ABSTRACT: The glycogen synthase kinase-3 (GSK-3) has been linked to the pathogenesis of colorectal cancer, diabetes, cardiovascular disease, acute myeloid leukemia (AML), and Alzheimer's disease (AD). The debate on the respective contributions of GSK-3α and GSK-3β to AD pathology and AML is ongoing. Thus, the identification of potent GSK-3α-selective inhibitors, endowed with favorable pharmacokinetic properties, may elucidate the effect of GSK-3α inhibition in AD and AML models. The analysis of all available crystallized GSK-3 structures provided a simplified scheme of the relevant hot spots responsible for ligand binding and potency. This resulted in the identification of novel scorpion shaped GSK-3 inhibitors. It is noteworthy, compounds **14d** and **15b** showed the highest GSK-3α selectivity reported so far. In addition, compound **14d** did not display significant inhibition of 48 out of 50 kinases in the test panel. The GSK-3 inhibitors were further profiled for efficacy and toxicity in the wild-type (wt) zebrafish embryo assay.

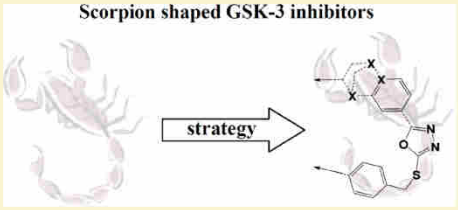

INTRODUCTION

Alzheimer's disease (AD), first described by Alois Alzheimer in 1906, is the most common dementia at old age. AD is characterized by the presence of two abnormal protein deposits: amyloid plaques composed of extracellular deposits of β-amyloid (Aβ) peptides and neurofibrillary tangles (NFTs) are formed by the accumulation of insoluble and hyperphosphorylated tau.[1−3] The 40−42 amino acid β-amyloid peptide is the major component of the amyloid deposits. It is produced from a larger protein, the amyloid precursor protein (APP), by proteolytic cleavage.[4] Tau is a soluble microtubule-binding protein which stabilizes the microtubules in axons.[2] Hyperphosphorylation of tau protein causes destabilization of microtubules and subsequent dissociation of tau, which in turn aggregates to form NFTs.[5] GSK-3 was identified ∼30 years ago and is a serine/threonine protein kinase that participates in a plethora of cellular processes, e.g., cell proliferation, microtubule dynamics, and gene transcription.[6−8] Several studies have linked glycogen synthase kinase-3 (GSK-3) to the primary abnormalities associated with AD, particularly the phosphorylation of tau.[4,9] Two closely related isoforms GSK-3α and GSK-3β are present in mammals.[10] They share 97% sequence similarity within their catalytic kinase domains.[7] GSK-3β has been proposed as the major kinase of tau phosphorylation, suggesting it as a potential, yet risky target for the therapy of AD.[1,5] Dysregulation of GSK-3β has been associated with diseases such as diabetes, Down's syndrome, bipolar disorder, colorectal cancer, and AD.[11] The inhibition of GSK-3α was suggested for the treatment of AD and other CNS diseases.[12−14] Furthermore, GSK-3α inhibition was proposed to modulate β-adrenergic signaling.[15] Recently, it was suggested that GSK-3α is involved in acute myeloid leukemia (AML), supporting a potential role for GSK-3α directed therapy.[16] Yet, the distinct contributions of both GSK-3 isoforms are still unknown. Appropriately, a number of pan-GSK-3α/β inhibitors have been disclosed because of the structure determination of GSK-3β.[17] Lithium chloride is the most thoroughly investigated GSK-3 inhibitor in AD animal models; it results in decreased tau hyperphosphorylation and decreased Aβ levels.[6] However, it is limited by a small therapeutic window. GSK-3 inhibitors were identified from remarkably different classes: organometallic compounds, paullones, indirubins, maleimides, thiadiazolidinones, L803-mts, ureas, and other small organic molecules.[4,10,18−24]

Received: March 5, 2012

dx.doi.org/10.1021/jm300309a | J. Med. Chem. XXXX, XXX, XXX−XXX

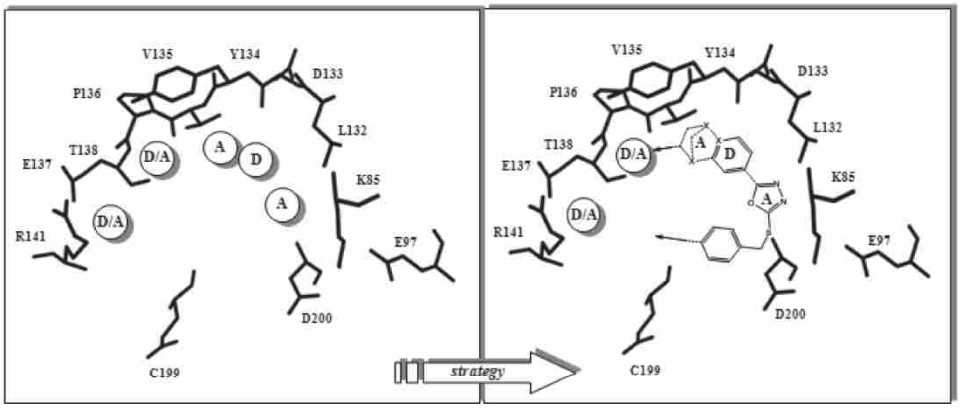

Figure 1. Synthesis strategy based on hot spot analysis of GSK-3 inhibition. The denoted acceptor (A) and donor (D) domains outline the necessary atoms respectively functional groups in the designated areas (left/right). The scaffold **I** used for the synthesis is marked on the right. X stands for heteroatoms.

Scheme 1[a]

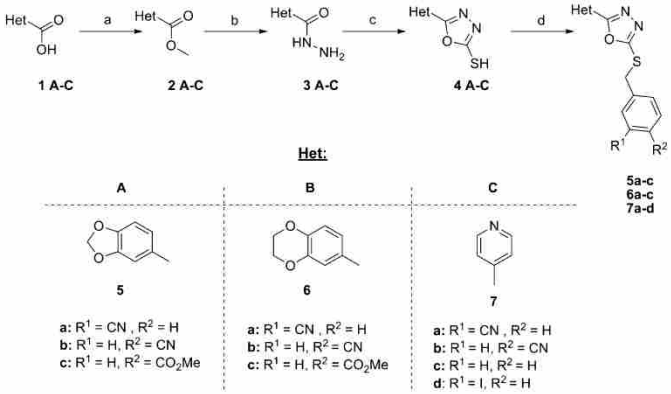

[a]Reagents and conditions: (a) MeOH, $SOCl_2$, 0−50 °C, 83−89%; (b) $NH_2NH_2{\cdot}H_2O$, EtOH, reflux, 67−75%; (c) CS_2, Et_3N, EtOH, reflux, 79−89%; (d) benzyl halides, 1N NaOH, DMF, rt, 41−84%.

All GSK-3 inhibitors, except for the thiadiazolidinones and L803-mts, are ATP competitive inhibitors and all of them inhibit the two isoforms, GSK-3α and GSK-3β, with similar potency.[6] The design of selective ligands remains a challenge despite several crystallized GSK-3 inhibitor complexes and substantial differences revealed by GSK-3α/GSK-3β sequence comparison as the major part of the ligand binding site is conserved.[17] Here we report the synthesis and optimization of novel GSK-3 inhibitors, along with their α/β selectivity and the evaluation of their in vivo efficacy in zebrafish embryos, which is an established model system for the validation of GSK-3 inhibitors. The oxadiazole moiety (scaffold **I**; Figure 1) was chosen as lead structure as it provided, if appropriately decorated, high inhibition of GSK-3β.[5,25,26]

The optimization process took advantage of the available cocrystallized GSK-3β inhibitor complexes and the analysis of the relevant hot spots (Figure 1). Most GSK-3 inhibitors occupy three or at most four acceptor/donor domains in the active site. Our main intention was the engagement with as many as possible acceptor/donor areas as depicted in Figure 1. Initially, we investigated the enlargement of **I** to reach R141. Subsequently, different substituents on the heterocyclic scaffold were explored in order to enhance the interaction with the enzyme backbone and to improve solubility at the same time. Most of the resulting compounds were tested for the selective inhibition of GSK-3α/β.

■ CHEMISTRY

The esterification of the carboxylic acids **1A−C** afforded the compounds **2A−C**,[27,28] which were converted to the hydrazides **3A−C**.[28,29] Reaction of the hydrazides **3A−C** with carbon disulfide (CS_2) resulted in the oxadiazoles **4A−C**.[30,31] The heterocyclic derivatives **5a−c**, **6a−c**, and **7a−c**[32] were prepared by benzylation of the mercaptanes **4A−C** (Scheme 1).[26]

dx.doi.org/10.1021/jm300309a | J. Med. Chem. XXXX, XXX, XXX−XXX

Scheme 2[a]

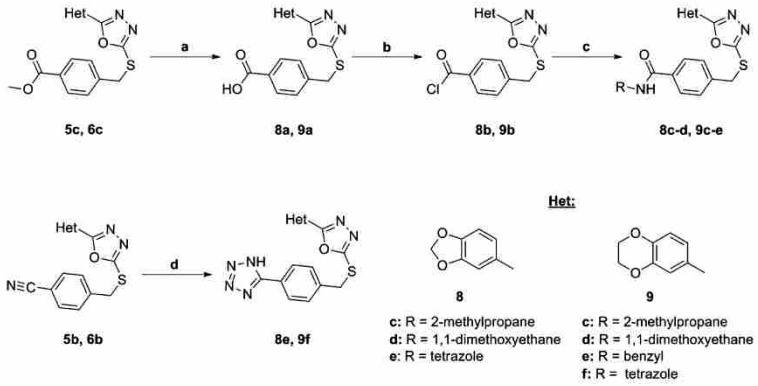

[a]Reagents and conditions: (a) 1N LiOH, THF, 60 °C, 83−91%; (b) $SOCl_2$, toluene, reflux; (c) amine, K_2CO_3, acetone, 0 °C to rt, 79−92%; (d) NaN_3, NH_4Cl, DMF, 100 °C, 67−79%.

Scheme 3[a]

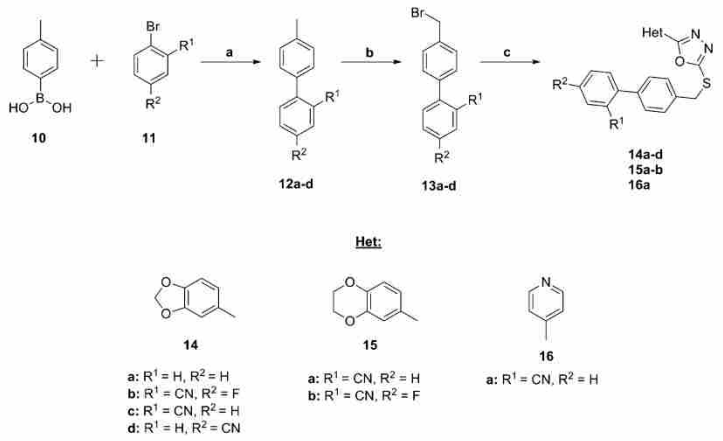

[a]Reagents and conditions: (a) aryl bromide, toluene, EtOH, $Pd(PPh_3)_4$, 2-tolylboronic acid, 2N Na_2CO_3 (aq), 80 °C; (b) NBS, AIBN, CCl_4, reflux; (c) **4**(**A**−**C**), 1N NaOH, DMF, rt, 53−75%.

Compound **7d** is commercially available. The esters **5c** and **6c** were converted to the carboxylic acids **8a** and **9a**, followed by treatment with thionyl chloride ($SOCl_2$) to form the acyl chlorides **8b** and **9b**.[33,34] Coupling of the acyl chlorides with primary amines gave the amides **8c−d** and **9c−e**.[34] The tetrazoles **8e** and **9f** were prepared from the nitriles **5b** and **6b** using sodium azide under microwave irradiation (Scheme 2).[35]

The biphenylic derivatives **13a−d** were prepared in two steps from the commercially available *p*-tolylboronic acid and substituted bromobenzenes. The 4′-(bromomethyl)biphenyl-2-carbonitrile is commercially available. The biphenylmethyl halides were coupled to the mercaptothiadiazoles **4A−C** to obtain the thioethers **14a−d**, **15a−b**, and **16a** (Scheme 3).[26] 3,4-Dihydroxybenzoic acid **17** was esterified to the methyl ester **18**, followed by cyclization with (±)-glycidyl tosylate or epibromohydrin to afford compound **19a**[36] as a mixture of enantiomers.[37−39] The hydrazide **21a** was prepared by methylation of **19a**, followed by the addition of hydrazine.[40] The reaction of the hydrazide **21a** with CS_2 gave the oxadiazole **22a**, which was coupled to 4′-(bromomethyl)biphenyl-2-carbonitrile to afford the thioether **23a**. The methyl ether in **23a** was cleaved by boron tribromide (BBr_3) to result in the alcohol **24a** (Scheme 4).[40] The compounds **23b−c** and **24a−b** were prepared under similar conditions; see Scheme 4. (*S*)-(+)-Glycidyl tosylate was used to obtain the *R*-enantiomer of compound **19b**.[37] The *S*-enantiomer of compound **19** was synthesized using (*R*)-(−)-glycidyl tosylate.[37] Mesylation of the alcohol **24b** and subsequent displacement of the mesylate by an amine afforded the acetal **26** (Scheme 4).[40]

dx.doi.org/10.1021/jm300309a | *J. Med. Chem.* XXXX, XXX, XXX−XXX

Scheme 4[a]

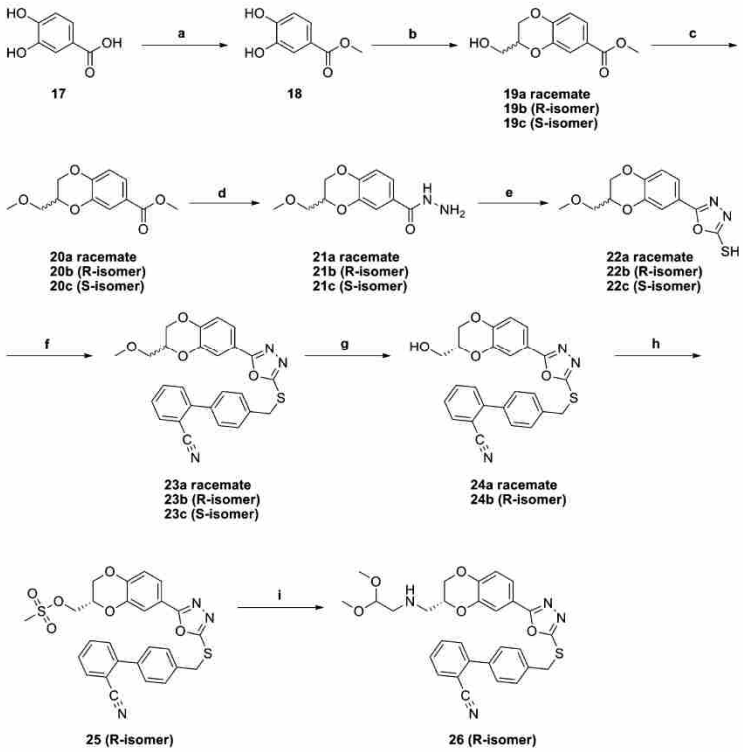

[a]Reagents and conditions: (a) $SOCl_2$, MeOH, 0−50 °C, 97%; (b) (*R*/*S*)-(±)-glycidyl tosylate or epibromohydrin, (*S*)-(+)-glycidyl tosylate or (*R*)-(−)-glycidyl tosylate, K_2CO_3, acetone or DMF, rt or 60 °C, 93−95%; (c) NaH, CH_3I, THF, 0 °C to rt, 68−71%; (d) $NH_2NH_2{\cdot}H_2O$, EtOH, reflux, 78−87%; (e) CS_2, Et_3N, EtOH, reflux, 81−91%; (f) biphenyl halide, 1N NaOH, DMF, rt, 84−88%; (g) BBr_3, DCM, −78 °C to rt; 73−79%; (h) CH_3SO_2Cl, Et_3N, DCM, 0 °C to rt, 98%; (i) amine, THF, Et_3N, 0 °C to reflux, 83%.

RESULTS AND DISCUSSION

Molecular Modeling. Compound **15a**, one of the most active inhibitors of the series, was docked, through Glide software, into the GSK-3β active site (PDB code: 3F88) with the aim to assess the ligand−protein interactions and to rationalize the SARs.[26] The docking experiments suggest that the oxadiazole ring positions itself in between the V70 and C199 side chains with one of the two nitrogens establishing an H-bond with the K85 side chain (Figure 2). The biphenyl branch forms a T-shaped interaction with P67 and hydrophobic contacts with the Q185 and Y140 carbons.[41] Furthermore, as shown in Figure 2, the CN substituent forms an H-bond with the T138 hydroxyl group. The latter interaction seems to improve the activity of our ligands, in fact, for example, **14c** is more active against GSK-3β than its analogue **14a**, which lacks the cyano group, and its analogue **14d**, equipped with the cyano group at the R2 site. As regards the **15a** binding mode, the dihydrobenzodioxine moiety establishes several hydrophobic interactions with L132, I62, A83, V110, and L188.

Moreover, one of the two oxygens of the dihydrodioxine ring forms an H-bond with the V135 NH in the hinge region, while

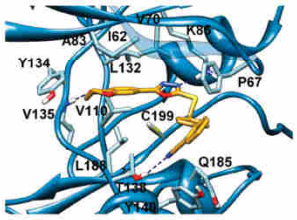

Figure 2. Molecular docking of compound **15a** into the X-ray structure of GSK-3β (PDB code: 3F88). This figure was prepared with Glide software.

the rest of the ring establishes hydrophobic contacts with the Y134. The latter interaction seems to be lost by **14c**, featuring the smaller benzodioxolane ring, while **16a**, a pyridine containing compound, forms a weaker H-bond with the same residue due to the position and the distance of the nitrogen atom of the pyridine ring from the NH of V135. The substitutions on the dihydrobenzodioxine moiety of **23** and **24**,

dx.doi.org/10.1021/jm300309a | J. Med. Chem. XXXX, XXX, XXX−XXX

respectively, do not provide any further interaction with the enzyme, as the groups point out into the solvent. The same holds true for **26**, where the bulky substituent on the dihydrobenzodioxine ring may negatively affect the horseshoe shape (scorpion shape). The proposed binding mode also clarifies the undesirable effect of the substitution of the fluorine atom at the R2 site of the biphenyl branch in **15b**, which is 37-fold less potent for GSK-3β in comparison to **15a**. In fact, the electron-withdrawing atom weakens the H-bond between the cyano substituent and the T138 hydroxyl group; moreover, it comes in proximity of the negative ring density of Y140, providing repulsive edgewise interaction. The good selectivity toward GSK-3α versus GSK-3β which was observed for several compounds and especially for compound **15b**, is far to be trivial to explain. The superposition of the GSK-3β crystallographic structure (PDB code: 3F88) with a homology model built with Prime software (Schrodinger) shows that the differences between the two isoforms are all located out of the binding site and especially in the loop at C-terminus fragment (see the Supporting Information). Thus, it is conceivable that the selectivity of our compounds may be due to subtle enzyme differences, which may affect the ligand entrance/exit processes. This process may include an antechamber site, a step known to play a pivotal role in the inhibitor/enzyme recognition process.[42,43] By analyzing the enzyme surface and the residue mutations, the antechamber site in the GSK-3α or GSK-3β could be represented by the loop at C-terminus fragment as highlighted in Figure S1 in the Supporting Information. Obviously, the latter is a pure speculative hypothesis that has to be confirmed by more advanced theoretical work, mutational analysis, and additional experiments.

Biological Assays and Structure−Activity Relationship (SAR) Studies. The synthesized compounds were tested for their inhibitory activity against GSK-3β in an in house in vitro assay and further profiled in a commercial system based on the Z'-LYTE technology, available from Invitrogen Life Technologies (Carlsbad, CA, USA), using human recombinant GSK-3α or GSK-3β as the enzyme source. Most compounds displayed significant inhibitory activity against GSK-3β at 10 μM, and several compounds exerted more than 50% inhibitory activity against GSK-3β at the initial concentration (10 μM). The potent compounds were selected for IC_{50} determination. We observed differences in the IC_{50} determination between the in-house and the commercial assay and decided to use the results of the commercial system for comparison.

The structure−activity analysis suggested interactions with the GSK-3 backbone, Y134/D133, and the polar binding pocket, K85/E97/D200, to be essential for potent inhibition. These interactions require an acceptor−donor−acceptor motif on the inhibitor. We generated a simplified illustration in which we denoted acceptor (A) and donor (D) domains and drafted scaffold **I** as lead structure (Figure 1). We examined the effect of three heterocycles **5**−**7** as potential hinge binders and different substituents on the *S*-benzyl group (Scheme 1). The oxadiazole derivatives of the heterocycles **5** and **6** provided several GSK-3 inhibitors with an IC_{50} below 100 nM (Table 1) and confirmed previously reported activity.[26] The pyridines **7a**−**c** displayed decreased activity in comparison to the heterocycles **5** and **6**; this may be due to the position of the pyridine moiety in the ATP binding pocket. Thus, they were not pursued further. The compounds **5a** and **6a** indicated that an electron-withdrawing group is required at the 3-position. We introduced the cyano and ester group at the 4-position in order to reach out to R141 and the correlated acceptor/donor domain and thus to engage the ATP binding pocket in its entirety. Our data indicated that the electron-withdrawing group at the 3-position was also tolerated at the 4-position. The oxadiazoles **5b** and **6b**−**c** showed comparable activity to the 3-substituted derivatives and indicated space in the ATP binding pocket. On the basis of these results, we further examined the para-position of our lead structure. The carboxylic acids **8a** and **9a** resulted in a 4-fold less inhibitory activity against GSK-3β at 10 μM concentration compared to their esters **5c** and **6c** (Scheme 2). In the case of **5c**, the percentage of GSK-3β activity increased from 17% of up to 81% (Table 2). In addition, compound **8e**, bearing a hydrophilic tetrazole at the 4-position (IC_{50} value of 107 nM for GSK-3α and 172 nM for GSK-3β), showed decreased inhibitory activity compared to the ester **6c** (Scheme 2). Conversion of the carboxylic acids to the amides **8c**−**d** and **9c**−**e** resulted in an increased activity. Especially, compound **8c** showed good inhibitory property against GSK-3β with a remaining kinase activity of 9% at 10 μM (Table 2). These results and the molecular modeling suggested that compounds containing polar groups at the 4-position were less active than compounds containing hydrophobic groups. Hence, we tried to elongate our compounds with a phenyl ring at the 4-position. Compounds bearing a phenyl group in the para-position showed very good inhibitory activity. The docking analysis of the biphenylic derivatives suggested several hydrophobic contacts, which may be responsible for the enhanced potency. Especially, compound **15a** with an IC_{50} value of <5 nM for GSK-3α and GSK-3β was found to be a potent inhibitor of GSK-3 (Table 3). Slightly decreased activity was observed for compound **14a** with an IC_{50} value of 9 nM for GSK-3α and 176 nM for GSK-3β. We observed an IC_{50} of 2 nM for GSK-3α and 22 nM for GSK-3β for structure **14b**, whereas **14c**, which lacks the fluorine substituent, resulted in slightly decreased IC_{50} values in comparison to **14b**.

The selectivity for the GSK-3α isoform was higher when the substituents were absent in the series **14a**−**c**. The absence of selectivity for GSK-3α in **15a** in comparison with **14c** may be explained by the interaction with Y134 (see Molecular Modeling), which seems to be lost in **14c**. Remarkably, compound **14d** displayed up to 52-fold selectivity in the inhibition of GSK-3α versus GSK-3β. This selectivity was even enhanced with compound **15b**, which is characterized by an IC_{50} of 2 nM for GSK-3α and 185 nM for GSK-3β. Thus, only the interplay respectively of a combination of different substituents was adequate to gain selectivity against one GSK-3 isoform. This observation will be helpful if a discrimination of one GSK-3 isoform is needed. In addition, the physiological functions and pathological roles of GSK-3α can be addressed in vitro and eventually in vivo with these tools. The biphenyl derivative **16a** from the pyridine series showed remarkably increased activity in comparison to the used reference **7d**, 20-fold for GSK-3α, and 19-fold for GSK-3β (Table 1). The effect of the second phenyl suggested an interaction with the glycine-rich loop, such an interaction was reported to have significant effects on binding potency and selectivity recently.[41] Furthermore, the SAR and molecular modeling suggested that an electron-withdrawing group in the ortho position of the second phenyl ring, such as the cyano-group, contributes to the inhibitory activity by interaction with the amino acid T138. We examined different linker systems on the dihydrobenzodioxine moiety with the aim to enhance the interaction with the backbone. Unfortunately, they do not provide any further

Table 1. Inhibitory Activity against GSK-3α and GSK-3β, IC_{50} (μM)

Compound	GSK-3α	GSK-3β	Compound	GSK-3α	GSK-3β
5a	0.015	0.065	**7a**	3.206	3.162
5b	0.015	0.130	**7b**	7.379	10.0
6a	0.095	0.086	**7c**	2.244	1.318
6b	0.045	0.166	**7d**	0.390	0.790
6c	0.012	0.036	**8e**	0.107	0.172

interaction (see Molecular Modeling). The effect of the methoxy group on compound **23a** resulted in an IC_{50} value of 54 nM for GSK-3α and 233 nM for GSK-3β, respectively, 195 nM and 758 nM for compound **23b**. In the case of **23c**, good inhibitory activity was observed against both isoforms of GSK-3, especially for GSK-3α. These results suggest that the *R*-enantiomer **23b** is the distomer of this compound, whereas the *S*-enantiomer **23c** was found to be the eutomer. Despite our expectations that an amine may improve the activity, compound **26** showed markedly reduced potency.

The potent GSK-3 inhibitors **6c**, **14a–d**, **15a–b**, **16a**, and **23a–c** were selected for selectivity profiling and tested against four structurally related protein kinases (Cdk5/p35, CK1ε, AurKA, and PKCα).

Good selectivity was obtained for all compounds tested. Particularly, the biphenyl derivatives **14c**, **15a**, and **16a** showed more than 2000-fold selectivity against these kinases (Table 4). Compound **14d** was not just GSK-3α selective, it was even more selective over the other kinases than compound **15b**. The broader selectivity of compound **14d** was screened at a concentration of 1 μM against 50 human protein kinases (Figure 3); 48 out of the 50 kinases in this panel showed an activity higher than 80%, whereas GSK-3α displayed a residual activity of 5% only. The only kinase which was also significantly inhibited by this compound was GSK-3β with a remaining activity of 27.2%. Therefore, it can be concluded that, within the test panel, compound **14d** is a selective inhibitor of GSK-3α. A bioavailability profile of compound **14d** was evaluated,

dx.doi.org/10.1021/jm300309a | J. Med. Chem. XXXX, XXX, XXX–XXX

Table 2. Inhibitory Activity against GSK-3β at 10 μM

Compound	GSK-3β activity in %	Compound	GSK-3β activity in %	Compound	GSK-3β activity in %
5c	17	**8c**	9	**9c**	37
6c	21	**8d**	31	**9d**	65
8a	81	**9a**	102	**9e**	71

and the results are shown in the Supporting Information. **14d** possesses a log *D* value of 3.58 and moderate metabolic stability. Nevertheless, the poor aqueous solubility and permeability are adverse properties which limit the potential use of the compound.

The biphenyl derivatives **14c–d**, **15a–b**, and **16a** were further tested for their in vivo activity on wild-type zebrafish embryos. We exposed the embryos to these compounds at early stages of development. The embryos were collected and maintained in E2 medium at ~28 °C. The compounds were added 5 h post fertilization (hpf), and the phenotypes compared at 44–48 hpf. Compound **14c** causes the eyeless phenotype at 0.5 μM and a stunted and crooked tail at 1 μM. Similar phenotypes were obtained for compound **15a** at 2.5 μM and for compound **16a** at 20 μM (Figure 4). This correlates with the observation that Wnt signaling, and thus GSK-3β plays a crucial role in the development of metazoan and that known GSK-3 inhibitors like LiCl and the ruthenium complex (*R*)-7 perturb the zebrafish development.[44,45] The zebrafish embryo assay provides evidence of exposure and cell penetration of the biphenyl derivatives, especially for compound **14c**. Interestingly, compounds **14d** and **15b** showed no effect on wild-type zebrafish embryos, suggesting that GSK-3α plays a minor role in the zebrafish Wnt signaling pathway. The lack of response in the zebrafish assay by compounds **14d** and **15b** may be explained by poor cell permeability. However, the structurally analogues compounds **14c** and **15a**, which are characterized by comparable solubility, did result in a GSK-3β-phenotype. Thus, the comparison of these compounds **14c**/**15a** and **14d**/**15b** does not support poor exposure and cell penetration as the dominant factors on the in vivo assay of the α-selective inhibitors. The inhibition of GSK-3α was proposed to regulate β-adrenergic signaling in mice, thus we monitored the heart development of the zebrafish embryo after administration of compound **14d** until day 5 (see the Supporting Information).[15,46] However, no effect was observed until the fifth day of development. All compounds displayed no lethality in our concentration range (<30 μM).

SH-SY5Y neuroblastoma cells stably transfected with Tau.P301L were incubated with increasing concentrations of compounds **14c** and **15a** (0, 30, and 100 μM) for 6 and 24 h. Cells were analyzed for total protein tau by Western blotting with antibody Tau5, directed against nonphosphorylated protein tau. In addition, the same samples were probed with a selection of phospho-specific antibodies that recognize typical GSK-3 dependent epitopes on protein tau. Moreover, the electrophoretic mobility of protein tau is a reliable index of the degree of phosphorylation of protein Tau.P301L: the lesser mobile isoforms carry the most phosphate groups (Figure 5).

Both compounds dose- and time-dependently decreased the phosphorylation of protein tau, expressed relatively to total tau, as demonstrated by the decreased immunoreaction with antibodies pS199, pT231, pS396, and pS404 in Western blotting (Figure 5). Moreover, the marked increase in electrophoretic mobility of the various phospho-isoforms of protein tau induced by treatment of the stably transfected SH-SY5Y cells corroborates their effectiveness in preventing phosphorylation on typical GSK-3 dependent epitopes. The comparison of the biphenyl derivatives indicated that compound **14c** is more effective in preventing phosphorylation than compound **15a**.

dx.doi.org/10.1021/jm300309a | *J. Med. Chem.* XXXX, XXX, XXX–XXX

Table 3. Inhibitory Activity of the Biphenyls against GSK-3α and GSK-3β, IC_{50} (μM)

Compound	GSK-3α	GSK-3β	Compound	GSK-3α	GSK-3β
14a	0.009	0.176	**15b**	0.002	0.185
14b	0.002	0.022	**16a**	0.019	0.041
14c	< 0.005	0.039	**23a**	0.054	0.233
14d	0.006	0.316	**23b**	0.195	0.758
15a	< 0.005	< 0.005	**23c**	0.015	0.129

This correlates with the observations made in the zebrafish embryo assay in which **14c** showed the best results.

CONCLUSION

On the basis of a simplified scheme of known and important interactions of GSK-3 inhibitors with the ATP binding pocket, we generated hypotheses for improved interaction of with this site. These hypotheses were challenged by three series of structurally closely related inhibitors which are all based on a central oxadiazole moiety. An appropriate decoration resulted in a more extended occupation of the ATP binding site. The most potent inhibitors displayed IC_{50} values in the low nanomolar range and good kinase selectivity versus four closely related kinases. Several inhibitors showed reported phenotypes in the zebrafish embryo assay without lethality at 30 μM. In addition, two inhibitors decreased the phosphorylation of tau protein in SH-SY5Y cells. The docking analysis of the potent inhibitors suggested an interaction with the glycine-rich loop, which was reported to have significant effects on the binding potency and selectivity by Li Feng et al.[41] To our knowledge, the selective inhibition of GSK-3α versus GSK-3β by the compounds **14d** and **15b** is the highest reported so far. In addition, compound **14d** did not show any strong inhibition for 48 out of 50 kinases. The contribution of GSK-3α and GSK-3β to the pathology of Alzheimer's disease is still subject of an ongoing debate.[47,48] Thus, these compounds may be useful tools and starting points for the synthesis of GSK-3α selective inhibitors with enhanced pharmacokinetic properties.

dx.doi.org/10.1021/jm300309a | J. Med. Chem. XXXX, XXX, XXX–XXX

Table 4. Kinase Selectivity of Several Derivatives

	IC_{50} (μM)					
compd	GSK-3α	GSK-3β	Cdk5/p35	CK1ε	AurKA	PKCα
6c	0.012	0.036	>100	>100	>100	>100
14a	0.009	0.176	>100	>100	>100	>100
14b	0.003	0.022	>100	20	30	>100
14c	<0.005	0.039	>100	>100	>100	>100
14d	0.006	0.316	>100	60	30	>100
15a	<0.005	<0.005	>100	>100	>100	>100
15b	0.002	0.185	>100	>100	5	>100
16a	0.019	0.041	>100	>100	>100	>100
23a	0.054	0.233	>100	>100	30	>100
23b	0.195	0.758	>100	>100	>100	>100
23c	0.015	0.129	>100	>100	>100	>100

EXPERIMENTAL SECTION

General Information. All reactions using anhydrous conditions were carried out under argon atmosphere with dry solvents unless otherwise noted. All commercial chemicals were used without further purification. The ^{1}H NMR spectra were recorded on a Bruker AC 300 spectrometer at 300 MHz and Bruker AC 500 spectrometer at 500 MHz. The ^{13}C NMR spectra were recorded on a Bruker AC 300 spectrometer at 75 MHz and Bruker AC 500 spectrometer at 125 MHz. Chemical shifts are reported as ppm downfield from Me_4Si. Abbreviations used to explain the multiplicities: s = singlet, d = doublet, t = triplet, q = quartet, n = nonett, m = multiplet, br = broad. Coupling constants (J values) are given in hertz (Hz). Mass spectrometry was performed on a Bruker−Franzen Esquire LC mass spectrometer and a MAT 95 double focusing sector field MS. Microwave experiments were carried out using a Biotage Initiator microwave apparatus. All microwave experiments were carried out in sealed microwave process vials utilizing the standard absorbance level (300 W maximum power). High performance liquid chromatographies (HPLC) were carried out on an Agilent 1100 (column: reversed phase, Zorbax Eclipse XDB-C18, 4.6 mm × 150 mm; 254 nm). Solvent gradient = 90% A at 0 min, 30% A at 2 min, 10% A at 5 min; solvent A = 0.1% trifluoroacetic acid in water; solvent B = acetonitrile; flow rate 1.0 mL/min; temperature 35 °C. Flash column chromatography was carried out using Merck silica gel 60 (40−63 and 15−40 μm) and 60G (5−40 μm). Thin-layer chromatography (TLC) was carried out using aluminum sheets precoated with silica gel 60 F254 (0.2 mm; E. Merck). All compounds that were evaluated in biological assays had >95% purity using the HPLC method described above.

General Procedure A: Coupling of Aromatic Rings by a Suzuki Reaction (12a−d).[49] To a solution of the aryl bromide **11** (5 mmol) in 15 mL of toluene/EtOH (1/1) was added 0.17 g (0.14 mmol) of $Pd(PPh_3)_4$, and the mixture was stirred under argon atmosphere. Then 2 N aqueous Na_2CO_3 (7.5 mL) and 0.80 g (6 mmol) of 2-tolylboronic acid **10** were added. The mixture was refluxed at 80 °C for 1−2 days until reaction was completed (TLC). After cooling to room temperature, the product was diluted with water and extracted with EtOAc. The organic layers were dried with $MgSO_4$, filtered, and concentrated. Purification was performed by column chromatography using a mixture of cyclohexane/EtOAc.

General Procedure B: Bromination at the Benzylic Position (13a−d).[49] To a stirred solution of the appropriately substituted toluene in CCl_4 (10 mL per mmol) were added 0.95 equiv of NBS and AIBN (5 mg per mmol). The reaction mixture was refluxed at 80 °C for about 40 h and then cooled to room temperature. The product was diluted with water and extracted with EtOAc. The organic layers were dried with $MgSO_4$, filtered, and concentrated. Purification was performed by column chromatography using a mixture of cyclohexane/EtOAc.

Methyl Benzo[*d*][1,3]dioxole-5-carboxylate (2A). To a stirred solution of benzo[*d*][1,3]dioxole-5-carboxylic acid (1.66 g, 10 mmol) in MeOH (20 mL) was added $SOCl_2$ (1.45 mL, 20 mmol) dropwise over 1 h at 0 °C. The mixture solution was further stirred 12 h at 50 °C. The mixture was cooled to room temperature and diluted with water (25 mL). MeOH was evaporated and the pH adjusted to ~6 with aqueous $NaHCO_3$. The mixture was extracted three times

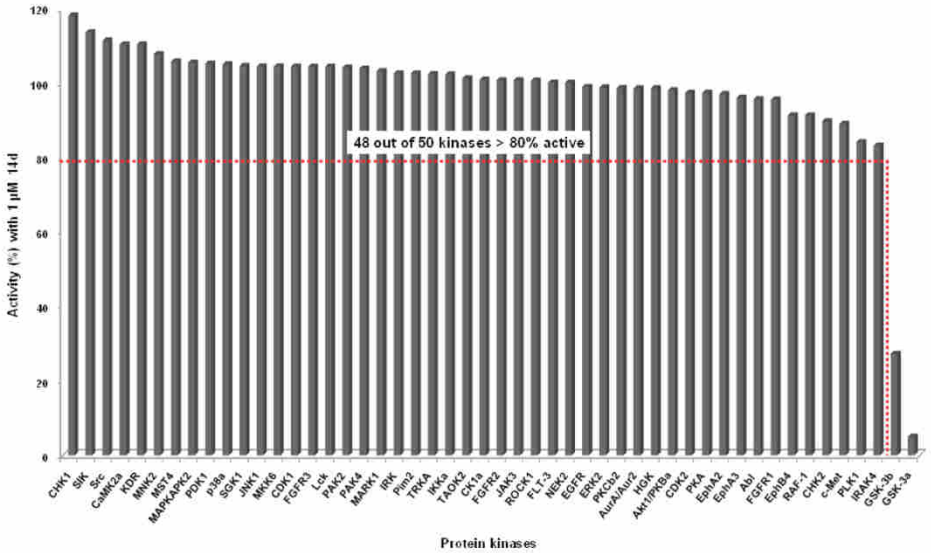

Figure 3. Screening of compound **14d** against a panel of human protein kinases. Each bar represents the activity of one individual protein kinase. Compound **14d** was tested at a concentration of 1 μM against 50 protein kinases. See Supporting Information for more details.

dx.doi.org/10.1021/jm300309a | *J. Med. Chem.* XXXX, XXX, XXX−XXX

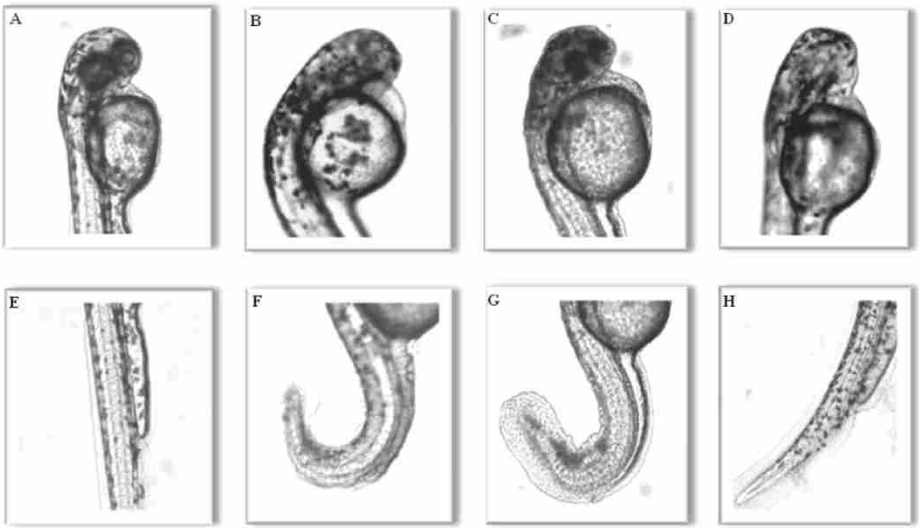

Figure 4. Effects on wild-type zebrafish embryos by compounds **14c**, **15a**, and **16a**. The embryos were collected and maintained in E2 medium at ~28 °C, compounds were added 5 hpf, and the phenotypes were compared at 44−48 hpf. (A,E) Head and tail of control embryos: DMSO (2%). (B,F) Head and tail of embryos treated with **14c**. This compound causes the eyeless phenotype at 0.5 μM and a stunted and crooked tail at 1.0 μM. (C,G) Head and tail of embryos treated with **15a**. A fluffy eye pigmentation and a stunted and crooked tail were observed at 2.5 μM. (D,H) Head and tail of embryos treated with **16a**. This compound causes the eyeless phenotype and a crooked tail at 20 μM.

with EtOAc and successively washed with brine. The organic layer was dried over $MgSO_4$ and concentrated under reduced pressure to give **2A** (1.6 g, 89%) as a colorless solid. ^{1}H NMR (DMSO-d_6, 500 MHz): δ [ppm] = 3.81 (3H, s), 6.14 (2H, s), 7.03 (1H, d, J = 8.1 Hz), 7.38 (1H, d, J = 1.7 Hz), 7.57 (1H, dd, J = 8.1 Hz, J = 1.7 Hz). ^{13}C NMR (DMSO-d_6, 125 MHz): δ [ppm] = 52.0, 102.1, 108.2, 108.5, 123.4, 125.0, 147.6, 151.4, 165.6. EI-MS: m/z = 180 (M^+).

The following compound **2B** was prepared in a similar manner to that described for **2A**.

Methyl 2,3-Dihydrobenzo[*b*][1,4]dioxine-6-carboxylate (2B). Yield 83%, colorless solid. ^{1}H NMR (DMSO-d_6, 500 MHz): δ [ppm] = 3.80 (3H, s), 4.19 (2H, m), 4.23 (2H, m), 6.80 (1H, m), 7.47 (2H, m). ^{13}C NMR (DMSO-d_6, 125 MHz): δ [ppm] = 50.5, 62.7, 63.2, 115.7, 117.6, 122.0, 141.7, 146.4, 165.2. EI-MS: m/z 194 (M^+).

Benzo[*d*][1,3]dioxole-5-carbohydrazide (3A). To a solution of **2A** (1.08 g, 6.0 mmol) in EtOH (30 mL) was added hydrazine hydrate (2.91 mL, 60 mmol), and the mixture was heated at reflux for 2 days. After cooling to room temperature, pure crystals are formed, collected by filtration, and washed several times with EtOH to give compound **3A** (0.72 g, 67%) as a colorless solid. ^{1}H NMR (DMSO-d_6, 500 MHz): δ [ppm] = 4.42 (2H, s), 6.07 (2H, s), 6.96 (1H, d, J = 8.1 Hz), 7.35 (1H, d, J = 1.7 Hz), 7.42 (1H, dd, J = 8.1 Hz, J = 1.7 Hz), 9.59 (1H, s). ^{13}C NMR (DMSO-d_6, 125 MHz): δ [ppm] = 101.5, 106.9, 107.8, 121.8, 127.2, 147.2, 149.5, 165.2. EI-MS: m/z = 180 (M^+).

Compound **3B** was prepared in a similar manner to that described for **3A**.

2,3-Dihydrobenzo[*b*][1,4]dioxine-6-carbohydrazide (3B). Yield 75%, light-yellow solid. ^{1}H NMR (methanol-d_4, 500 MHz): δ [ppm] = 4.28 (2H, m), 4.30 (2H, m), 6.89 (1H, d, J = 8.3 Hz), 7.30 (1H, dd, J = 8.3 Hz, J = 2.1 Hz), 7.33 (1H, d, J = 2.1 Hz), NH signals were not observed. ^{13}C NMR (methanol-d_4, 125 MHz): δ [ppm] = 65.9, 66.3, 117.9, 118.6, 121.9, 127.5, 145.2, 148.6, 169.6. EI-MS: m/z 194 (M^+).

5-(Benzo[*d*][1,3]dioxol-5-yl)-1,3,4-oxadiazole-2-thiol (4A). To a solution of **3A** (535 mg, 3.00 mmol) in EtOH (5 mL) were added carbon disulfide (397 μL, 6.60 mmol) and NEt_3 (469 μL, 3.30 mmol), and the mixture was heated at reflux overnight. The reaction mixture was diluted with EtOAc, and the organic layer was washed with 0.1 N HCl and brine and dried over Na_2SO_4. The solvent was evaporated under reduced pressure, and the obtained residue was recrystallized from cyclohexane/EtOAc to give **4A** (521 mg, 79%) as a pale-yellow solid. ^{1}H NMR (DMSO-d_6, 500 MHz): δ [ppm] = 6.14 (2H, s), 7.10 (1H, d, J = 8.1 Hz), 7.33 (1H, d, J = 1.6 Hz), 7.42 (1H, dd, J = 8.1 Hz, J = 1.6 Hz), SH signal was not observed. ^{13}C NMR (DMSO-d_6, 125 MHz): δ [ppm] = 102.1, 105.6, 109.1, 116.1, 121.5, 148.1, 150.6, 160.3, 177.2. EI-MS: m/z = 222 (M^+).

The compounds **4B**−**C** were prepared in a similar manner to that described for **4A**.

5-(2,3-Dihydrobenzo[*b*][1,4]dioxin-6-yl)-1,3,4-oxadiazole-2-thiol (4B). Yield 89%, light-brown solid. ^{1}H NMR (DMSO-d_6, 500 MHz): δ [ppm] = 4.32 (2H, m), 4.34 (2H, m), 7.05 (1H, d, J = 8.4 Hz), 7.30 (1H, d, J = 2.0 Hz), 7.36 (1H, dd, J = 8.4 Hz, J = 2.0 Hz), SH signal was not observed. ^{13}C NMR (DMSO-d_6, 125 MHz): δ [ppm] = 64.4, 64.8, 115.0, 115.7, 118.6, 120.0, 144.2, 147.3, 160.6, 177.6. EI-MS: m/z = 236 (M^+).

5-(Pyridin-4-yl)-1,3,4-oxadiazole-2-thiol (4C). Yield 83%, yellow solid. ^{1}H NMR (DMSO-d_6, 500 MHz): δ [ppm] = 7.81 (2H, dd, J = 4.4 Hz, J = 1.6 Hz), 8.81 (2H, dd, J = 4.4 Hz, J = 1.6 Hz), SH signal was not observed. ^{13}C NMR (DMSO-d_6, 125 MHz): δ [ppm] = 119.6, 129.7, 150.8, 158.7, 177.8. EI-MS: m/z = 179 (M^+).

3-((5-Benzo[*d*][1,3]dioxol-5-yl)-1,3,4-oxadiazol-2-ylthio)-methyl)benzonitrile (5a). To a solution of **4A** (55 mg, 0.25 mmol) and 1 N NaOH (0.25 mL, 0.25 mmol) in DMF (1 mL) was added 1-(bromomethyl)-3-methoxybenzene (75 mg, 0.38 mmol) at room temperature, and the mixture was stirred for 5 h. The precipitate formed was collected by filtration and washed once with less DMF (~1 mL) and thereafter several times with EtOH to give compound **5a** (55 mg, 64%) as a brown solid. ^{1}H NMR (DMSO-d_6, 500 MHz): δ [ppm] = 4.61 (2H, s), 6.16 (2H, s), 7.10 (1H, d, J = 8.1 Hz), 7.41 (1H, d, J = 1.4 Hz), 7.47 (1H, dd, J = 8.1 Hz, J = 1.5 Hz), 7.57 (1H, t,

dx.doi.org/10.1021/jm300309a | J. Med. Chem. XXXX, XXX, XXX−XXX

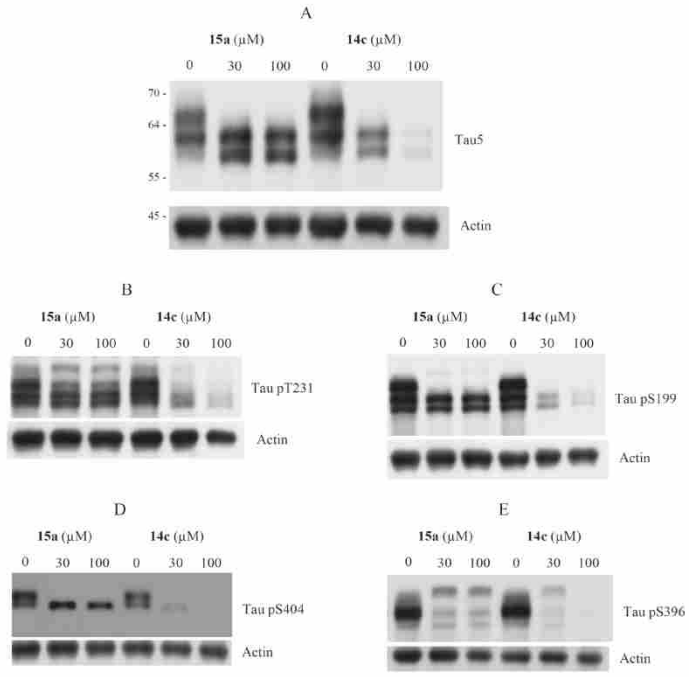

Figure 5. Western blotting for protein Tau.P301L expressed in stably transfected SH-SY5Y neuorblastoma cells, untreated (lanes marked 0) or treated for 6 h with compounds **14c** or **15a** (lanes marked 30 and 100 μM). Total protein tau was detected with antibody Tau5 (A). Phospho-epitopes on protein tau were detected with specific antibodies (B–E). Experiments were performed in triplicate, and representative blots are shown. Similar observations were obtained after 24 h of incubation. Note that compound **14c** specifically decreases the total concentration of protein tau, while levels of the internal marker (actin) remain unchanged.

J = 7.7 Hz), 7.76 (1H, d, J = 7.7 Hz), 7.84 (1H, d, J = 7.8 Hz), 7.96 (1H, s). ^{13}C NMR (DMSO-d_6, 125 MHz): δ [ppm] = 34.7, 102.1, 106.1, 109.1, 111.4, 116.6, 118.5, 121.7, 129.8, 131.4, 132.6, 133.9, 138.8, 148.1, 150.4, 162.2, 165.2. HPLC: 98%; t_R 7.21 min. EI-MS: m/z = 337 (M^+).

The compounds **5b–c**, **6a–c**, and **7a–c** were prepared in a similar manner to that described for **5a**. Note: Compounds which did not precipitate in solution were purified as follows. The reaction mixture was diluted with EtOAc and the organic layer was washed with water and brine, dried over $MgSO_4$, and concentrated in vacuo. The residue was purified by silica gel column chromatography (cyclohexane/EtOAc).

4-((5-Benzo[*d*][1,3]dioxol-5-yl)-1,3,4-oxadiazol-2-ylthio)-methyl)benzonitrile (5b). Yield 67%, brown solid. ^{1}H NMR (DMSO-d_6, 500 MHz): δ [ppm] = 4.64 (2H, s), 6.16 (2H, s), 7.11 (1H, d, J = 8.1 Hz), 7.42 (1H, d, J = 1.6 Hz), 7.48 (1H, dd, J = 8.1 Hz, J = 1.7 Hz) 7.68 (2H, d, J = 8.3 Hz), 7.82 (2H, d, J = 8.3 Hz). ^{13}C NMR (DMSO-d_6, 125 MHz): δ [ppm] = 35.2, 102.1, 106.1, 109.1, 110.4, 116.5, 118.6, 121.7, 130.0, 132.4, 142.8, 148.1, 150.5, 162.2, 165.2. HPLC: 95%; t_R 7.09 min. EI-MS: m/z = 337 (M^+).

Methyl 4-((5-(Benzo[*d*][1,3]dioxol-5-yl)-1,3,4-oxadiazol-2-ylthio)methyl Benzoate (5c). Yield 71%, pale-brown solid. ^{1}H NMR (DMSO-d_6, 500 MHz): δ [ppm] = 3.82 (3H, s), 4.63 (2H, s), 6.15 (2H, s), 7.10 (1H, d, J = 8.1 Hz), 7.41 (1H, d, J = 1.7 Hz), 7.48 (1H, dd, J = 8.1 Hz, J = 1.7 Hz), 7.62 (2H, d, J = 8.4 Hz), 7.92 (2H, d, J = 8.4 Hz). ^{13}C NMR (DMSO-d_6, 125 MHz): δ [ppm] = 35.4, 52.2, 102.2, 106.1, 109.2, 116.6, 121.7, 128.8, 129.4, 142.4, 148.1, 150.4, 162.3, 165.1, 165.9. HPLC: 96%; t_R 7.61 min. EI-MS: m/z = 370 (M^+).

3-((5-(2,3-Dihydrobenzo[*b*][1,4]dioxin-6-yl)-1,3,4-oxadiazol-2ylthio)methyl)benzonitrile (6a). Yield 73%, light-brown solid. ^{1}H NMR (DMSO-d_6, 500 MHz): δ [ppm] = 4.31 (2H, m), 4.34 (2H, m), 4.61 (2H, s), 7.05 (1H, d, J = 8.4 Hz), 7.39 (1H, d, J = 2.0 Hz), 7.42 (1H, dd, J = 8.4 Hz, J = 2.1 Hz), 7.57 (1H, t, J = 7.8 Hz), 7.77 (1H, dt, J = 7.8 Hz, J = 1.3 Hz), 7.84 (1H, dt, J = 7.8 Hz, J = 1.1 Hz), 7.96 (1H, t, J = 1.3 Hz). ^{13}C NMR (DMSO-d_6, 125 MHz): δ [ppm] = 35.2, 64.5, 64.7, 111.8, 115.5, 116.3, 118.5, 118.9, 120.4, 130.1, 131.8, 133.0, 134.4, 139.3, 144.2, 147.1, 162.7, 165.5. HPLC: 99%; t_R 7.53 min. EI-MS: m/z = 351 (M^+).

4-((5-(2,3-Dihydrobenzo[*b*][1,4]dioxin-6-yl)-1,3,4-oxadiazol-2-ylthio)methyl)benzonitrile (6b). Yield 56%, brown solid. ^{1}H NMR (DMSO-d_6, 500 MHz): δ [ppm] = 4.31 (2H, m), 4.34 (2H, m), 4.63 (2H, s), 7.05 (1H, d, J = 8.4 Hz), 7.37 (1H, d, J = 2.0 Hz), 7.41 (1H, dd, J = 8.4 Hz, J = 2.0 Hz), 7.67 (2H, d, J = 8.3 Hz), 7.81 (2H, d, J = 8.3 Hz). ^{13}C NMR (DMSO-d_6, 125 MHz): δ [ppm] = 35.3, 64.0, 64.4, 110.4, 115.0, 115.8, 118.2, 118.6, 119.9, 130.0, 132.4, 142.8, 143.8, 146.7, 162.2, 165.0. HPLC: 95%; t_R 7.49 min. EI-MS: m/z = 351 (M^+).

Methyl 4-((5-(2,3-Dihydrobenzo[*b*][1,4]dioxin-6-yl)-1,3,4-oxadiazol-2-ylthio)methyl) Benzoate (6c). Yield 49%, purple solid. ^{1}H NMR (DMSO-d_6, 500 MHz): δ [ppm] = 3.89 (3H, s), 4.36 (2H, m), 4.39 (2H, m), 4.67 (2H, s), 7.10 (1H, d, J = 8.4 Hz), 7.42 (1H, d, J = 2.0 Hz), 7.47 (1H, dd, J = 8.4 Hz, J = 2.0 Hz), 7.67 (2H, d, J = 8.3 Hz), 7.97 (2H, d, J = 8.3 Hz). ^{13}C NMR (DMSO-d_6, 125 MHz): δ [ppm] = 35.4, 52.1, 64.0, 64.4, 115.0, 115.8, 118.1, 120.0, 128.9, 129.4, 142.4, 143.8, 146.7, 162.3, 165.0, 165.8. HPLC: 99%; t_R 7.66 min.

dx.doi.org/10.1021/jm300309a | *J. Med. Chem.* XXXX, XXX, XXX–XXX

EI-MS: m/z = 384 (M^+). HRMS (EI): m/z calcd for $C_{19}H_{16}N_2O_5S$ 384.0780, found 384.0809.

3-((5-(Pyridin-4-yl)-1,3,4-oxadiazol-2-ylthio)methyl)-benzonitrile (7a). Yield 41%, yellow solid. ^{1}H NMR (DMSO-d_6, 500 MHz): δ [ppm] = 4.66 (2H, s), 7.58 (1H, t, J = 7.8 Hz), 7.78 (1H, dt, J = 7.7 Hz, J = 1.3 Hz), 7.86 (1H, t, J = 1.2 Hz), 7.88 (2H, dd, J = 4.4 Hz, J = 1.6 Hz), 7.99 (1H, t, J = 1.4 Hz), 8.82 (2H, dd, J = 4.4 Hz, J = 1.6 Hz). ^{13}C NMR (DMSO-d_6, 125 MHz): δ [ppm] = 34.8, 111.4, 118.5, 120.0, 129.8, 130.0, 131.5, 132.7, 134.0, 138.6, 150.9, 163.8, 164.4. HPLC: 96%; t_R 4.51 min. EI-MS: m/z = 294 (M^+).

4-((5-(Pyridin-4-yl)-1,3,4-oxadiazol-2-ylthio)methyl)-benzonitrile (7b). Yield 77%, pale-yellow solid. ^{1}H NMR (DMSO-d_6, 500 MHz): δ [ppm] = 4.69 (2H, s), 7.71 (2H, d, J = 8.2 Hz), 7.83 (2H, d, J = 8.2 Hz), 7.88 (2H, dd, J = 4.4 Hz, J = 1.6 Hz), 8.82 (2H, dd, J = 4.5 Hz, J = 1.5 Hz). ^{13}C NMR (DMSO-d_6, 125 MHz): δ [ppm] = 35.2, 110.5, 118.6, 120.0, 130.0, 130.1, 132.4, 142.6, 150.8, 163.9, 164.4. HPLC: 95%; t_R 4.51 min. EI-MS: m/z = 294 (M^+).

2-(Benzylthio)-5-(pyridin-4-yl)-1,3,4-oxadiazole (7c). Yield 79%, light-yellow solid. ^{1}H NMR (DMSO-d_6, 500 MHz): δ [ppm] = 4.62 (2H, s), 7.30 (1H, m), 7.36 (2H, m), 7.50 (2H, m), 7.90 (2H, dd, J = 4.4 Hz, J = 1.6 Hz), 8.82 (2H, dd, J = 4.4 Hz, 1.6 Hz). ^{13}C NMR (DMSO-d_6, 125 MHz): δ [ppm] = 35.8, 120.0, 127.8, 128.6, 129.1, 130.0, 136.4, 150.8, 163.6, 164.7. HPLC: 100%; t_R 4.89 min. EI-MS: m/z = 269 (M^+).

2-(3-Iodobenzylthio)-5-(pyridin-4-yl)-1,3,4-oxadiazole (7d). **7d** was used as reference. It is commercially available from Calbiochem (361541 GSK-3β Inhibitor II; CAS number, 478482-75-6).

4-((5-(Benzo[*d*][1,3]dioxol-5-yl)-1,3,4-oxadiazol-2-ylthio)-methyl)benzoic Acid (8a). Methyl 4-((5-(benzo[d][1,3]dioxol-5-yl)-1,3,4-oxadiazol-2-ylthio)methyl benzoate **5c** (300 mg, 0.81 mmol) was added in 5 mL of a 2 N lithium hydroxide−tetrahydrofuran solution. The reaction mixture was stirred overnight at 60 °C under an argon atmosphere. The reaction mixture was diluted with water and neutralized with 1 N HCl. Afterward, EtOAc was added and the organic layer was washed with water and brine, dried over $MgSO_4$, and concentrated in vacuo to give **8a** (239 mg, 83%) as a rose solid. ^{1}H NMR (DMSO-d_6, 500 MHz): δ [ppm] = 4.56 (2H, s), 6.08 (2H, s), 7.04 (1H, d, J = 8.1 Hz), 7.35 (1H, d, J = 1.6 Hz), 7.43 (1H, dd, J = 8.1 Hz, J = 1.7 Hz), 7.53 (2H, d, J = 8.2 Hz), 7.84 (2H, d, J = 8.2 Hz), 12.8 (1H, s, br). ^{13}C NMR (DMSO-d_6, 125 MHz): δ [ppm] = 35.4, 102.1, 106.1, 109.1, 116.6, 121.7, 129.1, 129.5, 130.4, 141.7, 148.1, 150.4, 162.4, 165.1, 166.9. HPLC: 99%; t_R 6.15 min. EI-MS: m/z = 356 (M^+).

Compound **9a** was prepared in a similar manner to that described for **8a**.

Methyl 4-((5-(2,3-Dihydrobenzo[*b*][1,4]dioxin-6-yl)-1,3,4-oxadiazol-2-ylthio)methyl)benzoic Acid (9a). Yield 91%, colorless solid. ^{1}H NMR (DMSO-d_6, 500 MHz): δ [ppm] = 4.31 (2H, m), 4.34 (2H, m), 4.62 (2H, s), 7.05 (1H, d, J = 8.4 Hz), 7.38 (1H, d, J = 2.0 Hz), 7.43 (1H, dd, J = 8.4 Hz, J = 2.1 Hz), 7.59 (2H, d, J = 8.3 Hz), 7.91 (2H, d, J = 8.3 Hz), 12.95 (1H, s). ^{13}C NMR (DMSO-d_6, 125 MHz): δ [ppm] = 35.4, 64.1, 64.4, 115.1, 115.7, 118.2, 119.8, 129.3, 129.5, 130.1, 141.9, 143.8, 146.7, 162.4, 165.0, 166.8. HPLC: 96%; t_R 6.22 min. EI-MS: m/z = 370 (M^+).

4-((5-(Benzo[*d*][1,3]dioxol-5-yl)-1,3,4-oxadiazol-2-ylthio)-methyl)-*N*-isobutylbenzamide (8c). A mixture of 4-((5-(benzo-[d][1,3]dioxol-5-yl)-1,3,4-oxadiazol-2-ylthio)methyl)benzoic acid **8a** (100 mg, 0.28 mmol) and thionyl chloride (30.5 μL, 0.42 mmol) was refluxed in dry toluene (1 mL) for about 2 h. Excess thionyl chloride was removed by repeated evaporation in vacuo with fresh dry toluene (3 × 1 mL). 2-Methylpropan-1-amine (27.8 μL, 0.28 mmol) and K_2CO_3 (38 mg, 0.28 mmol) were added in dry acetone (1 mL) cooled to 0 °C and stirred for 30 min. The crude acyl chloride was dissolved in dry acetone (0.5 mL) and added dropwise to the solution. After the addition was complete, stirring continued for 2 h. The reaction mixture was then diluted with water, extracted three times with EtOAc, and successively washed with brine. The organic layer was dried over $MgSO_4$ and concentrated under reduced pressure. The obtained residue was recrystallized from EtOH to give **8c** (90 mg, 81%) as a beige solid. ^{1}H NMR (DMSO-d_6, 500 MHz): δ [ppm] = 0.86 (6H, d, J = 6.7 Hz), 1.81 (1H, n, J = 6.7 Hz), 3.05 (2H, t, J = 6.7 Hz), 4.60 (2H, s), 6.16 (2H, s), 7.10 (1H, d, J = 8.1 Hz), 7.43 (1H, d, J = 1.6 Hz), 7.50 (1H, dd, J = 8.1 Hz, J = 1.7 Hz), 7.54 (2H, d, J = 8.2 Hz), 7.78 (2H, d, J = 8.3 Hz), 8.42 (1H, t, J = 5.7 Hz). ^{13}C NMR (DMSO-d_6, 125 MHz): δ [ppm] = 20.2, 28.0, 35.4, 46.6, 102.1, 106.1, 109.2, 116.6, 121.8, 127.5, 128.8, 134.1, 139.8, 148.1, 150.5, 162.4, 165.1, 165.8. HPLC: 95%; t_R 7.11 min. EI-MS: m/z = 411 (M^+).

The following compounds **8d** and **9c**−**e** were prepared in a similar manner to that described for **8c**.

4-((5-(Benzo[*d*][1,3]dioxol-5-yl)-1,3,4-oxadiazol-2-ylthio)-methyl)-*N*-(2,2-dimethoxyethyl)benzamide (8d). Yield 79%, light-yellow solid. ^{1}H NMR (DMSO-d_6, 500 MHz): δ [ppm] = 3.27 (6H, s), 3.33 (2H, br), 4.48 (1H, t, J = 5.6 Hz), 4.61 (2H, s), 6.16 (2H, s), 7.11 (1H, d, J = 8.1 Hz), 7.44 (1H, d, J = 1.7 Hz), 7.50 (1H, dd, J = 8.1 Hz, J = 1.7 Hz), 7.55 (2H, d, J = 8.1 Hz), 7.80 (2H, d, J = 8.1 Hz), 8.52 (1H, t, J = 5.7 Hz). ^{13}C NMR (DMSO-d_6, 125 MHz): δ [ppm] = 35.4, 41.1, 53.2, 101.8, 102.2, 106.2, 109.2, 116.6, 121.7, 127.5, 128.9, 133.5, 140.1, 148.1, 150.4, 162.4, 165.1, 166.0. HPLC: 95%; t_R 6.07 min. EI-MS: m/z = 443 (M^+).

4-((5-(2,3-Dihydrobenzo[*b*][1,4]dioxin-6-yl)-1,3,4-oxadiazol-2-ylthio)methyl)-*N*-isobutyl Benzamide (9c). Yield 92%, light-brown solid. ^{1}H NMR (DMSO-d_6, 500 MHz): δ [ppm] = 0.93 (6H, d, J = 6.7 Hz), 1.88 (1H, n, J = 6.7 Hz), 3.12 (2H, t, J = 6.6 Hz), 4.37 (2H, m), 4.39 (2H, m), 4.66 (2H, s), 7.10 (1H, d, J = 8.4 Hz), 7.45 (1H, d, J = 2.0 Hz), 7.48 (1H, dd, J = 8.4 Hz, J = 2.0 Hz), 7.60 (2H, d, J = 8.2 Hz), 7.85 (2H, d, J = 8.2 Hz), 8.46 (1H, t, J = 5.7 Hz). ^{13}C NMR (DMSO-d_6, 125 MHz): δ [ppm] = 20.2, 28.1, 35.4, 46.6, 64.1, 64.4, 115.0, 115.8, 118.1, 119.9, 127.4, 128.8, 134.1, 139.7, 143.8, 146.7, 162.4, 164.9, 165.8. HPLC: 96%; t_R 7.16 min. EI-MS: m/z = 425 (M^+).

4-((5-(2,3-Dihydrobenzo[*b*][1,4]dioxin-6-yl)-1,3,4-oxadiazol-2-ylthio)methyl)-*N*-(2,2-dimethoxy ethyl)benzamide (9d). Yield 84%, beige solid. ^{1}H NMR (DMSO-d_6, 500 MHz): δ [ppm] = 3.28 (6H, s), 3.35 (2H, d, J = 5.7 Hz), 4.31 (2H, m), 4.34 (2H, m), 4.50 (1H, t, J = 5.6 Hz), 4.61 (2H, s), 7.05 (1H, d, J = 8.3 Hz), 7.40 (1H, d, J = 2.0 Hz), 7.43 (1H, dd, J = 8.3 Hz, J = 2.0 Hz), 7.55 (2H, d, J = 8.2 Hz), 7.81 (2H, d, J = 8.2 Hz), 8.52 (1H, t, J = 5.8 Hz). ^{13}C NMR (DMSO-d_6, 125 MHz): δ [ppm] = 35.4, 41.1, 53.2, 64.0, 64.4, 101.8, 115.0, 105.8, 108.2, 119.9, 127.4, 128.8, 133.5, 140.0, 143.8, 146.7, 162.4, 164.9, 165.9. HPLC: 95%; t_R 6.13 min. EI-MS: m/z = 457 (M^+).

***N*-Benzyl-4-((5-(2,3-dihydrobenzo[*b*][1,4]dioxin-6-yl)-1,3,4-oxadiazol-2-ylthio)methyl)benzamide (9e).** Yield 89%, beige solid. ^{1}H NMR (DMSO-d_6, 500 MHz): δ [ppm] = 4.31 (2H, m), 4.34 (2H, m), 4.47 (2H, d, J = 5.9 Hz), 4.62 (2H, s), 7.05 (1H, d, J = 8.4 Hz), 7.23 (1H, m), 7.32 (4H, m), 7.40 (1H, d, J = 2.0 Hz), 7.43 (1H, dd, J = 8.3 Hz, J = 2.0 Hz), 7.56 (2H, d, J = 8.2 Hz), 7.86 (2H, d, J = 8.2 Hz), 9.01 (1H, t, J = 5.9 Hz). ^{13}C NMR (DMSO-d_6, 125 MHz): δ [ppm] = 35.4, 42.6, 64.1, 64.4, 115.1, 115.8, 118.3, 119.8, 126.7, 127.3, 127.5, 128.4, 128.8, 133.7, 139.6, 140.1, 143.8, 146.7, 162.4, 165.0, 165.8. HPLC: 95%; t_R 7.66 min. EI-MS: m/z = 459 (M^+).

2-(4-(1*H*-Tetrazol-5-yl)benzylthio)-5-(benzo[*d*][1,3]dioxol-5-yl)-1,3,4-oxadiazole (8e). 4-((5-Benzo[d][1,3]dioxol-5-yl)-1,3,4-oxadiazol-2-ylthio)methyl)benzonitrile **5b** (34 mg, 0.10 mmol), NaN_3 (78 mg, 1.20 mmol), and NH_4Cl (64 mg, 1.20 mmol) were added to 1 mL of DMF and stirred for 5 h at 100 °C under microwave irradiation. After cooling to room temperature, the reaction solution was added to water (2−3 mL), acidified with 2 N HCl, and extracted three times with ethyl acetate. The combined organic layers were dried over Na_2SO_4, filtered, and the solvent evaporated off to provide **8e** (25 mg, 67%) as a beige solid. ^{1}H NMR (DMSO-d_6, 500 MHz): δ [ppm] = 4.65 (2H, s), 6.15 (2H, s), 7.11 (1H, d, J = 8.1 Hz), 7.43 (1H, d, J = 1.6 Hz), 7.50 (1H, dd, J = 8.1 Hz, J = 1.7 Hz), 7.71 (2H, d, J = 8.3 Hz), 8.00 (2H, d, J = 8.3 Hz), NH signal was not observed. ^{13}C NMR (DMSO-d_6, 125 MHz): δ [ppm] = 35.4, 102.1, 105.0, 106.2, 108.9, 109.1, 116.6, 119.7, 121.7, 127.1, 130.0, 148.1, 150.4, 162.4, 165.1. HPLC: 96%; t_R 5.92 min. EI-MS: m/z = 380 (M^+).

Compound **9f** was prepared in a similar manner to that described for **8e**.

2-(4-(1*H*-Tetrazol-5-yl)benzylthio)-5-(2,3-dihydrobenzo[*d*]-[1,4]dioxin-5-yl)-1,3,4-oxadiazole (9f). Yield 79%, puce solid. ^{1}H NMR (DMSO-d_6, 500 MHz): δ [ppm] = 4.35 (2H, m), 4.38 (2H, m), 4.70 (2H, s), 7.10 (1H, d, J = 8.4 Hz), 7.43 (1H, d, J = 2.0 Hz),

dx.doi.org/10.1021/jm300309a | J. Med. Chem. XXXX, XXX, XXX−XXX

7.47 (1H, dd, J = 8.4 Hz, J = 2.1 Hz), 7.75 (2H, d, J = 8.3 Hz), 8.05 (2H, d, J = 8.3 Hz), NH signal was not observed. ^{13}C NMR (DMSO-d_6, 125 MHz): δ [ppm] = 35.5, 64.0, 64.4, 115.0, 115.8, 118.2, 119.9, 123.6, 127.1, 130.0, 140.1, 143.8, 146.7, 162.4, 165.1. HPLC: 95%; t_R 6.01 min. EI-MS: m/z = 394 (M^+).

The following compounds **14a**−**d**, **15a**−**b**, and **16a** were prepared in a similar manner to that described for **5a**.

2-(Benzo[*d*][1,3]dioxol-5-yl)-5-(biphenyl-4-ylmethylthio)-1,3,4-oxadiazole (14a). Yield 75%, beige solid. ^{1}H NMR (DMSO-d_6, 500 MHz): δ [ppm] = 4.55 (2H, s), 6.08 (2H, s), 7.04 (1H, d, J = 8.1 Hz), 7.28 (1H, m), 7.38 (3H, m), 7.45 (1H, dd, J = 8.1 Hz, J = 1.7 Hz), 7.48 (2H, d, J = 8.3 Hz), 7.58 (4H, m). ^{13}C NMR (DMSO-d_6, 125 MHz): δ [ppm] = 35.6, 102.1, 106.2, 109.1, 116.6, 121.7, 126.6, 126.8, 127.6, 128.9, 129.7, 135.8, 139.6, 148.1, 150.5, 162.6, 165.1. HPLC: 95%; t_R 9.12 min. EI-MS: m/z = 388 (M^+).

4′-((5-(Benzo[*d*][1,3]dioxol-5-yl)-1,3,4-oxadiazol-2-ylthio)-methyl)biphenyl-2-carbonitrile (14b). Yield 71%, brown solid. ^{1}H NMR (DMSO-d_6, 500 MHz): δ [ppm] = 4.66 (2H, s), 6.15 (2H, s), 7.11 (1H, d, J = 8.1 Hz), 7.45 (1H, d, J = 1.7 Hz), 7.51 (1H, dd, J = 8.1 Hz, J = 1.7 Hz), 7.57 (2H, d, J = 8.2 Hz), 7.65 (4H, m), 7.96 (1H, dd, J = 8.5 Hz, J = 2.3 Hz). ^{13}C NMR (DMSO-d_6, 125 MHz): δ [ppm] = 35.5, 102.1, 106.1, 109.1, 111.5, 111.6, 116.6, 117.3, 117.4, 120.3, 120.5, 121.0, 121.2, 121.7, 129.0, 129.4, 132.3, 132.4, 136.2, 137.5, 140.8, 140.9, 148.1, 150.4, 159.9, 161.9, 162.6, 165.1. HPLC: 95%; t_R 8.77 min. EI-MS: m/z = 431 (M^+). HRMS (EI): m/z calcd for $C_{23}H_{14}N_3O_3FS$ 431.0740, found 431.0728.

4-((5-(Benzo[*d*][1,3]dioxol-5-yl)-1,3,4-oxadiazol-2-ylthio)-methyl)-4-fluorobiphenyl-2-carbonitrile (14c). Yield 69%, gray solid. ^{1}H NMR (DMSO-d_6, 500 MHz): δ [ppm] = 4.66 (2H, s), 6.16 (2H, s), 7.11 (1H, d, J = 8.1 Hz), 7.45 (1H, d, J = 1.7 Hz), 7.51 (1H, dd, J = 8.1 Hz, J = 1.7 Hz), 7.56 (2H, d, J = 8.2 Hz), 7.65 (4H, m), 7.78 (1H, td, J = 7.7 Hz, J = 1.3 Hz), 7.95 (1H, dd, J = 7.7 Hz, J = 0.9 Hz). ^{13}C NMR (DMSO-d_6, 125 MHz): δ [ppm] = 35.5, 102.1, 106.1, 109.1, 110.1, 116.6, 118.5, 121.7, 128.3, 128.9, 129.4, 130.1, 133.5, 133.8, 137.2, 137.4, 140.0, 148.1, 150.4, 162.6, 165.1. HPLC: 96%; t_R 8.36 min. EI-MS: m/z = 413 (M^+). HRMS (EI): m/z calcd for $C_{23}H_{15}N_3O_3S$ 413.0835, found 413.0804.

4′-((5-(Benzo[*d*][1,3]dioxol-5-yl)-1,3,4-oxadiazol-2-ylthio)-methyl)biphenyl-4-carbonitrile (14d). Yield 51%, gray−brown solid. ^{1}H NMR (DMSO-d_6, 500 MHz): δ [ppm] = 4.63 (2H, s), 6.15 (2H, s), 7.10 (1H, d, J = 8.1 Hz), 7.43 (1H, d, J = 1.7 Hz), 7.51 (1H, dd, J = 8.1 Hz, J = 1.7 Hz), 7.61 (2H, d, J = 8.3 Hz), 7.73 (2H, d, J = 8.3 Hz), 7.87 (2H, d, J = 8.6 Hz), 7.91 (2H, d, J = 8.6 Hz). ^{13}C NMR (DMSO-d_6, 125 MHz): δ [ppm] = 35.9, 102.6, 106.6, 109.6, 110.6, 117.1, 119.3, 122.2, 127.7, 128.0, 130.3, 133.3, 138.0, 138.1, 144.5, 148.6, 150.9, 163.0, 165.5. HPLC: 97%; t_R 8.77 min. EI-MS: m/z = 413 (M^+). HRMS (EI): m/z calcd for $C_{23}H_{15}N_3O_3S$ 413.0835, found 413.0825.

4-((5-(2,3-Dihydrobenzo[*b*][1,4]dioxin-6-yl)-[1,3,4]oxadiazol-2-ylthio)methyl)biphenyl-2-carbonitrile (15a). Yield 74%, colorless solid. ^{1}H NMR (DMSO-d_6, 500 MHz): δ [ppm] = 4.31 (2H, m), 4.34 (2H, m), 4.65 (2H, s), 7.05 (1H, d, J = 8.4 Hz), 7.41 (1H, d, J = 2.0 Hz), 7.44 (1H, dd, J = 8.4 Hz, J = 2.0 Hz), 7.60 (6H, m), 7.79 (1H, td, J = 7.7 Hz, J = 1.2 Hz), 7.95 (1H, dd, J = 7.7 Hz, J = 0.9 Hz). ^{13}C NMR (DMSO-d_6, 125 MHz): δ [ppm] = 35.9, 64.4, 64.8, 110.5, 115.4, 116.3, 118.5, 118.8, 120.3, 128.6, 129.3, 129.7, 130.5, 133.8, 134.2, 137.5, 137.8, 144.1, 144.3, 147.1, 163.0, 165.3. HPLC: 100%; t_R 8.39 min. EI-MS: m/z 427 (M^+). HRMS (EI): m/z calcd for $C_{24}H_{17}N_3O_3S$ 427.0991, found 427.0962.

4′-((5-(2,3-Dihydrobenzo[*b*][1,4]dioxin-6-yl)-1,3,4-oxadiazol-2-ylthio)methyl)-4-fluorobiphenyl-2-carbonitrile (15b). Yield 29%, light-yellow solid. ^{1}H NMR (DMSO-d_6, 500 MHz): δ [ppm] = 4.32 (2H, m), 4.34 (2H, m) 4.65 (2H, s), 7.05 (1H, d, J = 8.4 Hz), 7.40 (1H, d, J = 2.1 Hz), 7.45 (1H, dd, J = 8.4 Hz, J = 2.1 Hz), 7.56 (2H, d, J = 8.2 Hz), 7.63 (2H, d, J = 8.2 Hz), 7.68 (2H, m), 7.97 (1H, dd, J = 9.0 Hz, J = 1.9 Hz). HPLC: 95%; t_R 8.76 min. EI-MS: m/z = 445 (M^+). HRMS (EI): m/z calcd for $C_{24}H_{16}N_3O_3FS$ 445.0897, found 445.0890.

4-((5-(Pyridine-4-yl)-1,3,4-oxadiazol-2-ylthio)methyl)-biphenyl-2-carbonitrile (16a). Yield 53%, colorless solid. ^{1}H NMR (DMSO-d_6, 500 MHz): δ [ppm] = 4.71 (2H, s), 7.58 (3H, m), 7.62 (1H, d, J = 7.7 Hz), 7.68 (2H, d, J = 8.1 Hz), 7.78 (1H, t, J = 7.7 Hz), 7.91 (2H, d, J = 4.1 Hz), 7.95 (1H, d, J = 7.7 Hz), 8.85 (2H, s, br). ^{13}C NMR (DMSO-d_6, 125 MHz): δ [ppm] = 35.4, 110.1, 118.5, 120.1, 128.2, 128.9, 129.4, 130.0, 130.1, 133.5, 133.7, 137.2, 137.3, 143.9, 150.8, 163.8, 164.8. HPLC: 99%; t_R 6.63 min. EI-MS: m/z = 370 (M^+). HRMS (EI): m/z calcd for $C_{21}H_{14}N_4OS$ 370.0889, found 370.0926.

Methyl 3,4-Dihydroxybenzoate (18). To a stirred solution of 3,4-dihydroxybenzoic acid (2.0 g, 13 mmol) in MeOH (25 mL) was added $SOCl_2$ (1.88 mL, 26 mmol) dropwise over 1 h at 0 °C. The solution was further stirred 12 h at 50 °C. The mixture was cooled to room temperature and diluted with water (30 mL). MeOH was evaporated and the pH adjusted to ∼6 with aqueous $NaHCO_3$. The mixture was extracted three times with EtOAc and successively washed with brine. The organic layer was dried over $MgSO_4$ and concentrated under reduced pressure to give **18** (2.1 g, 97%) as a colorless solid. ^{1}H NMR (DMSO-d_6, 500 MHz): δ [ppm] = 3.75 (3H, s), 6.80 (1H, d, J = 8.2 Hz), 7.31 (1H, dd, J = 8.2 Hz, J = 2.1 Hz), 7.35 (1H, d, J = 2.1 Hz), 9.35 (1H, s), 9.75 (1H, s). ^{13}C NMR (DMSO-d_6, 125 MHz): δ [ppm] = 51.5, 115.3, 116.2, 120.4, 121.7, 145.0, 150.4, 166.1. EI-MS: m/z = 168 (M^+).

Methyl 3-(Hydroxymethyl)-2,3-dihydrobenzo[*b*][1,4]-dioxine-6-carboxylate (19a). Methyl 3,4-dihydroxybenzoate **18** (0.8 g, 4.75 mmol) and K_2CO_3 (0.65 g, 4.75 mmol) were taken in dry acetone (10 mL) and stirred for 15 min at room temperature. Afterward, the solution was treated with epibromohydrin (0.40 mL, 4.75 mmol) and stirred overnight at 70 °C. The reaction mixture was diluted with water and extracted with EtOAc. The organic layer was washed with brine and dried over Na_2SO_4. The solvent was evaporated under reduced pressure and the crude product purified by silica gel column chromatography (DCM/EtOAc, 4:1) to give **19a** (1.01 g, 95%) as a colorless oil. ^{1}H NMR (DMSO-d_6, 500 MHz): δ [ppm] = 3.64 (2H, m), 3.80 (3H, s), 4.10 (1H, m), 4.20 (1H, m), 4.41 (1H, dd, J = 11.4 Hz, J = 2.3 Hz), 5.10 (1H, t, J = 5.7 Hz), 6.98 (1H, d, J = 8.4 Hz), 7.41 (1H, d, J = 2.0 Hz), 7.46 (1H, dd, J = 8.4 Hz, J = 2.0 Hz). ^{13}C NMR (DMSO-d_6, 125 MHz): δ [ppm] = 51.9, 59.7, 65.4, 73.6, 117.0, 117.9, 122.6, 122.7, 142.8, 147.4, 165.6. EI-MS: m/z = 224 (M^+).

Note: Alternatively (*R*/*S*)-(±)-glycidyl tosylate can be used to obtain compound **19a**. For more details see the synthesis of compound **19b**−**c**.

Methyl 3-(Methoxymethyl)-2,3-dihydrobenzo[*b*][1,4]-dioxine-6-carboxylate (20a). To a suspension of NaH (115 mg, 4.81 mmol) in 5 mL of anhydrous THF was added methyl 3-(hydroxymethyl)-2,3-dihydrobenzo[*b*][1,4]dioxine-6-carboxylate **19a** (900 mg, 4.01 mmol) at 0 °C. The mixture was stirred at room temperature for 30 min, followed by addition of methyl iodide (374 μL, 6.01 mmol). The reaction mixture was stirred at room temperature for 48 h, quenched with 10 mL of water, and extracted with ethyl acetate. The combined organic layer was dried over $MgSO_4$, the solvent was evaporated under reduced pressure, and the crude product purified by silica gel column chromatography (DCM/EtOAc, 20:1) to give **20a** (678 mg, 71%) as a colorless oil. ^{1}H NMR (DMSO-d_6, 500 MHz): δ [ppm] = 3.33 (3H, s), 3.60 (2H, m), 3.80 (3H, s), 4.09 (1H, m), 4.40 (2H, m), 6.99 (1H, m), 7.41 (1H, m), 7.47 (1H, m). ^{13}C NMR (DMSO-d_6, 125 MHz): δ [ppm] = 51.8, 58.7, 65.3, 70.3, 71.8, 117.0, 118.0, 122.7, 122.8, 142.6, 147.2, 165.5. EI-MS: m/z = 238 (M^+).

3-(Methoxymethyl)-2,3-dihydrobenzo[*b*][1,4]dioxine-6-carbohydrazide (21a). To a solution of **20a** (600 mg, 2.51 mmol) in EtOH (15 mL) was added hydrazine hydrate (731 μL, 15.06 mmol). and the mixture was heated at reflux for 2 days. After cooling to room temperature, the reaction mixture was diluted with water and extracted with EtOAc. The organic layer was washed with brine and dried over $MgSO_4$. The solvent was evaporated under reduced pressure and the crude product purified by silica gel column chromatography (MeOH/EtOAc, 1:10) to give **21a** (466 mg, 78%) as a colorless solid. ^{1}H NMR (DMSO-d_6, 500 MHz): δ [ppm] = 3.32 (3H, s), 3.59 (2H, m), 4.04 (1H, m), 4.36 (2H, m), 4.41 (2H, s), 6.92 (1H, d, J = 8.2 Hz), 7.35 (1H, dd, J = 8.2 Hz, J = 2.0 Hz), 7.37 (1H, d, J = 2.0 Hz), 9.52 (1H, s). ^{13}C NMR (DMSO-d_6, 125 MHz): δ [ppm] = 58.7, 65.1, 70.4, 71.8,

dx.doi.org/10.1021/jm300309a | J. Med. Chem. XXXX, XXX, XXX−XXX

115.8, 116.6, 120.3, 126.5, 142.3, 145.3, 165.1. EI-MS: m/z = 238 (M^+).

Compound **22a** was prepared in a similar manner to that described for **4A**.

5-(3-(Methoxymethyl)-2,3-dihydrobenzo[*b*][1,4]dioxin-6-yl)-1,3,4-oxadiazole-2-thiol (22a). Yield 81%, orange solid. ^{1}H NMR (DMSO-d_6, 500 MHz): δ [ppm] = 3.32 (3H, s), 3.61 (2H, m), 4.10 (1H, m), 4.43 (2H, m), 7.07 (1H, m), 7.32 (1H, m), 7.37 (1H, m), 14.60 (1H, s). ^{13}C NMR (DMSO-d_6, 125 MHz): δ [ppm] = 58.7, 65.3, 70.3, 72.1, 114.6, 115.6, 118.0, 119.7, 143.4, 146.4, 160.1, 177.4. EI-MS: m/z = 280 (M^+).

Compound **23a** was prepared in a similar manner to that described for **5a**.

4′-((5-(3-(Methoxymethyl)-2,3-dihydrobenzo[*b*][1,4]dioxin-6-yl)-1,3,4-oxadiazol-2ylthio)methyl)biphenyl-2-carbonitrile (23a). Yield 88%, colorless solid. ^{1}H NMR (DMSO-d_6, 500 MHz): δ [ppm] = 3.33 (3H, s), 3.61 (2H, m), 4.10 (1H, m), 4.44 (2H, m), 4.66 (2H, s), 7.07 (1H, m), 7.45 (2H, m), 7.57 (3H, m), 7.63 (3H, m), 7.78 (1H, td, J = 7.6 Hz, J = 1.2 Hz), 7.95 (1H, dd, J = 7.7 Hz, J = 1.1 Hz). ^{13}C NMR (DMSO-d_6, 125 MHz): δ [ppm] = 35.4, 58.7, 65.2, 70.3, 72.0, 110.1, 115.1, 116.2, 118.0, 118.5, 119.9, 128.2, 128.8, 129.4, 130.1, 133.5, 133.8, 137.1, 137.4, 143.3, 143.9, 146.2, 162.6, 164.9. HPLC: 100%; t_R 8.59 min. EI-MS: m/z = 471 (M^+). HRMS (EI): m/z calcd for $C_{26}H_{21}N_3O_4S$ 471.1253, found 471.1264.

4′-((5-(3-(Hydroxymethyl)-2,3-dihydrobenzo[*b*][1,4]dioxin-6-yl)-1,3,4-oxadiazol-2-ylthio) methyl)biphenyl-2-carbonitrile (24a). To a solution of 4′-((5-(3-(methoxymethyl)-2,3-dihydrobenzo-[*b*][1,4]dioxin-6-yl)-1,3,4-oxadiazol-2ylthio)methyl)biphenyl-2-carbonitrile **23a** (400 mg, 0.85 mmol) in 10 mL of DCM was added 1 N solution of BBr_3 in hexane (850 μL, 0.85 mmol) under argon atmosphere at −78 °C. The reaction mixture was stirred at the same temperature for 1 h and allowed to warm to room temperature and further stirred for 24 h. After treatment with saturated $NaHCO_3$ solution, the reaction mixture was extracted with ethyl acetate. The combined organic layers were dried over $MgSO_4$ and concentrated under reduced pressure. The crude product was purified by silica gel column chromatography (cyclohexane/EtOAc, 1:2) to give compound **24a** (283 mg, 73%) as a light-yellow solid. ^{1}H NMR (DMSO-d_6, 500 MHz): δ [ppm] = 3.59 (1H, s, br), 3.64 (2H, m), 4.10 (1H, m), 4.24 (1H, m), 4.42 (1H, dd, J = 11.5 Hz, J = 2.2 Hz), 4.65 (2H, s) 7.06 (1H, d, J = 8.3 Hz), 7.43 (2H, m), 7.60 (6H, m), 7.78 (1H, td, J = 7.7 Hz, J = 1.2 Hz), 7.94 (1H, dd, J = 7.7 Hz, J = 1.0 Hz). ^{13}C NMR (DMSO-d_6, 125 MHz): δ [ppm] = 35.4, 59.6, 65.4, 73.7, 110.1, 115.1, 116.1, 117.9, 118.5, 119.8, 128.2, 128.8, 129.4, 130.1, 133.4, 133.8, 137.1, 137.4, 143.5, 144.0, 146.2, 162.6, 165.0. HPLC: 96%; t_R 7.39 min. EI-MS: m/z = 457(M^+).

(*R*)-Methyl 3-(Hydroxymethyl)-2,3-dihydrobenzo[*b*][1,4]-dioxine-6-carboxylate (19b). To a round-bottom flask equipped with magnetic stirring and a nitrogen inlet was added methyl-3,4-dihydroxybenzoate **18** (1.0 g, 6 mmol), (2*S*)-(+)-glycidyl tosylate (1.37 g, 6 mmol), K_2CO_3(0.99 g, 7.2 mmol), and DMF (15 mL). This mixture was heated to 60 °C for 5 h. The mixture was cooled to room temperature, diluted with water, and extracted with EtOAc. The organic layer was washed with brine and dried over Na_2SO_4. The solvent was evaporated under reduced pressure and the crude product purified by silica gel column chromatography (DCM/EtOAc, 4:1) to give **19b** (1.25 g, 93%) as a colorless oil. ^{1}H NMR (DMSO-d_6, 500 MHz): δ [ppm] = 3.64 (2H, m), 3.80 (3H, s), 4.10 (1H, m), 4.20 (1H, m), 4.41 (1H, dd, J = 11.4 Hz, J = 2.3 Hz), 5.08 (1H, t, J = 5.7 Hz), 6.98 (1H, d, J = 8.4 Hz), 7.41 (1H, d, J = 2.0 Hz), 7.46 (1H, dd, J = 8.4 Hz, J = 2.0 Hz). ^{13}C NMR (DMSO-d_6, 125 MHz): δ [ppm] = 51.9, 59.7, 65.5, 73.6, 117.0, 117.9, 122.6, 122.7, 142.8, 147.4, 165.6. HPLC: 96%; t_R 2.44 min. EI-MS: m/z = 224 (M^+).

Compound **19c** was prepared in a similar manner to that described for **19b**. (2*R*)-(−)-glycidyl tosylate was used instead of (2*S*)-(+)-glycidyl tosylate to obtain the *S*-isomer.

(*S*)-Methyl 3-(Hydroxymethyl)-2,3-dihydrobenzo[*b*][1,4]-dioxine-6-carboxylate (19c). Yield 89%, as a colorless oil. ^{1}H NMR (DMSO-d_6, 500 MHz): δ [ppm] = 3.64 (2H, m), 3.80 (3H, s), 4.10 (1H, m), 4.20 (1H, m), 4.41 (1H, dd, J = 11.4 Hz, J = 2.3 Hz), 5.10 (1H, s, br), 6.98 (1H, d, J = 8.4 Hz), 7.41 (1H, d, J = 2.0 Hz), 7.46 (1H, dd, J = 8.4 Hz, J = 2.0 Hz). ^{13}C NMR (DMSO-d_6, 125 MHz): δ [ppm] = 51.9, 59.7, 65.5, 73.6, 117.0, 117.9, 122.6, 122.7, 142.8, 147.4, 165.6. EI-MS: m/z = 224 (M^+).

Compounds **20b−c** were prepared in a similar manner to that described for **20a**.

(*R*)-Methyl 3-(Methoxymethyl)-2,3-dihydrobenzo[*b*][1,4]-dioxine-6-carboxylate (20b). Yield 68%, as a colorless oil. ^{1}H NMR (DMSO-d_6, 500 MHz): δ [ppm] = 3.33 (3H, s), 3.60 (2H, m), 3.81 (3H, s), 4.09 (1H, m), 4.40 (2H, m), 6.99 (1H, d, J = 8.4 Hz), 7.42 (1H, d, J = 2.0 Hz), 7.47 (1H, dd, J = 8.4 Hz, J = 2.0 Hz). ^{13}C NMR (DMSO-d_6, 125 MHz): δ [ppm] = 51.9, 58.7, 65.3, 70.3, 71.8, 117.1, 117.9, 122.8, 122.9, 142.6, 147.3, 165.6. EI-MS: m/z = 238 (M^+).

(*S*)-Methyl 3-(Methoxymethyl)-2,3-dihydrobenzo[*b*][1,4]-dioxine-6-carboxylate (20c). After extraction and evaporation of the solvent, compound **20c** was used without further purification.

Compounds **21b−c** were prepared in a similar manner to that described for **21a**.

(*R*)-3-(Methoxymethyl)-2,3-dihydrobenzo[*b*][1,4]dioxine-6-carbohydrazide (21b). Yield 87%, as a colorless solid. ^{1}H NMR (DMSO-d_6, 500 MHz): δ [ppm] = 3.32 (3H, s), 3.59 (2H, m), 4.04 (1H, m), 4.36 (2H, m), 4.41 (2H, s), 6.92 (1H, d, J = 8.3 Hz), 7.35 (1H, dd, J = 8.3 Hz, J = 2.0 Hz), 7.37 (1H, d, J = 2.0 Hz), 9.57 (1H, s). ^{13}C NMR (DMSO-d_6, 125 MHz): δ [ppm] = 58.7, 65.1, 70.4, 71.7, 115.8, 116.6, 120.4, 126.6, 142.3, 145.3, 165.1. EI-MS: m/z = 238 (M^+).

(*S*)-3-(Methoxymethyl)-2,3-dihydrobenzo[*b*][1,4]dioxine-6-carbohydrazide (21c). Yield 92%, as a colorless solid. ^{1}H NMR (DMSO-d_6, 500 MHz): δ [ppm] = 3.32 (3H, s), 3.59 (2H, m), 4.04 (1H, m), 4.36 (2H, m), 4.41 (2H, s), 6.92 (1H, d, J = 8.3 Hz), 7.36 (1H, dd, J = 8.3 Hz, J = 2.0 Hz), 7.37 (1H, d, J = 2.0 Hz), 9.57 (1H, s). ^{13}C NMR (DMSO-d_6, 125 MHz): δ [ppm] = 58.7, 65.1, 70.4, 71.8, 115.8, 116.6, 120.4, 126.6, 142.3, 145.3, 165.2. EI-MS: m/z = 238 (M^+).

Compounds **22b−c** were prepared in a similar manner to that described for **4A**.

(*R*)-5-(3-(Methoxymethyl)-2,3-dihydrobenzo[*b*][1,4]dioxin-6-yl)-1,3,4-oxadiazole-2-thiol (22b). Yield 91%, orange solid. ^{1}H NMR (DMSO-d_6, 500 MHz): δ [ppm] = 3.33 (3H, s), 3.61 (2H, m), 4.10 (1H, m), 4.42 (2H, m), 7.07 (1H, m), 7.31 (1H, m), 7.37 (1H, m), 14.62 (1H, s). ^{13}C NMR (DMSO-d_6, 125 MHz): δ [ppm] = 58.8, 65.3, 70.2, 72.1, 114.6, 115.6, 118.0, 119.7, 143.3, 146.4, 160.1, 177.2. EI-MS: m/z = 280 (M^+).

(*S*)-5-(3-(Methoxymethyl)-2,3-dihydrobenzo[*b*][1,4]dioxin-6-yl)-1,3,4-oxadiazole-2-thiol (22c). Yield 91%, orange solid. ^{1}H NMR (DMSO-d_6, 500 MHz): δ [ppm] = 3.33 (3H, s), 3.61 (2H, m), 4.09 (1H, m), 4.39 (2H, m), 7.02 (1H, m), 7.24 (1H, m), 7.30 (1H, m), SH signal was not observed. ^{13}C NMR (DMSO-d_6, 125 MHz): δ [ppm] = 58.6, 65.3, 70.0, 72.1, 114.6, 115.6, 117.7, 119.7, 143.3, 146.4, 160.1, 177.2. EI-MS: m/z = 280 (M^+).

Compounds **23b−c** were prepared in a similar manner to that described for **5a**.

(*R*)-4′-((5-(3-(Methoxymethyl)-2,3-dihydrobenzo[*b*][1,4]-dioxin-6-yl)-1,3,4-oxadiazol-2-ylthio) methyl)biphenyl-2-carbonitrile (23b). Yield 84%, colorless solid. ^{1}H NMR (DMSO-d_6, 500 MHz): δ [ppm] = 3.38 (3H, s), 3.66 (2H, m), 4.15 (1H, m), 4.47 (2H, m), 4.71 (2H, s), 7.13 (1H, m), 7.50 (2H, m), 7.65 (6H, m), 7.82 (1H, td, J = 7.7 Hz, J = 1.3 Hz), 8.00 (1H, dd, J = 7.7 Hz, J = 0.9 Hz). ^{13}C NMR (DMSO-d_6, 125 MHz): δ [ppm] = 35.4, 58.7, 65.2, 70.4, 72.0, 110.1, 115.1, 116.2, 118.0, 118.4, 119.9, 128.2, 128.8, 129.4, 130.1, 133.5, 133.8, 137.2, 137.4, 143.2, 143.9, 146.2, 162.6, 164.9. HPLC: 99%; t_R 8.70 min. EI-MS: m/z = 471 (M^+).

(*S*)-4′-((5-(3-(Methoxymethyl)-2,3-dihydrobenzo[*b*][1,4]-dioxin-6-yl)-1,3,4-oxadiazol-2-ylthio) methyl)biphenyl-2-carbonitrile (23c). Yield 84%, colorless solid. ^{1}H NMR (DMSO-d_6, 500 MHz): δ [ppm] = 3.33 (3H, s), 3.61 (2H, m), 4.10 (1H, m), 4.42 (2H, m), 4.66 (2H, s), 7.07 (1H, m), 7.44 (2H, m), 7.60 (6H, m), 7.78 (1H, td, J = 7.6 Hz, J = 1.3 Hz), 7.94 (1H, dd, J = 7.7 Hz, J = 0.9 Hz). ^{13}C NMR (DMSO-d_6, 125 MHz): δ [ppm] = 35.2, 58.7, 65.2, 70.1, 71.9, 110.1, 115.1, 116.2, 117.9, 118.4, 119.9, 128.2, 128.6, 129.4, 130.1, 133.5, 133.8, 137.2, 137.4, 143.2, 143.9, 146.2, 162.6, 164.9.

dx.doi.org/10.1021/jm300309a | *J. Med. Chem.* XXXX, XXX, XXX−XXX

Table 5. Small Kinase Panel Values

kinase	enzyme conc (nM)	ATP conc (μM)	peptide used	peptide conc (μM)	buffer
GSK-3β	2	12.5	Ser/Thr 9 peptide	2	50 mM Hepes pH 7.5, 10 mM $MgCl_2$, 1 mM EGTA, 0.01% (w/v) Brij-35
GSK-3α	0.5	12.5	Ser/Thr 9 peptide	2	50 mM Hepes pH 7.5, 10 mM $MgCl_2$, 1 mM EGTA, 0.01% (w/v) Brij-35
CKIε	12	32	Ser/Thr 11 peptide	2	50 mM Hepes pH 7.5, 10 mM $MgCl_2$, 1 mM EGTA, 0.01% (w/v) Brij-35
Cdk5	10	12.5	Ser/Thr 12 peptide	2	50 mM Hepes pH 7.5, 10 mM $MgCl_2$, 1 mM EGTA, 0.01% (w/v) Brij-35
AurKA	20	10	Ser/Thr 1 peptide	2	50 mM Hepes pH 7.5, 10 mM $MgCl_2$, 1 mM EGTA, 0.01% (w/v) Brij-35
PKCα	0.15	10	Ser/Thr 7 peptide	2	50 mM Hepes pH 7.5, 10 mM $MgCl_2$, 1 mM EGTA, 0.01% (w/v) Brij-35

HPLC: 100%; t_R 8.65 min. EI-MS: m/z = 471 (M^+). HRMS (EI): m/z calcd for $C_{26}H_{21}N_3O_4S$ 471.1253, found 471.1269.

Compound **24b** was prepared in a similar manner to that described for **24a**.

(*R*)-4′-((5-(3-(Hydroxymethyl)-2,3-dihydrobenzo[*b*][1,4]-dioxin-6-yl)-1,3,4-oxadiazol-2-ylthio) methyl)biphenyl-2-carbonitrile (24b). Yield 79%, light-yellow solid. ^{1}H NMR (DMSO-d_6, 500 MHz): δ [ppm] = 3.40 (1H, s, br), 3.59 (2H, m), 4.04 (1H, m), 4.15 (1H, m), 4.34 (1H, dd, J = 11.5 Hz, J = 2.3 Hz), 4.57 (2H, s), 6.98 (1H, d, J = 8.3 Hz), 7.35 (2H, m), 7.53 (6H, m), 7.70 (1H, td, J = 7.7 Hz, J = 1.3 Hz), 7.85 (1H, dd, J = 7.7 Hz, J = 0.9 Hz). ^{13}C NMR (DMSO-d_6, 125 MHz): δ [ppm] = 35.4, 59.6, 65.4, 73.7, 110.1, 115.0, 116.1, 117.9, 118.5, 119.8, 128.2, 128.8, 129.3, 130.1, 133.4, 133.8, 137.1, 137.4, 143.5, 144.0, 146.2, 162.5, 164.9. HPLC: 95%; t_R 7.48 min. EI-MS: m/z = 457 (M^+).

(*S*)-((7-(5-(2′-Cyanobiphenyl-4-yl)methylthio)-1,3,4-oxadiazol-2-yl)-2,3-dihydrobenzo[*b*][1,4] dioxin-2-yl)-methylmethanesulfonate (25). To a solution of **24b** (238 mg, 0.52 mmol) in 10 mL of DCM was added Et_3N (0.72 mL, 5.2 mmol) followed by addition of methanesulfonyl chloride (402 μL, 5.2 mmol) at 0 °C. The reaction mixture was stirred at the same temperature for 1 h and further stirred at room temperature for 4 h. After treating with saturated $NaHCO_3$ solution, the reaction mixture was extracted with DCM. The combined organic layer was dried over $MgSO_4$, concentrated, and purified by column chromatography (EtOAc/cyclohexane, 1:1) to provide **25** (273 mg, 98%) yellow oil. ^{1}H NMR (DMSO-d_6, 500 MHz): δ [ppm] = 3.26 (3H, s), 4.17 (1H, m), 4.45 (1H, m), 4.50 (1H, dd, J = 11.6 Hz, J = 2.4 Hz), 4.55 (1H, dd, J = 11.6 Hz, J = 3.3 Hz), 4.62 (1H, m), 4.67 (2H, s), 7.11 (1H, d, J = 8.1 Hz), 7.48 (2H, m), 7.61 (6H, m), 7.77 (1H, td, J = 7.6 Hz, J = 1.3 Hz), 7.95 (1H, dd, J = 7.7 Hz, J = 0.8 Hz). ^{13}C NMR (DMSO-d_6, 125 MHz): δ [ppm] = 35.4, 36.8, 64.3, 67.8, 70.9, 110.1, 115.2, 116.4, 118.2, 118.5, 120.3, 128.2, 128.8, 129.4, 130.1, 133.5, 133.8, 137.1, 137.4, 142.7, 143.9, 145.9, 162.7, 164.9. HPLC: 96%; t_R 8.46 min. EI-MS: m/z = 535 (M^+).

(*R*)-4′-((5-(3-((2,2-Dimethoxyethylamino)methyl)-2,3-dihydrobenzo[*b*][1,4]dioxin-6-yl)-1,3,4-oxadiazol-2-ylthio)-methyl)biphenyl-2-carbonitrile (26). To a stirred solution of **25** (69 mg, 0.13 mmol) in 2 mL of THF was added 2,2-dimethoxyethylamine (140 μL, 1.3 mmol) and NEt_3 (180 μL, 1.3 mmol) at 0 °C, and the reaction mixture was stirred at room temperature for 5 days. The mixture was diluted with water and extracted with EtOAc. The organic layer was washed with brine and dried over $MgSO_4$. The solvent was evaporated under reduced pressure and the crude product purified by silica gel column chromatography (MeOH/EtOAc, 1:10) to give **26** (58 mg, 83%) as a dark-yellow oil. ^{1}H NMR (DMSO-d_6, 500 MHz): δ [ppm] = 1.91 (1H, m), 2.61 (2H, dd, J = 5.4 Hz, J = 0.7 Hz), 2.80 (2H, m), 3.18 (3H, s), 3.19 (3H, s), 4.00 (1H, m), 4.17 (1H, m), 4.30 (2H, m), 4.54 (2H, s), 6.87 (1H, m), 7.32 (2H, m), 7.44 (1H, dd, J = 7.6 Hz, J = 1.2 Hz), 7.46 (3H, m), 7.52 (2H, m), 7.64 (1H, td, J = 7.8 Hz, J = 1.3 Hz), 7.74 (1H, m). ^{13}C NMR (DMSO-d_6, 125 MHz): δ [ppm] = 36.7, 50.2, 52.1, 53.8, 53.9, 67.7, 74.1, 104.9, 111.8, 116.5, 117.8, 118.7, 119.1, 120.8, 129.0, 130.0, 130.4, 131.1, 134.1, 134.7, 138.4, 138.8, 144.7, 145.4, 147.6, 163.7, 166.3. HPLC: 95%; t_R 6.34 min. EI-MS: m/z = 544 (M^+).

GSK-3β in Vitro Assay. Purified GSK-3β (0.5 μg) was incubated in a reaction mixture of 50 mM Tris pH 7.3, 10 mM $MgAc_2$, 0.01% β-mercaptoethanol, ^{32}P[γ-ATP](100 μM, 0.5 μci/assay), and 100 μM of peptide substrate, pIRS-1 (RREGGMSRPAS(p)VDG (1). New molecules were added at various concentrations (1, 10, and 100 μM), and the reaction mixture was incubated for 15 min at 30 °C. The reactions were stopped, spotted on p81 paper (Whatman), washed with 10 mM phosphoric acid, and counted for radioactivity.[50] GSK-3β activity was calculated as the percentage of GSK-3β activity in the absence of inhibitor that was designated to 100%.

Small Kinase Panel. Compounds were serially diluted 1/3 in neat DMSO (10 serial dilutions), and these dilutions were further diluted 1/25 with reaction buffer. Then 2.5 μL of these solutions were added to the reaction mixture described below so that final compound concentration in the assay ranges from 100 μM to 5 nM in 1% (v/v) DMSO. When compounds showed high inhibition at 5 nM and therefore the data could not be fitted to the corresponding equation, they were re-evaluated in a new range from 400 nM to 20 pM (Table 5).

The enzymatic activity of the kinases was determined with a commercial system based on the Z′-LYTE technology, available from Invitrogen Life Technologies (Carlsbad, CA, USA), using human recombinant kinases as the enzyme source. This technology utilizes the fluorescence resonance energy transfer ("FRET") process between fluorescein and coumarin. The assay principle is based on the differential sensitivity of phosphorylated and nonphosphorylated peptide to proteolytic cleavage, which precludes the energy transfer process between the two fluorophores attached to both sides of the cleavage site. Hence, enzymatic phosphorylation will yield a phosphopeptide, which cannot be hydrolyzed by a suitable protease and energy transfer between the two fluorophores will occur. Opposingly, lack of phosphorylation will cause peptide hydrolysis hence lack of energy transfer as. The assay was performed in 96-well black plates, in a final volume of 10 μL, with components as detailed in Tables 1, 3, and 4.

In Vivo Activity on Zebrafish Embryos. The wt zebrafish was used in this study. The embryos were collected and placed into 24-well plates, 10 embryos per well, and maintained in E2 medium at ∼28 °C. Compounds were added 5 hpf (50% epiboly) and the embryos allowed to grow in chemical compound solution up to 2 days. The phenotypes were compared using the Axio Scope.A1 microscope system from Carl Zeiss at 44−48 hpf.[36,37,51]

Animal Husbandry. All animal experiment were conducted and documented according to the federal and local regulation. All embryo testing was stopped at day 5 of embryonic development.

SH-SY5Y Neuroblastoma Cells. SH-SY5Y neuroblastoma cells stably transfected with Tau.P301L in the pcDNA3 vector were grown to confluency in 6-well cluster plates (∼800000 cells/well) in DMEM-F12 medium supplemented with Glutamax and 15% fetal calf serum. The medium contained gentamycin (50 μg/mL) as general antibiotic and Geneticin (250 μg/mL) to maintain selection pressure on transfected cells. Cells were grown at 37 °C in a humidified incubator in an atmosphere of 5.0% CO_2 in air. Stock solutions of the

dx.doi.org/10.1021/jm300309a | J. Med. Chem. XXXX, XXX, XXX−XXX

compounds in DMSO were added to serum-free culture medium to the specified concentrations, using DMSO in the same final concentrations as control. Cells were incubated with the compounds at 37 °C for the indicated periods of time. After incubation, spent medium was removed and cells washed once with PBS containing Ca^{2+} and Mg^{2+}. The cells were rapidly harvested by mechanical scraping after addition of hot 62.5 mM Tris pH 6.8 buffer, containing 1% SDS (180 μL per well). Protein extracts were collected by aspiration and reduced and denatured by addition of 1% β-mercaptoethanol and boiling for 10 min. After separation by SDS-PAGE on 10% Tris-glycine SDS-PAGE, proteins were analyzed by Western blotting using the ECL-system.[52] In brief, after SDS-PAGE, the separated proteins were transferred to nitrocellulose filter-sheets, which were treated against nonspecific binding by incubation in 5% nonfat milk in Tris buffered saline (TBS: 10 mM Tris.HCl, pH 7.2, 0.9% sodium chloride, 0.1% Tween). Blots were subsequently incubated with primary antibodies specifically directed against total protein tau or against its selected phosphorylated epitopes, as specified in Results and Discussion and in the figure legends. After incubation with suitably labeled secondary antibodies, the resulting immune reactions were recorded and analyzed digitally with dedicated apparatus and software (LAS4000, Image-QuantTL, GE Healthcare, Brussels, Belgium). Data for tau and phospho-tau were normalized against actin, revealed by Western blotting of the same samples on the same blots.

Docking Simulations. Molecular docking of **15a** into the X-ray structure of GSK-3β (PDB code: 3F88) was carried out using the Glide 5.5 program.[53] Maestro 9.0.211 was employed as the graphical user interface, and Figure 2 was rendered by the Chimera software package.[54,55]

Ligand and Protein Setup. The inhibitor structure was first generated through the Dundee PRODRG2 server.[56] Then geometry optimized ligand was prepared using Lig-Prep 2.3 as implemented in Maestro. The target protein was prepared through the Protein Preparation Wizard of the graphical user interface Maestro and the OPLS-2001 force field. Water molecules were removed. Hydrogen atoms were added, and minimization was performed until the rmsd of all heavy atoms was within 0.3 Å of the crystallographically determined positions. The binding pocket was identified by placing a 20 Å cube centered on the mass center of the cocrystallized inhibitor. Molecular docking calculations were performed with the aid of Glide 5.5 in extra-precision (XP) mode, using Glidescore for ligand ranking.[57,58] For multiple ligand docking experiments, an output maximum of 5000 ligand poses per docking run with a limit of 100 poses for each ligand was adopted.

Homology Modeling. The homology model was built using the crystal structure of GSK-3β (PDB code: 3F88). The sequence identity between GSK-3α and GSK-3β is 61%. The alignment was performed by Prime, which calculates alignments using a combination of sequence and secondary structure information. The sequence of the human GSK-3α was obtained from the Universal Protein Resource (http://www.uniprot.org/) (code: P49840) and aligned using Prime. The homology model was inspected to ensure that the side chains of the conserved residues were aligned to the template.

■ ASSOCIATED CONTENT

Supporting Information

Homology modeling, in vitro pharmacology, bioavailability profile of compound **14d** and NMR data of compounds **5b**, **5c**, **6b**, **6c**, **14b**, **14c**, **14d**, **15a**, **15b**, **16a**, **23a**, **23b**, and **23c**. This material is available free of charge via the Internet at http://pubs.acs.org.

■ AUTHOR INFORMATION

Corresponding Author

*Phone: +496151-164531. Fax: +496151-163278. E-mail: schmidt_boris@t-online.de (B.S.); Fabio.Lo-Monte@gmx.de (F.L.).

Notes

The authors declare no competing financial interest.

■ ACKNOWLEDGMENTS

This work was supported by a collaborative project financed by the 7th Framework Program of the European Union (neuro.GSK3).

■ ABBREVIATIONS USED

ATP, adenosine triphosphate; AD, Alzheimer's disease; BBB, blood−brain barrier; Cdk, cyclin-dependent kinase; GSK-3, glycogen synthase kinase-3; DMF, dimethylformamide; DMSO, dimethyl sulfoxide; EtOAc, ethyl acetate; EtOH, ethanol; hpf, hours post fertilization; HPLC, high performance liquid chromatography; MeOH, methanol; SAR, structure−activity relationship

■ REFERENCES

(1) Engel, T.; Goni-Oliver, P.; Gómez de Barreda, E.; Lucas, J. J; Hernandez, F.; Avila, J. Lithium, a Potential Protective Drug in Alzheimer's Disease. *Neurodegenerative Dis.* **2008**, *5*, 247−249.

(2) Citron, M. Alzheimer's disease: strategies for disease modification. *Nature Rev. Drug Discovery* **2010**, *9*, 387−397.

(3) Mazanetz, M. P.; Fischer, P. M. Untangling tau hyperphosphorylation in drug design for neurodegenerative diseases. *Nature Rev. Drug Discovery* **2007**, *6*, 464−479.

(4) Cohen, P.; Goedert, M. GSK3 Inhibitors: Development and Therapeutic Potential. *Nature Rev. Drug Discovery* **2004**, *3*, 479−487.

(5) Saitoh, M.; Kunitomo, J.; Kimura, E.; Iwashita, H.; Uno, Y.; Onishi, T.; Uchiyama, N.; Kawamoto, T.; Tanaka, T.; Mol, C. D.; Dougan, D. R.; Textor, G. P.; Snell, G. P.; Takizawa, M.; Itoh, F.; Kori, M. 2-[3-[4-(Alkylsulfinyl)phenyl]-1-benzofuran-5-yl]-5-methyl-1,3,4-oxadiazole Derivatives as Novel Inhibitors of Glycogen Synthase Kinase-3β with Good Brain Permeability. *J. Med. Chem.* **2009**, *52*, 6270−6286.

(6) Martinez, A. Preclinical Efficacy on GSK-3 Inhibitors: Towards a Future Generation of Powerful Drugs. *Med. Res. Rev.* **2008**, *28*, 773−796.

(7) Frame, S.; Cohen, P. GSK3 takes centre stage more than 20 years after its discovery. *Biochem. J.* **2001**, *359*, 1−16.

(8) Cohen, P.; Frame, S. The renaissance of GSK3. *Nature Rev. Mol. Cell Biol.* **2001**, *2*, 769−775.

(9) Martinez, A.; Castro, A.; Dorronsoro, I.; Alonso, M. Glycogen Synthase Kinase 3 (GSK-3)—Inhibitors as New Promising Drugs for Diabetes, Neurodegeneration, Cancer and Inflammation. *Med. Res. Rev.* **2002**, *22*, 373−384.

(10) Bhat, R. V.; Budd Haeberlein, S. L.; Avila, J. Glycogen synthase kinase 3: a drug target for CNS therapies. *J. Neurochem.* **2004**, *89*, 1313−1317.

(11) Zou, H.; Zhou, L.; Li, Y.; Cui, Y.; Zhong, H.; Pan, Z.; Yan, Z.; Quan, J. Benzo[*e*]isoindole-1,3-diones as potential Inhibitors of Glycogen Synthase Kinase-3 (GSK-3). Synthesis, Kinase Inhibitory Activity, Zebrafish Phenotype, and Modeling of Binding Mode. *J. Med. Chem.* **2010**, *53*, 994−1003.

(12) Kaidanovich-Beilin, O.; Lipina, T. V.; Takao, K.; van Eede, M.; Hattori, S.; Laliberté, C.; Khan, M.; Pkamoto, K.; Chambers, J. W.; Fletcher, P. J.; MacAulay, K.; Doble, B. W.; Henkelman, M.; Miyakawa, T.; Roder, J.; Woodgett, J. R. Abnormalities in brain structure and behavior in GSK-3alpha mutant mice. *Mol. Brain* **2009**, *2*, 1−23.

(13) Alon, L. T.; Pietrokovski, S.; Barkan, S.; Avrahami, L.; Kaidanovich-Beilin, O.; Woodgett, J. R.; Barnea, A.; Eldar-Finkelman, H. Selective loss of glycogen synthase kinase-3α in birds reveals distinct roles for GSK-3 isozymes in tau phosphorylation. *FEBS Lett.* **2011**, *585*, 1158−1162.

(14) Phiel, C. J.; Wislon, C. A.; Lee, V. M.-Y.; Klein, P. S. GSK-3α regulates production of Alzheimer's disease amyloid-β peptides. *Nature* **2003**, *423*, 435−439.
(15) Zhou, J.; Lal, H.; Chen, X.; Shang, X.; Song, J.; Li, Y.; Kerkela, R.; Doble, B. W.; MacAulay, K.; DeCaul, M.; Koch, W. J.; Farber, J.; Woodgett, J.; Gao, E.; Force, T. GSK-3α directly regulates β-adrenergic signaling and the response of the heart to hemodynamic stress in mice. *J. Clin. Invest.* **2010**, *120*, 2280−2291.
(16) Banerji, V.; Frumm, S. M.; Ross, K. N.; Li, L. S.; Schinzel, A. C.; Hahn, C. K.; Kakoza, R. M.; Chow, K. T.; Ross, L.; Alexe, G.; Tolliday, N.; Inguilizian, H.; Galinsky, I.; Stone, R. M.; DeAngelo, D. J.; Roti, G.; Aster, J. C.; Hahn, W. C.; Kung, A. L.; Stegmaier, K. The intersection of genetic and chemical genomic screens identifies GSK-3α as a target in human acute myeloid leukemia. *J. Clin. Invest.* **2012**, *122*, 935−947.
(17) Dajani, R.; Fraser, E.; Roe, S. M.; Young, N.; Good, V.; Dale, T. C.; Pearl, L. H. Crystal Structure of Glycogen Synthase Kinase 3β: Structural Basis for Phosphate-Primed Substrate Specificity and Autoinhibition. *Cell* **2001**, *105*, 721−732.
(18) Leclerc, S.; Garnier, M.; Hoessel, R.; Marko, D.; Bibb, J. A.; Snyder, G. L.; Greengard, P.; Biernat, J.; Wu, Y. Z.; Mandelkow, E. M.; Eisenbrand, G.; Meijer, L. Indirubins inhibit glycogen synthase kinase-3 beta and CDK5/p25, two protein kinases involved in abnormal tau phosphorylation in Alzheimer's disease. A property common to most cyclin-dependent kinase inhibitors? *J. Biol. Chem.* **2001**, *276*, 251−260.
(19) Leost, M.; Schultz, C.; Link, A.; Wu, Y. Z.; Biernat, J.; Mandelkow, E. M.; Bibb, J. A.; Snyder, G. L.; Greengard, P.; Zaharevitz, D. W.; Gussio, R.; Senderowicz, A. M.; Sausville, E. A.; Kunick, C.; Meijer, L. Paullones are potent inhibitors of glycogen synthase kinase-3beta and cyclin-dependent kinase 5/p25. *Eur. J. Biochem.* **2000**, *267*, 5983−5994.
(20) Martinez, A.; Alonso, M.; Castro, A.; Perez, C.; Moreno, F. J. First non-ATP competitive glycogen synthase kinase 3 beta (GSK-3beta) inhibitors: thiadiazolidinones (TDZD) as potential drugs for the treatment of Alzheimer's disease. *J. Med. Chem.* **2002**, *45*, 1292−1299.
(21) Smith, D. G.; Buffet, M.; Fenwick, A. E.; Haigh, D.; Ife, R. J.; Saunders, M.; Slingsby, B. P.; Stacey, R.; Ward, R. W. 3-Anilino-4-arylmaleimides: potent and selective inhibitors of glycogen synthase kinase-3 (GSK-3). *Bioorg. Med. Chem. Lett.* **2001**, *11*, 635−639.
(22) Lo Monte, F.; Kramer, T.; Boländer, A.; Plotkin, B.; Eldar-Finkelman, H.; Fuertes, A.; Dominguez, J. M.; Schmidt, B. Synthesis and biological evaluation of glycogen synthase kinase 3 (GSK-3) inhibitors: a fast and atom efficient access to 1-aryl-3-benzylureas. *Bioorg. Med. Chem. Lett.* **2011**, *21*, 5610−5615.
(23) Eldar-Finkelman, H.; Martinez, A. GSK-3 inhibitors: preclinical and clinical focus on CNS. *Front. Mol. Neurosci.* **2011**, *4*, 1−18.
(24) Kramer, T.; Schmidt, B.; Lo Monte, F. Small-molecule inhibitors of GSK-3—Structural insights and their application to Alzheimer's disease models. *Int. J. Alzheimer's Dis.* **2012**, in press.
(25) Naerum, L.; Norskov-Lauritsen, L.; Olesen, P. H. Scaffold hopping and optimization towards libraries of glycogen synthase kinase-3 inhibitors. *Bioorg. Med. Chem. Lett.* **2002**, *12*, 1525−1528.
(26) Saitoh, M.; Kunitomo, J.; Kimura, E.; Hayase, Y.; Kobayashi, H.; Uchiyama, N.; Kawamoto, T.; Tanaka, T.; Mol, C. D.; Dougan, D. R.; Textor, G. S.; Snell, G. P.; Itoh, F. Design, synthesis and structure−activity relationships of 1,3,4-oxadiazole derivatives as novel inhibitors of glycogen synthase kinase-3beta. *Bioorg. Med. Chem.* **2009**, *17*, 2017−2029.
(27) Oertby, E.; Pictet, A. Derivatives of Piperonylic Acid. *Ber. Dtsch. Chem. Ges.* **1910**, *43*, 1336−1340.
(28) Yu, T.; Hsu, L.; Wu, S. *Huaxue Xuebao* **1958**, *24*, 170−173.
(29) Mc Fayden, J. S.; Stevens, T. S. New method for the conversion of acids into aldehydes. *J. Chem. Soc.* **1936**, 584−587.
(30) Konig, H. B.; Seifken, W.; Offe, H. A. Sulfur-containing derivatives of pyridine carboxylic acids and compounds derived therefrom. *Chem. Ber.* **1954**, *87*, 825−834.
(31) Mazzone, G.; Bonina, F.; Arrigo-Reina, R. Synthesis and pharmacological activities of some 2-(alkylaminoalkyl)mercapto-5-aryl-(1,3,4-oxadiazoles). *Farmaco, Ed. Sci.* **1977**, *32*, 414−429.
(32) Omar, R. H.; El-Fattah, B. A. Synthesis of certain pyridyl 1,3,4-oxadiazoles of biological interest and study of the cleavage of certain substituted oxadiazole rings with primary amines. *Egypt. J. Pharm. Sci.* **1985**, *24*, 49−56.
(33) Akwabi-Ameyaw, A.; Bass, J. Y.; Caldwell, R. D.; Caravella, J. A.; Chen, L.; Creech, K. L.; Deaton, D. N.; Madauss, K. P.; Marr, H. B.; McFadyen, R. B.; Miller, A. B.; Navas, F., III; Parks, D. J.; Spearing, P. K.; Todd, D.; Williams, S. P.; Wisely, G. B. FXR agonist activity of conformationally constrained analogs of GW 4064. *Bioorg. Med. Chem.* **2009**, *19*, 4733−4739.
(34) Dolezal, M.; Palek, L.; Vinsova, J.; Buchta, V.; Jampilek, J.; Kralova, K. Substituted Pyrazinecarboxamides: Synthesis and Biological Evaluation. *Molecules* **2006**, *11*, 242−256.
(35) Schmidt, B.; Meid, D.; Kieser, D. Safe and fast tetrazole formation in ionic liquids. *Tetrahedron* **2007**, *63*, 492−496.
(36) Funke, A.; Paulsen, A.; Cibrario, N. Chloromethyl- and aminomethyl(acetyl)benzodioxan isomers and derivatives resulting from oxidation of the acetyl group. *Bull. Soc. Chim. Fr.* **1958**, 470−473.
(37) Hormann, R. E.; Tice, C. M.; Chortyk, O.; Smith, H.; Meteyer, T. Diacylhydrazine ligands for modulating the expression of exogenous genes in mammalian systems via an ecdysone receptor complex. PCT-WO 2004/072254 2004, pp 1−120.
(38) Alksnis, A. F.; Surna, J. A. Preparation of Benzodioxane Derivatives. GB Patent 1109275 1965, pp 1−2.
(39) Satoh, Y.; Powers, C.; Toledo, L. M.; Kowalski, T. J.; Peters, P. A.; Kimble, E. F. Derivatives of 2-[[*N*-(Aminocarbonyl)-*N*-hydroxyamino]methyl]-1,4-benzodioxan as Orally Active 5-Lipoxygenase Inhibitors. *J. Med. Chem.* **1995**, *38*, 68−75.
(40) Lee, J. Y.; Park, Y. K.; Seo, S. H.; Yang, B.; Park, H.; Lee, Y. S. 7-Substituted-[1,4]dioxano[2,3-g]quinazolines as Inhibitors of Epidermal Growth Factor Receptor Kinase. *Arch. Pharm. Pharm. Med. Chem.* **2002**, *10*, 487−494.
(41) Feng, L.; Geisselbrecht, Y.; Black, S.; Wilbuer, A.; Atilla-Gokcumen, G. E.; Filippakopoulos, P.; Kräling, K.; Celik, M. A.; Harms, K.; Maksimoska, J.; Marmorstein, R.; Frenking, G.; Knapp, S.; Essen, L.; Meggers, E. Structurally Sophisticated Octahedral Metal Complexes as Highly Selective Protein Kinase Inhibitors. *J. Am. Chem. Soc.* **2011**, *133*, 5976−5986.
(42) Limongelli, V.; Marinelli, L.; Cosconati, S.; La Motta, C.; Sartini, S.; Mugnaini, L.; Da Settimo, F.; Novellino, E.; Parrinello, M. Sampling protein motion and solvent effect during ligand binding. *Proc. Natl. Acad. Sci. U.S.A.* **2012**, *109*, 1467−1472.
(43) Limongelli, V.; Bonomi, M.; Marinelli, L.; Gervasio, F. L.; Cavalli, A.; Novellino, E.; Parrinello, M. Molecular basis of cyclooxygenase enzymes (COXs) selective inhibition. *Proc. Natl. Acad. Sci. U.S.A.* **2010**, *107*, 5411−5416.
(44) Atilla-Gokcumen, G. E.; Williams, D. S.; Bregman, H.; Pagano, N.; Meggers, E. Organometallic Compounds with Biological Activity: A Very Selective and Highly Potent Cellular Inhibitor for Glycogen Synthase Kinase 3. *ChemBioChem* **2006**, *7*, 1443−1450.
(45) Paquet, D.; Bhat, R.; Sydow, A.; Mandelkow, E.; Berg, S.; Hellberg, S.; Fälting, J.; Distel, M.; Köster, R. W.; Schmid, B.; Haass, C. A zebrafish model of tauopathy allows in vivo imaging of neuronal cell death and drug evaluation. *J. Clin. Invest.* **2009**, *119*, 1382−1395.
(46) Azoulay-Alfaguter, I.; Yaffe, Y.; Licht-Murava, A.; Urbanska, M.; Jaworski, J.; Pietrokovski, S.; Hirschberg, K.; Eldar-Finkelman, H. Distinct molecular regulation of glycogen synthase kinase-3alpha isozyme controlled by its N-terminal region: functional role in calcium/calpain signaling. *J. Biol. Chem.* **2011**, *286*, 13470−13480.
(47) Jaworski, T.; Dewachter, I.; Lechat, B.; Gees, M.; Kremer, A.; Demedts, D.; Borghgreaf, P.; Devijver, H.; Kügler, S.; Patel, S.; Woodgett, J. R.; Van Leuven, F. GSK-3α/β kinases and amyloid production in vivo. *Nature* **2011**, *480*, E4−E5.
(48) Phiel, C. J.; Wislon, C. A.; Lee, V. M.-Y.; Klein, P. S. Phiel et al. reply. *Nature* **2011**, *480*, E6.

(49) Tromp, R. A.; van Ameijde, S.; Pütz, C.; Sundermann, C.; Sundermann, B; von Frijtag Drabbe Künzel, J. K.; IJzerman, P. Inhibition of Nucleoside Transport by New Analogues of 4-Nitrobenzylthioinosine: Replacement of the Ribose Moiety by Substituted Benzyl Groups. *J. Med. Chem.* **2004**, *47*, 5441−5450.
(50) Liberman, Z.; Eldar-Finkelman, H. Serine 332 phosphorylation of insulin receptor substrate-1 by glycogen synthase kinase-3 attenuates insulin signaling. *J. Biol. Chem.* **2005**, *280*, 4422−4428.
(51) Kimmel, C. B.; Ballard, W. W.; Kimmel, S. R.; Ullmann, B.; Schilling, T. F. Stages of Embryonic Development of the Zebrafish. *Dev. Dyn.* **1995**, *203*, 253−310.
(52) Dutschmann, M.; Menuet, C.; Stettner, G. M.; Gertreau, C.; Borghgraef, P.; Devijver, H.; Gielis, L.; Hilaire, G.; Van Leuven, F. Upper airway dysfunction of Tau.P301L mice correlates with tauopathy in midbrain and ponto-medullary brainstem nuclei. *J. Neurosci.* **2010**, *30*, 1810−1821.
(53) *Glide*, version 5.5; Schrödinger, LLC: New York, 2009.
(54) *Maestro*, version 9.0.211; Schrödinger, LLC: New York, 2009.
(55) Pettersen, E. F.; Goddard, T. D.; Huang, C. C.; Couch, G. S.; Greenblatt, D. M.; Meng, E. C.; Ferrin, T. E. UCSF chimera—a visualization system for exploratory research and analysis. *J. Comput. Chem.* **2004**, *25*, 1605−1612.
(56) Schuttelkopf, A. W.; van Aalten, D. M. PRODRG: a tool for high-throughput crystallography of protein−ligand complexes. *Acta Crystallogr., Sect. D: Biol. Crystallogr.* **2004**, *60*, 1355−1363.
(57) Friesner, R. A.; Murphy, R. B.; Repasky, M. P.; Frye, L. L.; Greenwood, J. R.; Halgren, T. A.; Sanschagrin, P. C.; Mainz, D. T. Extra precision glide: docking and scoring incorporating a model of hydrophobic enclosure for protein-ligand complexes. *J. Med. Chem.* **2006**, *49*, 6177−6196.
(58) Friesner, R. A.; Banks, J. L.; Murphy, R. B.; Halgren, T. A.; Klicic, J. J.; Mainz, D. T.; Repasky, M. P.; Knoll, E. H.; Shelley, M.; Perry, J. K.; Shaw, D. E.; Francis, P.; Shenkin, P. S. Glide: a new approach for rapid, accurate docking and scoring. 1. Method and assesment of docking accuracy. *J. Med. Chem.* **2004**, *47*, 1739−1749.

3.4 Strukturelle Optimierung von oxadiazolbasierten GSK-3-Inhibitoren

Der Inhalt dieses Kapitels wurde bereits veröffentlicht: Fabio Lo Monte, Thomas Kramer, Jiamin Gu, Martin Brodrecht, Johannes Pilakowski, Ana Fuertes, Juan Manuel Dominguez, Batya Plotkin, Hagit Eldar-Finkelman, Boris Schmidt, „*Structure-based optimization of oxadiazole-based GSK-3 Inhibitors*", Eur. J. Med. Chem. **2012**, *in press*, http://dx.doi.org/10.1016/j.ejmech.2012.06.006.

Mit freundlicher Genehmigung von *Elsevier*.

1,3,4-Oxadiazole wurden bereits mehrfach als Teil von potenten GSK-3 Inhibitoren publiziert und besitzen gegenüber 1,2,4-Oxadiazolen und anderen Heterozyklen bessere medizinalchemische Eigenschaften.[311] Die strukturelle Optimierung der oxadiazolbasierten GSK-3-Inhibitoren erfolgte in mehreren Abschnitten. Neben der Substitution des Oxadiazols durch ein Carbohydrazidmotiv wurde der heterozyklische Rest an sich modifiziert und das Biphenyl derivatisiert, Abb. 30.

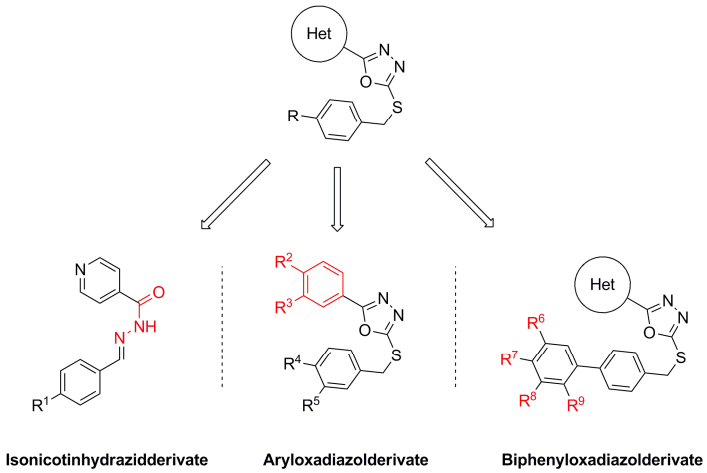

Abb. 30: Schematische Darstellung der Isonicotinhydrazidderivate (links), der Aryloxadiazolderivate (mitte) und der Biphenyloxadiazolderivate (rechts); Het = Benzodioxan-, Piperonyl- oder Pyridinrest; R-R^9 = unterschiedliche funktionelle Gruppen oder Alkyl-/Arylreste.

Zudem wurden Pyridin- und Benzothiazolamide als Kombination aus zwei GSK-3-Inhibitorstrukturmotiven: Harnstoffe und Oxadiazole, synthetisiert, Abb. 31. Damit sollen die Interaktionen der Harnstoffderivate (entlang der Gelenkregion der ATP-Bindungstasche) mit den Interaktionen der Biphenylderivate (mit der glycinreichen Schleife der ATP-Bindungstasche) kombiniert werden.

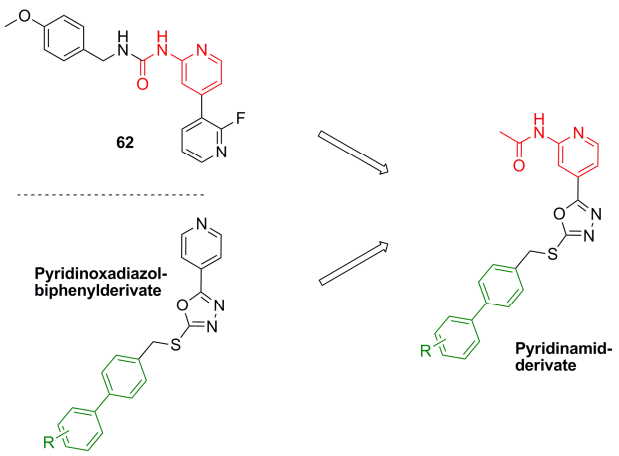

Abb. 31: Schematische Darstellung der Kombination zweier Strukturmotive am Beispiel des Pyridinamids. Kombiniert wurden **62** und Pyridinoxadiazolbiphenylderivate. R = funktionelle Gruppe, z. B. CN.

Alle Isonicotinhydrazide und Aryloxadiazolderivate erzielten bei einer Applikationsmenge von 10 µM pro Substanz im GSK-3 *in vitro* Assay entweder keine Inhibition oder nur eine vergleichsweise geringe Inhibition von maximal 50 %. Dahingegen inhibierten die Biphenyloxadiazolderivate GSK-3 bis in den einstelligen nanomolaren Bereich. Fast alle Biphenyle wiesen dabei eine Spezifität für GSK-3α auf. Der isoenzymspezifischste GSK-3α-Inhibitor ist **8g**. Er inhibierte GSK-3α 27-fach stärker als GSK-3β und zeigte keine inhibitorische Wirkung auf vier weitere Kinasen, CDK5/p35, CK1ε, AurKA und PKCα. Docking Studien der synthetisierten Inhibitoren in die ATP-Bindungstasche von GSK-3β (PDB Code: 3F88) ermöglichen einen Hinweis auf potentielle Interaktionen. Diese deuten darauf hin, dass Reste in para-Position des Biphenyls (α-selektiver Stachel) mit einem Aminosäurelager um Arg141 interagieren und somit eine mögliche α-Selektivität hervorrufen, Abb. 32. Diese Hypothese muss jedoch noch weiter untersucht werden. Eine Co-Kristallisation der Biphenyloxadiazolderivate mit GSK-3α und GSK-3β könnte dazu weitere Hinweise liefern.

Die Kombination von Strukturmotiven bekannter GSK-3-Inhibitoren erzielte im Falle der Pyridinamide verglichen mit den Pyridinderivaten ohne Amidrest eine Aktivitätssteigerung. Was für ein verbessertes Interaktionsmuster zwischen Inhibitor und ATP-Bindungstasche spricht. Das aktivste Pyridinamid ist mit einem IC_{50} von 2 nM für GSK-3α und 17 nM für GSK-3β **26d**, Abb. 33 rechts. Eine Docking Studie von **26d** in der ATP-Bindungstasche von GSK-3β (PDB Code: 3F88) ergab neben

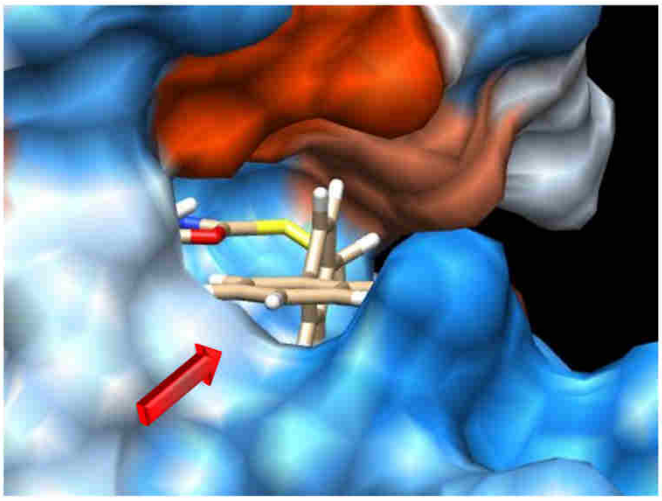

Abb. 32: Schematische Darstellung einer Docking Studien eines Biphenyloxadiazolderivats und GSK-3β. Der rote Pfeil weist auf die para-Position des Biphenylrestes und das Aminosäurelager um Arg141 hin (Verwendete Software: Molegro Virtual Docker 5; PDB Code = 3F88).[239]

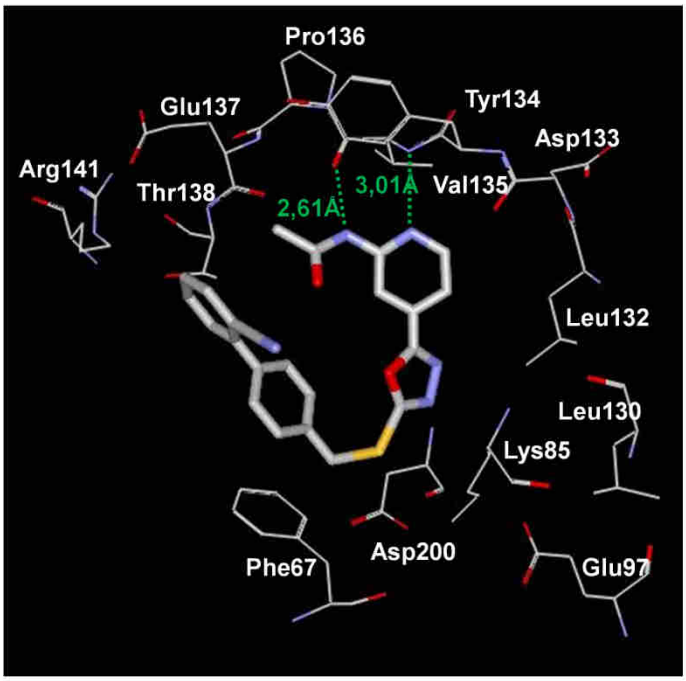

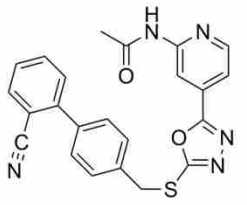

26d
IC_{50} (GSK-3α) = 2 nM
IC_{50} (GSK-3β) = 17 nM

Abb. 33: Links: Docking Studie von **26d** in die ATP-Bindungstasche von GSK-3β (Verwendete Software: Molegro Virtual Docker 5; PDB Code = 3F88); Rechts: Strukturformel von **26d** (Hinweis: Auf Grund der Veranschaulichung ist der Bindungswinkel der Methylenbrücke > 109.5°).[239]

einer möglichen Interaktion zwischen dem Pyridinstickstoff und dem NH des Tyr134 auch eine zwischen dem NH des Amids mit dem Val135 der Gelenkregion, Abb. 33 links. Die Selektivität von **26d** wurde in einem kleinen Kinase-Panel getestet. Gegenüber den vier Kinasen CDK5/p35, CK1ε, AurKA und PKCα zeigte **26d** keine inhibitorische Wirkung. Anschließend wurde **26d** in einem *zebrafish embryo*

phenotype assay auf seine *in vivo* Aktivität getestet. Bei einer Applikation von 30 μM entwickelten die Zebrafischembryos ein gekrümmtes bzw. verkürztes Rückgrat. Dies korreliert mit den Ergebnissen von *zebrafish embryo phenotype assays* durchgeführt mit bekannten GSK-3-Inhibitoren, wie **LiCl** und dem Rutheniumkomplex **(R)-7**.[309,310] Der Grund liegt in dem Einfluss von GSK-3β auf den WNT-Signalweg und somit auf die Entwicklung von Metazoan.

Das Benzothiazolamid **35** und zusätzlich synthetisierte, nicht veröffentlichte Benzothiazolderivate (Synthese siehe Kapitel: Experimenteller Teil – Ein Auszug) erwiesen sich als inaktiv gegenüber GSK-3α sowie GSK-3β. Eine Begründung dafür könnte eine zu direkte Positionierung des Amid-/Alkylrests in Richtung der Gelenkregion der ATP-Bindungstasche sein.

Die im Rahmen dieser Arbeit synthetisierten Verbindungen sind: **8a (BSc4733), 8f (BSc4675), 8h (BSc4673), 9e (BSc4671), 10b (BSc4679), 10f (BSc4677), 15a-d (BSc4676, BSc4673, BSc4675, BSc4674), 16a-d (BSc4679, BSc4672, BSc4678, BSc4677), 17a-d (BSc4668, BSc4667, BSc4664, BSc4666), 18a-d (BSc4671, BSc4670, BSc4665, BSc4669), 35 (BSc4680), 41 (BSc4735).**

ARTICLE IN PRESS

European Journal of Medicinal Chemistry xxx (2012) 1–15

Contents lists available at SciVerse ScienceDirect

European Journal of Medicinal Chemistry

journal homepage: http://www.elsevier.com/locate/ejmech

Original article

Structure-based optimization of oxadiazole-based GSK-3 inhibitors

Fabio Lo Monte [a,*], Thomas Kramer [a], Jiamin Gu [a], Martin Brodrecht [a], Johannes Pilakowski [a], Ana Fuertes [b], Juan Manuel Dominguez [b], Batya Plotkin [c], Hagit Eldar-Finkelman [c], Boris Schmidt [a,*]

[a] Clemens Schöpf – Institute of Organic Chemistry and Biochemistry, Technische Universität Darmstadt, Petersenstrasse 22, 64287 Darmstadt, Germany
[b] Noscira S.A., Drug Discovery, Tres Cantos 28760 Madrid, Spain
[c] Department of Human Molecular Genetics and Biochemistry, Sackler School of Medicine, Tel Aviv University, 69978 Tel Aviv, Israel

ARTICLE INFO

Article history:
Received 16 March 2012
Received in revised form
16 May 2012
Accepted 3 June 2012
Available online xxx

Keywords:
Glycogen synthase Kinase-3 (GSK-3)
Alzheimer's disease
Structure–activity relationship (SAR)
Reversible inhibition
Zebrafish phenotype

ABSTRACT

Inhibition of glycogen synthase kinase-3 (GSK-3) induces neuroprotective effects, e.g. decreases β-amyloid production and reduces tau hyperphosphorylation, which are both associated with Alzheimer's disease (AD). The two isoforms of GSK-3 in mammalians are GSK-3α and β, which share 98% homology in their catalytic domains. We investigated GSK-3 inhibitors based on 2 different scaffolds in order to elucidate the demands of the ATP-binding pocket [1]. Particularly, the oxadiazole scaffold provided potent and selective GSK-3 inhibitors. For example, the most potent inhibitor of the present series, the acetamide **26d**, is characterized by an IC_{50} of 2 nM for GSK-3α and 17 nM for GSK-3β. In addition, the benzodioxane **8g** showed up to 27-fold selectivity for GSK-3α over GSK-3β, with an IC_{50} of 35 nM for GSK-3α. Two GSK-3 inhibitors were further profiled for efficacy and toxicity in the wild-type (wt) zebrafish embryo assay to evaluate simultaneously permeability and safety.

1. Introduction

Alzheimer's disease (AD) is a neurodegenerative disorder and characterized by the presence of abnormal filamentous protein inclusions in nerve cells of the brain [2]. The neuropathological hallmarks of AD were first reported by Alois Alzheimer and date back to 1907 [3,4]. These inclusions are formed by extracellular amyloid deposits and intracellular microtubule-associated protein tau [5]. Early onset forms of familial Alzheimer's disease (FAD) have been linked to mutations in the amyloid precursor protein (APP), presenilin-1 (PS-1) and presenilin-2 (PS-2). These mutations adversely affect APP processing and result in the increased production of the 40-42 amino acid long β-amyloid (Aβ) peptides, which are the major component of amyloid deposits. Several risk factors have been associated with sporadic Alzheimer's disease (SAD). The most prevalent is aging and the presence of specific ApoE isoforms, which have been implicated in Aβ clearance. The activation of β-secretase may be involved in Aβ generation, which in combination with a deficiency in Aβ clearance will result in the accumulation of Aβ aggregates [2,6]. Partially phosphorylated tau in the normal adult brain features sequences that support association with tubulin, which entails the stabilization of microtubules. The pathological hyperphosphorylation of tau causes destabilization of microtubules, which in turn interferes with tubulin binding. The misfolding of hyperphosphorylated tau leads to the formation of insoluble neurofibrillary tangles (NFTs) and intraneuronal aggregates of paired helical filaments (PHFs) [7,8]. GSK-3 was shown to phosphorylate tau both *in vitro* and *in vivo* on multiple sites [7]. Several studies demonstrate that inhibition of GSK-3 induces decreased Aβ production and a reduction in tau hyperphosphorylation [9,10]. GSK-3 was identified in the late 1970s and is a constitutively active, ubiquitously expressed serine/threonine kinase, which participates in a number of physiological processes [2,11]. Two related isoforms of GSK-3 exist in mammals, GSK-3α and β, which share 98% homology in their catalytic domains and have similar biochemical properties [7,12]. The isoforms differ significantly outside of their catalytic domains at their N-terminal regions [13]. Furthermore, an alternative splice variant of GSK-3β: GSK-3β2, has been reported for rodents and humans [14,15]. The crystal structure of GSK-3β was determined in 2001 [16,17]. GSK-3 is highly enriched in the brain and several publications indicate that the GSK-3β isoform is a key kinase required for abnormal hyperphosphorylation of tau [18–20]. Lithium chloride was the first GSK-3 inhibitor to be discovered. However there are several other biological targets for lithium cations, which impose limits on the therapeutic window. Considering the homology of GSK-3α and β within the ATP-binding pocket it appears difficult to identify an

* Corresponding authors. Tel.: +49 6151 164531; fax: +49 6151 163278.
E-mail addresses: Fabio.Lo-Monte@gmx.de (F. Lo Monte), schmidt_boris@t-online.de (B. Schmidt).

0223-5234/$ – see front matter © 2012 Elsevier Masson SAS. All rights reserved.
http://dx.doi.org/10.1016/j.ejmech.2012.06.006

Please cite this article in press as: F. Lo Monte, et al., Structure-based optimization of oxadiazole-based GSK-3 inhibitors, European Journal of Medicinal Chemistry (2012), http://dx.doi.org/10.1016/j.ejmech.2012.06.006

inhibitor that differentiates the two isoforms. All GSK-3 inhibitors developed until now are able to inhibit the two isoforms with almost similar potency, except compound **Λ-OS1**, which showed up to 7-fold selectivity for GSK-3α and compound **15b**, which showed up to 92-fold selectivity for GSK-3α [21–24]. A plethora of GSK-3 inhibitors has been described and most of the effects were observed *in vitro* and cellular studies (Fig. 1) [5,25,26]. These studies and the ongoing patent filing indicate that GSK-3 is a potential drug target not just for the treatment of AD. Several research groups and pharmaceutical companies are interested in the discovery of novel GSK-3 inhibitors with good selectivity and bioavailability despite of the Wnt-pathway associated risks, which may result in adverse cell proliferation. In the present study, the 1,3,4-oxadiazole-moiety served as a scaffold for a variety of GSK-3 inhibitors. This particular heterocycle was chosen because it has favorable properties over 1,2,4-oxadiazoles and other five-membered heterocycles [27]. The inhibition potencies of these compounds were compared to those of the previously reported 1,3,4-oxadiazoles and substituted ureas in the attempt to identify additional heterocycles and substituents that enhance GSK-3 inhibition [1,28–30]. The resulting interactions with the ATP-binding pocket of GSK-3α and β were also investigated to generate a hypothesis for isoform discrimination. We employed the wild-type zebrafish embryo in order to validate the utility of these compounds *in vivo*.

2. Chemistry

The esterfication of the carboxylic acids **1a**, **b** afforded compounds **2a**, **b** which were converted to the hydrazides **3a**, **b**. The hydrazide **3c** was commercially available. Reaction of the hydrazides **3a**–**c** with carbon disulfide (CS_2) afforded the oxadiazoles **4a**–**c** (Scheme 1) [28,31,32].

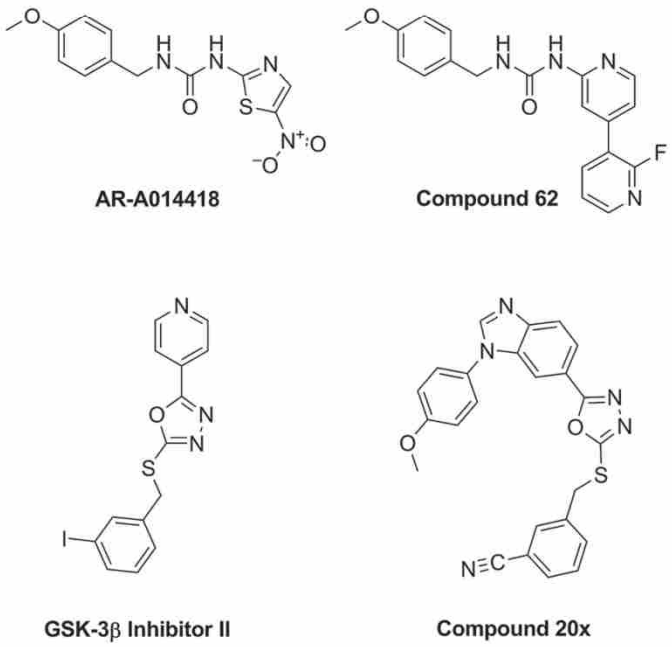

Fig. 1. Structures of previously reported GSK-3 inhibitors.

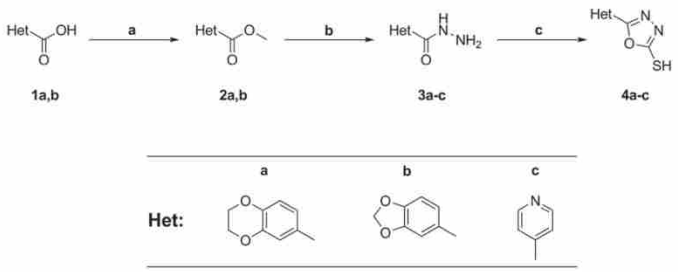

Scheme 1. Reagents and conditions: (a) MeOH, $SOCl_2$, 0 °C–50 °C, 83–89%; (b) $NH_2NH_2 \bullet H_2O$, EtOH, reflux, 67–75%; (c) CS_2, Et_3N, EtOH, reflux, 79–89%.

Please cite this article in press as: F. Lo Monte, et al., Structure-based optimization of oxadiazole-based GSK-3 inhibitors, European Journal of Medicinal Chemistry (2012), http://dx.doi.org/10.1016/j.ejmech.2012.06.006

The biphenyls **7a–h** were prepared in two steps from commercial *p*-tolylboronic acid and bromobenzene bearing substituents at the 1- to 4-position [33]. The biphenyl halides **7a–h** were coupled with the heterocycles **4a–c** to obtain the compounds **8a–h**, **9a–f** and **10a–f** (Scheme 2). The thioethers **15–18** (**a–d**) (Scheme 3) were synthesized similar to method described in Schemes 1 and 2 [28,34,35]. The hydrazones **20a–d** were prepared using isoniazid **19** (Scheme 4) and 4 different benzaldehydes [36–38]. The esterification of acid **21** to the ester **22** employed standard conditions, it was followed by reaction with acetic anhydride to provide the amide **23** (Scheme 5) [39,40]. The thioethers **26a–d** were synthesized according to the method described in Schemes 1 and 2. Esterfication of compound **27**, followed by cyclization gave compound **29** (Scheme 6) [41,42].

Compound **30** was obtained using the conditions described for compound **23** [40]. Saponification of the ester **30**, followed by reaction with *tert*-butyl carbazate, gave compound **32** [28,43]. Cleavage of the *tert*-butylamine in **32** by TFA and submission to the reaction conditions described in Schemes 1 and 2 provided the final product **35** [28]. Bromination of the 4-hydroxybenzoic acid **36**, gave compound **37** (Scheme 7) [44]. The dibenzofuran **38** was obtained by the combination of two reactions in a one-pot synthesis [45,46]. The final compound **41** was prepared in relation to the method described in Schemes 1 and 2. The structures of all compounds were verified by mass spectrometry, ^{1}H NMR and ^{13}C NMR.

3. Results and discussion

The synthesized compounds were evaluated for GSK-3 inhibition in a commercial system based on the Z′-LYTE® technology, available from Invitrogen Life Technologies (Carlsbad, CA, USA), using human recombinant GSK-3α or GSK-3β as the enzyme source and further for their inhibitory activity *in vitro* against GSK-3β. Several compounds displayed more than 50% inhibitory activity against GSK-3β at 10 μM concentration. We focussed our interest on inhibitors with potential occupation of the entire ATP-binding pocket, and thereby to enhance potency and selectivity (Fig. 2). Heterocycles featuring the oxadiazole ring typically interact within the green marked area of GSK3 (Fig. 2). Our goal was to extend our compounds to the area highlighted in blue. Furthermore, we tried to enhance the potential interaction with the backbone by replacing heterocycles with phenyl rings bearing different acceptors and to investigate the contribution deriving from the rigidity of a tricyclic system [26]. The 3 heterocyclic fragments **4a–c** were introduced as potential hinge binders in order to interact with the GSK-3 backbone: Asp133/Tyr134/Val135 (Scheme 1). The oxadiazole moiety is assumed to engage with the polar binding pocket, consisting of three amino acids (Lys85/Glu97/Asp200). Such interactions were previously reported for the GSK-3β inhibitor II and 20x (Fig. 1). We coupled the compounds **4a–c** to biphenyl systems bearing different substituents on the second phenyl ring (Scheme 2). Most of these compounds showed remarkable activities and selectivities (Table 1).

The compounds **8f** and **9a–e** were found to be potent inhibitors of both isoforms of GSK-3 as characterized by IC_{50} values in the low nanomolar range. In addition, all of them showed good selectivities against other kinases. Substituents in the ortho- and para-positions of structure **8** and **9** lead to potent inhibition of both isoforms as indicated for compound **8f** and **9e** with an IC_{50} value of 5 nM for GSK-3α respectively 14 nM and 32 nM for GSK-3β. We reasoned

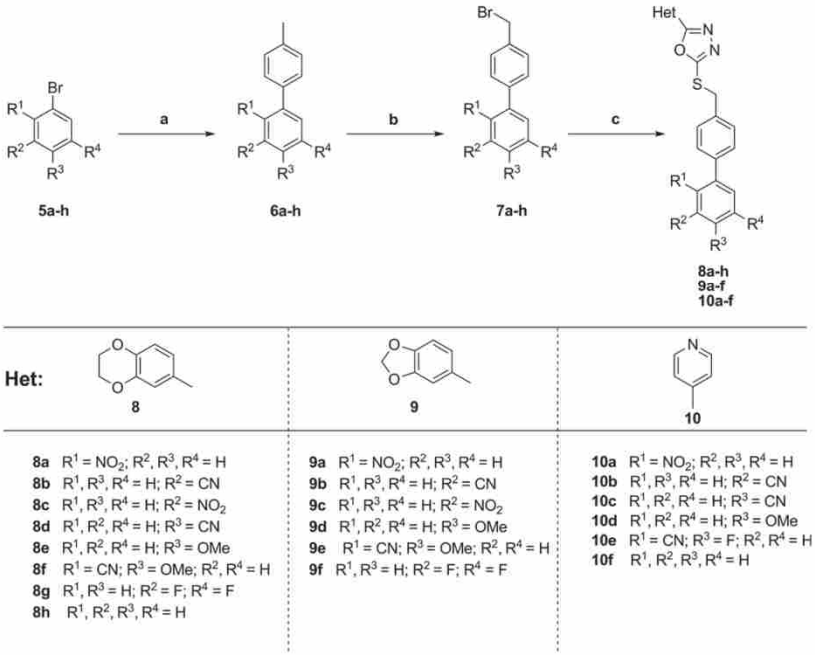

Scheme 2. Reagents and conditions: (a) aryl bomide, toluene, EtOH, $Pd(PPh_3)_4$, 2-tolylboronic acid, 2 N Na_2CO_3(aq.), 80 °C; (b) NBS, AIBN, CCl_4, reflux; (c) oxadiazoles (4a-c), 1 N NaOH, DMF, rt, 27–79%.

Please cite this article in press as: F. Lo Monte, et al., Structure-based optimization of oxadiazole-based GSK-3 inhibitors, European Journal of Medicinal Chemistry (2012), http://dx.doi.org/10.1016/j.ejmech.2012.06.006

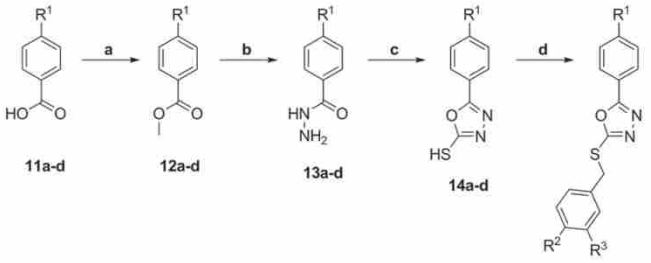

15a R^1, R^2, R^3 = H
15b R^1 = H, R^2 = 2-benzonitrile; R^3 = H
15c R^1 = H; R^2 = H, R^3 = OMe
15d R^1 = H; R^2 = H, R^3 = CN

16a R^1 = OMe; R^2, R^3 = H
16b R^1 = OMe, R^2 = 2-benzonitrile; R^3 = H
16c R^1 = OMe; R^2 = H, R^3 = OMe
16d R^1 = OMe; R^2 = H, R^3 = CN

17a R^1 = CN; R^2 = H, R^3 = H
17b R^1 = CN, R^2 = 2-benzonitrile; R^3 = H
17c R^1 = CN; R^2 = H, R^3 = OMe
17d R^1 = CN; R^2 = H, R^3 = CN

18a R^1 = NO_2; R^2 = H, R^3 = H
18b R^1 = NO_2, R^2 = 2-benzonitrile; R^3 = H
18c R^1 = NO_2; R^2 = H, R^3 = OMe
18d R^1 = NO_2; R^2 = H, R^3 = CN

Scheme 3. Reagents and conditions: Reagents and conditions: (a) MeOH, $SOCl_2$, 0 °C–50 °C, 68–76%; (b) $NH_2NH_2 \bullet H_2O$, EtOH, reflux, 81–89%; (c) CS_2, Et_3N, EtOH, reflux, 74–88%; (d) Benzyl halides, 1 N NaOH, DMF, rt, 32–71%.

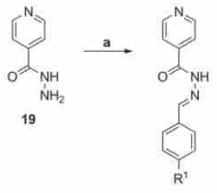

20a R^1= H
20b R^1 = OMe
20c R^1 = CN
20d R^1 = ethyl

Scheme 4. Reagents and conditions: (a) EtOH/H_2O, Aldehydes, rt, 83–97%.

that only the interplay respectively combination of different substituents is adequate to gain selectivity against one GSK-3 isoform. Compounds **8b** and **8g** enhance the selectivity for GSK-3α up to 27-fold. An inverse effect was observed for pyridine **10e** where a substituent in meta- and para-position leads to slightly increased selectivity for inhibition of GSK-3β. All compounds lacking the heterocycle (Scheme 3) or oxadiazole ring (Scheme 4) completely lost most of their ability to inhibit GSK-3 and resulted in a residual GSK-3β activity of more than 50% at 10 μM. We attempted the combination of different lead structures by the addition of an amide function at the pyridine and benzothiazole (Schemes 4 and 5). A similar moiety serves as an ambident moiety on Sorafenib. It was reported to establish hydrogen bonds with the same amide on the target hinge region either via the pyridyl nitrogen or through the carbonyl of the acetyl amide [47,48].

Thus the amide was expected to increase the interaction with the backbone of GSK-3 as observed in the tight binding of Compound **62** and **AR-A014418** (Fig. 1). We determined promising activities and selectivities for the pyridines **26a**, **26c** and **26d**. Especially compound **26d** with an IC_{50} value of 2 nM for GSK-3α and 17 nM for GSK-3β showed more than 5000-fold selectivity against Cdk5/p35, CK1ε, AurKA and PKCα (Table 1). However, the additional amide on the benzothiazole **35** reduced activity for both isoforms indicating too close proximity to the backbone. Moreover, the acetamide **26d** is characterized by a clogP of 2.90 and a tPSA of 103.0 $Å^2$. The letter value exceeds the limits for likely blood–brain

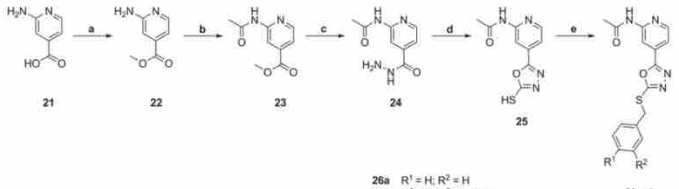

26a R^1 = H; R^2 = H
26b R^1 = H; R^2 = OMe
26c R^1 = H; R^2 = CN
26d R^1 = 2-benzonitrile; R^2 = H

Scheme 5. Reagents and conditions: (a) MeOH, $SOCl_2$, 0 °C–50 °C, 89%; (b) acetic anhydride, 105 °C, 69%; (c) $NH_2NH_2 \bullet H_2O$, EtOH, reflux, 74%; (d) CS_2, Et_3N, EtOH, reflux, 92%; (e) Benzyl halides, 1 N NaOH, DMF, rt, 37–68%.

Please cite this article in press as: F. Lo Monte, et al., Structure-based optimization of oxadiazole-based GSK-3 inhibitors, European Journal of Medicinal Chemistry (2012), http://dx.doi.org/10.1016/j.ejmech.2012.06.006

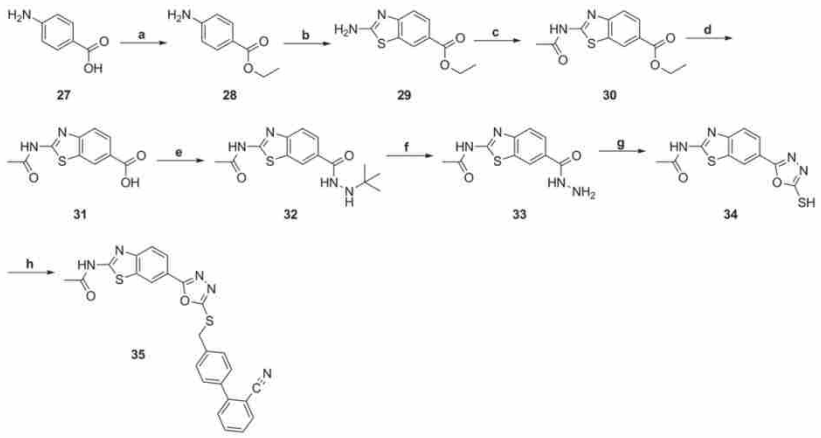

Scheme 6. Reagents and conditions: (a) EtOH, H_2SO_4, reflux, 91%; (b) CH_3COOH, KSCN, Br_2, rt, 67%; (c) acetic anhydride, 105 °C, 58%; (d) MeOH, 1 N NaOH, rt, 94%; (e) DMF, *tert*-Butyl carbazate, EDCI, HOBt•H_2O, rt, 77%; (f) TFA, rt, 99%; (g) CS_2, Et_3N, EtOH, reflux, 81%; (h) Benzyl halide, 1 N NaOH, DMF, rt, 47%.

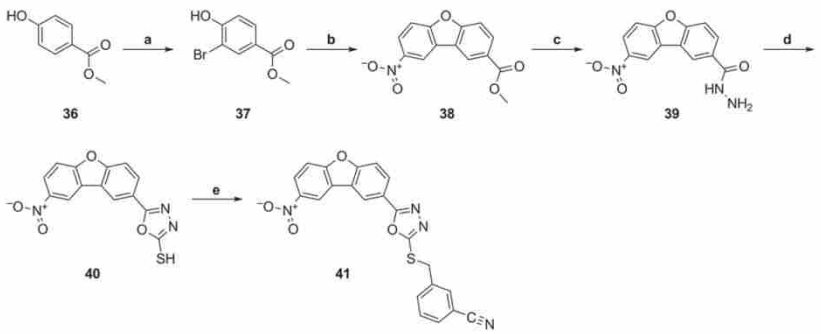

Scheme 7. Reagents and conditions: (a) DCM, Br_2, rt, 65%; (b) DMF, $Pd(OAc)_2$, K_2CO_3, 130 °C, 30%; (c) NH_2NH_2•H_2O, rt, 99%; (d) CS_2, Et_3N, EtOH, reflux, 48%; (e) Benzyl halide, 1N NaOH, DMF, rt, 44%.

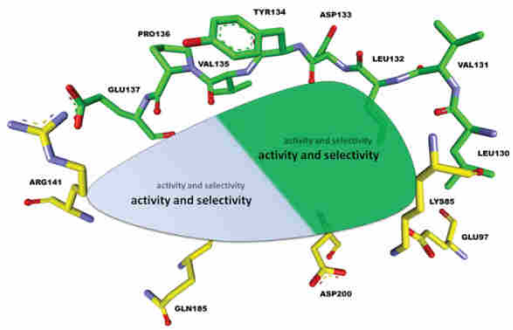

Fig. 2. Schematic overview of the GSK-3 ATP-binding pocket. The green marked area reveals the interaction site of the heterocycle and oxadiazole ring. The area we wanted to occupy with our structures is marked light blue. (For interpretation of the references to colour in this figure legend, the reader is referred to the web version of this article.)

barrier permeation. In addition, the structural rigidity of the dibenzofuran **41** resulted in loss of inhibitory activity against GSK-3.

A docking study of compound **9e** and **26d** into the PDB structure 3F88 of GSK-3β suggested a binding mode that uses the ATP-binding pocket in its entirety. The oxadiazole interacts in both cases with the polar pocket consisting of Lys85 and Asp200. For compound **9e** the amide functions leads to a binding mode along the hinge region of the ATP-binding pocket. The biphenyl system interacts with Ile62, Gly63, Phe67 and Val70, which form part of the flexible glycine-rich loop. The methoxy group of compound **9e** is located in close proximity to the salt bridge formed by Glu137 and Arg141, which may be responsible for the activity of this compound. Nevertheless, this structure does not provide insight into the selective inhibition of the GSK-3β isoforms as all amino acid residues shown in Fig. 3 are identical in both isoforms. Hence, only a complex of GSK-3β co-crystallized with one of these inhibitors, solved by X-ray crystallography, may provide the necessary insights. After evaluation of the *in vitro* activity and selectivity of these compounds the biphenyl derivatives **9e** and **26d** were.further tested for their *in vivo* activity on wt zebrafish embryos. We

Please cite this article in press as: F. Lo Monte, et al., Structure-based optimization of oxadiazole-based GSK-3 inhibitors, European Journal of Medicinal Chemistry (2012), http://dx.doi.org/10.1016/j.ejmech.2012.06.006

Table 1
Inhibitory activity against different kinases *in vitro* and *in silico* parameters (calc. with ChemDraw Ultra 9.0.1).

IC_{50} (μM)							clogP	tPSA(Å^2)
Compound	GSK-3α	GSK-3β	Cdk5/p35	CK1ε	AurKA	PKCα		
8a	0.004	0.090	>100	>100	>100	>100	4.62	112.2
8b	0.009	0.225	>100	>100	>100	>100	4.31	84.8
8c	0.015	0.164	>100	>100	>100	>100	4.62	112.2
8d	0.195	1.995	>100	>100	50.0	>100	4.31	84.8
8e	0.019	0.127	>100	>100	>100	>100	4.80	79.0
8f	0.005	0.032	>100	>100	>100	>100	4.56	98.9
8g	0.035	0.966	>100	>100	>100	>100	5.16	64.9
8h	0.051	0.234	>100	>100	>100	>100	4.88	64.9
9a	0.003	0.027	>100	>100	>100	>100	4.66	112.2
9b	0.004	0.029	>100	>100	>100	>100	4.35	84.8
9c	0.015	0.086	>100	>100	>100	>100	4.66	112.2
9d	0.007	0.075	>100	20.0	40.0	>100	4.84	79.0
9e	0.005	0.014	>100	50.0	45.0	>100	4.60	98.9
9f	0.051	0.195	>100	80.0	>100	>100	5.21	64.9
10a	0.027	0.164	>100	>100	5.0	>100	3.28	95.3
10b	0.046	0.084	>100	>100	60.0	>100	2.97	67.9
10c	0.077	0.153	>100	>100	>100	>100	2.97	67.9
10d	0.240	0.176	>100	>100	>100	>100	3.45	62.1
10e	0.324	0.056	>100	>100	>100	>100	3.11	67.9
10f	0.052	0.083	>100	>100	>100	>100	3.53	48.0
26a	0.020	0.035	>100	>100	60.0	>100	1.58	83.1
26c	0.017	0.019	>100	>100	>100	>100	1.01	103.0
26d	0.002	0.017	>100	>100	>100	>100	2.90	103.0

exposed the embryos to these compounds at early stages of development (Fig. 4). The embryos were collected and maintained in E2 medium at ~28 °C. The compounds were added 5 hpf (hour post fertilization), and the phenotypes were compared at 44-48 hpf. Compounds **9e** and **26d** cause a stunted and crooked tail at 30 μM. This correlates with the observation that Wnt signaling, and thus GSK-3β activity, plays a crucial role in the development of metazoan. This was demonstrated for the known GSK-3 inhibitors LiCl and the ruthenium complex (**R**)-**7**, which both perturb zebrafish development [49,50]. However, it must be noted that compound **9e** and **26d** were not completely dissolved in the E2-medium at 30 μM. Thus, an exact concentration cannot be stated for these compounds. Nevertheless, both compounds exerted no toxicity in the observation range (<30 μM).

4. Conclusion

In this report, we describe the synthesis and evaluation of oxadiazole-based GSK3 inhibitors. Occupation of the ATP-binding pocket in its entirety led to the identification of several potent and selective compounds. These compounds are characterized by IC_{50} values in the low nanomolar range and good selectivity versus other kinases. Surprisingly, we ascertained that the addition of different functional groups onto the biphenyl system was adequate to gain selectivity against one GSK-3 isoform. To the best of our knowledge the selectivity of compound **8g** for GSK-3α compared to GSK-3β is among the highest ever reported. These observations will be helpful, if the discrimination of one GSK-3 isoform is needed *in vivo*. The discriminating factor for this isoform selectivity is still unknown as the ATP-binding sites are almost identical in the two isoforms (Fig. 3). Differences in the amino acid sequence of the channels leading to the binding sites may hold a cue, but the lack of a crystallized GSK-3α makes this hypothesis highly speculative. Furthermore, amino acids in the second-sphere close to the ATP-binding pocket do vary for GSK-3α and thus may contribute to conformational changes. The interaction with the glycine-rich loop might have significant effects on the binding potencies and

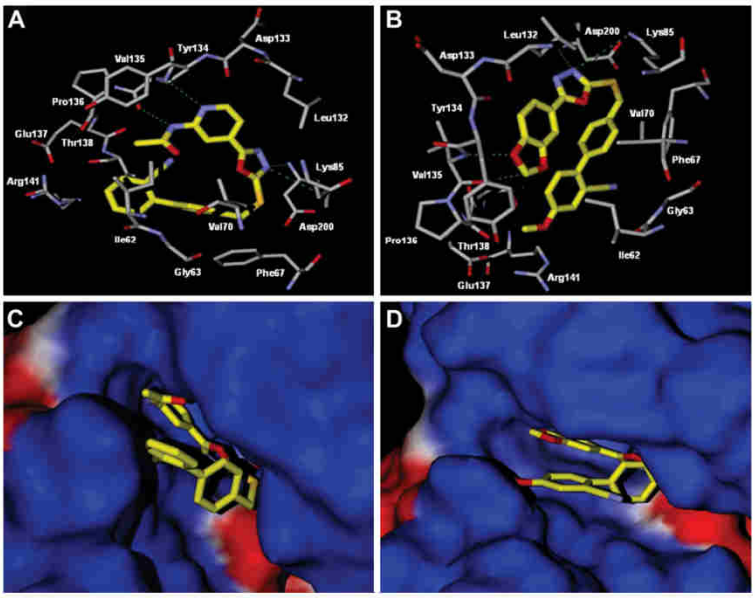

Fig. 3. Docking of compounds **9e** and **26d** into PDB structure 3F88 of GSK-3β; hydrogen bond interactions of compound **26d** (A) and **9e** (B) with the amino acids of the ATP-binding pocket; Surface illustration of the ATP-binding pocket with compound **26d** (C) and **9e** (D). The inhibitors are shown in yellow. These figures were prepared with Molegro Virtual Docker 5. (For interpretation of the references to colour in this figure legend, the reader is referred to the web version of this article.)

Please cite this article in press as: F. Lo Monte, et al., Structure-based optimization of oxadiazole-based GSK-3 inhibitors, European Journal of Medicinal Chemistry (2012), http://dx.doi.org/10.1016/j.ejmech.2012.06.006

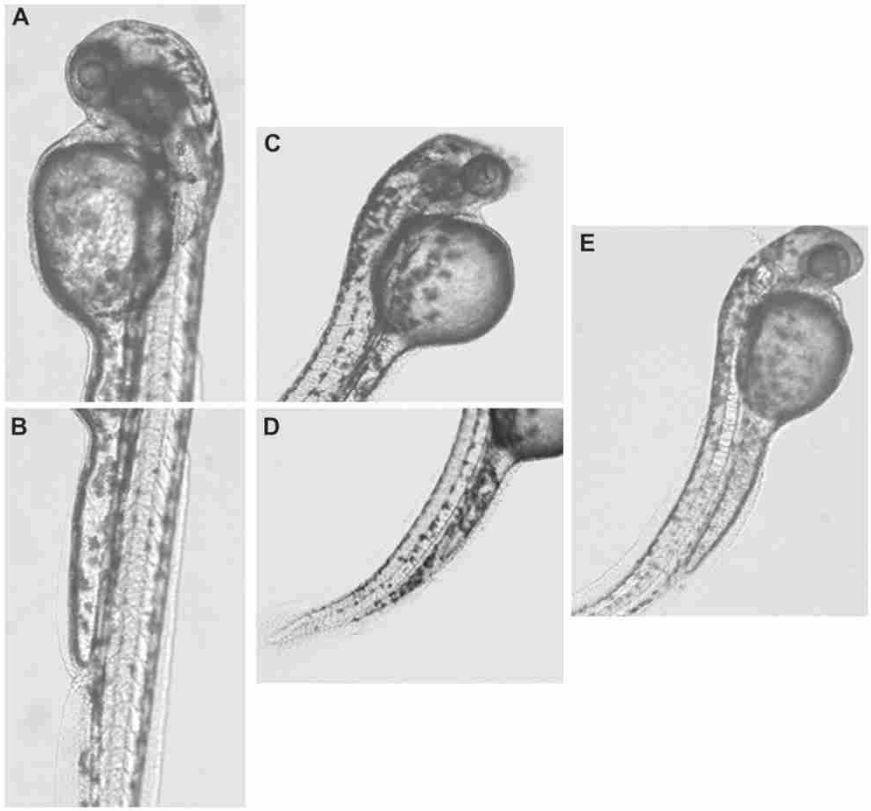

Fig. 4. Effect on the wild-type zebrafish embryo by compounds **9e** and **26d**. the embryos were collected and maintained in E2 medium at ~28 °C, compound was added 5 hpf, and the phenotypes were compared at 44–48 hpf. (A, B) Head and tail of control embryos - DMSO (2%). (C, D) Embryo treated with compound **9e**. this compound causes a stunted and crooked tail at 30 μM. (E) Embryo treated with compound **26d**. this compound causes a stunted and crooked tail at 30 μM.

selectivities of the biphenyl derivatives similar to the compounds reported by Li Feng *et al* [22]. The amide function in compound **26d** indicated a potential interaction with the backbone exploitable for further improvement. However, this moiety causes a significant contribution to the tPSA (103.0 $Å^2$) and thus impairs potential blood–brain barrier permeation. We exposed wt zebrafish embryos to two of these compounds at early stages of development and obtained desirable *in vivo* efficacy for compound **9e** and **26d**. We suppose that GSK-3α inhibition offers a new approach to reduce the formation of both amyloid plaques and neurofibrillary tangles and thus may be valuable in the treatment of AD [51]. On the basis of these results the derivatives **8b**, **8g** and **26d** were selected for further pharmacological and structural evaluations.

5. Experimental

5.1. Chemistry

All reactions under anhydrous conditions were carried out under argon atmosphere with dry solvents, unless otherwise noted. All the commercial chemicals were used without further purification. The ^{1}H NMR spectra were recorded on a Bruker AC 300 spectrometer at 300 MHz and Bruker AC 500 spectrometer at 500 MHz. The ^{13}C NMR spectra were recorded on a Bruker AC 300 spectrometer at 75 MHz and Bruker AC 500 spectrometer at 125 MHz. Chemical shifts are reported as ppm downfield from Me_4Si. Abbreviations used to explain the multiplicities: s = singlet, d = doublet, *t* = triplet, *q* = quartet, m = multiplet, br = broad. Coupling constants (*J* values) are given in hertz (Hz). Mass spectrometry was performed on a Bruker-Franzen Esquire LC mass spectrometer and a MAT 95 double focusing sector field MS. High performance liquid chromatographies were carried out on an Agilent 1100 (column: reversed phase, Zorbax Eclipse XDB-C8, 4.6 × 150 mm; 254 nm). Flash column chromatography was carried out using Merck silica gel 60 (40–63 and 15–40 μm) and 60G (5–40 μm). Thin-layer chromatography (TLC) was carried out using aluminum sheets precoated with silica gel 60 F254 (0.2 mm; E. Merck).

5.2. Methyl 2,3-dihydrobenzo[b][1,4]dioxine-6-carboxylate (**2a**)

To a stirred solution of 2,3-dihydrobenzo[*b*][1,4]dioxine-6-carboxylic acid **1a** (1.80 g, 10 mmol) in MeOH (20 mL) was added $SOCl_2$ (1.45 mL, 20 mmol) dropwise at 0 °C over 1 h. The mixture

Please cite this article in press as: F. Lo Monte, et al., Structure-based optimization of oxadiazole-based GSK-3 inhibitors, European Journal of Medicinal Chemistry (2012), http://dx.doi.org/10.1016/j.ejmech.2012.06.006

was further stirred 12 h at 50 °C. The solution was cooled to room temperature and diluted with water (25 mL). MeOH was evaporated and the pH adjusted to ~6 with aqueous $NaHCO_3$. The mixture was extracted three times with EtOAc and successively washed with brine. The organic layer was dried over $MgSO_4$ and concentrated under reduced pressure to give **2a** (1.6 g, 83%) as a colorless solid. ^{1}H NMR (DMSO-d_6, 500 MHz): δ [ppm] = 3.80 (3H, s), 4.19 (2H, m), 4.23 (2H, m), 6.80 (1H, m), 7.47 (2H, m). ^{13}C NMR (DMSO-d_6, 125 MHz): δ [ppm] = 50.5, 62.7, 63.2, 115.7, 117.6, 122.0, 141.7, 146.4, 165.2. EI-MS: m/z 194 (M^+).

*5.2.1. Compound **2b** was prepared in a similar manner to that described for **2a***

Methyl benzo[*d*][1,3]dioxole-5-carboxylate (**2b**). Yield 89%, colorless solid. ^{1}H NMR (DMSO-d_6, 500 MHz): δ [ppm] = 3.81 (3H, s), 6.14 (2H, s), 7.03 (1H, d, J = 8.1 Hz), 7.38 (1H, d, J = 1.6 Hz), 7.57 (1H, dd, J = 8.1 Hz, J = 1.7 Hz). ^{13}C NMR (DMSO-d_6, 125 MHz): δ [ppm] = 52.0, 102.1, 108.2, 108.5, 123.4, 125.0, 147.6, 151.4, 165.6. EI-MS: m/z = 180 (M^+).

*5.3. 2,3-Dihydrobenzo[b][1,4]dioxine-6-carbohydrazide (**3a**)*

To a solution of **2a** (1.16 g, 6.0 mmol) in EtOH (30 mL) was added hydrazine hydrate (2.91 mL, 60 mmol) and the mixture was heated at reflux for 2 days. After cooling to room temperature pure crystals are formed, collected by filtration and washed several times with EtOH to give compound **3a** (0.87 g, 75%) as a light yellow solid. ^{1}H NMR (DMSO-d_6, 500 MHz): δ [ppm] = 4.28 (2H, m), 4.30 (2H, m), 6.89 (1H, d, J = 8.4 Hz), 7.30 (1H, dd, J = 8.3 Hz, J = 2.1 Hz), 7.33 (1H, d, J = 2.1 Hz). ^{13}C NMR (DMSO-d_6, 125 MHz): δ [ppm] = 65.9, 66.3, 117.9, 118.6, 121.9, 127.5, 145.2, 148.6, 169.6. EI–MS: m/z 194 (M^+).

*5.3.1. Compound **3b** was prepared in a similar manner to that described for **3a***

Benzo[*d*][1,3]dioxole-5-carbohydrazide (**3b**). Yield 67%, colorless solid. ^{1}H NMR (DMSO-d_6, 500 MHz): δ [ppm] = 4.42 (2H, s), 6.07 (2H, s), 6.96 (1H, d, J = 8.1 Hz), 7.35 (1H, d, J = 1.7 Hz), 7.42 (1H, dd, J = 8.1 Hz, J = 1.7 Hz), 9.59 (1H, s). ^{13}C NMR (DMSO-d_6, 125 MHz): δ [ppm] = 101.5, 106.9, 107.8, 121.8, 127.2, 147.2, 149.5, 165.2. EI-MS: m/z = 180 (M^+).

*5.4. 5-(2,3-Dihydrobenzo[b][1,4]dioxin-6-yl)-1,3,4-oxadiazole-2-thiol (**4a**)*

To a solution of **3a** (582 mg, 3.00 mmol) in EtOH (5 mL) were added carbon disulfide (397 μL, 6.60 mmol) and Et_3N (469 μL, 3.30 mmol) and the mixture was heated at reflux overnight. The reaction mixture was diluted with EtOAc and the organic layer was washed with 0.1 N HCl, brine and dried over Na_2SO_4. The solvent was evaporated under reduced pressure, and the obtained residue was recrystallized from CH/EtOAc (1:2) to give **4a** (630 mg, 89%) as a light brown solid. ^{1}H NMR (DMSO-d_6, 500 MHz): δ [ppm] = 4.32 (2H, m), 4.34 (2H, m), 7.05 (1H, d, J = 8.4 Hz), 7.30 (1H, d, J = 2.0 Hz), 7.36 (1H, dd, J = 8.4 Hz, J = 2.0 Hz), 14.2 (1H, s, br). ^{13}C NMR (DMSO-d_6, 125 MHz): δ [ppm] = 64.4, 64.8, 115.0, 115.7, 118.6, 120.0, 144.2, 147.3, 160.6, 177.6. EI-MS: m/z = 236 (M^+).

*5.4.1. Compound **4b** was prepared in a similar manner to that described for **4a***

5-(Benzo[*d*][1,3]dioxol-5-yl)-1,3,4-oxadiazole-2-thiol (**4b**). Yield 79%, pale yellow solid. ^{1}H NMR (DMSO-d_6, 500 MHz): δ [ppm] = 6.14 (2H, s), 7.10 (1H, d, J = 8.1 Hz), 7.33 (1H, d, J = 1.6 Hz), 7.42 (1H, dd, J = 8.1 Hz, J = 1.6 Hz). ^{13}C NMR (DMSO-d_6, 125 MHz): δ [ppm] = 102.1, 105.6, 109.1, 116.1, 121.5, 148.1, 150.6, 160.3, 177.2. EI-MS: m/z = 222 (M^+).

*5.4.2. Compound **4c** was prepared in a similar manner to that described for **4a***

5-(Pyridin-4-yl)-1,3,4-oxadiazole-2-thiol (**4c**). Yield 83%, yellow solid. ^{1}H NMR (DMSO-d_6, 500 MHz): δ [ppm] = 7.81 (2H, dd, J = 4.4 Hz, J = 1.6 Hz), 8.81 (2H, dd, J = 4.4 Hz, J = 1.6 Hz). ^{13}C NMR (DMSO-d_6, 125 MHz): δ [ppm] = 119.6, 129.7, 150.8, 158.7, 177.8. EI-MS: m/z = 179 (M^+).

*5.5. General procedure for synthesis of compounds **6a–h** [33]*

To a solution of the aryl bromide (5 mmol) in 15 mL of toluene/EtOH (1/1) was added 0.17 g (0.14 mmol) of $Pd(PPh_3)_4$, and the mixture was stirred under argon atmosphere. Then 2 N aqueous Na_2CO_3 (7.5 mL) and 0.80 g (6 mmol) of 2-tolylboronic acid were added. The mixture was refluxed at 80 °C for 1–2 days until reaction was completed (TLC). After cooling to room temperature, the product was diluted with water and extracted with EtOAc. The organic layers were dried with $MgSO_4$, filtered, and concentrated. Purification was performed by column chromatography using a mixture of CH/EtOAc (9:1). The compounds were used, without structure determination, directly for the next step.

*5.6. General procedure for synthesis of compounds **7a–h** [33]*

To a stirred solution of the appropriately substituted toluene in CCl_4 (10 mL per mmol) were added 0.95 eq. of NBS and AIBN (5 mg per mmol). The reaction mixture was refluxed at 80 °C and then cooled to room temperature. The product was diluted with water and extracted with EtOAc. The organic layers were dried with $MgSO_4$, filtered, and concentrated. Purification was performed by column chromatography using a mixture of CH/EtOAc (6:1). The compounds were used, without structure determination, directly for the next step.

*5.7. General procedure for synthesis of compounds **8a–h**, **9a–f** and **10a–f***

To a solution of compound **4a–c** (0.25 mmol) and 1 N NaOH (0.25 mmol) in DMF (1 mL) was added the appropriate substituted biphenyl system (0.38 mmol) at room temperature, and the mixture was stirred for 5 h. The precipitate formed was collected by filtration and washed once with less DMF and thereafter several times with EtOH to give compounds **8a–h**, **9a–f** and **10a–f**.

Note: The compounds which did not precipitate from the solution were purified as follows. The reaction mixture was diluted with EtOAc and the organic layer was washed with water and brine, dried over $MgSO_4$ and concentrated *in vacuo*. The residue was purified by silica gel column chromatography (DCM/EtOAc – 20:1).

*5.7.1. 2,3-Dihydrobenzo[b][1,4]dioxin-6-yl-5-((2′-nitrobiphenyl-4-yl)methylthio)-1,3,4-oxadiazole (**8a**)*

Yield 77%, yellow solid. ^{1}H NMR (DMSO-d_6, 500 MHz): δ [ppm] = 4.31 (4H, m), 4.63 (2H, s), 7.10 (1H, d, J = 8.4 Hz), 7.35 (2H, m), 7.44 (1H, s), 7.41 (1H, d, J = 8.4 Hz), 7.53 (3H, m), 7.64 (1H, *t*, J = 7.8 Hz), 7.72 (1H, *t*, J = 7.6 Hz), 8.05 (1H, d, J = 8.1 Hz). ^{13}C NMR (DMSO-d_6, 125 MHz): 36.0, 64.5, 64.9, 115.5, 116.4, 118.6, 120.4, 124.5, 128.5, 129.4, 129.9, 132.3, 133.4, 135.0, 136.8, 137.4, 144.3, 147.2, 149.3, 163.1, 165.4. EI-MS: m/z = 447 (M^+).

*5.7.2. 4′-((5-(2,3-Dihydrobenzo[b][1,4]dioxin-6-yl)-1,3,4-oxadiazol-2-ylthio)methyl)-biphenyl-3-carbonitrile (**8b**)*

Yield 36%, colorless solid. ^{1}H NMR (DMSO-d_6, 500 MHz): δ [ppm] = 4.30 (4H, m), 4.62 (2H, s), 7.05 (1H, d, J = 8.5 Hz), 7.39

Please cite this article in press as: F. Lo Monte, et al., Structure-based optimization of oxadiazole-based GSK-3 inhibitors, European Journal of Medicinal Chemistry (2012), http://dx.doi.org/10.1016/j.ejmech.2012.06.006

(1H, d, J = 2.1 Hz), 7.44 (1H, dd, J = 8.5 Hz, J = 2.1 Hz), 7.59 (2H, d, J = 8.3 Hz), 7.66 (1H, m), 7.74 (2H, d, J = 8.3 Hz), 7.82 (1H, td, J = 6.6 Hz, J = 1.3 Hz), 8.02 (1H, d, J = 8.0 Hz), 8.14 (1H, s). ^{13}C NMR (DMSO-d_6, 125 MHz): δ [ppm] = 36.0, 64.5, 64.9, 112.6, 115.5, 116.4, 118.6, 119.2, 120.4, 127.6, 130.2, 130.6, 130.7, 131.6, 131.9, 137.6, 137.8, 141.1, 144.3, 147.2, 163.0, 165.4. EI-MS: m/z = 427 (M^+). HRMS (EI): m/z calcd for $C_{24}H_{17}N_3O_3S$ 427.0991, found 427.0976.

*5.7.3. 2-(2,3-Dihydrobenzo[b][1,4]dioxin-6-yl)-5-((3′-nitrobiphenyl-4-yl)methylthio)-1,3,4-oxadiazole (**8c**)*

Yield 37%, colorless solid. ^{1}H NMR (DMSO-d_6, 500 MHz): δ [ppm] = 4.32 (4H, m), 4.63 (2H, s), 7.05 (1H, d, J = 8.1 Hz), 7.39 (1H, d, J = 2.1 Hz), 7.44 (1H, dd, J = 8.4 Hz J = 2.1 Hz), 7.62 (2H, d, J = 8.5 Hz), 7.77 (3H, m), 8.13 (1H, m), 8.21 (1H, m), 8.42 (1H, m). ^{13}C NMR (DMSO-d_6, 125 MHz): δ [ppm] = 36.0, 64.5, 64.9, 115.5, 116.4, 118.6, 120.4, 121.5, 122.7, 127.7, 130.3, 130.9, 133.7, 137.6, 137.8, 141.7, 144.3, 147.2, 148.9, 163.0, 165.5. EI-MS: m/z = 447 (M^+).

*5.7.4. 4′-((5-(2,3-Dihydrobenzo[b][1,4]dioxin-6-yl)-1,3,4-oxadiazol-2-ylthio)methyl)-biphenyl-4-carbonitrile (**8d**)*

Yield 36%, colorless solid. ^{1}H NMR (DMSO-d_6, 500 MHz): δ [ppm] = 4.33 (4H, m), 4.62 (2H, s), 7.05 (1H, d, J = 8.3 Hz), 7.39 (1H, d, J = 2.1 Hz), 7.44 (1H, dd, J = 8.5 Hz, J = 2.1 Hz), 7.61 (2H, d, J = 8.5 Hz), 7.74 (2H, d, J = 8.5 Hz), 7.90 (4H, m). ^{13}C NMR (DMSO-d_6, 125 MHz): δ [ppm] = 36.0, 64.5, 64.9, 110.6, 115.5, 116.4, 118.6, 119.3, 120.4, 127.7, 128.0, 130.3, 133.3, 138.0, 138.1, 144.3, 144.5, 147.2, 163.0, 165.4. EI-MS: m/z = 427 (M^+).

*5.7.5. 2-(2,3-Dihydrobenzo[b][1,4]dioxin-6-yl)-5-((4′-methoxybiphenyl-4-yl)methylthio)-1,3,4-oxadiazole (**8e**)*

Yield 39%, colorless solid. ^{1}H NMR (DMSO-d_6, 500 MHz): δ [ppm] = 3.87 (3H, s), 4.31 (4H, m), 4.58, (2H, s), 7.01 (2H, d, J = 8.8 Hz), 7.04 (1H, d, J = 8.3 Hz), 7.43 (2H, m), 7.51 (2H, m), 7.58 (4H, m). ^{13}C NMR (DMSO-d_6, 125 MHz): δ [ppm] = 36.2, 55.6, 64.5, 64.9, 114.8, 115.5, 116.4, 118.6, 120.4, 126.6, 128.2, 130.0, 132.4, 135.5, 139.7, 144.3, 147.1, 159.4, 163.1, 165.4. EI-MS: m/z = 432 (M^+).

*5.7.6. 4′-((5-(2,3-Dihydrobenzo[b][1,4]dioxin-6-yl)-1,3,4-oxadiazol-2-ylthio)methyl)-4-methoxybiphenyl-2-carbonitrile (**8f**)*

Yield 50%, colorless solid. ^{1}H NMR (DMSO-d_6, 500 MHz): δ [ppm] = 3.85 (3H, s), 4.33 (4H, m), 4.64 (2H, s), 7.05 (1H, d, J = 8.4 Hz), 7.35 (1H, dd, J = 8.7 Hz, J = 2.8 Hz), 7.41 (1H, d, J = 2.0 Hz), 7.44 (1H, dd, J = 8.4 Hz, J = 2.1 Hz), 7.53 (4H, m), 7.61 (2H, d, J = 8.3 Hz). ^{13}C NMR (DMSO-d_6, 125 MHz): δ [ppm] = 36.0, 56.4, 64.5, 64.9, 111.3, 115.5, 116.4, 118.5, 118.6, 118.8, 120.4, 120.6, 129.3, 129.8, 131.9, 137.0, 137.4, 144.3, 147.2, 159.0, 163.1, 165.4. EI-MS: m/z = 457 (M^+). HRMS (EI): m/z calcd for $C_{25}H_{19}N_3O_4S$ 457.1097, found 457.1122.

*5.7.7. 2-((3′,5′-Difluorobiphenyl-4-yl)methylthio)-5-(2,3-dihydrobenzo[b][1,4]dioxin-6-yl)-1,3,4-oxadiazole (**8g**)*

Yield 41%, colorless solid. ^{1}H NMR (DMSO-d_6, 500 MHz): δ [ppm] = 4.33 (4H, m), 4.61 (2H, s), 7.05 (1H, d, J = 8.5 Hz), 7.22 (1H, m), 7.38 (1H, d, J = 2.1 Hz), 7.43 (3H, m), 7.57 (2H, d, J = 8.2 Hz), 7.73 (2H, d, J = 8.2 Hz). ^{13}C NMR (DMSO-d_6, 125 MHz): δ [ppm] = 36.0, 64.5, 64.9, 103.2, 110.1, 110.3, 115.5, 116.4, 118.6, 120.4, 127.5, 130.2, 137.4, 137.9, 143.7, 144.3, 147.2, 162.4, 163.0, 164.3, 165.4. EI-MS: m/z = 438 (M^+).

*5.7.8. 2-(Biphenyl-4-ylmethylthio)-5-(2,3-dihydrobenzo[b][1,4]dioxin-6-yl)-1,3,4-oxadi-azole (**8h**)*

Yield 38%, colorless solid. ^{1}H NMR (DMSO-d_6, 500 MHz): δ [ppm] = 4.31 (4H, m), 4.60 (2H, s), 7.03 (1H, d, J = 8.4 Hz), 7.33–7.68 (11H, m). ^{13}C NMR (DMSO-d_6, 125 MHz): δ [ppm] = 36.1, 64.5, 64.9, 115.5, 116.4, 118.6, 120.4, 127.1, 127.3, 127.5, 128.0, 129.4, 130.1, 136.4, 140.1, 144.3, 147.2, 163.1, 165.4. EI-MS: m/z = 402 (M^+).

*5.7.9. 2-(Benzo[d][1,3]dioxol-5-yl)-5-((2′-nitrobiphenyl-4-yl) methylthio)-1,3,4-oxadiazole (**9a**)*

Yield 27%, yellow solid. ^{1}H NMR (DMSO-d_6, 500 MHz): δ [ppm] = 4.62 (2H, s), 6.15 (2H, s), 7.11 (1H, d, J = 8.13 Hz), 7.32 (2H, d, J = 6.4 Hz), 7.42–7.66 (6H, m), 7.75 (1H, td, J = 7.6 Hz, J = 1.3 Hz), 7.97 (1H, dd, J = 8.0 Hz, J = 1.2 Hz). ^{13}C NMR (DMSO-d_6, 125 MHz): δ [ppm] = 36.0, 102.6, 106.6, 109.6, 117.1, 122.2, 124.5, 128.5, 129.4, 129.9, 132.3, 133.4, 135.0, 136.8, 137.3, 148.6, 149.3, 150.9, 163.1, 165.6. EI-MS: m/z = 433 (M^+).

*5.7.10. 4′-((5-(Benzo[d][1,3]dioxol-5-yl)-1,3,4-oxadiazol-2-ylthio) methyl)biphenyl-3-carbo-nitrile (**9b**)*

Yield 41%, off-white. ^{1}H NMR (DMSO-d_6, 500 MHz): δ [ppm] = 4.62 (2H, s), 6.16 (2H, s), 7.11 (1H, d, J = 8.1 Hz), 7.43 (1H, d, J = 1.7 Hz), 7.51 (1H, dd, J = 8.2 Hz, J = 1.7 Hz), 7.60 (2H, d, J = 8.2 Hz), 7.66 (1H, m), 7.73 (2H, d, J = 8.2 Hz), 7.82 (1H, d, J = 7.7 Hz), 8.01 (1H, d, J = 8.0 Hz), 8.14 (2H, m). ^{13}C NMR (DMSO-d_6, 125 MHz): δ [ppm] = 36.0, 102.5, 106.6, 109.61, 112.5, 117.0, 119.2, 122.1, 127.5, 130.2, 130.5, 130.6, 131.5, 131.8, 137.5, 137.8, 141.1, 148.5, 150.9, 163.0, 165.5. EI-MS: m/z = 413 (M^+). HRMS (EI): m/z calcd for $C_{23}H_{15}N_3O_3S$ 413.0835, found 413.0828.

*5.7.11. 2-(Benzo[d][1,3]dioxol-5-yl)-5-((3′-nitrobiphenyl-4-yl) methylthio)-1,3,4-oxadiazole (**9c**)*

Yield 48%, grey/brown solid. ^{1}H NMR (DMSO-d_6, 500 MHz): δ [ppm] = 4.64 (2H, s), 6.16 (2H, s), 7.11 (1H, d, J = 8.6 Hz), 7.44 (1H, d, J = 1.7 Hz), 7.52 (1H, dd, J = 8.1 Hz, J = 1.6 Hz), 7.63 (2H, d, J = 8.4 Hz), 7.77 (3H, m), 8.14 (1H, m), 8.22 (1H, m), 8.43 (1H, m). ^{13}C NMR (DMSO-d_6, 125 MHz): δ [ppm] = 36.0, 102.6, 106.6, 109.6, 117.1, 121.5, 122.2, 122.7, 127.7, 130.4, 131.0, 133.7, 137.6, 137.8, 141.4, 148.6, 148.9, 150.9, 163.0, 165.6. EI-MS: m/z = 433 (M^+).

*5.7.12. 2-(Benzo[d][1,3]dioxol-5-yl)-5-((4′-methoxybiphenyl-4-yl) methylthio)-1,3,4-oxadi-azole (**9d**)*

Yield 48%, grey/brown solid. ^{1}H NMR (DMSO-d_6, 500 MHz): δ [ppm] = 3.79 (3H, s), 4.60 (2H, s), 6.16 (2H, s), 7.01 (2H, dd, J = 2.1 Hz, J = 8.8 Hz), 7.11 (1H, d, J = 8.2 Hz), 7.44 (1H, d, J = 1.8 Hz), 7.52 (3H, m), 7.59 (4H, m). ^{13}C NMR (DMSO-d_6, 125 MHz): δ [ppm] = 36.2, 53.6, 102.6, 106.6, 109.6, 114.8, 117.1, 122.2, 126.7, 128.2, 130.0, 132.4, 135.5, 139.7, 148.6, 150.9, 159.4, 163.1, 165.5. EI-MS: m/z = 418 (M^+).

*5.7.13. 4′-((5-(Benzo[d][1,3]dioxol-5-yl)-1,3,4-oxadiazol-2-ylthio) methyl)-4-methoxybiphe-nyl-2-carbonitrile (**9e**)*

Yield 47%, off-white. ^{1}H NMR (DMSO-d_6, 500 MHz): δ [ppm] = 3.86 (3H, s), 4.64 (2H, s), 6.16 (2H, s), 7.11 (1H, d, J = 8.2 Hz), 7.35(1H, dd, J = 8.7 Hz, J = 2.8 Hz), 7.45 (1H, d, J = 1.7 Hz), 7.52 (5H, m), 7.61 (2H, d, J = 8.3 Hz). ^{13}C NMR (DMSO-d_6, 125 MHz): δ [ppm] = 35.9, 56.3, 102.6, 106.6, 109.6, 111.3, 117.1, 118.5, 118.8, 120.6, 122.2, 129.3, 129.8, 131.9, 137.0, 137.3, 137.4, 148.6, 150.9, 159.0, 163.1, 165.6. EI-MS: m/z = 443 (M^+). HRMS (EI): m/z calcd for $C_{24}H_{17}N_3O_4S$ 443.0940, found 443.0902.

*5.7.14. 2-(Benzo[d][1,3]dioxol-5-yl)-5-((3′,5′-difluorobiphenyl-4-yl) methylthio)-1,3,4-oxa-diazole (**9f**)*

Yield 50%, grey/brown solid. ^{1}H NMR (DMSO-d_6, 500 MHz): δ [ppm] = 4.62 (2H, s), 6.16 (2H, s), 7.11 (1H, d J = 8.1 Hz), 7.22 (1H, m), 7.44 (3H, m), 7,52 (1H, dd, J = 8.1 Hz, J = 1.8 Hz), 7.58 (2H, d, J = 8.3 Hz), 7.73 (2H, d, J = 8.3 Hz). ^{13}C NMR (DMSO-d_6, 125 MHz): δ [ppm] = 35.9, 102.6, 103.2, 106.6, 109.6, 110.1, 110.3, 117.1, 122.2, 127.5, 130.2, 137.4, 137.9, 143.7, 148.6, 150.9, 162.3, 163.0, 164.2, 165.6. EI-MS: m/z = 424 (M^+).

Please cite this article in press as: F. Lo Monte, et al., Structure-based optimization of oxadiazole-based GSK-3 inhibitors, European Journal of Medicinal Chemistry (2012), http://dx.doi.org/10.1016/j.ejmech.2012.06.006

*5.7.15. 2-((2′-Nitrobiphenyl-4-yl)methylthio)-5-(pyridine-4-yl)-1,3,4-oxadiazole (**10a**)*

Yield 79%, yellow solid. ^{1}H NMR (DMSO-d$_6$, 500 MHz): δ [ppm] = 4.7 (2H, s), 7.3 (2H, d, J = 8.2 Hz), 7.5 (1H, d, J = 7.7 Hz), 7.6 (2H, d, J = 8.2 Hz), 7.6 (1H, *t*, J = 7.8 Hz), 7.8 (1H, *t*, J = 7.6 Hz), 7.9 (2H, d, J = 6.1 Hz), 8.0 (1H, d, J = 8.1 Hz), 8.8 (2H, d, J = 6.1 Hz). ^{13}C NMR (DMSO-d$_6$, 125 MHz): δ [ppm] = 36.0, 120.5, 124.6, 128.5, 129.4, 130.0, 130.5, 132.2, 133.4, 135.0, 136.9, 137.2, 149.3, 151.4, 164.3, 165.3. EI-MS: m/z = 390 (M$^+$).

*5.7.16. 4′-((5-(Pyridine-4-yl)-1,3,4-oxadiazol-2-ylthio)methyl) biphenyl-3-carbonitrile (**10b**)*

Yield 53%, yellow solid. ^{1}H NMR (DMSO-d$_6$, 500 MHz): δ [ppm] = 4.68 (2H, s), 7.64 (3H, m), 7.74 (2H, d), 7.82 (1H, dt, J = 7.7 Hz, J = 1.3 Hz), 7.90 (2H, dd, J = 4.5 Hz, J = 1.7 Hz), 8.01 (1H, m), 8.15 (1H, m), 8.82 (2H, dd, J = 4.5 Hz, J = 1.7 Hz). ^{13}C NMR (DMSO-d$_6$, 125 MHz): δ [ppm] = 36.0, 112.6, 119.2, 120.4, 127.6, 130.3, 130.5, 130.6, 130.7, 131.6, 131.9, 137.3, 137.9, 141.1, 151.4, 164.2, 165.2. EI-MS: m/z = 370 (M$^+$).

*5.7.17. 4′-((5-(Pyridine-4-yl)-1,3,4-oxadiazol-2-ylthio)methyl) biphenyl-4-carbonitrile (**10c**)*

Yield 32%, colorless solid. ^{1}H NMR (DMSO-d$_6$, 500 MHz): δ [ppm] = 4.69 (2H, s), 7.64 (2H, d, J = 8.1 Hz), 7.75 (2H, d, J = 8.1 Hz), 7.86-7.93 (6H, m), 8.82 (2H, m). ^{13}C NMR (DMSO-d$_6$, 125 MHz): δ [ppm] = 35.9, 110.6, 119.3, 120.4, 127.8, 128.0, 130.4, 130.5, 133.3, 137.8, 138,1, 144.5, 151.4, 165.2, 164.3. EI-MS: m/z = 370 (M$^+$).

*5.7.18. 2-((4′-Methoxybiphenyl-4-yl)methylthio)-5-(pyridine-4-yl)-1,3,4-oxadiazole (**10d**)*

Yield 37%, colorless solid. ^{1}H NMR (DMSO-d$_6$, 500 MHz): δ [ppm] = 3.79 (3H, s), 4.66 (2H, s), 7.01 (2H, d, J = 8.6 Hz), 7.55 (2H, d, J = 8.2 Hz), 7.60 (4H, m), 7.90 (2H, d, J = 5.8 Hz), 8.82 (2H, d, J = 5.8 Hz). ^{13}C NMR (DMSO-d$_6$, 125 MHz): δ [ppm] = 36.1, 55.6, 114.8, 120.4, 126.8, 128.2, 130.1, 130.5, 132.4, 135.3, 139.8, 151.4, 159.5, 164.2, 165.3. EI-MS: m/z = 375 (M$^+$).

*5.7.19. 4-Fluoro-4′-((5-(pyridine-4-yl)-1,3,4-oxadiazol-2-ylthio) methyl)biphenyl-2-carbonit-rile (**10e**)*

Yield 31%, yellow solid. ^{1}H NMR (DMSO-d$_6$, 500 MHz): δ [ppm] = 4.71 (2H, s), 7.57 (2H, d, J = 1.8 Hz), 7.67 (4H, m), 7.90 (2H, dd, J = 4.4 Hz, J = 1.7 Hz), 7.97 (1H, m), 8.82 (2H, dd, J = 4.4 Hz, J = 1.7 Hz). ^{13}C NMR (DMSO-d$_6$, 125 MHz): δ [ppm] = 35.9, 112.1, 117.9, 120.5, 121.0, 121.5, 129.5, 129.9, 130.5, 132.9, 136.8, 137.8, 141.3, 151.4, 164.3, 165.3. EI-MS: m/z = 388 (M$^+$). HRMS (EI): m/z calcd for $C_{21}H_{13}N_4OFS$ 388.0795, found 388.0825.

*5.7.20. 2-(Biphenyl-4-ylmethylthio)-5-(pyridine-4-yl)-1,3,4-oxadiazole (**10f**)*

Yield 32%, yellow solid. ^{1}H NMR (DMSO-d$_6$, 500 MHz): δ [ppm] = 4.67 (2H, s), 7.36 (1H, m), 7.46 (2H, m), 7.66-7.70 (6H, m), 7.9 (2H, d, J = 6.1 Hz), 8.8 (2H, d, J = 6.1 Hz). ^{13}C NMR (DMSO-d$_6$, 125 MHz): δ [ppm] = 36.1, 120.5, 127.1, 127.3, 128.0, 129.4, 130.2, 130.5, 136.2, 140.0, 140.1, 151.4, 164.1, 165.3. EI-MS: m/z = 345 (M$^+$).

*5.8. Compounds **12a–d** were prepared in a similar manner to that described for **2a***

The compounds were used, without structure determination, directly for the next step.

*5.9. Compounds **13a–d** were prepared in a similar manner to that described for **3a***

The compounds were used, without structure determination, directly for the next step.

*5.10. Compounds **14a–d** were prepared in a similar manner to that described for **4a***

The compounds were used, without structure determination, directly for the next step.

*5.11. Compounds **15–18** (**a–d**) were prepared in a similar manner to that described for compounds **8a–h**, **9a–f** and **10a–f***

*5.11.1. 2-(Benzylthio)-5-phenyl-1,3,4-oxadiazole (**15a**)*

Yield 67%, colorless solid. ^{1}H NMR (DMSO-d$_6$, 500 MHz): δ [ppm] = 4.59 (2H, s), 7.29 (1H, m), 7.35 (2H, m), 7.48 (2H, m), 7.60 (3H, m), 7.95 (2H, m). ^{13}C NMR (DMSO-d$_6$, 125 MHz): δ [ppm] = 35.9, 122.9, 126.3, 127.7, 128.5, 129.0, 129.4, 132.0, 136.5, 163.2, 165.2. EI-MS: m/z = 268 (M$^+$).

*5.11.2. 4′-((5-Phenyl-1,3,4-oxadiazol-2-ylthio)methyl)biphenyl-2-carbonitrile (**15b**)*

Yield 58%, colorless solid. ^{1}H NMR (DMSO-d$_6$, 300 MHz): δ [ppm] = 4.68 (2H, s), 7.53-7.69 (9H, m, br), 7.78 (1H, td, J = 7.7 Hz, J = 1.4 Hz), 7.95 (3H, m). ^{13}C NMR (DMSO-d$_6$, 75 MHz): δ [ppm] = 35.4, 110.0, 118.4, 122.9, 126.3, 128.2, 128.8, 129.3, 130.0, 131.9, 133.4, 133.8, 137.1, 137.3, 143.9, 163.2, 165.2. EI-MS: m/z = 369 (M$^+$).

*5.11.3. 2-(3-Methoxybenzylthio)-5-phenyl-1,3,4-oxadiazole (**15c**)*

Yield 51%, colorless solid. ^{1}H NMR (DMSO-d$_6$, 500 MHz): δ [ppm] = 3.72 (3H, s), 4.55 (2H, s), 6.84 (1H, m), 7.05 (2H, m), 7.26 (1H, *t*, J = 7.8 Hz), 7.62 (3H, m), 7.97 (2H, m). ^{13}C NMR (DMSO-d$_6$, 125 MHz): δ [ppm] = 35.9, 55.0, 113.2, 114.6, 121.1, 122.9, 126.3, 129.4, 129.6, 132.0, 138.0, 159.2, 163.2, 165.2. EI-MS: m/z = 298 (M$^+$).

*5.11.4. 3-((5-Phenyl-1,3,4-oxadiazol-2-ylthio)methyl)benzonitrile (**15d**)*

Yield 38%, colorless solid. ^{1}H NMR (DMSO-d$_6$, 500 MHz): δ [ppm] = 4.63 (2H, s), 7.60 (4H, m), 7.77 (1H, d, J = 7.7 Hz), 7.85 (1H, d, J = 7.9 Hz), 7.94 (2H, m), 7.98 (1H, s). ^{13}C NMR (DMSO-d$_6$, 125 MHz): δ [ppm] = 34.8, 111.3, 118.4, 122.9, 126.3, 129.3, 129.7, 131.4, 132.0, 132.6, 133.9, 138.8, 162.9, 165.3. EI-MS: m/z = 293 (M$^+$).

*5.11.5. 2-(Benzylthio)-5-(4-methoxyphenyl)-1,3,4-oxadiazole (**16a**)*

Yield 63%, colorless solid. ^{1}H NMR (DMSO-d$_6$, 500 MHz): δ [ppm] = 3.85 (3H, s), 4.56 (2H, s), 7.13 (2H, m), 7.28 (1H, m), 7.33 (2H, m), 7.47 (2H, m), 7.89 (2H, m). ^{13}C NMR (DMSO-d$_6$, 125 MHz): δ [ppm] = 35.9, 55.5, 114.8, 115.3, 127.7, 128.2, 128.5, 128.9, 136.6, 162.0, 162.3, 165.1. EI-MS: m/z = 298 (M$^+$).

*5.11.6. 4′-((5-(4-Methoxyphenyl)-1,3,4-oxadiazol-2-ylthio)methyl) biphenyl-2-carbonitrile (**16b**)*

Yield 71%, orange solid. ^{1}H NMR (DMSO-d$_6$, 300 MHz): δ [ppm] = 4.62 (2H, s), 7.22-7.43 (3H, m, br), 7.50 (2H, m), 8.22 (2H, m), 8.41 (2H, m). ^{13}C NMR (DMSO-d$_6$, 75 MHz): δ [ppm] = 35.8, 124.5, 127.7, 127.7, 128.4, 128.5, 129.0, 136.3, 149.1, 163.8, 164.7. EI-MS: m/z = 399 (M$^+$).

*5.11.7. 2-(3-Methoxybenzylthio)-5-(4-methoxyphenyl)-1,3,4-oxadiazole (**16c**)*

Yield 57%, colorless solid. ^{1}H NMR (DMSO-d$_6$, 500 MHz): δ [ppm] = 3.72 (3H, s), 3.85 (3H, s), 4.53 (2H, s), 6.84 (1H, m), 7.03 (2H, *t*, J = 5.0 Hz), 7.13 (2H, m), 7.25 (1H, *t*, J = 7.9 Hz), 7.90 (2H, m).

Please cite this article in press as: F. Lo Monte, et al., Structure-based optimization of oxadiazole-based GSK-3 inhibitors, European Journal of Medicinal Chemistry (2012), http://dx.doi.org/10.1016/j.ejmech.2012.06.006

^{13}C NMR (DMSO-d$_6$, 125 MHz): δ [ppm] = 35.9, 55.0, 55.5, 113.2, 114.6, 114.8, 115.3, 121.1, 128.2, 129.6, 138.0, 159.2, 162.0, 162.4, 165.1. EI-MS: *m*/*z* = 328 (M$^+$).

*5.11.8. 3-((5-(4-Methoxyphenyl)-1,3,4-oxadiazol-2-ylthio)methyl) benzonitrile (**16d**)*

Yield 41%, colorless solid. ^{1}H NMR (DMSO-d$_6$, 500 MHz): δ [ppm] = 3.84 (3H, s), 4.60 (2H, s), 7.13 (1H, m), 7.57 (2H, *t*, *J* = 7.8 Hz), 7.76 (1H, dt, *J* = 7.7 Hz, *J* = 1.3 Hz), 7.83 (1H, m), 7.88 (2H, m), 7.96 (1H, *t*, *J* = 1.5 Hz). ^{13}C NMR (DMSO-d$_6$, 125 MHz): δ [ppm] = 34.8, 55.5, 111.3, 114.8, 115.2, 118.4, 128.2, 129.7, 131.4, 132.6, 133.9, 138.8, 162.0, 165.3. EI-MS: *m*/*z* = 323 (M$^+$).

*5.11.9. 4-(5-(Benzylthio)-1,3,4-oxadiazol-2-yl)benzonitrile (**17a**)*

Yield 32%, colorless solid. ^{1}H NMR (DMSO-d$_6$, 300 MHz): δ [ppm] = 4.61 (2H, s), 7.31 (3H, m), 7.49 (2H, d, *J* = 7.3 Hz), 8.09 (4H, td, *J* = 8.2 Hz, *J* = 0.9 Hz). ^{13}C NMR (DMSO-d$_6$, 75 MHz): δ [ppm] = 35.8, 114.0, 118.0, 126.9, 127.0, 127.7, 128.5, 129.0, 133.3, 136.4, 164.0, 164.4. EI-MS: *m*/*z* = 293 (M$^+$).

*5.11.10. 4′-((5-Phenyl-1,3,4-oxadiazol-2-ylthio)methyl)biphenyl-2-carbonitrile (**17b**)*

Yield 53%, orange solid. ^{1}H NMR (DMSO-d$_6$, 500 MHz): δ [ppm] = 4.72 (2H, s), 7.48 (1H, m), 7.51 (1H, m), 7.57 (2H, m), 7.62 (2H, m), 7.67 (1H, dt, *J* = 7.7 Hz, *J* = 1.3 Hz), 7.79 (1H, dd, *J* = 7.7 Hz, *J* = 0.9 Hz), 7.81 (2H, m), 8.13 (2H, m). ^{13}C NMR (DMSO-d$_6$, 125 MHz): δ [ppm] = 36.4, 111.2, 115.1, 117.8, 118.5, 127.1, 127.4, 127.8, 129.2, 129.5, 129.9, 132.8, 132.9, 133.8, 136.0, 138.0, 144.6, 164.3, 165.1. EI-MS: *m*/*z* = 394 (M$^+$).

*5.11.11. 4-(5-(3-Methoxybenzylthio)-1,3,4-oxadiazol-2-yl) benzonitrile (**17c**)*

Yield 47%, colorless solid. ^{1}H NMR (DMSO-d$_6$, 500 MHz): δ (ppm) = 3.77 (3H, s), 4.49 (2H, s), 6.82 (1H, dd, *J* = 8.3 Hz, *J* = 2.0 Hz), 6.97 (1H, m), 7.00 (1H, d, *J* = 7.6 Hz), 7.23 (1H, *t*, *J* = 7.9 Hz), 7.75 (2H, m), 8.08 (2H, m). ^{13}C NMR (DMSO-d$_6$, 125 MHz): δ (ppm) = 36.9, 55.3, 113.8, 114.7, 115.1, 117.9, 121.4, 127.1, 127.5, 129.9, 132.9, 136.7, 159.9, 164.3, 165.3. EI-MS: *m*/*z* = 323 (M$^+$).

*5.11.12. 3-((5-(4-Cyanophenyl)-1,3,4-oxadiazol-2-ylthio)methyl) benzonitrile (**17d**)*

Yield 45%, colorless solid. ^{1}H NMR (DMSO-d$_6$, 300 MHz): δ [ppm] = 4.47 (2H, s), 7.40 (1H, *t*, *J* = 7.8 Hz), 7.52 (1H, m), 7.70 (4H, m), 8.03 (2H, dt, *J* = 6.8 Hz, *J* = 0.9 Hz). ^{13}C NMR (DMSO-d$_6$, 75 MHz): δ [ppm] = 34.9, 112.2, 114.5, 117.1, 117.6, 126.4, 126.5, 129.0, 131.1, 131.9, 132.2, 133.0, 136.8, 163.8, 163.9. EI-MS: *m*/*z* = 318 (M$^+$).

*5.11.13. 2-(Benzylthio)-5-(4-nitrophenyl)-1,3,4-oxadiazole (**18a**)*

Yield 46%, light yellow solid. ^{1}H NMR (DMSO-d$_6$, 300 MHz): δ [ppm] = 4.62 (2H, s), 7.32 (3H, m), 7.49 (2H, m), 8.21 (2H, m), 8.41 (2H, m). ^{13}C NMR (DMSO-d$_6$, 75 MHz): δ [ppm] = 35.8, 124.5, 127.7, 127.7, 128.4, 128.5, 129.0, 136.3, 149.1, 163.8, 164.7. EI-MS: *m*/*z* = 313 (M$^+$).

*5.11.14. 4′-((5-(4-Nitrophenyl)-1,3,4-oxadiazol-2-ylthio)methyl) biphenyl-2-carbonitrile (**18b**)*

Yield 58%, orange solid. ^{1}H NMR (DMSO-d$_6$, 500 MHz): δ [ppm] = 4.71 (2H, s), 7.60 (4H, m), 7.68 (2H, d, *J* = 8.2 Hz), 7.78 (1H, dt, *J* = 7.7 Hz, *J* = 1.2 Hz), 7.94 (1H, dd, *J* = 7.7 Hz, *J* = 0.9 Hz), 8.22 (2H, m), 8.41 (2H, m). ^{13}C NMR (DMSO-d$_6$, 125 MHz): δ [ppm] = 35.9, 110.5, 118.9, 125.0, 128.2, 128.7, 129.0, 129.4, 129.9, 130.5, 134.0, 134.3, 137.7, 137.7, 144.4, 149.6, 164.4, 165.2. EI-MS: *m*/*z* = 414 (M$^+$).

*5.11.15. 2-(3-Methoxybenzylthio)-5-(4-nitrophenyl)1,3,4-oxadiazole (**18c**)*

Yield 33%, yellow solid. ^{1}H NMR (DMSO-d$_6$, 500 MHz): δ (ppm) = 3.73 (3H, s), 4.59 (2H, s), 6.86 (1H, m), 7.07 (2H, m), 7.27 (1H, *t*, *J* = 7.9 Hz), 8.23 (2H, m), 8.40 (2H, m). ^{13}C NMR (DMSO-d$_6$, 125 MHz): 35.8, 55.0, 113.3, 114.6, 121.2, 124.5, 127.7, 128.4, 129.7, 137.8, 149.1, 159.2, 163.9, 154.7. EI-MS: *m*/*z* = 343 (M$^+$).

*5.11.16. 3-((5-(4-Nitrophenyl)-1,3,4-oxadiazol-2-ylthio)methyl) benzonitrile (**18d**)*

Yield 47%, orange solid. ^{1}H NMR (DMSO-d$_6$, 300 MHz): δ [ppm] = 4.66 (2H, s), 7.58 (1H, *t*, *J* = 7.8 Hz), 7.76 (1H, m), 7.86 (1H, m), 7.99 (1H, dd, *J* = 2.3 Hz, *J* = 1.1 Hz), 8.20 (2H, m), 8.41 (2H, m). ^{13}C NMR (DMSO-d$_6$, 75 MHz): δ [ppm] = 34.7, 111.3, 118.4, 124.5, 127.7, 128.4, 129.7, 131.4, 132.6, 134.0, 138.6, 149.1, 164.0, 164.4. EI-MS: *m*/*z* = 338 (M$^+$).

*5.12. General procedure for synthesis of compounds **20a**–**d** [52]*

The appropriate benzaldehyde (1.0 eq.) was dissolved in 5 mL EtOH and isoniazid (1.0 eq.) was added slowly to the solution. The reaction mixture was stirred at room temperature for 16 h. The solvent was removed under vacuum and the residue was purified by recrystallization in EtOH.

*5.12.1. (E)-N′-benzylideneisonicotinohydrazide (**20a**)*

Yield 85%, colorless solid. ^{1}H NMR (DMSO-d$_6$, 500 MHz): δ [ppm] = 7.47 (3H, m), 7.76 (2H, m), 7.83 (2H, dd, *J* = 4.3 Hz, *J* = 1.5 Hz), 8.47 (1H, s), 8.79 (2H, dd, *J* = 4.5 Hz, *J* = 1.5 Hz), 12.09 (1H, s). ^{13}C NMR (DMSO-d$_6$, 125 MHz): δ [ppm] = 121.4, 127.1, 128.7, 130.2, 133.9, 140.3, 148.9, 150.2, 161.5. EI-MS: *m*/*z* = 225 (M$^+$).

*5.12.2. (E)-N′-(4-Methoxybenzylidene)isonicotinohydrazide (**20b**)*

Yield 97%, yellow solid. ^{1}H NMR (DMSO-d$_6$, 500 MHz): δ [ppm] = 3.83 (3H, s), 7.03 (2H, d, *J* = 9.0 Hz), 7.70 (2H, d, *J* = 9.0 Hz), 7.81 (2H, dd, *J* = 4.5 Hz, *J* = 1.5 Hz), 8.42 (1H, s), 8.78 (2H, dd, *J* = 4.5 Hz, *J* = 1.5 Hz), 11.93 (1H, s). ^{13}C NMR (DMSO-d$_6$, 125 MHz): δ [ppm] = 55.24, 114.31, 121.3, 126.4, 128.2, 140.5, 148.8, 150.2, 161.0, 161.3. EI-MS: *m*/*z* = 255 (M$^+$).

*5.12.3. (E)-N′-(4-Cyanobenzylidene)isonicotinohydrazide (**20c**)*

Yield 83%, colorless solid. ^{1}H NMR (DMSO-d$_6$, 500 MHz): δ [ppm] = 7.83 (2H, dd, *J* = 4.3 Hz, *J* = 1.5 Hz), 7.94 (4H, s), 8.51 (1H, s), 8.80 (2H, dd, *J* = 4.5 Hz, *J* = 1.5 Hz), 12.27 (1H, s). ^{13}C NMR (DMSO-d$_6$, 125 MHz): δ [ppm] = 112.1, 118.4, 121.4, 127.7, 128.3, 132.6, 140.0, 146.9, 150.2, 161.8. EI-MS: *m*/*z* = 250 (M$^+$).

*5.12.4. (E)-N′-(4-Ethylbenzylidene)isonicotinohydrazide (**20d**)*

Yield 96%, colorless solid. ^{1}H NMR (DMSO-d$_6$, 500 MHz): δ [ppm] = 1.20 (3H, *t*, *J* = 7.5 Hz), 2.65 (2H, m), 7.32 (2H, d, *J* = 8.1 Hz), 7.67 (2H, d, *J* = 8.1 Hz), 7.82 (2H, dd, *J* = 4.5 Hz, *J* = 1.8 Hz), 8.44 (1H, s), 8.78 (2H, dd, *J* = 4.5 Hz, *J* = 1.8 Hz), 11.99 (1H, s). ^{13}C NMR (DMSO-d$_6$, 125 MHz): δ [ppm] = 15.2, 28.0, 121.4, 127.2, 128.2, 131.4, 140.4, 146.4, 149.0, 150.2, 161.4. EI-MS: *m*/*z* = 253 (M$^+$).

*5.13. Compound **22** was prepared in a similar manner to that described for **2a***

Methyl 2-aminoisonicotinate (**22**). Yield 89%, colorless solid. ^{1}H NMR (DMSO-d$_6$, 500 MHz): δ [ppm] = 3.84 (3H, s), 6.28 (2H, s), 6.87 (1H, dd, *J* = 5.2 Hz, *J* = 1.5 Hz), 6.96 (1H, m), 8.05 (1H, dd, *J* = 5.2 Hz, *J* = 0.6 Hz). ^{13}C NMR (DMSO-d$_6$, 125 MHz): δ [ppm] = 52.4, 107.4, 110.0, 137.8, 148.9, 160.5, 165.7. EI-MS: *m*/*z* = 152 (M$^+$).

Please cite this article in press as: F. Lo Monte, et al., Structure-based optimization of oxadiazole-based GSK-3 inhibitors, European Journal of Medicinal Chemistry (2012), http://dx.doi.org/10.1016/j.ejmech.2012.06.006

*5.14. Methyl 2-acetamidoisonicotinate (**23**)*

A solution of compound **22** (760 mg, 5 mmol) in acetic anhydride (20 mL) was heated at 80 °C for 6 h. The reaction was cooled to room temperature and the precipitate formed was filtered off and well washed with water to obtain compound **23** (0.67 g, 69%)as yellow solid. ^{1}H NMR (DMSO-d_6, 500 MHz): δ [ppm] = 2.12 (3H, s), 3.89 (3H, s), 7.52 (1H, dd, J = 5.0 Hz, J = 1.4 Hz), 8.48 (1H, d, J = 5.0 Hz), 8.57 (1H, s), 10.74 (1H, s). ^{13}C NMR (DMSO-d_6, 125 MHz): δ [ppm] = 23.8, 52.7, 112.2, 117.9, 138.6, 149.0, 153.0, 165.1, 169.6. EI-MS: m/z = 154 (M^+).

*5.15. Compound **24** was prepared in a similar manner to that described for **3a***

N-(4-(Hydrazinecarbonyl)pyridin-2-yl)acetamide (**24**). Yield 74%, light yellow solid. ^{1}H NMR (DMSO-d_6, 500 MHz): δ [ppm] = 2.11 (3H, s), 4.58 (2H, s), 7.38 (1H, dd, J = 5.1 Hz, J = 1.5 Hz), 8.38 (1H, dd, J = 5.1 Hz, J = 0.7 Hz), 8.41 (1H, s), 9.99 (1H, s), 10.59 (1H, s). ^{13}C NMR (DMSO-d_6, 125 MHz): δ [ppm] = 23.9, 111.3, 116.2, 142.8, 148.2, 152.7, 164.2, 169.3. EI-MS: m/z = 194 (M^+).

*5.16. Compound **25** was prepared in a similar manner to that described for **4a***

N-(4-(5-Mercapto-1,3,4-oxadiazol-2-yl)pyridin-2-yl)acetamide (**25**). Yield 92%, yellow solid. ^{1}H NMR (DMSO-d_6, 500 MHz): δ [ppm] = 2.14 (3H, s), 7.49 (1H, dd, J = 5.1 Hz, J = 1.5 Hz), 8.53 (1H, dd, J = 5.1 Hz, J = 0.7 Hz), 8.54 (1H, s), 10.82 (1H, s), 14.90 (1H, s). ^{13}C NMR (DMSO-d_6, 125 MHz): δ [ppm] = 23.9, 108.8, 114.9, 131.4, 149.4, 153.0, 158.8, 169.8, 177.7. EI-MS: m/z = 236 (M^+).

*5.17. Compounds **26a–d** were prepared in a similar manner to that described for compounds **8a–h, 9a–f** and **10a–f***

*5.17.1. N-(4-(5-(Benzylthio)-1,3,4-oxadiazol-2-yl)pyridin-2-yl) acetamide (**26a**)*

Yield 68%, colorless solid. ^{1}H NMR (DMSO-d_6, 500 MHz): δ [ppm] = 2.15 (3H, s), 4.61 (2H, s), 7.30 (1H, m), 7.36 (2H, m), 7.51 (2H, m), 7.58 (1H, dd, J = 5.1 Hz, J = 1.5 Hz), 8.52 (1H, dd, J = 5.1 Hz, J = 0.8 Hz), 8.63 (1H, s), 10.80 (1H, s). ^{13}C NMR (DMSO-d_6, 125 MHz): δ [ppm] = 24.0, 35.9, 109.2, 115.4, 127.8, 128.6, 129.1, 131.7, 136.4, 149.4, 153.0, 163.8, 164.4, 169.8. EI-MS: m/z = 326 (M^+).

*5.17.2. **N**-(4-(5-(3-Methoxybenzylthio)-1,3,4-oxadiazol-2-yl) pyridin-2-yl)acetamide (**26b**)*

Yield 51%, yellow solid. ^{1}H NMR (DMSO-d_6, 500 MHz): δ [ppm] = 2.14 (3H, s), 3.73 (3H, s), 4.58 (2H, s), 6.86 (1H, m), 7.07 (2H, m), 7.27 (1H, m), 7.58 (1H, dd, J = 5.1 Hz, J = 1.5 Hz), 8.52 (1H, dd, J = 5.1 Hz, J = 0.7 Hz), 8.63 (1H, s), 10.80 (1H, s). ^{13}C NMR (DMSO-d_6, 125 MHz): δ [ppm] = 24.0, 35.9, 55.0, 109.2, 113.3, 114.6, 115.4, 121.2, 129.7, 131.8, 137.8, 149.4, 153.0, 159.3, 163.8, 164.7, 169.8. EI-MS: m/z = 356 (M^+).

*5.17.3. **N**-(4-(5-(Benzylthio)-1,3,4-oxadiazol-2-yl)pyridin-2-yl) acetamide (**26c**)*

Yield 37%, colorless solid. ^{1}H NMR (DMSO-d_6, 500 MHz): δ [ppm] = 2.14 (3H, s), 4.64 (2H, s), 7.57 (2H, m), 7.77 (1H, d, J = 7.8 Hz), 7.87 (1H, d, J = 7.8 Hz), 7.97 (1H, s), 8.51 (1H, d, J = 5.1 Hz), 8.61 (1H, s), 10.81 (1H, s). ^{13}C NMR (DMSO-d_6, 125 MHz): δ [ppm] = 23.9, 34.8, 109.2, 111.4, 115.4, 118.5, 129.8, 131.5, 131.8, 132.6, 134.1, 138.6, 149.5, 153.0, 163.9, 164.4, 169.8. EI-MS: m/z = 351 (M^+). HRMS (EI): m/z calcd for $C_{17}H_{13}N_5O_2S$ 351.0791, found 351.0787.

*5.17.4. N-(4-(5-((2'-Cyanobiphenyl-4-yl)methylthio)-1,3,4-oxadiazol-2-yl)pyridin-2-yl)acet-amide (**26d**)*

Yield 62%, light yellow solid. ^{1}H NMR (DMSO-d_6, 500 MHz): δ [ppm] = 2.14 (3H, s), 4.70 (2H, s), 7.56-7.61 (5H, m), 7.68 (2H, d, J = 8.2 Hz), 7.78 (1H, td, J = 7.6 Hz, J = 1.3 Hz), 7.94 (1H, dd, J = 7.6 Hz, J = 1.1 Hz), 8.52 (1H, dd, J = 5.1 Hz, J = 0.7 Hz), 8.64 (1H, s), 10.80 (1H, s). ^{13}C NMR (DMSO-d_6, 125 MHz): δ [ppm] = 23.9, 35.5, 109.3, 110.1, 115.4, 118.5, 128.3, 128.9, 129.4, 130.1, 131.8, 133.5, 133.9, 137.2, 144.0, 149.5, 153.1, 163.9, 164.7, 169.8. EI-MS: m/z = 427 (M^+). HRMS (EI): m/z calcd for $C_{23}H_{17}N_5O_2S$ 427.1104, found 427.1104.

*5.18. Ethyl 4-aminobenzoate (**28**)*

To a solution of compound **27** (3.4 g, 25 mmol) in ethanol (30 mL) was added dropwise concentrated sulfuric acid (2.4 mL). The mixture was heated under reflux for 6 h. The resulting solution was diluted with water (200 mL) and made neutral by addition of concentrated ammonia water. The precipitation was collected by filtration and then washed with water and subsequently dried to afford compound **28** (3.68 g, 91%) as colorless solid. The compound was used, without structure determination, directly for the next step.

*5.19. Ethyl 2-aminobenzo[d]thiazole-6-carboxylate (**29**)*

Compound **28** (2.0 g, 12 mmol) was dissolved in 16 mL of acetic acid, and to the resulting solution was suspended potassium thiocyanate (4.67 g, 48 mmol). A solution of 0.61 mL of bromine in 8 ml of acetic acid was slowly added, and the reaction mixture was stirred at room temperature overnight. Water was added and the mixture was made neutral by addition of aqueous ammonium hydroxide. The precipitation was collected by filtration and then washed with water and subsequently dried to afford compound **29** (1.80 g, 67%) as light yellow solid. The compound was used, without structure determination, directly for the next step.

*5.20. Compound **30** was prepared in a similar manner to that described for **23***

Ethyl 2-acetamidobenzo[*d*]thiazole-6-carboxylate (**30**). Yield 58%, light brown solid. The compound was used, without structure determination, directly for the next step.

*5.21. 2-Acetamidobenzo[d]thiazole-6-carboxylic acid (**31**)*

A solution of compound **30** (1.0 g, 3.8 mmol), 1 N NaOH (40 mL), and MeOH (15 mL) was stirred at room temperature for 4 h and then the solvent was evaporated. To the resulting aqueous layer was added water (10 mL) and the solution acidified with 1 N HCl to pH 2. The resulting solid was collected by filtration and washed with water. The solid was dried to afford compound **31** (0.84 g, 94%) as light brown solid. The compound was used, without structure determination, directly for the next step.

*5.22. N-(6-(2-tert-Butylhydrazinecarbonyl)benzo[d]thiazol-2-yl) acetamide (**32**)*

To a solution of **31** (0.80 g, 3.3 mmol), *tert*-butyl carbazate (0.47 g, 3.6 mmol) and 1-(3-dimethylaminopropyl)-3-ethylcarbodiimide hydrochloride (EDCI) (0.74 g, 3.9 mmol) in DMF (10 mL) was added 1-hydroxybenzotriazole hydrate (HOBt•H_2O) (0.59 g, 3.9 mmol) and the mixture stirred overnight at room temperature. The reaction mixture was diluted with EtOAc and the organic layer was washed with water and brine, dried over

Please cite this article in press as: F. Lo Monte, et al., Structure-based optimization of oxadiazole-based GSK-3 inhibitors, European Journal of Medicinal Chemistry (2012), http://dx.doi.org/10.1016/j.ejmech.2012.06.006

Na_2SO_4 and concentrated *in vacuo*. The residue was recrystallized in EtOAc/CH to give **32** (0.79 g, 77%) as light brown solid. The compound was used, without structure determination, directly for the next step.

*5.23. N-(6-(Hydrazinecarbonyl)benzo[d]thiazol-2-yl)acetamide (**33**)*

A solution of **32** (0.75 g, 2.4 mmol) in trifluoroacetic acid (5 mL) was stirred at room temperature for 1 h. The solvent was concentrated to give **33** (0.59 g, 99%) as colorless solid. The compound was used, without structure determination, directly for the next step.

*5.24. Compound **34** was prepared in a similar manner to that described for **4a***

*5.24.1. N-(6-(5-Mercapto-1,3,4-oxadiazol-2-yl)benzo[d]thiazol-2-yl)acetamide (**34**)*

Yield 81%, light brown solid. The compound was used, without structure determination, directly for the next step.

*5.25. Compounds **35** was prepared in a similar manner to that described for compounds **8a–h**, **9a–f** and **10a–f***

*5.25.1. N-(6-(5-((2′-Cyanobiphenyl-4-yl)methylthio)-1,3,4-oxadiazol-2-yl)benzo[d]thiazol-2-yl)acetamide (**35**)*

Yield 47%, light brown solid. ^{1}H NMR (DMSO-d_6, 500 MHz): δ [ppm] = 2.23 (3H, s), 4.69 (2H, s), 7.59 (4H, m), 7.67 (2H, d, J = 8.3 Hz), 7.78 (1H, td, J = 7.7 Hz, J = 1.4 Hz), 7.88 (1H, d, J = 8.5 Hz), 7.94 (1H, dd, J = 7.8 Hz, J = 1.1 Hz), 8.01 (1H, dd, J = 8.5 Hz, J = 1.8 Hz), 8.64 (1H, d, J = 1.5 Hz), 12.56 (1H, s). ^{13}C NMR (DMSO-d_6, 125 MHz): δ [ppm] = 22.7, 35.5, 110.0, 117.8, 118.4, 120.6, 121.0, 124.3, 128.2, 128.9, 129.4, 130.0, 132.4, 133.5, 133.8, 137.1, 137.3, 143.9, 151.1, 160.7, 162.9, 165.4, 169.7. EI-MS: m/z = 483 (M^+).

*5.26. Methyl 3-bromo-4-hydroxybenzoate (**37**)*

To a solution of **36** (3.15 g, 20.7 mmol) in DCM (230 mL) was added slowly at −5 °C a solution of bromine (1.1 mL, 21 mmol) in DCM (50 mL). The mixture was stirred for 4.5 h at room temperature. The reaction mixture was diluted with EtOAc and the organic layer was washed with water and brine, dried over $MgSO_4$ and concentrated *in vacuo*. The residue was purified by silica gel column chromatography (DCM/EtOAc) to give **37** (3.10 g, 65%) as colorless solid. The compound was used, without structure determination, directly for the next step.

*5.27. Methyl 8-nitrodibenzo[b,d]furan-2-carboxylate (**38**)*

A mixture of compound **37** (0.51 g, 2.2 mmol), 1-fluoro-4-nitrobenzene (0.36 g, 2.2 mmol) and Palladium(II) acetate (0.05 g, 0.22 mmol) in *N,N*-dimethylacetamide (2 mL) was stirred overnight at 130 °C. The reaction mixture was diluted with EtOAc (20 mL) and filtered over celite. The solvent was removed *in vacuo* and the resulting oil was diluted with water (7 mL). The precipitate formed was collected by filtration and recrystallized in EtOH to give compound **38** (0.18 g, 30%) as colorless solid. The compound was used, without structure determination, directly for the next step.

*5.28. 8-Nitrodibenzo[b,d]furan-2-carbohydrazide (**39**)*

To compound **38** (160 mg, 0.59 mmol) was added hydrazine hydrate (1.5 mL) and the mixture was heated at reflux for 6 h. After cooling to room temperature pure crystals are formed, collected by filtration and washed several times with EtOH to give compound **39** (158 mg, 99%) as a yellow solid. The compound was used, without structure determination, directly for the next step.

*5.29. Compound **40** was prepared in a similar manner to that described for **4a***

5-(8-Nitrodibenzo[*b*,*d*]furan-2-yl)-1,3,4-oxadiazole-2-thiol (**40**). Yield 48%, light brown solid. The compound was used, without structure determination, directly for the next step.

*5.30. Compound **41** was prepared in a similar manner to that described for compounds **8a–h**, **9a–f** and **10a–f***

*5.30.1. 3-({[5-(8-Nitrodibenzo[b,d]furan-2-yl)-1,3,4-oxadiazol-2-yl] sulfanyl}methyl)benzonitril (**41**)*

Yield 44%, yellow solid. ^{1}H NMR (DMSO-d_6, 500 MHz): δ [ppm] = 4.71 (2H, s), 7.63 (1H, *t*, J = 7.8 Hz), 7.81 (1H, m), 7.96 (1H, m), 8.03 (3H, m), 8.25 (1H, d, J = 8.7 Hz), 8.58 (1H, d, J = 9.1 Hz), 9.11 (1H, s), 9.42 (1H, s). ^{13}C NMR (DMSO-d_6, 125 MHz): δ [ppm] = 35.7, 64.5, 114.0, 119.7, 122.3, 125.0, 128.3, 130.7, 132.4, 133.6, 134.9. EI-MS: m/z = 428 (M^+).

5.31. Determination of GSK-3 inhibition

GSK-3β in vitro assay: Purified GSK-3β (0.5 μg) was incubated in a reaction mixture of 50 mM Tris pH 7.3, 10 mM MgAc, 0.01% β-mercaptoethanol, ^{32}P[γ-ATP](100 μM, 0.5 μci/assay), and 100 μM of peptide substrate, pIRS-1 (RREGGMSRPAS(p)VDG). New molecules were added at various concentrations (1, 10 and 100 μM), and the reaction mixture was incubated for 15 min at 30 °C. The reactions were stopped, spotted on p81 paper (Whatman), washed with 10 mM phosphoric acid, and counted for radioactivity [53].GSK-3β activity was calculated as the percentage of GSK-3β activity in the absence of inhibitors that was designated to 100%.

Kinase Panel: Compounds are serially diluted 1/3 in neat DMSO (10 serial dilutions) and these dilutions are further diluted 1/25 with reaction buffer. 2.5 μL of these solutions are added to the reaction mixture described below so that final compound concentration in the assay ranges from 100 μM to 5 nM in 1% (v/v) DMSO. The enzymatic activity of the kinases is determined with a commercial system based on the Z′-LYTE® technology, available from Invitrogen Life Technologies (Carlsbad, CA, USA), using human recombinant kinases as the enzyme source.

Kinase	Enzyme conc. (nM)	ATP conc. (μM)	Peptide used	Peptide conc. (μM)	Buffer
GSK-3β	2	12.5	Ser/Thr 9 peptide	2	50 mM Hepes pH 7.5, 10 mM $MgCl_2$, 1 mM EGTA, 0.01% (w/v) Brij-35
GSK-3α	0.5	12.5	Ser/Thr 9 peptide	2	"
CKIε	12	32	Ser/Thr 11 peptide	2	"
Cdk5	10	12.5	Ser/Thr 12 peptide	2	"
AurKA	20	10	Ser/Thr 1 peptide	2	"
PKCα	0.15	10	Ser/Thr 7 peptide	2	"

Please cite this article in press as: F. Lo Monte, et al., Structure-based optimization of oxadiazole-based GSK-3 inhibitors, European Journal of Medicinal Chemistry (2012), http://dx.doi.org/10.1016/j.ejmech.2012.06.006

This technology utilizes the fluorescence resonance energy transfer ("FRET") process between fluorescein and coumarin. The assay principle is based on the differential sensitivity of phosphorylated and non-phosphorylated peptide to proteolytic cleavage, which precludes the energy transfer process between the two fluorophores attached to both sides of the cleavage site. Hence, enzymatic phosphorylation will yield a phosphopeptide, which cannot be hydrolyzed by a suitable protease and energy transfer between the two fluorophores will occur. Opposingly, lack of phosphorylation will cause peptide hydrolysis hence lack of energy transfer as. The assay is performed in 96-well black plates, in a final volume of 10 μL.

5.32. Determination of the in vivo activity on wt zebrafish embryos

In Vivo Activity on Zebrafish Embryos: The wt zebrafish was used in this study. The embryos were collected and placed into 24-well plates, ten embryos per well and maintained in E2 medium at ~28 °C. Compounds were added 5 hpf (50% epiboly) and the embryos allowed to grow in chemical compound solution up to 2 days. The phenotypes were compared using the Axio Scope.A1 microscope system from Carl Zeiss at 44–48 hpf [49,50,54].

5.33. Docking simulations

Molecular docking of **9e** and **26d** into the X-ray structure of GSK-3β (PDB code: 3F88) was carried out using Molegro Virtual Docker 5.

Acknowledgments

This work was supported by a collaborative project financed by the 7th Framework Program of the European Union: NeuroGSK3.

Appendix A. Supplementary information

Supplementary data related to this article can be found online at http://dx.doi.org/10.1016/j.ejmech.2012.06.006.

References

[1] F. Lo Monte, T. Kramer, A. Boländer, B. Plotkin, H. Eldar-Finkelman, A. Fuertes, J. Dominguez, B. Schmidt, Synthesis and biological evaluation of glycogen synthase kinase 3 (GSK-3) inhibitors: an fast and atom efficient access to 1-aryl-3-benzylureas, Bioorg. Med. Chem. Lett. 21 (2011) 5610–5615.
[2] C. Hooper, R. Killick, S. Lovestone, The GSK3 hypothesis of Alzheimer's disease, J. Neurochem. 104 (2008) 1433–1439.
[3] A. Alzheimer, Über eine eigenartige Erkankung der Hirnrinde, Allgemeine Zeitschrift Für Psychiatrie Und Psychisch-gerichtliche Medizin (Berlin) 64 (1907) 146–148.
[4] A. Alzheimer, R.A. Stelzmann, H.N. Schnitzlein, F.R. Murtagh, An English translation of Alzheimer's 1907 paper, "Über eine eigenartige Erkankung der Hirnrinde", Clin. Anat. 8 (1995) 429–431.
[5] P. Cohen, M. Goedert, GSK3 inhibitors: development and therapeutical potential, Nat. Rev. Drug Discov. 3 (2004) 479–487.
[6] F. Hernández, J. Avila, The role of glycogen synthase kinase 3 in the early stages of Alzheimers' disease, FEBS Lett. 582 (2008) 3848–3854.
[7] Eldar-Finkelman, Glycogen synthase kinase 3: an emerging therapeutic target, Trends Mol. Med. 8 (2002) 126–132.
[8] M. Mazanetz, P. Fischer, Untangling tau hyperphosphorylation in drug design for neurodegenerative diseases, Nat. Rev. Drug Discov. 6 (2007) 464–479.
[9] L. Chico, L. Van Eldik, D. Watterson, Targeting protein kinases in central nervous system disorders. 892–909, Nat. Rev. Drug Discov. 8 (2009).
[10] L. Meijer, M. Flajolet, P. Greengard, Pharmacological inhibitors of glycogen synthase kinase 3, TRENDS. Pharmacol. Sci. 25 (2004) 471–480.
[11] A. Martinez, C. Gil, D.I. Perez, Glycogen synthase kinase 3 inhibitors in the next horizon for Alzheimer's disease treatment, Int. J. of Alzheimer's Disease 2011 (2011) 1–7.
[12] K.F. Lau, C.C.J. Miller, B.H. Anderton, P.C. Shaw, Expression analysis of glycogen synthase kinase-3 in human tissues, J. Pept. Res. 54 (1999) 85–91.
[13] S. Frame, P. Cohen, GSK3 takes centre stage more than 20 years after its discovery, Biochem. J. 359 (2001) 1–16.
[14] E. Hur, F. Zhou, GSK3 signalling in neural development, Nat. Rev. Neurosci. 11 (2010) 539–551.
[15] F. Mukai, K. Ishiguro, Y. Sano, S.C. Fujita, Alternative splicing isoform of tau protein kinase I/glycogen synthase kinase 3 beta, J. Neurochem. 81 (2002) 1073–1083.
[16] E. ter Haar, J.T. Coll, D.A. Austen, H. Hsiao, L. Swenson, J. Jain, Structure of GSK3β reveals a primed phosphorylation mechanism, Nat. Struct. Biol. 8 (2001) 593–596.
[17] R. Dajani, E. Fraser, S.M. Roe, N. Young, V. Good, T.C. Dale, L.H. Pearl, Crystal structure of glycogen synthase kinase 3: structural basis for phosphate-primed substrate specificity and autoinhibition, Cell 105 (2001) 721–732.
[18] A. Takashima, Drug development targeting the glycogen synthase kinase-3β (GSK-3β)-mediated signal transduction pathway: role of GSK-3β in adult brain, J. Pharmacol. Sci. 109 (2009) 174–178.
[19] L. Serenó, M. Coma, M. Rodriguez, P. Sánchez-Ferrer, M.B. Sánchez, I. Gich, J.M. Agulló, J. Avila, M. Pérez, C. Guardia-Laguarta, J. Clarimón, A. Lleó, T. Gómez-Isla, A novel GSK-3β inhibitor reduces Alzheimer's pathology and rescues neuronalloss in vivo, Neurobiol. Dis. 35 (2009) 359–367.
[20] H. Yamaguchi, K. Ishiguro, T. Uchida, A. Takashima, C.A. Lemere, K. Imahori, Preferential labeling of Alzheimer neurofibrillary tangles with antisera for tau protein kinase (TPK) I/glycogen synthase kinase-3β and cyclin-dependent kinase 5, a component of TPK II, Acta Neuropathol. 92 (1996) 232–241.
[21] A. Martinez, A. Castro, I. Dorronsoro, M. Alonso, Glycogen synthase kinase 3 (GSK-3) inhibitors as new promising drugs for diabetes, neurodegeneration, cancer, and inflammation, Med. Res. Rev. 22 (2002) 373–384.
[22] L. Feng, Y. Geisselbrecht, S. Blanck, A. Wilbuer, G.E. Atilla-Gokcumen, P. Filippakopoulos, K. Krling, M.A. Celik, K. Harms, J. Maksimoska, R. Marmorstein, G. Frenking, S. Knapp, L. Essen, E. Meggers, Structurally sophisticated octahedral metal complexes as highly selective protein kinase inhibitors, J. Am. Chem. Soc. 133 (2011) 5976–5986.
[23] R.V. Bhat, S.L. Budd Haeberlein, J. Avila, Glycogen synthase kinase 3: a drug target for CNS therapies, J. Neurochem. 89 (2004) 1313–1317.
[24] F. Lo Monte, T. Kramer, J. Gu, U. Rao Anumala, L. Marinelli, V. La Pietra, E. Novellino, B. Franco, D. Demedts, F. Van Leuven, A. Fuertes, J.M. Dominguez, B. Plotkin, H. Eldar-Finkelman, B. Schmidt, Identification of glycogen synthase Kinase-3 inhibitors with a selective sting for glycogen synthase Kinase-3α, J. Med. Chem. 55 (2012) 4407–4424.
[25] T. Kramer, B. Schmidt, F. Lo Monte, Small-molecule inhibitors of GSK-3-Structural insights and their application to Alzheimer's disease models, Int. J. of Alzheimer's Disease (2012). accepted, http://www.hindawi.com/journals/ijad/aip/381029/.
[26] B. Voigt, M. Krug, C. Schächtele, F. Totzke, A. Hilgeroth, Probing novel 1-Aza-9-oxafluorenes as selective GSK-3β inhibitors, ChemMedChem 3 (2008) 120–126.
[27] J. Boström, A. Hogner, A. Llinás, E. Wellner, A.T. Plowright, Oxadiazoles in medicinal chemistry, J. Med. Chem. 55 (2012) 1817–1830.
[28] M. Saitoh, J. Kunitomo, E. Kimura, Y. Hayase, H. Kobayashi, N. Uchiyama, T. Kawamoto, T. Tanaka, C.D. Mol, D.R. Dougan, G.S. Textor, G.P. Snell, F. Itoh, Design, synthesis and structure–activity relationships of 1,3,4-oxadiazole derivatives as novel inhibitors of glycogen synthase kinase-3β, Bioorg. Med. Chem. 17 (2009) 2017–2029.
[29] L. Naerum, L. Norskov-Lauritsen, P.H. Olesen, Scaffold hopping and optimization towards libraries of glycogen synthase kinase-3 inhibitors, Bioorg. Med. Chem. Lett. 12 (2002) 1525–1528.
[30] R. Bhat, X. Xue, S. Berg, S. Hellberg, M. Ormö, Y. Nilsson, A. Radesäter, E. Jerning, P. Markgren, M. Nylöf, T. Borgegard, A. Giménez-Cassina, F. Hernández, J.J. Lucas, J. Díaz-Nido, J. Avila, Structural insights and biological effects of glycogen synthase kinase 3-specific inhibitor AR-A014418, J. Biol. Chem. 278 (2003) 45937–45945.
[31] H.B. Konig, W. Seifken, H.A. Offe, Sulfur-containing derivatives of pyridine carboxylic acids and compounds derived therefrom, Chem. Berichte 87 (1954) 825–834.
[32] G. Mazzone, F. Bonina, R. Arrigo-Reina, Synthesis and pharmacological activities of some 2-(alkylaminoalkyl)mercapto-5-aryl-(1,3,4-oxadiazoles), Farmaco, Ed. Scient 32 (1977) 414–429.
[33] R.A. Tromp, S. van Ameijde, C. Pütz, C. Sundermann, B. Sundermann, J.K. von Frijtag Drabbe Künzel, P. IJzerman, Inhibition of nucleoside transport by new analogues of 4-nitrobenzylthioinosine: replacement of the ribose moiety by substituted benzyl groups, J. Med. Chem. 47 (2004) 5441–5450.
[34] S. Chao, S. Li, X. Hui, P. Xu, L. Dong, Synthesis and antibacterial activities of 2-phenyl-5-[[2'-cyano(1,1'-biphenylyl)-4-]methyl]mercapto-1,3,4-oxadiazole, Xinxiang Yixueyuan Xuebao 23 (2006) 5–6.
[35] S. Giri, H. Singh, L.D.S. Yadav, Studies in oxadiazoles. Synthesis of some 2-mercapto-1,3,4-oxadiazoles and related compounds as potential fungicides, Agr. Biol. Chem. 40 (1976) 17–21.
[36] M.C. da Silva Lourenco, M. de Lima Ferreira, M.V.N. de Souza, M.A. Peralta, T.R.A. Vasconcelos, M. das Gracas Henriques, Synthesis and anti-mycobacterial activity of (E)-N'-(monosubstituted-benzylidene)isonicotinohydrazide derivatives, Eur. J. Med. Chem. 43 (2008) 1344–1347.
[37] I. Ninomiya, O. Yamamoto, Photochemistry of isonicotinohydrazide and its analogs in alcohol, Heterocycles 4 (1976) 475–481.
[38] R.R. Shah, R.D. Mehta, A.R. Parikh, Studies on isoniazid derivatives. Preparation and antimicrobial activity of 2-aryl-3-(pyridylcarbomyl)-5-carboxymethyl-4-thiazolidinones, J. Ind. Chem. Soc. 62 (1985) 255–257.
[39] S.K. Boovanahalli, X. Jin, Y. Jin, J.H. Kim, N.T. Dat, Y. Hong, J.H. Lee, S. Jung, K. Lee, J.J. Lee, Synthesis of (aryloxyacetylamino)-isonicotinic/nicotinic acid

Please cite this article in press as: F. Lo Monte, et al., Structure-based optimization of oxadiazole-based GSK-3 inhibitors, European Journal of Medicinal Chemistry (2012), http://dx.doi.org/10.1016/j.ejmech.2012.06.006

analogues as potent hypoxia-inducible factor (HIF)-1a inhibitors, Bioorg. Med. Chem. Lett. 17 (2007) 6305–6310.
[40] M.A. Chowdhury, K.R.A. Abdellatif, Y. Dong, M. Rahman, D. Das, M.R. Suresh, E.E. Knaus, Synthesis of 1-(methanesulfonyl- and aminosulfonylphenyl)acetylenes that possess a 2-(N-difluoromethyl-1,2-dihydropyridin-2-one pharmacophore): evaluation as dual inhibitors of cyclooxygenases and 5-lipoxygenase with anti-inflammatory activity, Bioorg. Med. Chem. Lett. 19 (2009) 584–588.
[41] Q. Zheng, F. Zhang, K. Cheng, Y. Yang, Y. Chen, Y. Qian, H. Zhang, L. Li, C. Zhou, S. An, Q. Jiao, H. Zhu, Synthesis, biological evaluation and molecular docking studies of amide-coupled benzoic nitrogen mustard derivatives as potential antitumor agents, Bioorg. Med. Chem. 18 (2010) 880–886.
[42] A. Molinos-Gómez, X. Vidal, M. Maymó, D. Velasco, J. Martorell, F. López-Calahorra, Tautomeric enhancement of the hyperpolarizability in new acridine-benzothiazolylamine based NLO chromophores, Tetrahedron 61 (2005) 9075–9081.
[43] K. Yamazaki, Y. Kaneko, K. Suwa, S. Ebara, K. Nakazawa, K. Yasuno, Synthesis of potent and selective inhibitors of Candida albicans N-myristoyltransferase based on the benzothiazole structure, Bioorg. Med. Chem. 13 (2005) 2509–2522.
[44] P. Basabe, A. Diego, S. Delgado, D. Díez, I.S. Marcos, J.G. Urones, Short and efficient synthesis of (+)-subersic acids, Tetrahedron 59 (2003) 9173–9177.
[45] M. Ebisawa, M. Ueno, Y. Oshimo, Y. Kondo, Synthesis of dictyomedins using phosphazene base catalyzed diaryl ether formation, Tetrahedron Lett. 48 (2007) 8918–8921.
[46] L. Campeau, M. Parisien, A. Jean, K. Fagnou, Catalytic direct arylation with aryl chlorides, bromides, and iodides: intramoleculas studiel leading tn new intermolecular reactions, J. Am. Chem. Soc. 128 (2006) 581–590.
[47] H.V. Namboodiri, M. Bukhtiyarova, J. Ramcharan, M. Karpusas, Y. Lee, E.B. Springman, Analysis of Imatinib and Sorafenib binding to p38a compared with c-Abl and b-Raf provides structural insights for understanding the selectivity of inhibitors targeting the DFG-Out form of protein kinases, Biochemistry 49 (2010) 3611–3618.
[48] J.R. Simard, M. Getlik, C. Grütter, V. Pawar, S. Wulfert, M. Rabiller, D. Rauh, Development of a fluorescent-tagged kinase assay system for the detection and characterization of allosteric kinase inhibitors, J. Am. Chem. Soc. 131 (2009) 13286–13296.
[49] D. Paquet, R. Bhat, A. Sydow, E. Mandelkow, S. Berg, S. Hellberg, J. Fälting, M. Distel, R.W. Köster, B. Schmid, C. Haass, A zebrafish model of tauopathy allows in vivo imaging of neuronal cell death and drug evaluation, J. Clin. Invest. 119 (2009) 1382–1395.
[50] G.E. Atilla-Gokcumen, D.S. Williams, H. Bregman, N. Pagano, E. Meggers, Organometallic compounds with biological activity: a very selective and highly potent cellular inhibitor for glycogen synthase kinase 3, ChemBioChem 7 (2006) 1443–1450.
[51] C.J. Phiel, C.A. Wilson, V.M.Y. Lee, P.S. Klein, GSK-3 alpha regulates production of Alzheimer's disease amyloid-beta peptides, Nature 423 (2003) 435–439.
[52] M. Cristina da Silva Lourenco, M. de Lima Ferreira, M. Vinícius Nora de Souza, M. Amado Peralta, T. Rocha Alves Vasconcelos, M.O. das Gracas, M. Henriques, Synthesis and anti-mycobacterial activity of (E)-N'-(monosubstituted-benzylidene)isonicotinohydrazide derivatives, Eur. J. Med. Chem. 43 (2008) 1344–1347.
[53] Z. Liberman, H. Eldar-Finkelman, Serine 332 phosphorylation of insulin receptor substrate-1 by glycogen synthase kinase-3 attenuates insulin signaling, J. Biol. Chem. 280 (2005) 4422–4428.
[54] C.B. Kimmel, W.W. Ballard, S.R. Kimmel, B. Ullmann, T.F. Schilling, Stages of embryonic development of the zebrafish, develop, Dynamics 203 (1995) 253–310.

Please cite this article in press as: F. Lo Monte, et al., Structure-based optimization of oxadiazole-based GSK-3 inhibitors, European Journal of Medicinal Chemistry (2012), http://dx.doi.org/10.1016/j.ejmech.2012.06.006

3.5 Verbindungen als Glykogen Synthase Kinase-3 (GSK-3) Inhibitoren für die Behandlung von GSK-3-vermittelten Erkrankungen

Die in den Kapiteln 5.3 und 5.4 aufgeführten Strukturen wurden (neben weiteren Produkten) vor ihrer Veröffentlichung bereits zum Patent angemeldet.

Deutsche Patentanmeldung Nr.: DE 10 2011 106 990.2

Patentanmelder: Technische Universität Darmstadt

Erfinder: Prof. Boris Schmidt, Dr. Fabio Lo Monte, Dipl.-Chem. Thomas Kramer, Prof. Hagit Edar-Finkelman, Prof. Fred Van Leuven

Titel: Verbindungen als Glykogen Synthase Kinase-3 (GSK-3) Inhibitoren für die Behandlung von GSK-3-vermittelten Erkrankungen

Allgemeine Formal (I):

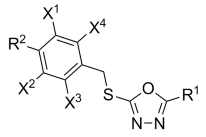

Allgemeine Formel (I)

Im Folgenden sind Auszüge dieses Patents angefügt.

Verbindungen als Glykogen Synthase Kinase 3 (GSK-3) Inhibitoren für die Behandlung von GSK-3-vermittelten Erkrankungen

Beschreibung

Die vorliegende Erfindung betrifft Verbindungen, die als selektive Liganden der Glykogen Synthase Kinase 3 (GSK-3) wirken und für die Behandlung von GSK-3-vermittelten Erkrankungen verwendet werden können. Die erfindungsgemäßen Verbindungen wirken als Inhibitoren der Glykogen Synthase Kinase 3 (GSK-3).

GSK-3 ist eine hoch konservierte Familie von Serin/Threoninproteinkinasen. Beim Menschen kodieren zwei Gene zwei unterschiedliche, aber eng miteinander verbundenen GSK-3 Formen, die so genannte GSK-3α und GSK-3β. Sie zeigen insgesamt 84% Identität und 98% Identität innerhalb ihrer katalytischen Domäne, der Hauptunterschied zwischen den beiden Proteinkinasen besteht in einem Glycin-reichen Abschnitt in der N-terminalen Domäne von GSK-3α. Dennoch hat sich in embryonal letalen Phänotypen der GSK-3β gezeigt, dass beide Formen der GSK-3 nicht funktionell austauschbar sind.

GSK-3 spielt eine wichtige Funktion im Wnt-Signalweg. Durch die Stimulation des Wnt-Signalweges wird GSK-3 inaktiviert, wodurch sich β-Catenin im Zellkern ansammelt, um dort mit TCF / LEF einen Transkriptionsfaktor zu formen, der eine Vielzahl von Genen reguliert. GSK-3 phosphoryliert unter anderem den Zellzyklusregulator β-Catenin, Cyclin D1, Cyclin E, p21CIP1 und c-Myc, wodurch diese Ubiquitin-abhängig abgebaut werden. In Abwesenheit von Insulin phosphoryliert aktive GSK-3 die Glykogen-Synthase und eIF2B, wodurch diese inaktiviert werden. Die Bindung von Insulin an seinen Plasmamembran Rezeptor führt zur Aktivierung von PKB / Akt, was wiederum zur Phosphorylierung und Inaktivierung von GSK-3 führt. Folglich sind dadurch die Glykogen-Synthase und eIF2B aktiviert, wodurch die Glykogen und Protein-Synthese stimuliert werden. GSK-3 hat weiterhin pro-apoptotische Funktion in neuronalen Zellen. Im Gegensatz dazu ist GSK-3 auch für das Überleben von Zellen beschrieben worden. In GSK-3β-Knockout-Mäusen führte die TNFα-induzierte Apoptose von Hepatozyten zu einem frühen Tod während der Embryonalentwicklung der Mäuse. Zudem wird der GSK-3 und CK1 eine Funktion bei der Regelung der zirkadianen Uhr bei Drosophila und in Säugetieren nachgesagt. Schließlich spielt sowohl die GSK-3 Aktivität/Inaktivität als

auch die räumliche Verteilung eine wesentliche Rolle während der Entwicklung, insbesondere im Rahmen der Polaritätsbestimmung.

Kaum ein anderes Enzym besitzt einen so großen Einfluss auf eine Vielzahl zellulärer Vorgänge wie GSK-3. Unter anderem wurde ein Einfluss von GSK-3 auf folgende physiologischen Funktionen beschrieben: den Wnt und Hedgehog Signalweg, in der Transkription, der Regulation des Zellteilungszyklus, der Antwort auf DNA-Schäden, der Regulation des Zelltods und dem Überleben der Zelle, kardiovaskuläre und neuronale Funktionen, dem Insulin-Transduktionsweg, der Differenzierung, Regulation des zirkadianen Rhythmus und der Entwicklung/Erhaltung von Stammzellen. Bis heute wurden rund 40 Substrate identifiziert, die von GSK-3 phosphoryliert werden.

Fünf Studien haben die Suche nach pharmakologischen Inhibitoren der GSK-3 besonders angeregt: Erstens, die Stimmungsstabilisierenden Eigenschaften von Lithium, dem ersten GSK-3-Inhibitor überhaupt. Zweitens die Insulin-mimetischen Eigenschaften von GSK-3-Inhibitoren. Drittens die Wechselwirkung von GSK-3 mit Presenilin-1, die GSK-3-abhängigen Amyloid-β Produktion und abnorme tau-Phosphorylierung in der Alzheimer-Krankheit. Viertens, die Beteiligung der GSK-3 im neuronalen Zelltod und der Neuroprotektion durch GSK-3-Inhibitoren und fünftens die Aufrechterhaltung der Pluripotenz von embryonalen Stammzellen in der Abwesenheit von Feeder-Zellen durch GSK-3-Inhibitoren. Über 30 GSK-3-Inhibitoren wurden bisher identifiziert. An der Identifizierung neuer GSK-3-Inhibitoren besteht daher nach wie vor ein fortlaufend großes Interesse.

Zu den Krankheiten, die mit GSK-3 Inhibitoren behandelt werden können, gehören insbesondere die Alzheimer-Krankheit und andere Tauopathien, Asthma, bipolare affektive Störungen, Depression, Nervenzelltod und Schlaganfall, Parkinson, Huntington, Skelettmuskelatrophie, Kardioprotektion, Haarverlust, verringerte Spermienmotilität, Diabetes und damit in Zusammenhang stehende Folgeerkrankungen, z.B. Syndrom X und Adipositas, Erkrankungen, die durch einzellige Parasiten verursacht werden, transmissible spongiforme Enzephalopathie, Schizophrenie, Krankheiten des zirkadianen Rhythmus und Krebs.

Im Stand der Technik sind bereits einige GSK-3 Inhibitoren und ihr therapeutisches Potential beschrieben worden. In einem Review von Cohen and Goedert, *Nat. Rev. Drug. Discov.*, 2004, 3: 480-87, wurden einige potentielle GSK-3 Inhibitoren, wie z.B. SB 216763, SB 415286, CHIR 98014, CHIR 99021, AR A014418, 1-Azakenpaullone

und Bis-7-indolylmaleimide für eine Vielzahl von therapeutischen Anwendungen beschrieben.

Im Stand der Technik sind (R)-Roscovitin, Aloisin A, Indirubin-3´-oxim, Pyrazolpyridin, Aminothiazol, Alsterpaullon und 1-Aza-9-oxafluoren als GSK-3 Inhibitoren identifiziert worden.

Obwohl bereits einige GSK-3 Inhibitoren im Stand der Technik bekannt sind, spielt die GSK-3 bei klassischen Krankheiten wie Alzheimer und Krebs eine so entscheidende Rolle, dass weiterhin und auch zukünftig ein großes Interesse daran besteht, weitere GSK-3 Inhibitoren zu identifizieren.

Aufgabe der vorliegenden Erfindung ist es daher, weitere Verbindungen bereitzustellen, die in der Lage sind, die GSK-3 zu inhibieren.

Diese Aufgabe wird erfindungsgemäß durch die technische Lehre der unabhängigen Ansprüche gelöst. Weitere vorteilhafte Ausgestaltungen der Erfindung ergeben sich aus den abhängigen Ansprüchen, der Beschreibung, den Figuren sowie den Beispielen.

Überraschend wurde gefunden, dass die Verbindungen gemäß allgemeiner Formel (I) Inhibitoren der Glykogen Synthase Kinase 3 (GSK-3) sind und damit auch für die Prophylaxe und Behandlung von GSK-3-vermittelten Erkrankungen geeignet sind.

Somit betrifft die vorliegende Erfindung Verbindungen der allgemeinen Formel (I)

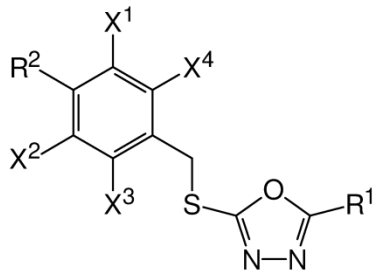

worin

R^1 für einen der folgenden Reste steht:

3.6 Zusätzlich bearbeitete Themen - neben dem Schwerpunkt der GSK-3-Inhibitoren

Im Zuge der vorliegenden Dissertation wurden weitere Themenkomplexe veröffentlicht: *Small Molecule Kinase Inhibitors for LRRK2 and Their Application to Parkinson´s Disease Models*, *Modification of a promiscuous inhibitor shifts the inhibition from g-secretase to FLT-3* und *2-Styrylindolium based fluorescent probes visualize neurofibrillary tangles in Alzheimer´s disease*.

3.6.1 *Small molecule* Kinase Inhibitoren für die *leucine-rich repeat kinase 2* (LRRK2) und ihre Anwendung in Modellen der Parkinson Krankheit

Der Inhalt dieses Kapitels wurde bereits veröffentlicht: Thomas Kramer*, Fabio Lo Monte*, Stefan Göring, Ghislaine Marlyse Okala Amombo, Boris Schmidt, „*Small Molecule Kinase Inhibitors for LRRK2 and Their Application to Parkinson´s Disease Models*", ACS Chem. Neurosci. **2012**, *3*, 151-160, doi: 10.1021/cn200117j.

Mit freundlicher Genehmigung von *American Chemical Society (ACS)*.

Die Parkinson Krankheit (Morbus Parkinson; *Parkinson´s disease*; PD) ist hinter der Alzheimer-Krankheit die zweithäufigste neurodegenerative Erkrankung. Diverse Genmutationen konnten bereits mit PD in Verbindung gebracht werden. Die häufigste Ursache für die sporadische und familiäre PD sind jedoch Mutationen des Gens PARK8. Im Menschen ist es zuständig für die Kodierung der *leucine-rich repeat kinase 2* (LRRK2), wodurch die LRRK2 zu einem potentiellen therapeutischen Zielenzym zur Behandlung von PD wurde.

LRRK2 ist ein großer Proteinkomplex bestehend aus mehreren Domänen zur Proteininteraktion und mehreren enzymatischen Domänen. In jeder konnten bereits diverse Punktmutationen detektiert werden. Die am häufigsten vorkommende Punktmutation in PD-Patienten ist die Gly2019Ser. Sie befindet sich in der Kinasedomäne von LRRK2 und ist für deren gesteigerte Aktivität verantwortlich. Zur

Hemmung der gesteigerten Kinaseaktivität wurden bereits einige ATP-kompetitive Kinaseinhibitoren veröffentlicht, Abb. 34. Diese wiesen teilweise eine inhibitorische Aktivität im nanomolaren Bereich auf und konnten Ihre Selektivität in breitaufgestellten Kinase-Paneln unter Beweis stellen. Einer der limitierenden Faktoren war deren mangelnde Hirngängigkeit.

Obwohl die ATP-kompetitive Inhibition der LRRK2 noch ein sehr junges Forschungsgebiet ist, kann auf Grund der anwachsenden, letztjährigen Patentanzahl (z. B. Glaxo Group Limited und Cellzome Limited) von einem gesteigerten Interesse seitens der akademischen und industriellen Forschung ausgegangen werden.

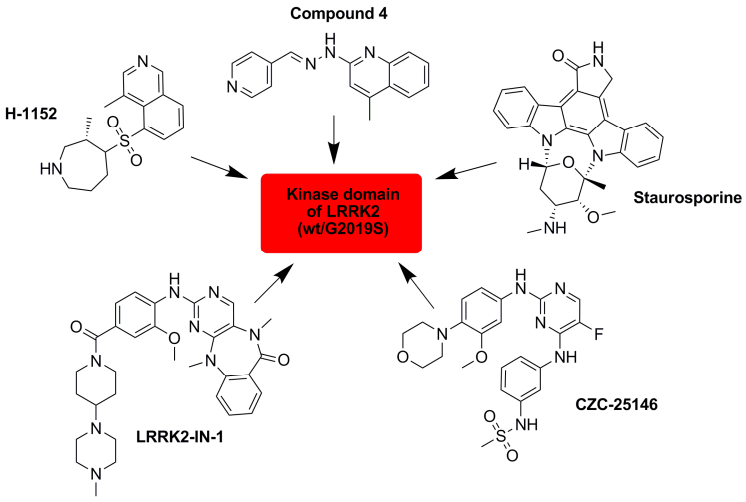

Abb. 34: Schematische Darstellung einer Auswahl publizierter, ATP-kompetitiver LRRK2-Inhibitoren.

ACS Chemical Neuroscience

Review

pubs.acs.org/acschemicalneuroscience

Small Molecule Kinase Inhibitors for LRRK2 and Their Application to Parkinson's Disease Models

Thomas Kramer,[†] Fabio Lo Monte,[†] Stefan Göring, Ghislaine Marlyse Okala Amombo, and Boris Schmidt*

Clemens Schöpf - Institute of Organic Chemistry and Biochemistry, Technische Universität Darmstadt, 64287 Darmstadt, Germany

ABSTRACT: Parkinson's disease (PD) is the second most common neurodegenerative disorder. Several single gene mutations have been linked to this disease. Mutations in the gene encoding leucine-rich repeat kinase 2 (LRRK2) indicate LRRK2 as promising therapeutic target for the treatment of PD. LRRK2 mutations were observed in sporadic as well as familial PD patients and have been investigated intensively. LRRK2 is a large and complex protein, with multiple enzymatic and protein-interaction domains, each of which is effected by mutations. The most common mutation in PD patients is G2019S. Several LRRK2 inhibitors have been reported already, although the crystal structure of LRRK2 has not yet been determined. This review provides a summary of known LRRK2 inhibitors and will discuss recent in vitro and in vivo results of these inhibitors.

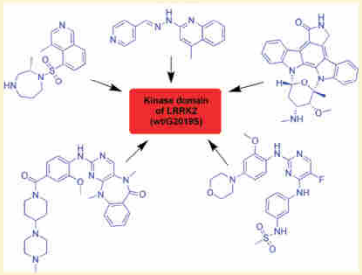

KEYWORDS: *Parkinson's disease, leucine-rich repeat kinase 2 (LRRK2), LRRK2 inhibitors, mutations, animal models*

Parkinson's disease (PD) is the second most prevalent neurodegenerative disorder after Alzheimer's disease, effecting up to ~4% of the population over 80.[1,2] PD is characterized by a large number of motoric and non-motoric symptoms. Four of them are designated as cardinal features: tremor at rest, rigidity, akinesia, and postural instability.[3] PD patients usually develop dementia during the course of the disease and gradually develop depression. The National Institute for Health and Clinical Excellence (NICE, U.K.) published guidelines for the diagnosis and management of patients with PD, which is used by most experts.[2,4] The typical hallmarks of PD in post-mortem brain tissue are loss of dopaminergic neurons of the substantia nigra, associated with the formation of fibrillar aggregates composed of α-synuclein and other proteins (e.g. Lewy bodies).[5,6] Presently, there is no cure for PD and the mainstay therapy is still the drug levodopa (L-Dopa).[2,7] L-Dopa is highly effective in reducing motor symptoms; nevertheless, there are two major problems, the side-effects and that patients become therapy resistant.[7,8] Adenosine A2a receptor antagonists have been shown to reduce PD-like features in animal studies through interaction with the specific dopamine receptor subtype D2 in the basal ganglia, making it more sensitive to dopamine. The adenosine A2a receptor antagonists SYN-115 from Synosia Therapeutics is currently in a phase IIb trial.[7] Other approaches are the metabotropic glutamate receptors (mGluRs), which are members of the G-protein-coupled receptor (GPCR) superfamily. They participate in the modulation of synaptic transmission and neuronal excitability throughout the central nervous system. Several studies indicate the therapeutic utility of mGluR ligands in neurological and psychiatric disorders and make mGluRs promising targets for non-dopaminergic drug discovery in PD. $mGluR_5$ is the target of drug development programmes at major pharmaceutical companies, e.g. Roche and Novartis.[7,9,10]

Several single gene mutations have been identified and linked to PD, for example, DJ-1, UCH-L1, SNCA, PRKN, and LRRK2.[1,2,5,11−14] However, mutations in the LRRK2 gene are the most common cause of familial and sporadic late-onset PD.[15] Since the LRRK2 gene mutations have been linked to PD, several inhibitors were reported to inhibit this kinase. We reviewed the literature and summarized the relevant data.

■ LRRK2: STRUCTURE AND MUTATIONS

The leucine-rich repeat kinase 2 (LRRK2) encodes a large multidomain protein with 2527 amino acids. Several independent domains have been established or predicted for the LRRK2 protein, including an ankyrin-like (ANK) domain, a leucine-rich repeat (LRR) domain, a Ras (renin-angiotensin system) of complex (Roc) domain, which belongs to the Ras GTPase family, followed by a C-terminal of ROC (COR) domain, a kinase (Kinase) domain, and a C-terminal WD40 domain (Figure 1).[16−18]

Beside the structural homology to the MAP kinase kinase kinases (MAPKKK) LRRK2 shares other biochemical features with MAPKKK, like autophosphorylation and interaction with kinase-specific chaperones.[19] LRRK2 is expressed in various brain regions and in several other organs, for example, in the lung, kidney, and heart.[20−22] LRRK2 efficiently phosphorylates

Received: November 25, 2011
Accepted: January 18, 2012

dx.doi.org/10.1021/cn200117j | *ACS Chem. Neurosci.* XXXX, XXX, XXX−XXX

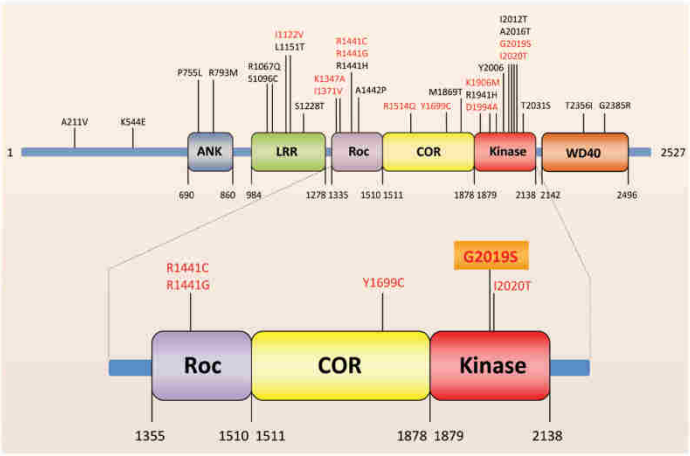

Figure 1. Schematic illustration of domains and most common PD-linked point mutations of LRRK2. Red marked mutations have been linked to altered kinase activity. ANK, ankyrin-like domain; LRR, leucin-rich repeat domain; Roc, Ras of complex domain, which belongs to the Ras GTPase family; COR, C-terminal of Roc domain; Kinase, kinase domain; WD40, C-terminal WD40 domain. The five putatively pathogenic mutations are enlarged.

moesin at Thr[558] in vitro, raising the idea that moesin may be a physiological substrate of LRRK2. Moreover, ezrin and radixin are phosphorylated by LRRK2, which are involved in moesin binding actin.[23,24] LRRK2 predominantly exists as a dimer under native conditions. The wild-type (wt) LRRK2 dimer displays increased kinase activity versus its monomeric counterpart.[25,26] More than 20 LRRK2 mutations have been linked to autosomal-dominant parkinsonism, and five of them are considered definitely pathogenic (R1441C, R1441G, Y1699C, G2019S, I2020T).[17,18,27] The most common mutation, which is present in more than 85% of PD patients carrying LRRK2 mutations, is G2019S.[28] In some ethnic groups the frequency of the LRRK2-G2019S mutation has been found to be even higher. For example, 13−40% of all PD patients in the Ashkenazi Jewish and northern African Arab population have this mutation, whereas in the Asian population this mutation is much less common.[17,28] The G2019S, R1441C, and R1441G mutations increase the LRRK2 kinase activity and both the kinase as well as the GTPase activities of LRRK2 are required to induce cell death.[6,29−32] The GTPase domain-associated R1441C mutation in combination with the G2019S kinase domain mutation increased the kinase activity up to 7-fold relative to wild-type protein.[33] It was reported that expression of G2019S mutant in Drosophila dendritic arborization neurons causes several dendrite defects, including tau mislocalization in dendrites, tau hyperphosphorylation at the T^{212}/S^{214} sites, dendrite degeneration, and microtubule fragmentation.[34] Furthermore, the LRRK2-G2019S mutant caused a progressive degeneration of nigral dopaminergic neurons in rats.[35] In addition, the autokinase activity of the LRRK2 mutant I2020T was found to be increased in comparison to wild-type.[19] Mutations within or near the GTPase domain including R1514Q, Y1699C, and I1371V increase kinase activity, while the alteration of the lysine residue K1347A leads to an ablation of this. The I1122V mutation in the LRR domain nominally increases kinase activity, whereas the D1994A and K1906M mutations in the kinase domain are able to diminish respectively to inhibit kinase activity.[31] Replacing the kinase domain with a "kinase-dead" version blocks inclusion body formation and delays cell death.[36] In addition, LRRK2 is able to phosphorylate MAPKKK 3, 4, 6, and 7 in vitro. This indicates that MAPKKK are molecular targets of LRRK2 mutants, whereby LRRK2 could be linked to neurotoxicity, cellular stress, and apoptosis.[37,38] LRRK2 provides a potential therapeutic target utilizing the knowledge gained in neuroprotective kinase inhibition.

■ IN VIVO MODELS AND STUDIES

Several studies using in vivo models of LRRK2 fostered the understanding of neurobiology, pathogenesis, and utility of potential therapeutics. The Drosophila model revealed that a LRRK2 loss-of-function mutant leads to significantly impaired locomotive activity and that LRRK2 is critical for the integrity of dopaminergic neurons (DA).[39] Another study showed that transgenic Drosophila harboring G2019S, Y1699C, or G2385 LRRK2 variants exhibit late-onset loss of DA and reduced lifespan.[40] Liu et al. used the GAL4/UAS system to generate transgenic Drosophila expressing either wild-type human LRRK2 or LRRK2-G2019S. They reported that expression of either wild-type human LRRK2 or LRRK2-G2019S in the photoreceptor cells caused retinal degeneration. Furthermore, they observed that expression of LRRK2 or LRRK2-G2019S in neurons produced adult-onset selective loss of dopaminergic neurons and locomotor dysfunction.[41,42] Overexpression of human LRRK2 wild-type, R1441C, and G2019S in DA of transgenic *C. elegans* models was sufficient to induce neurodegeneration and behavioral deficits, whereas knockout of the *C. elegans* LRRK2 homologue, LRK-1, prevents the LRRK2-induced neurodegeneration.[43] The blockage of zebrafish LRRK2 protein by morpholinos caused embryonic lethality and severe development defects such as growth retardation and loss of neurons. In addition, the deletion of the WD40 domain of zebrafish LRRK2 by morpholinos revealed Parkinsonism-like

Table 1. Staurosporine and Derivatives as LRRK2 Inhibitors

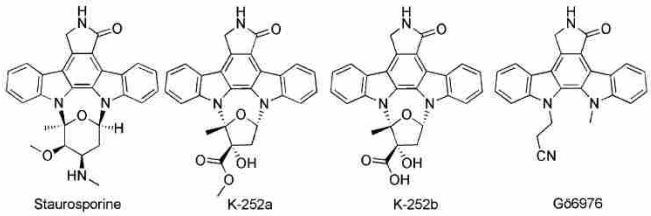

		IC_{50}					
no.	name	wild-type LRRK2	LRRK2-G2019S	substrate	selectivity[a]	in vivo	lit.
1	Staurosporine	~1 nM;[b] 2 nM;[b] 8.2 nM;[d] 40 nM[e]	0.2 nM;[f] 1.8 nM;[c] 40 nM[e]	GST-moesin; LRRKtide; MBP[g]	2		58, 60−62
2	K-252a	~25 nM;[b] 3.6 nM[c]	2.8 nM[c]	LRRKtide			60, 61
3	K-252b	~50 nM[b]		LRRKtide			61
4	Gö6976	~250 nM[b]		LRRKtide			61

[a]Number of all kinases, including LRRK2. [b]Goat GST-LRRK2. [c]GST-LRRK2 (970−2527; wt/G2019S). [d]full-length LRRK2. [e]GST-LRRK2 (wt/G2019S). [f]Full-length Strep-tag LRRK2 (G2019S). [g]Myelin basic protein (MBP).

phenotypes, including loss of dopaminergic neurons in the diencephalon and locomotion defects.[44] Remarkably, another research group failed to reproduce the phenotypic loss of dopaminergic neurons in zebrafish.[45] Nevertheless, the zebrafish model may be a useful vertebrate model. The presence of a LRRK2 protein excess in LRRK2 wild-type and G2019S mice showed exacerbated α-synuclein A53T-mediated cytotoxicity. This result raised the idea that inhibition of LRRK2 expression may provide an applicable strategy to ameliorate α-synuclein-induced neurodegeneration in PD.[46] Expression of full-length LRRK2 wild-type did not induce any significant neuronal loss in the nigrostriatal system of adult rats, whereas expression of human LRRK2-G2019S mutant causes progressive degeneration of nigral dopaminergic neurons.[35] Bacterial artificial chromosome (BAC) transgenic mice expressing LRRK2 wild-type, LRRK2-R1441G, and LRRK2-G2019S have shown evidence of neurodegeneration.[24,47,48] Furthermore, the LRRK2-R1441G BAC transgenic mice revealed tau to be hyperphosphorylated in brain tissues.[48] However, LRRK2 knockout mice lacking the kinase domain of LRRK2 are viable and live a normal life span. Thus, LRRK2 is not essential for mouse development and maintenance of DA.[49] However, expression of the human LRRK2-G2019S mutation in transgenic mice is sufficient to recreate the slowly progressive degeneration of dopaminergic neurons that forms the hallmark pathology of familial and sporadic PD.[50] Several mice studies investigated the potential of LRRK2 as therapeutic strategy for the treatment of PD.[51−57] Two independent lines of LRRK2 germ-line deletion mice indicated that LRRK2 plays an essential role in the regulation of protein homeostasis during aging. Therefore, the authors concluded that LRRK2 inhibition may not represent a suitable therapeutic strategy for the treatment of PD.[54] Another research group created inducible transgenic rats expressing LRRK2 with G2019S substitution and recapitulated the initiation process of dopaminergic dysfunction. However, the mutation was not sufficient to develop dopaminergic neurodegeneration or to induce neuron death in transgenic rats.[57] Data obtained from a R1441C knockin mouse suggested that this mutation impairs stimulated dopamine neurotransmission and D2 receptor function. The R1441C mutation could represent pathogenic precursors preceding dopaminergic degeneration in PD brains.[53] A novel herpes simplex virus (HSV) amplicon-based mouse model of LRRK2 dopaminergic neurotoxicity was developed to determine the efficacy of several LRRK2 kinase inhibitors. Nonetheless, a significant loss of tyrosine hydroxylase-positive neurons was induced due to HSV amplicon-mediated delivery of LRRK2-G2019S, whereas the HSV amplicon-mediated delivery of LRRK2-D1994A caused no neuronal loss. The injection of the LRRK2 kinase inhibitors can attenuate the loss of tyrosine hydroxylase-positive neurons induced by HSV-G2019S. Thus, the inhibition of LRRK2 kinase activity may hold potential to protect against LRRK2 toxicity and consequently for the treatment of neurodegeneration in PD.[58] Hence, LRRK2 kinase inhibition holds potential for the treatment of PD. In the following, we will give a summary of small molecule LRRK2 kinase inhibitors. The inhibition effect of $ROCO^{LRRK2}$ fragments will not be discussed.[59]

■ SMALL MOLECULE KINASE INHIBITORS FOR LRRK2

LRRK2 is a large protein with several discrete domains. It surfaced as a therapeutic target when the kinase activity and the most common LRRK2 mutation, G2019S, were associated with neurotoxicity and PD. The first LRRK2 inhibitors derived from library screening efforts were mostly ATP-competitive. There are only few inhibitors, which were specifically developed to inhibit LRRK2. Thus, the majority of the compounds inhibits more than one kinase at the concentration indicated in the tables. The data in Table 1 derived from a limited number of in vitro assays using wild-type LRRK2 and G2019S-LRRK2. These assays vary in the concentration of LRRK2-constructs, substrate, and ATP; thus, the mere comparison of IC_{50} is misleading. The high sensitive assays utilize radioisotopes, which allow detection of both autophosphorylation and substrate phosphorylation, but are less suitable for high-throughput screening (HTS). High-throughput capability was achieved by time-resolved fluorescence resonance energy transfer (TF-FRET) and the amplified luminescent proximity homogeneous (AlphaScreen) assays.[62] Although truncated LRRK2 and its full-length analog display similar phosphorylation activity, differences have been noticed. This may be a

dx.doi.org/10.1021/cn200117j | ACS Chem. Neurosci. XXXX, XXX, XXX−XXX

Table 2. Maleimide Derivatives as LRRK2 Inhibitors

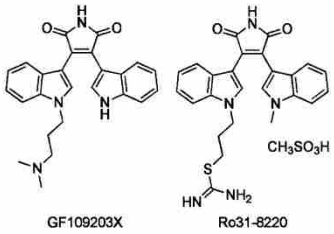

		IC50					
no.	name	wild-type LRRK2	LRRK2-G2019S	substrate	selectivity[a]	in vivo	lit.
5	GF109203X	2190 nM[b]	2620 nM[b]	MBP[c]	2		58
6	Ro31-8220	2671 nM;[d] 50 nM[b]	1922 nM;[d] 5160 nM[b]	LRRKtide; MBP[c]	2		58, 60

[a]Number of all kinases, including LRRK2. [b]GST-LRRK2 (wt/G2019S). [c]Myelin basic protein (MBP). [d]GST-LRRK2 (970-2527; wt/G2019S).

Table 3. 5-Iodotubericidin as LRRK2 Inhibitor

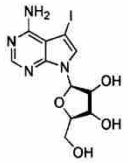

		IC50					
no.	name	wild-type LRRK2	LRRK2-G2019S	substrate	selectivity[a]	in vivo	lit.
7	5-iodo-tubericidin	14780 nM[b]	3410 nM[b]	MBP[c]	2		58

[a]Number of all kinases, including LRRK2. [b]GST-LRRK2 (wt/G2019S). [c]Myelin basic protein (MBP).

Table 4. Sorafenib as LRRK2 Inhibitor

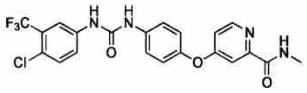

		IC50					
no.	name	wild-type LRRK2	LRRK2-G2019S	substrate	selectivity[a]	in vivo	lit.
8	sorafenib	5580 nM[b]	1230 nM[b]	MBP[c]	2	*C. elegans*; Drosophila	58

[a]Number of all kinases, including LRRK2. [b]GST-LRRK2 (wt/G2019S). [c]Myelin basic protein (MBP).

result from the utilization of different substrates, for example, LRRKtide and myelin basic protein (MBP).[60,63]

Staurosporine (**1**) is one of the widely used kinase inhibitors. This unselective compound equipotently inhibited both wild-type LRRK2 and LRRK2-G2019S (truncated and full-length) with an IC_{50} ranging from 0.2 to 40 nM (Table 1).[58,60−62] Its inhibitory effect concerning LRRK2 was determined in different in vitro assays, for example, radioactive, TF-FRET, and AlphaScreen assay. These assays utilized different substrates such as synthetic peptides, for example, LRRKtide and potential physiological substrates: GST-Moesin. Staurosporine (**1**) had a similar inhibitory profile against LRRK1/LRRK2 autophosphorylation and MBP phosphorylation.[58] Its isoindolinone derivatives K-252a/b (**2**/**3**) and Gö6976 (**4**) also inhibited wild-type LRRK2 and LRRK2-G2019S in the nanomolar range, whereas the maleimide analoga GF109203X (**5**) and Ro31-8220 (**6**) inhibited wild-type and LRRK2-G2019S in the low micromolar range only (Table 2).[58,60,61] Ro31-8220 (**6**) is remarkable for the potent inhibition of MBP phosphorylation with an IC_{50} of 50 nM in the TF-FRET assay.

The inhibitory potency of 5-Iodotubericidin (**7**) (Table 3) and Sorafenib (**8**) (Table 4) was more than 4-fold higher for LRRK2-G2019S compared to wild-type LRRK2.[58] Sorafenib (**8**) was up to 50% more selective for wild-type LRRK2 than for wild-type LRRK1. LRRK2-G2019S induced toxicity in rat primary cortical neuronal cultures (TUNEL assay) was completely protected by 5 μM of Sorafenib (**8**). Furthermore, it protected against LRRK2-G2019S-induced neurodegeneration in *C. elegans* and in Drosophila.[64]

The indolinones GW5074 (**9**) and Indirubin-3′-monoxime (**10**) were ∼3-fold more active concerning LRRK2-G2019S than its corresponding wild-type. GW5074 (**9**) and Indirubin-3′-monoxime (**10**) inhibited LRRK2-G2019S with IC_{50}'s of 880 nM and ∼1.3 μM, respectively.[58,61] They inhibited the closely related LRRK1 and LRRK2 in a similar manner. GW5074 (**9**) and Indirubin-3′-monoxime (**10**) inhibited LRRK2-mediated

dx.doi.org/10.1021/cn200117j | ACS Chem. Neurosci. XXXX, XXX, XXX−XXX

Table 5. Indolinone Dervivatives as LRRK2 Inhibitors

		IC_{50}					
no.	name	wild-type LRRK2	LRRK2-G2019S	substrate	selectivity[a]	in vivo	lit.
9	Raf-1 kinase inhibitor I (GW5074)	~500 nM;[b] 3150 nM[c]	880 nM[c]	LRRKtide; MBP[d]	2	HSV[g] amplicon-based mouse model	58, 61
10	Indirubin-3′-monooxime	4830 nM[c]	1310 nM[c]	MBP[d]	2	HSV[g] amplicon-based mouse model	58
11	Sunitinib	79 nM;[e] 15 nM[f]	19 nM;[e] 26 nM[f]	Nictide; LRRKtide	85		60, 63, 65

[a]Number of all kinases, including LRRK2. [b]Goat GST-LRRK2. [c]GST-LRRK2 (wt/G2019S). [d]Myelin basic protein (MBP). [e]GST-LRRK2 (1326−2527; wt/G2019S). [f]GST-LRRK2 (970−2527; wt/G2019S). [g]Herpes simplex virus.

Table 6. Quinoline Derivatives as LRRK2 Inhibitors

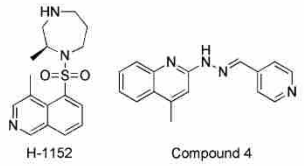

		IC_{50}					
no.	name	wild-type LRRK2	LRRK2-G2019S	substrate	selectivity[a]	in vivo	lit.
12	H-1152	244 nM[b]	600 nM;[c] 150 nM[b]	GST-Moesin; Nictide	85		62, 63, 65
13	Compound 4		4100 nM[d]		13		67

[a]Number of all kinases, including LRRK2. [b]GST-LRRK2 (1326-2527; wt/G2019S). [c]full-length Strep-tag LRRK2 (G2019S). [d]GST-LRRK2 (G2019S).

phosphorylation of LRRKtide and MBP, and additionally the phosphorylation of the eukaryotic translation initiation factor 4E-binding protein (4E-BPI), a putative physiological LRRK2 substrate. Furthermore, they attenuated LRRK2-G2019S induced cell injury and cell death. GW5074 (**9**) rescued the reduction of the density of tyrosine hydroxylase-positive fibers in a herpes simplex virus (HSV) amplicon-based mouse model of LRRK2 dopaminergic neurotoxicity. In addition, GW5074 (**9**) prevented LRRK2-G2019S induced inflammation, increase in isolectin B_4 (ILB4)-positive cells in the striatum and substantia nigra pairs compacta.[58] Both Sorafenib (**8**) and GW5074 (**9**) were found to protect against LRRK2-G2019S-induced neurodegeneration in *C. elegans* and in Drosophila.[64] The well-known kinase inhibitor Sunitinib (**11**) was also investigated concerning its ability to inhibit LRRK2 (Table 5). It inhibited the LRRK2-mediated phosphorylation of Nictide and LRRKtide with an IC_{50} of 15−79 nM (truncated wild-type and LRRK2-G2019S).[60,63,65] The selectivity of Sunitinib (**11**) was profiled in a panel of 85 kinases. Sunitinib (**11**) inhibits LRRK2-G2019S, its wild-type, and 12 further kinases at 1 μM by more than 80%.[60,63,65] However, the less selective Sunitinib (**11**) is capable to suppress the activity of full-length LRRK2 expressed from Swiss-3T3 fibroblast cells.[63] The apparent potency of Sunitinib (**11**) to inhibit wild-type LRRK2 drops to an IC_{50} of 370 nM at cellular ATP concentration (1 mM).[66] In addition, studies of endogenous LRRK2 activity and phosphorylation in EBV-transformed lymphoblastoid cells, derived from a PD patient harboring a homozygous LRRK2-G2019S mutation, revealed that Sunitinib (**11**) inhibited the phosphorylation of Ser^{910} and Ser^{935} more potently than in wild-type cells.[65] A comparable result was observed for the inhibitor H-1152 (**12**) (Table 6). H-1152 (**12**) is a known ROCK2 inhibitor. This compound was profiled in a panel of 85 kinases and found to inhibit Aurora B kinase, BRSK2, wild-type LRRK2, and LRRK2-G2019S at the relevant concentration. H-1152 (**12**) displayed IC_{50}'s ranging from 150 to 600 nM in radioisotope or AlphaScreen phosphorylation assays of wild-type LRRK2 and LRRK2-G2019S. Unfortunately, the structure determination of the LRRK2 kinase domain by X-ray crystallography was not reported yet. A docking analysis of H-1152 (**12**) utilized homology modeling of LRRK2, by superimposing the protein C_α atoms of the LRRK2 model with the reported ROCK1-H-1152 complex. This analysis indicated a backbone interaction with the NH atom of Ala^{1950} (PDB code of ROCK1-H-1152 not published). Furthermore, the two methyl groups of H-1152 (**12**) were observed to make lipophilic contacts with the ATP binding site. The amino acid Ala^{2016} was found to be close to H-1152 (**12**). This can

Table 7. Y-27632 as LRRK2 Inhibitor

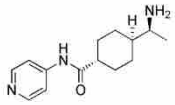

no.	name	IC_{50} wild-type LRRK2	IC_{50} LRRK2-G2019S	substrate	selectivity[a]	in vivo	lit.
14	Y-27632	2300 nM[b]	1800 nM;[c] 1000 nM[b]	GST-Moesin; Nictide	85		62, 63

[a]Number of all kinases, including LRRK2. [b]GST-LRRK2 (1326-2527; wt/G2019S). [c]Full-length Strep-tag LRRK2 (G2019S).

Table 8. Anthracene and Phenanthrene Derivatives as LRRK2 Inhibitors

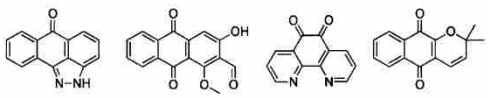

SP600125 Damnacanthal LDN-73794 LDN-22684

no.	name	IC_{50} wild-type LRRK2	IC_{50} LRRK2-G2019S	substrate	substrate selectivity[a]	in vivo	lit.
15	SP600125	3100 nM[b]	5000 nM[b]	MBP[c]	2		58
16	Damnacanthal	7810 nM[b]	9450 nM[b]	MBP[c]	2		58
17	LDN-73794	3500 nM[d]		PLK-peptide	2		68
18	LDN-22684[e]	6900 nM[f]	6100 nM[f]	PLK-peptide			69

[a]Number of all kinases, including LRRK2. [b]GST-LRRK2 (wt/G2019S). [c]Myelin basic protein (MBP). [d]Purified from BAC-transgenic mouse brain. [e]Non-ATP competitive. [f]Human LRRK2 (970-2527; wt/G2019S).

Table 9. Pyrimidine Derivatives as LRRK2 Inhibitors

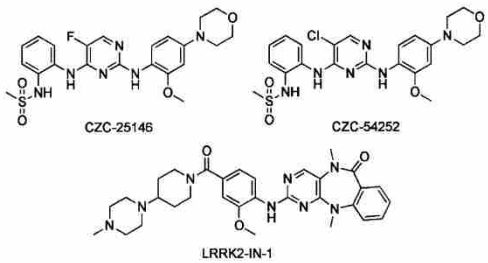

CZC-25146 CZC-54252 LRRK2-IN-1

no.	name	IC_{50} wild-type LRRK2	IC_{50} LRRK2-G2019S	substrate	selectivity[a]	in vivo	lit.
19	CZC-25146	4.76 nM[b]	6.87 nM[b]	LRRKtide	LRRKtide	male CD-1 mice	71
20	CZC-54252	1.28 nM[b]	1.85 nM[b]	LRRKtide	LRRKtide	male CD-1 mice	71
21	LRRK2-IN-1	13 nM[c]	6 nM[c]	Nictide	Nictide	Male C57BL/6 mice	70

[a]Number of all kinases, including LRRK2. [b]Human LRRK2 (wt/G2019S). [c]GST-LRRK2 (1326−2527; wt/G2019S).

contribute to crucial drug resistance, because the IC_{50} of H-1152 (**12**) for the LRRK2 mutant A2016T increased up to ~30-fold.[63] Another commercially available quinoline derivative, Compound 4 (**13**), inhibited the autophosphorylation of LRRK2-G2019S with an IC_{50} of 4.1 μM (Table 6). It was screened in a small kinase panel of 13 kinases at 10 μM concentration. There was no other inhibitory effect, except for MLK1.[67] This observation can be rationalized by the similarity of the kinase domains of MLK and LRRK2. Compound 4 (**13**) was analyzed in a homology model of LRRK2 using the structure of the transforming growth factor-beta (TGF-β) activated kinase 1 (TAK1; PDB code: 2EVA). This homology model of the LRRK2 kinase domain with inhibitor Compound 4 (**13**) indicated hydrogen bond interactions between Compound 4 (**13**) and Ala[1950]. It was found that the 4-pyridine ring was located in the solvent exposed region of LRRK2. Moreover, a comparison of ATP and Compound 4 (**13**) docking revealed that the 4-methyl quinoline moiety overlapped with the adenine rings of ATP. The treatment of murine dopaminergic SN4741 cells with 10 μM of Compound 4 (**13**) restored their cell survival rates in an oxidative stress-induced test to the level of the control cells. The neurotoxicity test with primary rat cortical neuronal cells revealed cell survival rates of 85% at 10 μM and a significantly increased toxicity at 100 μM.[67] In a kinase panel of 85 kinases the known ROCK inhibitor Y-27632 (**14**) was found to additionally inhibit PRK2,

Table 10. Pharmocokinetic Profile of the Currently Best Published LRRK2 inhibitors CZC-25146 and LRRK2-IN-1[a]

name	route	dose (mg/kg)	T_{max} (h)	C_{max} (ng/mL)	$AUC_{0-\infty}$ (h·ng/mL)	$T_{1/2}$ (h)	CL (mL/min/kg)	V_{ss} (L/kg)	F (%)	BBB penetration (%)	lit.
CZC-25146 (male CD-1 mice)	IV	1	0	154	419−434	1.6	2.3	5.4		4	71
	PO	5	0.25	1357	2878−2894	1			133		
LRRK2-IN-1 (male C57BL/6 mice)	IV	1			2974	4.47	5.6	1.71		not efficiently	70
	PO	10	1.0	1618	14758				49.3		

[a]IV = intravenous injection; PO = oral delivery; T_{max} = time of maximum plasma concentration; C_{max} = maximum plasma concentration; $AUC_{0-\infty}$ = area under the curve (measure of exposure); $T_{1/2}$ = half life; CL = plasma clearance; V_{ss} = volume of distribution; F = oral bioavailability; BBB = blood-brain barrier.

MNK1, wild-type LRRK2 and LRRK2-G2019S at 10 μM (Table 7). Y-27632 (**14**) inhibited truncated LRRK2-G2019S with an IC_{50} of 1 μM in a radioisotope assay. Furthermore, the full-length Strep-tag LRRK2-G2019S was inhibited with an IC_{50} of 1.8 μM in an AlphaScreen assay.[62,63] The anthracene and phenanthrene derivatives SP60012 (**15**), Damnacanthal (**16**), LDN-73794 (**17**), and LDN-22684 (**18**) inhibited LRRK2-G2019S and wild-type LRRK2 in the low micromolar range (Table 8).[58,68,69] LDN-73794 (**17**) was confirmed to be ATP competitive, whereas LDN-22684 (**18**) was found to be a non-ATP competitive inhibitor. Further studies revealed LDN-22684 (**18**) to be neither GTP competitive nor substrate competitive. Hence, it was deduced that LDN-22684 (**18**) is an allosteric LRRK2 inhibitor.[68,69] Three compounds were especially developed to inhibit LRRK2, namely, CZC-25146 (**19**), CZC-54252 (**20**), and LRRK2-IN-1 (**21**) (Table 9).[70,71] CZC-25146 (**19**) and CZC-54252 (**20**) inhibited the activity of recombinant human wild-type LRRK2 with an IC_{50} ranging from ∼1 to ∼5 nM. The G2019S mutant was inhibited with an IC_{50} ranging from ∼2 to ∼7 nM in a TF-FRET assay. In addition, they were screened against a kinase panel of 185 kinases and exhibited good selectivity. CZC-25146 (**19**) inhibited five other kinases, PLK4, GAK, TNK1, CAMKK2, and PIP4K2C, with high potency only, but none of them have been classified as predictors of genotoxicity or hematopoietic toxicity.[72,73] Furthermore, it prevents mutant LRRK2-induced injury of cultured rodent and human neurons with mid-nanomolar potency. In vivo pharmacology established a volume of distribution of 5.4 L/kg and a clearance of 2.3 L/h/kg for CZC-25146 (**19**). Unfortunately, it exhibited a poor brain penetration of just 4% (Table 10).[71]

A HTS and subsequent lead optimization provided the LRRK2 inhibitor LRRK2-IN-1 (**21**). It inhibited both truncated wild-type LRRK2 and LRRK2-G2019S with IC_{50} values of 13 and 6 nM, but LRRK2-A2016T and LRRK2-A2016T+G2019S mutants were found to be ∼400-fold more resistant to LRRK2-IN-1 (**21**) (Table 9).[70] This was explained by a molecular docking study of LRRK2-IN-1 (**21**) bound to a homology model of LRRK2 (A2016T), which revealed an unfavorable steric interaction as observed for H-1152 (**12**). The confirmed reversible ATP competitive inhibitor LRRK2-IN-1 (**21**) was selective in kinase panels containing more than 470 kinases. Surprisingly, under the same conditions as employed for LRRK2, LRRK2-IN-1 lacked inhibition of LRRK1. The kinase panels revealed additional inhibition of DCLK1, DCLK2, as well as MAPK7 and supported IC_{50}'s of greater than 1 μM for AURKB, CHEK2, MKNK2, MYLK (smMLCK), NUAK1, PLK1, and RPS6KA2. LRRK2-IN-1 (**21**) induced a similar dose-dependent Ser^{910} and Ser^{935} dephosphorylation and loss of 14−3−3 binding to endogenous LRRK2 in human-derived neuroblastoma SHSY5Y cells and mouse Swiss3T3 cells. Pharmacokinetic studies of LRRK2-IN-1 (**21**) revealed a half-life of 4.5 h and a bioavailability of 49.3% in mice (Table 10). An insufficient blood-brain barrier (BBB) permeation was concluded from the LRRK2 phosphorylation status in the kidney versus brain, which imposes limits on this "useful first-generation 'tool'".[70]

So far, just a small number of LRRK2 inhibitors have been synthesized and profiled in kinase panels. The best of the reported compounds display both high activity and selectivity. However, these reported best-in-class compounds do not pass the BBB efficiently, which limits their potential in animal models of PD. Maybe the patent literature holds additional treasures, waiting to be released.[74−79]

■ CONCLUSION AND PERSPECTIVES

The importance of the G2019S mutation in the kinase domain of LRRK2 derives from the association with the second most common neurodegenerative disease: Parkinson's disease. The late-onset sporadic classical PD affects almost 2% of the world population over 65 years of age.[80] The availability of suitable HTS assay formats such as TF-FRET or AlphaScreen provided first inhibitors of LRRK2 activity with moderate selectivity. Lead optimization resulted in first generation tools and second-generation inhibitors, which displayed promising pharmacokinetic properties, but are limited by insufficient brain uptake or brain activity. The increase in patent applications (e.g., Glaxo Group Limited and Cellzome Limited) indicates a target on the rise. TTT-3002, a drug candidate of TauTaTis, exhibited good results in LRRK2 inhibition. A phase I clinical trial of TTT-3002 is expected to start in 2011.[74−79,81]

The clinical development of LRRK2 inhibitors is impaired by the lack of public data of relevant pharmacology, biology, and even biomarkers. Moreover, the gain of function in LRRK2 mutations may require fundamentally different dosing regimes for mutation carriers versus other PD patients resulting in personalized medicine. This dosage may very up to 100-fold, implying genomic profiling, patient stratification and a wide therapeutic window. Several in vivo invertebrate models indicate neurotoxic hyperactivity of LRRK2 kinase, but the number of LRRK2 kinase activity studies in mouse models is rather limited. New LRRK2 animal models may provide essential information for target validation and suitable biomarkers for end point identification in drug development. Passage of the blood-brain barrier remains a challenge, yet LRRK2 function may be important outside the CNS. Moreover, the consequences of LRRK2 inhibition are not sufficiently established in animal models or humans to conclude a safe inhibition rate in mutation carriers or normal PD patients nor to rule out therapy resistance in gain of function mutations.

Furthermore, just a small number of substrates has been reported to date and this may increase. Hence, an effective and safe inhibition of LRRK2 kinase activity has yet to be confirmed in vivo, in vitro. Any novel therapy must be evaluated against established PD therapies, which results in either extended or large clinical trials. A robust and approved biomarker may enable shorter or smaller trials; however, this may take years to develop and to gain approval.[82−84] Recently, the LRRK-2 phosphorylation sites Ser^{910}, Ser^{935}, Ser^{955}, and Ser^{973} were suggested as biomarkers for LRRK2 because the treatment of LRRK2 expressing cells with LRRK2-IN-1 (**21**) revealed these phosphorylations to be disrupted. However, the kinases and phosphatases responsible for the regulation of these phosphorylation sites have yet to be identified.[85]

Type-I-kinase inhibitors are notorious for their selectivity problems, which frequently cause adverse events in humans. In addition, drug resistance or diminished activity has been observed, which may be caused by kinase domain mutations. LRRK2 features many mutations, which imposes problems to find a useful drug candidate.[63,70] A new generation of kinase inhibitors, called type-II-inhibitors, may reduce some of these problems.[86,87] They bind to the ATP site and extend into an adjacent allosteric site. This allosteric site is not as highly conserved as the ATP binding site and may provide a strategy to obtain improved selectivity. LRRK2 is a particularly challenging target: the G2019S gain of function mutation requires very efficient inhibition to reduce the activity to the wild-type level. The lack of brain permeable inhibitors leaves an open fundamental question: how much G2019S LRRK2 inhibition is required in vivo? In summary, it can be stated that LRRK2 inhibition provides potential to treat PD, albeit further research and clarification is inevitable.

■ AUTHOR INFORMATION

Corresponding Author

*Fax: +496151-163278. Telephone: +496151-164531. E-mail: schmidt_boris@t-online.de.

Author Contributions

†These authors contributed equally to this work.

Funding

This work was supported by the Technische Universität Darmstadt.

Notes

The authors declare no competing financial interest.

■ REFERENCES

(1) Ross, O. A., and Farrer, M. J. (2005) Pathophysiology, pleiotrophy and paradigm shifts: genetic lessons from Parkinson's disease. *Biochem. Soc. Trans. 33*, 586−590.

(2) Davie, C. A. (2008) A review of Parkinson's disease. *Br. Med. Bull. 86*, 109−127.

(3) Jankovic, J. (2008) Parkinson's disease: clinical features and diagnosis. *J. Neurol. Neurosurg. Psychiatry 79*, 368−376.

(4) Clarke, C. E. (2007) Parkinson's disease. *BMJ - Clin. Rev. 335*, 441−445.

(5) Zimprich, A., Biskup, S., Leitner, P., Lichtner, P., Farrer, M., Lincoln, S., Kachergus, J., Hulihan, M., Uitti, R. J., Calne, D. B., Stoessl, A. J., Pfeiffer, R. F., Patenge, N., Carbajal, I. C., Vieregge, P., Asmus, F., Müller-Myhsok, B., Dickson, D. W., Meitinger, T., Strom, T. M., Wszolek, Z. K., and Gasser, T. (2004) Mutations in LRRK2 cause autosomal-dominant parkinsonism with pleomorphic pathology. *Neuron 44*, 601−607.

(6) Berwick, D. C., and Harvey, K. (2011) LRRK2 signaling pathways: the key to unlocking neurodegeneration? *Trends Cell Biol. 21*, 257−265.

(7) Smith, K. (2010) Treatment frontiers. *Nature - Parkinson's Disease Outlook 466*, 15−18.

(8) Poewe, W. (2006) The natural history of Parkinson's disease. *J. Neurol. 253*, VII/2−VII/6.

(9) Duty, S. (2010) Therapeutic potential of targeting group III metabotropic glutamate receptors in the treatment of Parkinson's disease. *Br. J. Pharmacol. 161*, 271−287.

(10) Niswender, C. M., and Conn, P. J. (2010) Metabotropic glutamate receptors: physiology, pharmacology, and disease. *Annu. Rev. Pharmacol. Toxicol. 50*, 295−322.

(11) Paisán-Ruíz, C., Jain, S., Evans, E. W., Gilks, W. P., Simón, J., van der Brug, M., López de Munain, A., Aparicio, S., Martínez Gil, A., Khan, N., Johnson, J., Martinez, J. R., Nicholl, D., Carrera, I. M., Pena, A. S., de Silva, R., Lees, A., Martí-Massó, J. F., Pérez-Tur, J., Wood, N. W., and Singleton, A. B. (2004) Cloning of the gene containing mutations that cause PARK8-linked Parkinson's disease. *Neuron 44*, 595−600.

(12) Valente, E. M., Abou-Sleiman, P. M., Caputo, V., Muqit, M. M. K., Harvey, K., Gispert, S., Ali, Z., Del Turco, D., Bentivoglio, A. R., Healy, D. G., Albanese, A., Nussbaum, R., González-Maldonado, R., Deller, T., Salvi, S., Cortelli, P., Gilks, W. P., Latchman, D. S., Harvey, R. J., Dallapiccola, B., Auburger, G., and Wood, N. W. (2004) Hereditary early-onset Parkinson's disease caused by mutations in PINK1. *Science 304*, 1158−1160.

(13) Bonifati, V., Rizzu, P., van Baren, M. J., Schaap, O., Breedveld, G. J., Krieger, E., Dekker, M. C. J., Squitieri, F., Ibanez, P., Joosse, M., van Dongen, J. W., Vanacore, N., van Swieten, J. C., Brice, A., Meco, G., van Duijn, C. M., Oostra, B. A., and Heutink, P. (2003) Mutations in the DJ-1 gene associated with autosomal recessive early-onset parkinsonism. *Science 299*, 256−259.

(14) Kitada, T., Asakawa, S., Hattori, N., Matsumine, H., Yamamura, Y., Minoshima, S., Yokochi, M., Mizuno, Y., and Shimizu, N. (1998) Mutations in the parkin gene cause autosomal recessive juvenile parkinsonism. *Nature 392*, 605−608.

(15) Tan, E. K., and Schapire, A. H. (2011) LRRK2 as a therapeutic target in Parkinson's disease. *Eur. J. Neurol. 18*, 545−546.

(16) Deng, J., Lewis, P. A., Greggio, E., Sluch, E., Beilina, A., and Cookson, M. R. (2008) Structure of the ROC domain from the Parkinson's disease-associated leucine-rich repeat kinase 2 reveals a dimeric GTPase. *Proc. Natl. Acad. Sci. U.S.A. 105*, 1499−1504.

(17) Giasson, B. I., and Van Deerlin, V. M. (2008) Mutations in LRRK2 as a cause of Parkinson's disease. *Neurosignals 16*, 99−105.

(18) Mata, I. F., Wedemeyer, W. J., Farrer, M. J., Taylor, J. P., and Gallo, K. A. (2006) LRRK2 in Parkinson's disease: protein domains and functional insights. *Trends Neurosci. 29*, 286−293.

(19) Gloeckner, C. J., Kinkl, N., Schumacher, A., Braun, R. J., ÓNeill, E., Meitinger, T., Kolch, W., Prokisch, H., and Ueffing, M. (2006) The Parkinson disease causing LRRK2 mutation I2020T is associated with increased kinase activity. *Hum. Mol. Genet. 15*, 223−232.

(20) Li, X., Tan, Y., Poulose, S., Olanow, C. W., Huang, X., and Yue, Z. (2007) Leucine-rich repeat kinase 2 (LRRK2)/PARK8 possesses GTPase activity that is altered in familial Parkinson's disease R1441C/G mutants. *J. Neurochem. 103*, 238−247.

(21) Biskup, S., Moore, D. J., Celsi, F., Higashi, S., West, A. B., Andrabi, S. A., Kurkinen, K., Yu, S., Savitt, J. M., Waldvogel, H. J., Faull, R. L. M., Emson, P. C., Torp, R., Ottersen, O. P., Dawson, T. M., and Dawson, V. L. (2006) Localization of LRRK2 to membranous and vesicular structures in mammalian brain. *Ann. Neurol. 60*, 557−569.

(22) Giasson, B. I., Covy, J. P., Bonini, N. M., Hurtig, H. I., Farrer, M. J., Trojanowski, J. Q., and Van Deerlin, V. M. (2006) Biochemical and pathological characterization of Lrrk2. *Ann. Neurol. 59*, 315−322.

(23) Jaleel, M., Nichols, R. J., Deak, M., Campbell, D. G., Gillardon, F., Knebel, A., and Alessi, D. R. (2007) LRRK2 phosphorylates moesin at threonine-558: characterization of how Parkinson's disease mutants affect kinase activity. *Biochem. J. 405*, 307−317.

(24) Li, T., Yang, D., Sushchky, S., Liu, Z., and Smith, W. (2011) Models for LRRK2-Linked Parkinsonism. *Parkinson's Dis. 2011*, 1−16.
(25) Berger, Z., Smith, K. A., and La Voie, M. J. (2010) Membrane localization of LRRK2 is associated with increased formation of the highly active LRRK2 dimer and changes in its phosphorylation. *Biochemistry 49*, 5511−5523.
(26) Greggio, E., Zambrano, I., Kaganovich, A., Beilina, A., Taymans, J., Daniels, V., Lewis, P., Jain, S., Ding, J., Syed, A., Thomas, K. J., Baekelandt, V., and Cookson, M. R. (2008) The Parkinson disease-associated leucine-rich repeat kinase 2 (LRRK2) is a dimer that undergoes intramolecular autophosphorylation. *J. Biol. Chem. 283*, 16906−16914.
(27) Taylor, J. P., Mata, I. F., and Farrer, M., J. (2006) LRRK2: a common pathway for parkinsonism, pathogenesis and prevention? *Trends Mol. Med. 12*, 76−82.
(28) Seol, W. (2010) Biochemical and molecular features of LRRK2 and its pathophysiological roles in Parkinson's disease. *BMB Rep. 43*, 233−244.
(29) Cookson, M. R. (2010) The role of leucine-rich repeat kinase 2 (LRRK2) in Parkinson's disease. *Nat. Rev. Neurosci. 11*, 791−797.
(30) West, A. B., Moore, D. J., Biskup, S., Bugayenko, A., Smith, W. W., Ross, C. A., Dawson, V. L., and Dawson, T. M. (2005) Parkinson's disease-associated mutations in leucine-rich repeat kinase 2 augment kinase activity. *Proc. Natl. Acad. Sci. U.S.A. 102*, 16842−16847.
(31) West, A. B., Moore, D. J., Choi, C., Andrabi, S. A., Li, X., Dikeman, D., Biskup, S., Zhang, Z., Lim, K., Dawson, V. L., and Dawson, T. M. (2007) Parkinson's disease-associated mutations in LRRK2 link enhanced GTP-binding and kinase activities to neuronal toxicity. *Hum. Mol. Genet. 16*, 223−232.
(32) Xiong, Y., Coombes, C. E., Kilaru, A., Li, X., Gitler, A. D., Bowers, W. J., Dawson, V. L., Dawson, T. M., and Moore, D. J. (2010) GTPase activity plays a key role in the pathobiology of LRRK2. *PLoS Genet. 6*, e1000902.
(33) Webber, P. J., Smith, A. D., Sen, S., Renfrow, M. B., Mobley, J. A., and West, A. B. (2011) Autophosphorylation in the Leucine-Rich Repeat Kinase 2 (LRRK2) GTPase Domain Modifies Kinase and GTP-Binding Activities. *J. Mol. Biol. 412*, 94−100.
(34) Lin, C., Tsai, P., Wu, R., and Chien, C. (2010) LRRK2 G2019S mutation induces dendrite degeneration through mislocalization and phosphorylation of tau by recruiting autoactivated GSK3ß. *J. Neurosci. 30*, 13138−13149.
(35) Dusonchet, J., Kochubey, O., Stafa, K., Yound, S. M. Jr, Zufferey, R., Moore, D. J., Schneider, B. L., and Aebischer, P. (2011) A rat model of progressive nigral neurodegeneration induced by the Parkinson's disease-associated G2019S mutation in LRRK2. *J. Neurosci. 31*, 907−912.
(36) Greggio, E., Jain, S., Kingsbury, A., Bandopadhyay, R., Lewis, P., Kaganovich, A., van der Brug, M. P., Beilina, A., Blackinton, J., Thomas, K. J., Ahmad, R., Miller, D. W., Kesavapany, S., Singleton, A., Lees, A., Harvey, R. J., Harvey, K., and Cookson, M. R. (2006) Kinase activity is required for the toxic effects of mutant LRRK2/dardarin. *Neurobiol. Dis. 23*, 329−341.
(37) Hsu, C. H., Chan, D., Greggio, E., Saha, S., Guillily, M. D., Ferree, A., Raghavan, K., Shen, G. C., Segal, L., Ryu, H., Cookson, M. R., and Wolozin, B. (2010) MKK6 binds and regulates expression of Parkinson's disease-related protein LRRK2. *J. Neurochem. 112*, 1593−1604.
(38) Gloeckner, C. J., Schumacher, A., Boldt, K., and Uefffing, M. (2009) The Parkinson disease-associated protein kinase LRRK2 exhibits MAPKKK activity and phosphorylates MKK3/6 and MKK4/7, in vitro. *J. Neurochem. 109*, 959−968.
(39) Lee, S. B., Kim, W., Lee, S., and Chung, J. (2007) Loss of LRRK2/PARK8 induces degeneration of dopaminergic neurons in Drosophila. *Biochem. Biophys. Res. Commun. 358*, 534−539.
(40) Ng, C., Mok, S. Z. S., Koh, C., Ouyang, X., Fivaz, M. L., Tan, E., Dawson, V. L., Dawson, T. M., Yu, F., and Lim, K. (2009) Parkin protects against LRRK2 G2019S mutant-induced dopaminergic neurodegeneration in Drosophila. *J. Neurosci. 29*, 11257−11262.
(41) Liu, Z., Wang, X., Yu, Y., Li, X., Wang, T., Jiang, H., Ren, Q., Jiao, Y., Sawa, A., Moran, T., Ross, C. A., Montell, C., and Smith, W. W. (2008) A Drosophila model for LRRK2-linked parkinsonism. *Proc. Natl. Acad. Sci. U.S.A. 105*, 2693−2698.
(42) Smith, W. W. (2010) Leucine-rich kinase 2 (LRRK2) Drosophila Model For Parkinsońs Disease: Wildtype1 (WT1) and G2019S Mutant Flies. U.S. 2010/0175140 A1.
(43) Yao, C., El Khoury, R., Wang, W., Byrd, T. A., Pehek, E. A., Thacker, C., Zhu, X., Smith, M. A., Wilson-Delfosse, A. L., and Chen, S. G. (2010) LRRK2-mediated neurodegeneration and dysfunction of dopaminergic neurons in a Caenorhabditis elegans model of Parkinson's disease. *Neurobiol. Dis. 40*, 73−81.
(44) Sheng, D., Qu, D., Kwok, K. H. H., Ng, S. S., Lim, A. Y. M., Aw, S. S., Lee, C. W. H., Sung, W. K., Lufkin, T., Jesuthasan, S., Sinnakaruppan, M., and Liu, J. (2010) Deletion of the WD40 domain of LRRK2 in Zebrafish causes Parkinsonism-like loss of neurons and locomotive defect. *PLoS Genet. 6*, e1000914.
(45) Ren, G., Xin, S., Zhong, H., and Lin, S (2011) Disruption of LRRK2 does not cause specific loss of dopaminergic neurons in zebrafish. *PLoS Genet. 6*, e20630.
(46) Lin, X., Parisiadou, L., Gu, X., Wang, L., Shim, H., Sun, L., Xie, C., Long, C., Yang, W., Ding, J., Chen, Z. Z., Gallant, P. E., Tao-Cheng, J., Rudow, G., Troncoso, J. C., Liu, Z., Li, Z., and Cai, H. (2009) Leucine-rich repeat kinase 2 regulates the progression of neuropathology induced by Parkinson's-disease-related mutant alpha-synuclein. *Neuron 64*, 807−827.
(47) Li, X., Patel, J. C., Wang, J., Avshalumov, M. V., Nicholson, C., Buxbaum, J. D., Elder, G. A., Rice, M. E., and Yue, Z. (2010) Enhanced striatal dopamine transmission and motor performance with LRRK2 overexpression in mice is eliminated by familial Parkinson's disease mutation G2019S. *J. Neurosci. 30*, 1788−1797.
(48) Li, Y., Liu, W., Oo, T. F., Wang, L., Tang, Y., Jackson-Lewis, V., Zhou, C., Geghman, K., Bogdanov, M., Przedborski, S., Beal, M. F., Burke, R. E., and Li, C. (2009) Mutant LRRK2(R1441G) BAC transgenic mice recapitulate cardinal features of Parkinson's disease. *Nat. Neurosci. 12*, 826−828.
(49) Andreas-Mateos, E., Mejias, R., Sasaki, M., Li, X., Lin, B. M., Biskup, S., Zhang, L., Banerjee, R., Thomas, B., Yang, L., Liu, G., Beal, M. F., Huso, D. L., Dawson, T. M., and Dawson, V. L. (2009) Unexpected lack of hypersensitivity in LRRK2 knock-out mice to MPTP (1-methyl-4-phenyl-1,2,3,6-tetrahydropyridine). *J. Neurosci. 29*, 15846−15850.
(50) Ramonet, D., Daher, J. P. L, Lin, B. M., Stafa, K., Kim, J., Banerjee, R., Westerlund, M., Pletnikova, O., Glauser, L., Yang, L., Liu, Y., Swing, D. A., Beal, M. F., Troncoso, J. C., McCaffery, J. M., Jenkins, N. A., Copeland, N. G., Galter, D., Thomas, B., Lee, M. K., Dawson, T. M., Dawson, V. L., and Moore, D. J. (2011) Dopaminergic neuronal loss, reduced neurite complexity and autophagic abnormalities in transgenic mice expressing G2019S mutant LRRK2. *PloS ONE 6*, e18568.
(51) Melrose, H. L., Dächsel, J. C., Behrouz, B., Lincoln, S. J., Yue, M., Hinkle, K. M., Kent, C. B., Korvatska, E., Taylor, J. P., Witten, L., Liang, Y. Q., Beevers, J. E., Boules, M., Dugger, B. N., Serna, V. A., Gaukhman, A., Yu, X., Castanedes-Casey, M., Braithwaite, A. T., Ogholikhan, S., Yu, N., Bass, D., Tyndall, G., Schellenberg, G. D., Dickson, D. W., Janus, C., and Farrer, M. J. (2010) Impaired dopaminergic neurotransmission and microtubule-associated protein tau alterations in human LRRK2 transgenic mice. *Neurobiol. Dis. 40*, 503−517.
(52) Melrose, H. L., Kent, C. B., Taylor, J. P., Dachsel, J. C., Hinkle, K. M., Lincoln, S. J., Mok, S. S., Culvenor, J. G., Masters, C. L., Tyndall, G. M., Bass, D. I., Ahmed, Z., Andorfer, C. A., Ross, O. A., Wszolek, Z. K., Delldonne, A., Dickson, D. W., and Farrer, M. J. (2007) A comparative analysis of leucine-rich repeat kinase 2 (Lrrk2) expression in mouse brain and Lewy body disease. *Neuroscience 147*, 1047−1058.
(53) Tong, Y., Pisani, A., Martella, G., Karouani, M., Yamaguchi, H., Pothos, E. N., and Shen, J. (2009) R1441C mutation in LRRK2

impairs dopaminergic neurotransmission in mice. *Proc. Natl. Acad. Sci. U.S.A. 106*, 14622−14627.
(54) Tong, Y., Yamaguchi, H., Giaime, E., Boyle, S., Kopan, R., Kelleher, R. J. III, and Shen, J. (2010) Loss of leucine-rich repeat kinase 2 causes impairment of protein degradation pathways, accumulation of alpha-synuclein, and apoptotic cell death in aged mice. *Proc. Natl. Acad. Sci. U.S.A. 107*, 9879−9884.
(55) Wang, L., Xie, C., Greggio, E., Parisiadou, L., Shim, H., Sun, L., Chandran, J., Lin, X., Lai, C., Yang, W., Moore, D. J., Dawson, T. M., Dawson, V. L., Chiosis, G., Cookson, M. R., and Cai, H. (2008) The chaperone activity of heat shock protein 90 is critical for maintaining the stability of leucine-rich repeat kinase 2. *J. Neurosci. 28*, 3384−3391.
(56) Winner, B., Melrose, H. L., Zhao, C., Hinkle, K. M., Yue, M., Kent, C., Braithwaite, A. T., Ogholikhan, S., Aigner, R., Winkler, J., Farrer, M. J., and Gage, F. H. (2011) Adult neurogenesis and neurite outgrowth are impaired in LRRK2 G2019S mice. *Neurobiol. Dis. 41*, 706−716.
(57) Zhou, H., Huang, C., Tong, J., Hong, W. C., Liu, Y., and Xia, X. (2011) Temporal expression of mutant LRRK2 in adult rats impairs dopamine reuptake. *Int. J. Biol. Sci. 7*, 753−761.
(58) Lee, B. D., Shin, J., VanKampen, J., Petrucelli, L., West, A. B., Ko, H. S., Lee, Y., Maguire-Zeiss, K. A., Bowers, W. J., Federoff, H. J., Dawson, V. L., and Dawson, T. M. (2010) Inhibitors of leucine-rich repeat kinase-2 protect against models of Parkinson's disease. *Nat. Med. 16*, 998−1000.
(59) Klein, C. L., Rovelli, G., Springer, W., Schall, C., Gasser, T., and Kahle, P. J. (2009) Homo- and heterodimerization of ROCO kinases: LRRK2 kinase inhibition by the LRRK2 ROCO fragment. *J. Neurochem. 111*, 703−715.
(60) Anand, V. S., Reichling, L. J., Lipinski, K., Stochaj, W., Duan, W., Kelleher, K., Pungaliya, P., Brown, E. L., Reinhart, P. H., Somber, R., Hirst, W., Riddle, S. M., and Braithwaite, S. P. (2009) Investigation of leucine-rich repeat kinase 2: enzymological properties and novel assays. *FEBS J. 276*, 466−478.
(61) Covy, J. P., and Giasson, B. I. (2009) Identification of compounds that inhibit the kinase activity of leucine-rich repeat kinase 2. *Biochem. Biophys. Res. Commun. 378*, 473−477.
(62) Pedro, L., Padrós, J., Beaudet, L., Schubert, H.-D., Gillardon, F., and Dahan, S. (2010) Development of a high-throughput AlphaScreen assay measuring full-length LRRK2(G2019S) kinase activity using moesin protein substrate. *Anal. Biochem. 404*, 45−51.
(63) Nichols, R. J., Dzamko, N., Hutti, J. E., Cantley, L. C., Deak, M., Moran, J., Bamborough, P., Reith, A. D., and Alessi, D. R. (2009) Substrate specificity and inhibitors of LRRK2, a protein kinase mutated in Parkinson's disease. *Biochem. J. 424*, 47−60.
(64) Liu, Z., Hamamichi, S., Lee, B. D., Yang, D., Ray, A., Caldwell, G. A., Caldwell, K. A., Dawson, T. M., Smith, W. W., and Dawson, V. L. (2011) Inhibitors of LRRK2 kinase attenuate neurodegeneration and Parkinson-like phenotypes in Caenorhabditis elegans and Drosophila Parkinson's disease models. *Hum. Mol. Genet. 20*, 3933−3942.
(65) Dzamko, N., Deak, M., Hentati, F., Reith, A. D., Prescott, A. R., Alessi, D. R., and Nichols, R. J. (2010) Inhibition of LRRK2 kinase activity leads to dephosphorylation of Ser(910)/Ser(935), disruption of 14−3-3 binding and altered cytoplasmic localization. *Biochem. J. 430*, 405−413.
(66) Reichling, L. J., and Riddle, S. M. (2009) Leucine-rich repeat kinase 2 mutants I2020T and G2019S exhibit altered kinase inhibitor sensitivity. *Biochem. Biophys. Res. Commun. 384*, 255−258.
(67) Yun, H., Heo, H. Y., Kim, H. H., DooKim, N., and Seol, W. (2011) Identification of chemicals to inhibit the kinase activity of leucine-rich repeat kinase 2 (LRRK2), a Parkinson's disease-associated protein. *Bioorg. Med. Chem. Lett. 21*, 2953−2957.
(68) Liu, M., Dobson, B., Glicksman, M. A., Yue, Z., and Stein, R. L. (2010) Kinetic mechanistic studies of wild-type leucine-rich repeat kinase 2: characterization of the kinase and GTPase activities. *Biochemistry 49*, 2008−2017.
(69) Liu, M., Poulose, S., Schuman, E., Zaitsev, A. D., Dobson, B., Auerbach, K., Seyb, K., Cuny, G. D., Glicksman, M. A., Stein, R. L., and Yue, Z. (2010) Development of a mechanism-based high-throughput screen assay for leucine-rich repeat kinase 2--discovery of LRRK2 inhibitors. *Anal. Biochem. 404*, 186−192.
(70) Deng, X., Dzamko, N., Prescott, A., Davies, P., Liu, Q., Yang, Q., Lee, J.-D., Patricelli, M. P., Nomanbhoy, T. N., Alessi, D. R., and Gray, N. S. (2011) Characterization of a selective inhibitor of the Parkinson's disease kinase LRRK2. *Nat. Chem. Biol. 7*, 203−205.
(71) Ramsden, N., Perrin, J., Ren, Z., Lee, B. D., Zinn, N., Dawson, V. L., Tam, D., Bova, M., Lang, M., Drewes, G., Bantscheff, M., Bard, F., Dawson, T. M., and Hopf, C. (2011) Chemoproteomics-Based Design of Potent LRRK2-Selective Lead Compounds That Attenuate Parkinson's Disease-Related Toxicity in Human Neurons. *ACS Chem. Biol. 6*, 1021−1028.
(72) Olaharski, A. J., Bitter, H., Gonzaludo, N., Kondru, R., Goldstein, D. M., Zabka, T. S., Lin, H., Singer, T., and Kolaja, K. (2010) Modeling bone marrow toxicity using kinase structural motifs and the inhibition profiles of small molecular kinase inhibitors. *Toxicol. Sci. 118*, 266−275.
(73) Olaharski, A. J., Gonzaludo, N., Bitter, H., Goldstein, D., Kirchner, S., Uppal, H., and Kolaja, K. (2009) Identification of a kinase profile that predicts chromosome damage induced by small molecule kinase inhibitors. *PLoS Comput. Biol. 5*, e1000446.
(74) Chan, B., Estrada, A., Sweeney, Z., and Mciver, E. G. (2011) Pyrazolopyridines as inhibitors of the kinase LRRK2. WO 2011/141756 A1.
(75) Kim, J. W., Lee, J., Song, H.-J., Kim, Y., Lee, H. K., Choi, J.-S., Lim, S.-H., and Chang, S. (2011) Kinase Inhibitors. WO 2011/053861 A1.
(76) Lee, J., Song, H.-J., Koh, J. S., Lee, L. K., Kim, Y., Chang, S., Kim, H. W., Chang, S., Lim, S.-H., Choi, J.-S., Kim, J.-H., and Kim, S.-W. (2011) Kinase Inhibitors. WO 2011/060295 A1.
(77) Mciver, E. G., Smiljanic, E., Harding, D. J., and Hough, J. (2010) Compounds (I). WO 2010/106333 A1.
(78) Nichols, P. L., Eatherton, A. J., Bamborough, P., Jandu, K. S., Philips, O. J., and Andreotti, D. (2011) WO 2011/038872 A1.
(79) Ramsden, N. (2009) Use Of LRRK2 Inhibitors For Neuro-degenerative Disease. WO 2009/127642 A2.
(80) Correia Guedes, L., Ferreira, J. J., Rosa, M. M., Coelho, M., Bonifati, V., and Sampaio, C. (2010) Worldwide frequency of G2019S LRRK2 mutation in Parkinson's disease: A systematic review. *J. Prak. Rel. Dis. 16*, 237−242.
(81) http://www.tautatis.com/home.html (2011).
(82) Yue, Z. (2012) Genetic mouse models for understanding LRRK2 biology, pathology and pre-clinical application. *Parkinsonism Relat. Disord. 18* (Suppl 1), S180−182.
(83) Yue, Z., and Lachenmayer, M. L. (2011) Genetic LRRK2Models of Parkinson's Disease: Dissecting the Pathogenic Pathway and Exploring Clinical Applications. *Movement Disord. 26*, 1386−1397.
(84) http://www.pdonlineresearch.org/ (2012).
(85) Doggett, E. A., Zhao, J., Mork, C. N., Hu, D., and Nichols, R. J. (2012) Phosphorylation of LRRK2 serines 955 and 973 is disrupted by Parkinsońs disease mutations and LRRK2 pharmacological inhibition. *J. Neurochem. 120*, 37−45.
(86) Davis, M. I., Hunt, J. P., Herrgard, S., Ciceri, P., Wodicka, L. M., Pallares, G., Hocker, M., Treiber, D. K., and Zarrinkar, P. P. (2011) Comprehensive analysis of kinase inhibitor selectivity. *Nat. Biotechnol. 29*, 1046−1051.
(87) Rauh, D. (2010) Inaktive Kinasekonformationen stabilisieren. *Nachr. Chem. 58*, 118−121.

3.6.2 Modifikation einer Inhibitorleitstruktur weg von der γ-Sekretase und hin zur *FMS-like tyrosine Kinase-3* (FLT-3) Inhibition

Der Inhalt dieses Kapitels wurde bereits bei Bioorg. Med. Chem. Lett. veröffentlicht (**2012**): Ghislaine Marlyse Okala Amombo*, Thomas Kramer*, Fabio Lo Monte*, Stefan Göring, Matthias Fach, Steven Smith, Stephanie Kolb, Robert Schubenel, Karlheinz Baumann, Boris Schmidt, „*Modification of a promiscuous inhibitor shifts the inhibition from γ-secretase to FLT-3*", http://dx.doi.org/10.1016/j.bmcl.2012.10.016.

Mit freundlicher Genehmigung von *Elsevier*.

Die akute myeloische Leukämie (AML) ist eine aggressive hämatologische Erkrankung mit einer langfristigen Überlebensrate von 25 bis 70 % bei Patienten unter 60 Jahren. Bei Patienten älter als 60 Jahren sind es sogar nur 5 %. Häufig auftretende molekulare Abnormalitäten sind die aktivierend wirkenden Mutationen in der *FMS-like tyrosine Kinase-3* (FLT-3). Dabei sind neben den *internal tandem duplications* (ITDs) die Punktmutationen in der Protein-Tyrosin-Kinase-Domäne 2 zu nennen. Es wurden bereits diverse ATP-kompetitive FLT-3-Inhibitoren synthetisiert. Manche befinden sich derzeit in einer präklinischen oder klinischen Phase, Abb. 35.

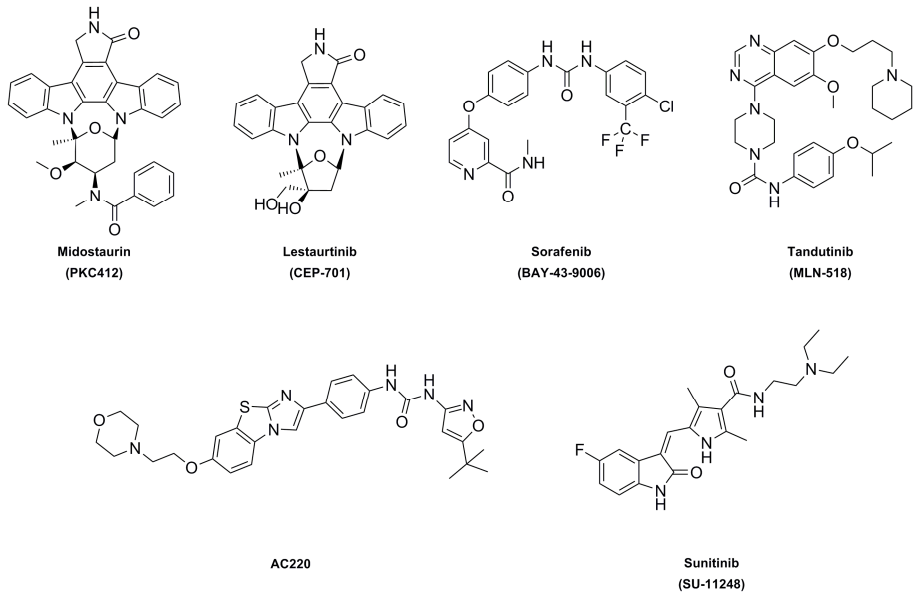

Abb. 35: Graphische Darstellung einer Auswahl von FLT-3 Inhibitoren, die sich in einer präklinischen oder klinischen Phase der Entwicklung befinden.

Während der Arbeit auf dual spezifischen CK1/γ-Sekretase-Inhibitoren wurden mehrere von ihnen in einem Kinase-Panel auf ihre Selektivität getestet. Dabei

zeigten zwei der auf einer Indolinonstruktur basierenden Substanzen eine inhibitorische Aktivität gegenüber FLT-3. Mit dem Ziel die Aktivität gegenüber FLT-3 zu verbessern und gegenüber der γ-Sekretase zu vermindern, wurden systematisch mehrere Substanzen synthetisiert und in einem FLT-3 *in vitro* Assay getestet. Die synthetisierten Produkte erzielten zum größten Teil eine sehr gute FLT-3-Inhibition. Die gegenüber der γ-Sekretase selektivsten FLT-3-Inhibitoren waren **16i** (FLT-3-Inhibitionsratio von 96 %; IC_{50} ($A\beta_{42}$) > 40 μM) und **16n** (FLT-3-Inhibitionsratio von 87 %; IC_{50} ($A\beta_{42}$) > 160 μM), Abb. 36. Der aktivste FLT-3-Inhibitor war das Indolinon **16e** mit einem IC_{50} von 4.1 nM, Abb. 36.

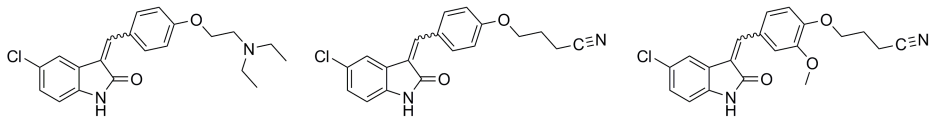

16e
IC_{50} (FLT-3) = 4.1 nM
IC_{50} (γ-Sekretase) = 17.7 μM

16i
FLT-3 Inhibitionsratio = 96%
IC_{50} (γ-Sekretase) = >40 μM

16n
FLT-3 Inhibitionsratio = 87%
IC_{50} (γ-Sekretase) = >160 μM

Abb. 36: Strukturformeln der indolinonbasierten FLT-3-Inhibitoren **16e**, **16i** und **16n**.

Dessen Selektivität wurde nicht nur gegenüber der γ-Sekretase (IC_{50} ($A\beta_{42}$) = 17.7 μM), sondern auch in einem 50 Kinasen umfassenden Panel bestimmt. Dort wurde neben FLT-3 nur die Serin-/Threoninkinase HGK (MAP4K4) (> 20 % Restaktivität) und die Tyrosinkinase JAK3 (> 60 % Restaktivität) inhibiert. Die Bestimmung einer möglichen Toxizität vom Indolinon **16e** wurde in einem *zebrafish embryo phenotype assay* durchgeführt. Es konnte keine Sterblichkeit noch phänotypische Veränderungen festgestellt werden. In einer Dockingstudie von **16e**, gedockt in die ATP-Bindungstasche von FLT-3 (PDB Code = 1RJB), konnten mögliche Interaktionen mit den Aminosäuren Lys644, Met665, Phe691 und Phe830 detektiert werden. Da der ClogP von **16e** mit 5.28 relativ hoch ist und damit beispielsweise eine verringerte Löslichkeit einhergeht, liegt der zukünftige Fokus auf der Verbesserung der pharmakologischen Parameter kommender FLT-3-Inhibitoren.

Die im Rahmen dieser Arbeit synthetisierten Verbindungen sind: **16a (BSc4540), 16c (BSc4534), 16d (BSc4538), 16i (BSc4536), 16q (BSc4532).**

Accepted Manuscript

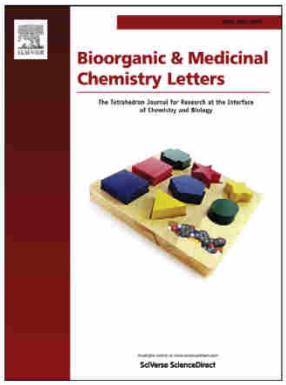

Modification of a promiscuous inhibitor shifts the inhibition from γ-secretase to FLT-3

Ghislaine Marlyse Okala Amombo, Thomas Kramer, Fabio Lo Monte, Stefan Göring, Matthias Fach, Steven Smith, Stephanie Kolb, Robert Schubenel, Karlheinz Baumann, Boris Schmidt

PII: S0960-894X(12)01283-8
DOI: http://dx.doi.org/10.1016/j.bmcl.2012.10.016
Reference: BMCL 19638

To appear in: *Bioorganic & Medicinal Chemistry Letters*

Received Date: 14 August 2012
Revised Date: 28 September 2012
Accepted Date: 1 October 2012

Please cite this article as: Amombo, G.M.O., Kramer, T., Monte, F.L., Göring, S., Fach, M., Smith, S., Kolb, S., Schubenel, R., Baumann, K., Schmidt, B., Modification of a promiscuous inhibitor shifts the inhibition from γ-secretase to FLT-3, *Bioorganic & Medicinal Chemistry Letters* (2012), doi: http://dx.doi.org/10.1016/j.bmcl.2012.10.016

Graphical Abstract

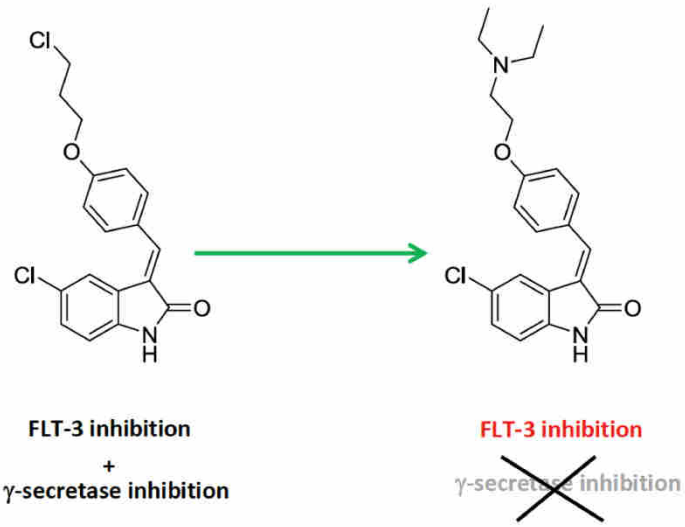

Modification of a promiscuous inhibitor shifts the inhibition from γ-secretase to FLT-3

Ghislaine Marlyse Okala Amombo[a,*], Thomas Kramer[a,*], Fabio Lo Monte[a,*], Stefan Göring[a], Matthias Fach[a], Steven Smith[a], Stephanie Kolb[a], Robert Schubenel[b], Karlheinz Baumann[b] and Boris Schmidt[a,†]

[a] Clemens Schöpf-Institute of Organic Chemistry and Biochemistry, Technische Universität Darmstadt, Petersenstr. 22, D-64287 Darmstadt, Germany

[b] F. Hoffmann-La Roche Ltd., Pharmaceutical Division, Preclinical Research CNS, Bldg. 70/345, CH-4070 Basel, Switzerland

[*] These authors contributed equally to this work.

[†] Corresponding author. Tel.: +49 6151 163075; fax: +49 6151 163278

E-mail address: Schmidt_boris@t-online.de (B. Schmidt).

+ Electronic supplementary information (ESI) available: Experimental section and assay conditions.

Keywords: Acute myeloid leukemia, FLT-3, kinase inhibitor, γ-secretase

Abstract

The inhibition of FLT-3 activity is an interesting target for the treatment of acute myeloid leukemia (AML). The serendipitous identification of FLT-3 inhibitors from a CK1/γ-secretase programme provided compounds with dual inhibitory activity. We analyzed the structure activity relationship of these inhibitors and derivatized them to arrive at compounds with reduced impact on γ-secretase activity and enhanced FLT-3 inhibition.

Acute myeloid leukemia (AML) is an aggressive haematological malignancy with long-term survival rates of 25%-70% in patients younger than 60 years and only 5%-15% in older patients.[1,2] Activating mutations of FLT-3 (FMS-like tyrosine kinase-3) are abundant molecular abnormalities found in AML.[3] FLT-3 is essential for the

normal function of stem cells and the immune system and is primarily expressed in immature hematopoietic cells.[4] It contains an extracellular ligand binding domain, a transmembrane domain, and an intracellular juxtamembrane domain followed by the tyrosine kinase domain, which is interrupted by a kinase insert region.[5,6] Internal-tandem duplications (ITDs) and tyrosine kinase domain (TKD) point mutations are the two major classes of activating FLT-3 mutations identified in AML patients.[7] FLT-3/ITD mutations were estimated to occur in ~23% of *de novo* AML.[8] Several ATP-competitive FLT-3 inhibitors have been developed for a targeted therapy of this disease.[9] The FLT-3 inhibitors are derived from different structural classes and some of them displayed high potential in preclinical and clinical trials, Scheme 1.[5-10]

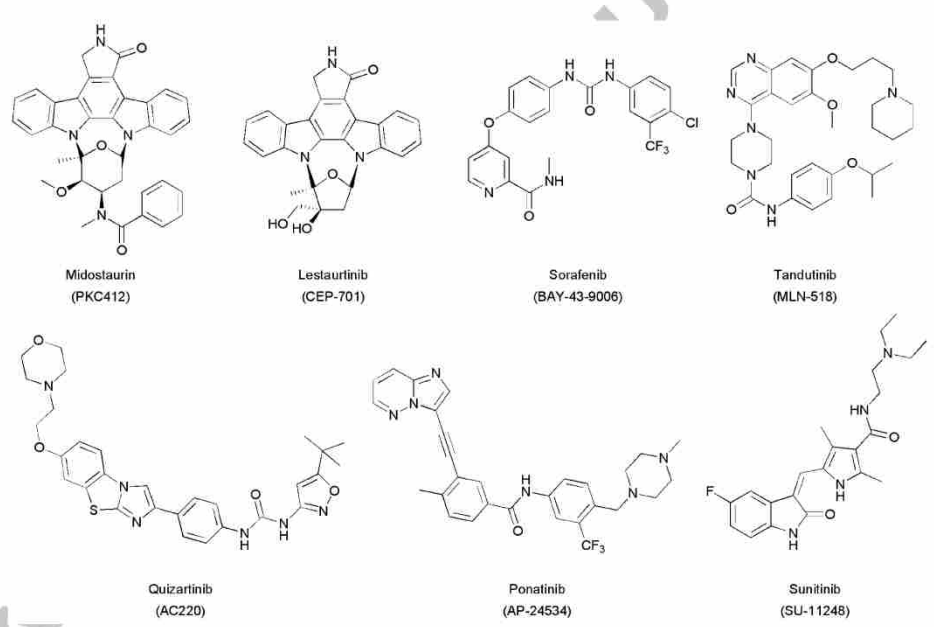

Scheme 1: FLT-3 inhibitors evaluated in preclinical or clinical trials.[5-7,9,10]

The published data suggest that FLT-3 is an attractive therapeutic target for the development of kinase inhibitors for AML and other associated diseases.[11]

Working on the structure activity relationship of the indolinone scaffold of dual CK1/γ-secretase inhibitors in the context of Alzheimer´s disease we additionally profiled the compounds for kinase selectivity. Serendipitously FLT-3 was part of the kinase panel and two substances displayed significant inhibition (98% and 89% at 10 μM) of this tyrosine kinase, Scheme 2.[11]

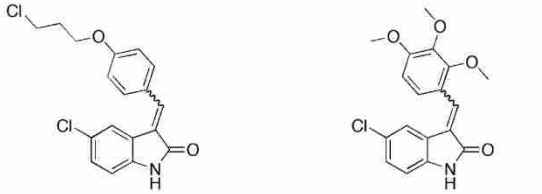

1 (98% FLT-3 inhibition at 10 μM) 2 (89% FLT-3 inhibition at 10 μM)

Scheme 2: Screening hits of potential FLT-3 inhibibitors in a kinase panel of 43 kinases.[11]

Regarding this and the fact that FLT-3 is not known to exert effects on the amyloid precursor protein metabolism we focused on optimizing the FLT-3 inhibitory activity of **1** and reducing its modulation of γ-secretase activity. Primary objective of our research was to decrease the effect on γ-secretase and to improve meanwhile the inhibitory activity against FLT-3. The structure of **1** guided the variation of the structure-activity relationship (SAR) study.

The Knoevenagel condensation of indolinones and aldehydes provides a rapid and efficient method to generate a chemical diversity. The Koevenagel products were obtained from microwave irradiated reaction mixtures within 30 minutes, which was followed by rapid purification. In the first step alkyl or aryl benzyl halides were coupled with 4-hydroxybenzaldhydes **3** under basic conditions to obtain a series of elongated benzaldehydes **4a-n** for the subsequent Knoevenagel condensation.[11,12] A further nucleophilic substitution of the chlorides **4k,l** resulted in the tertiary amines **5a,b**, potential intermediate iminium salts were hydrolysed in the aqueous work up.[11] The ether **7** was formed in a microwave heated reactor by substitution of an aromatic fluoride **6** with a 4-(4-methyl-1*H*-imidazole-1-yl)phenol.[13] The 4-fluoro-benzaldehyde **8** was substituted to its corresponding sulfonyl **9** and imidazol benzaldehyde **10**, Scheme 3.[13,14] The phenylimidazoles **7** and **10** were prepared to evaluate this motif, which is frequently employed on γ-secretase modulators.[15] The opportunity to obtain fluorescent derivatives was addressed by two derivatives: A) a two step synthesis resulted in the azobenzene derivative **12**, the 4-aminobenzaldehyde **11** was converted to its diazonium derivative via diazotation and the final azobenzene **12** was formed by an azo coupling reaction.[16] B) The 9-methyl-9*H*-carbazole **13** was converted to the bulky aldehyde **14** in a two step procedure under Vilsmeier-Haack conditions, Scheme 3.[17]

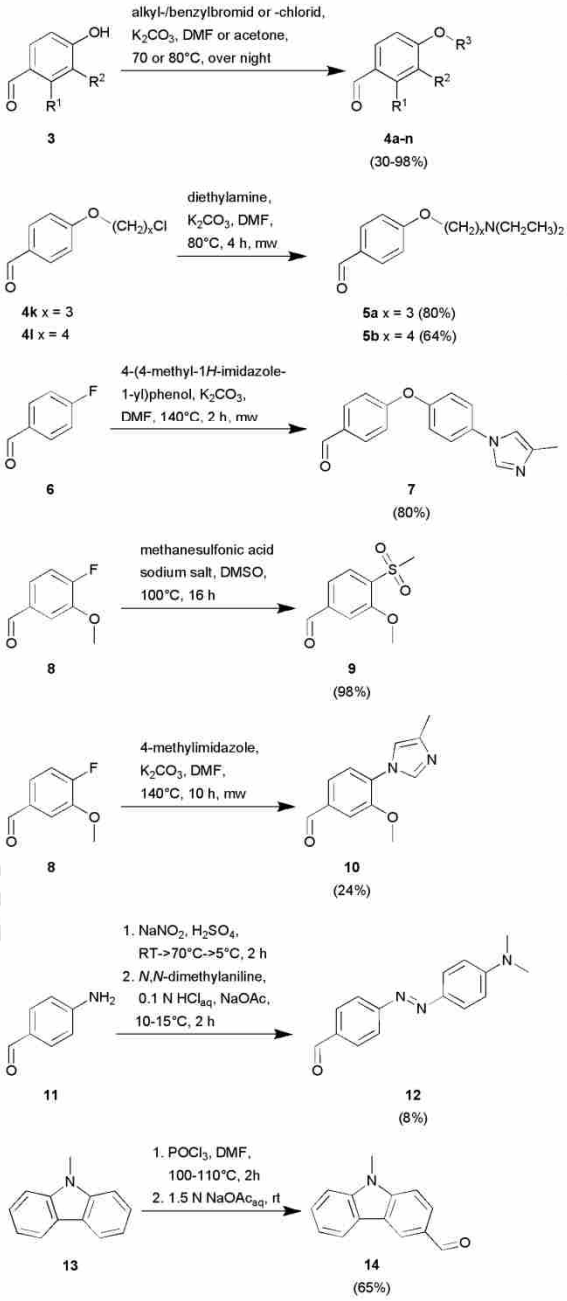

Scheme 3: Aldehyde syntheses (R^1 = H, OMe; R^2 = H, OMe; R^3 = alkyl/benzyl moieties).[11-14,16,17]

Commercial aldehydes and the previously synthesized benzaldehydes (scheme 3) were coupled with the indolinones **15a,b** under microwave supported Knoevenagel conditions, Scheme 4.[11] The resulting products **16a-x** were obtained in yields up to 97%, Table 1. This class of compounds was shown to isomerize within two days in methanol, thus no attempts were made to separate the isomers.[11] A further reduction of compound **16e** resulted in 77% yield of product **16y**, Scheme 5a. Finally, the product **16i** was derivatized to obtain the tetrazole **16z** in a moderate yield of 62%, Scheme 5b.[18]

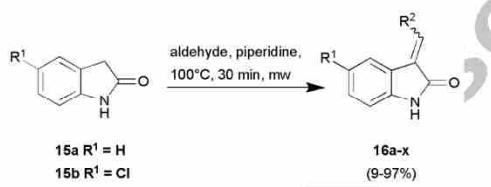

15a R^1 = H
15b R^1 = Cl

16a-x
(9-97%)

Scheme 4: Synthesis of indolinone derivatives under microwave conditions (R^2 = Phenyl moieties).[11,19-22]

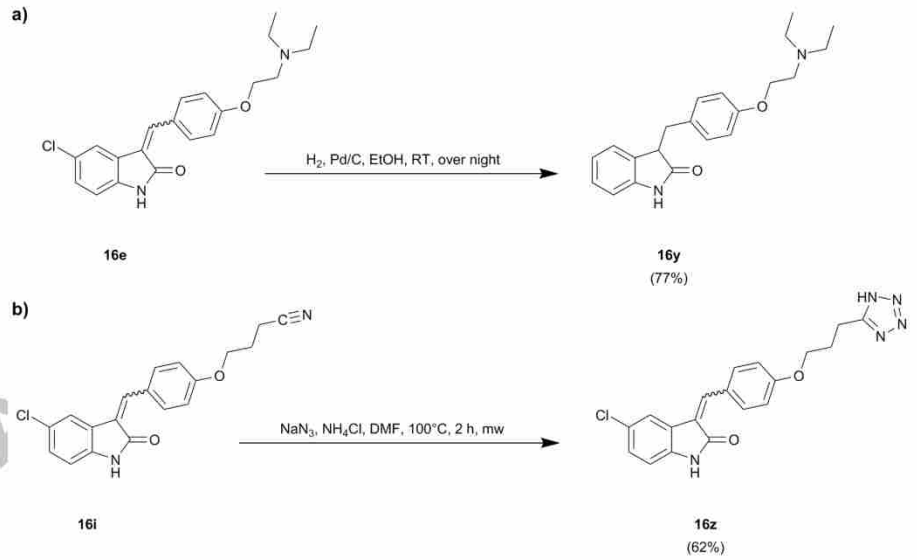

16e

16y
(77%)

16i

16z
(62%)

Scheme 5: Post-Knoevenagel modifications: a) Reduction with H_2 and Pd/C; b) Tetrazole synthesis under microwave conditions.[18]

Table 1: Synthesized indolinones, their chemical properties and *in vitro* assay results.[23,24]

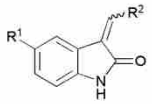

1-2, 16a-x, 16z

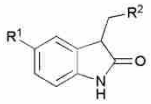

16y

Compound	R^1	R^2	FLT-3 Inhibition -ratio[a]	IC_{50} of $A\beta_{42}$ LPECL Assay[b]	Toxicity (μM)[c]	Yield (%)	ClogP[d]
Staurosporine[e]	-	-	100%	n.t.[f]	n.t.[f]	-	4.19
Sunitinib[e]	-	-	100%	n.t.[f]	n.t.[f]	-	3.00
1	Cl	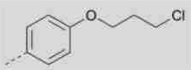	98%	4.7 μM	Y (40)	-	5.04
2	Cl	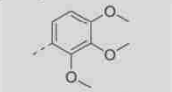	89%	-	-	-	3.50
16a	Cl	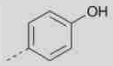	94%	47.6 μM	N (40)	28	3.53
16b	Cl	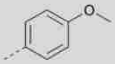	85%	>40 μM	N (40)	88	4.12
16c	Cl	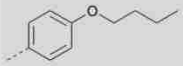	79%	>40 μM	N (40)	83	5.71
16d	Cl	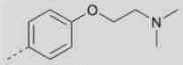	99%	7.6 μM	N (40)	65	4.22
16e	Cl	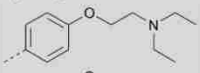	100%	17.7 μM	Y (40)	55	5.28
16f	H	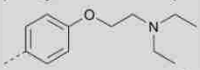	97%	-	-	95	4.31
16g	Cl	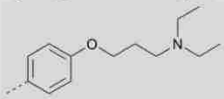	99%	-	-	80	5.63
16h	Cl	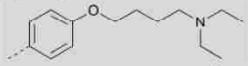	99%	-	-	64	5.56
16i	Cl	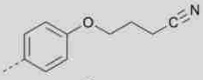	96%	>40 μM	Y (40)	90	3.94
16j	Cl	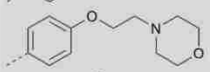	96%	11.3 μM	N (40)	84	4.24
16k	Cl	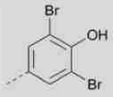	97%	15.0 μM	N (40)	97	5.10
16l	Cl	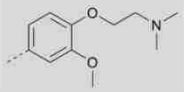	98%	11.5 μM	Y (40)	31	3.96
16m	Cl	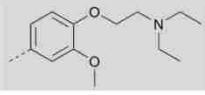	99%	11.5 μM	Y (40)	42	5.02

16n	Cl	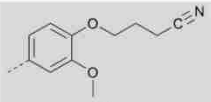	87%	>160 μM	N (160)	67	3.68
16o	Cl	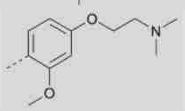	100%	10.0 μM	N (40)	71	4.31
16p	Cl	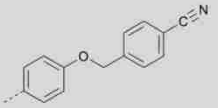	75%	27.3 μM	N (40)	93	5.32
16q	Cl	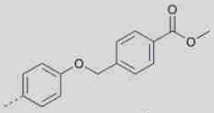	58%	38.8 μM	N (40)	70	5.86
16r	Cl	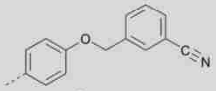	77%	>40 μM	N (40)	48	5.32
16s	Cl	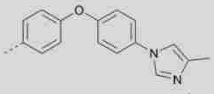	83%	5.4 μM	Y (10)	41	5.88
16t	H	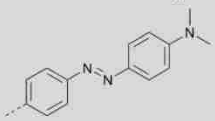	77%	>80 μM	N (80)	9	5.55
16u	Cl	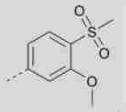	48%	7.3 μM	Y (20)	85	2.49
16v	Cl	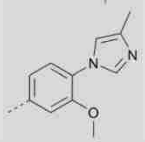	74%	6.7 μM	Y (80)	55	4.25
16w	Cl	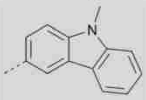	69%	19.8 μM	N (80)	17	6.04
16x	H	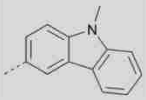	78%	27.6 μM	Y (80)	15	5.07
16y	H	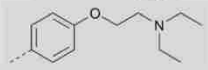	47%	-	-	77	3.87
16z	Cl	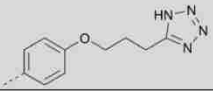	83%	17.7 μM	Y (40)	62	3.76

[a] Percent of control (Staurosporine) specific activity ((measured specific activity/control specific activity) x 100); activity at a concentration of 10 μM; [b] Aβ liquid phase electrochemiluminescence (LPECL) assay, H4 APP#9 cells; [c] Determined in H4-cells, Y = Yes, N = No; [d] Calculated by ChemDraw Ultra (9.0.1); [e] Control; [f] n.t. = not tested.

Human recombinant FLT-3 was used in the FLT-3 *in vitro* kinase assay to ascertain the inhibitory activity. The concentration of the phosphorylated substrate peptide phospho-Ulight-CAGAGAIETDKEYYTVKD (Starting unphosphorylated peptide concentration: 100 nM) was determined after 90 min incubation time at room temperature by the LANCE detection method.[24] All experiments were carried out as technical replicates, the average of two such replicates is listed in Table 1.

The results are expressed as a percent of control (Staurosporine) specific activity ((measured specific activity/control specific activity) x 100) obtained in the presence of the test compounds (10 μM), Table 1. The previously described liquid phase electrochemiluminescence (LPECL) assay was used to measure the $A\beta_{42}$ isoform to evaluate the compounds for their potency in inhibiting γ-secretase activity, Table 1.[23]

To confirm the FLT-3 inhibition-ratio observed at 10 μM concentration we determined the IC_{50} values of compounds **16e,j,l,n**. The 4 compounds showed potent inhibition of FLT-3 activity: IC_{50} = 4.1 nM for **16e**, IC_{50} = 14.0 nM for **16j**, IC_{50} = 29.0 nM for **16l** and IC_{50} = 17.0 nM for **16n**, which exceeded the IC_{50} in the $A\beta_{42}$ generation assay by 3 powers of 10. These activities indicated that we have differentiated FLT-3 inhibition from γ-secretase inhibition.

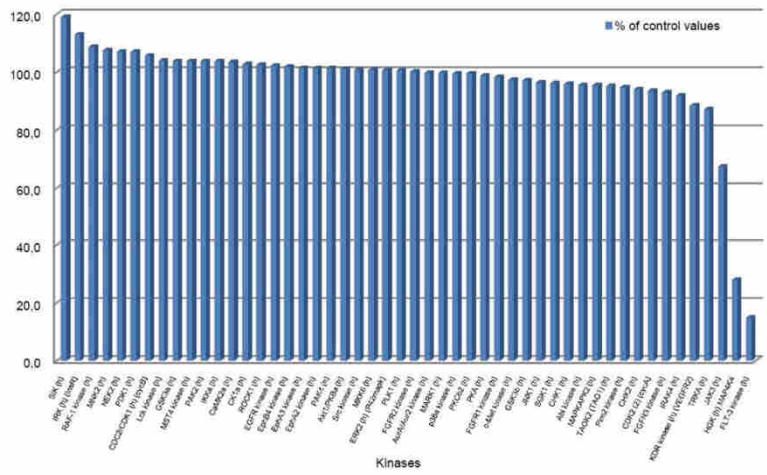

Figure 1: Screening of compound **16e** against a panel of human protein kinases. Each bar represents the activity of one individual protein kinase (Determination method: Percent of control (Staurosporine) specific activity [(measured specific activity/control specific activity) x 100]). Compound **16e** was tested at a concentration of 1 μM against 50 protein kinases. See the Supporting Information for more details.[24]

The most potent γ-secretase inhibitors **16s,v** feature a phenylimidazole, which is frequently encountered in γ-secretase modulators. However, both compounds display reduced FLT-3 inhibition. As indolinones are well known as kinase inhibitors[25,26] we determined the broader selectivity of our most active FLT-3 inhibitor **16e.** The selectivity of compound **16e** was evaluated at a concentration of 1 µM against 50 human protein kinases, Figure 1. Most of the 50 kinases in this panel showed a residual activity higher than 80%, whereas FLT-3 displayed a residual activity of only 14.7%. The only kinases, which were also significantly inhibited by this compound, were the Ser/Thr kinase HGK (MAP4K4) and the Tyr kinase JAK3.

In addition to the H4 APP#9 cell-based toxicity assay, we evaluated the compounds in a zebrafish embryo phenotype assay, which enabled toxicity determination in whole organisms.[27] The embryos were collected and maintained in E2 medium at 28°C. Compound **16e** was added 4-5 hpf (hours post fertilization) and the phenotypes were compared after 48 hpf. Compound **16e** causes a development delay at 20 µM, Figure 2. Compared to the control, zebrafish embryos treated with **16e** were still covered by the chorion. Nevertheless, they did not reveal other abnormalities. The zebrafish embryo assay did not reveal lethality and peculiarities at a concentration below 20 µM of **16e**.

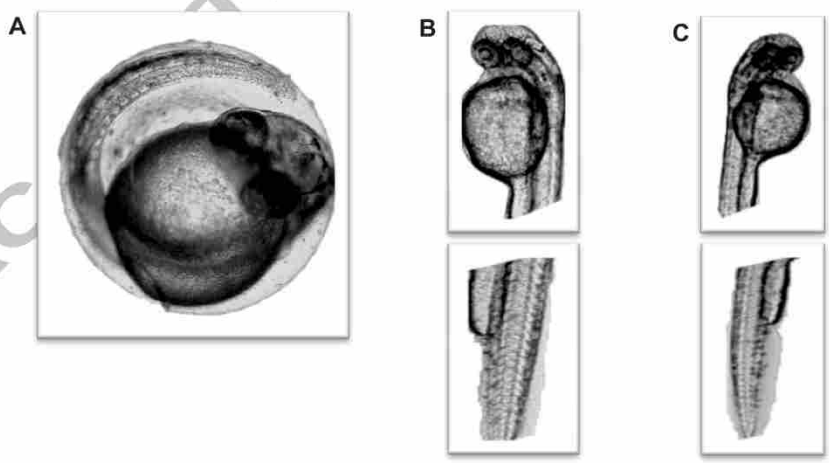

Figure 2: Exposure of zebrafish embryos to A) 20 µM of **16e**, B) 5 µM of **16e**, C) control. The embryos were collected and maintained in E2 medium at 28°C. Compound **16e** was added 4-5 hpf (hours post fertilization) and the phenotypes were compared after 48 hpf.

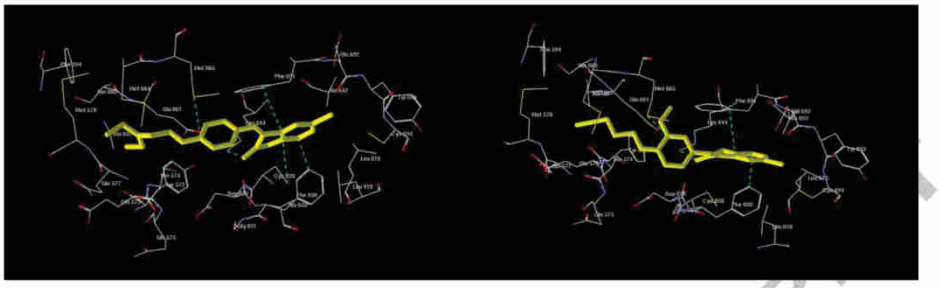

Figure 3: Docking of compound **16e** (left) and **16n** (right) into the PDB crystal structure 1RJB of FLT-3; important interactions are highlighted; Software: Molegro Virtual Docker 5.

The docking studies (Molegro Virtual Docker 5) of the FLT-3 crystal structure (PDB: 1RJB) and compounds **16e** and **16n** revealed potential inhibitor-enzyme interactions, Figure 3.[8] In both cases the docking result indicates four potential interactions. The indolinone motif interacts edge-to-face with the Phe830 of the DFG motif. In addition, the indolinone fits to the FLT-3 hinge region by face-to-face interplay with Phe691 and the hydrogen bonding with Lys644.[8] The phenyl group of the inhibitors interacts with Met665.[28] In addition to these interactions, the rigidity of the bridge between the indolinone and the phenyl moiety may contribute to potent FLT-3 inhibition. Therefore, we synthesized compounds **16e** and **16y**, which differ in orientation and rotational flexibility of the aryl substituent. The FLT-3 *in vitro* assay results of compounds **16e** (FLT-3 inhibition-ratio = 100%) and **16y** (FLT-3 inhibition-ratio = 47%) revealed a 2-fold increased FLT-3 inhibition-ratio for **16e** and exemplifying the influence of rigidity. A FLT-3 inhibition comparison of all compounds revealed that an electron donor motif is needed at the end of the elongated, variable alkyl chain. For example compound **16c**, which lacks this motif, showed a decreased inhibition activity compared to **16d,i**. This may be explained by a polar area formed by Glu573 and Gln577, which is in close vicinity. A comparison of the FLT-3 inhibition results and the docking studies offers the possible suggestion that the benzylidene indolinone moiety may occupy the entrance of the ATP-binding site (compound **16a,b,k**) and the elongated alkyl chain ranging from C_2 (**16e**) to C_4 (**16h**) could act as a flexible "anchor" in the inner side of the ATP-binding pocket, e.g. **16d-j**. Furthermore, a comparison of the FLT-3 inhibition results of Table 1 revealed that bulky residues at the phenyl moiety lead to a decreased inhibitory activity.

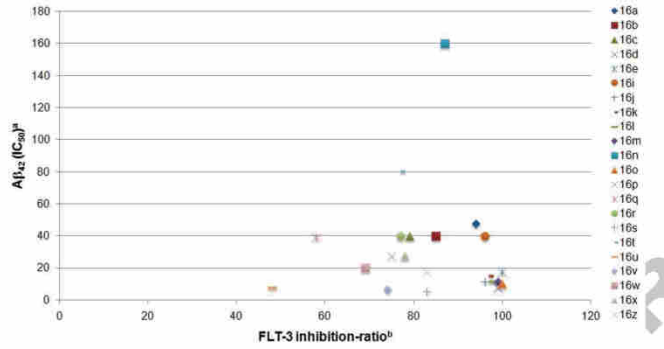

Figure 4: Correlation plot of FLT-3 activity inhibition and $A\beta_{42}$ inhibition (IC_{50}): [a] Values at 40 μM are determined as >40, see Table 1; [b] Determination method: Percent of control (Staurosporine) specific activity [(measured specific activity/control specific activity) x 100]).

The inhibitory activity of the synthesized compounds in the γ-secretase assay cannot be correlated to the FLT-3 inhibition-ratio, Figure 4. In the case of compounds **16i** (FLT-3 Inhibition-ratio = 96%; IC_{50} ($A\beta_{42}$) >40 μM) and **16n** (FLT-3 Inhibition-ratio = 87%; IC_{50} ($A\beta_{42}$) >160 μM) we expected the same result, but surprisingly, they were not active against the γ-secretase, Table 1 and Figure 4. In comparison with other compounds, e.g. **16d,l** and **16p,r**, the nitrile and alkyl chain combination is important for this selectivity.

Conclusion: we have identified several potent FLT-3 inhibitors based on the scaffold of the screening hit **1,** which display neglible activity on γ–secretase inhibition. The most active compound **16e** did not display significant toxicity in H4 APP#9 cells and the zebrafish embryo phenotype assay. This lack of apparent toxicity may be due to lack of permeation, yet permeation is indicated by the activity in the $A\beta_{42}$ generation assay. The combination of FLT-3 *in vitro* results and docking studies revealed likely enzyme-inhibitor interactions with the amino acids Lys644, Met665, Phe691 and Phe830. Further improvement of these FLT-3 inhibitors will focus on the reduction of the logP to enhance to pharmacokinetic properties. Our most active FLT-3 inhibitor **16e** exhibits a ClogP value of 5.28, Table 1, which implies impaired solubility.

Supplementary data

Supplementary data associated with this article can be found, in the online version, at …

References and notes

1. Kindler, T.; Lipka, D. B.; Fischer, T. *Blood* **2010**, *116*, 5089.
2. Levis, M.; Small, D. *Expert Opin. Investig. Drugs* **2003**, *12*, 1951.
3. Pratz, K. W.; Levis, M. J. *Curr. Drug Targets* **2010**, *11*, 781.
4. Griffith, J.; Black, J.; Faerman, C.; Swenson, L.; Wynn, M.; Lu, F.; Lippke, J.; Saxena, K. *Mol. Cell* **2004**, *13*, 169.
5. Advani, A. S. *Curr. Pharm. Des.* **2005**, *11*, 3449.
6. Paz, K.; Zhu, Z. *Expert Opin. Ther. Targets* **2005**, *9*, 1147.
7. Zarrinkar, P. P.; Gunawardane, R. N.; Cramer, M. D.; Gardner, M. F.; Brigham, D.; Belli, B.; Karaman, M. W.; Pratz, K. W.; Pallares, G.; Chao, Q.; Sprankle, K. G.; Patel, H. K.; Levis, M.; Armstrong, R. C.; James, J.; Bhagwat, S. S. *Blood* **2009**, *114*, 2984.
8. Mahboobi, S.; Uecker, A.; Sellmer, A.; Cenac, C.; Hocher, H.; Pongratz, H.; Eichhorn, E.; Hufsky, H.; Trumpler, A.; Sicker, M.; Heidel, F.; Fischer, T.; Stocking, C.; Elz, S.; Bohmer, F. D.; Dove, S. *J. Med. Chem.* **2006**, *49*, 3101.
9. Pemmaraju, N.; Kantarjian, H.; Ravandi, F.; Cortes, J. *Cancer* **2011**, *117*, 3293.
10. www.clinicaltrials.gov **July 2012**.
11. Höttecke, N.; Liebeck, M.; Baumann, K.; Schubenel, R.; Winkler, E.; Steiner, H.; Schmidt, B. *Bioorg. Med. Chem. Lett.* **2010**, *20*, 2958.
12. Strohfeldt, K.; Müller-Bunz, H.; Pampillón, C.; Sweeney, N. J.; Tacke, M. *Eur. J. Inorg. Chem.* **2006**, 4621.
13. Fischer, C.; Munoz, B.; Zultansky, S.; Methot, J.; Zhou, H.; Brown, W. C., WO 2008/156580 A1, **2008**.
14. Ulman, A.; Urankar, E. *J. Org. Chem.* **1989**, *54*, 4691.
15. Schmidt, B.; Baumann, S.; Braun, H. A.; Larbig, G. *Curr. Top Med. Chem.* **2006**, *6*, 377.
16. Perez-Moreno, J.; Zhao, Y.; Clays, K.; Kuzyk, M. G.; Shen, Y.; Qiu, L.; Hao, J.; Guo, K. *J. Am. Chem. Soc.* **2009**, *131*, 5084.
17. Langendoen, A.; Plug, J. P. M.; Koomen, G.-J.; Pandit, U. K. *Tetrahedron* **1989**, *45*, 1759.
18. Lo Monte, F.; Kramer, T.; Boländer, A.; Plotkin, B.; Eldar-Finkelman, H.; Fuertes, A.; Dominguez, J.; Schmidt, B. *Bioorg. Med. Chem. Lett.* **2011**, *21*, 5610.
19. Angell, R.; Reynolds, K.; Lumley, J., WO 2004069998 A2, **2004**.
20. Bouerat, L. M. E.; Fensholdt, J.; Nielsen, S. F.; Liang, X.; Havez, S. E.; Andersson, E. C.; Jensen, L.; Hansen, J. R., WO 2005058309 A1, **2005**.

21. Jiang, T.; Kuhen, K. L.; Wolff, K.; Yin, H.; Bieza, K.; Caldwell, J.; Bursulaya, B.; Tuntland, T.; Zhang, K.; Karanewsky, D.; He, Y. *Bioorg. Med. Chem. Lett.* **2006**, *16*, 2109.
22. Wood, E.; Crosby, R. M.; Dickerson, S.; Frye, S. V.; Griffin, R.; Hunter, R.; Jung, D. K.; McDonald, O. B.; McNutt, R.; Mahony, W. B.; Peel, M. R.; Ray, J.; Lackey, K. *Anti-Cancer Drug Des.* **2001**, *16*, 1.
23. Narlawar, R.; Perez Revuelta, B. I.; Haass, C.; Steiner, H.; Schmidt, B.; Baumann, K. *J. Med. Chem.* **2006**, *49*, 7588.
24. www.cerep.fr.
25. Chen, C. H.; Lee, O.; Yao, C. N.; Chuang, M. Y.; Chang, Y. L.; Chang, M. H.; Wen, Y. F.; Yang, W. H.; Ko, C. H.; Chou, N. T.; Lin, M. W.; Lai, C. P.; Sun, C. Y.; Wang, L. M.; Chen, Y. C.; Hseu, T. H.; Chang, C. N.; Hsu, H. C.; Lin, H. C.; Shih, Y. C.; Chou, S. H.; Hsu, Y. L.; Tseng, H. W.; Liu, C. P.; Tu, C. M.; Hu, T. L.; Tsai, Y. J.; Chen, T. S.; Lin, C. L.; Chiou, S. J.; Liu, C. C.; Hwang, C. S. *Bioorg. Med. Chem. Lett.* **2010**, *20*, 6129.
26. Prakash, C. R.; Raja, S. *Mini Rev. Med. Chem.* **2012**, *12*, 98.
27. Nagel, R. *ALTEX* **2002**, *19 Suppl 1*, 38.
28. Salonen, L. M.; Ellermann, M.; Diederich, F. *Angew. Chem.* **2011**, *123*, 4908.

3.6.3 2-Styrylindolium basierte, fluoreszierende Substanzen zur Visualisierung von Neurofibrillenbündeln (NFTs) in der Alzheimer-Krankheit

Der Inhalt dieses Kapitels wurde bereits bei Bioorg. Med. Chem. Lett. veröffentlicht (**2012**): Jiamin Gu, Upendra Rao Anumala, Fabio Lo Monte, Thomas Kramer, Roland Heyny von Haußen, Jana Hölzer, Valérie Goetschy-Meyer, Gerhard Mall, Ingrid Hilger, Christian Czech, Boris Schmidt, „*2-Styrylindolium based fluorescent probes visualize neurofibrillary tangles in Alzheimer´s disease*", http://dx.doi.org/10.1016/j.bmcl.2012.09.109.

Mit freundlicher Genehmigung von *Elsevier*.

In der folgenden Publikation wurden wasserlösliche, fluoreszierende 2-Styrylindoliumderivate als neuartige Markierungsreagenzien für Neurofibrillenbündeln synthetisiert. Diese wurden zunächst in einem *liver hepatocellular carcinoma cell assay* und in einem *zebrafish embryo phenotype assay* auf ihre Toxizität getestet. Dabei wurde nur bei dem Marker **11** eine leichte Toxizität festgestellt. Anschließend erfolgten die qualitativen Markierungsexperimente, in denen Gehirnschnitte des Hippocampus von Alzheimer Patienten mit den Farbstoffen versetzt wurden. Diese wurden mittels Fluoreszenzmikroskopie ausgewertet. Es wurden die NFTs markiert. Zudem ergab sich ein gutes Kontrastbild im Vergleich zur Markierung der Aβ-Plaques und des Hintergrunds. Um dies genauer zu untersuchen, wurden die 2-Styrylindoliumderivate **9** und **11** auf ihre Tau- und $A\beta_{40}$-Affinität getestet, Abb. 37. Die erhaltenen Tau-Affinitätswerte sind um ein vielfaches höher gegenüber zuvor publizierten, fluoreszierenden Markern, wie **Methoxy-X04** oder **^{11}C-PIB**. Jedoch konnte kein signifikanter Unterschied zur $A\beta_{40}$-Affinität festgestellt werden.

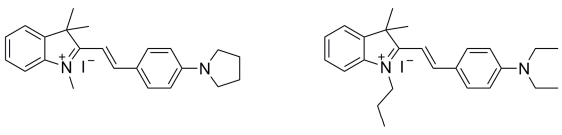

9
EC_{50} = 8.31 μM
IC_{50} (Tau-Affinität) = 5.10 nM
IC_{50} ($A\beta_{40}$-Affinität) = ND

11
EC_{50} = 0.93 μM
IC_{50} (Tau-Affinität) = 1.41 nM
IC_{50} ($A\beta_{40}$-Affinität) = 1.37 nM

Abb. 37: Strukturformel der fluoreszierenden 2-Styrylindoliumderivate **9** und **11**. Die EC_{50} Bestimmung erfolgte in einem *liver hepatocellular carcinoma cell assay*. Die Affinitäten wurde in einem *Thiazine Red R*-Verdrängungsassay ermittelt. ND = *not determined*.

Nichtsdestotrotz sind die synthetisierten wasserlöslichen und fluoreszierenden 2-Styrylindoliumderivate mögliche Marker für weitere *in vivo* Studien zur Evaluation der pathologischen Ablagerungen der Alzheimer-Krankheit als auch für die *post mortem* Detektion von NFTs in Gehirnen von Alzheimer Patienten.

Im Rahmen dieser Arbeit wurde die Toxizität der PET-Sonden mit einem *zebrafish embryo phenotype assay* bestimmt.

Accepted Manuscript

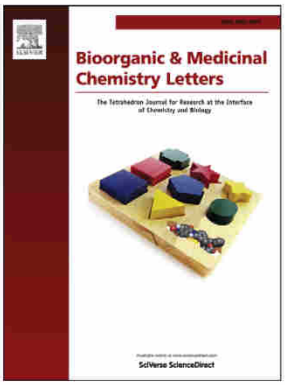

2-Styrylindolium based fluorescent probes visualize neurofibrillary tangles in Alzheimer's disease

Jiamin Gu, Upendra Rao Anumala, Fabio Lo Monte, Thomas Kramer, Roland Heyny von Haußen, Jana Hölzer, Valérie Goetschy-Meyer, Gerhard Mall, Ingrid Hilger, Christian Czech, Boris Schmidt

PII: S0960-894X(12)01264-4
DOI: http://dx.doi.org/10.1016/j.bmcl.2012.09.109
Reference: BMCL 19619

To appear in: *Bioorganic & Medicinal Chemistry Letters*

Received Date: 21 June 2012
Revised Date: 27 September 2012
Accepted Date: 29 September 2012

Please cite this article as: Gu, J., Anumala, U.R., Monte, F.L., Kramer, T., Haußen, R.H.v., Hölzer, J., Goetschy-Meyer, V., Mall, G., Hilger, I., Czech, C., Schmidt, B., 2-Styrylindolium based fluorescent probes visualize neurofibrillary tangles in Alzheimer's disease, *Bioorganic & Medicinal Chemistry Letters* (2012), doi: http://dx.doi.org/10.1016/j.bmcl.2012.09.109

ELSEVIER

Bioorganic & Medicinal Chemistry Letters
journal homepage: www.elsevier.com

2-Styrylindolium based fluorescent probes visualize neurofibrillary tangles in Alzheimer's disease

Jiamin Gu[a], Upendra Rao Anumala[a], Fabio Lo Monte[a], Thomas Kramer[a], Roland Heyny von Haußen[b], Jana Hölzer[c], Valérie Goetschy-Meyer[d], Gerhard Mall[b], Ingrid Hilger[c], Christian Czech[d], Boris Schmidt[a,*]

[a]Clemens Schöpf Institute of Chemistry and Biochemistry, Technische Universität Darmstadt, Petersenstrasse 22, Darmstadt 64287, Germany
[b]Institute of Pathology, Klinikum Darmstadt, Grafenstrasse 9, Darmstadt 64283, Germany
[c]Institute of Diagnostic and Interventional Radiology I, Jena University Hospital – Friedrich Schiller Universität Jena, Erlanger Allee 10 , Jena 07747, Germany
[d]F. Hoffmann-La Roche AG, Grenzacherstrasse 124, Gebäude 93/3.44, Basel 4070, Switzerland

ARTICLE INFO

Article history:
Received
Revised
Accepted
Available online

Keywords:
Alzheimer's disease
Neurofibrillary tangles
Zebrafish
Cytotoxicity
Imaging

ABSTRACT

We evaluated 2-styrylindolium derivatives (**6-11**) as novel and selective probes for neurofibrillary tangles (NFTs) on brain sections of AD patients. The staining experiments indicated that these compounds may bind selectively to NFTs in the presence of ß-amyloid (Aß) plaques. Cell free binding assays confirmed that 2-[2-[4-(1-pyrrolidinyl)phenyl]ethenyl]-1,3,3-trimethyl-3H-indolium iodide (**9**) and 2-[2-[4-(diethylamino)phenyl]ethenyl]-1-butyl-3,3-dimethyl-3H-indolium iodide (**11**) display excellent affinities to Tau-aggregates (IC_{50} values of 5.1 and 1.4 nM, respectively) in the displacement of *Thiazin Red R*. These probes have good solubility in distilled water and low or no cytotoxicity in zebrafish embryo and liver hepatocellular carcinoma cell assays.

Alzheimer's disease (AD) is the most common form of dementia, which is a progressive neurodegenerative disorder associated with memory loss, spatial disorientation, and gradual deterioration of intellectual capacity.[1-3] Age is the major risk factor for disease progression, and most individuals with the disease are age 65 or older. After age 65, the possibility of developing dementia roughly doubles every five years. It was estimated that 36 million people live with Alzheimer's disease and other dementias worldwide in 2011. This number is expected to rise to 66 million by 2030 and 115 million by 2050.[4]

The presence of two abnormal proteins in patients' brains: senile plaques (SPs) and neurofibrillary tangles (NFTs) are the characteristic hallmarks of AD.[5,6] SPs are composed of ß-amyloid peptide (Aß), a fragment of the amyloid peptide precursor protein (APP), whereas the intracellular NFTs are comprised of hyperphosphorylated aggregates of the twisted strands of Tau protein.[7-9] Diagnostic probes which specifically bind to Aß plaques and NFTs are considered to be a significant advance not only to diagnosis but as an enabling tool for drug development. Several probes have been developed in order to detect Aß plaques pathology in the brains of patients with AD by either single-photon emission computed tomography (SPECT) or positron emission tomography (PET),[10-15] whereas few probes for NFTs have been reported yet.[16-19,41] Noninvasive *in vivo* imaging of Aß plaques in the brain is well established, yet limited by the late onset of detectable amyloid deposition and a plateau phase in plaque load in late stage AD. The presence of ß-amyloid in the human retina was demonstrated by several groups and monitored in the mouse retina by fluorescence microscopy after high dosage of curcumin.[20,21] Systemic application of curcumin to humans at the necessary concentration is likely to cause adverse events as curcumin is photo labile and toxic to most human cell lines > 50 µmol/L. Recent reports suggest Tau pathology to be a more reliable biomarker for AD.[8,22] These results showed that the number of NFTs in the brain correlates better with the progress

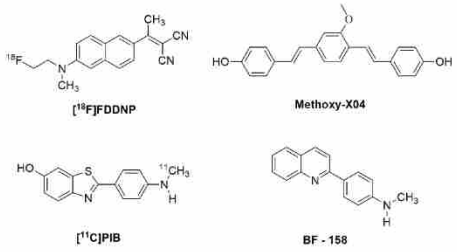

Figure 1. Chemical structures of [^{18}F]FDDNP, Methoxy-X04, [^{11}C]PIB and BF-170.

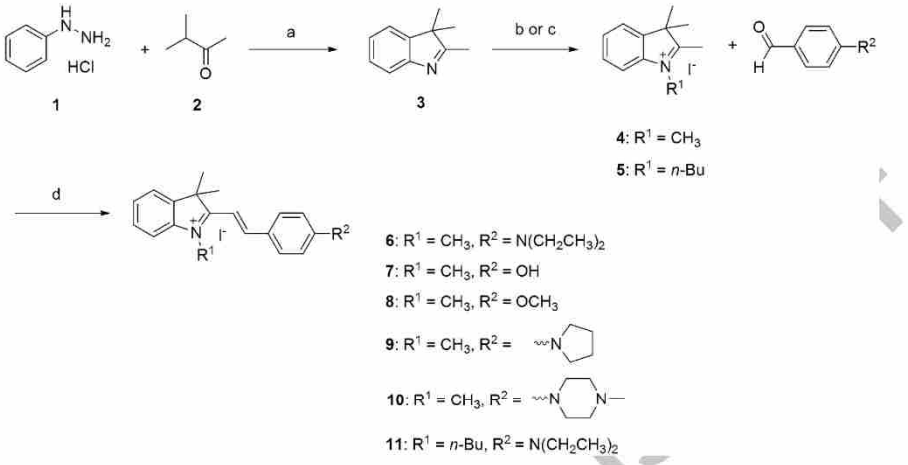

Scheme 1. Synthesis of 2-styrylindolium derivatives (**6**-**11**). Reagents and conditions: (a) 1.0 equiv **1**, 1.25 equiv **2**, CH_3COOH, 120°C, 16h; (b) 1.0 equiv **3**, 2.0 equiv methyl iodide, CH_3CN, reflux, 12h; (c) 1.0 equiv **3**, 1.5 equiv 1-iodobutane, 2-butanone, reflux, 12 h; (d) 1.0 equiv **4** or **5**, 1.1 equiv corresponding aldehyde, EtOH, reflux, 12 h.

of dementia in AD patients and does not reach a plateau as reported for amyloid pathology. Thus, *in vivo* imaging of NFTs or Aß plaques in the human retina may provide an efficient diagnosis of AD in the early, presymptomatic stages. Current data suggest [^{18}F]FDDNP,[16] Methoxy-X04,[17] [^{11}C]PIB,[18] benzimidazole and quinoline derivatives[19] as candidates for *in vivo* imaging of Tau pathology. However, these probes display equipotent affinity for both Aß plaques and NFTs. Moreover, these probes do not display the appropriate fluorescence to be applied to human tissue or they display undesirable pharmacokinetic properties, e.g. the very low clearance of Methoxy-XO4 in rodents. This lack of suitable NFTs-specific fluorescent probes imposes a limit on the *in vivo* quantification of neurofibrillary pathology. Therefore, the challenge remains to develop fluorescent probes with improved affinity and selectivity to NFTs. In this study, we present a series of highly water-soluble 2-styrylindolium probes with excellent affinities to NFTs and moderate toxicity. The probes may be applied to the imaging of retinal NFTs in AD animal models.

In order to eliminate potentially unsafe compounds in the early development process and to prioritize compounds for further studies, we profiled the fluorescent probes in the *in vitro* liver hepatocellular carcinoma cell assay (HepG2) and in the zebrafish embryo development assay, which has become a major model in neurobiology and toxicology.[23,24] The incubation with liver cells provides information on the detoxification of the fluorophores *in vivo* in human tissue. The transparent body of the zebrafish embryo constitutes an important advantage of this model as it enables to observe and analyze several parameters by microscopy. The morphological and molecular basis tissues are identical or similar to other vertebrates including human beings. However, this model does not include pathological Tau-aggregates.[25-27]

The lead structure was selected from a set of established highly fluorescent dyes and evaluated for the silk dying properties versus wool reserve, which indicates ß-sheet binding of the dye. The cyanines were advanced due to their structural analogy to known Tau ligands and evaluated against 5 other lead structures, such as bis-stilbenes[41] and squaric acid derivatives. The bis-stilbenes displayed limited solubility and the squaric acid derivatives did not display sufficient binding affinity.[28] The synthesis of the 2-styrylindolium derivatives employed known methods or slight modifications [29-33] thereof, which are depicted in Scheme 1. The phenylhydrazine hydrochloride and 3-methyl-2-butanone were condensed to form the intermediate hydrazone and converted by Fischer indole synthesis to obtain the 2,3,3-trimethylindolenine **3**. Methylation of the indolenine in acetonitrile under reflux formed the indolium **4** in quantitative yield. The indolenine and 1-iodobutane were refluxed in ethylmethylketone to obtain the indolium **5**. The key transformation to the target 2-styrylindolium derivatives (**6**-**11**) compounds was achieved by the Knoevenagel condensation of the *N*-alkylated indolium backbone with the corresponding aldehyde in ethanol under reflux. The products were isolated in good yields ranging from 77 to 96 % (Table 1) by standard chromatographic purification on silica gel. The ^{1}H-NMR spectrum revealed that the two doublets at 8.40-8.26 and 7.54-7.19 ppm correspond to trans configured olefinic protons with a large coupling constant (15.5-16.5 Hz).

Table 1.
Yields, properties and toxicity (EC_{50}) of probes **6**–**11**.

Compound	Yield[a]	MW[b]	cLog P[c]	EC_{50} µM[d]
6	92%	460.39	2.14	8.57
7	83%	405.27	0.81	ND
8	77%	419.30	1.34	10.93
9	96%	458.38	1.79	8.31
10	91%	487.42	1.28	ND
11	96%	502.47	3.58	0.93

ND, not determined
[a]Isolated yields.
[b]Determined by CS ChemOffice 10.0.
[c]Log P values were calculated using the Molinspiration Cheminformatics software (V2011. 04).
[d]EC_{50} declares the dye concentration in which 50 % of the cells died after incubation with the probe.

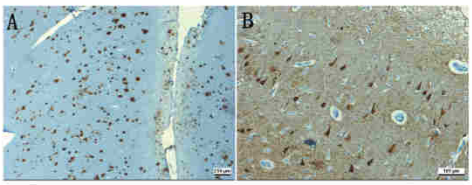

Figure 2. Immunohistochemical staining of hippocampal sections: τ antibody AT8 (B) Aβ-plaques with antibody amyloid A4 (A). See Fig. 3.

To ensure that the tissues contain both tau and Aß aggregates, we conducted a immunohistochemical staining of the tissues. Figure 2 shows that the tissues contain a rich amount of both tau and Aß aggregates. The qualitative selective binding of the fluorescent probes to NFTs was evaluated in the primary screen on hippocampal sections of human AD brain tissue and analyzed by fluorescence microscopy. This low throughput screen secured binding of the probes to Tau-aggregates in human AD pathology, as different Tau isoforms may result in different binding site on *in vitro* aggregates or Tau transgenic mouse models.[34] The 2-styryl-indolium probes stain NFTs in human tissue (Figure 3) and provide a good contrast versus Aß plaques and background, especially probes **9** and **11**. These probes displayed excellent staining of NFTs (Figure 3, D and F) in comparison to Aß plaques (Figure 3, G and H). The results suggested a good affinity to the NFTs, which required quantification in a ligand binding assay to both aggregated amyloid and Tau. Remarkably, the probes **6-11** stained NFTs in human tissue strongly as observed by fluorescent microscopy, whereas plaques in the same brain preparations were stained just weakly. This observation stands in contrast to the activity in the *Thiazine Red R* displacement assay, where compound **11** displayed almost equipotent affinity to $Aß_{40}$-aggregates and Tau-aggregates (4R). The lack of potent plaque staining in the human tissue preparations may be due to interference with the fluorescence properties upon plaque binding, e.g. a fluorescence reduction or changes in the Stokes shift, which limit the detection by the DAPI- or FITC-filter employed in fluorescence microscopy. However, these results indicated that 2-styrylindolium probes **6-11** may be useful for the post mortem detection of NFTs in the brain of AD patients.

Probes with appropriate lipophilicity and low molecular weight may display sufficient permeability to cross the blood-brain barrier (BBB) and rapid clearance from the body when used as an *in vivo* probes.[12, 35] The calculated log *P* values of all these compounds were found to be in the range of 0.81 and 3.58. Besides, the molecular weight of that 2-styrylindolium iodide salts are below 505 Daltons (Table 1).[36] These properties are in the range of accepted lipophilicity criteria for BBB permeation after intravenous injection. The solubilities of the *N*-methylated probes **6-10** are higher than 0.5 g/L in distilled water. The *N*-butylated probe **11** displays a solubility of > 0.1 g/L at 25°C. The solubility of established imaging agents: FDDNP, Methoxy-X04 and BF-158, is in the same range or inferior to the solubility of these 2-styrylindolium derivatives.

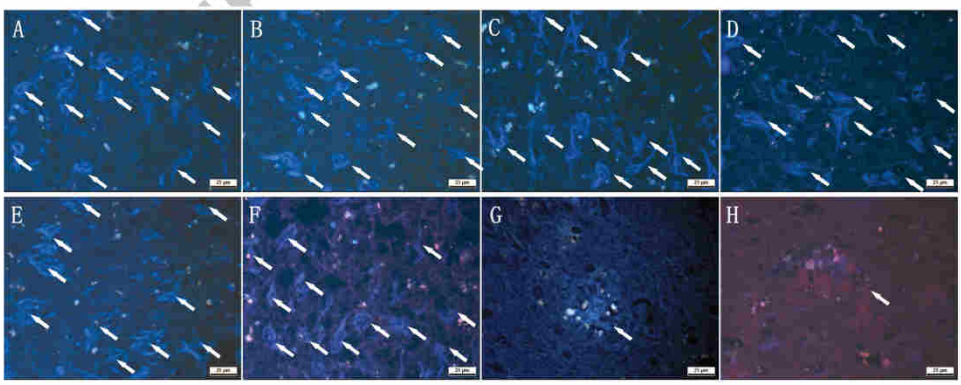

Figure 3. Neuropathological staining of brain sections from the hippocampus of an AD patient (A-H). Probes **6** (A), **7** (B), **8** (C), **9** (D), **10** (E) and **11** (F) are clearly stained neurofibrillary tangles. In contrast, the probes **9** (G) and **11** (H) faintly stained with Aß plaques. (Tissues: hippocampus; Patient: male, 71 years old, CERAD-Score: 3; NFTs-level: V).

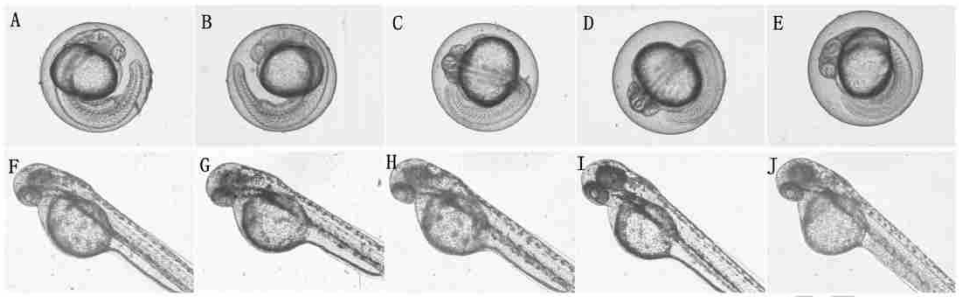

Figure 4. *In vivo* cytotoxicity studies with embryos of zebrafish after 24 (A-E) and 72 (F-G) hpf at 10 μM resp.. Controls (A and F), Probe **6** (B and G), **8** (C and H), **9** (D and I) and **11** (E and J).

The affinity of the probes to aggregated tau protein was determined by displaced of the reference dye Thiazine Red R, hence IC_{50} data obtained in the competition assay are reported rather than Ki values. *Thiazine Red R* was selected as reference ligand for the displacement assay, because it was previously shown to be superior to thioflavin S or immune histochemical detection of aggregated Tau and $Aß_{40}$.[37,41] It was shown to be an accurate maker for ß-pleated sheet structures and to reliably stain Aß plaques and diffuse NFTs (K_d for aggregated $Aß_{40}$ = 49 nM and K_d for aggregated tau = 18 nM). It was reported that the *in vitro* binding affinity (K_i) of Methoxy-X04 is 26.8 nM.[17] The same compound was measured in *Thiazine Red R* assay and IC_{50} values are shown in Table. 2. Unfortunately, the affinity of most probes to Tau-aggregates could not be quantified due to spectral overlap with the reference ligand *Thiazine Red R*. Moreover it interfered with the acquisition of dose dependent fluorescence increase of the bound probe, which was employed to exclude potent protein disaggregating dyes. The affinity of the probes **9** and **11** to Tau-aggregates was determined indirectly (IC_{50} values of 5.1 and 1.4 nM) in the displacement assay for Tau affinity versus the reference ligand *Thiazine Red R* using aggregated recombinant human microtubule associated tau protein purified from *E. coli* and aggregated synthetic $Aß_{40}$ as reported previously.[41] *Thiazine Red R* was added at the concentration corresponding to the K_d of the respective aggregated protein binding site to induce a fluorescent signal that can be inhibited by the addition of a displacer compound. (K_d for aggregated tau =18 nM, and K_d for aggregated A = 49 nM.) To determine the affinity of a displacer compound to the thiazine red binding sites of the aggregated proteins, the compound was added at different concentrations to the assay mixture ranging from 0.1 to 10 000 nM. Compounds were also measured together with the aggregated proteins, but in the absence of *Thiazine Red R*. Net fluorescence was calculated by subtracting the fluorescence of the wells without *Thiazine Red R* from the fluorescence of wells containing *Thiazine Red R*.

Remarkably, the pyrrolidyl substituent results in higher affinity than the *N,N*-diethyl derivative. This may be due to the locked conformation of the *N*-alkyl chain. The displacement ability of these 2-styrylindolium derivatives was compared against the known probes: Methoxy-X04, FDDNP, PIB and BF-158 under the same assay conditions (Table. 2). Significantly, the 2-styrylindolium derivatives **9** and **11** displayed ~50-7000 fold higher affinity to Tau-aggregates. It indicates sufficient affinity of the probes for imaging of Tau-aggregates *in vivo*. Furthermore, the series may be radiolabeled with $^{11}CH_3$, ^{18}F and ^{123}I at either the O or N position and evaluated as positron emission tomography (PET) and single photon emission tomography (SPECT) radioligands for NFT- imaging *in vivo*.

Table 2.
Competitive *Thiazine Red R* displacement from Tau /$Aß_{40}$ aggregates for probes **9**, **11**, Methoxy-X04, FDDNP, PIB and BF158.

Compound	Aggr.Tau-IC_{50}/nM	Aggr. $Aß_{40}$-IC_{50}/nM
9	5.10	ND
11	1.41	1.37
Methoxy-X04	246	140
FDDNP	1635	1467
PIB	3255	5190
BF-158	>10000	>10000

ND, not determined due to spectral overlap with the reference compound in the displacement assay.

Four of the 2-styrylindolium compounds (**6**, **8**, **9** and **11**) have been further evaluated at different concentrations in the zebrafish embryo development assay. The embryos developed well and no lesions were found at the different concentrations up to 10 μM at 24 hours post-fertilization (hpf). After 72 hpf, only the juvenile fish incubated with compound **11** showed small lesions in the yolk sac (Figure 4, J). The HepG2 cell proliferation assay of these four compounds was used to evaluate the cytotoxicity in human cells. The effective doses (EC_{50}) were calculated via the best-fitted trendline of cell vitality as a function of dye concentration. Compounds **6**, **8**, **9** and **11** showed EC_{50} values of 8.57, 10.93, 8.31 and 0.93 μM, respectively, after 24 h incubation (Table. 1). Compound **11** displayed higher cytotoxicity in both assays than other compounds in this series. Both cytotoxicity studies suggested that 2-styrylindolium probes have no or negligible cytotoxicity against zebrafish embryos and HepG2 at the concentration employed for the histology experiments on human AD brain tissue (1 μM).

Taken together these results suggest that 2-styrylindolium compounds should be advanced to *in vivo* mice experiments in transgenic mice. However, the 4R Tau transgenic mice available to the project are all based on the 4R Tau repeat and deposit very little amounts of Tau. Moreover, these 4R Tau mouse models seem to be void of the Tau-aggregate binding site present in humans.[38-39] The presence of at least two different binding sites on Tau-aggregates was demonstrated for the Tau probe THK523 recently.[40]

In conclusion, we have developed a series of water soluble 2-styrylindolium probes for fluorescent imaging of NFTs in human Alzheimer's disease brain. The results of the *in vitro* fluorescent staining protocol using brain sections of AD patient indicated

potent NFT imaging and low nonspecific binding. The cytotoxicity experiments with zebrafish embryos and HepG2 cells suggest that these probes may be suitable for further *in vivo* applications. This indicates sufficient safety for *in vivo* evaluation in mouse models.

Acknowledgments

This work was supported by grants from German Federal Ministry of Education and Research (Bundesministerium für Bildung und Forschung, Germany, 13N10636).

References and notes

1. Citron, M. *Nat. Rev. Drug Discov.* **2010**, *9*, 387.
2. Monaccelli, A. M.; Cushman, L. A.; Kavcic, V.; Duffy, C. J. *Neurology* **2003**, *61*, 1491.
3. Jakob-Roetne, R.; Jacobsen, H. *Angew. Chem. Int. Ed. Engl.* **2009**, *48*, 3030.
4. Prince, M.; Bryce, R.; Ferri, C. WorldAlzheimerReport2011. 2011;
5. Selkoe, D. J. *Physiol. Rev.* **2001**, *81*, 741.
6. Ittner, L. M.; Gotz, J. *Nat. Rev. Neurosci.* **2011**, *12*, 67.
7. LaFerla, F. M. *Biochem. Soc. Trans.* **2010,** *38*, 993.
8. Bruno, B.; Pickhardt, M.; Schmidt, B.; Mandelkow, E.-M.; Waldmann, H.; Mandelkow, E. *Angew. Chem. Int. Ed.* **2008**, *48*, 1740.
9. Binder, L. I.; Guillozet-Bongaarts, A. L.; Garcia-Sierra, F.; Berry, R. W. *Biochim. Biophys. Acta.* **2005**, *1739*, 216;
10. Flaherty, D. P.; Walsh, S. M.; Kiyota, T.; Dong, Y.; Ikezu, T.; Vennerstrom, J. L. *J. Med. Chem.* **2007**, *50*, 4986.
11. Mathis, C. A.; Wang, Y. M.; Holt, D. P.; Huang, G. F.; Debnath, M. L.; Klunk, W. E. *J. Med. Chem.* **2003**, *46*, 2740.
12. Sutharsan, J.; Dakanali, M.; Capule, C. C.; Haidekker, M. A.; Yang, J.; Theodorakis, E. A. *ChemMedChem* **2010**, *5*, 56.
13. Cui, M.; Ono, M.; Kimura, H.; Liu, B.; Saji, H. *Bioorg. Med. Chem. Lett.* **2011**, *21*, 4193.
14. Zhuang, Z. P.; Kung, M. P.; Kung, H. F. *J. Med. Chem.* **2006**, *49*, 2841.
15. Zha, Z.; Choi, S. R.; Ploessl, K.; Lieberman, B. P.; Qu, W.; Hefti, F.; Mintun, M.; Skovronsky, D.; Kung, H. F. *J. Med. Chem.* **2011**, *54*, 8085.
16. Braskie, M. N.; Klunder, A. D.; Hayashi, K. M.; Protas, H.; Kepe, V.; Miller, K. J.; Huang, S. C.; Barrio, J. R.; Ercoli, L. M.; Siddarth, P.; Satyamurthy, N.; Liu, J.; Toga, A. W.; Bookheimer, S. Y.; Small, G. W.; Thompson, P. M. *Neurobiol. Aging* **2010**, *31*, 1669.
17. Klunk, W. E.; Bacskai, B. J.; Mathis, C. A.; Kajdasz, S. T.; McLellan, M. E.; Frosch, M. P.; Debnath, M. L.; Holt, D. P.; Wang, Y.; Hyman, B. T. *J. Neuropathol. Exp. Neurol.* **2002**, *61*, 797.
18. Mathis, C. A.; Bacskai, B. J.; Kajdasz, S. T.; McLellan, M. E.; Frosch, M. P.; Hyman, B. T.; Holt, D. P.; Wang, Y.; Huang, G. F.; Debnath, M. L.; Klunk, W. E. *Bioorg. Med. Chem. Lett.* **2002**, *12*, 295.
19. Okamura, N.; Suemoto, T.; Furumoto, S.; Suzuki, M.; Shimadzu, H.; Akatsu, H.; Yamamoto, T.; Fujiwara, H.; Nemoto, M.; Maruyama, M.; Arai, H.; Yanai, K.; Sawada, T.; Kudo, Y. *J. Neurosci.* **2005**, *25*, 10857.
20. Koronyo, Y.; Salumbides, B. C.; Black, K. L.; Koronyo-Hamaoui, M. *Neurodegener. Dis.* **2012**, *10*, 285.
21. Koronyo-Hamaoui, M.; Koronyo, Y.; Ljubimov, A. V.; Miller, C. A.; Ko, M. K.; Black, K. L.; Schwartz, M.; Farkas, D. L. *Neuroimage* **2011**, *54*, S204.
22. Taghavi, A.; Nasir, S.; Pickhardt, M.; Heyny-von Haußen, R.; Mall, G.; Mandelkow, E.; Mandelkow, E.-M.; Schmidt, B. *J. Alz. Dis.* **2011**, *27*, 835.
23. Zon, L. I.; Peterson, R. T. *Nat. Rev. Drug. Discov.* **2005**, *4*, 35.
24. Ko, S. K.; Chen, X.; Yoon, J.; Shin, I. *Chem. Soc. Rev.* **2011**, 40, 2120.
25. Kimmel, C. B.; Ballard, W. W.; Kimmel, S. R.; Ullmann, B.; Schilling, T. F. *Dev. Dyn.* **1995**, *203*, 253.
26. Paquet, D.; Bhat, R.; Sydow, A.; Mandelkow, E. M.; Berg, S.; Hellberg, S.; Falting, J.; Distel, M.; Koster, R. W.; Schmid, B.; Haass, C. *J. Clin. Invest.* **2009**, *119*, 1382.
27. Lamason, R. L.; Mohideen, M. A.; Mest, J. R.; Wong, A. C.; Norton, H. L.; Aros, M. C.; Jurynec, M. J.; Mao, X.; Humphreville, V. R.; Humbert, J. E.; Sinha, S.; Moore, J. L.; Jagadeeswaran, P.; Zhao, W.; Ning, G.; Makalowska, I.; McKeigue, P. M.; O'Donnell, D.; Kittles, R.; Parra, E. J.; Mangini, N. J.; Grunwald, D. J.; Shriver, M. D.; Canfield, V. A.; Cheng, K. C. *Science* **2005,** 310, 1782;
28. Kieser, D. Ph.D. Dissertation, Technische Universität Darmstadt, 2011.
29. Lindsey, J. S.; Brown, P. A.; Siesel, D. A. *Tetrahedron* **1989**, *45*, 4845.
30. Wang, J.; Cao, W. F.; Su, J. H.; Tian, H.; Huang, Y. H.; Sun, Z. R. *Dyes and Pigments* **2003**, *57*, 171.
31. Mancois, F.; Pozzo, J. L.; Pan, J.; Adamietz, F.; Rodriguez, V.; Ducasse, L.; Castet, F.; Plaquet, A.; Champagne, B. *Chem. Eur. J.* **2009**, *15*, 2560.
32. Berezin, M. Y.; Guo, K.; Teng, B.; Edwards, W. B.; Anderson, C. J.; Vasalatiy, O.; Gandjbakheche, A.; Griffiths, G. L.; Achilefu, S. *J. Am. Chem. Soc.* **2009**, *131*, 9198.
33. Boto, R. E. F.; El-Shishtawy, R. M.; Santos, P. F.; Reis, L. V.; Almeida, P. *Dyes and Pigments* **2007,** *73*, 195.
34. Zhang, W.; Arteaga, J.; Cashion, D. K.; Chen, G.; Gangadharmath, U.; Gomez, L. F.; Kasi, D.; Lam, C.; Liang, Q.; Liu, C.; Mocharla, V. P.; Mu, F.; Sinha, A.; Szardenings, A. K.; Wang, E.; Walsh, J. C.; Xia, C.; Yu, C.; Zhao, T.; Kolb, H. C. *J. Alzheimers Dis.* **2012**, accepted. DOI: 10.3233/JAD-2012-120712
35. Ryu, E. K.; Chen, X. *Front. Biosci.* **2008**, *13*, 777.
36. Log *P* values were calculated by the Molinspiration Cheminformatics software; http://www.molinspiration.com/ (V2011. 04).
37. Uchihara, T.; Nakamura, A.; Yamazaki, M.; Mori, O. *Acta. Neuropathol.* **2000**, *100*, 385.
38. Cashion, D. K.; Chen, G.; Kasi, D.; Kolb, H. C.; Liu, C.; Sinha, A.; Szardenings, A. K.; Wang, E.; Yu, C.; Zhang, W.; Gangadharmath, U. B.; Walsh, J. C. WO 2011119565, 2011.
39. Mohorko, N.; Repovs, G.; Popovic, M.; Kovacs, G. G.; Bresjanac, M. *J. Neuropathol. Exp. Neurol.* **2010**, *69*, 405.
40. Fodero-Tavoletti, M. T.; Okamura, N.; Furumoto, S.; Mulligan, R. S.; Connor, A. R.; McLean, C. A.; Cao, D.; Rigopoulos, A.; Cartwright, G. A.; O'Keefe, G.; Gong, S.; Adlard, P. A.; Barnham, K. J.; Rowe, C. C.; Masters, C. L.; Kudo, Y.; Cappai, R.; Yanai, K.; Villemagne, V. L. *Brain* **2011**, *134*, 1089.
41. Boländer, A.; Kieser, D.; Voss, C.; Bauer, S.; Schön, C.; Burgold, S.; Bittner, T.; Hölzer, J.; Heyny-von Haußen, R.; Mall, G.; Goetschy, V.; Czech, C.; Knust, H.; Berger, R.; Herms, J.; Hilger, I.; Schmidt, B. *J. Med. Chem.* 2012, **DOI:** 10.1021/jm300653b

Supplementary Material

Supplementary data associated with this article can be found, in the online version, at XXX.

*Graphical Abstract (for review)

Graphical Abstract

To create your abstract, type over the instructions in the template box below.
Fonts or abstract dimensions should not be changed or altered

2-Styrylindolium based fluorescent probes for neurofibrillary tangles in Alzheimer's disease

Leave this area blank for abstract info.

Jiamin Gu, Upendra Rao Anumala, Fabio Lo Monte, Thomas Kramer, Roland Heyny von Haußen, Jana Hölzer, Valérie Goetschy-Meyer, Gerhard Mall, Ingrid Hilger, Christian Czech, Boris Schmidt

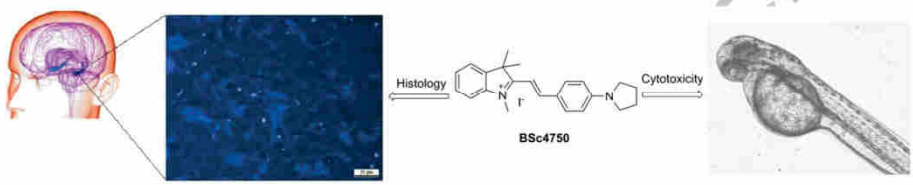

4 Zusammenfassung

Am Anfang galt es die publizierten Forschungsergebnisse auf dem Gebiet der ATP-kompetitiven GSK-3-Inhibitoren zusammenzufassen. Dabei konnten für die Aktivität und Selektivität von ATP-kompetitiven GSK-3-Inhibitoren essentielle Bindungspartner bestimmt werden, Abb. 38 links. In der Rückgratregion der ATP-Bindungstasche von GSK-3 sind es Asp133, Tyr134 und Val135. Im polaren Bereich sind es Lys85, Glu97 und Asp200. Bei der Interaktion mit der glycinreichen Schleife spielt der aromatische Rest des Phe67 eine wesentliche Rolle. Im Fall der Region in Richtung „Ausgang“ sind die Aminosäuren Thr138, Arg141 und Gln185 zu nennen.

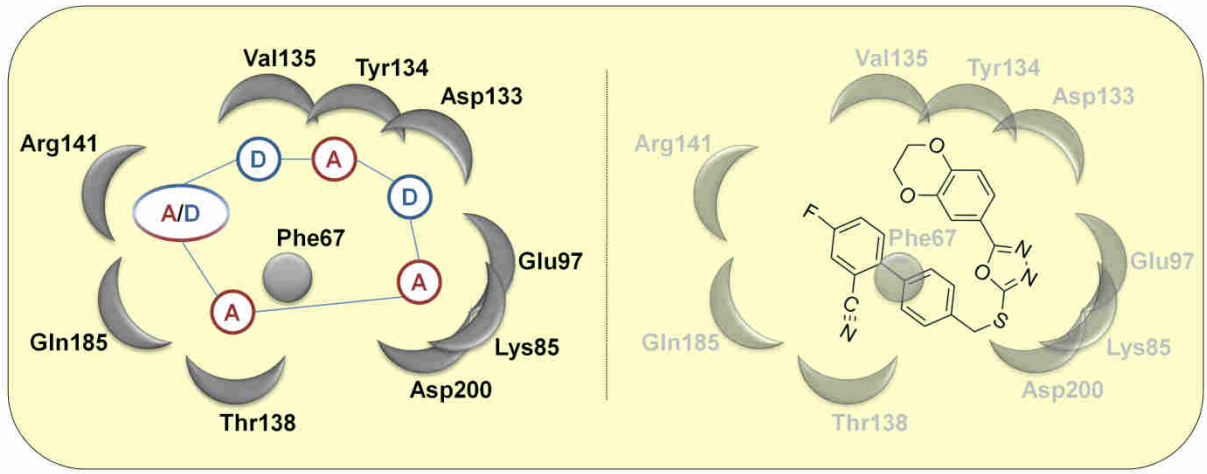

Abb. 38: Schematische Darstellung der ATP-Bindungstasche von GSK-3. Hervorgehoben sind die für die Aktivität und Selektivität von potentiellen ATP-kompetitiven Inhibitoren wichtigen Aminosäuren. Links: Eine regionale Einteilung potentieller Inhibitoren in Wasserstoffakzeptoren (A) und Wasserstoffdonatoren (D). Rechts: Zur Veranschaulichung wurde mit **15b** ein potenter GSK-3-Inhibitor eingefügt. Mit dem Strukturmotiv von **15b** werden alle wichtigen Interaktionen ausgefüllt.

Um theoretische Daten experimentell zu untermauern, diente das Strukturmotiv der 1-Aryl-3-benzylharnstoffe als Basis. Die gezielte Verwendung unterschiedlicher *building blocks*, die Etablierung einer chromatographiefreien Aufarbeitung und die weitere Derivatisierung durch Suzukireaktionen bzw. Mikrowellen-unterstützte Reaktionsführung ermöglichte die Synthese diverser Harnstoffe innerhalb kürzester Zeit. Die erhaltenen Strukturaktivitätsbeziehungen stimmten mit den theoretischen Daten überein. Darüber hinaus konnten Harnstoffe mit gesteigerter Aktivität (zweistelliger nanomolarer Bereich) und geringerer Toxizität im Vergleich zur Referenz **AR-A014418** synthetisiert werden. Die Synthese von Imidazo[4,5-*b*]pyridin-2-aminderivaten als EU-Projektziel, mögliche patentierbare Leitstruktur und

heterozyklische Strukturvarianz zum Harnstoffmotiv war erfolgreich, Abb. 39. Jedoch wiesen diese eine verringerte Löslichkeit sowie eine geringe Aktivität bezüglich GSK-3 auf. Ein neuer Ansatz war die Synthese und biochemische Evaluation von Oxadiazolbenzylen (**11**). Dafür konnte eine relativ schnelle, kostengünstige Synthese etabliert werden, Abb. 40.

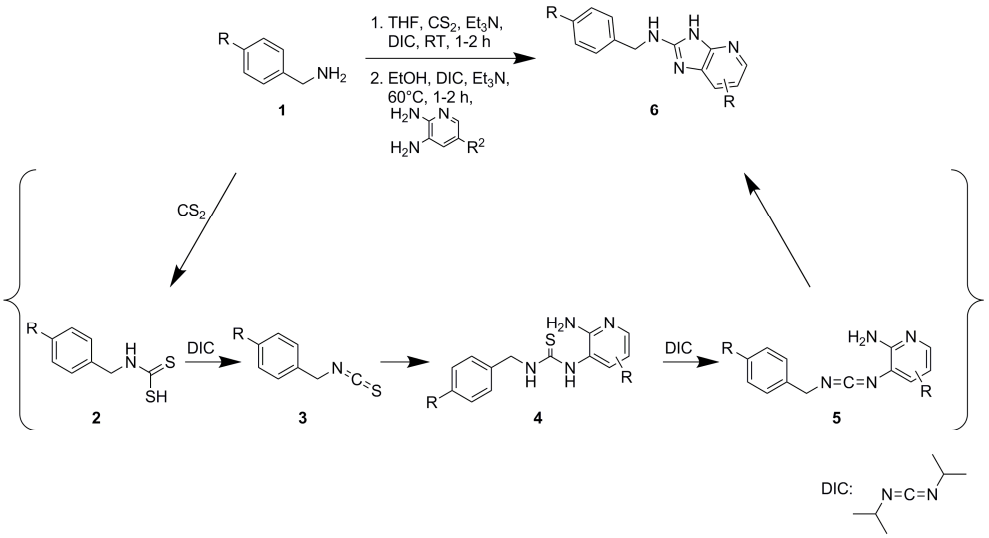

Abb. 39: Etablierte Syntheseroute von Imidazo[4,5-*b*]pyridin-2-aminderivaten (**6**); R = alkylische/ funktionelle Reste.

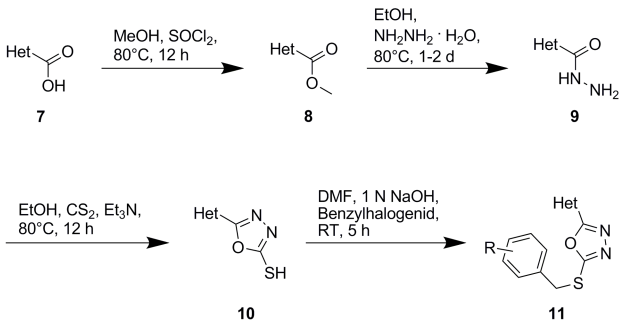

Abb. 40: Etablierte Syntheseroute von Oxadiazolbenzylen (**5**); Het = Heterozyklen; R = alkylische/ arylische/funktionelle Reste.

Die dabei erhaltenen biphenylischen Derivate inhibieren GSK-3 größtenteils im einstelligen nanomolaren Bereich und erzielten eine nie zuvor realisierte isoenzymatische Selektivität bzgl. GSK-3α (bis zu 92-fach gegenüber GSK-3β). Dockingstudien von Oxadiazolbiphenylderivaten konnten zwar eine sehr gute Interaktion mit den relevanten Aminosäuren der ATP-Bindungstasche nachweisen, Abb. 38 rechts, jedoch keinen Aufschluss über deren α-Selektivität liefern. Eine Symbiose des Harnstoff- und Oxadiazolbiphenylmotivs sollte das Interaktionsmuster, Abb. 38 links, noch weiter intensivieren. Im Fall eines Pyridinamidderivates, Abb. 31,

scheint dieses erfolgreich gewesen zu sein. Es resultierten verglichen mit den Derivaten ohne Amid eine Löslichkeits- und Aktivitätssteigerung (10-fach höhere GSK-3α-Inhibition). Die *in vivo* Aktivität der Oxadiazolbiphenylderivate wurde in einem eigens vor Ort etablierten *zebrafish embryo phenotype assay* bestätigt. Es konnten die für eine GSK-3-Inhibition typischen Veränderungen, wie fehlende Augenpigmentierung und ein verkürztes bzw. gekrümmtes Rückgrat der Zebrafischembryos, bestimmt werden. Abschließend konnte durch die Applikation von Oxadiazolbiphenylderivaten in stabil mit Tau.P301L transfizierten SH-SY5L-Neuroblastomzellen eine verringerte Phosphorylierung am Tau-Protein erzielt werden. Die Oxadiazolderivate wurden bereits zum Patent angemeldet.

Um neue Kinase-/Diagnostikprojekte zu initiieren und zu etablieren wurde im Fall von LRRK2 eine Datenanalyse durchgeführt. Die wichtigsten Daten wurden zusammengefasst und zukünftige Syntheseprojekte vorbereitet. Zudem wurde eine gezielte Derivatisierung von dualspezifischen CK1/γ-Sekretase-Inhibitoren, die eine inhibitorische Aktivität bezüglich FLT-3 aufwiesen, durchgeführt. Die dabei synthetisierten selektiven Indolinonderivate hemmen FLT-3 mit IC_{50} Werten im niedrigen zweistelligen bis zum einstelligen nanomolaren Bereich. Im Fall der NFT-Marker ergaben die wasserlöslichen, fluoreszierenden 2-Styrylindoliumderivate weitaus bessere Tau-Affinitätswerte als zuvor publizierte Marker, wie **Methoxy-X04** oder **^{11}C-PIB**.

5 Ausblick

Die Verbesserung der pharmakologischen Eigenschaften der Oxadiazolbiphenyle ist eines der zukünftigen Ziele. Eines der Parameter, die dabei ins Gewicht fallen, ist der ClogP. Dieser sollte laut der Lipinski „*rule of five*“ und dem CNS-MPO-Modell weniger als 5 betragen. Der ClogP einer Vielzahl der synthetisierten Oxadiazolbiphenyle liegt in dem Bereich um 5 und ist somit grenzwertig. Möglichkeiten zur Erniedrigung des ClogP wären beispielsweise die Oxidation des Schwefels zum Sulfonyl (**12**) oder der Austausch eines Phenylrings des Biphenyls durch einen Heterozyklus (**13**-**14**), Abb. 41.

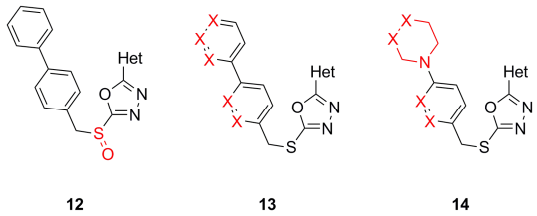

Abb. 41: Potentielle Derivatisierungsstellen zur Verbesserung des pharmakologischen Profils der Oxadiazolbiphenylderivate; Het = Heterozyklen; X = Heteroatom.

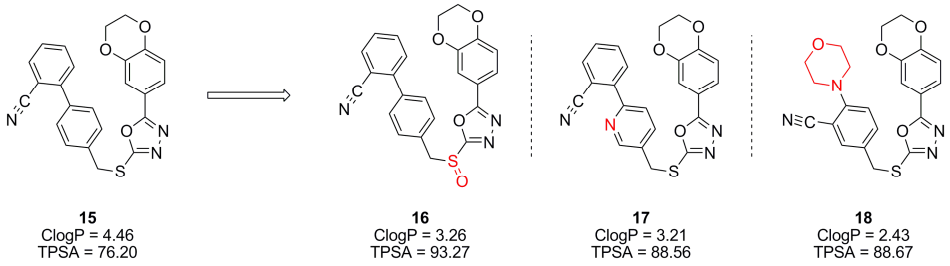

Abb. 42: Potentielle Derivatisierung zur Verbesserung des pharmakologischen Profils am konkreten Beispiel des Oxadiazolbiphenylderivats **15**.

Eine Berechnung des ClogP am konkreten Beispiel des Oxadiazolbiphenylderivats **15** ergab eine signifikante Erniedrigung in allen Fällen (**16**-**18**), Abb. 42. Zudem befindet sich der berechnete TPSA im bevorzugten Rahmen von 40 bis 90 (CNS-MPO). Desweiteren könnte eine Substitution am Biphenylrest die Löslichkeit verbessern, Abb. 43. Dabei stellen Löslichkeitslinker, wie Ethylenglykolreste oder alkylierte Amine, eine Möglichkeit dar. Neben der Löslichkeitsverbesserung könnte eine Substitution in para-Position weitere Einblicke in deren isoenzymatische Selektivität bringen, Abb. 43 A), D).

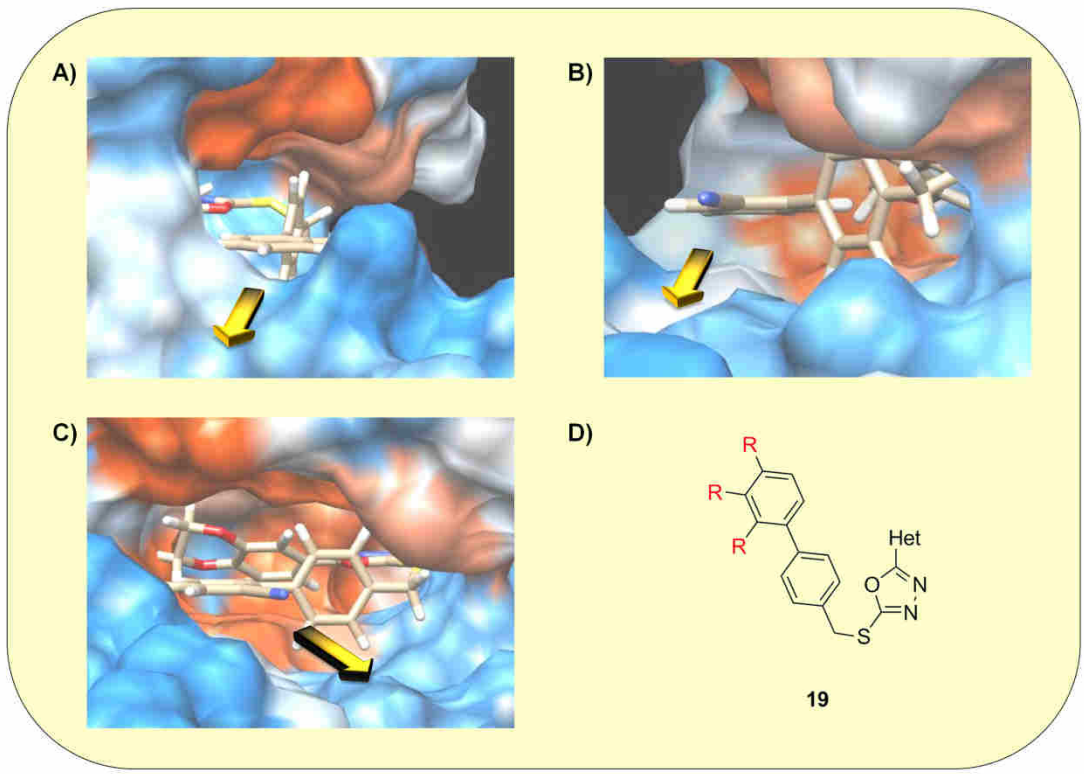

Abb. 43: Schematische Darstellung potentieller Substitutionsmöglichkeiten/-richtungen am Biphenyl **19** in einer Dockingstudie vom Oxadiazolbiphenylderivat **15** gedockt in die ATP-Bindungstasche von GSK-3β (Verwendete Software: Molegro Virtual Docker 5 und Chimera 1.6.2; PDB Code = 3F88).[239]

Darüber hinaus könnten Co-Kristallisationen nicht isoenzymspezifischer Oxadiazolbiphenylderivate mit GSK-3α und GSK-3β verglichen mit denen von GSK-3α-selektiven Strukturanaloga entscheidende Konformationsänderungen aufdecken. Diese würden eventuell eine zielgerichtetere Synthese von GSK-3α- und GSK-3β-spezifischen Inhibitoren ermöglichen. Zudem könnte eine Substitution des para-ständigen Fluors in Verbindung **15b** durch ^{18}F für *in vitro*/*in vivo* Markierungen verwendet werden. Die Oxadiazolbiphenylderivate weisen zwar eine für ATP-kompetitive Kinaseinhibitoren typische Struktur auf, jedoch sollte dies in kinetischen Studien noch belegt werden.

Neuartige GSK-3-Inhibitoren könnten eventuell auf der Basis von Pyridin-/Pyrimidin-derivaten **20**/**23** erzielt werden, Abb. 44. Die in Abb. 44 links dargestellten Pyridinderivate **24**/**25** weisen einen sehr niedrigen ClogP auf. Wenn sich die ersten Grundstrukturen als relativ aktiv gegenüber GSK-3 erweisen, stünde einer späteren Derivatisierung auch mit hydrophoberen Resten (die glycinreiche Schleife betreffend) nichts im Wege.

Das GSK-3 bis heute ein pharmazeutisches Target ist, beweist die permanente Veröffentlichung neuer Inhibitoren. Selbst eine Reihe neuer Harnstoffe wurde erst kürzlich patentiert.[312] Wird der Zusammenhang von GSK-3 mit den diversen metabolischen Mechanismen in Betracht gezogen, ist dies nur allzu verständlich.

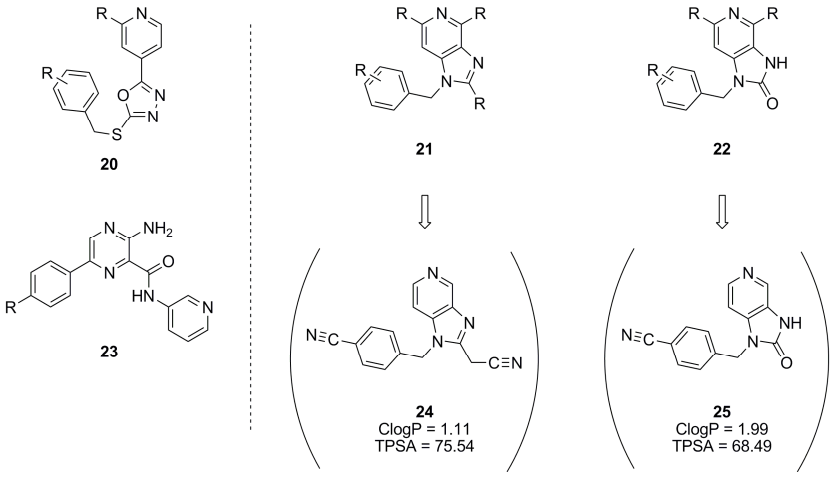

Abb. 44: Links: Referenzstrukturmotiv publizierter GSK-3-Inhibitoren; Rechts: Potentielle Pyridinderivate als mögliche GSK-3-Inhibitoren.[313-315]

6 Experimenteller Teil – Ein Auszug

Die verwendeten Chemikalien wurden bei den Anbietern Acros Organics, Alfa Aesar, Apollo Scientific, Fischer Scientific, Fluka, Merck, ABCR und Sigma-Aldrich erworben. Die absoluten Lösungsmittel wie beispielsweise DMF und THF wurden von Acros Organics in mit Septum versiegelten Flaschen gekauft und direkt eingesetzt. Wasserfreies Methanol und Ethanol wurden durch Destillation über Magnesium erhalten und über 3 Å Molekularsieb gelagert.

Zur Säulenchromatographie wurde Kieselgel 60 mit Korngrößen zwischen 0,04-0,06 mm der Firma Merck verwendet. Die Dünnschichtchromatographie (DC) wurde unter Verwendung von DC-Aluminiumfolien mit Kieselgel 60 F254 der Firma Merck durchgeführt. Die entwickelten DC-Chromatogramme wurden unter UV-Licht (254 und 366 nm) ausgewertet. Zum Einfärben der Platten wurde bei Bedarf eine Ninhydrin-, Vanillin- oder Kaliumpermanganatlösung sowie Iod verwendet (1. 1 g Ninhydrin in 180 mL EtOH und 10 mL Essigsäure; 2. 1 g Vanillin in 170 mL MeOH, 20 mL Essigsäure und 10 mL konz. Schwefelsäure; 3. Kaliumpermanganat 1 gew.% in dest. Wasser; 4. Elementares Iod). HPLC-Messungen erfolgten an einem Agilent 1100 (Säule: *reversed phase*, Zorbax Eclipse XDBC8, 4.6 x 150 mm, Wellenlängendetektion bei 254 nm). Als Laufmittel wurde Acetonitril und Wasser in verschiedenen Gradientenmischungen verwendet.

Sämtliche Messungen der ^{1}H und ^{13}C-NMR-Spektren wurden mit den Spektrometern ARX 300 und DRX 500 der Firma Bruker Biospin GmbH aufgenommen. Die jeweilige Messfrequenz und das verwendete Lösungsmittel sind den spektroskopischen Daten in Klammern vorangestellt. Die chemischen Verschiebungen δ sind in ppm tieffeldverschoben zu Tetramethylsilan als interner Standard (δ = 0 ppm) angegeben. Zur Bezeichnung der Feinstrukturen der Protonensignale wurden folgende Abkürzungen verwendet: s (Singulett), d (Duplett) und t (Triplett). Die Kopplungskonstanten *J* werden in Hz angegeben. Die Auswertung der Spektren erfolgte mit der Software MestReNova der Firma Mestrelab Research. Zur Bestimmung der massenspektrometrischen Daten wurden ESI-MS-Spektren mit einem Bruker-Franzen Esquire LC Massenspektrometer und EI-MS-Spektren mit

einem doppelt fokussierenden Massenspektrometer MAT 95 aufgenommen. Die detektierten Ionenmassen m/z werden in u angegeben.

6.1 Ein Auszug der *supporting information* zur Publikation aus Kapitel 5.2

Supplementary Material (ESI) for Bioorganic & Medicinal Chemistry Letters

Supporting Information

Synthesis and biological evaluation of glycogen synthase kinase 3 (GSK-3) inhibitors: a fast and atom efficient access to 1-aryl-3-benzylureas

Fabio Lo Monte*[a], Thomas Kramer*[a], Alexander Boländer[a], Batya Plotkin[b], Hagit Eldar-Finkelman[b], Ana Fuertes[c], Juan M. Dominguez[c] and Boris Schmidt†[a]

[a] Clemens Schöpf - Institute of Organic Chemistry and Biochemistry, Technische Universität Darmstadt, 64287 Darmstadt, Hessen, Germany, Fax: ı496151-163278; Tel: ı496151-164531;
[b] Department of Human Molecular Genetics and Biochemistry, Sackler School of Medicine, Tel Aviv University, Tel Aviv 69978, Israel,
[c] Noscira S. A. Tres Cantos 28760, Madrid, Spain
† E-mail: schmidt_boris@t-online.de
*These authors contributed equally to this work.

Content:

General procedure

1.) Synthesis of the urea derivatives

The amine (0.80 mmol) was added to a stirred mixture of 5 ml saturated sodium bicarbonate solution ($NaHCO_3$) and 5 ml dichloromethane (DCM) at 0 °C. Afterwards triphosgene (0.28 mmol) was added slowly. After 2.5 h at 0 °C 10 ml of DCM were added and the organic layer separated from the aqueous phase. The aqueous phase was washed twice with 10 ml of DCM. The combined organic layers were washed with ammonium chloride (NH_4Cl) and brine and later dried over sodium sulfate, filtered and concentrated to approximately 0.5 ml.

To the residue was added dry tetrahydrofuran (THF, 1.5 ml). It was added dropwise to a solution of n-buthyllithium (0.80 mmol, 1.6 M in n-Hexane) deprotonated amine (0.80 mmol) in 1.5 ml tetrahydrofuran and stirred at room temperature overnight. The reaction solution was added to a vigorous stirred water to give the solid crude urea. The solid was filtered off and recrystallised from methanol or ethanol.

2.) Suzuki coupling

An urea derivative with a bromo substituent (0.15 mmol), boronic acid (0.19 mmol), sodium ethoxide (0.31 mmol) and 1 mol-% of palladium acetate or 1 mol-% of tetrakis(triphenylphosphine)palladium(0) were suspended in 1 ml dry ethanol and stirred for 0.5 - 3 h at 110 °C. Afterwards the solution was filtered and the solvent evaporated. The residue was added to water and extracted three times with ethyl acetate. The combined organic layers were dried over sodium sulfate, filtered and the solvent was evaporated. The solid was recrystallised from ethanol or methanol.

3.) Microwave synthesis

Entry **9**, 1**2**, **13** or **29** (0.10 mmol), sodium azide (NaN_3, 1.20 mmol) and ammonium chloride (NH_4Cl, 1.20 mmol) were added to 1 ml of *N*,*N*-dimethylformamide (DMF) and stirred for 2 h at 100 °C under microwave irradiation. After cooling to room temperature the reaction solution was added to water, acidified with 2 N HCl and extracted three times with ethyl acetate. The combined organic layers were dried over sodium sulfate, filtered and the solvent evaporated off to provide the product.

GSK-3β *in vitro* assay

Purified GSK-3β (0.5 µg) was incubated in a reaction mixture of 50 mM Tris pH 7.3, 10 mM MgAc, 0.01% β-mercaptoethanol, ^{32}P[γ-ATP](100µM, 0.5 µci/assay), and 100 µM of peptide substrate, pIRS-1 (RREGGMSRPAS(p)VDG (1). **New molecules** were added at various concentrations (1, 10 and 100 µM), and the reaction mixture was incubated for 15 min at 30^{o}C. The reactions were stopped, spotted on p81 paper (Whathman), washed with 10 mM phosphoric acid, and counted for radioactivity as described (1). GSK-3β activity was calculated as the percentage of GSK-3β activity in the absence of inhibitors that was designated to 100%.

Kinase Panel:

Compounds are serially diluted 1/3 in neat DMSO (10 serial dilutions) and these dilutions are further diluted 1/25 with reaction buffer. 2.5µl of these solutions are added to the reaction mixture described below so that final compound concentration in the assay ranges from 100 µM to 5 nM in 1% (v/v) DMSO. The enzymatic activity of the kinases is determined with a commercial system based on the Z'-LYTE® technology, available from Invitrogen Life Technologies (Carlsbad, CA, USA), using human recombinant kinases as the enzyme source. This technology utilizes the fluorescence resonance energy transfer ("FRET") process between fluorescein and coumarin. The assay principle is based on the differential sensitivity of phosphorylated and non-phosphorylated peptide to proteolytic cleavage, which precludes the energy transfer process between the two fluorophores attached to both sides of the cleavage site. Hence, enzymatic phosphorylation will yield a phosphopeptide, which cannot be hydrolyzed by a suitable protease and energy transfer between the two fluorophores will occur. Opposingly, lack of phosphorylation will cause peptide hydrolysis hence lack of energy transfer as.
The assay is performed in 96-well black plates, in a final volume of 10 µl, with components as detailed in Table 1.

Table 1

Kinase	Enzyme conc. (nM)	ATP conc. (μM)	Peptide used	Peptide conc. (μM)	Buffer
GSK3β	0.54	26	Ser/Thr 9 peptide	2	50 mM Hepes pH 7.5, 10 mM $MgCl_2$, 1 mM EGTA, 0.01% (w/v) Brij-35
CKIε	18.84	32	Ser/Thr 11 peptide	2	50 mM Hepes pH 7.5, 10 mM $MgCl_2$, 1 mM EGTA, 0.01% (w/v) Brij-35
Cdk5	15.9	12.5	Ser/Thr 12 peptide	2	50 mM Hepes pH 7.5, 10 mM $MgCl_2$, 1 mM EGTA, 0.01% (w/v) Brij-35
AurKA	20	10	Ser/Thr 1 peptide	2	50 mM Hepes pH 7.5, 20 mM $MgCl_2$, 1 mM EGTA, 0.01% (w/v) Brij-35
PKCα	1.04	1	Ser/Thr 7 peptide	2	50 mM Hepes pH 7.5, 10 mM $MgCl_2$, 1 mM EGTA, 0.01% (w/v) Brij-35

6.2 Synthese des Thioharnstoffderivats zu Kapitel 5.2.1

AAV 1 für die Synthese der Thioharnstoffderivate (26)

1.0 eq. des 6-Aminonicotiononitrils wird in trockenem THF (2-3 mL) gelöst. Es werden 1.3 eq. Natriumhydrid (60%) hinzugegeben. Die Reaktionslösung wird 30 min. bei RT gerührt. Anschließend wird sie auf 0°C abgekühlt. Ein Lösung des 1-(Isothiocyanatomethyl)-4-methoxybenzens (1.0 eq.) gelöst in 1 mL trockenem THF wird bei gleichbleibender Temperatur von 0°C langsam zugetropft. Die resultierende Reaktionslösung wird über Nacht bei RT gerührt. Nach erfolgter Umsetzung wird die Reaktionslösung auf Wasser (50-100 mL) gegeben. Die Suspension wird filtriert. Der Feststoff wird mit Wasser gewaschen und in EtOH umkristallisiert.

Produktbeispiel: *1-(5-Cyanopyridin-2-yl)-3-(4-methoxybenzyl)thioharnstoff* (**BSc4247**)

Es resultieren 67% eines farblosen Feststoffs.

HPLC t_R: 6.92 min.

^{1}H-NMR (300 MHz, DMSO-d6): δ [ppm] = 3.72 (3H, s), 4.82 (2H, d, *J* = 5.4 Hz), 6.91 (2H, d, *J* = 8.5 Hz), 7.29 (3H, m), 8.17 (1H, dd, *J* = 8.7 Hz, *J* = 2.1 Hz), 8.64 (1H, d, *J* = 1.8 Hz), 11.11 (1H, s), 11.61 (1H, t, *J* = 5.2 Hz).

^{13}C-NMR (75 MHz, DMSO-d6): δ [ppm] = 47.5, 55.0, 101.7, 112.6, 113.8, 117.1, 128.7, 129.6, 141.5, 150.7, 155.1, 158.4, 179.5.

EI-MS: m/z: 298 (M^+).

6.3 Synthese der Guanidinderivate zu Kapitel 5.2.1

AAV 2 für die Synthese der Guanidinderivate (27)

1.0 eq. des Thioharnstoffs **26** und 1.5 eq. des Alkyl-/Benzylhydroxylamins werden in 1 mL trockenem DMF gelöst. Hinzugefügt werden 4.0 eq. TEA und 1.1 eq. $HgCl_2$. Die Reaktionssuspension wird über Nacht bei RT gerührt. Anschließend wird sie mit EE (20 mL) aufgenommen und über Celite® filtriert. Das Lösungsmittel wird im Vakuum entfernt und der Rückstand wird säulenchromatographisch gereinigt (EE/Cy – 1.5 : 1).

Produktbeispiel: *(E/Z)-1-(5-Cyanopyridin-2-yl)-2-methoxy-3-(4-methoxybenzyl) guanidin* (**BSc4470**)

Es resultieren 86% eines leicht gelblichen Feststoffs.

R_f: 0.50.

HPLC t_R: 3.62 min.

^{1}H-NMR (500 MHz, DMSO-d6): δ (ppm) = 9.34 (s, 1H), 9.11 (s, 1H), 8.54 (d, *J* = 2.3 Hz, 1H), 8.50 (d, *J* = 2.0 Hz, 1H), 8.03 (dd, *J* = 8.8, 2.3 Hz, 1H), 7.95 (t, *J* = 5.7 Hz, 1H), 7.86 (dd, *J* = 8.8, 2.1 Hz, 1H), 7.32 (d, *J* = 8.9 Hz, 1H), 7.29 (d, *J* = 8.7 Hz, 2H), 7.10 (d, *J* = 8.4 Hz, 1H), 6.97 (d, *J* = 8.9 Hz, 1H), 6.90 (d, *J* = 8.6 Hz, 2H), 6.81 (d, *J* = 8.5 Hz, 2H), 6.52 (t, *J* = 6.4 Hz, 1H), 4.17 (d, *J* = 5.6 Hz, 2H), 4.11 (d, *J* = 6.4 Hz, 1H), 3.74 (s, 3H), 3.70 (s, 2H), 3.64 (s, 2H), 3.62 (s, 3H).

^{13}C-NMR (126 MHz, DMSO-d6): δ (ppm) = 158.28, 158.18, 158.07, 155.98, 152.43, 151.06, 148.72, 148.05, 140.70, 140.23, 132.28, 131.33, 128.65, 128.16, 118.12, 117.59, 113.69, 113.59, 112.40, 109.10, 99.91, 98.34, 60.83, 60.55, 55.00, 44.40, 43.85.

EI-MS: m/z: 311 (M^+).

6.4 Synthese der Imidazo[4,5-*b*]pyridin-2-aminderivate zu Kapitel 5.2.1

AAV 3 für die Synthese der Imidazo[4,5-*b*]pyridin-2-aminderivate (28)

Zu einer Lösung bestehend aus 1 mL trockenem THF, 1.0 eq. eines Benzylamins und 3.3 eq. TEA wird 1eq. CS_2 hinzugefügt. Die Reaktionslösung wird 1-2 h bei RT gerührt. 1.2 eq. DIC werden hinzugefügt und über Nacht bei RT gerührt. Die Reaktionslösung wird filtriert und zu einer Lösung bestehend aus 1 mL trockenem EtOH, 1.1 eq. eines Diaminopyridins und 1.0 eq. DIC hinzu getropft. Anschließend wird die Reaktionslösung bei 60°C für 4-5 h gerührt. Die entstandene Suspension wird kalt filtriert und der Rückstand in EtOH umkristallisiert.

Produktbeispiel: *6-Bromo-N-(4-methoxybenzyl)-1H-imidazo[4,5-b]pyridin-2-amin* (**BSc4458**)

Es resultieren 48% eines leicht gräulichen Feststoffs.

HPLC t_R: 2.93 min.

^{1}H-NMR (300 MHz, DMSO-d6): δ (ppm) = 7.91 (s, 1H), 7.58 (s, 1H), 7.53 (d, *J* = 2.0 Hz, 1H), 7.29 (d, *J* = 8.7 Hz, 2H), 6.88 (d, *J* = 8.7 Hz, 2H), 4.45 (d, *J* = 6.1 Hz, 2H), 3.71 (s, 3H) (Hinweis: NH nicht erkennbar).

^{13}C-NMR (75 MHz, DMSO-d6): δ (ppm) = 128.56, 113.67, 55.03, 44.70 (Hinweis: Heterozyklische C-Atome nicht erkennbar).

EI-MS: m/z: 332 (M^+).

6.5 Synthese der Amid-/Sulfonamidderivate zu Kapitel 5.2.1

AAV 4 für die Synthese der Amid-/Sulfonamidderivate (29/30)

Eine Lösung bestehend aus 1.0 eq. eines Thiazolamins bzw. Benzothiazolamins 3.0 eq. TEA, einer katalytischen Menge an DMAP und 1 mL trockenem DCM bzw. EE wird auf 4°C abgekühlt. Es wird bei gleichbleibender Temperatur eine Lösung aus 2 eq. eines Benzoylchlorids bzw. 1.0 eq. eines Sulfonylchlorids gelöst in 1 mL trockenem DCM bzw. EE langsam hinzugetropft. Anschließend wird die Reaktionslösung bei 40°C über Nacht gerührt. Nach erfolgter Umsetzung wird die Reaktionslösung mit 30 mL DCM bzw. EE aufgenommen und mit einer gesättigten Natriumchloridlösung gewaschen. Das organische Lösungsmittel wird mit Natriumsulfat versetzt, filtriert und im Vakuum entfernt. Der resultierende Feststoff wird in einem Lösungsmittelgemisch aus EE und Cy umkristallisiert.

Amidproduktbeispiel: *4-Nitro-N-(5-nitrothiazol-2-yl)benzamid* (**BSc4475**)

Es resultieren 74% eines orangefarbenen Feststoffs.

HPLC t_R: 6.69 min.

^{1}H-NMR (300 MHz, DMSO-d6): δ (ppm) = 8.58 (s, 1H), 8.38 - 8.29 (m, 4H) (Hinweis: NH Signal nicht erkennbar).

^{13}C-NMR (75 MHz, DMSO-d6): δ (ppm) = 170.71, 169.21, 149.03, 144.94, 141.75, 138.25, 129.68, 123.36.

EI-MS: m/z: 294 (M^+).

Sulfonamidproduktbeispiel: *4-Nitro-N-(5-nitrothiazol-2-yl)benzensulfonamid* (**BSc4468**)

Es resultieren 68% eines gelben Feststoffs.

HPLC t_R: 6.14 min.

^{1}H-NMR (500 MHz, DMSO-d6): δ (ppm) = 8.36 - 8.29 (m, 2H), 8.24 (s, 1H), 8.06 - 7.99 (m, 2H). (Hinweis: NH Signal nicht erkennbar).

^{13}C NMR (126 MHz, DMSO-d6): δ (ppm) = 146.55, 127.28, 124.10 (Hinweis: Nur aromatische C-Atome erkennbar).

EI-MS: m/z: 330 (M^+).

6.6 Ein Auszug der *supporting information* zur Publikation aus Kapitel 5.3

SUPPORTING INFORMATION

Identification of Glycogen Synthase Kinase-3 Inhibitors with a Selective Sting for Glycogen Synthase Kinase-3α

Fabio Lo Monte,[a,] Thomas Kramer,[a] Jiamin Gu,[a] Upendra Rao Anumala,[a] Luciana Marinelli,[b] Valeria La Pietra,[b] Ettore Novellino,[b] Bénédicte Franco,[c] David Demedts,[c] Fred Van Leuven,[c] Ana Fuertes,[d] Juan Manuel Dominguez,[d] Batya Plotkin,[e] Hagit Eldar-Finkelman[e] and Boris Schmidt[a,]**

[a] Clemens Schöpf - Institute of Organic Chemistry and Biochemistry, Technische Universität Darmstadt, 64287 Darmstadt, Germany

[b] Dipartimento di Chimica Farmaceutica e Tossicologica, Università di Napoli "Federico II", 80131 Napoli, Italy

[c] Experimental Genetics Group, Department of Human Genetics, Katholieke Universiteit Leuven, 3000 Leuven, Belgium

[d] Noscira S.A., Drug Discovery, Tres Cantos 28760 - Madrid, Spain

[e] Department of Human Molecular Genetics and Biochemistry, Sackler School of Medicine, Tel Aviv University, 69978 Tel Aviv, Israel

* To whom correspondence should be addressed. Phone: +496151-164531.
Fax: +496151-163278.
E-Mail: schmidt_boris@t-online.de; Fabio.Lo-Monte@gmx.de

Table of contents

Homology Modeling

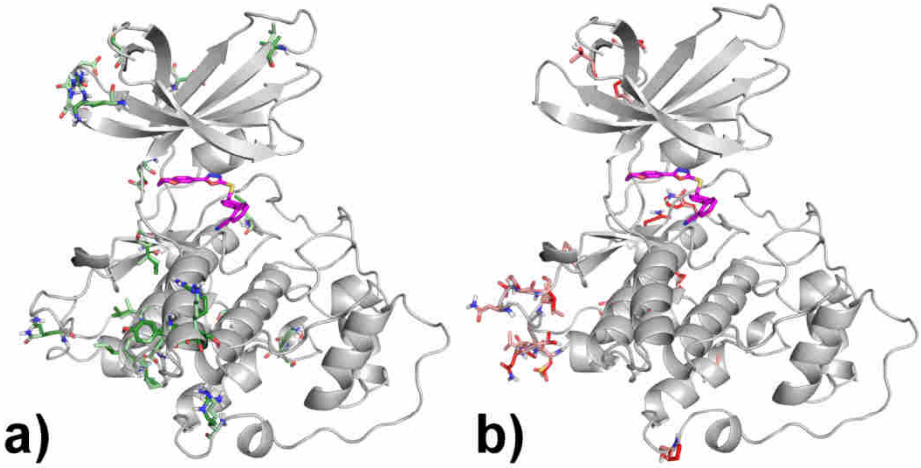

Figure S1. Superposition of 3D structure of GSK-3β (PDB code 3F88) and the homology-based 3D structure of GSK-3α. Both proteins are shown as white cartoons; conservative mutations are displayed as forest and light green stick, for GSK-3β and GSK-3α respectively (**a**), while non-conservative mutations are represented as red and pink sticks, for GSK-3β and GSK-3α respectively (**b**). It is evident that the majority of the mutations are located at the loop at the C-terminus fragment of the proteins (D345-T363 in GSK-3β and R407-A427 in GSK-3α).

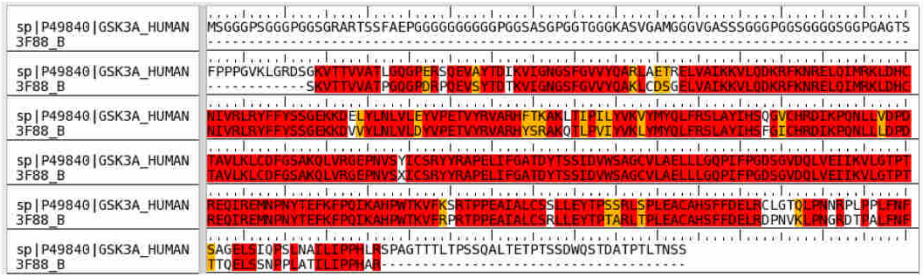

Figure S2. Alignment between GSK-3α (Swiss-Prot code: P49840) and GSK-3β sequences (PDB code: 3F88). Identical residues are colored in red, conservative residues in orange, while non-conservative residues are not painted. Gaps are represented as dashes.

***In Vitro* Pharmacology: Screening of compound 14d**

The ExpresS Diversity kinase profile is a fast turnaround profile conducted by Cerep. Percentage kinase activities with compound **14d** at one concentration (1 μM) in panels of human protein kinases determined by Cerep. Measurements were performed in duplicate and the average was taken.

CHK1	118,1		**FGFR2**	100,8
SIK	113,6		**JAK3**	100,8
Src	111,4		**ROCK1**	100,7
CaMK2α	110,4		**FLT-3**	100,2
KDR	110,4		**NEK2**	100,2
MNK2	107,8		**EGFR**	99
MST4	105,8		**ERK2**	98,9
MAPKAPK2	105,5		**PKCb2**	98,7
PDK1	105,2		**AurA/Aur2**	98,6
p38α	105		**HGK**	98,6
SGK1	104,6		**Akt1/PKBα**	98,1
JNK1	104,5		**CDK2**	97,4
MKK6	104,5		**PKA**	97,4
CDK1	104,4		**EphA2**	97,1
FGFR3	104,4		**EphA3**	96,1
Lck	104,4		**Abl**	95,7
PAK2	104,2		**FGFR1**	95,6
PAK4	103,9		**EphB4**	91,4
MARK1	103,2		**RAF-1**	91,4
IRK	102,6		**CHK2**	89,8
Pim2	102,6		**c-Met**	89,1
TRKA	102,4		**PLK1**	84,2
IKKα	102,3		**IRAK4**	83,3
TAOK2	101,3		**GSK-3β**	27,2
CK1α	100,9		**GSK-3α**	5

Assay Kinases	Source	Substrate/Stimulus/Tracer	Incubation	Measured Component
Abl kinase (h)	human recombinant (insect cells)	ATP + Ulight-TK peptide (100 nM)	60 min RT	phospho-Ulight-TK-peptide
Akt1/PKBα (h)	human recombinant (insect cells)	ATP + CREBtide (CKRREILSRRPSYRK) (25 nM)	60 min RT	phospho-CREBtide (CKRREILSRRPSYRK)
AurA/Aur2 kinase (h)	human recombinant (Sf21 cells)	ATP + Ulight-RRRSLLE (100 nM)	15 min RT	phospho-Ulight-RRRSLLE
CaMK2α *(h)*	human recombinant	ATP + Ulight-CGSGSGRPRTSSFAEG (50 nM)	30 min RT	phospho-Ulight-CGSGSGRPRTSSFAEG
CDC2/CDK 1 (h) (cycB)	human recombinant (insect cells)	ATP + Ulight-CFFKNIVTPRTPPPSQGK-amide (100 nM)	15 min RT	phospho-Ulight-CFFKNIVTPRTPPPSQGK-amide
CDK2 *(h)* (cycA)	human recombinant	ATP + Ulight-CFFKNIVTPRTPPPSQGK-amide (50 nM)	30 min RT	phospho-Ulight-CFFKNIVTPRTPPPSQGK-amide
CHK1 *(h)*	human recombinant (insect cells)	ATP + CREBtide (CKRREILSRRPSYRK) (25 nM)	30 min RT	phospho-CREBtide (CKRREILSRRPSYRK)
CHK2 *(h)*	human recombinant (insect cells)	ATP + CREBtide (CKRREILSRRPSYRK) (25 nM)	15 min RT	phospho-CREBtide (CKRREILSRRPSYRK)
CK1α *(h)*	human recombinant	ATP + Ulight-ARTKQTARKSTGGKAPRKQLAGCG (25 nM)	60 min RT	phospho-Ulight-ARTKQTARKSTGGKAPRKQLAGCG
c-Met kinase *(h)*	human recombinant (insect cells)	ATP + Ulight-CAGAGAIETDKEYYTVKD (25 nM)	60 min RT	phospho-Ulight-CAGAGAIETDKEYYTVKD
EGFR kinase *(h)*	human recombinant (insect cells)	ATP + Ulight-CAGAGAIETDKEYYTVKD (100 nM)	15 min RT	phospho-Ulight-CAGAGAIETDKEYYTVKD
EphA2 kinase *(h)*	human recombinant	ATP + Ulight-TK peptide (50 nM)	30 min RT	phospho-Ulight-TK-peptide
EphA3 kinase *(h)*	human recombinant	ATP + Ulight-TK peptide (50 nM)	60 min RT	phospho-Ulight-TK-peptide
EphB4 kinase *(h)*	human recombinant (insect cells)	ATP + Ulight-TK peptide (100 nM)	90 min RT	phospho-Ulight-TK-peptide

ERK2 *(h)* ($P42^{mapk}$)	human recombinant (*E. coli*)	ATP + Ulight-CFFKNIVTPRTPPPSQGK-amide (100 nM)	15 min RT	phospho-Ulight-CFFKNIVTPRTPPPSQGK-amide
FGFR1 kinase *(h)*	human recombinant (insect cells)	ATP + Ulight-CAGAGAIETDKEYYTVKD (100 nM)	60 min RT	phospho-Ulight-CAGAGAIETDKEYYTVKD
FGFR2 kinase *(h)*	human recombinant	ATP + Ulight-CAGAGAIETDKEYYTVKD (25 nM)	15 min RT	phospho-Ulight-CAGAGAIETDKEYYTVKD
FGFR3 kinase *(h)*	human recombinant	ATP + Ulight-CAGAGAIETDKEYYTVKD (100 nM)	90 min RT	phospho-Ulight-CAGAGAIETDKEYYTVKD
FLT-3 kinase *(h)*	human recombinant (insect cells)	ATP + Ulight-CAGAGAIETDKEYYTVKD (100 nM)	90 min RT	phospho-Ulight-CAGAGAIETDKEYYTVKD
GSK3α *(h)*	human recombinant	ATP + Ulight-CFFKNIVTPRTPPPSQGK-amide (100 nM)	60 min RT	phospho-Ulight-CFFKNIVTPRTPPPSQGK-amide
GSK3β *(h)*	human recombinant	ATP + Ulight-CFFKNIVTPRTPPPSQGK-amide (100 nM)	90 min RT	phospho-Ulight-CFFKNIVTPRTPPPSQGK-amide
HGK *(h)* (MAP4K4)	human recombinant	ATP + Ulight-FLGFTYVAP (50 nM)	90 min RT	phospho-Ulight-FLGFTYVAP
IKKα *(h)*	human recombinant (Sf21 cells)	ATP + Ulight-IkappaB-alpha (100 nM)	30 min RT	phospho-Ulight-IkappaB-alpha
IRAK4 *(h)*	human recombinant (insect cells)	ATP + Ulight-FLGFTYVAP (50 nM)	90 min RT	phospho-Ulight-FLGFTYVAP
IRK *(h)* (InsR)	human recombinant	ATP + Ulight-Poly GAT[EAY(1:1:1)]n (50 nM)	10 min RT	phospho-Ulight-Poly GAT[EAY(1:1:1)]n
JAK3 *(h)*	human recombinant	ATP + Ulight-CAGAGAIETDKEYYTVKD (100 nM)	60 min RT	phospho-Ulight-CAGAGAIETDKEYYTVKD
JNK1 *(h)*	human recombinant (*E. coli*)	ATP + Ulight-CFFKNIVTPRTPPPSQGK-amide (100 nM)	60 min RT	phospho-Ulight-CFFKNIVTPRTPPPSQGK-amide
KDR kinase *(h)* (VEGFR2)	human recombinant (Sf9 cells)	ATP + Ulight-CAGAGAIETDKEYYTVKD (100 nM)	60 min RT	phospho-Ulight-CAGAGAIETDKEYYTVKD
Lck kinase *(h)*	human recombinant (insect cells)	ATP + Ulight-Poly GAT[EAY(1:1:1)]n (25 nM)	30 min RT	phospho-Ulight-Poly GAT[EAY(1:1:1)]n
MAPKAPK 2 *(h)*	human recombinant (*E. coli*)	ATP + CREBtide (CKRREILSRRPSYRK) (25 nM)	15 min RT	phospho-CREBtide (CKRREILSRRPSYRK)
MARK1 *(h)*	human recombinant	ATP + Ulight-RRRSLLE (50 nM)	30 min RT	phospho-Ulight-RRRSLLE
MKK6 *(h)*	human recombinant	ATP + inactive p38a (50 nM)	10 min RT	phospho-p38a
MNK2 *(h)*	human recombinant (Sf21 cells)	ATP + CREBtide (CKRREILSRRPSYRK) (25 nM)	90 min RT	phospho-CREBtide (CKRREILSRRPSYRK)

MST4 kinase *(h)*	human recombinant	ATP + Ulight TM- PKC (50 nM)	30 min RT	Phospho-Ulight-TM-PKC
NEK2 *(h)*	human recombinant (insect cells)	ATP + Ulight-FLGFTYVAP (50 nM)	60 min RT	phospho-Ulight-FLGFTYVAP
p38α kinase *(h)*	human recombinant (*E. coli*)	ATP + Ulight-CFFKNIVTPRTPPPSQGK-amide (100 nM)	60 min RT	phospho-Ulight-CFFKNIVTPRTPPPSQG Kamide
PAK2 *(h)*	human recombinant (Sf9 cells)	ATP + Ulight-RRRSLLE (50 nM)	60 min RT	phospho-Ulight-RRRSLLE
PAK4 *(h)*	human recombinant (insect cells)	ATP + Ulight-RRRSLLE (50 nM)	30 min RT	phospho-Ulight-RRRSLLE
PDK1 *(h)*	human recombinant (insect cells)	ATP + Ulight-FLGFTYVAP (400 nM)	90 min RT	phospho-Ulight-FLGFTYVAP
Pim2 kinase *(h)*	human recombinant (insect cells)	ATP + CREBtide (CKRREILSRRPSYRK) (25 nM)	60 min RT	phospho-CREBtide (CKRREILSRRPSYRK)
PKA *(h)*	human recombinant (*E. coli*)	ATP + Ulight-RRRSLLE (50 nM)	10 min RT	phospho-Ulight-RRRSLLE
PKCβ2 *(h)*	human recombinant	ATP + CREBtide (CKRREILSRRPSYRK) (25 nM)	15 min RT	phospho-CREBtide (CKRREILSRRPSYRK)
PLK1 *(h)*	human recombinant	ATP + Ulight-FLGFTYVAP (40 nM)	60 min RT	phospho-Ulight-FLGFTYVAP
RAF-1 kinase *(h)*	human recombinant	ATP + Ulight-ARTKQTARKSTGGKAPRKQL AGCG (50 nM)	180 min RT	phospho-Ulight-ARTKQTARKSTGGKAP RKQ LAGCG
ROCK1 *(h)*	human recombinant	ATP + Ulight-RRRSLLE (50 nM)	30 min RT	phospho-Ulight-RRRSLLE
SGK1 *(h)*	human recombinant	ATP + Ulight-RRRSLLE (50 nM)	30 min RT	phospho-Ulight-RRRSLLE
SIK *(h)*	human recombinant (Sf21 cells)	ATP + CREBtide (CKRREILSRRPSYRK) (25 nM)	90 min RT	phospho-CREBtide (CKRREILSRRPSYRK)
Src kinase *(h)*	human recombinant (insect cells)	ATP + Ulight-Poly GAT[EAY(1:1:1)]n (5 nM)	10 min RT	phospho-Ulight-Poly GAT[EAY(1:1:1)]n
TAOK2 (TAO1) *(h)*	human recombinant	ATP + Ulight-FLGFTYVAP (40 nM)	60 min RT	phospho-Ulight-FLGFTYVAP
TRKA *(h)*	human recombinant (insect cells)	ATP + Ulight-Poly GAT[EAY(1:1:1)]n (5 nM)	10 min RT	phospho-Ulight-Poly GAT[EAY(1:1:1)]n

Bioavailability profile of compound 14d (conducted by Cerep)

Assay	Technique	Test concentration	Incubation	Detection mode
Aqueous solubility (PBS, pH 7.4)	shake-flask	200 µM	24hr/RT	HPLC-UV/VIS
Partition coefficient (log D, n-octanol /PBS, pH 7.4)	shake-flask	100 µM	60min/RT	HPLC-UV/VIS
Protein binding (plasma, human)	Equilibrium dialysis	10 µM	Overnight (18 ± 2hr) 37°C	HPLC-MS/MS

Assay	Source	Incubation	Detection mode
A-B permeability (Caco-2, pH 6.5/7.4)	Caco-2 cell line	0 and 60 min 37°C	HPLC-MS/MS

Assay	Source	Subtrate	Incubation	Measured Component	Detection mode
Metabolic stability (liver microsomes, human)	Human liver microsomes (0.3 mg/mL)	Test compound	0 and 60 min 37°C	Test compound	HPLC-MS/MS

Assay	Test Concentration (M)	Result
Partition coefficient (logD, n-octanol/PBS, pH 7.4)	1.0E-04	3.58
Protein binding (plasma, human)	1.0E-05	91% Protein Bound 121% Recovery
A-B permeability (Caco-2, pH 6.5/7.4)	1.0E-05	<0.1 Permeability 68% Recovery
Metabolic stability (liver microsomes, human)	1.0E-06	25% Parent Remaining
Aqueous solubility (PBS, pH 7.4)	2.0E-04	Below the limit of quantitation

Monitoring of the heart development on zebrafish embryos

The wt zebrafish was used in this study. The embryos were collected and placed into 24-well plates, ten embryos per well and maintained in E2 medium at ~28°C. Compounds were added 5 hpf (50% epiboly) and the embryos allowed to grow in chemical compound solution up to 5 days. The phenotypes were compared using the Axio Scope.A1 microscope system from Carl Zeiss at 48, 72 and 96 hpf. The heart beat was counted for one minute and compared to the control. - **Animal husbandry.** All animal experiments were conducted and documented according to the federal and local regulation. Due to the federal law and regulation all embryo testing was stopped at day 5 of embryonic development.

NMR Data of compounds 5b, **5c**, **6b**, **6c**, **14b**, **14c**, **14d**, **15a**, **15b**, **16a**, **23a**, **23b** and **23c**

The ^{1}H-NMR spectra were recorded on a Bruker AC 300 spectrometer at 300 MHz and Bruker AC 500 spectrometer at 500 MHz. The ^{13}C-NMR spectra were recorded on a Bruker AC 300 spectrometer at 75 MHz and Bruker AC 500 spectrometer at 125 MHz.

6.7 Synthese der Benzothiazolderivate zu Kapitel 5.4

AAV 5 für die Synthese von 2-Bromobenzo[*d*]thiazolen (31)

Eine Lösung aus 1.0 eq. eines Benzothiazol-2-amins, 2.1 eq. Kupfer(II)-bromid und 250 ml Acetonitril werden auf 0 °C gekühlt und mit 2.0 eq. *tert*.-Butylnitrit versetzt. Die Reaktionslösung wird über Nacht bei RT gerührt. Anschließend wird sie auf 250 ml dest. Wasser gegeben und es wird mit EE extrahiert. Die vereinigten organischen Phasen werden mit gesättigter Natriumchloridlösung vorgetrocknet, anschließend mit Natriumsulfat versetzt und filtriert. Das organische Lösungsmittel wird im Vakuum entfernt. Der resultierende Feststoff wird in einem Lösungsmittelgemisch aus EE und Cy umkristallisiert und ohne weitere Analytik weiter umgesetzt.

AAV 6 für die Synthese von Benzo[*d*]thiazol-2-aminen (32)

Zu einer Lösung bestehend aus 1.0 eq. eines 2-Bromobenzothiazolderivates in 10 mL DMF werden 10 eq. eines Alkyl-/Arylamins hinzugegeben. Anschließend wird die Reaktionslösung 2 h bei 100 °C gerührt. Das Reaktionsgemisch wird auf RT abgekühlt und mit 100 ml EE aufgenommen. Die organische Phase wird dreimal mit 0.1 N Salzsäure gewaschen. Die vereinigten organischen Phasen werden mit gesättigter Natriumchloridlösung vorgetrocknet, anschließend mit Natriumsulfat versetzt und filtriert. Das organsiche Lösungsmittel wird im Vakuum entfernt. Der resultierende Feststoff wird in einem Lösungsmittelgemisch aus EE und Cy umkristallisiert und ohne weitere Analytik weiter umgesetzt.

AAV 7 für die Synthese von 2-Aminobenzo[*d*]thiazol-6-carbohydraziddderivaten (33)

Eine Lösung bestehend aus 1.0 eq. eines Benzothiazol-2-amins und 0.5 mL Hydrazinhydrat wird 2 h bei 130°C gerührt. Anschließend wird die Reaktionsmischung auf RT abgekühlt. Die Reaktionsmischung über Nacht bei 4°C gelagert. Das Fällungsprodukt wird abfiltriert, mit wenig kaltem Ethanol gewaschen und ohne weitere Analytik weiter umgesetzt.

AAV 8 für die Synthese von 5-(2-Aminobenzo[*d*]thiazol-6-yl)-1,3,4-oxadiazol-2-thiolen (34)

Eine Lösung bestehend aus 0.5 mL EtOH, 1.0 eq. eines 2-Aminobenzo[*d*]thiazol-6-carbohydrazidderivats, 1.1 eq. TEA und 2.2 eq. CS_2 wird über Nacht refluxiert. Die Reaktionsmischung wird auf RT abgekühlt, mit wenig EE aufgenommen und mit 0.1 N Salzsäure gewaschen. Die organische Phase wird mit gesättigter Natriumchloridlösung vorgetrocknet, anschließend mit Natriumsulfat versetzt und filtriert. Das organsiche Lösungsmittel wird im Vakuum entfernt. Der resultierende Feststoff wird in einem Lösungsmittelgemisch aus EE und Cy umkristallisiert und ohne weitere Analytik weiter umgesetzt.

AAV 9 für die Synthese von 3-((5-(2-Aminobenzo[*d*]thiazol-6-yl)-1,3,4-oxadiazol-2-ylthio)methyl)benzonitrilen (35)

Eine Lösung bestehend aus 0.8 mL DMF, 1.0 eq. **34** und 1.1 eq. 1.0 N Natronlauge wird 30 min. bei RT gerührt. Anschließend werden 1.1 eq. 3-Cyanobenzylbromid hinzugegeben und für 48 h bei RT gerührt. Die Reaktionsmischung wird auf 2.0 mL EE gegeben und mit dest. Wasser gewaschen. Die organische Phase wird mit gesättigter Natriumchloridlösung vorgetrocknet, anschließend mit Natriumsulfat versetzt und filtriert. Das organsiche Lösungsmittel wird im Vakuum entfernt. Der resultierende Feststoff wird in einem Lösungsmittelgemisch aus EE und Cy umkristallisiert.

Produktbeispiel: *3-((5-(2-(3-Methoxybenzylamino)benzo[d]thiazol-6-yl)-1,3,4-oxadiazol-2-ylthio)methyl)benzonitril* (**BSc4798**)

Es resultieren 4% eines leicht bräunlichen Feststoffs.

HPLC t_R: 7.83 min.

^{1}H-NMR (500 MHz, DMSO-d6): δ (ppm) = 3.74 (s, 3H), 4.61 (m, 4H), 6.84 (m, 1H), 6.96 (m, 2H), 7.27 (t, *J* = 8.1 Hz, 1H), 7.54 (m, 2H), 7.80 (m, 3H), 7.97 (s, 1H), 8.30 (d, *J* = 1.8 Hz, 1H), 8.88 (t, *J* = 5.8 Hz, 1H).

EI-MS: m/z: 485 (M^+).

Hinweis: Aufgrund der geringen Löslichkeit und Substanzmenge wurde auf ein ^{13}C-NMR verzichtet.

7 Literaturverzeichnis

1. Assauer, R.; Strasser, P. In *Wie ausgewechselt: Verblassende Erinnerungen an mein Leben*; Riva, 2012.
2. Alzheimer, A. *Allg. Z. Psychiat. Psych.-Gerichtl. Med.* **1907,** *64*, 146-8.
3. Alzheimer, A.; Stelzmann, R. A.; Schnitzlein, H. N.; Murtagh, F. R. *Clin. Anat.* **1995,** *8*, 429-31.
4. Perrin, R. J.; Fagan, A. M.; Holtzman, D. M. *Nature* **2009,** *461*, 916-22.
5. Dubois, B.; Feldman, H. H.; Jacova, C.; Dekosky, S. T.; Barberger-Gateau, P.; Cummings, J.; Delacourte, A.; Galasko, D.; Gauthier, S.; Jicha, G.; Meguro, K.; O'Brien, J.; Pasquier, F.; Robert, P.; Rossor, M.; Salloway, S.; Stern, Y.; Visser, P. J.; Scheltens, P. *Lancet Neurol.* **2007,** *6*, 734-46.
6. McKhann, G.; Drachman, D.; Folstein, M.; Katzman, R.; Price, D.; Stadlan, E. M. *Neurology* **1984,** *34*, 939-44.
7. AFI. *Alzheimer Forschung Initiative e.V.: Faktenblatt 2 - Zahlen und Fakten* **2012**.
8. DAG. *Deutsche Alzheimer Gesellschaft: Das Wichtigste 1 - Die Epidemiologie der Demenz* **2010**.
9. WHO; ADI. **2012**.
10. Ballard, C.; Gauthier, S.; Corbett, A.; Brayne, C.; Aarsland, D.; Jones, E. *Lancet* **2011,** *377*, 1019-31.
11. Galluzzi, K. E.; Appelt, D. M.; Balin, B. J. *J. Am. Osteopath. Assoc.* **2010,** *110*, S37-42.
12. Osborn, G. G.; Saunders, A. V. *J. Am. Osteopath. Assoc.* **2010,** *110*, S16-26.
13. Hernandez, F.; Gomez de Barreda, E.; Fuster-Matanzo, A.; Lucas, J. J.; Avila, J. *Exp. Neurol.* **2010,** *223*, 322-5.
14. Martinez, A.; Gil, C.; Perez, D. I. *Int. J. Alzheimers Dis.* **2011,** *2011*, 280502.
15. *www.clinicaltrials.gov* **2012**.
16. Ferri, C. P.; Prince, M.; Brayne, C.; Brodaty, H.; Fratiglioni, L.; Ganguli, M.; Hall, K.; Hasegawa, K.; Hendrie, H.; Huang, Y.; Jorm, A.; Mathers, C.; Menezes, P. R.; Rimmer, E.; Scazufca, M. *Lancet* **2005,** *366*, 2112-7.
17. Reitz, C.; Brayne, C.; Mayeux, R. *Nat. Rev. Neurol.* **2011,** *7*, 137-52.
18. WHO. *World Health Report 2003 - Shaping the future.* **2003**.
19. Dillen, K.; Annaert, W. *Int. Rev. Cytol.* **2006,** *254*, 215-300.
20. Duce, J. A.; Tsatsanis, A.; Cater, M. A.; James, S. A.; Robb, E.; Wikhe, K.; Leong, S. L.; Perez, K.; Johanssen, T.; Greenough, M. A.; Cho, H. H.; Galatis, D.; Moir, R. D.; Masters, C. L.; McLean, C.; Tanzi, R. E.; Cappai, R.; Barnham, K. J.; Ciccotosto, G. D.; Rogers, J. T.; Bush, A. I. *Cell* **2010,** *142*, 857-67.
21. Priller, C.; Bauer, T.; Mitteregger, G.; Krebs, B.; Kretzschmar, H. A.; Herms, J. *J. Neurosci.* **2006,** *26*, 7212-21.
22. Turner, P. R.; O'Connor, K.; Tate, W. P.; Abraham, W. C. *Prog. Neurobiol.* **2003,** *70*, 1-32.
23. LaFerla, F. M.; Green, K. N.; Oddo, S. *Nat. Rev. Neurosci.* **2007,** *8*, 499-509.
24. Kojro, E.; Fahrenholz, F. *Subcell. Biochem.* **2005,** *38*, 105-27.
25. Lichtenthaler, S. F.; Haass, C. *J. Clin. Invest.* **2004,** *113*, 1384-7.
26. Haass, C.; Lemere, C. A.; Capell, A.; Citron, M.; Seubert, P.; Schenk, D.; Lannfelt, L.; Selkoe, D. J. *Nat. Med.* **1995,** *1*, 1291-6.
27. Bitan, G.; Kirkitadze, M. D.; Lomakin, A.; Vollers, S. S.; Benedek, G. B.; Teplow, D. B. *PNAS USA* **2003,** *100*, 330-5.
28. Bitan, G.; Vollers, S. S.; Teplow, D. B. *J. Biol. Chem.* **2003,** *278*, 34882-9.
29. DeMattos, R. B.; Bales, K. R.; Cummins, D. J.; Dodart, J. C.; Paul, S. M.; Holtzman, D. M. *PNAS USA* **2001,** *98*, 8850-5.
30. Jarrett, J. T.; Berger, E. P.; Lansbury, P. T., Jr. *Biochemistry* **1993,** *32*, 4693-7.
31. Younkin, S. G. *J. Physiol. Paris* **1998,** *92*, 289-92.
32. Alonso, A. C.; Zaidi, T.; Grundke-Iqbal, I.; Iqbal, K. *PNAS USA* **1994,** *91*, 5562-6.
33. Grundke-Iqbal, I.; Iqbal, K.; Tung, Y. C.; Quinlan, M.; Wisniewski, H. M.; Binder, L. I. *PNAS USA* **1986,** *83*, 4913-7.
34. Himmelstein, D. S.; Ward, S. M.; Lancia, J. K.; Patterson, K. R.; Binder, L. I. *Pharmacol. Ther.* **2012,** *136*, 8-22.
35. Iqbal, K.; Grundke-Iqbal, I.; Zaidi, T.; Merz, P. A.; Wen, G. Y.; Shaikh, S. S.; Wisniewski, H. M.; Alafuzoff, I.; Winblad, B. *Lancet* **1986,** *2*, 421-6.
36. Jakob-Roetne, R.; Jacobsen, H. *Angew. Chem.* **2009,** *121*, 3074-105.
37. Hanger, D. P.; Anderton, B. H.; Noble, W. *Trends Mol. Med.* **2009,** *15*, 112-9.
38. Mazanetz, M. P.; Fischer, P. M. *Nat. Rev. Drug Discov.* **2007,** *6*, 464-79.
39. Wang, J. Z.; Grundke-Iqbal, I.; Iqbal, K. *Eur J. Neurosci.* **2007,** *25*, 59-68.
40. Mandelkow, E. M.; Stamer, K.; Vogel, R.; Thies, E.; Mandelkow, E. *Neurobiol. Aging* **2003,** *24*, 1079-85.
41. Stamer, K.; Vogel, R.; Thies, E.; Mandelkow, E.; Mandelkow, E. M. *J. Cell Biol.* **2002,** *156*, 1051-63.
42. Brunden, K. R.; Trojanowski, J. Q.; Lee, V. M. *Nat. Rev. Drug Discov.* **2009,** *8*, 783-93.
43. Ittner, L. M.; Gotz, J. *Nat. Rev. Neurosci.* **2011,** *12*, 65-72.
44. Karran, E.; Mercken, M.; De Strooper, B. *Nat. Rev. Drug Discov.* **2011,** *10*, 698-712.
45. Kremer, A.; Louis, J. V.; Jaworski, T.; Van Leuven, F. *Front. Mol. Neurosci.* **2011,** *4*, 17.
46. Selkoe, D. J. *Nat. Med.* **2011,** *17*, 1060-5.
47. Small, S. A.; Duff, K. *Neuron* **2008,** *60*, 534-42.
48. Phiel, C. J.; Wilson, C. A.; Lee, V. M.; Klein, P. S. *Nature* **2003,** *423*, 435-9.
49. Benilova, I.; Karran, E.; De Strooper, B. *Nat. Neurosci.* **2012,** *15*, 349-57.
50. Cowan, C. M.; Quraishe, S.; Mudher, A. *Biochem. Soc. Trans.* **2012,** *40*, 693-7.
51. Larson, M. E.; Lesne, S. E. *J. Neurochem.* **2012,** *120 Suppl. 1*, 125-39.
52. Walsh, D. M.; Klyubin, I.; Fadeeva, J. V.; Cullen, W. K.; Anwyl, R.; Wolfe, M. S.; Rowan, M. J.; Selkoe, D. J. *Nature* **2002,** *416*, 535-9.
53. Walsh, D. M.; Selkoe, D. J. *Neuron* **2004,** *44*, 181-93.
54. Ward, S. M.; Himmelstein, D. S.; Lancia, J. K.; Binder, L. I. *Biochem. Soc. Trans.* **2012,** *40*, 667-71.
55. Clavaguera, F.; Bolmont, T.; Crowther, R. A.; Abramowski, D.; Frank, S.; Probst, A.; Fraser, G.; Stalder, A. K.; Beibel, M.; Staufenbiel, M.; Jucker, M.; Goedert, M.; Tolnay, M. *Nat. Cell Biol.* **2009,** *11*, 909-13.
56. de Calignon, A.; Polydoro, M.; Suarez-Calvet, M.; William, C.; Adamowicz, D. H.; Kopeikina, K. J.; Pitstick, R.; Sahara, N.; Ashe, K. H.; Carlson, G. A.; Spires-Jones, T. L.; Hyman, B. T. *Neuron* **2012,** *73*, 685-97.
57. Matthews, F. E.; Brayne, C.; Lowe, J.; McKeith, I.; Wharton, S. B.; Ince, P. *PLoS Med.* **2009,** *6*, e1000180.
58. Braak, H.; Braak, E. *Acta Neuropathol..* **1991,** *82*, 239-59.
59. Braak, H.; Braak, E.; Bohl, J. *Eur. Neurol.* **1993,** *33*, 403-08.

60. Delaère, P.; He, Y.; Fayet, G.; Duyckaerts, C.; Hauw, J.-J. *Neurobiol. Aging* **1993,** *14*, 191-4.
61. Mackenzie, I. R.; McLachlan, R. S.; Kubu, C. S.; Miller, L. A. *Neurology* **1996,** *46*, 425-9.
62. Sjöbeck, M.; Englund, E. *Dementia Geriatr. Cognit. Disord.* **2001,** *12*, 211-8.
63. Snowdon, D. A. *Gerontologist* **1997,** *37*, 150-6.
64. Thal, D. R.; Rub, U.; Orantes, M.; Braak, H. *Neurology* **2002,** *58*, 1791-800.
65. Bertram, L.; Lill, C. M.; Tanzi, R. E. *Neuron* **2010,** *68*, 270-81.
66. Bekris, L. M.; Yu, C. E.; Bird, T. D.; Tsuang, D. W. *J. Geriatr. Psychiatry Neurol.* **2010,** *23*, 213-27.
67. *www.molgen.vib-ua.be/ADMutations/* **2012**.
68. De Strooper, B.; Saftig, P.; Craessaerts, K.; Vanderstichele, H.; Guhde, G.; Annaert, W.; Von Figura, K.; Van Leuven, F. *Nature* **1998,** *391*, 387-90.
69. Scheuner, D.; Eckman, C.; Jensen, M.; Song, X.; Citron, M.; Suzuki, N.; Bird, T. D.; Hardy, J.; Hutton, M.; Kukull, W.; Larson, E.; Levy-Lahad, E.; Viitanen, M.; Peskind, E.; Poorkaj, P.; Schellenberg, G.; Tanzi, R.; Wasco, W.; Lannfelt, L.; Selkoe, D.; Younkin, S. *Nat. Med.* **1996,** *2*, 864-70.
70. Corder, E. H.; Saunders, A. M.; Strittmatter, W. J.; Schmechel, D. E.; Gaskell, P. C.; Small, G. W.; Roses, A. D.; Haines, J. L.; Pericak-Vance, M. A. *Science* **1993,** *261*, 921-3.
71. Kurz, A.; Altland, K.; Lautenschlager, N.; Zimmer, R.; Busch, R.; Gerundt, I.; Lauter, H.; Muller, U. *J. Neurol.* **1996,** *243*, 452-6.
72. Poirier, J.; Davignon, J.; Bouthillier, D.; Kogan, S.; Bertrand, P.; Gauthier, S. *Lancet* **1993,** *342*, 697-9.
73. Evans, K. C.; Berger, E. P.; Cho, C. G.; Weisgraber, K. H.; Lansbury, P. T., Jr. *PNAS USA* **1995,** *92*, 763-7.
74. Ma, J.; Yee, A.; Brewer, H. B., Jr.; Das, S.; Potter, H. *Nature* **1994,** *372*, 92-4.
75. Rebeck, G. W.; Reiter, J. S.; Strickland, D. K.; Hyman, B. T. *Neuron* **1993,** *11*, 575-80.
76. Schmechel, D. E.; Saunders, A. M.; Strittmatter, W. J.; Crain, B. J.; Hulette, C. M.; Joo, S. H.; Pericak-Vance, M. A.; Goldgaber, D.; Roses, A. D. *PNAS USA* **1993,** *90*, 9649-53.
77. Hanson, L. G. *Concepts in Magnetic Resonance Part A* **2008,** *32A*, 329-40.
78. Rooney, W. G.; Johnson, G.; Li, X.; Cohen, E. R.; Kim, S.-G.; Ugurbil, K.; Springer Jr., C. S. *Magnetic Resonance in Medicine* **2007,** *57*, 308-18.
79. de Leon, M. J.; DeSanti, S.; Zinkowski, R.; Mehta, P. D.; Pratico, D.; Segal, S.; Rusinek, H.; Li, J.; Tsui, W.; Saint Louis, L. A.; Clark, C. M.; Tarshish, C.; Li, Y.; Lair, L.; Javier, E.; Rich, K.; Lesbre, P.; Mosconi, L.; Reisberg, B.; Sadowski, M.; DeBernadis, J. F.; Kerkman, D. J.; Hampel, H.; Wahlund, L. O.; Davies, P. *Neurobiol. Aging* **2006,** *27*, 394-401.
80. Fox, N. C.; Warrington, E. K.; Rossor, M. N. *Lancet* **1999,** *353*, 2125.
81. Hampel, H.; Burger, K.; Teipel, S. J.; Bokde, A. L.; Zetterberg, H.; Blennow, K. *Alzheimers Dement.* **2008,** *4*, 38-48.
82. Holland, D.; Brewer, J. B.; Hagler, D. J.; Fennema-Notestine, C.; Dale, A. M. *PNAS USA* **2009,** *106*, 20954-9.
83. Teipel, S. J.; Ewers, M.; Wolf, S.; Jessen, F.; Kolsch, H.; Arlt, S.; Luckhaus, C.; Schonknecht, P.; Schmidtke, K.; Heuser, I.; Frolich, L.; Ende, G.; Pantel, J.; Wiltfang, J.; Rakebrandt, F.; Peters, O.; Born, C.; Kornhuber, J.; Hampel, H. *Psychiatry Res.* **2010,** *182*, 244-50.
84. Vemuri, P.; Whitwell, J. L.; Kantarci, K.; Josephs, K. A.; Parisi, J. E.; Shiung, M. S.; Knopman, D. S.; Boeve, B. F.; Petersen, R. C.; Dickson, D. W.; Jack, C. R., Jr. *Neuroimage* **2008,** *42*, 559-67.
85. Apostolova, L. G.; Dutton, R. A.; Dinov, I. D.; Hayashi, K. M.; Toga, A. W.; Cummings, J. L.; Thompson, P. M. *Arch. Neurol.* **2006,** *63*, 693-9.
86. Mungas, D.; Harvey, D.; Reed, B. R.; Jagust, W. J.; DeCarli, C.; Beckett, L.; Mack, W. J.; Kramer, J. H.; Weiner, M. W.; Schuff, N.; Chui, H. C. *Neurology* **2005,** *65*, 565-71.
87. Carlson, N. E.; Moore, M. M.; Dame, A.; Howieson, D.; Silbert, L. C.; Quinn, J. F.; Kaye, J. A. *Neurology* **2008,** *70*, 828-33.
88. Chetelat, G.; Landeau, B.; Eustache, F.; Mezenge, F.; Viader, F.; de la Sayette, V.; Desgranges, B.; Baron, J. C. *Neuroimage* **2005,** *27*, 934-46.
89. Devanand, D. P.; Pradhaban, G.; Liu, X.; Khandji, A.; De Santi, S.; Segal, S.; Rusinek, H.; Pelton, G. H.; Honig, L. S.; Mayeux, R.; Stern, Y.; Tabert, M. H.; de Leon, M. J. *Neurology* **2007,** *68*, 828-36.
90. Likeman, M.; Anderson, V. M.; Stevens, J. M.; Waldman, A. D.; Godbolt, A. K.; Frost, C.; Rossor, M. N.; Fox, N. C. *Arch. Neurol.* **2005,** *62*, 1410-5.
91. Chen, S.; Li, X. *Comput. Math. Methods Med.* **2012,** *2012*, 613465.
92. Kwong, K. K.; Belliveau, J. W.; Chesler, D. A.; Goldberg, I. E.; Weisskoff, R. M.; Poncelet, B. P.; Kennedy, D. N.; Hoppel, B. E.; Cohen, M. S.; Turner, R.; et al. *PNAS USA* **1992,** *89*, 5675-9.
93. Ogawa, S.; Lee, T. M.; Kay, A. R.; Tank, D. W. *PNAS USA* **1990,** *87*, 9868-72.
94. Patwardhan, M. B.; McCrory, D. C.; Matchar, D. B.; Samsa, G. P.; Rutschmann, O. T. *Radiology* **2004,** *231*, 73-80.
95. Silverman, D. H.; Small, G. W.; Chang, C. Y.; Lu, C. S.; Kung De Aburto, M. A.; Chen, W.; Czernin, J.; Rapoport, S. I.; Pietrini, P.; Alexander, G. E.; Schapiro, M. B.; Jagust, W. J.; Hoffman, J. M.; Welsh-Bohmer, K. A.; Alavi, A.; Clark, C. M.; Salmon, E.; de Leon, M. J.; Mielke, R.; Cummings, J. L.; Kowell, A. P.; Gambhir, S. S.; Hoh, C. K.; Phelps, M. E. *JAMA* **2001,** *286*, 2120-7.
96. Small, G. W.; Bookheimer, S. Y.; Thompson, P. M.; Cole, G. M.; Huang, S. C.; Kepe, V.; Barrio, J. R. *Lancet Neurol.* **2008,** *7*, 161-72.
97. Mathis, C. A.; Wang, Y.; Holt, D. P.; Huang, G. F.; Debnath, M. L.; Klunk, W. E. *J. Med. Chem.* **2003,** *46*, 2740-54.
98. Rowe, C. C.; Ng, S.; Ackermann, U.; Gong, S. J.; Pike, K.; Savage, G.; Cowie, T. F.; Dickinson, K. L.; Maruff, P.; Darby, D.; Smith, C.; Woodward, M.; Merory, J.; Tochon-Danguy, H.; O'Keefe, G.; Klunk, W. E.; Mathis, C. A.; Price, J. C.; Masters, C. L.; Villemagne, V. L. *Neurology* **2007,** *68*, 1718-25.
99. Klunk, W. E.; Engler, H.; Nordberg, A.; Wang, Y.; Blomqvist, G.; Holt, D. P.; Bergstrom, M.; Savitcheva, I.; Huang, G. F.; Estrada, S.; Ausen, B.; Debnath, M. L.; Barletta, J.; Price, J. C.; Sandell, J.; Lopresti, B. J.; Wall, A.; Koivisto, P.; Antoni, G.; Mathis, C. A.; Langstrom, B. *Ann. Neurol.* **2004,** *55*, 306-19.
100. Mintun, M. A.; Larossa, G. N.; Sheline, Y. I.; Dence, C. S.; Lee, S. Y.; Mach, R. H.; Klunk, W. E.; Mathis, C. A.; DeKosky, S. T.; Morris, J. C. *Neurology* **2006,** *67*, 446-52.
101. Clark, C. M.; Schneider, J. A.; Bedell, B. J.; Beach, T. G.; Bilker, W. B.; Mintun, M. A.; Pontecorvo, M. J.; Hefti, F.; Carpenter, A. P.; Flitter, M. L.; Krautkramer, M. J.; Kung, H. F.; Coleman, R. E.; Doraiswamy, P. M.; Fleisher, A. S.; Sabbagh, M. N.; Sadowsky, C. H.; Reiman, E. P.; Zehntner, S. P.; Skovronsky, D. M. *JAMA* **2011,** *305*, 275-83.
102. Garber, K. *Nat. Biotechnol.* **2012,** *30*, 575.
103. Braak, H.; Braak, E. *Neurobiol. Aging* **1997,** *18*, 351-7.
104. *www.amyvid.com* **2012**.

105. Buckner, R. L.; Snyder, A. Z.; Shannon, B. J.; LaRossa, G.; Sachs, R.; Fotenos, A. F.; Sheline, Y. I.; Klunk, W. E.; Mathis, C. A.; Morris, J. C.; Mintun, M. A. *J. Neurosci.* **2005,** *25*, 7709-17.
106. Choi, S. R.; Golding, G.; Zhuang, Z.; Zhang, W.; Lim, N.; Hefti, F.; Benedum, T. E.; Kilbourn, M. R.; Skovronsky, D.; Kung, H. F. *J. Nucl. Med.* **2009,** *50*, 1887-94.
107. Kung, H. F.; Choi, S. R.; Qu, W.; Zhang, W.; Skovronsky, D. *J. Med. Chem.* **2010,** *53*, 933-41.
108. Lin, K. J.; Hsu, W. C.; Hsiao, I. T.; Wey, S. P.; Jin, L. W.; Skovronsky, D.; Wai, Y. Y.; Chang, H. P.; Lo, C. W.; Yao, C. H.; Yen, T. C.; Kung, M. P. *Nucl. Med. Biol.* **2010,** *37*, 497-508.
109. Wong, D. F.; Rosenberg, P. B.; Zhou, Y.; Kumar, A.; Raymont, V.; Ravert, H. T.; Dannals, R. F.; Nandi, A.; Brasic, J. R.; Ye, W.; Hilton, J.; Lyketsos, C.; Kung, H. F.; Joshi, A. D.; Skovronsky, D. M.; Pontecorvo, M. J. *J. Nucl. Med.* **2010,** *51*, 913-20.
110. Zhang, W.; Arteaga, J.; Cashion, D. K.; Chen, G.; Gangadharmath, U.; Gomez, L. F.; Kasi, D.; Lam, C.; Liang, Q.; Liu, C.; Mocharla, V. P.; Mu, F.; Sinha, A.; Szardenings, A. K.; Wang, E.; Walsh, J. C.; Xia, C.; Yu, C.; Zhao, T.; Kolb, H. C. *J. Alzheimers Dis.* **2012**.
111. Szardenings, A. K.; Zhang, W.; Kolb, H. C.; Cashion, D. K.; Chen, G.; Kasi, D.; Liu, C.; Sinha, A.; Wang, E.; Yu, C.; Gangadharmath, U. B.; Walsh, J. C.; SIEMENS MEDICAL SOLUTIONS USA, INC. (Malvern, PA, US), 2011.
112. Jack, C. R., Jr.; Dickson, D. W.; Parisi, J. E.; Xu, Y. C.; Cha, R. H.; O'Brien, P. C.; Edland, S. D.; Smith, G. E.; Boeve, B. F.; Tangalos, E. G.; Kokmen, E.; Petersen, R. C. *Neurology* **2002,** *58*, 750-7.
113. Nordberg, A.; Rinne, J. O.; Kadir, A.; Langstrom, B. *Nat. Rev. Neurol.* **2010,** *6*, 78-87.
114. Whitwell, J. L.; Josephs, K. A.; Murray, M. E.; Kantarci, K.; Przybelski, S. A.; Weigand, S. D.; Vemuri, P.; Senjem, M. L.; Parisi, J. E.; Knopman, D. S.; Boeve, B. F.; Petersen, R. C.; Dickson, D. W.; Jack, C. R., Jr. *Neurology* **2008,** *71*, 743-9.
115. Barrio, J. R.; Satyamurthy, N.; Huang, S. C.; Petric, A.; Small, G. W.; Kepe, V. *Acc Chem Res* **2009,** *42*, 842-50.
116. Small, G. W.; Kepe, V.; Ercoli, L. M.; Siddarth, P.; Bookheimer, S. Y.; Miller, K. J.; Lavretsky, H.; Burggren, A. C.; Cole, G. M.; Vinters, H. V.; Thompson, P. M.; Huang, S. C.; Satyamurthy, N.; Phelps, M. E.; Barrio, J. R. *N. Engl. J. Med.* **2006,** *355*, 2652-63.
117. Hansson, O.; Zetterberg, H.; Buchhave, P.; Andreasson, U.; Londos, E.; Minthon, L.; Blennow, K. *Dement. Geriatr. Cogn. Disord.* **2007,** *23*, 316-20.
118. Motter, R.; Vigo-Pelfrey, C.; Kholodenko, D.; Barbour, R.; Johnson-Wood, K.; Galasko, D.; Chang, L.; Miller, B.; Clark, C.; Green, R.; et al. *Ann. Neurol.* **1995,** *38*, 643-8.
119. Fagan, A. M.; Mintun, M. A.; Mach, R. H.; Lee, S. Y.; Dence, C. S.; Shah, A. R.; LaRossa, G. N.; Spinner, M. L.; Klunk, W. E.; Mathis, C. A.; DeKosky, S. T.; Morris, J. C.; Holtzman, D. M. *Ann. Neurol.* **2006,** *59*, 512-9.
120. Ewers, M.; Buerger, K.; Teipel, S. J.; Scheltens, P.; Schroder, J.; Zinkowski, R. P.; Bouwman, F. H.; Schonknecht, P.; Schoonenboom, N. S.; Andreasen, N.; Wallin, A.; DeBernardis, J. F.; Kerkman, D. J.; Heindl, B.; Blennow, K.; Hampel, H. *Neurology* **2007,** *69*, 2205-12.
121. Vandermeeren, M.; Mercken, M.; Vanmechelen, E.; Six, J.; van de Voorde, A.; Martin, J. J.; Cras, P. *J. Neurochem.* **1993,** *61*, 1828-34.
122. Fagan, A. M.; Roe, C. M.; Xiong, C.; Mintun, M. A.; Morris, J. C.; Holtzman, D. M. *Arch. Neurol.* **2007,** *64*, 343-9.
123. Hansson, O.; Zetterberg, H.; Buchhave, P.; Londos, E.; Blennow, K.; Minthon, L. *Lancet Neurol.* **2006,** *5*, 228-34.
124. Li, G.; Sokal, I.; Quinn, J. F.; Leverenz, J. B.; Brodey, M.; Schellenberg, G. D.; Kaye, J. A.; Raskind, M. A.; Zhang, J.; Peskind, E. R.; Montine, T. J. *Neurology* **2007,** *69*, 631-9.
125. Tapiola, T.; Alafuzoff, I.; Herukka, S. K.; Parkkinen, L.; Hartikainen, P.; Soininen, H.; Pirttila, T. *Arch. Neurol.* **2009,** *66*, 382-9.
126. Deane, R.; Du Yan, S.; Submamaryan, R. K.; LaRue, B.; Jovanovic, S.; Hogg, E.; Welch, D.; Manness, L.; Lin, C.; Yu, J.; Zhu, H.; Ghiso, J.; Frangione, B.; Stern, A.; Schmidt, A. M.; Armstrong, D. L.; Arnold, B.; Liliensiek, B.; Nawroth, P.; Hofman, F.; Kindy, M.; Stern, D.; Zlokovic, B. *Nat. Med.* **2003,** *9*, 907-13.
127. Deane, R.; Wu, Z.; Sagare, A.; Davis, J.; Du Yan, S.; Hamm, K.; Xu, F.; Parisi, M.; LaRue, B.; Hu, H. W.; Spijkers, P.; Guo, H.; Song, X.; Lenting, P. J.; Van Nostrand, W. E.; Zlokovic, B. V. *Neuron* **2004,** *43*, 333-44.
128. Shibata, M.; Yamada, S.; Kumar, S. R.; Calero, M.; Bading, J.; Frangione, B.; Holtzman, D. M.; Miller, C. A.; Strickland, D. K.; Ghiso, J.; Zlokovic, B. V. *J. Clin. Invest.* **2000,** *106*, 1489-99.
129. Zlokovic, B. V.; Deane, R.; Sagare, A. P.; Bell, R. D.; Winkler, E. A. *J. Neurochem.* **2010,** *115*, 1077-89.
130. Schupf, N.; Tang, M. X.; Fukuyama, H.; Manly, J.; Andrews, H.; Mehta, P.; Ravetch, J.; Mayeux, R. *PNAS USA* **2008,** *105*, 14052-7.
131. Graff-Radford, N. R.; Crook, J. E.; Lucas, J.; Boeve, B. F.; Knopman, D. S.; Ivnik, R. J.; Smith, G. E.; Younkin, L. H.; Petersen, R. C.; Younkin, S. G. *Arch. Neurol.* **2007,** *64*, 354-62.
132. Mayeux, R.; Tang, M. X.; Jacobs, D. M.; Manly, J.; Bell, K.; Merchant, C.; Small, S. A.; Stern, Y.; Wisniewski, H. M.; Mehta, P. D. *Ann. Neurol.* **1999,** *46*, 412-6.
133. Mehta, P. D.; Pirttila, T.; Patrick, B. A.; Barshatzky, M.; Mehta, S. P. *Neurosci. Lett.* **2001,** *304*, 102-6.
134. Vanderstichele, H.; Van Kerschaver, E.; Hesse, C.; Davidsson, P.; Buyse, M. A.; Andreasen, N.; Minthon, L.; Wallin, A.; Blennow, K.; Vanmechelen, E. *Amyloid* **2000,** *7*, 245-58.
135. Plassman, B. L.; Williams, J. W., Jr.; Burke, J. R.; Holsinger, T.; Benjamin, S. *Ann. Intern. Med.* **2010,** *153*, 182-93.
136. Valenzuela, M. J.; Sachdev, P. *Psychol. Med.* **2006,** *36*, 441-54.
137. Carlson, M. C.; Helms, M. J.; Steffens, D. C.; Burke, J. R.; Potter, G. G.; Plassman, B. L. *Alzheimers Dement.* **2008,** *4*, 324-31.
138. Fratiglioni, L.; Wang, H. X. *J. Alzheimers Dis.* **2007,** *12*, 11-22.
139. Ball, K.; Berch, D. B.; Helmers, K. F.; Jobe, J. B.; Leveck, M. D.; Marsiske, M.; Morris, J. N.; Rebok, G. W.; Smith, D. M.; Tennstedt, S. L.; Unverzagt, F. W.; Willis, S. L. *JAMA* **2002,** *288*, 2271-81.
140. Angevaren, M.; Aufdemkampe, G.; Verhaar, H. J. J.; Aleman, A.; Vanhees, L. *The Cochrane Library* **2008**.
141. Abbott, R. D.; White, L. R.; Ross, G. W.; Masaki, K. H.; Curb, J. D.; Petrovitch, H. *JAMA* **2004,** *292*, 1447-53.
142. Gustafson, D.; Rothenberg, E.; Blennow, K.; Steen, B.; Skoog, I. *Arch. Intern. Med.* **2003,** *163*, 1524-8.
143. Razay, G.; Vreugdenhil, A. *BMJ* **2005,** *331*, 455; author reply 455.
144. Stewart, R.; Masaki, K.; Xue, Q. L.; Peila, R.; Petrovitch, H.; White, L. R.; Launer, L. J. *Arch. Neurol.* **2005,** *62*, 55-60.
145. Gustafson, D. R.; Backman, K.; Waern, M.; Ostling, S.; Guo, X.; Zandi, P.; Mielke, M. M.; Bengtsson, C.; Skoog, I. *Neurology* **2009,** *73*, 1559-66.
146. Profenno, L. A.; Porsteinsson, A. P.; Faraone, S. V. *Biol. Psychiatry* **2010,** *67*, 505-12.
147. Anstrey, K. J.; Mack, H. A.; Cherbuin, N. *Am. J. Geriatr. Psychiatry* **2009,** *17*, 542-55.
148. Lee, Y.; Back, J. H.; Kim, J.; Kim, S. H.; Na, D. L.; Cheong, H. K.; Hong, C. H.; Kim, Y. G. *Int. Psychogeriatr.* **2010,** *22*, 174-87.

149. Traber, M. G.; van der Vliet, A.; Reznick, A. Z.; Cross, C. E. *Clin. Chest Med.* **2000,** *21*, 173-87.
150. Craft, S. *Curr. Alzheimer Res.* **2007,** *4*, 147-52.
151. Gao, C.; Holscher, C.; Liu, Y.; Li, L. *Rev. Neurosci.* **2012,** *23*, 1-11.
152. Leibson, C. L.; Rocca, W. A.; Hanson, V. A.; Cha, R.; Kokmen, E.; O´Brien, P. C.; Palumbo, P. J. *Ann. N. Y. Acad. Sci.* **1997,** *826*, 422-7.
153. Luchsinger, J. A.; Tang, M. X.; Stern, Y.; Shea, S.; Mayeux, R. *Am. J. Epidemiol.* **2001,** *154*, 635-41.
154. Ott, A.; Stolk, R. P.; van Harskamp, F.; Pols, H. A.; Hofman, A.; Breteler, M. M. *Neurology* **1999,** *53*, 1937-42.
155. Cheung, Z. H.; Gong, K.; Ip, N. Y. *J. Neurosci.* **2008,** *28*, 4872-7.
156. Weishaupt, J. H.; Kussmaul, L.; Grotsch, P.; Heckel, A.; Rohde, G.; Romig, H.; Bahr, M.; Gillardon, F. *Mol. Cell. Neurosci.* **2003,** *24*, 489-502.
157. Deane, R.; Wu, Z.; Zlokovic, B. V. *Stroke* **2004,** *35*, 2628-31.
158. Kalaria, R. N. *Nutr. Rev.* **2010,** *68*, S74-S87.
159. McGuinness, B.; Todd, S.; Passmore, A. P.; Bullock, R. *J. Neurol. Neurosurg. Psychiatry* **2008,** *79*, 4-5.
160. Anstey, K. J.; Lipnicki, D. M.; Low, L. F. *Am. J. Geriatr. Psychiatry* **2008,** *16*, 343-54.
161. Kivipelto, M.; Solomon, A. *Acta Neurol. Scand.* **2006,** *114*, 50-7.
162. McGuinness, B.; Craig, D.; Bullock, R.; Passmore, P. *Cochrane Database Syst. Rev.* **2009**, CD003160.
163. Francis, P. T.; Palmer, A. M.; Snape, M.; Wilcock, G. K. *J. Neurol. Neurosurg. Psychiatry* **1999,** *66*, 137-47.
164. Ibach, B.; Haen, E. *Curr. Pharm. Des.* **2004,** *10*, 231-51.
165. Davis, K. L.; Thal, L. J.; Gamzu, E. R.; Davis, C. S.; Woolson, R. F.; Gracon, S. I.; Drachman, D. A.; Schneider, L. S.; Whitehouse, P. J.; Hoover, T. M.; et al. *N. Engl. J. Med.* **1992,** *327*, 1253-9.
166. Hansen, R. A.; Gartlehner, G.; Webb, A. P.; Morgan, L. C.; Moore, C. G.; Jonas, D. E. *Clin. Interv. Aging* **2008,** *3*, 211-25.
167. Mori, E.; Hashimoto, M.; Krishnan, K. R.; Doraiswamy, P. M. *Alzheimer Dis. Assoc. Disord.* **2006,** *20*, S19-26.
168. Seow, D.; Gauthier, S. *Can. J. Psychiatry* **2007,** *52*, 620-9.
169. Birks, J.; Grimley Evans, J.; Iakovidou, V.; Tsolaki, M.; Holt, F. E. *Cochrane Database Syst. Rev.* **2009**, CD001191.
170. Birks, J.; Harvey, R. J. *Cochrane Database Syst. Rev.* **2006**, CD001190.
171. Loy, C.; Schneider, L. *Cochrane Database Syst. Rev.* **2006**, CD001747.
172. Waldemar, G.; Gauthier, S.; Jones, R.; Wilkinson, D.; Cummings, J.; Lopez, O.; Zhang, R.; Xu, Y.; Sun, Y.; Knox, S.; Richardson, S.; Mackell, J. *Int. J. Geriatr. Psychiatry* **2011,** *26*, 150-7.
173. Rockwood, K.; Fay, S.; Song, X.; MacKnight, C.; Gorman, M. *CMAJ* **2006,** *174*, 1099-105.
174. Rockwood, K.; Stolee, P.; Howard, K.; Mallery, L. *Neuroepidemiology* **1996,** *15*, 330-8.
175. Reisberg, B.; Doody, R.; Stoffler, A.; Schmitt, F.; Ferris, S.; Mobius, H. J. *N. Engl. J. Med.* **2003,** *348*, 1333-41.
176. Koch, H. J.; Szecsey, A.; Haen, E. *Curr. Pharm. Des.* **2004,** *10*, 253-9.
177. Scarpini, E.; Scheltens, P.; Feldman, H. *Lancet Neurol.* **2003,** *2*, 539-47.
178. Gauthier, S.; Loft, H.; Cummings, J. *Int. J. Geriatr. Psychiatry* **2008,** *23*, 537-45.
179. Wilcock, G. K.; Ballard, C. G.; Cooper, J. A.; Loft, H. *J. Clin. Psychiatry* **2008,** *69*, 341-8.
180. Lopez, O. L.; Becker, J. T.; Wahed, A. S.; Saxton, J.; Sweet, R. A.; Wolk, D. A.; Klunk, W.; Dekosky, S. T. *J. Neurol. Neurosurg. Psychiatry* **2009,** *80*, 600-7.
181. Potter, P. E. *J. Am. Osteopath. Assoc.* **2010,** *110*, S27-36.
182. Ballard, C.; Hanney, M. L.; Theodoulou, M.; Douglas, S.; McShane, R.; Kossakowski, K.; Gill, R.; Juszczak, E.; Yu, L. M.; Jacoby, R. *Lancet Neurol.* **2009,** *8*, 151-7.
183. Ballard, C.; Howard, R. *Nat. Rev. Neurosci.* **2006,** *7*, 492-500.
184. de la Torre, J. C. *J. Alzheimers Dis.* **2011,** *24*, 657-68.
185. Selkoe, D. J. *J. Alzheimers Dis.* **2001,** *3*, 75-80.
186. Citron, M. *Nat. Rev. Drug Discov.* **2010,** *9*, 387-98.
187. Hawkes, C. A.; McLaurin, J. *Expert Rev. Neurother.* **2007,** *7*, 1535-48.
188. Schenk, D.; Hagen, M.; Seubert, P. *Curr. Opin. Immunol.* **2004,** *16*, 599-606.
189. Hock, C.; Konietzko, U.; Streffer, J. R.; Tracy, J.; Signorell, A.; Muller-Tillmanns, B.; Lemke, U.; Henke, K.; Moritz, E.; Garcia, E.; Wollmer, M. A.; Umbricht, D.; de Quervain, D. J.; Hofmann, M.; Maddalena, A.; Papassotiropoulos, A.; Nitsch, R. M. *Neuron* **2003,** *38*, 547-54.
190. Panza, F.; Frisardi, V.; Solfrizzi, V.; Imbimbo, B. P.; Logroscino, G.; Santamato, A.; Greco, A.; Seripa, D.; Pilotto, A. *Immunotherapy* **2012,** *4*, 213-38.
191. Bard, F.; Cannon, C.; Barbour, R.; Burke, R. L.; Games, D.; Grajeda, H.; Guido, T.; Hu, K.; Huang, J.; Johnson-Wood, K.; Khan, K.; Kholodenko, D.; Lee, M.; Lieberburg, I.; Motter, R.; Nguyen, M.; Soriano, F.; Vasquez, N.; Weiss, K.; Welch, B.; Seubert, P.; Schenk, D.; Yednock, T. *Nat. Med.* **2000,** *6*, 916-9.
192. Hartman, R. E.; Izumi, Y.; Bales, K. R.; Paul, S. M.; Wozniak, D. F.; Holtzman, D. M. *J. Neurosci.* **2005,** *25*, 6213-20.
193. Eckman, E. A.; Eckman, C. B. *Biochem. Soc. Trans.* **2005,** *33*, 1101-5.
194. Jacobsen, J. S.; Comery, T. A.; Martone, R. L.; Elokdah, H.; Crandall, D. L.; Oganesian, A.; Aschmies, S.; Kirksey, Y.; Gonzales, C.; Xu, J.; Zhou, H.; Atchison, K.; Wagner, E.; Zaleska, M. M.; Das, I.; Arias, R. L.; Bard, J.; Riddell, D.; Gardell, S. J.; Abou-Gharbia, M.; Robichaud, A.; Magolda, R.; Vlasuk, G. P.; Bjornsson, T.; Reinhart, P. H.; Pangalos, M. N. *PNAS USA* **2008,** *105*, 8754-9.
195. Gervais, F.; Paquette, J.; Morissette, C.; Krzywkowski, P.; Yu, M.; Azzi, M.; Lacombe, D.; Kong, X.; Aman, A.; Laurin, J.; Szarek, W. A.; Tremblay, P. *Neurobiol. Aging* **2007,** *28*, 537-47.
196. Beher, D.; Bettati, M.; Checksfield, G. D.; Churcher, I.; Doughty, V. A.; Oakley, P. J.; Quddus, A.; Teall, M. R.; Wrigley, J. D.; Merck Sharp & Dohme Limited, UK, 2005.
197. Kounnas, M. Z.; Danks, A. M.; Cheng, S.; Tyree, C.; Ackerman, E.; Zhang, X.; Ahn, K.; Nguyen, P.; Comer, D.; Mao, L.; Yu, C.; Pleynet, D.; Digregorio, P. J.; Velicelebi, G.; Stauderman, K. A.; Comer, W. T.; Mobley, W. C.; Li, Y. M.; Sisodia, S. S.; Tanzi, R. E.; Wagner, S. L. *Neuron* **2010,** *67*, 769-80.
198. Stanton, M. G.; Hubbs, J.; Sloman, D.; Hamblett, C.; Andrade, P.; Angagaw, M.; Bi, G.; Black, R. M.; Crispino, J.; Cruz, J. C.; Fan, E.; Farris, G.; Hughes, B. L.; Kenific, C. M.; Middleton, R. E.; Nikov, G.; Sajonz, P.; Shah, S.; Shomer, N.; Szewczak, A. A.; Tanga, F.; Tudge, M. T.; Shearman, M.; Munoz, B. *Bioorg. Med. Chem. Lett.* **2010,** *20*, 755-8.
199. Van Broeck, B.; Chen, J. M.; Treton, G.; Desmidt, M.; Hopf, C.; Ramsden, N.; Karran, E.; Mercken, M.; Rowley, A. *Br. J. Pharmacol.* **2011,** *163*, 375-89.
200. Milano, J.; McKay, J.; Dagenais, C.; Foster-Brown, L.; Pognan, F.; Gadient, R.; Jacobs, R. T.; Zacco, A.; Greenberg, B.; Ciaccio, P. J. *Toxicol. Sci.* **2004,** *82*, 341-58.

201. Wong, G. T.; Manfra, D.; Poulet, F. M.; Zhang, Q.; Josien, H.; Bara, T.; Engstrom, L.; Pinzon-Ortiz, M.; Fine, J. S.; Lee, H. J.; Zhang, L.; Higgins, G. A.; Parker, E. M. *J. Biol. Chem.* **2004,** *279*, 12876-82.
202. Trojanowski, J. Q.; Lee, V. M. *FASEB J.* **1995,** *9*, 1570-6.
203. Iqbal, K.; Liu, F.; Gong, C. X.; Grundke-Iqbal, I. *Curr. Alzheimer Res.* **2010,** *7*, 656-64.
204. Lee, V. M.; Goedert, M.; Trojanowski, J. Q. *Annu. Rev. Neurosci.* **2001,** *24*, 1121-59.
205. Thal, D. R.; Holzer, M.; Rub, U.; Waldmann, G.; Gunzel, S.; Zedlick, D.; Schober, R. *Exp. Neurol.* **2000,** *163*, 98-110.
206. Lee, V. M.; Trojanowski, J. Q. *J. Alzheimers Dis.* **2006,** *9*, 257-62.
207. Schneider, A.; Mandelkow, E. *Neurotherapeutics* **2008,** *5*, 443-57.
208. Bulic, B.; Pickhardt, M.; Schmidt, B.; Mandelkow, E. M.; Waldmann, H.; Mandelkow, E. *Angew. Chem. Int. Ed. Engl.* **2009,** *48*, 1740-52.
209. Gong, C. X.; Iqbal, K. *Curr. Med. Chem.* **2008,** *15*, 2321-8.
210. Kramer, T.; Schmidt, B.; Lo Monte, F. *Int. J. Alzheimers Dis.* **2012,** *2012*, 381029.
211. Dominguez, J. M.; Fuertes, A.; Orozco, L.; del Monte-Millan, M.; Delgado, E.; Medina, M. *J. Biol. Chem.* **2012,** *287*, 893-904.
212. Eldar-Finkelman, H.; Martinez, A. *Front. Mol. Neurosci.* **2011,** *4*, 32.
213. Phukan, S.; Babu, V. S.; Kannoji, A.; Hariharan, R.; Balaji, V. N. *Br. J. Pharmacol.* **2010,** *160*, 1-19.
214. Mangialasche, F.; Solomon, A.; Winblad, B.; Mecocci, P.; Kivipelto, M. *Lancet Neurol.* **2010,** *9*, 702-16.
215. Tobinick, E.; Gross, H.; Weinberger, A.; Cohen, H. *MedGenMed* **2006,** *8*, 25.
216. Tobinick, E. L.; Gross, H. *BMC Neurol.* **2008,** *8*, 27.
217. Tobinick, E. L.; Gross, H. *J. Neuroinflammation* **2008,** *5*, 2.
218. Winblad, B. G.; Minthon, L.; Floesser, A.; Imbert, G.; Dumortier, T.; He, Y.; Maguire, P.; Karlsson, M.; Östlund, H.; Lundmark, J.; Orgogozo, J. M.; Graf, A.; Andreasen, N. *Alzheimer Dement.* **2009,** *5*, 113-4.
219. Dubois, B.; Feldman, H. H.; Jacova, C.; Cummings, J. L.; Dekosky, S. T.; Barberger-Gateau, P.; Delacourte, A.; Frisoni, G.; Fox, N. C.; Galasko, D.; Gauthier, S.; Hampel, H.; Jicha, G. A.; Meguro, K.; O'Brien, J.; Pasquier, F.; Robert, P.; Rossor, M.; Salloway, S.; Sarazin, M.; de Souza, L. C.; Stern, Y.; Visser, P. J.; Scheltens, P. *Lancet Neurol.* **2010,** *9*, 1118-27.
220. Gates, N.; Valenzuela, M. *Curr. Psychiatry Rep.* **2010,** *12*, 20-7.
221. *www.happy-neuron.de // www.happy-neuron.com* **2012**.
222. *www.proteinkinase.info* **2012**.
223. *www.cellsignal.com* **2012**.
224. Kaidanovich-Beilin, O.; Woodgett, J. R. *Front. Mol. Neurosci.* **2011,** *4*, 40.
225. Ubersax, J. A.; Ferrell, J. E., Jr. *Nat. Rev. Mol. Cell Biol.* **2007,** *8*, 530-41.
226. Embi, N.; Rylatt, D. B.; Cohen, P. *Eur. J. Biochem.* **1980,** *107*, 519-27.
227. Cohen, P.; Frame, S. *Nat. Rev. Mol. Cell Biol.* **2001,** *2*, 769-76.
228. Frame, S.; Cohen, P. *Biochem. J.* **2001,** *359*, 1-16.
229. Kockeritz, L.; Doble, B.; Patel, S.; Woodgett, J. R. *Curr. Drug Targets* **2006,** *7*, 1377-88.
230. Lei, P.; Ayton, S.; Bush, A. I.; Adlard, P. A. *Int. J. Alzheimers Dis.* **2011,** *2011*, 189246.
231. Woodgett, J. R. *EMBO J.* **1990,** *9*, 2431-8.
232. Ferrer, I.; Barrachina, M.; Puig, B. *Acta Neuropathol.* **2002,** *104*, 583-91.
233. Perez-Costas, E.; Gandy, J. C.; Melendez-Ferro, M.; Roberts, R. C.; Bijur, G. N. *PLoS One* **2010,** *5*, e8911.
234. Yao, H. B.; Shaw, P. C.; Wong, C. C.; Wan, D. C. *J. Chem. Neuroanat.* **2002,** *23*, 291-7.
235. Dajani, R.; Fraser, E.; Roe, S. M.; Young, N.; Good, V.; Dale, T. C.; Pearl, L. H. *Cell* **2001,** *105*, 721-32.
236. Alon, L. T.; Pietrokovski, S.; Barkan, S.; Avrahami, L.; Kaidanovich-Beilin, O.; Woodgett, J. R.; Barnea, A.; Eldar-Finkelman, H. *FEBS Lett.* **2011,** *585*, 1158-62.
237. ter Haar, E.; Coll, J. T.; Austen, D. A.; Hsiao, H. M.; Swenson, L.; Jain, J. *Nat. Struct. Biol.* **2001,** *8*, 593-6.
238. Palomo, V.; Soteras, I.; Perez, D. I.; Perez, C.; Gil, C.; Campillo, N. E.; Martinez, A. *J. Med. Chem.* **2011,** *54*, 8461-70.
239. Saitoh, M.; Kunitomo, J.; Kimura, E.; Hayase, Y.; Kobayashi, H.; Uchiyama, N.; Kawamoto, T.; Tanaka, T.; Mol, C. D.; Dougan, D. R.; Textor, G. S.; Snell, G. P.; Itoh, F. *Bioorg. Med. Chem.* **2009,** *17*, 2017-29.
240. Hanks, S. K.; Quinn, A. M. *Methods Enzymol.* **1991,** *200*, 38-62.
241. Hanks, S. K.; Quinn, A. M.; Hunter, T. *Science* **1988,** *241*, 42-52.
242. Buescher, J. L.; Phiel, C. J. *J. Biol. Chem.* **2010,** *285*, 7957-63.
243. Medina, M.; Wandosell, F. *Int. J. Alzheimers Dis.* **2011,** *2011*, 479249.
244. Frame, S.; Cohen, P.; Biondi, R. M. *Mol. Cell* **2001,** *7*, 1321-7.
245. Stambolic, V.; Woodgett, J. R. *Biochem. J.* **1994,** *303 (Pt 3)*, 701-4.
246. Sutherland, C.; Leighton, I. A.; Cohen, P. *Biochem. J.* **1993,** *296 (Pt 1)*, 15-9.
247. Ding, Q.; Xia, W.; Liu, J. C.; Yang, J. Y.; Lee, D. F.; Xia, J.; Bartholomeusz, G.; Li, Y.; Pan, Y.; Li, Z.; Bargou, R. C.; Qin, J.; Lai, C. C.; Tsai, F. J.; Tsai, C. H.; Hung, M. C. *Mol. Cell* **2005,** *19*, 159-70.
248. Thornton, T. M.; Pedraza-Alva, G.; Deng, B.; Wood, C. D.; Aronshtam, A.; Clements, J. L.; Sabio, G.; Davis, R. J.; Matthews, D. E.; Doble, B.; Rincon, M. *Science* **2008,** *320*, 667-70.
249. Hughes, K.; Nikolakaki, E.; Plyte, S. E.; Totty, N. F.; Woodgett, J. R. *EMBO J.* **1993,** *12*, 803-8.
250. Kim, L.; Liu, J.; Kimmel, A. R. *Cell* **1999,** *99*, 399-408.
251. Buch, I.; Fishelovitch, D.; London, N.; Raveh, B.; Wolfson, H. J.; Nussinov, R. *Biochemistry* **2010,** *49*, 10890-901.
252. Cohen, P.; Goedert, M. *Nat. Rev. Drug Discov.* **2004,** *3*, 479-87.
253. Cole, A.; Frame, S.; Cohen, P. *Biochem. J.* **2004,** *377*, 249-55.
254. Chou, H. Y.; Howng, S. L.; Cheng, T. S.; Hsiao, Y. L.; Lieu, A. S.; Loh, J. K.; Hwang, S. L.; Lin, C. C.; Hsu, C. M.; Wang, C.; Lee, C. I.; Lu, P. J.; Chou, C. K.; Huang, C. Y.; Hong, Y. R. *Biochemistry* **2006,** *45*, 11379-89.
255. Stoothoff, W. H.; Cho, J. H.; McDonald, R. P.; Johnson, G. V. *J. Biol. Chem.* **2005,** *280*, 270-6.
256. Yost, C.; Farr, G. H., 3rd; Pierce, S. B.; Ferkey, D. M.; Chen, M. M.; Kimelman, D. *Cell* **1998,** *93*, 1031-41.
257. Bijur, G. N.; Jope, R. S. *Neuroreport* **2003,** *14*, 2415-9.
258. Franca-Koh, J.; Yeo, M.; Fraser, E.; Young, N.; Dale, T. C. *J. Biol. Chem.* **2002,** *277*, 43844-8.
259. Hoshi, M.; Takashima, A.; Noguchi, K.; Murayama, M.; Sato, M.; Kondo, S.; Saitoh, Y.; Ishiguro, K.; Hoshino, T.; Imahori, K. *PNAS USA* **1996,** *93*, 2719-23.
260. Azoulay-Alfaguter, I.; Yaffe, Y.; Licht-Murava, A.; Urbanska, M.; Jaworski, J.; Pietrokovski, S.; Hirschberg, K.; Eldar-Finkelman, H. *J. Biol. Chem.* **2011,** *286*, 13470-80.
261. Meares, G. P.; Jope, R. S. *J. Biol. Chem.* **2007,** *282*, 16989-7001.
262. Thomas, G. M.; Frame, S.; Goedert, M.; Nathke, I.; Polakis, P.; Cohen, P. *FEBS Lett.* **1999,** *458*, 247-51.
263. Doble, B. W.; Woodgett, J. R. *J. Cell Sci.* **2003,** *116*, 1175-86.

264. Eldar-Finkelman, H. *Trends Mol. Med.* **2002,** *8*, 126-32.
265. Gould, T. D.; Zarate, C. A.; Manji, H. K. *J. Clin. Psychiatry* **2004,** *65*, 10-21.
266. Hernandez, F.; Avila, J. *FEBS Lett.* **2008,** *582*, 3848-54.
267. Hooper, C.; Killick, R.; Lovestone, S. *J. Neurochem.* **2008,** *104*, 1433-9.
268. Hur, E. M.; Zhou, F. Q. *Nat. Rev. Neurosci.* **2010,** *11*, 539-51.
269. Jope, R. S.; Yuskaitis, C. J.; Beurel, E. *Neurochem. Res.* **2007,** *32*, 577-95.
270. Luo, J. *Cancer Lett.* **2009,** *273*, 194-200.
271. Ougolkov, A. V.; Billadeau, D. D. *Future Oncol.* **2006,** *2*, 91-100.
272. Aplin, A. E.; Gibb, G. M.; Jacobsen, J. S.; Gallo, J. M.; Anderton, B. H. *J. Neurochem.* **1996,** *67*, 699-707.
273. Kirschenbaum, F.; Hsu, S. C.; Cordell, B.; McCarthy, J. V. *J. Biol. Chem.* **2001,** *276*, 30701-7.
274. Kirschenbaum, F.; Hsu, S. C.; Cordell, B.; McCarthy, J. V. *J. Biol. Chem.* **2001,** *276*, 7366-75.
275. Terracciano, C.; Nogalska, A.; Engel, W. K.; Askanas, V. *J. Neurochem.* **2010,** *112*, 389-96.
276. Chico, L. K.; Van Eldik, L. J.; Watterson, D. M. *Nat. Rev. Drug Discov.* **2009,** *8*, 892-909.
277. Lipinski, C. A.; Lombardo, F.; Dominy, B. W.; Feeney, P. J. *Adv. Drug Deliv. Rev.* **2001,** *46*, 3-26.
278. Wager, T. T.; Hou, X.; Verhoest, P. R.; Villalobos, A. *ACS Chem. Neurosci.* **2010,** *1*, 435-49.
279. Bech, P. *Psychother. Psychosom.* **2006,** *75*, 265-9.
280. Jope, R. S. *Trends Pharmacol. Sci.* **2003,** *24*, 441-3.
281. Rowe, M. K.; Wiest, C.; Chuang, D. M. *Neurosci. Biobehav. Rev.* **2007,** *31*, 920-31.
282. Conde, S.; Perez, D. I.; Martinez, A.; Perez, C.; Moreno, F. J. *J. Med. Chem.* **2003,** *46*, 4631-3.
283. Perez, D. I.; Conde, S.; Perez, C.; Gil, C.; Simon, D.; Wandosell, F.; Moreno, F. J.; Gelpi, J. L.; Luque, F. J.; Martinez, A. *Bioorg. Med. Chem.* **2009,** *17*, 6914-25.
284. Perez, D. I.; Palomo, V.; Perez, C.; Gil, C.; Dans, P. D.; Luque, F. J.; Conde, S.; Martinez, A. *J. Med. Chem.* **2011,** *54*, 4042-56.
285. Grutter, C.; Simard, J. R.; Mayer-Wrangowski, S. C.; Schreier, P. H.; Perez-Martin, J.; Richters, A.; Getlik, M.; Gutbrod, O.; Braun, C. A.; Beck, M. E.; Rauh, D. *ACS Chem. Biol.* **2012,** *7*, 1257-67.
286. Ilouz, R.; Kowalsman, N.; Eisenstein, M.; Eldar-Finkelman, H. *J. Biol. Chem.* **2006,** *281*, 30621-30.
287. Ilouz, R.; Pietrokovski, S.; Eisenstein, M.; Eldar-Finkelman, H. *J. Mol. Biol.* **2008,** *383*, 999-1007.
288. Licht-Murava, A.; Plotkin, B.; Eisenstein, M.; Eldar-Finkelman, H. *J. Mol. Biol.* **2011,** *408*, 366-78.
289. Hamann, M.; Alonso, D.; Martin-Aparicio, E.; Fuertes, A.; Perez-Puerto, M. J.; Castro, A.; Morales, S.; Navarro, M. L.; Del Monte-Millan, M.; Medina, M.; Pennaka, H.; Balaiah, A.; Peng, J.; Cook, J.; Wahyuono, S.; Martinez, A. *J. Nat. Prod.* **2007,** *70*, 1397-405.
290. Plotkin, B.; Kaidanovich, O.; Talior, I.; Eldar-Finkelman, H. *J. Pharmacol. Exp. Ther.* **2003,** *305*, 974-80.
291. Huse, M.; Kuriyan, J. *Cell* **2002,** *109*, 275-82.
292. Johnson, L. N.; Lowe, E. D.; Noble, M. E.; Owen, D. J. *FEBS Lett.* **1998,** *430*, 1-11.
293. Zuccotto, F.; Ardini, E.; Casale, E.; Angiolini, M. *J. Med. Chem.* **2010,** *53*, 2681-94.
294. *www.merckmillipore.com* **2012**.
295. Banerji, V.; Frumm, S. M.; Ross, K. N.; Li, L. S.; Schinzel, A. C.; Hahn, C. K.; Kakoza, R. M.; Chow, K. T.; Ross, L.; Alexe, G.; Tolliday, N.; Inguilizian, H.; Galinsky, I.; Stone, R. M.; DeAngelo, D. J.; Roti, G.; Aster, J. C.; Hahn, W. C.; Kung, A. L.; Stegmaier, K. *J. Clin. Invest.* **2012,** *122*, 935-47.
296. Jaworski, T.; Dewachter, I.; Lechat, B.; Gees, M.; Kremer, A.; Demedts, D.; Borghgraef, P.; Devijver, H.; Kugler, S.; Patel, S.; Woodgett, J. R.; Van Leuven, F. *Nature* **2011,** *480*, E4-5; Discussion E6.
297. Feng, L.; Geisselbrecht, Y.; Blanck, S.; Wilbuer, A.; Atilla-Gokcumen, G. E.; Filippakopoulos, P.; Kraling, K.; Celik, M. A.; Harms, K.; Maksimoska, J.; Marmorstein, R.; Frenking, G.; Knapp, S.; Essen, L. O.; Meggers, E. *JACS* **2011,** *133*, 5976-86.
298. Bhat, R.; Xue, Y.; Berg, S.; Hellberg, S.; Ormo, M.; Nilsson, Y.; Radesater, A. C.; Jerning, E.; Markgren, P. O.; Borgegard, T.; Nylof, M.; Gimenez-Cassina, A.; Hernandez, F.; Lucas, J. J.; Diaz-Nido, J.; Avila, J. *J. Biol. Chem.* **2003,** *278*, 45937-45.
299. Noble, W.; Planel, E.; Zehr, C.; Olm, V.; Meyerson, J.; Suleman, F.; Gaynor, K.; Wang, L.; LaFrancois, J.; Feinstein, B.; Burns, M.; Krishnamurthy, P.; Wen, Y.; Bhat, R.; Lewis, J.; Dickson, D.; Duff, K. *PNAS USA* **2005,** *102*, 6990-5.
300. Selenica, M. L.; Jensen, H. S.; Larsen, A. K.; Pedersen, M. L.; Helboe, L.; Leist, M.; Lotharius, J. *Br. J. Pharmacol.* **2007,** *152*, 959-79.
301. *www.noscira.com* **2012**.
302. del Ser, T. *Alzheimer´s Dementia* **2010,** *6*.
303. Luna-Medina, R.; Cortes-Canteli, M.; Sanchez-Galiano, S.; Morales-Garcia, J. A.; Martinez, A.; Santos, A.; Perez-Castillo, A. *J. Neurosci.* **2007,** *27*, 5766-76.
304. Martinez, A.; Alonso, M.; Castro, A.; Dorronsoro, I.; Gelpi, J. L.; Luque, F. J.; Perez, C.; Moreno, F. J. *J. Med. Chem.* **2005,** *48*, 7103-12.
305. Martinez, A.; Alonso, M.; Castro, A.; Perez, C.; Moreno, F. J. *J. Med. Chem.* **2002,** *45*, 1292-9.
306. Baumann, S., TU Darmstadt, 2009.
307. Larbig, G., TU Darmstadt, 2007.
308. Zhou, J.; Lal, H.; Chen, X.; Shang, X.; Song, J.; Li, Y.; Kerkela, R.; Doble, B. W.; MacAulay, K.; DeCaul, M.; Koch, W. J.; Farber, J.; Woodgett, J.; Gao, E.; Force, T. *J. Clin. Invest.* **2010,** *120*, 2280-91.
309. Atilla-Gokcumen, G. E.; Williams, D. S.; Bregman, H.; Pagano, N.; Meggers, E. *ChemBioChem* **2006,** *7*, 1443-50.
310. Paquet, D.; Bhat, R.; Sydow, A.; Mandelkow, E. M.; Berg, S.; Hellberg, S.; Falting, J.; Distel, M.; Koster, R. W.; Schmid, B.; Haass, C. *J. Clin. Invest.* **2009,** *119*, 1382-95.
311. Bostrom, J.; Hogner, A.; Llinas, A.; Wellner, E.; Plowright, A. T. *J. Med. Chem.* **2012,** *55*, 1817-30.
312. Turner, S.; Mack, H.; Bakker, M. H. M.; Van Gaalen, M.; Hoft, C.; Hornberger, W.; Abbott GmbH & Co. KG, 2012.
313. Berg, S.; Bergh, M.; Hellberg, S.; Hogdin, K.; Lo-Alfredsson, Y.; Soderman, P.; von Berg, S.; Weigelt, T.; Ormo, M.; Xue, Y.; Tucker, J.; Neelissen, J.; Jerning, E.; Nilsson, Y.; Bhat, R. *J. Med. Chem.* **2012**.
314. Lo Monte, F.; Kramer, T.; Gu, J.; Anumala, U. R.; Marinelli, L.; La Pietra, V.; Novellino, E.; Franco, B.; Demedts, D.; Van Leuven, F.; Fuertes, A.; Dominguez, J. M.; Plotkin, B.; Eldar-Finkelman, H.; Schmidt, B. *J. Med. Chem.* **2012,** *55*, 4407-24.
315. Lo Monte, F.; Kramer, T.; Gu, J.; Brodrecht, M.; Pilakowski, J.; Fuertes, A.; Dominguez, J. M.; Plotkin, B.; Eldar-Finkelman, H.; Schmidt, B. *Eur J. Med. Chem.* **2012**.

8 Anhang

Thomas Kramer 29.10.2012

Bornheimer Landwehr 91

60385 Frankfurt am Main

Eidesstattliche Erklärung

Ich erkläre hiermit an Eides Statt, dass ich meine Dissertation selbständig und nur mit den angegebenen Hilfsmitteln angefertigt habe.

Thomas Kramer

Thomas Kramer

Bornheimer Landwehr 91

60385 Frankfurt am Main

29.10.2012

Erklärung

Ich erkläre hiermit, noch keinen Promotionsversuch unternommen zu haben.

Thomas Kramer

Curriculum Vitae

PERSÖNLICHES

Name	Thomas Kramer
Adresse	Bornheimer Landwehr 91 60385 Frankfurt am Main
Nationalität	Deutsch
Telefonnummer	+49/17670065061
E-Mail-Adresse	th.b.kramer@gmx.de

BERUFLICHER WERDEGANG

seit 10/2008 **Promotion**

Themenschwerpunkt: Synthese von Kinase-Inhibitoren, gefördert durch das *European 7th Framework Programme*, Technische Universität Darmstadt, organische/medizinische Chemie, Arbeitskreis von Herrn Prof. Dr. Boris Schmidt

01/2008 - 09/2008 **Chemiker bei der Baxter Oncology GmbH**

Bereich Research & Development der Wirkstoffproduktion, Schwerpunkt: Scale-up, Baxter Oncology GmbH Bielefeld

10/2007 - 12/2007 **Wissenschaftlicher Angestellter**

Aufgabengebiet: Synthese von Farbstoff-gekoppelten Sonden zur Proteindetektion, Universität Bielefeld, organische/bioorganische Chemie, Arbeitskreis von Herrn Prof. Dr. Norbert Sewald

10/1999 - 09/2007 **Studium Diplom-Chemie**
Diplom Note: „gut“; Diplomarbeit Note: „sehr gut“

Thema der Diplomarbeit: Molekulare Werkzeuge zur Charakterisierung von Sulfatasen, Universität Bielefeld, organische/bioorganische Chemie, Arbeitskreis von Herrn Prof. Dr. Norbert Sewald

11/1998 - 08/1999 **Wehrdienst**

Obergefreiter an der Artellerieschule Idar-Oberstein bzw. Blücher Kaserne Münster (Westf.)

07/1998 **Abitur**
Note: 2,8

Allgemeine Hochschulreife am Gymnasium Ochtrup

NEBENTÄTIGKEITEN

09/2010 - 08/2011	Ehrenamtlicher Unternehmensbetreuer der AG konaktiva GbR der Technischen Universität Darmstadt
02/2007 - 08/2007	Mitarbeiter in Technik und Verwaltung, Chemikalienlager, Universität Bielefeld
03/2003 - 09/2006	Studentische Hilfskraft, Chemikalienlager, Universität Bielefeld
10/2002 - 02/2003	Studentische Hilfskraft, Praktikum Organische Chemie II, Universität Bielefeld

AKADEMISCHE WEITERBILDUNG

01/2011	Von der Erfindung zum Patent
01/2011	Führungskompetenzen für Wissenschaftler und Wissenschaftlerinnen
09/2010	Teilnahme an der 5th Summer School „Medicinal Chemistry“
10/2009 - 02/2010	Projektmanagement I
04/2009 - 07/2009	Analytik und Qualitätskontrolle im chemischen und pharmazeutischen Unternehmen (Merck KGaA)
10/2008 - 02/2009	Management von Forschung und Entwicklung in der chemischen Industrie (Merck KGaA)

ZUSATZQUALIFIKATIONEN/ FACHKENNTNISSE

Sprachen	Deutsch (Muttersprache) Englisch (fließend in Wort und Schrift)
EDV	MS/Mac Office (Word, Excel, Powerpoint, Outlook/Entourage) Patent-/Literaturrecherche, z.B. mittels SciFinder Molegro Virtual Docker
Fachkenntnisse	Grundlagen der medizinalchemischen Forschung: Optimierung einer Leitstruktur, Auswertung von Struktur-Aktivitätsuntersuchungen, Molecular Modelling, biochemische Untersuchungsmethoden (z.B. SDS-Page, Western Blot) Sehr gute theoretische und praktische Kenntnisse der organischen Synthesechemie (z.B. Heterozyklen-, Peptid- und Medizinalchemie) und gängiger analytischer Methoden (z.B. NMR, MS, IR, HPLC, LC, DC) Erfahrungen in der der Handhabung von Schlenck-Techniken und metallorganischer Verbindungen Führungserfahrung durch Betreuung von Praktikanten sowie Bachelor-, Master- und Diplomarbeiten

PUBLIKATIONEN/PATENTE

Wissenschaftliche Publikationen

T. Kramer, B. Schmidt and F. Lo Monte. Small-molecule inhibitors of GSK-3 – Structural insights and their application to Alzheimer´s disease models. *Int. J. Alzheimers Dis.* 2012, *im Druck*.

F. Lo Monte, **T. Kramer**, J. Gu, U. R. Anumala, L. Marinelli, V. La Pietra, E. Novellino, B. Franco, D. Demedts, F. Van Leuven, A. Fuertes, J. M. Dominguez, B. Plotkin, H. Eldar-Finkelman and B. Schmidt. Identification of Glycogen Synthase Kinase-3 Inhibitors with a Selective Sting for Glycogen Synthase Kinase-3α. *J. Med. Chem.* 2012, *55*, 4407-4424.

F. Lo Monte, **T. Kramer**, J. Gu, M. Brodrecht, J. Pilakowski, A. Fuertes, J. M. Dominguez, B. Plotkin, H. Eldar-Finkelman and B. Schmidt. Structure-based optimization of oxadiazole-based GSK-3 inhibitors. *Eur. J. Med. Chem.* 2012, *im Druck*.

F. Lo Monte*, **T. Kramer***, A. Boländer, B. Plotkin, H. Eldar-Finkelman, A. Fuertes, J. Dominguez, B. Schmidt. Synthesis and biological evaluation of glycogen synthase kinase-3 (GSK-3) inhibitors: An fast and atom efficient access to 1-aryl-3-benzylureas. *Bioorg. Med. Chem. Lett.* 2011, *21*, 5610-5615.

T. Kramer*, F. Lo Monte*, S. Göring, G. M. Okala Amombo, B. Schmidt. Small Molecule Kinase Inhibitors for LRRK2 and Their Application to Parkinson´s Disease Models. *ACS Chem. Neurosci.* 2012, *3*, 151-160.

G. M. Okala Amombo*, **T. Kramer***, F. Lo Monte*, S. Göring, M. Fach, S. Smith, S. Kolb, R. Schubenel, K. Baumann, B. Schmidt. Modification of a promiscuous inhibitor shifts the inhibition from γ-secretase to FLT-3. *Bioorg. Med. Chem. Lett.* veröffentlicht im Oktober 2012.

J. Gu, U. R. Anumala, F. Lo Monte, **T. Kramer**, R. H. von Haußen, J. Hölzer, V. Goetschy-Meyer, G. Mall, I. Hilger, C. Czech, B. Schmidt. 2-Styrylindolium based fluorescent probes visualize neurofibrillary tangles in Alzheimer´s disease. *Bioorg. Med. Chem. Lett.* veröffentlicht im Oktober 2012.

Patente

Patentanmeldung 2011, Nr.: DE 10 2011 106 990.2

VORTRÄGE/POSTERPRÄSENTATIONEN

Vorträge

„The A is GSK-3α, but what was the Q?", *3th neuro.GSK3 consortium meeting*, 26.-27.01.2012, Leuven, Belgien

„Potential Inhibitors for Alzheimer´s disease", *Doktorandenworkshop des Promotionskollegs der Technischen Universität Darmstadt*, 07.07.2010, Darmstadt

„Overview of known glycogen synthase kinase 3β (GSK-3β) inhibitors and our current results", *1th neuro.GSK3 consortium meeting*, 05.-06.11.2012, Darmstadt

Posterpräsentationen

F. Lo Monte*, T. Kramer*, A. Boländer, B. Plotkin, H. Eldar-Finkelman, A. Fuertes, J. Dominguez und B. Schmidt, „GSK-3 inhibitors in Alzheimer's disease", *International Conference on Alzheimer´s Disease (ICAD) 2011*, 17.-20.07.2011, Paris, Frankreich

T. Kramer*, F. Lo Monte*, A. Boländer, B. Plotkin, H. Eldar-Finkelman, A. Fuertes, J. Dominguez und B. Schmidt, „GSK-3 inhibitors in Alzheimer´s disease – a structure-activity relationship study", *Doktorandenworkshop des Promotionskollegs der Technischen Universität Darmstadt*, 13.07.2011, Darmstadt

F. Lo Monte*, T. Kramer*, A. Boländer, B. Plotkin, H. Eldar-Finkelman und B. Schmidt, „GSK-3 inhibitors in Alzheimer´s disease", *5th Summer School Medicinal Chemistry – „Medicinal Chemistry: Molecular Recognition – Ligand Receptor Interactions"*, 13.-15.09.2010, Regensburg

Thomas Kramer

Frankfurt am Main, 29. Oktober 2012